TERRE & ENVIRONNEMENT

Osman PARLAK

Geochemistry and geochronology of the Mersin ophiolite within the eastern Mediterranean tectonic frame (southern Turkey)

1996

Volume 6

Institut Forel
Département de Minéralogie
Département de Géologie et Paléontologie

Section des Sciences de la Terre, Université de Genève

UNIVERSITÉ DE GENÈVE
Département de Minéralogie

FACULTÉ DES SCIENCES
Professeur Michel Delaloye

Geochemistry and geochronology of the Mersin ophiolite within the Eastern Mediterranean tectonic frame (Southern Turkey)

THÈSE

présentée à la Faculté des Sciences de l'Université de Genève pour obtenir le grade de Docteur ès Sciences, mention Sciences de la Terre

Par

Osman PARLAK

d'Adana (Turquie)

Thèse No 2824

Genève
1996

La Faculté des Sciences, sur le préavis de Messieurs M. DELALOYE, professeur ordinaire et directeur de thèse (Département de minéralogie), E. BINGÖL, profeseur et codirecteur de thèse (Université Çukurova, Adana, Turquie), P.A. FLOYD, professeur (Université de Keele, Grande-Bretagne), J. BERTRAND, professeur titulaire (Département de minéralogie) et B. SINGER, docteur (Département de minéralogie), autorise l'impression de la présente thèse, sans exprimer d'opinion sur les propositions qui y sont énoncées.

Genève, le 20 juin 1996

Thèse - 2824 -

Le Doyen, Eric DOELKER

Parlak, O.: Geochemistry and geochronology of the Mersin ophiolite within the eastern Mediterranean tectonic frame (Southern Turkey).

Terre&Environnement, vol. 6, ix + 242 pp. (1996)

ISBN 2-940153-05-1
Section des Sciences de la Terre, Université de Genève, 13 Rue des Maraichers, CH-1211 Genève 4, SUISSE
Téléphone: ++41-22-702-6611, Téléfax: ++41-22-320-5732

TABLE OF CONTENTS

* This chapter "Introduction and summary of the results" is written in French in accordance with the instructions for publication of PhD theses of the Faculté des Sciences, Université de Genève.

ACKNOWLEDGEMENTS

I would like to thank my research supervisor, Prof. Michel Delaloye, for allowing me the opportunity to enter the domain of scientific research, and for his encouragement, and technical and financial support which permitted that this work be accomplished.

I would like to thank Prof. Erguzer Bingol (co-supervisor) for introducing me to the Mersin ophiolite and his valuable discussions throughout the project.

I would like to thank the members of my Ph.D. dissertation committee, Prof. Michel Delaloye, Prof. Erguzer Bingol, Prof. Jean Bertrand, Dr. Peter Floyd and Dr. Bradley Singer, for productive discussions about the research that lead to the manuscript chapters of my dissertation.

I am grateful to Prof. Cavit Demirkol and Prof. Aziz Ertunc in the Geology Department at Çukurova University in Turkey, without their help this study could not have been completed. I would like to express my appreciation to Hüseyin Kozlu for his productive discussions in the field.

I would like to express my thanks for the analytical work in the laboratory of Department of Mineralogy at the Universities of Geneva and Lausanne; especially to Fabio Capponi and Michèle Senn-Berger (XRF analyses); Dr. P. Voldet (REE analyses); Dr. D. Fontignie and Marcelle Falcheri ($^{87}Sr/^{86}Sr$ and $^{143}Nd/^{144}Nd$ isotope measurements); Dr. B. Singer ($^{40}Ar/^{39}Ar$ incremental heating analyses); Christian Kasper (K-Ar analyses); Drs. T. Feeley and F. Bussy (Microprobe analyses); J.M. Bocard and V. Cornut (thin section preparation).

My warmest thanks go out to Ö.Faruk Çelik, Alican Kop, Mustafa Açlan and Ertan Bol for their appreciated assistance during the field study.

Thanks and appreciation go to my friends and colleagues in the Mineralogy Department especially J. Berthoud, U. Eigenmann, M. Doppler, R. Marschik, M. Ferrés, A. Moscariello, M. Chiaradia, F. Costa, F. Lieben for interesting discussions and shared experience.

I acknowledge financial support from the Swiss National Science Foundation (Grant No= (20-40240.94/1).

Finally I deeply thank the support, encouragement, and patience of my family and my fiancée, Derya Erdem, during my study.

ABSTRACT

The Mersin ophiolite, which is one of the Cretaceous ophiolitic massifs situated on the southern flank of the Tauride belt in southern Turkey, is bounded tectonicaly by the sinistral Ecemis fault to the east, the Bolkardag metamorphics to the north and covered by Miocene carbonates to the south and west. The Mersin ophiolite having approximately 6 km thick oceanic crustal section presents, from bottom to top, following units: Subophiolitic metamorphics, mantle tectonites, ultramafic and mafic cumulates, basaltic lavas and associated deep marine sediments. All this units rest tectonicaly on the ophiolitic melange.

Ophiolitic melange in the study area comprises continental margin units, rift-related sediments, platform carbonates, serpantinized harzburgites and fragments of subophiolitic metamorphic rocks. Subophiolitic metamorphic rocks observed beneath the mantle tectonites as a thin slice (>100 m) consist mainly of amphibolite, amphibolitic schist, micaschist, marble, calcschist. These metamorphic rocks yielding an age range between 92 and 96 Ma ($^{40}Ar/^{40}Ar$) are deformed and cut by post metamorphic diabase dikes which give slightly younger ages (89-63 Ma from $^{40}Ar/^{40}Ar$). These results suggest that intraoceanic thrusting (compressional event) was completed rapidly (~ 4 Ma) and converted into extensional regime (perhaps in less than 3 m.y.) during which postkinematic dike emplacement occured. Major and trace element analyses indicate that ocean island or seamount basaltic rocks are possible rock assemblages from which subophiolitic metamorphics were derived. Cumulative rocks having over 3 km thickness start with dunite, wherlite and clinopyroxenite at the bottom and pass into gabbroic rocks. The cumulates exhibiting adcumulate and mesocumulate texture show some accumulation features such as cyclic sedimentation, size grading, graded layering, and igneous lamination in the magma chamer. Limited cryptic variation in plagioclase (An_{95-91})-olivine (Fo_{91-80})-clinopyroxene (Mg_{93-77}), absence of evidence of zoning in intercumulus and cumulus minerals, crystallization of clinopyroxene before plagioclase all indicate that high pressure fractionation was present in the Mersin ophiolite magma chamber. Volcanic suites in the study area are characterized by alkaline (Upper Jurassic-Early Cretaceous) and tholeiitic (Late Cretaceous ?) basaltic rocks in terms of major, trace element and mineral chemistry. Alkali basalts show the features of ocean island/seamount basalts whereas the tholeiitic basalts are characterized by island arc basalts.

The ophiolite body is cross-cut at all structural levels by numerous mafic dyke intrusions. The dykes do not intrude the underlying melange or platform carbonates. Therefore dike emplacement postdate the formation of the ophiolite and metamorphic sole but predate the final obduction onto the Tauride platform. The post-metamorphic dyke swarms suggest geochemical character of Island Arc Tholeiites (IAT).

Not only structural data observed in the subophiolitic metamorphic rocks but vergence of large scale faults and asymetric folding also show that the Mersin ophiolite obducted onto the active continental margin of the Taurides from southern branch of the Neotethys in southern Turkey.

CHAPITRE 1

INTRODUCTION ET RÉSUMÉ DES RÉSULTATS*

1.1. Introduction

Les ophiolites sont interprétées comme des fragments de lithosphère océanique obductés sur les continents. Leur origine est liée au développement de la croûte océanique le long des rides. Ce concept est maintenant largement accepté; il est basé sur l'existence des complexes filoniens (Gass, 1967; Coleman, 1971; Dewey and Bird, 1971). L'étude des ophiolites est primordiale pour permettre la reconstruction des anciennes limites entre les plaques.

L'océan appelé Néo-Téthys est un bassin océanique d'âge mésozoïque qui s'est développé entre la plateforme afro-arabe au sud et la plateforme eurasienne au nord. Lors de l'ouverture de la Néo-Téthys, la Paléo-Téthys, d'âge paléozoïque à mésozoïque, était déjà en phase de fermeture.

Les ophiolites rencontrées en Méditerranée orientale et appartenant à la Néo-Tethys sont réparties sur deux axes. L'un comprend les ophiolites du Troodos à Chypre, du Kizildag en Turquie, du Baer Bassit en Syrie, du Semail en Oman. Elles affleurent le long de la zone de collision continent à continent nommée "Zone Bitlis-Zagros". Elles représentent les fragments d'une vraie croûte océanique possédant une vraie "pseudo-stratigraphie" (Dilek and Moores, 1990). L'autre axe est composé d'éléments démembrés et déformés situés de part et d'autre de l'axe de la chaîne des Taurides (Juteau, 1980). Ces ophiolites forment les massifs lyciens, les massifs de Beysehir, d'Alihoca, de Mersin, de Pozanti-Karsanti. Ils sont généralement accompagnés d'une semelle métamorphique et d'un mélange tectonique (Fig. 1.1a).

1.1.1. Objectifs de la recherche

De nombreuses études géochimiques ont montré une similitude dans l'environnement tectonique de ces ophiolites téthysiennes formées durant la fin du Crétacé (Pearce et al., 1984; Parlak et al., in review; Robertson, 1994; Yaliniz et al., 1994). Pearce et al. (1984); elles suggèrent que les ophiolites de la Méditerranée orientale se sont formées dans un environnement tectonique situé au-dessus de la zone de subduction (supra-subduction zone). La caractéristique la plus controversée rencontrée pour les ophiolites néotéthysiennes de Turquie et des régions avoisinantes concerne le nombre de zones de racines dont elles dériverrient. Sengor et Yilmaz (1981), Robertson et Dixon (1984) prétendent que deux

*This chapter "Introduction and summary of the results" is written in French in accordance with the instructions for publication of PhD theses of the Faculté des Sciences, Université de Genève.

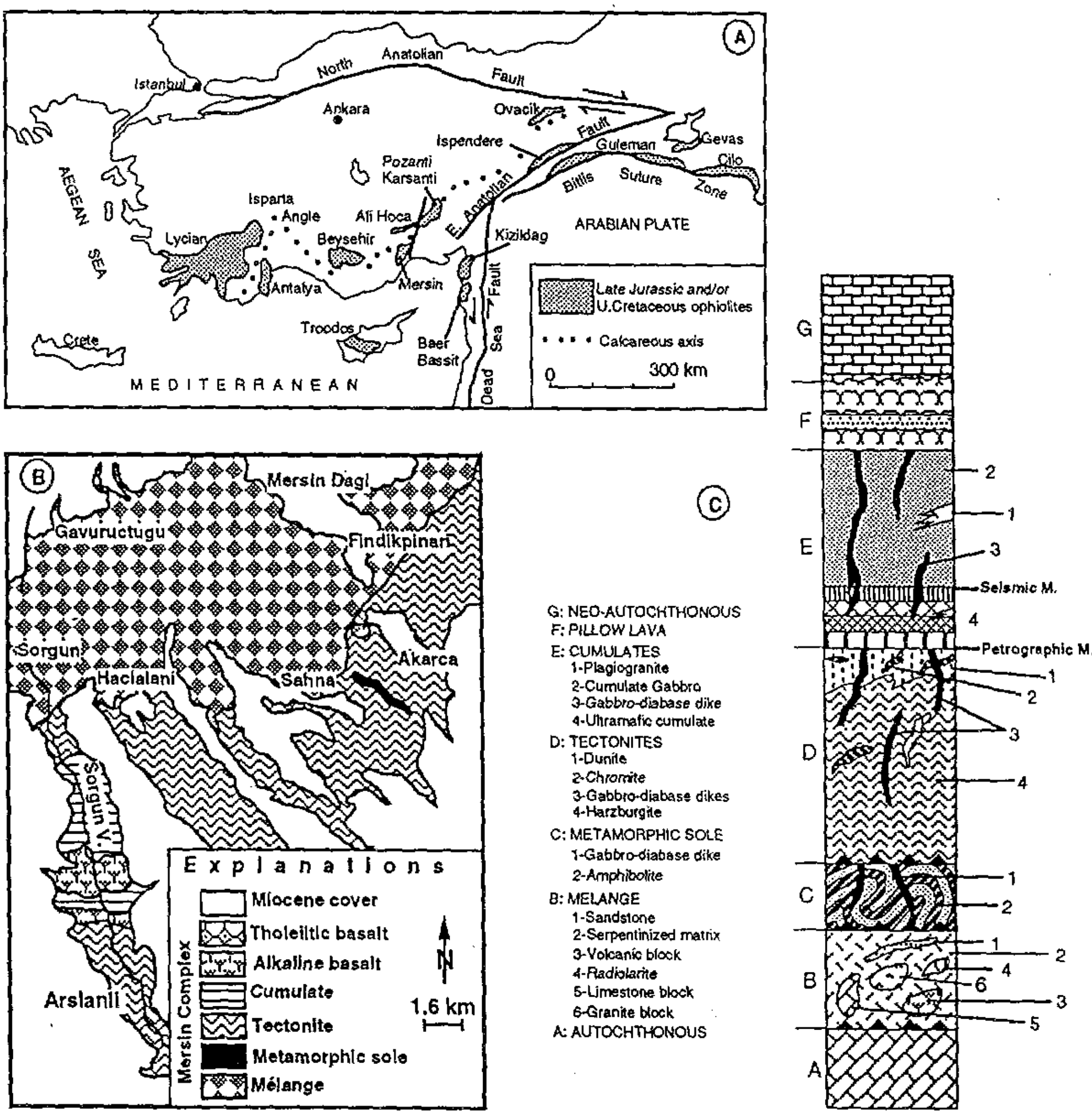

Figure 1.1. a. Massifs ophiolitiques du sud de la Turquie (modifié de Dilek et Moores, 1990). **b.** Carte géologique simplifiée de l'ophiolite de Mersin. **c.** Colonne stratigraphique détaillée des roches de l'ophiolite de Mersin.

bassins principaux étaient actifs, l'un au nord, formé de plusieurs bras, l'autre au sud, plus simple, formant la branche sud de la Néo-Téthys. En revanche, d'autres auteurs, en particulier Ricou et al. (1984) et Whitechurch et al. (1984), pensent que ces ophiolites se sont formées dans un bassin unique situé au centre de la Turquie.

La présente recherche développe trois thèmes particuliers:

1) Présentation détaillée des caractéristiques principales d'une ophiolite de type « supra-subduction zone » rencontrée dans la Néo-Tethys de Turquie. Dans ce but, des recherches

géochimiques (éléments majeurs, trace, Terres-Rares) et une analyse chimique des différentes phases minérales ont été menées soit sur les termes extrusifs soit sur les roches plutoniques de l'ophiolite de Mersin.

2) Utilisation des éléments de géologie structurale que l'on peut reconnaître dans la semelle métamorphique et dans le mélange pour tenter de déterminer la polarité de l'obduction de ce massif ophiolitique. Pour résoudre ce problème des déterminations d'âge K-Ar et $^{40}Ar/^{39}Ar$ ont été effectuées sur des concentrés d'amphiboles provenant de la semelle métamorphique afin de déterminer le temps de résidence intra-océanique et la période à laquelle se sont produites les injections de dykes.

3) Présentation d'un modèle pour l'évolution de l'ophiolite de Mersin dans le cadre du processus de collision en rassemblant les différentes données récoltées.

1.1.2. Situation géographique et géologique

Le complexe ophiolitique de Mersin (MOC) est situé à 30-35 km au N-NW de Mersin et Erdemli dans le sud de la Turquie. Il présente une section de croûte océanique d'environ 6 km d'épaisseur. Il est situé sur le flanc sud du Bolkardag le long de la chaîne du Taurus. Les affleurements les mieux conservés de cette section de croûte océanique peuvent être observés dans le vallée de Sorgun orientée NW-SE. L'ophiolite de Mersin est limitée à l'est par la faille d'Ecemis et au nord par les roches métamorphiques du Bolkardag. Elle est recouverte au sud et à l'ouest par les roches sédimentaires detritiques et carbonatées du Miocène.

Ce complexe présente trois éléments structuraux distincts: un mélange ophiolitique, une semelle métamorphique sub-ophiolitique et une croûte océanique où il manque le complexe filonien (Juteau, 1980; Parlak et al., 1994, 1995a) (Fig. 1.1b-c).

Le mélange ophiolitique représente l'unité inférieur de la pile tectonique. Il est principalement constitué par des éléments provenant de la marge continentale, des sédiments liés au rift, des blocs de calcaire qui ne sont pas enracinés, des basaltes, des harzburgites, des gabbros serpentinisés, des roches métamorphiques sub-ophiolitiques et des blocs granitiques. La lithologie et l'organisation structurale des éléments du mélange montrent clairement l'ouverture, le development et la fermeture de la Néo-Tethys en Turquie du sud. Cette unité est recouverte tectoniquement par la semelle métamorphique qui a subi un métamorphisme prograde puis rétrograde du faciès amphibolite au faciès schiste vert. Les roches métamorphiques sub-ophiolitiques, formées durant la mise en place intra-océanique, ont enregistré une déformation polyphasée et sont recoupées par un très grand nombre de dykes diabasiques (Parlak et al., 1995c). Des éléments de la semelle métamorphique, qui avoisinent 50 à 70 m d'épaisseur, sont bien exposés soit au-dessous des tectonites harzburgitiques rencontrés au fond des vallées, soit parmi des éléments du mélange ophiolitique et des tectonites provenant du manteau. La lithosphère océanique observée dans l'ophiolite de Mersin est une des plus complètes de toute la chaîne des Taurus. A l'exception du complexe filonien, elle comprend des tectonites harzburgitiques, des cumulats ultramafiques et mafiques ainsi que deux générations distinctes de basaltes qui se différencient par leur âge et leur affinité géochimique et des dykes isolés. Ces deux générations sont des basaltes alcalins d'âge Jurassique supérieur à Crétacé inférieur et des basaltes tholéitiques d'âge Crétacé supérieur. Un très grand nombre de dykes diabasiques et microgabbroïques, de composition tholéitique, se sont mis en place dans les tectonites harzburgitiques.

1.2. Les volcanites

Les roches volcaniques se présentent en deux groupes distincts, soit en ce qui concerne la géochimie, soit en ce qui concerne la structure. Le premier est représenté par des laves basaltiques intercalées avec des radiolarites et des calcaires pélagiques (Jurassique sup.-Crétacé inf.) tandis que le deuxième est représenté par des laves en coussins basaltiques et des diabases (Crétacé sup.). Le volcanisme tholéiitique basaltique co-génétique avec la formation de la croûte océanique néo-téthysienne a été reconnu pour la première fois dans l'ophiolite de Mersin. Les basaltes tholéiitiques présentant une structure intersertale sont caractérisés par un assemblage minéralogique très constant comprenant clinopyroxène (25-30%), baguettes de plagioclase albitisé (40-45 %) et oxydes de Fe-Ti (5 %) dans une matrice vitreuse altérée (30 à 35 %). Les diabases associées aux basaltes ont une texture doléritique mais la même composition minéralogique (augite-plagioclase). Les basaltes alcalins diffèrent des basaltes tholéitiques par leur clinopyroxène à forte concentration en TiO_2 (2-4 %). Ces basaltes de structure porphyritique, dont la taille des grains peut atteindre 0.5 à 1.8 mm, sont intercalés avec des cherts, des radiolarites et des calcaires pélagiques.

Les roches volcaniques et les diabases ont subi un métamorphisme de faible intensité ayant altéré l'assemblage primaire des minéraux et faisant apparaître des zéolites dans un contexte de faciès schistes verts. Ces minéraux secondaires comprennent de l'albite, de la chlorite, de l'épidote, du quartz et de la calcite.

1.2.1. Géochimie

Les roches volcaniques de l'ophiolite de Mersin peuvent aussi être subdivisées en deux groupes sur la base de leur composition en éléments en trace (Winchester et Floyd, 1977): l'un alcalin, l'autre sub-alcalin à tholéitique (Fig. 1.2).

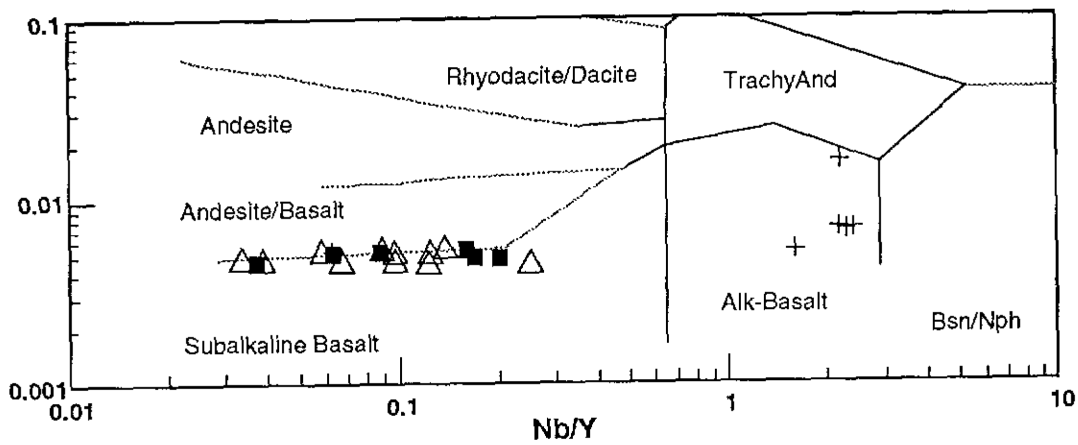

Figure 1.2. Discrimination des différents types de roches de l'ophiolite de Mersin, basée sur les éléments en trace immobiles (d'après Winchester et Floyd, 1977). Les triangles et les carrés pleins représentent les basaltes et les diabases du Crétacé Supérieur, et les croix les basaltes du Jurassique Supérieur-Crétacé Inférieur.

Les basaltes alcalins présentent de faibles teneurs en silice et des teneurs élevées en titane, en calcium et phosphore. Ils présentent des concentrations importantes en éléments en trace incompatibles Zr, Nb, Y, Ba et Sr et en éléments de transition Cr, Ni et V. Les basaltes tholéitiques et les diabases qui se sont formés d'une façon cogénétique dans l'ophiolite de Mersin sont caractérisés par de fortes teneurs en SiO_2, de faibles teneurs en TiO_2, en P_2O_5 et CaO en comparaison aux basaltes alcalins. Les tholéiites sont appauvries en éléments incompatibles Zi, Y, Nb, mais enrichies en LIL (Ba et Sr) et en éléments de transition (Cr, Ni, V). Les basaltes tholéiitiques ne montrent pas d'enrichissement en TiO_2 associé à l'augmentation du rapport FeO/MgO caractéristique des roches volcaniques dans l'environnement d'arcs insulaires (Miyashiro, 1973) (Fig. 1.3).

Les concentrations en terres rares sont présentées dans la Figure 1.4. Les basaltes alcalins montrent un certain enrichissement en LREE avec un rapport La/Yb normalisé compris entre 14,1 et 14,8. Ils ressemblent aux basaltes alcalins des Azores (White et al., 1979; Schilling, 1975), à ceux des îles de la Mer Rouge (Gass et Smewing, 1973), à des basaltes alcalins du mélange d'Ankara (Floyd, 1993), aux basaltes alcalins triasiques de la région d'Antalya (Robertson et Waldron, 1990) et à ceux de la région de Pozanti-Karsanti (Catakli, 1983). Ces basaltes alcalins et les sédiments qui leur sont associés ont été interprétés comme la source probable de la semelle sub-ophiolitique.

Les basaltes tholéiitiques et les diabases présentent une courbe de terres rares pratiquement horizontale (Fig. 1.4) avec un taux de fractionnement (La/Yb compris entre

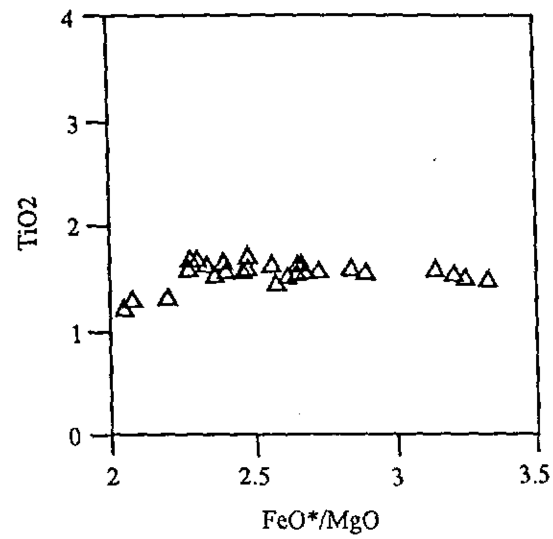

Figure 1.3. Rappport en poids TiO2 vs. FeO*/MgO pour les basaltes tholéiitiques et les diabases de l'ophiolite de Mersin.

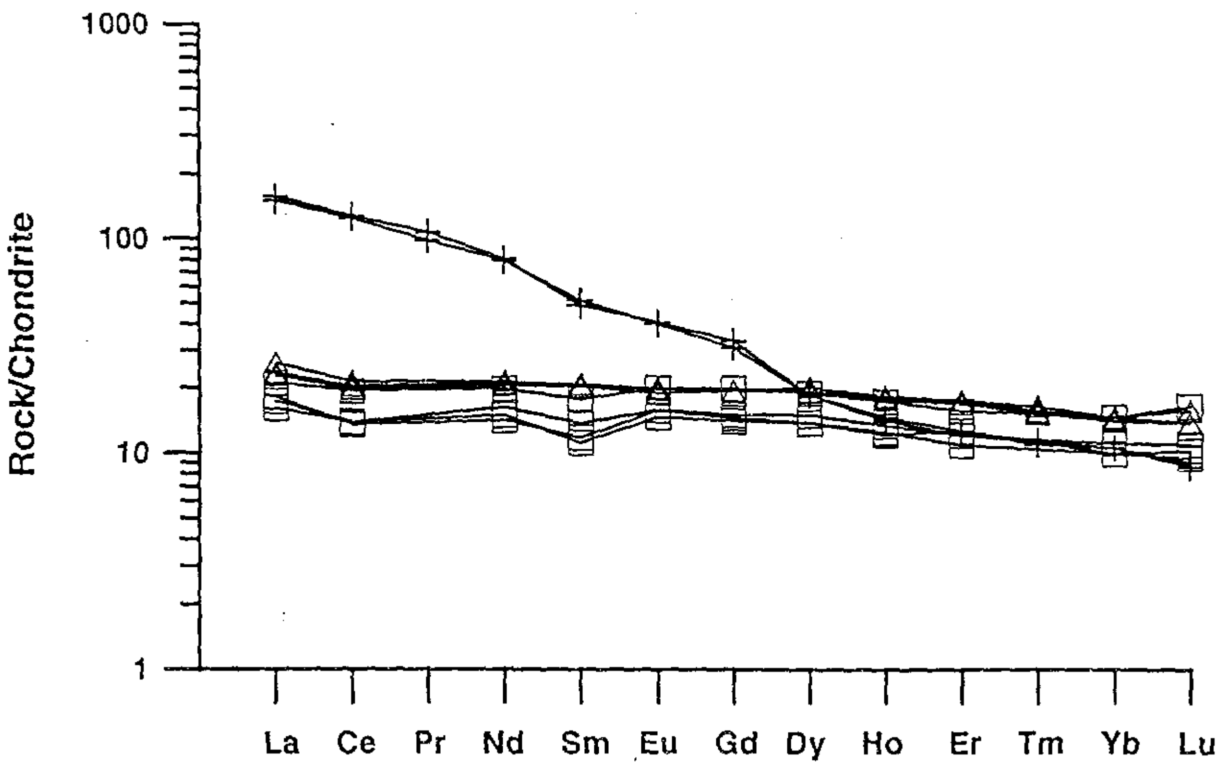

Figure 1.4. Abondance des Terres Rares normalisées aux chondrites, pour les basaltes alcalins (croix), les basaltes tholéiitiques (triangles) et les diabases (carrés). (valeurs de normalisation de Sun et McDonough, 1989).

1,4 et 1,9) en désaccord avec les valeurs des N-MORB (La/Yb de l'ordre de 0,6; Sun et al., 1979). Cette allure de la courbe des terres rares très plate est souvent observée dans les tholéiites d'arcs insulaires comme en Papouasie Nouvelle Guinée, aux îles Salomon, et l'île Macquarie (Jakes and Gill, 1970). Dans les unités de l'ophiolite de Mersin, il n'y a pas d'anomalie négative en Europium, suggérant que durant la période précoce de fractionnation, l'olivine était la phase minérale dominante par rapport au plagioclase. Les faibles concentrations en Ni et en Cr viennent à l'appui de cette hypothèse (Jakes et Gill, 1970). Les caractéristiques propres aux arcs insulaires de tous les massifs ophiolitiques de la Méditerranée orientale, y compris Oman (Alabaster et al., 1982; Searle et al., 1980), Troodos (Desmons et al., 1980), Baer-Bassit (Parrot, 1977), Hatay (Delaloye et Wagner, 1984), Sarikaman (Yaliniz et al., 1994) pour la Turquie ainsi que l'ophiolite de Bay of Island (Elthon, 1991) ne sont pas différentes de celles de l'ophiolite de Mersin.

Pour identifier l'environnement tectonique des roches basaltiques de l'ophiolite de Mersin, des diagrammes de discrimination tectono-magmatiques basés sur les éléments immobiles ont été utilisés. Dans le diagramme triangulaire Nb, Zr, Y (Meschede, 1986), les basaltes tholéitiques et les diabases se regroupent dans le domaine des N-MORB et des VAB, tandis que les basaltes alcalins se situent dans le domaine WBA (Fig. 1.5a). Le diagramme ternaire Zr/Y vs Zr (Pearce et Norry, 1979), divise les roches volcaniques en deux groupes: les basaltes tholéitiques et les diabases sont situés à l'interface entre les MORB et les IAB, tandis que les basaltes alcalins se placent dans le champ des WBA (Fig. 1.5b). Dans la Figure 1.5c, la relation Ti vs V est utilisée pour les basaltes tholéitiques. Ces basaltes présentent un caractère de transition dû à une concentration élevée en vanadium entre les MORB et les basaltes d'arc. Il peut être mis en relation avec la fugacité de l'oxygène qui parait être plus importante dans les magmas d'arcs (Shervais, 1982).

Les différences entre les basaltes alcalins et les basaltes tholéitiques, tout au moins en ce qui concerne la géochimie et l'âge permettent de penser que les basaltes alcalins associés aux calcaires et aux radiolarites et présentant les caractéristiques des basaltes d'îles océaniques se sont formés durant l'ouverture progressive de l'océan sous forme d'un "seamount" situé sur la croûte océanique pendant une période s'étendant entre le Jurassique supérieur et le Crétacé inférieur.

Les basaltes tholéiitiques présentent des caractéristiques d'arc insulaire et doivent s'être formés au Crétacé supérieur, en même temps que le volcanisme basaltique, dans un domaine de zone "supra-subduction".

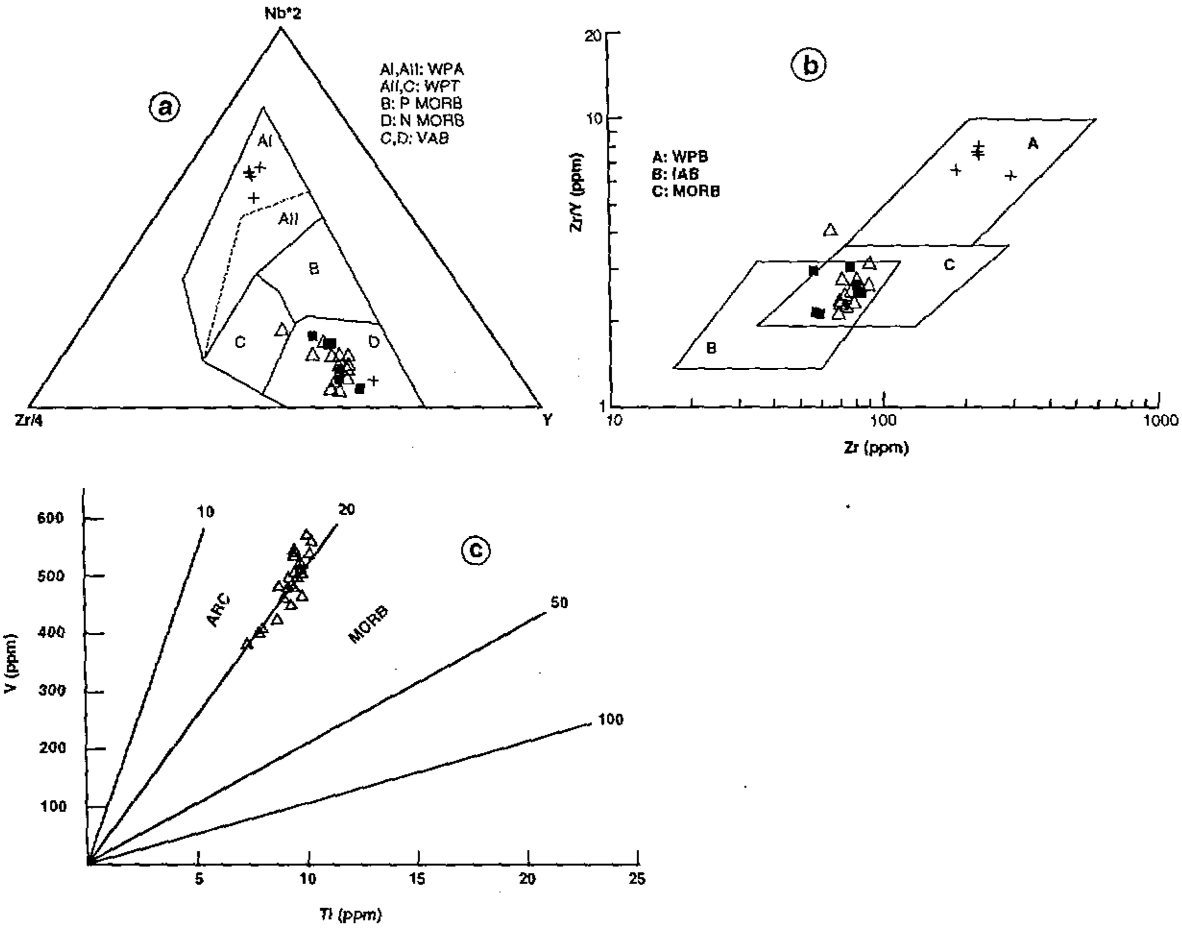

Figure 1.5. a. Diagramme Nb-Zr-Y pour la discrimination tectono-magmatique des basaltes tholéiitiques, diabases et basaltes alcalins de l'ophiolite de Mersin (d'après Meschede, 1986). Les triangles et les carrés pleins représentent les basaltes tholéiitiques et les diabases respectivement, et les croix les basaltes alcalins. **b.** Diagramme Zr/Y vs. Zr pour la discrimination des roches basaltiques (d'après Pearce et Norry, 1979). (symboles comme sur la figure 5a). **c.** Diagramme Ti vs. V pour les basaltes tholéiitiques et les diabases (d'apres Shervais, 1982).

1.2.2. Chimie des minéraux

Les clinopyroxènes des roches alcalines sont des diopsides (Ca_{53-49} Mg_{9-6} Fe_{38-42}). Ils sont riches en TiO_2 et Al_2O_3; Mg*(Mg/Mg+Fe) est compris entre 0,7 et 1,8. En revanche, les clinopyroxènes des basaltes tholéitiques et des diabases sont des augites (Ca_{37-40} Mg_{18-16} Fe_{45-41}). Ils sont pauvres en SiO_2 et Al_2O_3 si on les compare aux clinopyroxènes des basaltes alcalins. Mg* varie entre 0,71 et 0,75.

Il est connu que des différences chimiques importantes peuvent exister entre les pyroxènes que l'on rencontre dans les différents associations tectoniques (Nisbet and Pearce, 1977). Elles ont été observées dans les roches de l'ophiolite de Mersin en ce qui concerne la composition des clinopyroxènes comme de la composition des roches totales. Dans le diagramme Ti en fonction de Ca + Mg, basé sur la formule chimique des phénocristaux de clinopyroxène, on peut distinguer les caractères tholéitiques et alcalins des roches basaltiques (Leterrier et al., 1982) (Fig. 1.6).

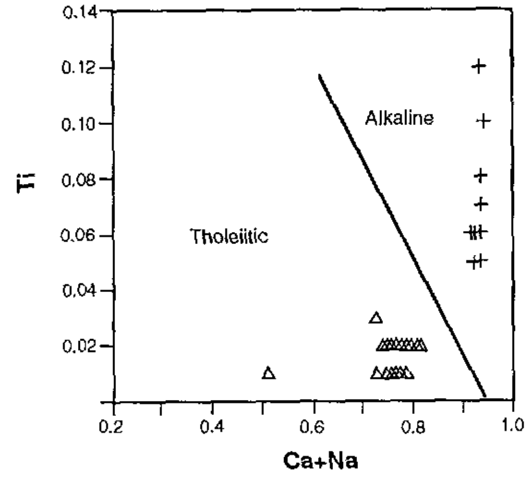

Figure 1.6. Caractérisation du parentage magmatique des roches basaltiques de l'ophiolite de Mersin en utilisant les phénocristaux de clinopyroxène (d'après Leterrier et al., 1982). Les triangles représentent les clinopyroxènes des basaltes tholéiitiques et les croix ceux des basaltes alcalins.

1.3. Les cumulats

Les cumulats ont plus de 3 km d'épaisseur. Ils débutent par 800 m de roche ultramafique et se poursuivent par 2500 m environ de roches gabbroïques. Ils présentent des contacts tectoniques avec les harzburgites à leur base et avec les basaltes au sommet. Des structures polycycliques de cumulat sont observées entre les roches mafiques et les roches ultramafiques. Les cumulats ultramafiques qui montrent des structures de type adcumulat sont caractérisés par des dunites, des wehrlites et des pyroxénites. Les cumulats mafiques consistent principalement en gabbros, leucogabbros, gabbros à olivine et anorthosite qui constituent à peu près les deux tiers de toute la section des cumulats. Soit sur le terrain, soit sous le microscope, les cumulats mafiques sont très frais et présentent des structures d'adcumulats et de mésocumulats. Des granoclassements et des figures de sédimentation apparaissent dans les cumulats mafiques et ultramafiques. La polarité granulométrique est toujours positive, indiquant un contrôle gravifique du dépôt des cumulats. Les laminations et les alternances centimétriques sont communes. Il n'y a pas de structures entrecroisées qui pourraient indiquer la présence de courants magmatiques importants dans la chambre.

On peut observer dans la Figure 1.7 que les phases cumulus sont l'olivine, le chrome-spinelle, le clinopyroxène et le plagioclase, tandis que les phases post-cumulus sont l'orthopyroxène, le clinopyroxène, le plagioclase et l'olivine. Les ordres de cristallisation sont les suivants: dans les cumulats ultramafiques, olivine + chromite, olivine + clinopyroxène, clinopyroxène et, dans les cumulats mafiques, olivine + plagioclase + clinopyroxène, plagioclase + clinopyroxène + orthopyroxène, plagioclase.

1.3.1. Géochimie

Les compositions chimiques des clinopyroxènes, de l'olivine et du plagioclase des roches plutoniques sont présentées à la Figure 1.8. Le peu de variations chimiques observées dans les minéraux de cette importante section indique que la cristallisation s'est faite à partir d'un magma de composition relativement uniforme avec des remplissages successifs de la chambre magmatique à partir d'un magma primitif.

Les rapports Mg/Fe élevés des phases mafiques et ultramafiques, les plagioclases riches en calcium et l'absence de zonation des minéraux cumulus et intercumulus sont la preuve de processus de cristallisation dans un contexte de haute température.

La composition des minéraux des cumulats mafiques et ultramafiques montrent des caractéristiques différentes de celles que l'on peut observer dans les MORB de basse pression (Dungan et al., 1978; Fisk et al., 1980; Elthon, 1981). Selon certains auteurs, l'existence de réactions de phase à basse pression (~1 atmosphère) sont étayées par la présence d'une fractionation importante de l'olivine, avec ou sans plagioclase, qui a précédé la cristallisation du pyroxène. Cette situation appauvrit les liquides résiduels en MgO, le Mg* du clinopyroxène est abaissé, l'olivine est généralement appauvrie (< 82) et l'orthopyroxène a un Mg* encore plus faible (< à 74) (Elthon et al., 1982; Burns, 1985). De plus, une cristallisation de MORB à basse pression se caractériserait par la présence de dunite, de troctolite et de gabbro à olivine (Elthon et al., 1982; Pearce et al., 1984).

Les ultramafites de Mersin sont en contradiction avec la cristallisation à basse pression traditionnelle car elles présentent des dunites, des wehrlites, des clinopyroxénites et des gabbros. Le Mg* élevé des olivines (89-80), des clinopyroxènes (95-77) et des orthopyroxènes (77-68) dans les cumulats ultramafiques et mafiques ainsi que la teneur en anorthite du plagioclase (96-90) des gabbros montrent l'incompatibilité avec une cristallisation à basse pression d'un magma de type MORB. Dans la Figure 1.9, le Mg* des olivines et des clinopyroxènes montre que les valeurs obtenues dans les roches de Mersin diffèrent des champs qui sont définis par les expériences à une atmosphère, mais recouvrent les champs des xénolithes provenant du manteau et ayant cristallisé à haute pression (7-10 kbars). Ces données sont aussi en accord avec celles qui ont été publiées par Elthon et al. (1982) ou Elthon (1991) sur des roches de North Arm Mountains qui ont

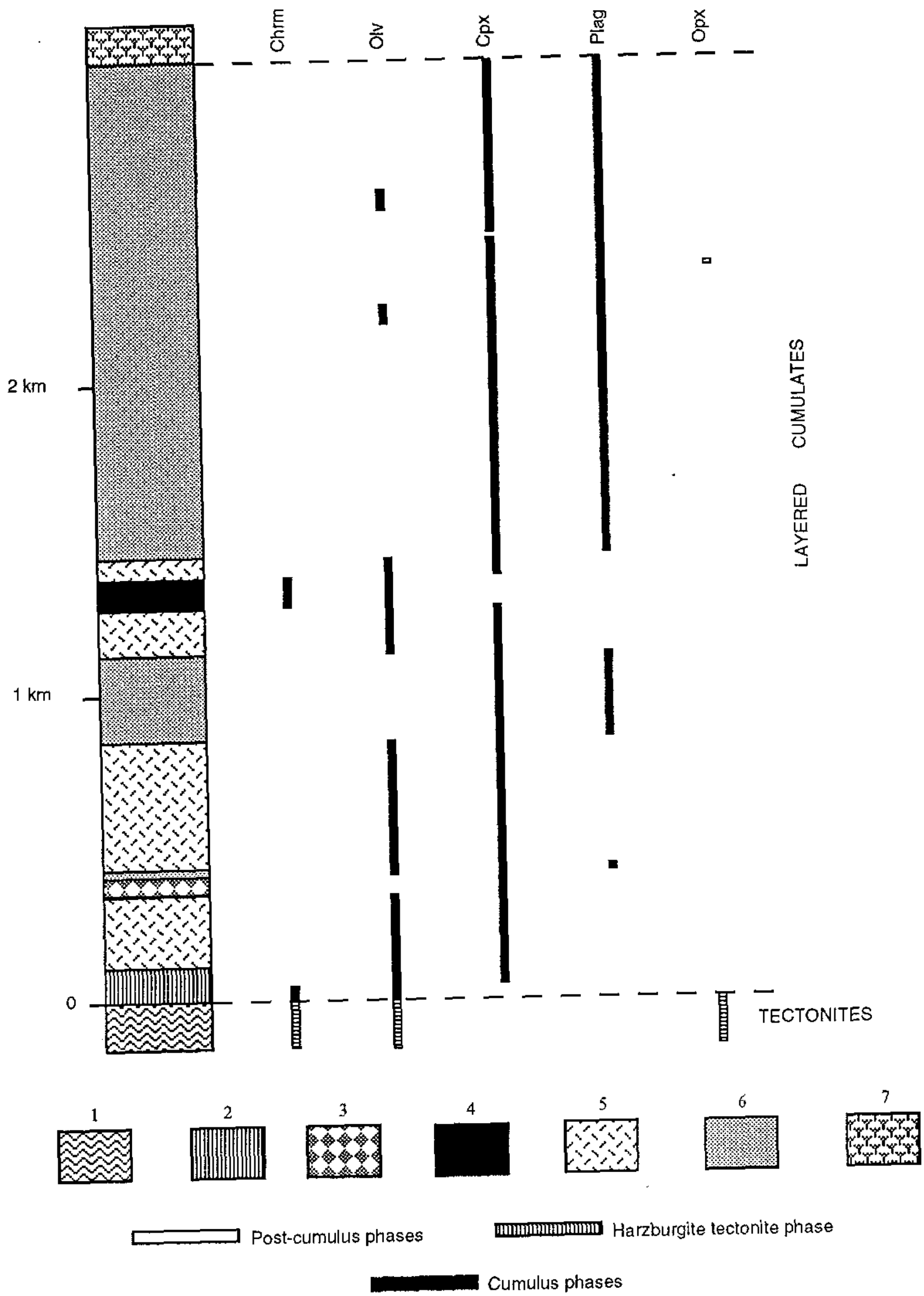

Figure 1.7. Distribution des phases dans les cumulats: 1- Tectonites du manteau, 2- Zone d'altération des dunites et des wherlites, 3- Clinopyroxénite, 4- Dunite, 5- Wherlite, 6- Gabbro, 7- Basalte.

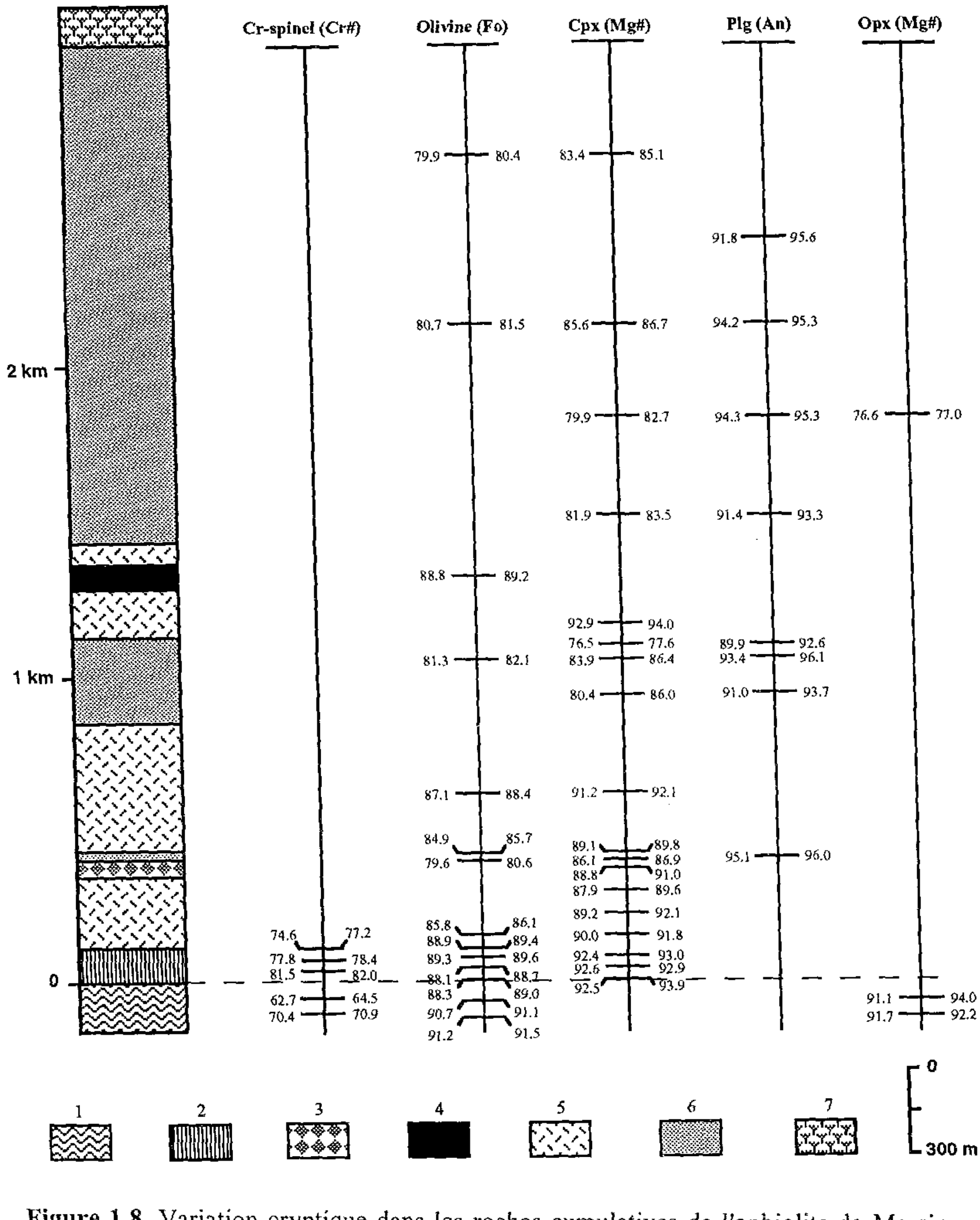

Figure 1.8. Variation cryptique dans les roches cumulatives de l'ophiolite de Mersin. (Légende comme sur la figure 7). Les nombres représentent les valeurs minimale et maximale pour des échantillons individuels.

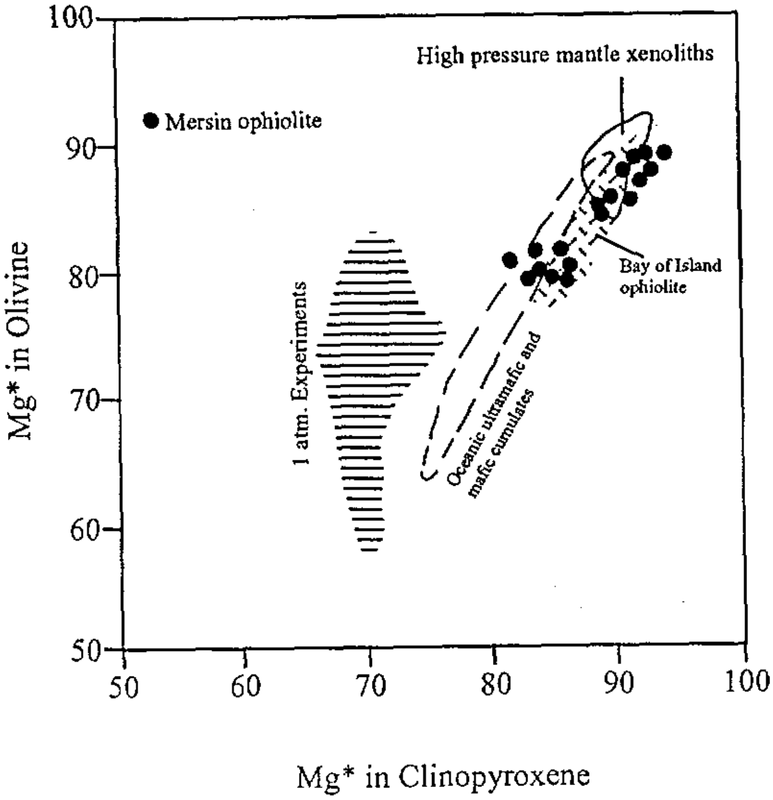

Figure 1.9. Mg# vs. (100*Mg/Mg+Fe) pour les olivines et les pyroxènes qui coéxistent dans les cumulats mafiques et ultramafiques de l'ophiolite de Mersin. Les différents champs ont été définis par Elthon et al. (1982).

cristallisé dans un environnement d'arc insulaire « suprasubduction zone » à haute pression. Cette cristallisation à haute pression des phases mafiques et ultramafiques est également en accord avec les variations chimiques très faibles rencontrées tout au long de cette section de l`-ophiolite épaisse de 3 km (Parlak et al., 1995b).

Comme les pyroxènes dans leurs phases cumulus et intercumulus ne sont pas zonés, il faut en déduire que la vitesse de refroidissement du magma dans la chambre a été lente (Flower et al., 1977b).

La composition chimique des plagioclases et des pyroxènes dans les gabbros-cumulats illustrée dans la Figure 1.10a montre que le plagioclase très calcique et le clinopyroxène très magnésien sont en bon accord avec des gabbros que l'on rencontre dans un environnement d'arc. La Figure 1.10b présente les variations de composition de l'olivine et du plagioclase pour Mersin, pour le Troodos (Hébert et Laurent, 1990) et d'autres massifs (Hébert 1985; Beard, 1986). La composition minéralogique des roches plutoniques de Mersin présente une fractionation très limitée par rapport à l'anorthite et la forstérite. Elle diffère certainement de la composition des cumulats océaniques qui sont, eux, très fractionnés (Fig. 1.10b). L'ophiolite de Mersin présente des similitudes très fortes avec certaines roches des Petites Antilles (Arculus et Wills, 1980) avec le volcan Agrigan dans l'arc des

Mariannes (Stern, 1979) et avec le Troodos qui s'est mis en place dans un environnement d'arc (Hébert et Laurent, 1990). Les analyses d'éléments majeurs, en traces, des Terres Rares ainsi que la géochimie des minéraux des roches basaltiques de l'ophiolite de Mersin suggèrent également une affinité d'arc. Les chambres magmatiques à la base d'un arc

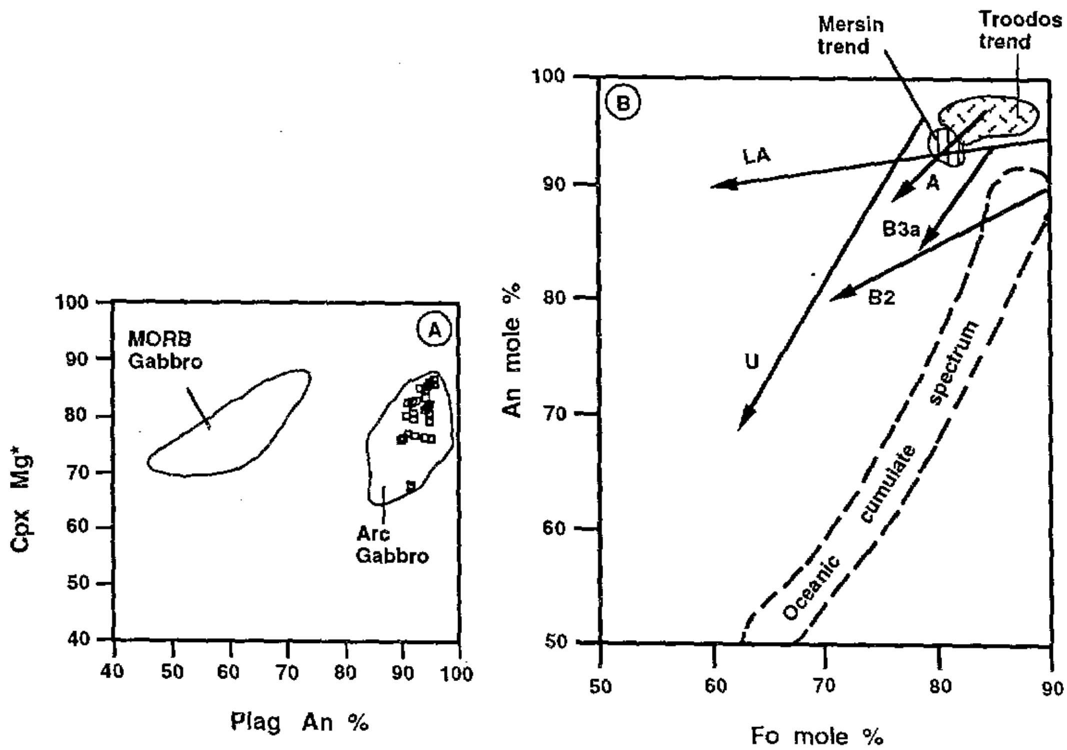

Figure 1.10. a. Composition des plagioclases et des pyroxènes qui co-éxistent dans les cumulats de gabbros de l'ophiolite de Mersin (champs définis d'après Burns, 1985).
b. Co-variation de l'olivine et du plagioclase de la suite plutonique de l'ophiolite de Mersin et de divers contextes tectoniques connus (Hébert, 1985; Beard, 1986; Hébert et Laurent, 1990). LA: Petites Antilles (Arculus and Wills, 1980), A: Volcan Agrigan, arc Mariane (Stern, 1979), B2 et B3a: Volcan Boisa, Papua (Gust et Johnson, 1981), U: Volcan Usa, Japon (Fujimaki, 1986).

immature permettent en effet la cristallisation de séquences de cumulats mafiques et ultramafiques à haute pression dans lesquelles l'olivine et le spinelle sont suivis par le pyroxène puis par le plagioclase, tandis que dans les ophiolites de type MORB le plagioclase cristallise avant le pyroxène (Burns, 1985; Coleman, 1986). A l'intérieur de la séquence plutonique de Mersin, les niveaux dunitiques passant à des wehrlites et des pyroxénites montrent les mêmes caractéristiques que elles observées dans les chambres magmatiques de type arc insulaire, tels qu'elles sont décrites par ex. dans le Border Range Ultramafic and Mafic Complex (Burns, 1985).

1.4. Les roches métamorphiques sub-ophiolitiques

Ces roches présentent une zonation métamorphique inverse allant des faciès à amphibolite aux faciès schiste vert. Elles apparaissent d'une manière discontinue à la base de la séquence ophiolitique sur le flanc sud du Bolkardag. Ces roches métamorphiques, plissées et imbriquées, présentent des déformations polyphasées. Elles sont coupées par des dykes diabasiques non métamorphiques. La séquence métamorphique comprend les associations suivantes: amphibolite et schiste amphibolitique, schiste à amphibole et épidote, micaschiste quartzique, calcschiste et marbre.

1.4.1. Géochimie

Par contre, le spectre des terres rares obtenu à partir de l'analyse d'un dyke est presque horizontal. Sm et Eu présentent une légère anomalie négative (Fig. 1.11). Il est similaire à ceux des basaltes d'arrière-arc et à ceux des tholéites d'arc insulaire (Cullers et Graf, 1984). Il y a un léger enrichissement en terres rares légères par rapport aux MORB normaux qui peuvent être interprétés comme la source des dykes. Cette interprétation a déjà été invoquée pour les autres complexes ophiolitiques de la Méditerranée orientale qui appartiennent tous à une zone « supra-subduction » (Pearce, 1980; Pearce et al., 1984). Les diagrammes des terres rares des amphibolites montrent l'enrichissement en terres rares légères observé dans les WPB (Fig. 1.11) ou dans les basaltes d'îles océaniques telles que celles des Açores (White et al., 1979) et dans les basaltes alcalins du mélange d'Ankara (Floyd, 1993).

Les métamorphites associées à l'ophiolite de Mersin semblent provenir de deux sources différents. Le premier serait responsable de la formation d'amphibolites dont le diagramme terres rares et les diagrammes normalisés au MORB sont comparables avec ceux des îles océaniques et ceux des basaltes de seamount (WPB). Le second serait responsable des dykes isolés montrant une tendance N-MORB et VAB pour ce qui a trait en éléments en traces et en Terres Rares. Les mêmes remarques peuvent être faites à propos des diagrammes Nb-Zr-Y de Meschede (1986) (Fig. 1.12a), et du diagramme Ti-Zr-Y de Pearce et Cann (1973) (Fig. 1.12b). Le protolithe le plus probable pour les amphibolites et les roches métapélitiques est un environnement d'îles océaniques et de seamount associé à des sédiments pélagiques.

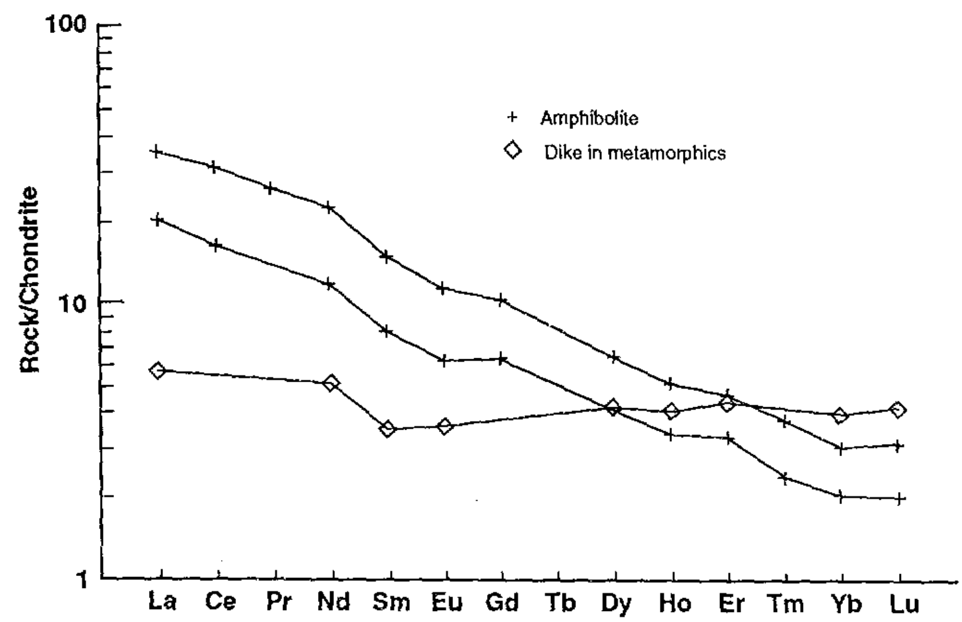

Figure 1.11. Spectre des Terres Rares normalisées des amphibolites et de dyke.

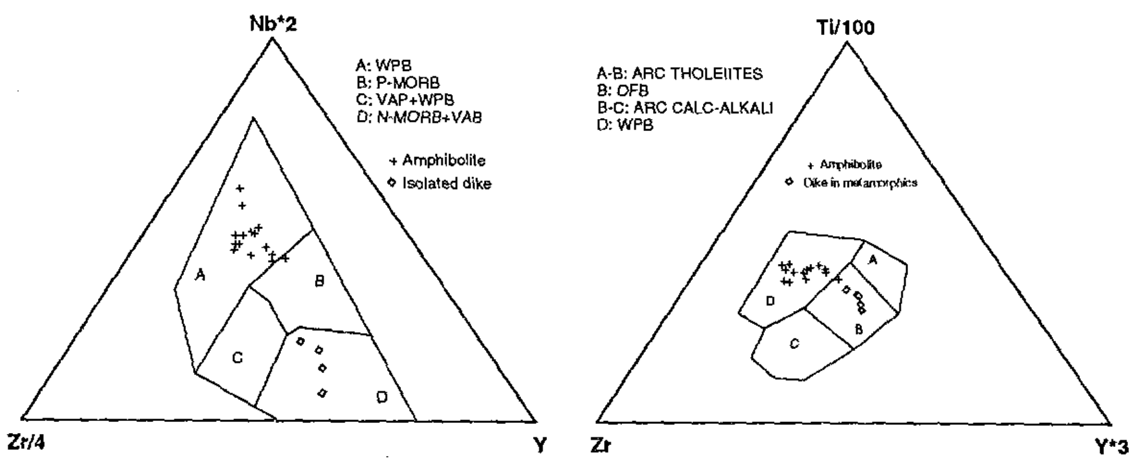

Figure 1.12. a. Diagramme discriminant Ti-Zr-Y pour les dykes et les amphibolites de l'ophiolite de Mersin (d'après Pearce et Cann, 1973). **b.** Diagramme Nb-Zr-Y de discrimation tectono-magmatique pour les dykes et les amphibolites de l'ophiolite de Mersin (d'après Meschede, 1986).

1.4.2. Géochronologie

La géochronologie $^{40}Ar/^{39}Ar$ a été utilisée pour les roches de la semelle métamorphique et pour les dykes afin de déterminer la séquence de ces deux événements caractéristiques de l'ophiolite de Mersin. L'âge de fermeture obtenu sur les amphiboles de la semelle métamorphique indique que leur refroidissement s'est effectué durant une période comprise entre 96,0±0,7 Ma et 91,6±0,3Ma. Les spectres d'âge obtenus sur les amphiboles suggèrent qu'il s'agit d'un refroidissement rapide (McDougall et Harrison, 1988). En revanche, les trois dykes diabasiques qui coupent la semelle métamorphique présentent des âges isochrones un peu plus jeunes de 89,6±0,7 Ma, 88,3±0,7 et 86,3±0,5 Ma. Les spectres d'âge obtenus par chauffages successifs montrent également un refroidissement rapide de ces intrusion. Ces âges sont donc proches des âges de cristallisation. Un dyke diabasique échantillonné dans les tectonites présente un âge de 63,8±0,9 Ma. On peut en conclure que l'injection des dykes s'est poursuivie jusqu'au Paléocène inférieur (Fig. 1.13). L'obduction de l'ophiolite de Mersin sur la chaîne du Taurus s'est terminée à la fin du Paléocène.

1.4.3. Géologie structurale

Les métamorphites montrent des structures migmatitiques bien développées et des rubanages métamorphiques définis par l'alternance de niveaux riches en épidote et de niveaux carbonatés. Une foliation de type régional S_1 orientée NW-SE associée à une linéation des minéraux L_1 et des plis de premier ordre F_1 ont été produits durant la déformation. Ces premières déformations ont été replissées par des plis F_2 orientés NW-SE. On obtient ainsi des textures imbriquées tout à fait typiques.

D'autres structures, telles que l'asymétrie des ocelles de calcite, la vergence et l'asymétrie des plis F_1, l'acquisition de structures ductiles ou cassantes, la vergence des plis F_2 et les chevauchements des structures, indiquent d'une manière sûre une déformation différente du plissement principal du Taurus et un sens de tension dirigé vers le NE. De l'analyse structurale, on peut conclure que l'ophiolite de Mersin a été obductée par-dessus les terrains mésozoïques du Bolkardag selon une direction SE-NW. Le sens de déformation des roches métamorphiques sub-ophiolitiques est compatible avec la vergence à large échelle des unités qui incluent l'ophiolite de Mersin.

1.5. Le mélange ophiolitique

Le mélange ophiolitique de Mersin représente un assemblage de roches très différentes, d'âges différents, et ayant des relations lithostratigraphiques variées. Il comprend des unités provenant de la marge continentale, d'assemblages rencontrés dans les rifts, de fragments de plateforme, des unités métamorphiques et des éléments d'ophiolites. Les contacts entre ces unités sont tectoniques.

Les unités provenant de la marge continentale sont limités dans leur extension et sont caractérisés par des grès turbiditiques, des argiles, des marbres, des marnes et des radiolarites. Les fragments de plateforme sont représentés par des blocs calcaires généralement orientés EW et d'âge compris entre le Permien et le Crétacé supérieur. Les roches associées au rift comprennent des éléments variés tels que des tufs acides intercalés avec des calcaires pélagiques d'âge carnien-norien. Ils précisent l'âge de la première étape de block-faulting et de l'apparition du volcanisme dans la chaîne du Taurus. On rencontre également des calcaires, des cherts à radiolaires, des grès à plantes et des laves en coussins mafiques. Le mélange ophiolitique contient encore des serpentinites, des laves en coussins basaltiques très altérées, des gabbros, des éléments de roches métamorphiques. Un affleurement de granite présente les caractéristiques géochimiques d'un VAG. L'âge K-Ar déterminé sur la muscovite altérée de ce granite est de l'ordre de 330 à 390 Ma.

Le processus de rifting et de formation du bassin océanique s'est probablement arrêté il y a 94 Ma, date de la formation de la semelle amphibolitique et du début de la fermeture du bassin. La formation du mélange ophiolitique a débuté au Crétacé supérieur déjà, durant l'obduction de la croûte océanique sur la marge continentale et s'est achevée au Paléocène supérieur. Des sédiments du Paléocène supérieur présentant des caractères transgressifs se sont déposés sur l'ophiolite avec une discordance angulaire marquée.

1.6. Conclusions

Les résultats géochimiques, structuraux et géochronologiques obtenus sur les différentes roches de l'ophiolite de Mersin, permettent de l'insérer dans le contexte géotectonique de la Méditerranée orientale. Le début de la phase de rifting affectant la Néo-Téthys a débuté entre le Trias supérieur et le Jurassique inférieur (Sengör and Yilmaz, 1981; Robertson and Dixon, 1984). Les calcaires micritiques intercalés entre les roches volcaniques alcalines et les tufs observés dans le mélange ont produit les fossiles suivants: Meandrspira sp., Glomospira sp., Aulotortus sp., Duostominidae sp., Frendicularia sp., Involutina sp., Trochamina et des Algues. Ces fossiles permettent de limiter la période d'océanisation au Trias supérieur (Carnien-Norien), tout au moins en ce qui concerne la région étudiée. Robertson and Woodcock (1982) signalent un âge Anisien-Carnien pour la phase d'ouverture de l'océan ayant donné lieu aux ophiolites d'Antalya. Les grès à plantes du Trias supérieur qui affleurent dans la chaine du Taurus (Özgül, 1976) prouvent aussi l'existence d'une sédimentation en eau peu profonde et le début d'une période d'extension crustale (Fig. 1.13).

L'extension continue de bassins marins dans la Néo-Téthys, soit dans sa branche nord soit dans sa branche sud (Sengör and Yilmaz, 1981), s'est poursuivie durant le Jurassique et le Crétacé inférieur. Cette période est dominée par le dépôt de calcaires et de formations terrigènes, de sédiments pélagiques et hémi-pélagiques siliceux fins (Robertson and Woodcock, 1982; Özgül, 1976, 1984). Un volcanisme de type basaltique alcalin (îles océaniques et seamonts) s'est développé durant le Jurassique supérieur et le Crétacé inférieur (Parlak et al., publication soumise), il est associé à des calcaires siliceux et des radiolarites.

A la fin de l'ouverture de l'Atlantique Sud (Smith et al., 1981) datée du début du Crétacé supérieur, l'extension a cessé et la convergence des plaques afro-arabique et eurasienne a débuté. En raison de la permanence de cette collision, la subduction induite dans la branche sud de la Néo-Téthys a donné lieu, dès le Crétacé supérieur, à un magmatisme ophiolitiques associé à l'arc insulaire ou situé au-dessus de la zone de subduction (Pearce et al., 1984; Jones et al., 1991; Robertson, 1994). L'ophiolite de Mersin s'est formée dans la branche sud de la Néo-Téthys. La géochimie des roches volcaniques et la chimie des minéraux des cumulats mafiques et ultramafiques montrent clairement que cette ophiolite s'est formée au-dessus de la zone de subduction (Parlak et al., 1996). Une phase de compression intra-océanique, apparue très tôt, a permis la formation de la semelle amphibolitique qui avait déjà été refroidie au-dessous de 500°C entre 96 et 91 Ma. La géochimie des roches de cette semelle indique que le volcanisme sous-marin se produisait dans un environnement d'arc ou de seamount (Fig. 1.13).

Ce magmatisme a produit des réseaux de filons qui se sont mis en place dans la semelle, dans les tectonites et dans les cumulats. Ces filons ne sont pas métamorphiques; ils sont donc plus jeunes que les amphibolites. Un même contexte a été décrit dans l'ophiolite de Pozanti-Karsanti toute proche (Lytwyn and Casey, 1995). L'âge absolu mesuré sur les filons est compris entre 89 et 86 Ma. Des injections d'âge danien (63 Ma) ont également été observés dans d'autres parties de l'ophiolite, montrant par là la présence de l'activité volcanique durant le Paléocène inférieur dans la chaîne du Taurus, peu avant l'obduction.

La formation sédimentaire la plus ancienne qui repose en discordance sur l'ophiolite est un calcaire marno-gréseux à Alvéolines du Paléocène supérieur (Avsar, 1992) (Fig.1.13).

Les caractéristiques structurales observées dans les différentes roches de l'ophiolite permettent de conclure à l'existence d'une obduction dirigée SW-NE. Celle-ci s'est effectuée sur la chaîne du Taurus, à partir de la branche sud de la Néo-Téthys, à la fin du Paléocène inférieur.

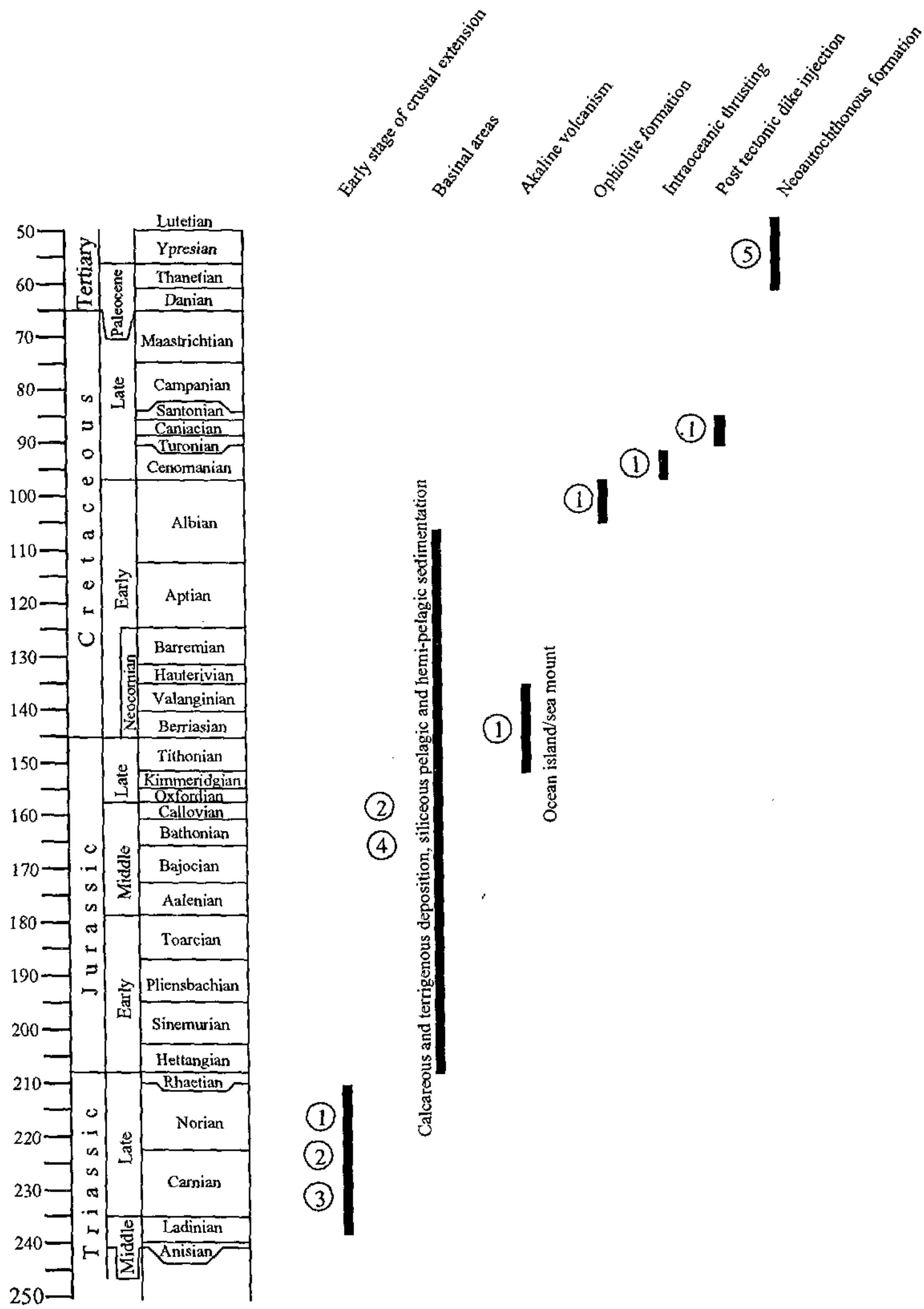

Figure 1.13. Résumé de l'histoire évolutive de l'ophiolite de Mersin (voir texte pour discussion). Les nombres indiquent les références: (1) cette étude, (2) Robertson et Woodcock (1982), (3) Sengor et Yilmaz (1981), (4) Özgül (1976, 1984), (5) Avsar (1992).

Références

Alabaster, T., Pearce, J.A. and Malpas, J., 1982; The volcanic stratigraphy and petrogenesis of the Oman ophiolite complex. Contr. Mineral. Petrol., 81, 168-183.

Arculus, R.J. and Wills, K.J.A., 1980; The petrology of plutonic blocks and inclusions from the Lesser Antilles island arc. J. Petrol., 21, 743-99.

Avsar, N., 1992; Namrun (Içel) yöresi Paleojen bentik foraminifer faunası, M.T.A. Bull., 114, 127-144.

Beard, J.S., 1986; Characteristic mineralogy of arc-related cumulate gabbros: Implications for the tectonic setting of gabbroic plutons and for andesite genesis. Geology 14, 848-851.

Burns, L.E., 1985; The Border Ranges ultramafic and mafic complex, south-central Alaska: cumulate fractionates of island-arc volcanics. Canad. J. Earth Sci., 22, 1020-1038.

Çataklı, A.S., 1983; Assemblage ophiolitique et roches aasociées de la partie occidentale du massif de Pozanti-Karsanti, Taurus Cilicien-Turquie. These de doctorat, Nancy-France, 760p.

Coleman, R.G., 1971; Plate tectonic emplacement of upper mantle peridotites along the continental edges. J. Geophys. Res., 76, 1212-1222.

Coleman, R.G., 1986; Ophiolites and accretion of the North American Cordillera. Bull. Soc. géol. France, 8, 961-968.

Cullers; R.L. and Graf, J.L., 1984; Rare earth elements in igneous rocks of the continental crust: predominantly basic and ultrabasic rocks. In Henderson (ed.), Rare earth element geochemistry, Elsevier-Amsterdam, 510p.

Delaloye, M. and Wagner, J.J., 1984; Ophiolites and volcanic activity near the western edge of the Arabian plate. In: Dixon, J.E. and Robertson, A.H.F. (eds.). Geological Evolution of the Eastern Mediterranean. Geol. Soc. Spec. Publ. London, 17, 225-233.

Desmons, J., Delaloye, M., Desmet, A., Gagny, C., Rocci, G., and Voldet, P., 1980; Trace and REE abundance in Troodos lavas and sheeted dikes, Cyprus. Ofioliti, 5, 35-56.

Dewey, J.F., and Bird, J.M., 1971; Origin and emplacement of the ophiolite suite: Appalachian ophiolites in Newfounland. J. Geophys. Res., 76, 3179-3206.

Dilek, Y. and Moores, E.M., 1990; Regional tectonics of the eastern Mediterranean ophiolites. In: Malpas J, Moores E, Panayiotou A, Xenophontos C (eds), Ophiolites-oceanic crustal analogues. Proceedings of Troodos ophiolite symposium-1987, 295-309.

Dungan, M.A., Long, P.E. and Rhodes, J.M., 1978; The petrology, mineral chemistry, and one atmosphere phase relations of basalts from site 395. Initial Rep. Deep Sea Drill. Proj., 45, 461-472.

Elthon, D., 1981; 1 atm phase equilibria of basalts from the Tortuga ophiolite complex, with implications for magma chamber processes. Chapman Conference on the Generation of the Oceanic Lithosphere-AGU.

Elthon, D., Casey, J.F. and Komor, S., 1982; Mineral chemistry of ultramafic cumulates from the North Arm Mountain Massif of the Bay of Islands Ophiolite: Evidence for high-pressure crystal fractionation of oceanic basalts. J. Geophys. Res., 87, 8717-34.

Elthon, D., 1991; Geochemical evidence for formation of the Bay of Island ophiolite above subduction zone. Nature, 354, 140-143.

Fisk, M.R., Schilling, J.G. and Sigurdsoon, H., 1980; An experimental investigation of Iceland and Reykjanes Ridge tholeiites, I, Phase relations. Contr. Mineral. Petrol., 74, 361-374.

Flower, M.F.J., Robinson, P.T., Schmincke, H.U. and Ohnmacht, W., 1977; Magma fractionation systems beneath the Mid-Atlantic Ridge at 36-37^{o}N. Contr. Mineral. Petrol., 64, 167-195.

Floyd, P.A., 1993; Geochemical discrimination and petrogenesis of alkalic basalt sequences in part of the Ankara melange, central Turkey. J. Geol. Soc. London, 150, 541-550.

Fujimaki, H., 1986; Fractional crystallization of the basaltic suite of Usu volcano, southwest Hokkaido Japan, and its relationships with the associated felsic suite. Lithos, 19, 129-140.

Gass, I.G., 1967; The ultrabasic volcanic assemblages of the Troodos massif, Cyprus. In: Wyllie, P.J. (ed.), Ultramafic and related rocks, John Wiley, Newyork, 121-134.

Gass, I.G., and Smewing, J.D., 1973; Intrusion, extrusion and metamorphism at constructive margins; evidence from the Troodos massif, Cyprus. Nature, 242, 26-29.

Gust, D.A., and Johnson, R.W., 1981; Amphibole bearing cumulates from Boisa island, Papua New Guinea: evaluation of the role of fractional crystallization in an andesitic volcano. J. Geol., 89, 219-232.

Hébert, R., 1985; Pétrologie des roches ignées océaniques et comparison avec les complexs ophiolitiques du Québec, de Chypre et de L'Apennin: Thèse d'Etat, Université de Bretagne Occidentale, Brest, 542p.

Hébert, R. and Laurent, R., 1990; Mineral chemistry of the plutonic section of the Troodos ophiolite: New consraints for genesis of arc-related ophiolites. In: Malpas J, Moores E, Panayiotou A, Xenophontos C (eds), Ophiolites-oceanic crustal analogues. Proceedings of Troodos ophiolite symposium-1987, 149-163.

Jakes, P., and Gill, J., 1970; Rare earth elements and the island arc tholeiitic series. Earth and Planet. Sci. Lett., 9, 17-28.

Jones, G., Robertson, A.H.F. and Cann, J.R., 1991; Supra-subduction zone origin of the Pindos ophiolite, Northwestern Greece. In: Peters, T., Nicolas, A. and Coleman, R.G. (eds.), Ophiolite genesis and evolution of the oceanic lithosphere. Proceedings of the International Conference, Muscat, 7-18 January 1990, 771-801.

Juteau, T., 1980; Ophiolites of Turkey. Ofioliti, 2, 199-238.

Leterrier, J., Maury, R.C., Thonon, P., Girard, D., and Marchal, M., 1982; Clinopyroxene composition as a method of identification of the magmatic affinities of paleo-volcanic series. Earth and Planet. Sci. Lett., 59, 139-154.

Lytwyn, J. N., and Casey, J.F., 1995; The geochemistry of postkinematic mafic dike swarms and subophiolitic metabasites, Pozanti-Karsanti ophiolite, Turkey: evidence for ridge subduction. Bull. geol. Soc. Amer., 107, 7, 830-850.

McDougall, I., and Harrison, T.M., 1988; Geochronology and thermochronology by the $^{40}Ar/^{39}Ar$ method. Oxford monographs on geology and geophysics no. 9. Oxford university press, p.208.

Meschede, M., 1986; A method of discriminating between different types of mid-oceanic ridge basalts and continental tholeiites with the Nb-Zr-Y diagram. Chem. Geol., 56, 207-218.

Miyashiro, A., 1973; The Troodos ophiolite complex was probably formed in an island arc, Earth and Planet. Sci. Lett., 19, 218-224.

Nisbet, E.G., and Pearce, J.A., 1977; Clinopyroxene composition in mafic lavas from different tectonic settings. Contr. Mineral. Petrol., 63, 149-160.

Özgül, N., 1976; Torosların bazı jeoloji özellikleri. T.J.K. Bull., 19, 65-78.

Özgül, N., 1984; Stratigraphy and tectonic evolution of the central Taurides. In: Tekeli, O. and Göncüoglu, M.C. (eds.), Geology of the Taurus belt. Proceedings of international symposium on the geology of the Taurus belt, 1983, Ankara-Turkey, 77-90.

Parlak, O., Delaloye, M., and Bingol, E., 1994; The main features of the Mersin ophiolite-S. Turkey, Abstracts of International Volcanological Congress (IAVCEI-94) 160p., 12-16 September, Ankara-Turkey.

Parlak, O., Bozkurt, E., Delaloye, M., and Bingöl, E., 1995a; The obduction direction of the Mersin ophiolite: Structural evidence from sub-ophiolitic metamorphics in the Central Tauride Belt, Southern Turkey. Abstracts of Second International Turkish Geology Workshop 85p, 6-8 September, Sivas-Turkey.

Parlak, O., Delaloye, M., and Bingöl, E., 1995b; Magma chamber process in Mersin ophiolite, S. Turkey. Abstracts of International Ophiolite Symposium 109p, 18-23 September, Pavia-Italy.

Parlak, O., Delaloye, M., and Bingol, E., 1995c; Origin of sub-ophiolitic metamorphic rocks beneath the Mersin ophiolite, S. Turkey. Ofioliti, 20, 2, 97-110.

Parlak, O., Delaloye, M., and Bingol, E., (in review) Geochemistry of volcanic rocks in the Mersin ophiolite and their tectonic significance in the eastern Mediterranean geology, in IESCA-1995 Proceedings, Int.ernational Earth Sciences Colloquium on the Eagean Region.

Parlak, O., Delaloye, M., and Bingol, E., 1996; Mineral chemistry of ultramafic and mafic cumulates as an indicator of the arc related origin of the Mersin ophiolite (southern Turkey). Geol. Rdsch., 85.

Parrot, J.F., 1977; Assemblage ophiolitique du Baer-Bassit et termes effusifs du volcano-sédimentaire. Pétrologie d'un fragment de la croûte téthysienne charriée sur la plate-forme syrienne. Trav. et Doc. ORSTOM Paris, 72, 333 pp.

Pearce, J.A., and Cann, J.R., 1973; Tectonic setting of basic volcanic rocks determined using trace element analysis. Earth and Planet. Sci. Lett., 19, 290-300.

Pearce, J.A., and Norry, M.J., 1979; Petrogenetic implications of Ti, Zr, Y and Nb variations in volcanic rocks. Contr. Mineral. Petrol., 69, 33-47.

Pearce, J.A., 1980; Geochemical evidence for the genesis and eruptive setting of lavas from Tethyan ophiolites. In: Panayiotou, A. (ed.), Ophiolites, Cyprus, 751-757.

Pearce, J.A., Lippard, S.J., and Roberts, S., 1984; Characteristics and tectonic significance of supra-subduction zone ophiolites. In: Kokelaar BP, Howells MF (eds.), Marginal Basin Geology, 77-94. Blackwell Scientific-Oxford.

Ricou, L.E., Marcoux, J., and Whitechurch, H., 1984; The Mesozoic organization of the Taurides: one or several ocean basins?. In: Dixon, J.E. and Robertson, A.H.F. (eds.), The geological evolution of the eastern Mediterranean. Geol. Soc. Spec. Publ. London, 17, 349-361.

Robertson, A.H.F., and Woodcock, N.H., 1982; Sedimentary history of the south-western segment of the Mesozoic-Tertiary Antalya continental margin, south-west Turkey, Eclogae Geol. Helv., 75, 3, 517-562, .

Robertson, A.H.F., and Dixon, J.E., 1984; Introduction: aspects of the geological evolution of the eastern Mediterranean. In: Dixon, J.E. and Robertson, A.H.F. (eds.), The geological evolution of the eastern Mediterranean. Geol. Soc. Spec. Publ. London, 17, 1-75.

Robertson, A.H.F., and Waldron, J., 1990; Geochemistry and tectonic setting of Late Triassic and Late Jurassic-Early Cretaceous basaltic extrusives from the Antalya Complex, SW Turkey. In: Savasçin, Y. and Eronat, A.H. (eds.), International Earth Sciences Congress on Aegean Regions-Turkey, IESCA-1990 proceedings, 2, 279-299.

Robertson, A.H.F., 1994; Role of the tectonic facies concept in orogenic analysis and its application to Tethys in the eastern Mediterranean region. Earth-Sci. Rev., 37, 139-213.

Schilling, J.G., 1975; Azores mantle blob: rare earth evidence. Earth and Planet. Sci. Lett., 25, 103.

Searle, M.P., Lippard, S.J., Smewing, J.D., and Rex, D.C., 1980; Volcanic rocks beneath the Semail ophiolite nappe in the northern Oman mountains and their significance in the Mesozoic evolution of Tethys. J. geol. Soc. London, 137, 589-604.

Sengör, A.M.C., and Yılmaz, Y., 1981; Tethyan evolution of Turkey: Plate tectonic approach. Tectonopysics 75, 181-241.

Shervais, J.W., 1982; Ti-V plots and the petrogenesis of modern and ophiolitic lavas. Earth and Planet. Sci. Lett., 59, 101-118.

Smith, A.G., Hurley, A.M. and Briden, J.C., 1981; Phanerozoic palaeocontinental maps. Cambridge, Cambridge University Press, 102p.

Stern, R.J., 1979; On the origin of andesite in the northern Mariana island arc: implications from agrigan. Contr. Mineral. Petrol., 68, 207-219.

Sun, S.S., Nesbitt, R.W. and Sharaskin, A.Y., 1979; Geochemical characteristics of Mid-Ocean Ridge Basalts. Earth and Planet. Sci. Lett., 44, 119-138.

Sun, S.S., and McDonough, W.F., 1989. Chemical and isotopic systematics of oceanic basalts: implication for mantle composition and processes. In Saunders, A.D. and Norry, M.J. (eds), Magmatism in the ocean basins. Geol. Soc. Spec. Publ. London, 42, 313-345.

Whitechurch, H., Juteau, T., and Montigny, R., 1984; Role of the Eastern Mediterranean ophiolites (Turkey, Syria, Cyprus) in the history of the Neo-Tethys. In: Dixon, J.E. and Robertson, A.H.F. (eds.). Geological Evolution of the Eastern Mediterranean. Geol. Soc. Spec. Publ. London, 17, 301-317.

Winchester, J.A., and Floyd, P.A., 1977; Geochemical discrimination of different magma series and their differentiation products using immobile elements. Chem. Geol., 20, 325-343.

White, W.M., Tapia, M.D.M., and Schilling, J.G., 1979; The petrology and geochemistry of the Azores islands. Contr. Mineral. Petrol., 69, 201-213.

Yalınız, M.K., Göncüoglu, M.C., and Floyd, P.A., 1994; Geochemical characteristics and geodynamic interpretation of the Supra-subduction Sarıkaman ophiolite, Central Anatolia. Abstracts of International Volcanological Congress (IAVCEI-94) 162p. 12-16 September, Ankara-Turkey.

CHAPTER 2

GENERAL OVERVIEW OF THE EASTERN MEDITERRANEAN OPHIOLITES

2.1. Introduction

Ophiolites have been interpreted as on-land fragments of oceanic lithosphere developed as a result of sea floor spreading at oceanic spreading centers.The concept of an oceanic spreading center origin for ophiolites has been widely accepted based mainly on the presence of a sheeted dike complex (Gass, 1967; Coleman, 1971; Dewey and Bird, 1971). Ophiolites have a great importance in reconstruction of ancient plate boundaries since their acceptance as on-land fragments of oceanic lithosphere. The Neotethys represents a Mesozoic oceanic basin which evolved between the Afro-Arabian platform to the south and the Eurasian platform to the north while the Paleozoic-early Mesozoic paleotethys was consuming (Sengör and Yilmaz, 1981). The Neotethyan ocean is divided into two basinal areas from which Tethyan ophiolites were derived onto continental margins during Late Cretaceous in Turkey (Sengor and Yilmaz, 1981; Robertson and Dixon, 1984). These ocean basins are so-called the multi-armed northern branch of Neotethys that includes intra-Pontide, Izmir-Ankara, inner-Tauride oceans and a relatively more simple southern branch of Neotethys.

The ophiolitic massifs cropping out in Turkey are distinguished as three different groups, namely North Anatolian ophiolite belt, Peri-Arabic ophiolite belt and Tauride ophiolite belt (Juteau, 1980). All of which have their specific character (Fig. 2.1). The North Anatolian and Tauride ophiolites (except the Antalya ophiolite) are thought to be derived from the Northern branch of the Neotethys whereas the Peri-Arabic belt ophiolites belong to the southern branch of the Neotethyan ocean basin (Sengor and Yilmaz, 1981; Robertson and Dixon, 1984; Whitechurch et al., 1984; Dilek and Moores, 1991).

2.2. North Anatolian ophiolite belt

This belt consists of a series of E-W trending ophiolite bodies in northern Turkey (Fig. 2.1). The most distinctive feature of these ophiolite bodies, particularly in the western part, is the occurence of HP-LT glaucophane, lawsonite and jadeite bearing blueschists paragenesis (Okay, 1980, 1984; Juteau, 1980). These bodies are also intruded by numerous plutons and dikes of diorite, granodiorite and tonalite which are Tertiary in age (Juteau, 1980).

Figure 2.1. Distribution of ophiolitic massifs in Turkey (Juteau, 1980).

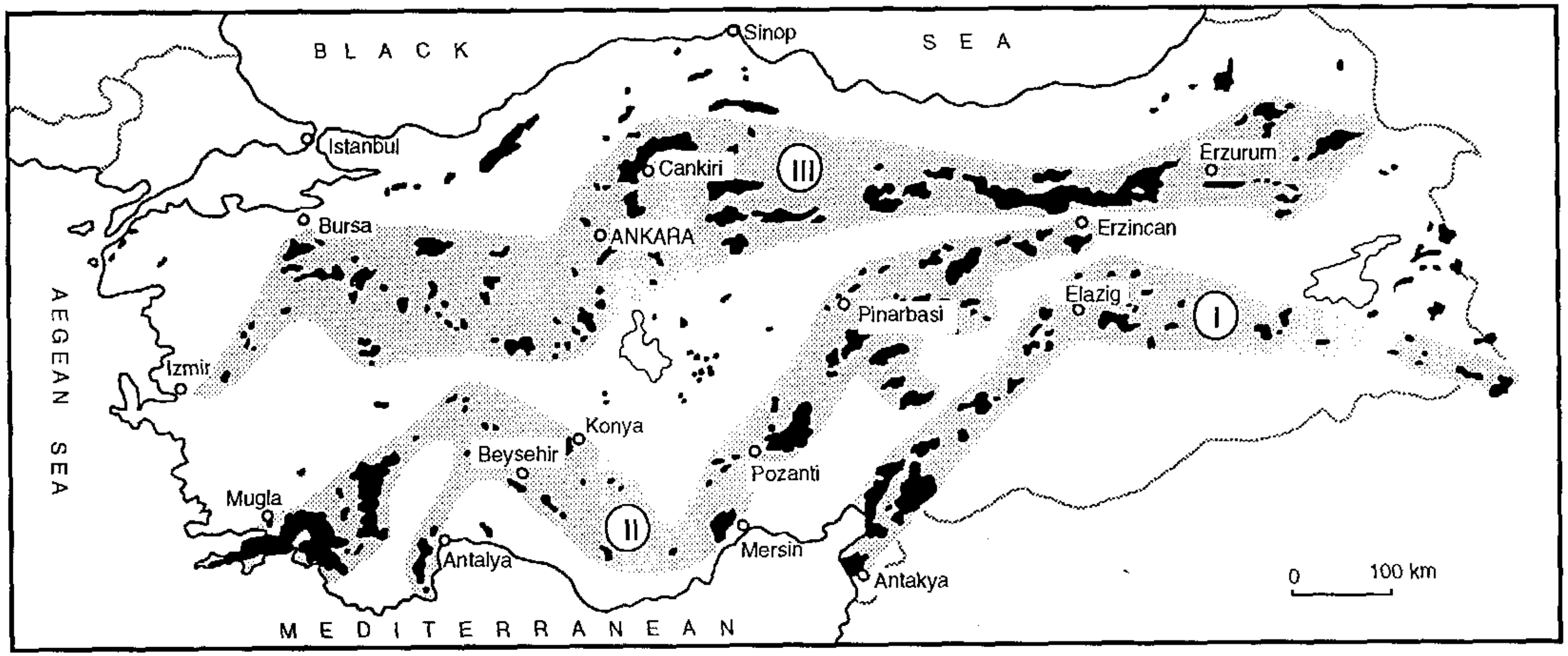

I - The southern (Peri-Arabic) ophiolite belt   II - The median (Tauric) ophiolite belt   III - The northern ophiolite belt

Ophiolites of this northern belt consist mainly of metamorphosed and serpentinized harzburgites, dunites, layered metagabbros, isolated diabase dikes that cut all the ophiolite suite, rare metamorphic sole(s) and dismembered volcanic associated with sedimentary units. They are generally associated with a tectonic melange (Juteau, 1980).

2.3. Peri-Arabic ophiolite belt

Peri-Arabic belt starts from Oman ophiolite in the east and continues westward along the Zagros crushed zone-Bitlis suture zone then ends up by Troodos ophiolite (Ricou, 1971). Cretaceous ophiolites along the Turkish segment of the Peri-Arabic belt exposed nearly in E-W trending discontinuous belts around the Arabian promontory are possible remnants of the Neotethyan oceanic lithosphere (Fig. 2.2). The tectonic position of the ophiolites in the southern belt between the Afro-Arabian platform on the south and E-W trending microcontinents of possible Gondwana origin on the north suggests that Neotethyan oceanic crust in the southern strand developed after distruption and rifting-off the northern margin of the Afro-Arabia (Sengor and Yilmaz, 1981; Dilek and Moores, 1990). The onset of this continental rifting is interpreted to have occurred around the Late Triassic time as suggested by the existence of Upper Triassic alkaline lavas and rift-related terrigenous sedimentary rocks associated with the ophiolites (Delaloye and Wagner, 1984; Whitechurch et al., 1984)

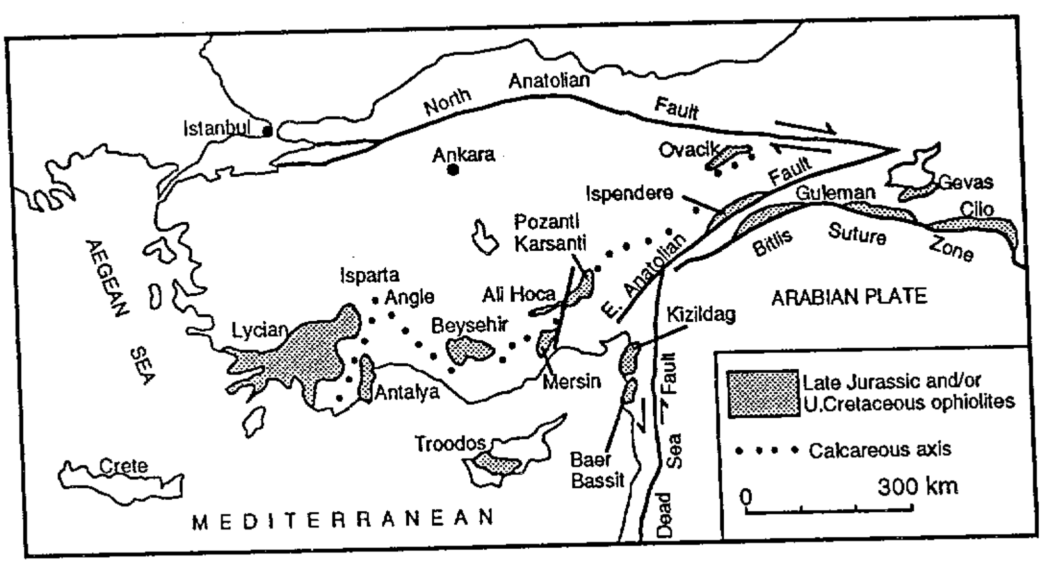

Figure 2.2. Main tectonic elements and distribution of the ophiolitic complexes in the eastern Mediterranean (Dilek and Moores, 1990).

2.3.1. Baer-Bassit ophiolite

The Baer-Bassit ophiolite (NW Syria) belongs to the southernmost or "external" belt of Tethyan ophiolite nappes thrust onto the northern border of the Arabian platform during Maastrichtian time. It is situated in front of Cyprus, and represents an eastward prolongation of its formations and structures, thus forming the western end of the "peri-Arabic ophiolite crescent" (Ricou, 1971).

The Baer-Bassit ophiolitic massif consists mainly of mantle tectonites and cumulates, layered gabbros, sheeted diabasic complex, plagiogranite and two different levels of pillow-lavas. It also comprises an infra-peridotitic metamorphic sole and a volcano-sedimentary series (Parrot, 1980) (Fig. 2.3a).

2.3.2. Hatay (Kızıldag) ophiolite

The Cretaceous Kizildag ophiolite in southern Turkey represents a remnant of oceanic lithosphere formed in a southern strand of the Mesozoic Neotethys (Dilek et al., 1991).

During the last decade, many studies have been carried out on the geology and tectonic evolution of the Hatay ophiolite (Selcuk, 1981; Piskin et al., 1986; Dilek et al., 1991; Dilek and Delaloye, 1992; Piskin et al., 1990). According to their definitions, the geological units are divided, in the Hatay area, into three groups such as autochthonous units, allochthonous units and neo-autochthonous units (Fig. 2.3b).

Autochthonous units, which can be interpreted as part of the Arabian plate, are characterized by platform type sediments of Mesozoic age. Allochthonous units are indicated by the ophiolitic rocks which can be subdivided into tectonites, cumulates, isotropic gabbros, sheeted dike complex, pillow-lavas and volcano-sedimentary rocks.

The Hatay ophiolite is considered as complete in accordance with the Penrose conference definition. The oceanic crust is rather thin like that in slow-spreading systems. Erendil (1984) suggested a paleospreading rate of 2 cm/year.

The ophiolite sequence and the basement rocks are covered transgressively by sedimentary terrains whose total thickness is estimated as about 3000 m and form the neoautochthonous units. The timing of the transgression is from Upper Cretaceous to Miocene.

2.3.3. Troodos ophiolite

The Troodos massif comprises two parts separated by the more or less E-W striking Arakapas fault zone. The northern part constituting the principal part of the Troodos massif mainly consists of peridotite-serpentinite overlain by mafic-ultramafic plutonic complex,

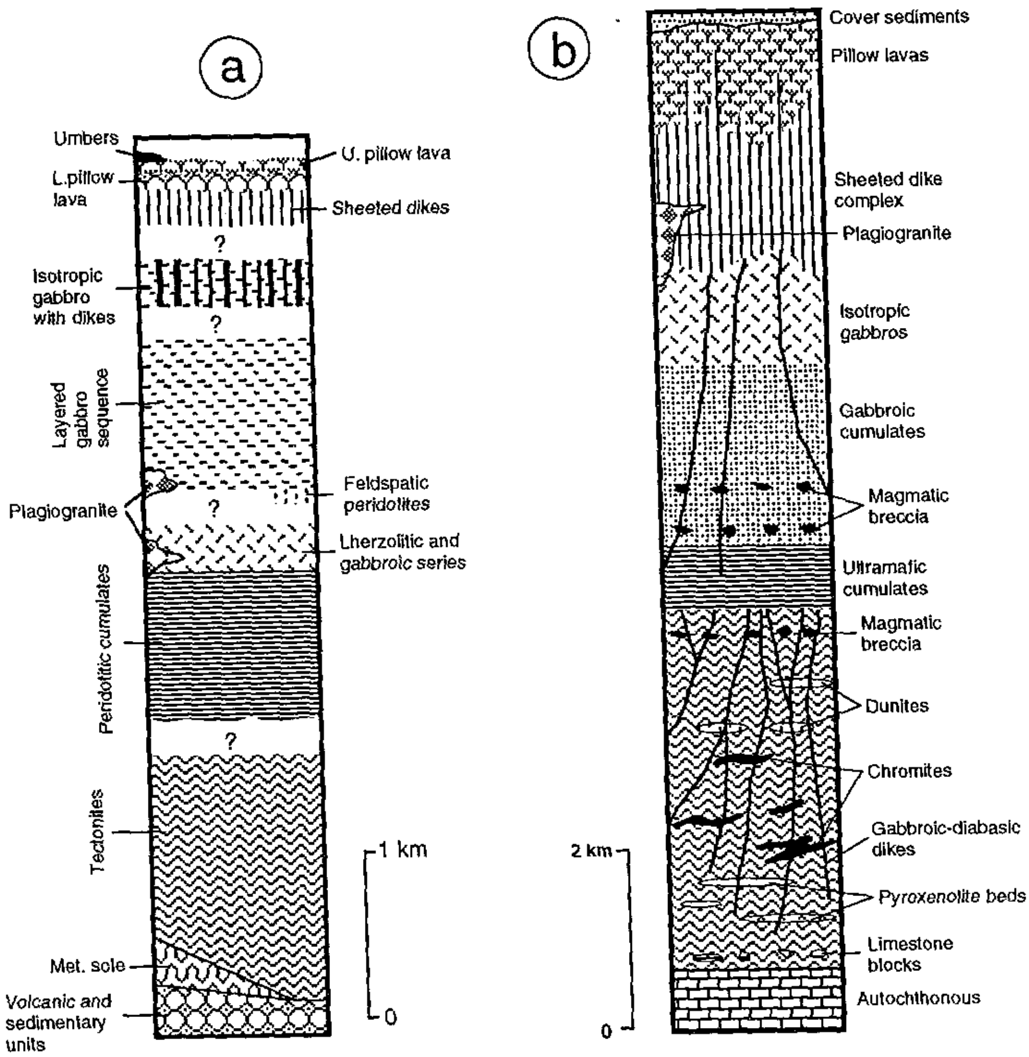

Figure 2.3. a. Synthetic log of the Baer-Bassit ophiolite (Parrot, 1980). **b.** Synthetic section of the Hatay (Kizildag) ophiolite (Selcuk, 1981).

sheeted dike complex, extrusive rocks and overlying sediments (Fig. 2.4). Axial grabens and normal faults parallel to the grabens within the sheeted dike complex and extrusive sequence are indication of oceanic spreading centers (Varga and Moores, 1985). Arakapas fault zone is interpreted as a possible fossile transform fault (Moores and Vine, 1971; Murton and Gass, 1986). Geochemical studies of intrusive and extrusive rocks contrasting with the structural studies imply a calc-alkaline trend for these rocks, showing a subduction-related origin (Moores et al., 1984; Pearce et al., 1984).

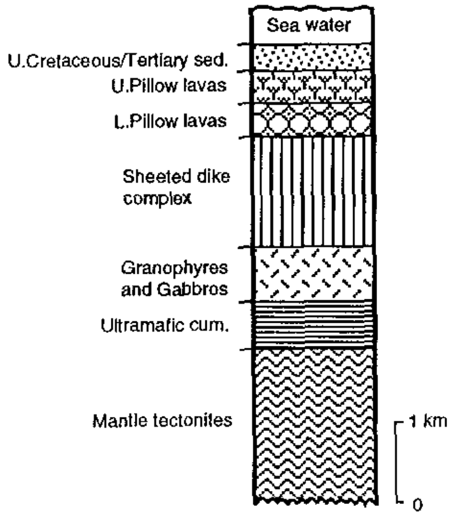

Figure 2.4. Troodos ophiolite units (Gass and Smewing, 1973).

2.4. Tauride ophiolite belt

The Tauride ophiolites (Fig. 2.1) are complex, gathering several tectonic units of miscellaneous ages, including from bottom to top;

-volcanic and sedimentary units, including alkaline basaltic pillow-lavas and associated sediments of Upper Triassic age, probable fragments of a first Tethyan proto-oceanic crust;

-units of metamorphic rocks, typically located as a tectonic sole under the peridotites, probable witnessing of early slicing events in the oceanic crust before obduction;

-unit made of coarse-grained tholeiitic rocks of probable Cretaceous (Cenonian ?) age, including foliated harzburgitic tectonites, non-deformed ultramafic and mafic cumulates and, in one case (Antalya) a dike complex. Metamorphics, tectonites and cumulates are intersected by numerous isolated tholeiitic diabase dikes (Juteau, 1980).

2.4.1. Pozanti-Karsanti ophiolite

This ophiolite is situated 100 km north of Adana on the eastern flank of the Tauride chain, just between Pozanti and Farasa. It is seen on the 1/500.000 scale geological map of Turkey that geometrically the Pozanti-Karsanti ophiolitic massif having NE-SW trend was offset from Mersin ophiolite by the sinistral movement of the Ecemis fault.

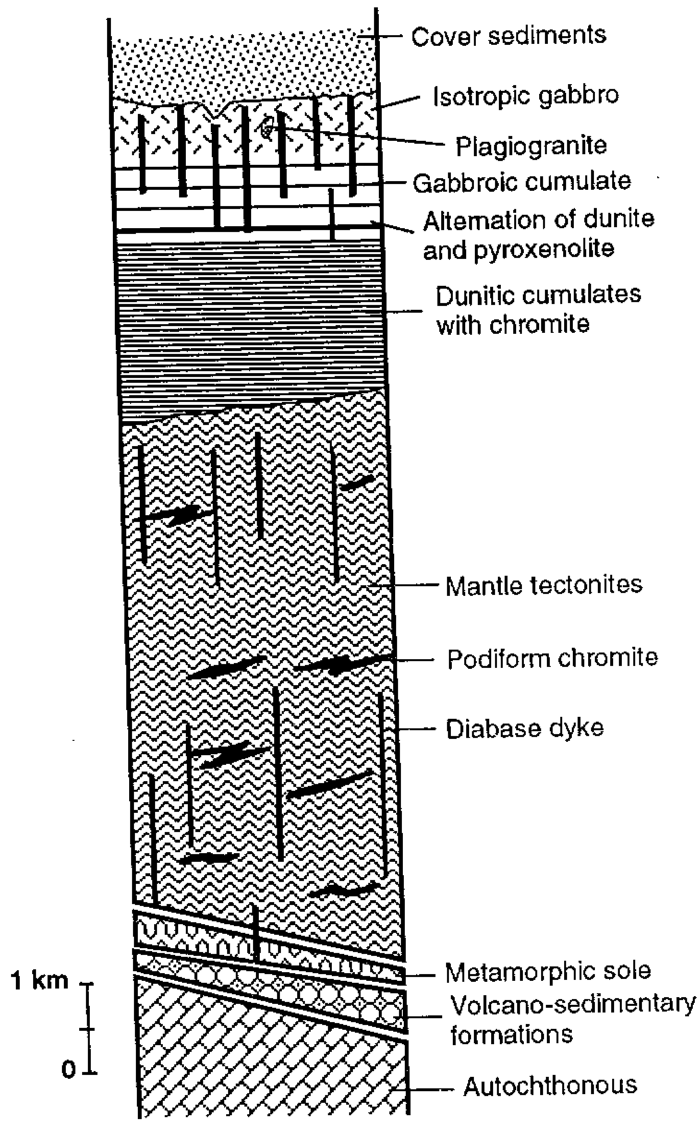

Figure 2.5. Synthetic log of Pozanti-Karsanti ophiolitic massif (Bingol, 1978).

The definition of the rock units, bottom to top, is based on the study of Bingöl (1978) in the eastern part of the massif (Fig. 2.5).

-Autochthonous series: The basement, on which Pozanti-Karsanti ophiolite thrusted during the Upper Cretaceous, is characterized by platform type carbonates ranging from Lower Paleozoic to Upper Cretaceous age in the region.

-Volcano-sedimentary unit: Radiolarite, limestone, clayey sediments, cherts and basaltic volcanic rocks form the volcano-sedimentary units in the massif. This unit was tectonically overlain by ultramafic rocks of the ophiolitic massif during the thrusting onto the continental platform.

-Metamorphic slices: Amphibolites are the dominant rock type within the metamorphics. It also comprises quartzites, micaschists, epidotes. These rocks are rarely cut by diabase dikes. Mineral paragenesis and the conditions of metamorphism indicate that they formed within the greenschist facies during the intra-oceanic thrusting.

-Tectonites and cumulates cut by tholeiitic diabase dikes represent the basic and ultrabasic rocks of the Pozanti-Karsanti ophiolitic massif. Tectonites having 6 km thickness are characterized by harzburgites (85%) and dunites. Both of which show the same deformation style namely mylonitic texture at the bottom and tectonite-cumulate character at the top of the ultramafics. Three different types of rock are seen in the cumulates; from bottom to top these are dunites, pyroxenites and gabbros. The Pozanti-Karsanti ophiolite is overlain unconformably by the sedimentary sequence of the Oligocene-Miocene Pozanti-Karsanti basin.

2.4.2. Mersin ophiolite

The Mersin ophiolite crops out on the southern flank of the Bolkardag within the nearly N-S trending deep valleys under the tabular Miocene carbonates (Fig. 2.6b). Mersin ophiolites includes tectonic slices of serpentinized harzburgite, layered ultramafic and mafic rocks both of which intruded by isolated gabbro and diabase dikes, basaltic pillow-lavas and associated deep marine sediments. Tectonites are underlain by metamorphic rocks composed of amphibolite, marble, quartzites cut by numerous gabbroic and diabasic dikes which in turn overlies a melange sequence (Juteau, 1980; Dilek and Moores, 1990).

2.4.3. Alihoca ophiolite

A narrow, dismembered and deformed ophiolitic sequence is present in the north of the Bolkardag (Fig. 2.6b). The Alihoca complex comprises serpentinised peridotites, gabbros and basalts intruded by diorites, quartz-diorites and tonalites (Calapkulu, 1985). In its southern margin, the complex has a tectonic contact with the marbles of the Bolkardag marked by exposures of the glaucophane-greenschist facies (Juteau, 1980). Alihoca ophiolite is overlain by the calc-alkaline andesitic series of Ciftehan including flyschoid sediments of Upper Cretaceous-Paleocene age.

2.4.4. Beysehir ophiolite nappes

After the curvature of Isparta angle, the Lycian nappes extend eastward to the ophiolitic massif of Beysehir (Fig. 2.6a). Beysehir ophiolite consists of harzburgitic tectonites underlain by metamorphic rocks (yielding 95 Ma) (Thuizat et al., 1981), isolated diabase dikes intersecting the peridotites, alkaline basaltic pillow-lavas associated with Upper Triassic pelagic sediments (Juteau, 1980).

2.4.5. Lycian ophiolitic nappe

The Lycian nappes are thrusted over a relatively autochthonous unit of Beydaglari carbonate platform (Fig. 2.6a). They exhibit, from bottom to top, typical "Tauric" ophiolite organization such as:

-a huge sheet of coarse-grained ultramafic tectonites including a banded complex of the harzburgite-dunite-orthopyroxenite intersected by isolated tholeiitic diabase dikes,

-tectonites are underlain by the metamorphic sole (amphibolite-quartzite) yielding 104 Ma (Thuizat et al., 1981); some of the metamorphics are also cut by the diabase dikes,

-non-deformed cumulate rocks have discontinuous exposures in the Lycian nappes,

-truncated sedimentary and volcanic units form the upper most unit of the Lycian nappes.

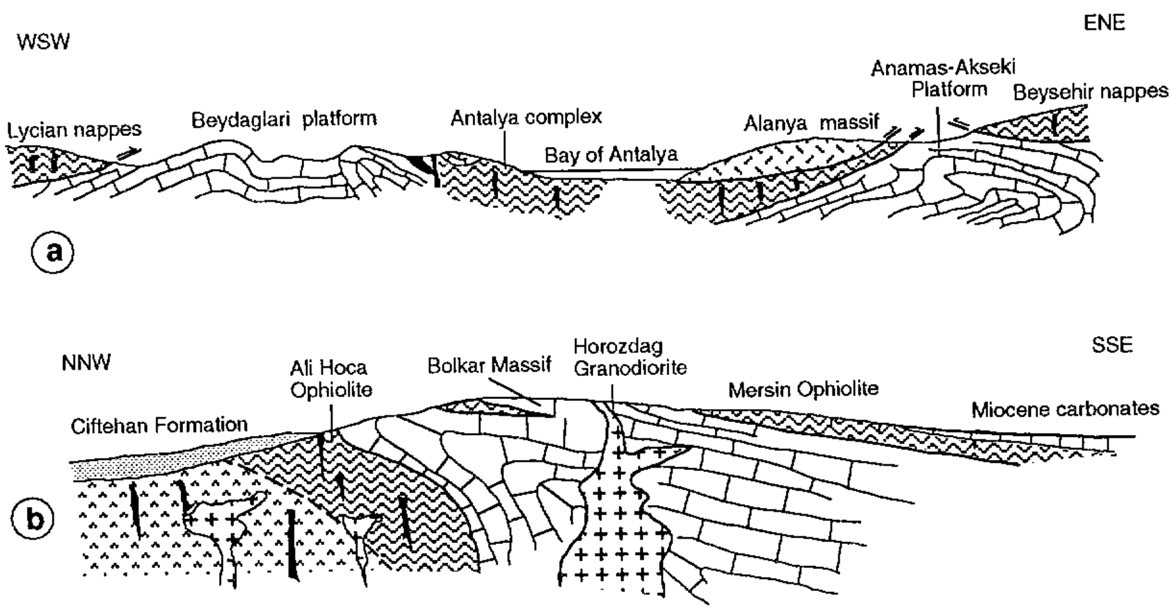

Figure 2.6. a. Schematic geologic cross section from Lycian nappes in the west to the Beysehir nappes in the east (Dilek and Moores, 1990). **b.** Schematic cross section running from Alihoca ophiolite in the north and Mersin ophiolite in the south of Bolkardag (Dilek and Moores, 1990).

2.4.6. Antalya ophiolite complex

The Antalya ophiolite complex belongs to the median unit of the so-called Antalya nappe, one of the biggest nappe systems in the western Taurides (Lefevre, 1967; Brunn et al., 1971; Marcoux and Poisson, 1972). Detailed mapping of Juteau (1968, 1970, 1975) done in the region has shown that the ophiolitic complex can be divided into two main units (Fig. 2.7) as:

a coarse-grained unit comprising tectonites-cumulates and dike complex, intersected by tholeiitic diabase dikes, crop out within three different massifs namely, from south to north, the Adrasan, the Cirali-Tekirova and the Kemer massifs. These massifs are separated, and in places covered, by erosional remnants of the upper Antalya nappe, by neo-autochthonous deposits, or by long sand beaches. The Adrasan massif is entirely composed of ultramafic tectonites comprising the following lithologies: harzburgites, dunites and associated podiform chromites. All these are intersected by isolated diabase dikes. The massif of Cirali-Tekirova includes two petrographic units: a sole of harzburgitic tectonites and non-deformed ultramafic and mafic layered cumulates. The northern massif of Kemer consists of a dike complex made of tholeiitic diabase, quartz-diabase and plagiogranites (Juteau, 1980).

A volcanic unit mainly composed of pillow-lavas and showing primary contact with the Upper Triassic "Alakir çay" sedimentary unit (Marcoux, 1970).

Metamorphic rocks, namely amphibolites, quartzites and marbles, appear as small tectonic slices in the ophiolitic zone of the Alakir çay valley.

2.5. Comparison of the eastern Mediterranean ophiolites

Tauride and peri-Arabic belt ophiolites in southern Turkey are those on which the attention of numerous authors have been focussed (Juteau, 1970; 1975; 1980; Juteau et al., 1977; Robertson and Dixon, 1984; Delaloye and Wagner, 1984; Whitechurch et al., 1984; Yilmaz, 1984; Ricou et al., 1984; Dilek and Moores, 1990; Piskin et al., 1990; Dilek and Delaloye, 1992; Lytwyn and Casey, 1993; Lytwyn and Casey, 1995; Polat and Casey, 1995) during more than the last two-decades in the eastern Mediterranean region. All these studies deal essentially with geochemistry, geochronology and structural setting of the Turkish ophiolites within the eastern Mediterranean geotectonic context. Here, a comparison summary will be given for these ophiolites based on the above-mentioned references.

Ophiolites in southern Turkey are situated along two lineaments namely *Tauride* that is associated with a metamorphic sole and an ophiolitic melange and *peri-Arabic* belt that presents a complete ophiolite succession.

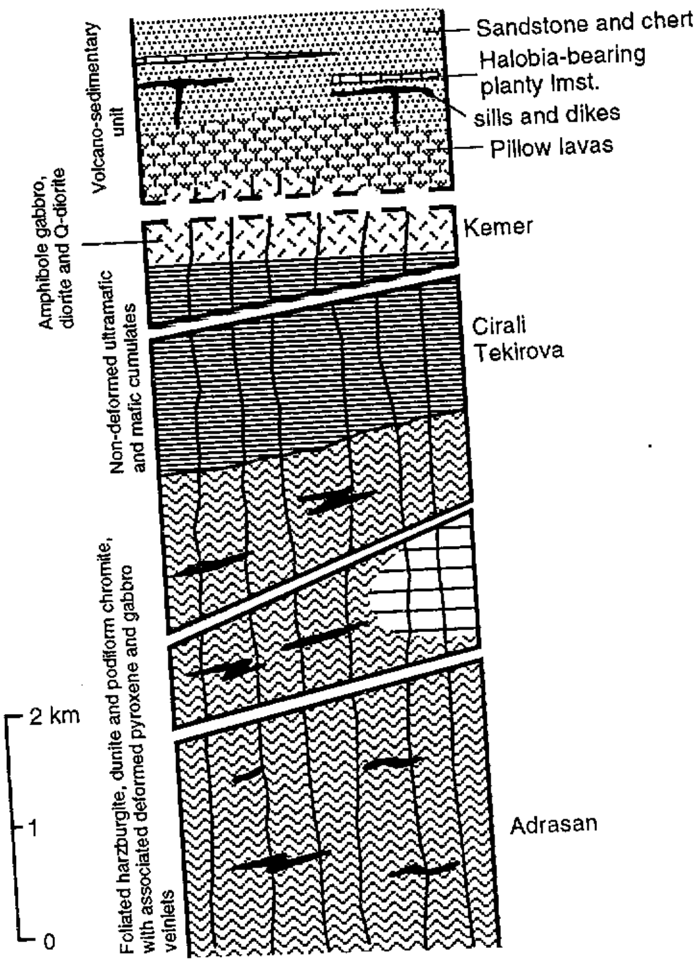

Figure 2.7. Synthetic log of the Antalya ophiolite complex (Juteau, 1977).

a) All ophiolites in the Tauride belt possess a thin sheet of metamorphic rocks that are folded, imbricated, and cut by numerous post-metamorphic tholeiitic microgabbroic-diabasic dike swarms. These metamorphic rocks are represented mainly by amphibolite, marble, amphibolitic schists, epidote-amphibolite schists, micaschists. Whereas, except Baer-Bassit, peri-Arabic belt ophiolites do not possess any metamorphic sole (Fig. 2.8).

b) Taurus type ophiolites exhibit a thick ultramafic-mafic cumulate sequence ranging from 3 to 5 km. In contrast, the cumulate sequence of the peri-Arabic belt ophiolites is represented by a small amount of ultramafic and mafic rocks (maximum 1 km thick) (Fig. 2.8).

c) Except Antalya, Taurus type ophiolites do not have a sheeted dyke complex whereas the peri-Arabic belt ophiolites do contain well-developed sheeted dyke complexes (Fig. 2.8).

d) Cogenetic tholeiitic pillow lavas are not preserved in Tauride type ophiolites due to submarine erosion or tectonic events during obduction onto the continent (Whitechurch et al., 1984). On the other hand alkaline basaltic pillow lavas and associated terrigeneous sediments ranging from Upper Triassic to Upper Cretaceous in age are exposed at the base of the Tauride ophiolites. This tectonic slice is also exposed in the Troodos and Baer-Bassit ophiolites (Fig. 2.8).

e) One of the main characteristics of the Tauride belt ophiolites is that they are intruded by numerous low-K tholeiitic diabase dikes at all structural levels whereas in Hatay and Troodos ophiolites isolated diabase dike swarms are rarely seen (Fig. 2.8).

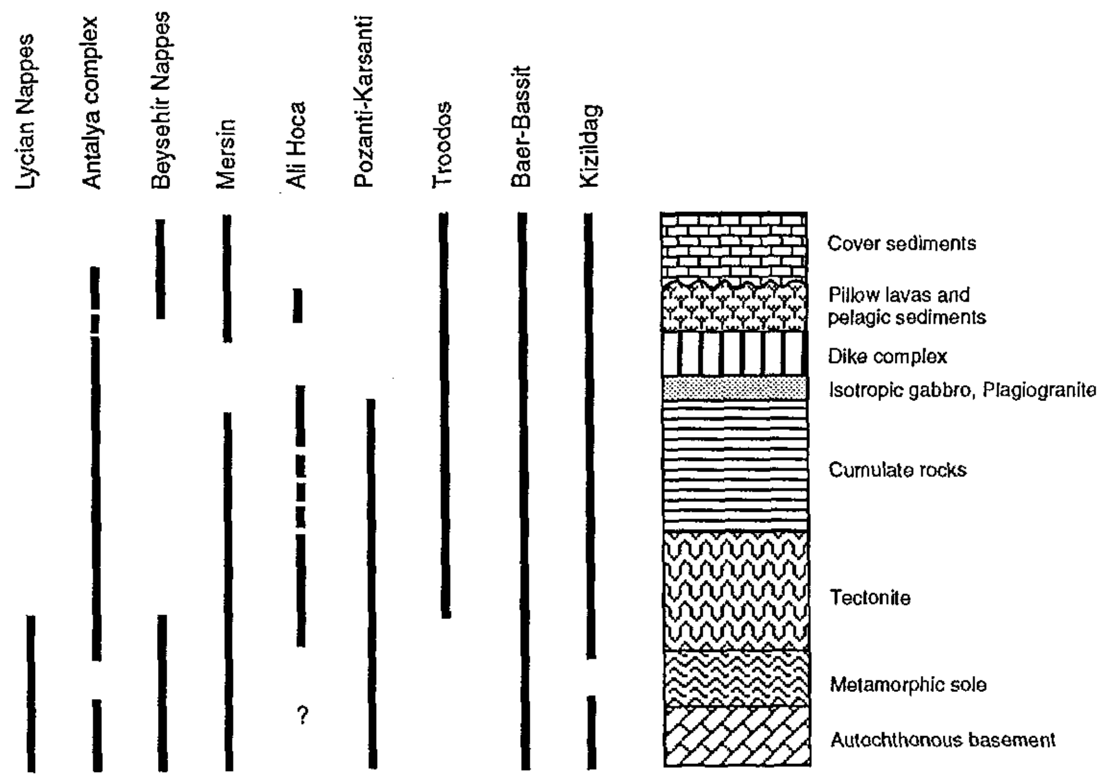

Figure 2.8. Schematic comparison of the eastern Mediterranean ophiolites with expanded ophiolite assemblage (from Dilek and Moores, 1990).

References

Bingöl, A.F., 1978; Pétrologie du massif ophiolitique de Pozanti-Karsanti (Taurus cilicien,Turquie): étude de la partie orientale. Thése 3e cycle, Univ. Strasbourg, 227p.

Brunn, J.H., Argyriadis, J.F., Graciansky, P.C., Gutnic, M., Juteau, T., Marcoux, J., Monod, O., and Poisson, A., 1971; Outline of the Geology of the Western Taurides. In: A.S. Campbell (ed.), Geology and History of Turkey. Petroleum Exploration Soc. of Libya, Tripoli, 225-255.

Calapkulu, F., 1985; Les observations sur la tectonique des plaques dans la région de Bolkardag (Turquie). In: Izdar, E. and Nakoman, E. (eds.), Procedings of the VI Colloquim on geology of the Aegean region, Izmir-Turkey, II. edition: 81-97.

Coleman, R.G., 1971; Plate tectonic emplacement of upper mantle peridotites along the continental edges. J. Geophys. Res., 76, 1212-1222.

Delaloye, M., and Wagner, J.J., 1984; Ophiolites and volcanic activity near the western edge of the Arabian plate. In: Dixon, J.E. and Robertson, A.H.F. (eds.), The geological evolution of the eastern Mediterranean. Geol. Soc. Spec. Publ. London, 17, 225-233.

Dewey, J.F., and Bird, J.M., 1971; Origin and emplacement of the ophiolite suite: Appalachian ophiolites in Newfounland. J. Geophys. Res., 76, 3179-3206.

Dilek, Y., and Moores, E.M., 1990; Regional tectonics of the eastern Mediterranean ophiolites. In: Malpas, J., Moores, E.M., Panayiotou, A. and Xenophontos, C. (eds.), Ophiolites and Oceanic crustal analogues. Nicosia, Geol. Surv. Dept., Cyprus, 295-309.

Dilek, Y., Moores, E.M., Delaloye, M., and Karson, J.A., 1991; Amagmatic extension and tectonic denudation in the Kizildag ophiolite, southern Turkey: Implications for the evolution of Neo-tethyan oceanic crust. In: Peters, T.J., Nicolas, A. and Coleman, R.G. (eds.), Ophiolite genesis and evolution of the oceanic lithosphere, 485-500, Ministry of Petroleum and Minerals, Sultanate of Oman.

Dilek, Y., and Delaloye, M., 1992; Structure of the Kizildag ophiolite, a slow-spread Cretaceous ridgesegment north of the Arabian promontory. Geology, 20, 19-22.

Erendil, M., 1984; Petrology and structure of the upper crustal units of the Kizildag ophiolite. In: Tekeli, O. and Göncüoglu, M.C. (eds.), Geology of the Taurus belt. Proceedings of the international symposium-1983, Ankara-Turkey, 269-284.

Gass, I.G., 1967; The ultrabasic volcanic assemblages of the Troodos massif, Cyprus. In Wyllie, P.J. (ed.), Ultramafic and related rocks, John Wiley, Newyork, 121-134.

Gass, I.G., and Smewing, J.D., 1973; Intrusions, extrusions and metamorphism at the constructive plate margins: evidence from the Troodos massif, Cyprus. Nature, 242, 26-29.

Juteau, T., 1968; Commentaire de la carte géologique des ophiolite de la region de Kumluca (Taurus Lycian, Turquie méridionale): cadre structural, modes de gisement et description des principaux faciés du cortège ophiolitique. M.T.A. Enst. Bull., Ankara, 70, 70-91.

Juteau, T., 1970; Pétrogenèse des ophiolites des nappes d`Antalya (Taurus Lycian oriental, Turquie). Leur liaison avec une phase d`expansion océanique active au Trias supérieur. Sci. de la Terre, Nancy, 15, 265-288.

Juteau, T., 1975; Les ophiolites des nappes d`Antalya (Taurides occidentales, Turquie). Pétrologie d`un fragment de l`ancienne croute océanique téthysienne. Sci. de la Terre, Nancy, Mém., 32, 692p.

Juteau, T., Nicolas, A., Dubessy, J., Fruchard, J.C., and Bouchez, J.L., 1977; Structural relationships in the Antalya ophiolitic complex, Turkey: Possible model for an oceanic ridge. Bull. geol. Soc. Amer., 88, 1740-1748.

Juteau, T., 1980; Ophiolites of Turkey. In: G. Rocci (ed.), Tethyan ophiolites. Ofioliti, 2, 199-237.

Lefevre, R., 1967; Une nouvelle element de la geologie du Taurus Lycien: Les nappes d`Antalya (Turquie): Comptes Rendus de L`Academie des sciences, 7, 1365-1368.

Lytwyn, J.N., and Casey, J.F., 1993; The geochemistry and petrogenesis of volcanics and sheeted dikes from the Hatay (Kizildag) ophiolite, southern Turkey: possible formation with the Troodos ophiolite, Cyprus, along for-arc spreading centers. Tectonophysics, 223, 237-272.

Lytwyn, J.N., and Casey, J.F., 1995; The geochemistry of postkinematic mafic dike swarms and subophiolitic metabasites, Pozanti-Karsanti ophiolite, Turkey: evidence for ridge subduction. Bull. geol. Soc. Amer., 107, 7, 830-850.

Marcoux, J., 1970; Age Carnien de termes effusifs du cortége ophiolitique des nappes d`Antalya (Taurus Lycien occidental, Turquie). C.R. Acad. Sci. Fr., 271, 285-287.

Marcoux, J., and Poisson, A., 1972; Une nouvelle unité structurale majeure dans les nappes d`Antalya: la nappe inférieure et ses séries Mésozoiques radiolaritique (Taurides occidentales, Turquie). C.R. Acad. Sci., Paris, 271, 285-287.

Moores, E.M., and Vine, F.J., 1971; The Troodos massif, Cyprus and other ophiolites as oceanic crust: evaluation and implications. Phil. Trans. r. Soc. London, 268, 443-446.

Moores, E.M., Robinson, P.T., Malpas, J., and Xenophontos, C., 1984; Model for the origin of the Troodos massif, Cyprus and other mideast ophiolites. Geology, 12, 500-503.

Murton, B.J., and Gass, I.G., 1986; Western Limasol Forest complex, Cyprus: part of an Upper Cretaceous leaky transform fault. Geology, V.14, Kluwer academic publ., The Netherlands, 367p.

Okay, A.I., 1980; The petrology of blueschists in north-west Turkey, north-east of Tavsanli. Unpublished Ph.D. thesis, University of Cambridge, England.

Okay, A.I., 1984; Distribution and characteristics of the north-west Turkish blueschists. In: Dixon, J.F. and Robertson, A.H.F. (eds.), The Geological Evolution of the Eastern Mediterranean. Geol. Soc. Spec. Publ. London, 17, 455-466.

Parrot, J.F., 1980; The Baer-Bassit (NW Syria) ophiolitic area. In: G.Rocci (ed.), Tethyan ophiolites. Ofioliti, 2, 279-295.

Pearce, J.A., Lippard, S.J., and Roberts, S., 1984; Characteristics and tectonic significance of supra-subduction zone ophiolites. In: B.P. Kokelaar and M.F. Howels (eds.), Marginal basin geology. Geol. Soc. Spec. Publ. London, 16, 77-94.

Piskin, Ö., Delaloye, M., Selcuk, H., and Wagner, J.J., 1986; Guide to Hatay Geology (SE-Turkey). Ofioliti, 11, 87-104.

Piskin, Ö., Delaloye, M., Moritz,R., and Wagner, J.J., 1990; Geochemistry and Geothermometry of the Hatay complex,Turkey: Implications for the genesis of the ophiolite complex. In: Malpas, J., Moores, E.M., Panayiotou, A. and Xenophontos, C. (eds.), Ophiolites and Oceanic crustal analogues. Nicosia, Geol. Surv. Dept. Cyprus, 329-337.

Polat, A., and Casey, J.F., 1995; A structural record of the emplacement of the Pozanti-Karsanti ophiolite onto the Menderes-Taurus block in the late Cretaceous, eastern Taurides, Turkey. J. Struct. Geol., 17, 12, 1673-1688.

Ricou, L.E., 1971; Le croissant ophiolitique péri-arabe, une ceinture de nappes mises en place au Crétacé supériur. Rev. Géogr. phys. Géol. Dyn., 13, 327-349.

Ricou, L.E., Marcoux, J., and Whitechurch, H., 1984; The Mesozoic organization of the Taurides: one or several ocean basins? In: Dixon, J.E. and Robertson, A.H.F. (eds.), The geological evolution of the eastern Mediterranean. Geol. Soc. Spec. Publ. London, 17, 349-359.

Robertson, A.H.F., and Dixon, J.E., 1984; Introduction: aspects of the geological evolution of the eastern Mediterranean. In: Dixon, J.E., and Robertson, A.H.F., (eds.), The geological evolution of the eastern Mediterranean, Geol. Soc. London Spec. Publ., 17, 1-74.

Selcuk, H., 1981; Etude géologique de la partie meridionale du Hatay (Turquie). Thése no.1977, Dépt. de Minéralogie, Université de Genève, 116 p.

Sengor, A.M.C., and Yilmaz, Y., 1981; Tethyan evolution of Turkey: a plate tectonic approach. Tectonophysics, 75, 181-241.

Thuizat R., Whitechurch, H., Montigny, R., and Juteau, T., 1981; K-Ar dating of some infra-ophiolitic metamorphic soles from the eastern Mediterranean: New evidence for oceanic thrusting before obduction. Earth and Planet. Sci. Lett., 52, 302-310.

Varga, R.J., and Moores, E.M., 1985; Spreading structure of the Troodos ophiolite, Cyprus. Geology, V.13, 846-850.

Whitechurch, H., Juteau, T., and Montigny, R., 1984; Role of the eastern mediterranean ophiolites (Turkey, Syria, Cyprus) in the history of the Neo-tethys. In: Dixon, J.E. and Robertson, A.H.F. (eds.), The geological evolution of the eastern Mediterranean. Geol. Soc. Spec. Publ. London, 17, 301-317.

Yilmaz, P.O., 1984; Fossil and K-Ar data for the age of the Antalya complex, SW Turkey. In: Dixon, J.E. and Robertson, A.H.F. (eds.), The geological evolution of the eastern Mediterranean. Geol. Soc. Spec. Publ. London, 17, 335-347.

CHAPTER 3

MERSIN OPHIOLITE OCEANIC CRUSTAL SECTION

Abstract

Mersin ophiolite, which is bounded by the Ecemis fault to the east, the Bolkardag metamorphics to the north, and capped by Miocene carbonates to the west and south, represents a remnant of Mesozoic Neo-Tethyan oceanic crust in Southern Turkey.

Volcanic rocks present two discrete geochemical and structural features. The first one is represented by basaltic pillow lavas intercalated with radiolarites and pelagic limestones (Late Jurassic-Early Cretaceous), whereas the second one is represented by basaltic pillow lavas and diabase (Late Cretaceous ?). Basaltic rocks associated with deep marine sediments show an alkaline affinity. Major and trace element compositions suggest that these volcanic rocks formed in a within plate basalt setting. REE chemistry of these volcanic rocks, which shows LREE enrichment, also confirms the formation in an ocean island /sea mount (WPB) environment. In addition, clinopyroxene compositions of these alkaline basalts show also a within plate alkaline affinity. Basalts and diabases of the second group, which exhibit similar geochemical features, differ from the above mentioned group by their tholeiitic affinity. Composition of clinopyroxenes also confirms this tholeiitic character. Major and trace element chemistry suggests that these rocks have the chemical features of a supra-subduction zone setting. Flat-lying REE patterns of basalts and diabases are also an indicative of an arc-related environment.

Cumulate rocks, occupying an area of approximately 15 km^2, crop out within the N-S oriented Sorgun valley (Mersin) in the western part of the ophiolitic massif. Cumulates have over 3 km thickness. They start with 800 m of ultramafic rocks at the bottom and continue into 2500 m of gabbroic rocks. They show tectonic contacts with mantle harzburgites at their base and with basaltic rocks at the top. Polycyclic cumulate feature is observed in the mafic and ultramafic cumulate rocks. Ultramafic cumulates, showing adcumulate-heteradcumulate texture, consist mainly of dunite, wehrlite and pyroxenite. Igneous lamination, size grading and rhythmic layering are observed as accumulation features in the ultramafic cumulates. Mafic cumulates, mainly of gabbro, leucogabbro, olivine gabbro and anorthosite, constitute more than 2/3 of the whole cumulate section. Mafic cumulate rocks are fresh and present adcumulate, mesocumulate and orthocumulate texture. Size grading and rhythmic layering are also seen in mafic cumulates. Crystallization order is olivine (Fo_{91-80})±chromian spinel (Cr# 60-80), clinopyroxene (Mg# 95-77), plagioclase ($An_{95.6-91.6}$) and orthopyroxene (Mg# 68-77). Mineral

chemistry of ultramafic and mafic cumulates suggest that highly magnesian olivines, clinopyroxenes and absence of plagioclase in the basal ultramafic cumulates are in good agreement with products of high-pressure crystal fractionation of primary basaltic melts beneath an island arc environment.

The ophiolite body is cross-cut at all structural levels by numerous mafic dyke intrusions. The dykes do not intrude the underlying melange or platform carbonates. Therefore dike emplacement postdate the formation of the ophiolite and metamorphic sole but predate the final obduction onto the Tauride platform. The post-metamorphic dyke swarms suggest geochemical character of Island Arc Tholeiites (IAT).

Overall geochemical as well as structural features suggest a supra-subduction zone tectonic setting for the Mersin ophiolite in the southern branch of Neotethys in southernTurkey.

3.1. Introduction

Ophiolites were defined in Penrose Conference (Geotimes, 1972) and have been interpreted as oceanic lithosphere fragment obducted onto continental margins during orogenic processes (Gass, 1967; Coleman, 1971; Dewey and Bird, 1971).

The Eastern Mediterranean ophiolites are situated within two discontinuous belts, namely the "Peri-Arabic belt" of Ricou (1971) and the "median Tauric ophiolite belt" in southern Turkey. In Southern Turkey , the Peri-Arabic belt (Kizildag in Turkey, Baer-Bassit in Syria and Trodoos in Cyprus) presents complete and undeformed ophiolite pseudostratigraphies whereas the median Tauric belt ophiolites (Lycian, Antalya, Beysehir, Alihoca, Pozanti-Karsanti and Mersin), characterized by dismembered oceanic lithosphere lithologies, are commonly associated with widespread melange and sub-ophiolitic metamorphic rocks in the north and south of the Taurus calcareous axis (Juteau, 1980; Dilek and Moores, 1990) (Fig. 3.1a).

Alkaline volcanic rocks can be observed tectonically either below or above the ophiolitic massifs all over the Tauride belt (Whitechurch et al., 1984). These volcanic rocks are Late Triassic in age and interpreted as the product of initial rifting stage in Tauride belt (Juteau, 1970; Juteau et al., 1973; Lapierre and Rocci, 1976; Marcoux, 1976; Robertson and Woodcock, 1981). The absence of tholeiitic lavas in the Tauride belt has been interpreted as the effect of extensive submarine erosion event (Whitechurch et al., 1984). Recent studies show that besides alkaline volcanic rocks, tholeiitic volcanic sequences have been also observed in the Antalya complex (Robertson and Waldron, 1990) and the Pozanti-Karsanti ophiolite (Çatakli, 1983). In this study tholeiitic basalts, interpreted as products of ocean floor spreading, exist in the Mersin ophiolite situated on the southern flank of the Bolkardag in southern Turkey.

Ultramafic and mafic cumulates within ophiolite complexes and those recovered from Mid-Oceanic Ridge centers are the result of differentiation in magma chambers. Improvement of petrogenetic studies of layered magmatic rocks have been started mainly from the pioneering studies of Hess (1960), Jackson (1961) and Wager and Brown (1968). In the last two decade studies carried on magmatic cumulates of the well-preserved eastern Mediterranean ophiolites such as Oman (Browning, 1984; Pallister and Hopson, 1980, 1981), Troodos (Thy, 1987a-b,1990; Hébert and Laurent, 1990), Hatay (Piskin et al., 1990) and Antalya (Juteau and Whitechurch, 1980) in Turkey or other well-known ophiolites such as Bay of Island (Church and Riccio, 1977; Elthon et al., 1982; 1984), have highlighted very much on magma fractionation and magma chamber evolution in different geotectonic settings. The data so far available on the magmatic cumulates of the eastern Mediterranean ophiolites indicate that evidence of high pressure fractionation exists beneath an island arc tectonic setting (Pearce et al., 1984; Hebert and Laurent, 1990; Parlak et al., 1995a). Cumulate sequence of the Mersin ophiolite is one of the well-preserved magmatic suite in Turkey which show gravity controlled structures such as magmatic lamination, size grading, graded layering and rhytmic cyclicity. They resemble to those found in Antalya and Hatay ophiolites in the southern Turkey. The mineral chemistry of plutonic suite as well as the geochemistry of volcanic rocks in the Mersin ophiolite show close similarity to other ophiolitic massifs of the surrounding region (Fig. 3.1a).

Numerous isolated tholeiitic microgabbroic-diabasic dykes, presenting uniform mineralogical and chemical compositions, intersect metamorphic soles and oceanic lithospheric units all over the Tauride belt in southern Turkey (Juteau, 1980; Whitechurch et al., 1984).

The aim of the present paper is to discuss the geochemistry of the volcanic rocks, ultramafic-mafic cumulates and isolated dike swarms, and consider their tectonic significance in the evolution of the NeoTethyan ocean in Eastern Mediterranean.

3.2. Geological setting

Mersin ophiolite, which is bounded by the Ecemis fault to the east, the Bolkardag metamorphics to the north, and capped by Miocene carbonates to the west and the south, represents a remnant of the Mesozoic Neo-Tethyan oceanic lithosphere in southern Turkey. Except for a sheeted dyke complex, it comprises the following ophiolitic pseudostratigraphy: mantle tectonites, ultramafic-mafic cumulates, basaltic pillow lavas and associated deep marine sediments (Fig. 3.1b-c).

Basaltic rocks are situated at three localities in the study area (Fig. 3.1b). Two of these outcrops are seen in the Sorgun valley and the third one is located at Findikpinari village. Field observations and geochemical studies show that these volcanic rocks differ from each other. Volcanic rocks in the Sorgun valley are seen as two nappe-packages between harzburgitic tectonite and cumulate (Fig. 3.1b). These rocks have been extensively deformed during the obduction onto the continental margin. The volcanic rocks are basaltic lava flows and pillow lavas intercalated with pelagic cherty limestones and radiolarites

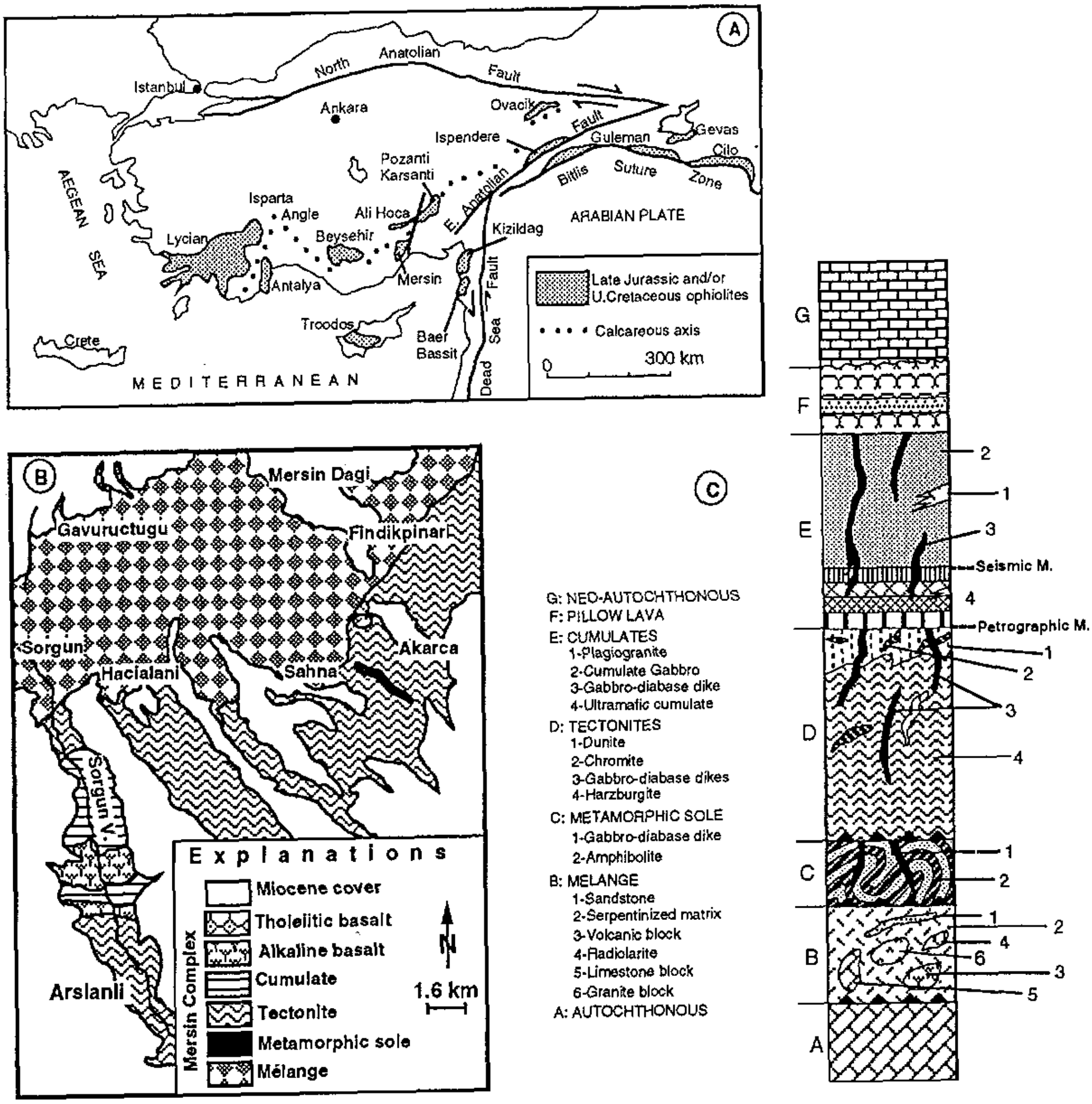

Figure 3.1. a. Ophiolitic massifs in southern Turkey (taken from Dilek and Moores, 1990). **b.** Simplified geological map of the Mersin ophiolite. **c.** Detailed stratigraphic column of the rock units in the Mersin ophiolite.

(Plate 3.1c-d). The radiolarites (*Archaeodictyomitra apiara* and *Ristola cf. boessi* determined by Holdsworth, B.K. at Keele University-England) yielded Late Jurassic-Early Cretaceous age range. However, basaltic rocks near Findikpinari are represented by pillow lavas and underlying diabases that are thought to be Late Cretaceous in age (Plate 3.1a-b). These diabases, oriented approximately N70E, are interpreted as feeder dykes of the basaltic volcanism during the formation of the oceanic crust. Because of the limited outcrop size, it is not possible to interprete these diabase tubes, which do not show any cross-cutting relationships, as the remnant sheeted dyke complex do. The outcrop of these rocks is very small, covered by a harzburgitic envelope which protected the basaltic rocks from alteration effects. They present well preserved pillow structures and the maximum diameter of a pillow is about 50 cm. In the field, some secondary mineralizations (pyrite, calcite, quartz, etc.) filling the vesicles of the pillow basalts can be seen. There is no dike intrusion within both type of volcanic units.

Well preserved ultramafic and mafic cumulates rocks are only seen within the roughly N-S oriented Sorgun valley in the western part of the massif (Fig. 3.1b). The measured detailed stratigraphic section of the cumulates, which was over 3000 m thickness, starts at the bottom with ultrabasic cumulates (800 m) and gradually passes up into gabbroic rocks (2500 m). Basal ultramafic cumulates mainly characterized by adcumulate texture start with dunites in which stratiform chromites are observed in diffrent levels. Dunites are gradually followed by well layered wehrlites which in turn are gradually overlain by clinopyroxenites.The mafic cumulates with mesocumulate and orthocumulate texture start at the bottom with olivine gabbro and continue into gabbro, leucogabbro and anorthosite. In the upper part of the gabbroic cumulates, poorly developed late stage magma chamber differentiation products cut also country rock as plagiogranitic inclusion. Igneous lamination, mono-mineralic size grading, and rhythmic layering have been observed as gravity controlled accumulation structures in the ultramafic and mafic cumulates (Parlak et al., 1995a).

Numerous micro-gabbroic-diabasic dikes intrude the mantle tectonites, cumulates and metamorphic sole (Plate 3.5 a-b-c-d). They show variable attitude of the layering such as E-W/60S, N65E/50NW, N70W/33NE.

3.3. Basaltic units

3.3.1. Petrographic summary

Two different types of volcanic activity, based on both their field relations and their geochemical signatures, have been observed in the Mersin ophiolite. Tholeiitic basaltic volcanism, which is cogenetic with the formation of oceanic crust in Neo-Tethys, was first recognized in the Mersin ophiolite. Tholeiitic basalts showing intersertal texture are characterized by constant mineralogical assemblages such as euhedral-subhedral clinopyroxene (25-30 %) with a grain size of 0.7-2.6 mm, laths of albitized plagioclase (40-45 %) with a grain size of 0.8-7.6 mm and Fe-Ti oxides (5 %) in an altered glassy-matrix (30-35 %). Diabase beneath the basalts exhibiting doleritic texture has the same mineral composition (augite-plagioclase).

The alkaline basalts differ from tholeiitic types by their high-Ti euhedral clinopyroxenes (15-20 %) with a grain size of 0.5-1.8 mm. These basaltic rocks, with porphyritic texture, are intercalated with radiolarian cherts and pelagic limestones. Fe-Ti oxides are also present. All the volcanic rocks and diabases have undergone low grade metamorphism (possibly on the sea floor) which have altered the primary mineral assemblage to phases stable at zeolite and lower greenschist facies conditions. Secondary phases include albite, chlorite, epidote, silica and calcite.

3.3.2. Analytical method

Major and trace element analyses have been carried out on 26 tholeiitic basalts and diabases, and 6 alkaline basalts. 7 tholeiitic basalts and diabases and 2 alkaline volcanics have been analysed for REE concentrations. Major and trace element analyses have been carried out by XRF on glass beads fused from ignited powders to which $Li_2B_4O_7$ was added (1:5), in a gold-platinum crucible at 1150^{o} C. REE analysis was done by ICP-AES technique (Voldet 1993). Microprobe analysis of pyroxene was carried out using a Camebax SX-50 instrument in the Mineralogy Department at Lausanne University. The analytical conditions for the elements (K, Mg, Ca, Na, Mn, Cr, Al, Si, Fe, Ti) were 30 seconds of counting interval, beam current 20 mA, and acceleration voltage 15 kV.

Sr and Rb concentrations were determined using a Philips 1410 XRF spectrometer at Geneva University. Sm and Nd concentrations were measured by ICP-AES with an analytical error ±5-10% at Geneva University. Sr and Nd were isolated from the same sample dissolution by using $HF+HNO_3$ method of Hart and Brooks (1974). 500 mg powder of each sample was loaded into a 15 ml Teflon bomb capsule. Four ml of concentrated HF and 0.5 ml of concentrated HNO_3 were added, and the bomb was sealed in an aluminum jacket at 200^{o}C for 5 hours. Then the HF and HNO_3 were evaporated to dryness. Dissolution was further assured and HF eliminated by evaporating twice with 1 ml 6M HCl at 130^{o}C. The samples were then dissolved in 1 ml of 2.5M HCl, centrifuged, and the solution loaded on column for separation of Sr and Nd. Sr and Nd isotopic ratios were determined at the University of Geneva on a 7-collectors Finnigan MAT 262 thermal ionization mass spectrometer with extended geometry and stigmatic focussing. The data are recalculated with reference to the following standards: Eimer and Amend

$^{87}Sr/^{86}Sr$=0.7080 and La Jolla standard $^{143}Nd/^{144}Nd$=0.511835. Sr and Nd isotopic ratios were corrected for mass fractionation assuming $^{86}Sr/^{88}Sr$=0.1194 and $^{146}Nd/^{144}Nd$=0.721903 respectively. The mean value of standard for Eimer and Amend $^{87}Sr/^{86}Sr$=0.708001±06 (2σ) and for La Jolla $^{143}Nd/^{144}Nd$= 0.511797±04 (2σ) during the period of data acquisition.

3.3.3. Whole rock chemistry

Representative major, trace and REE chemical analyses of alkaline and tholeiitic basalts and diabases are documented in Table 3.1. Effects of alteration can be clearly observed in the loss on ignition values of alkaline basalts (LOI≈ 3.23-6.53 %), tholeiitic basalts and diabases (LOI≈ 3.11-5.67 %). Selected incompatible trace elements, in particular Zr, Nb, Y, and REE have been shown to be the least mobile during alteration processes (Thompson, 1973; Pearce and Cann, 1973; Humpris and Thompson, 1978; Hart, 1970). These incompatible elements are good indicators to characterize petrological affinities and the past tectonic environment of volcanic rocks (Pearce and Cann, 1973; Floyd and Winchester, 1975; Pearce and Norry, 1979).

Volcanic rocks in the Mersin ophiolite can be classified as two distinct groups namely alkaline and sub-alkaline/tholeiitic basalts (Fig. 3.2) based on their trace element concentrations (Winchester and Floyd, 1977).

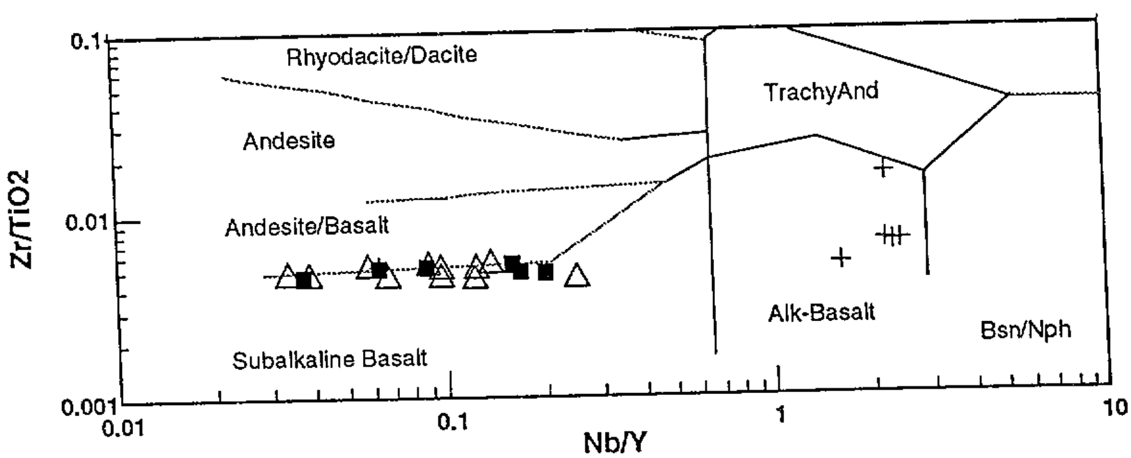

Figure 3.2. Discrimination of different rock types in the Mersin ophiolite based on immobile trace elements (after Winchester and Floyd, 1977). Triangle and filled-square representing Late Cretaceous basalt and diabase respectively, cross showing Late Jurassic-Early Cretaceous basalt.

Table 3.1. Major, trace and REE analyses of volcanic rocks in the Mersin ophiolite, S. Turkey

Sample	Alkaline Basalts						Tholeiitic Basalts													
No	277	283	285	289	290	291	134	135	137	138	143	211	212	213	214	215	375	376	377	378
SiO2	49.66	42.67	47.22	44.70	44.92	44.65	47.76	49.62	47.59	51.32	46.36	48.06	50.04	56.97	49.81	49.31	46.75	46.17	48.13	48.66
Al2O3	14.23	13.97	14.65	14.49	14.66	14.43	13.64	14.56	14.50	13.92	14.57	14.66	14.36	12.93	13.87	14.02	13.94	14.10	15.31	15.10
TiO2	1.43	3.54	1.83	3.25	3.23	3.21	1.52	1.56	1.54	1.56	1.65	1.64	1.60	1.46	1.58	1.61	1.59	1.60	1.73	1.71
FeO	12.00	14.13	12.00	12.46	12.92	12.03	14.62	14.27	14.83	12.79	15.04	14.16	14.55	11.53	14.00	14.13	14.81	13.97	14.48	14.27
CaO	8.27	8.95	6.81	8.59	8.01	9.08	6.87	6.10	8.73	4.85	7.90	5.58	5.08	3.91	6.37	7.03	6.22	6.57	4.05	4.34
MgO	6.39	8.50	2.75	6.05	5.95	5.27	5.57	5.39	4.62	4.43	5.87	6.09	5.88	4.49	5.15	4.97	6.01	6.16	5.87	6.26
Na2O	4.13	3.07	5.71	3.75	4.15	4.09	4.07	3.67	2.66	4.88	3.84	4.13	4.02	4.18	3.12	2.94	4.35	4.73	5.39	5.19
K2O	0.44	0.48	0.68	1.30	1.17	1.37	0.79	0.92	1.40	1.95	0.10	0.90	0.75	1.94	1.66	1.69	0.77	0.12	0.17	0.07
MnO	0.28	0.29	0.33	0.19	0.19	0.19	0.18	0.15	0.15	0.20	0.21	0.19	0.17	0.20	0.16	0.15	0.20	0.21	0.17	0.17
P2O5	0.11	0.50	0.74	0.64	0.63	0.62	0.16	0.17	0.13	0.15	0.14	0.13	0.15	0.14	0.15	0.15	0.14	0.15	0.15	0.15
LOI	3.25	3.23	6.53	3.67	3.26	3.99	4.47	3.68	4.07	3.75	4.34	4.59	3.91	3.15	4.31	4.12	4.90	5.67	3.89	4.11
Total	100.18	99.34	99.25	99.07	99.09	98.95	99.65	100.12	100.23	99.81	100.02	100.13	100.51	100.90	100.18	100.12	99.69	99.45	99.34	100.03
Ba	120	326	208	553	521	523	139	0	0	0	126	95	118	96	98	109	77	102	110	80
Ni	70	93	7	59	49	40	0	15	8	8	0	10	5	0	3	2	7	7	4	6
V	379	333	0	250	248	249	458	480	477	446	461	509	537	419	485	495	477	502	557	534
Cr	153	220	22	142	104	65	14	28	20	22	14	31	20	23	19	23	24	25	29	20
Nb	2	45	101	66	66	67	2	3	1	3	4	1	0	4	0	0	5	3	2	4
Zr	73	185	293	223	225	225	69	70	71	77	73	76	74	65	73	69	80	78	89	90
Y	32	28	46	29	30	28	30	31	26	31	33	30	32	16	30	33	29	34	34	29
Sr	136	462	428	626	612	590	178	188	192	235	112	226	205	185	183	201	224	273	363	307
Rb	17	8	16	14	17	22	23	25	40	54	3	27	19	46	40	37	21	4	5	5
La				37.2		35.5			6.2						5.6	5.4				
Ce				78.3		75.8			13.1						12.5	12.1				
Pr				10.2		9.3			n.d						n.d	n.d				
Nd				37.8		37			10.1						9.8	9.6				
Sm				7.5		7.9			3.1						3.2	3.1				
Eu				2.37		2.32			1.16						1.15	1.1				
Gd				6.9		6.4			4						4	4				
Tb				n.d		n.d			n.d						n.d	n.d				
Dy				4.7		4.7			4.9						5.1	4.9				
Ho				0.83		0.8			1						1.04	1.02				
Er				2.1		2			2.8						2.9	2.9				
Tm				0.28		0.29			0.39						0.4	0.42				
Yb				1.8		1.8			2.4						2.5	2.5				
Lu				0.23		0.22			0.35						0.35	0.4				

n.d: not determined, Total Fe is expressed as FeO

Table 3.1. (continued)

Sample	Tholeiitic Basalts			Tholeiitic Diabases								
No	379	380	381	136	139	140	142	144	366	367	368	369
SiO2	45.63	47.44	47.03	46.63	48.62	49.98	48.56	47.71	50.92	50.58	49.36	50.42
Al2O3	13.62	15.40	14.64	14.80	14.08	14.75	13.74	13.84	14.47	14.12	14.60	14.25
TiO2	1.55	1.69	1.67	1.65	1.34	1.59	1.23	1.32	1.59	1.51	1.64	1.59
FeO	14.52	14.90	14.56	15.95	13.01	13.49	12.16	12.80	13.58	11.69	14.10	14.12
CaO	6.90	4.60	5.73	6.02	9.09	6.65	10.42	10.01	6.20	9.51	6.24	5.97
MgO	6.15	6.47	6.08	5.99	5.95	5.61	5.97	6.18	5.08	3.60	5.33	4.49
Na2O	4.38	4.66	4.59	4.15	4.28	4.73	3.67	3.21	5.18	4.23	5.07	4.89
K2O	0.94	0.10	0.18	0.07	0.11	0.07	0.07	0.04	0.10	0.03	0.06	0.04
MnO	0.20	0.19	0.20	0.23	0.17	0.16	0.17	0.17	0.17	0.16	0.19	0.15
P2O5	0.15	0.15	0.15	0.15	0.10	0.14	0.10	0.11	0.14	0.13	0.14	0.14
LOI	5.09	4.44	5.00	3.91	3.11	3.15	4.59	3.94	3.03	4.29	3.45	3.38
Total	99.13	100.04	99.83	99.55	99.86	100.32	101.08	99.33	100.45	99.85	100.18	99.44
Ba	81	104	98	0	117	82	54	0	83	97	98	71
Ni	11	6	7	7	13	29	28	32	8	5	5	2
V	493	566	515	502	404	541	378	396	531	457	520	503
Cr	29	32	26	24	79	65	95	97	36	21	24	21
Nb	4	4	2	0	0	5	1	0	5	5	3	2
Zr	77	83	81	79	56	76	57	59	80	79	84	80
Y	32	32	28	31	19	25	27	28	30	31	34	32
Sr	212	308	312	120	140	128	146	86	154	78	98	60
Rb	26	7	4	5	2	4	3	3	3	4	1	2
La					4.3	5	3.8	4.1				
Ce					8.3	11.8	8.5	8.5				
Pr					n.d	n.d	n.d	n.d				
Nd					6.6	9.3	7	7.6				
Sm					1.8	2.7	1.7	2.1				
Eu					0.91	1.16	0.85	0.92				
Gd					3	4.1	2.9	3.1				
Tb					n.d	n.d	n.d	n.d				
Dy					3.5	4.8	3.5	3.8				
Ho					0.71	0.98	0.69	0.76				
Er					1.8	2.6	2.1	2				
Tm					n.d	n.d	n.d	n.d				
Yb					1.7	2.5	1.7	1.9				
Lu					0.24	0.42	0.26	0.28				

Alkaline basalts are represented by low SiO_2 (42-49 %), high TiO_2 (1.4-3.5 %), CaO (7-9 %), P_2O_5 (0.5-0.7 %). They are also characterized by high concentrations of incompatible trace elements (Zr: 73-225 ppm, Nb:45-101 ppm, Y: 28-46 ppm), LIL elements (Ba: 120-550 ppm, Sr: 136-626 ppm) and transition elements (Cr: 22-150 ppm, Ni: 40-90 ppm, V: 250-380 ppm). Incompatible trace element ratios for the alkaline basalts are Zr/Nb: 3-4, Zr/Y: 6.5-8, Y/Nb: 0.4-0.6.

The tholeiitic basalts and diabases, formed as a co-genetic extrusive sequence of the Mersin ophiolite, are characterized by high SiO_2 (45-51 %), low TiO_2 (1.2-1.7 %), P_2O_5 (0.1-0.15 %), CaO (4-10 %) compared to the alkaline basalts. These tholeiitic rocks are also represented by depleted incompatible trace elements (Zr: 65-90 ppm, Y: 16-34 ppm, Nb: 1-5 ppm), enriched LIL elements (Ba: 54-139 ppm, Sr: 60-363 ppm) and their transition element concentrations (low Cr: 21-97 ppm, Ni: 2-32 ppm, high V: 378-566 ppm). Incompatible element ratios for the tholeiitic basalts and diabases are Zr/Nb: 15.2-44.5, Zr/Y: 2.1-4.1, Y/Nb: 4-30. The one important feature of the tholeiitic basalts is that they do not show any increment in TiO_2 values with increasing FeO*/MgO ratio which is the characteristic feature of volcanic rocks in Island Arc volcanic suites (Miyashiro, 1973) (Fig. 3.3).

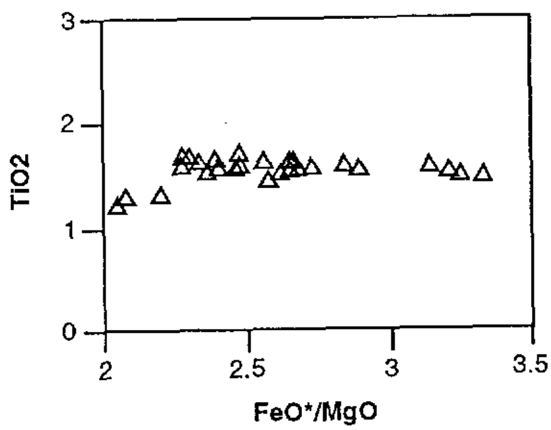

Figure 3.3. TiO_2 versus FeO*/MgO weight ratio for tholeiitic basalts and diabases in the Mersin ophiolite.

Distinct compositional variations can easily be detected from trace element concentrations of these two groups. Using co-variation of Zr-Y and Zr-Nb, alkaline basaltic rocks show enrichment in Nb, Y and Zr compared to tholeiitic basaltic rocks (Fig. 3.4a-b). Enrichment of HFS (Zr, Y, Nb) and LIL (Ba, Sr) elements in alkali basalts suggests that they were derived from the deeper mantle under the influence of metasomatic fluids (Saunders and Tarney, 1984) or probably a plume source. The HFS (Zr, Nb, Y) element depletion in the tholeiitic basalts that formed in an island arc setting is attributed to effects of subducted oceanic crust. It is believed that the mantle wedge above subduction zone is not subject to re-enrichment of HFS elements by metasomatism from the deeper mantle (Saunders and Tarney, 1984). There is also considerable variation in the trace element ratios (Zr/Y-Zr/Nb; Y/Nb-Zr/Nb) within the groups (Fig. 3.4c-d). Tholeiitic basalts and diabases show the same chemical tendency whereas alkaline basalts lie in a separate field. In Figure 4d, alkaline and tholeiitic rocks show the same trend indicating a source mixing but the ages (Late Jurassic-Early Cretaceous and Late Cretaceous) of the two suites are different. These distinct variations suggest derivation from mantle sources of different compositions (White et al., 1979; Humphris and Thompson, 1983).

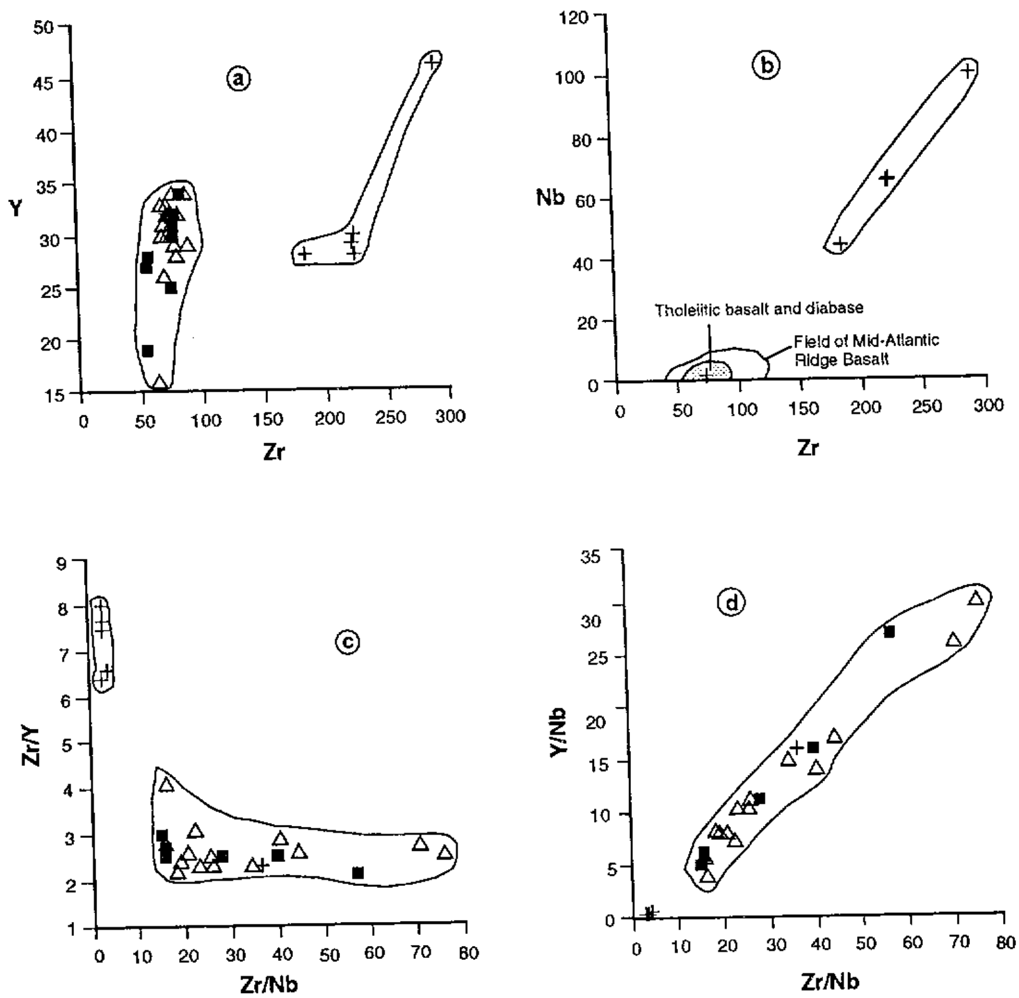

Figure 3.4. a-b) Covariation of incompatible trace elements in basalts from the Mersin ophiolite. Note that Zr, Y and Nb depletion in tholeiitic suite are due to subducted slab component within suprasubduction zone, whereas enrichment of these elements in alkali basalts is attributed to source derived from deeper mantle. **c-d)** Relation between incompatible trace element ratios in basalts

Chondrite-normalized REE abundances of the tholeiitic basalts-diabases and alkali basalts are shown in Figure 3.5. Alkali basalts demonstrate LREE enrichment ($[La/Yb]_N$ ratios between 14.1-14.8) which resemble alkali basalts of the Azores (White et al., 1979; Schilling, 1975), some islands of the Red Sea (Gass and Smewing, 1973), alkali basalts in the Ankara melange (Floyd, 1993), Late Triassic alkaline rocks in Antalya (Robertson and Waldron, 1990), and in Pozanti-Karsanti (Çatakli, 1983). These alkali basalts and the associated sediments have been interpreted as a possible protolith of the sub-ophiolitic metamorphic rocks beneath the Mersin ophiolite (Parlak et al., 1995b). Tholeiitic basalts and diabases present flat-chondrite normalized REE patterns (Fig. 3.5). It shows small REE fractionation ($[La/Yb]_N$ ratios between 1.4-1.9) which is not in agreement with typical depleted LREE patterns of N-MORB ($[La/Yb]_N$ ratios of about 0.6; Sun et al., 1979). These flat-lying REE patterns are typically observed in island arc tholeiitic series such as in Papua-New Guinea, Solomon Island, Macquarie Island (Jakes and Gill, 1970). In the lava units of the Mersin ophiolite, there is no negative Eu anomalies which may suggest that during early fractionation olivine was the dominant mineral phase relative to plagioclase in island arc and low concentration of Ni (0-15 ppm), Cr (20-30 ppm) does support this interpretation (Jakes and Gill, 1970). Arc-related nature of all the ophiolitic massifs in the eastern Mediterranean region, including Oman ophiolite (Alabaster et al., 1982; Searle et al., 1980), Troodos ophiolite (Desmons et al., 1980), Baer Bassit in Syria (Parrot, 1977), Hatay ophiolite (Delaloye and Wagner, 1984), Sarikaman ophiolite (Yaliniz et al., 1994) in Turkey, and Bay of Island ophiolite (Elthon, 1991), demonstrate the same geochemical features like Mersin ophiolite.

MORB-normalized trace element patterns of selected tholeiitic basalts-diabases and alkali basalts are presented in Figure 3.6. The alkali basalts are represented by humped patterns which can be compared to ocean island basalts like in Azores (White, 1985; Weaver, 1991) and ocean island/ seamount basalt sequences in the Ankara melange in Turkey (Floyd, 1993) whereas the tholeiitic basalts and diabases are characterized by distinct patterns. They show LIL element (Sr, K, Rb, Ba) enrichment relative to HFS elements (Nb, Ce, Zr, Sm, Ti, Y, Yb) (Fig. 3.6). This features might be due to secondary alteration or, as Pearce et al (1984), Saunders and Tarney (1984) explained, modification of mantle source region for island arc basalts because of subduction derived aqueous and siliceous fluids which caused additional enrichment in LIL elements. The patterns of the tholeiitic basalts and diabases show the characteristic features of the Supra-Subduction Zone (SSZ) ophiolites (Pearce et al., 1984). Degree of partial melting in the mantle source is approximately 35-40% (Pearce, 1980) (Fig. 3.7a). This evidence shows that high degree of partial melting requires water input from subducted oceanic crust in the arc-related lavas of the Mersin ophiolite. Spreading half-rate of the oceanic crust is estimated as 3 cm/y based on the Zr/Y-Zr diagram of Pearce (1980) (Fig. 3.7b).

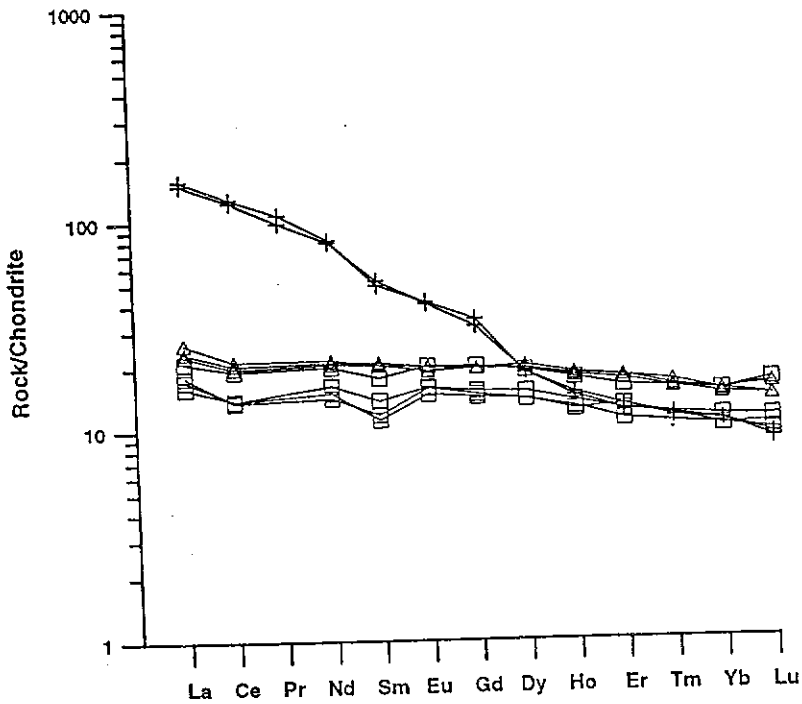

Figure 3.5. Chondrite normalized REE abundance in alkali (cross) basalts and tholeiitic basalts (triangle), diabases (square) (Normalizing values from Sun and McDonough, 1989).

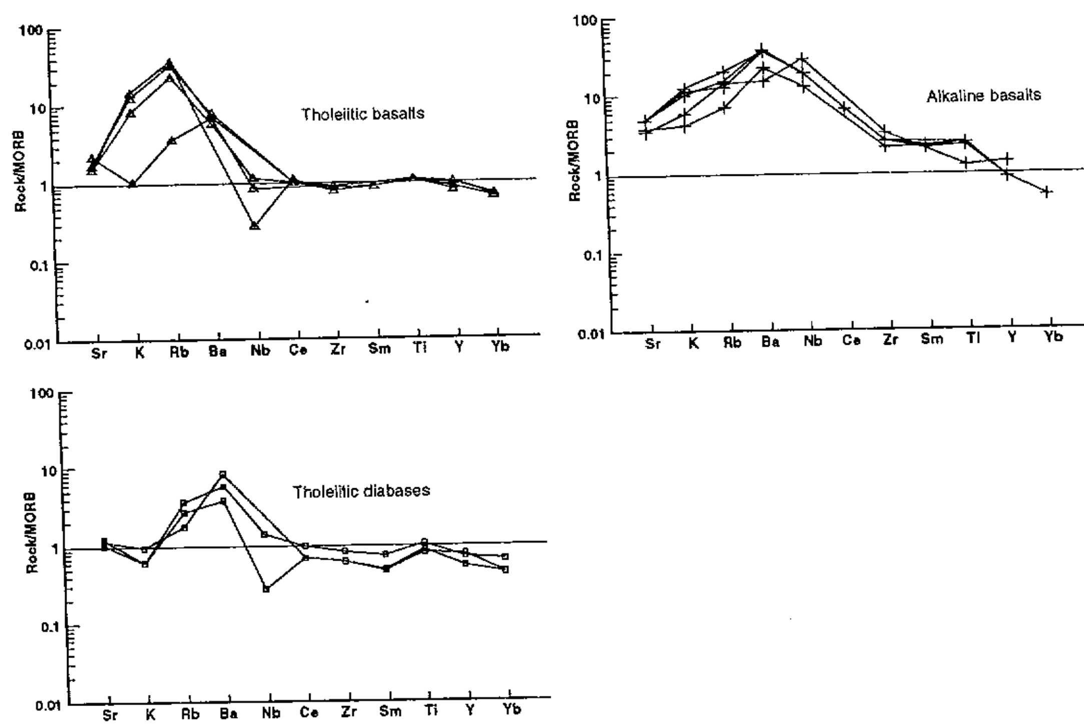

Figure 3.6. MORB normalized trace element patterns of the basaltic rocks in the Mersin ophiolite (normalizing values from Pearce, 1982).

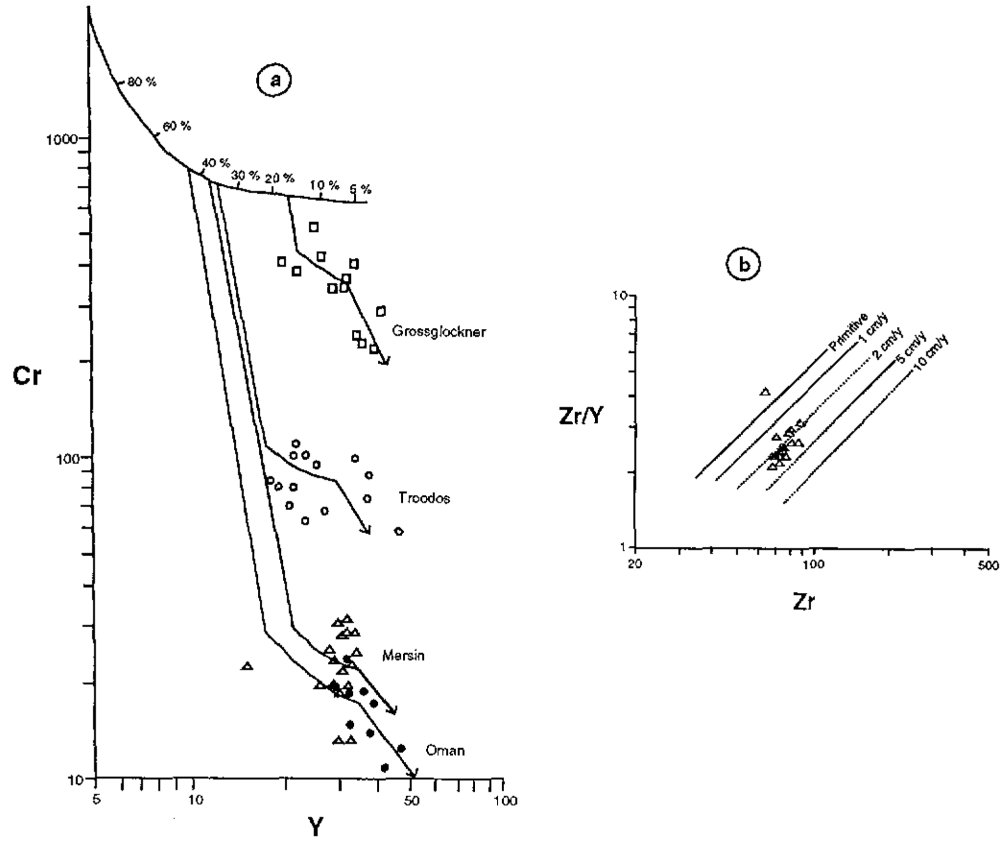

Figure 3.7. a. Cr-Y partial melting diagram of tholeiitic basalts (triangle) from the Mersin ophiolite (after Pearce, 1980). **b.** Zr/Y versus Zr diagram showing spreading half rate of the tholeiitic basalts (triangle) for the Mersin ophiolite (after Pearce, 1980).

3.3.4. Mineral chemistry

Representative microprobe analyses of clinopyroxenes are listed in Table 3.2. Clinopyroxenes from alkaline rocks are characterized by euhedral diopside crystals ($Ca_{53-49}Mg_{9-6}Fe_{38-42}$). They contain high TiO_2 (4.20-1.76 %) and Al_2O_3 (8.59-4.42 %). Mg number (Mg/Mg+Fe) ranges from 0.7 to 0.8. The clinopyroxenes in tholeiitic basalt and diabase are augites ($Ca_{37-40}Mg_{45-41}Fe_{18-16}$). They have low TiO_2 (0.52-0.88 %) and Al_2O_3 (2.24-3.86 %) compared to clinopyroxenes from alkaline basalts. Mg number (Mg/Mg+Fe) varies between 0.71 and 0.75.

Significant chemical differences exist between clinopyroxenes of different tectonic settings (Nisbet and Pearce, 1977).Differences are observed between the volcanic successions in the Mersin ophiolite from the composition of clinopyroxenes as well as from the whole rock chemistry. Ti versus Ca+Na diagram based on the atomic formula of clinopyroxene phenocrysts distinguishes the alkaline and tholeiitic characters of the basaltic rocks (Leterrier et al. 1982) (Fig. 3.8a). The triangular diagram of Nisbet and Pearce (1977), using TiO_2-MnO-Na_2O clinopyroxene composition also discriminates two

Table 3.2. Representative microprobe analyses of pyroxenes in alkaline-tholeiitic basalts and diabases from Mersin ophiolite, S. Turkey

Sample	Alkaline Basalts								Tholeiitic Basalts						Tholeiitic Diabases				
No	289-1	289-2	289-3	289-4	289-5	289-6	289-7	289-8	211-1	211-2	211-3	214-1	214-2	214-3	140-1	140-2	140-3	140-4	140-5
SiO2	43.60	49.11	48.59	47.27	48.55	46.28	49.14	46.80	51.01	50.05	49.74	49.82	50.30	50.36	51.46	51.46	49.50	50.79	51.09
Al2O3	8.59	4.56	5.14	6.26	5.27	7.02	4.42	6.36	2.24	3.34	3.53	3.86	3.59	3.21	2.37	2.25	3.93	2.55	2.38
TiO2	4.20	1.94	1.89	1.91	1.76	2.65	2.02	2.52	0.52	0.64	0.81	0.87	0.79	0.73	0.56	0.48	0.88	0.64	0.52
Fe2O3	4.09	2.31	2.27	3.18	2.57	2.86	2.46	3.22											
FeO	4.68	4.82	4.27	3.32	3.71	4.05	4.83	4.22	11.34	10.68	10.90	10.97	10.95	10.20	9.92	9.81	11.44	10.47	10.11
MnO	0.15	0.13	0.12	0.10	0.06	0.13	0.15	0.11	0.24	0.32	0.28	0.32	0.25	0.32	0.23	0.32	0.30	0.24	0.28
MgO	11.29	13.71	13.73	13.23	13.75	12.70	13.93	12.82	15.61	14.64	15.19	15.27	15.32	15.38	16.11	16.13	15.27	15.42	15.77
Cr2O3	0.00	0.00	0.52	0.64	0.88	0.37	0.01	0.18	0.03	0.00	0.13	0.12	0.14	0.08	0.12	0.08	0.16	0.03	0.01
CaO	22.08	22.68	22.63	22.62	22.93	22.67	22.43	22.64	18.20	20.01	19.28	18.44	18.43	19.34	19.42	18.94	18.12	19.87	19.21
Na2O	0.58	0.43	0.42	0.41	0.38	0.40	0.37	0.38	0.30	0.34	0.26	0.29	0.29	0.26	0.20	0.24	0.28	0.26	0.24
K2O	0.00	0.00	0.00	0.12	0.08	0.00	0.11	0.10	0.03	0.00	0.00	0.00	0.00	0.00	0.01	0.02	0.00	0.00	0.02
H2O									0.49	0.00	0.00	0.04	0.00	0.13	0.00	0.29	0.13	0.00	0.39
Total	99.25	99.69	99.58	99.04	99.92	99.12	99.86	99.36	100.01	100.02	100.12	100.00	100.06	100.01	100.40	100.02	100.01	100.27	100.02
Si	1.65	1.83	1.81	1.77	1.80	1.74	1.83	1.76	1.85	1.86	1.85	1.85	1.87	1.86	1.90	1.88	1.83	1.88	1.85
Al IV	0.35	0.17	0.19	0.23	0.20	0.26	0.17	0.24	0.09	0.14	0.15	0.15	0.13	0.13	0.10	0.09	0.17	0.11	0.11
Al VI	0.03	0.03	0.04	0.05	0.03	0.05	0.02	0.04	0.00	0.01	0.00	0.02	0.02	0.00	0.00	0.00	0.00	0.00	0.00
Ti	0.12	0.05	0.05	0.05	0.05	0.07	0.06	0.07	0.01	0.02	0.02	0.02	0.02	0.02	0.02	0.01	0.02	0.02	0.01
Fe+3	0.12	0.06	0.06	0.09	0.07	0.08	0.07	0.09	0.32	0.12	0.12	0.12	0.08	0.16	0.08	0.21	0.17	0.11	0.27
Fe+2	0.15	0.15	0.13	0.10	0.12	0.13	0.15	0.13	0.02	0.21	0.22	0.22	0.26	0.16	0.22	0.09	0.18	0.21	0.04
Mn	0.00	0.00	0.00	0.00	0.00	0.00	0.00	0.00	0.01	0.01	0.01	0.01	0.01	0.01	0.01	0.01	0.01	0.01	0.01
Mg	0.64	0.76	0.76	0.74	0.76	0.71	0.77	0.72	0.84	0.81	0.84	0.84	0.85	0.84	0.89	0.88	0.84	0.85	0.85
Cr	0.00	0.00	0.02	0.02	0.03	0.01	0.00	0.01	0.00	0.00	0.00	0.00	0.00	0.00	0.00	0.00	0.00	0.00	0.00
Ca	0.90	0.91	0.90	0.91	0.91	0.91	0.89	0.91	0.71	0.80	0.77	0.73	0.73	0.76	0.77	0.74	0.72	0.79	0.75
Na	0.04	0.03	0.03	0.03	0.03	0.03	0.03	0.03	0.02	0.02	0.02	0.02	0.02	0.02	0.01	0.02	0.02	0.02	0.02
K	0.00	0.00	0.00	0.01	0.00	0.00	0.01	0.00	0.00	0.00	0.00	0.00	0.00	0.00	0.00	0.00	0.00	0.00	0.00
OH									0.12	0.00	0.00	0.01	0.00	0.03	0.00	0.07	0.03	0.00	0.09
Ens	37.78	41.81	42.29	42.12	42.50	40.51	42.42	40.66	44.36	41.60	43.01	43.81	43.96	43.72	45.05	45.53	43.78	43.18	44.54
Fors	9.07	8.48	7.60	6.11	6.54	7.49	8.50	7.71	18.46	17.54	17.76	18.17	18.03	16.78	15.92	16.05	18.89	16.83	16.47
Wol	53.14	49.71	50.11	51.77	50.96	52.00	49.08	51.63	37.17	40.86	39.23	38.02	38.01	39.50	39.03	38.42	37.33	39.99	38.99

Numbers of ions on the basis of 6 (O)

different magma types in the Mersin ophiolite (Fig. 3.8b). The clinopyroxenes from tholeiitic basalts may show the effects of orogenic component within island arc environment (Leterrier et al., 1982). In Figure 3.8c, clinopyroxenes from the arc-related tholeiitic basalts in the Mersin ophiolite clearly indicate the existence of an arc related orogenic component.

The clinopyroxene geothermometer of Kretz (1982) have been applied on the tholeiitic basalt to estimate the average magma temperature during the submarine volcanism. The temperatures range from 1016 to 1124 ^{o}C with an error of ±27 ^{o}C.

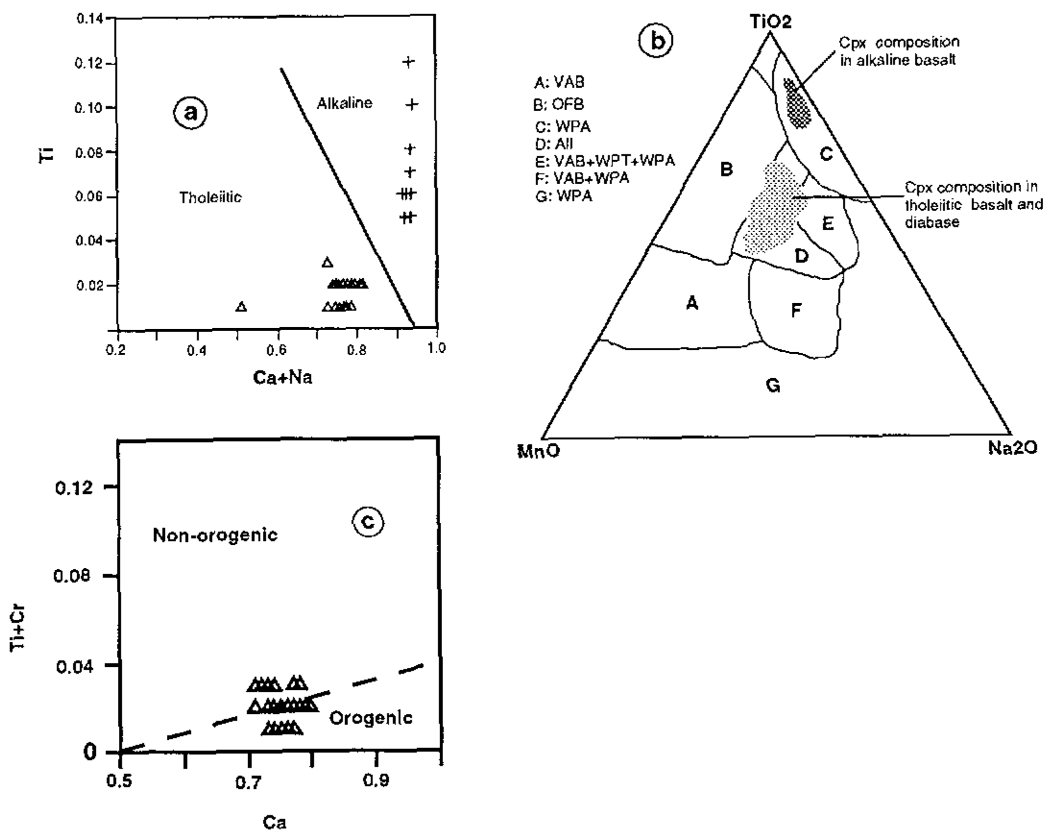

Figure 3.8. a. Characterization of magmatic parentage of the basaltic rocks in the Mersin ophiolite using the Cpx phenocrysts (after Leterrier et al., 1982). Triangles showing Cpx from tholeiitic basalts, crosses illustrates Cpx from alkali basalts. **b.** Triangular diagram of TiO_2-MnO-Na_2O discriminating Cpx from different magma types (after Leterrier et al., 1982). **c.** Ti+Cr versus Ca plot of the Cpx from the tholeiitic basalts indicating volcanic arc component (after Leterrier et al., 1982).

3.3.5. $^{87}Sr/^{86}Sr$ and $^{143}Nd/^{144}Nd$ isotopic compositions

The results of $^{87}Sr/^{86}Sr$ and $^{143}Nd/^{144}Nd$ isotope analyses of 15 tholeiitic basalt samples are given in Table 3.3. Measured $^{87}Sr/^{86}Sr$ and $^{143}Nd/^{144}Nd$ ratios in the tholeiitic volcanics have been corrected assuming a crystallization age of 100 m.y. for the Mersin ophiolite oceanic crust.

$^{87}Sr/^{86}Sr$ ratio of the Maastrichtian seawater varies between 0.707754 and 0.707821 (McLaughlin et al., 1995) and for the Cretaceous is between (0.70715-0.70775) (Burke et al., 1982). Moreover all ocean island alkaline basalts contain high concentrations of Nd and Sr compared to tholeiitic island arc basalts in the Mersin ophiolite. These alkali basalts might have been in close association with the late Cretaceous island arc basalts. Sr contained in hydrothermal fluids derived both from alkali rocks and seawater would cause a strong shift in Sr isotopic composition of the rock. The very high $^{87}Sr/^{86}Sr$ ratios, ϵSr in the altered volcanic rocks of the Mersin ophiolite are consistent with a high degree of hydrothermal interaction with seawater. Due to overprinting of rock Sr with seawater Sr it becomes impossible to determine the primary magmatic $^{87}Sr/^{86}Sr$ ratio in these rocks.

The corrected $^{143}Nd/^{144}Nd$ ratios of the tholeiitic volcanics are given in Table 3.3. Nd isotopic ratios show limited variation, ranging from 0.512694 to 0.512742. ϵNd values are between 3.6 and 4.5. ϵNd values are thought to be less sensitive to seawater contamination than ϵSr values (McCulloch et al., 1981). This is attributed to the low concentration of Nd in seawater of $3x10^{-6}$ ppm (Høgdahl et al., 1968; Goldberg, 1965; Piepgras et al., 1979) compared to 8 ppm for Sr. Therefore no change in $^{143}Nd/^{144}Nd$ ratios in altered oceanic basalts have been observed (DePaolo and Wasserburg, 1977; O'Nions et al., 1977). McCulloch et al. (1981) pointed out that W/R Nd ratio is required to be bigger than 10^5 to affect ϵNd values (Fig. 3.9). ϵNd and ϵSr values from the tholeiitic volcanics in the Mersin ophiolite are plotted in Figure 3.9. For comparison the Semail ophiolite values (McCulloch et al., 1980-1981) and present day values of oceanic rocks (O'Nions et al., 1977; DePaolo and Wasserburg, 1977) are also plotted. The data points from Semail ophiolite clearly show that the Nd values are similar whereas the Sr isotopic compositions are shifted drastically to high values (McCulloch et al., 1980-1981). The Sr isotopic compositions in the Mersin ophiolite have been modified probably by hydrothermal alteration and Cretaceous seawater contamination. The ϵNd values have been shifted to lower values than they are assumed (Fig. 3.9). As noted earlier, already formed ocean island basalts during Late Jurassic-Early Cretaceous in the ocean basin were probably subducted when the late Cretaceous island arc tholeiitic basalts formed in supra-subduction zone environment. This subducted component might cause the shift in ϵNd values as a result of this source mixing.

Table 3.3. Sr and Nd isotopic data for the tholeiitic arc volcanics of the Mersin ophiolite.

Sample	Sr	Rb	Sm	Nd	$^{87}Rb/^{86}Sr$	$^{147}Sm/^{144}Nd$	$(^{87}Sr/^{86}Sr)_m$	$(^{87}Sr/^{86}Sr)_i$	$(^{143}Nd/^{144}Nd)_m$	$(^{143}Nd/^{144}Nd)_i$	εSr_i	εNd_i
OP-134	178	23	2.6	9.8	0.373	0.161	0.707713 ± 11	0.707182 ± 11	0.512819 ± 04	0.512714 ± 04	39.7	4.0
OP-135	188	25	3.1	11.2	0.384	0.168	0.707873 ± 08	0.707327 ± 08	0.512836 ± 06	0.512726 ± 06	41.8	4.2
OP-137	192	40	3.1	10.1	0.602	0.186	0.708545 ± 08	0.707689 ± 08	0.512815 ± 11	0.512694 ± 11	46.9	3.6
OP-138	235	54	2.8	10.0	0.664	0.169	0.708611 ± 08	0.707667 ± 08	0.512850 ± 04	0.512739 ± 04	46.6	4.5
OP-143	112	3	2.8	10.7	0.077	0.158	0.708056 ± 07	0.707946 ± 07	0.512846 ± 07	0.512742 ± 07	50.6	4.5
OP-211	226	27	2.6	9.9	0.345	0.159	0.707636 ± 07	0.707145 ± 07	0.512840 ± 03	0.512736 ± 03	39.2	4.4
OP-212	205	19	3.7	11.0	0.268	0.204	0.707647 ± 08	0.707266 ± 08	0.512832 ± 08	0.512699 ± 08	40.9	3.7
OP-213	185	46	3.2	9.6	0.719	0.202	0.708492 ± 06	0.707471 ± 06	0.512853 ± 06	0.512721 ± 06	43.8	4.1
OP-375	224	21	3.5	10.7	0.271	0.198	0.707631 ± 08	0.707246 ± 08	0.512843 ± 04	0.512714 ± 04	40.6	4.0
OP-376	273	4	3.5	10.3	0.042	0.206	0.707253 ± 07	0.707193 ± 07	0.512842 ± 05	0.512708 ± 05	39.9	3.9
OP-377	363	5	3.4	10.3	0.040	0.200	0.707281 ± 11	0.707224 ± 11	0.512862 ± 08	0.512731 ± 08	40.3	4.3
OP-378	307	5	3.5	10.9	0.047	0.194	0.707303 ± 11	0.707236 ± 11	0.512847 ± 05	0.512720 ± 05	40.5	4.1
OP-379	212	26	3.5	10.5	0.354	0.202	0.707718 ± 07	0.707214 ± 07	0.512834 ± 05	0.512702 ± 05	40.2	3.8
OP-380	308	7	3.7	11.1	0.066	0.202	0.707263 ± 08	0.707170 ± 08	0.512845 ± 07	0.512713 ± 07	39.5	4.0
OP-381	312	4	3.8	10.9	0.037	0.211	0.707349 ± 09	0.707296 ± 09	0.512841 ± 05	0.512703 ± 05	41.3	3.8

T=100 Ma (late Cretaceous), $\lambda=1.42\times10^{-11}$ for Sr and $\lambda=6.54\times10^{-12}$ for Nd were used

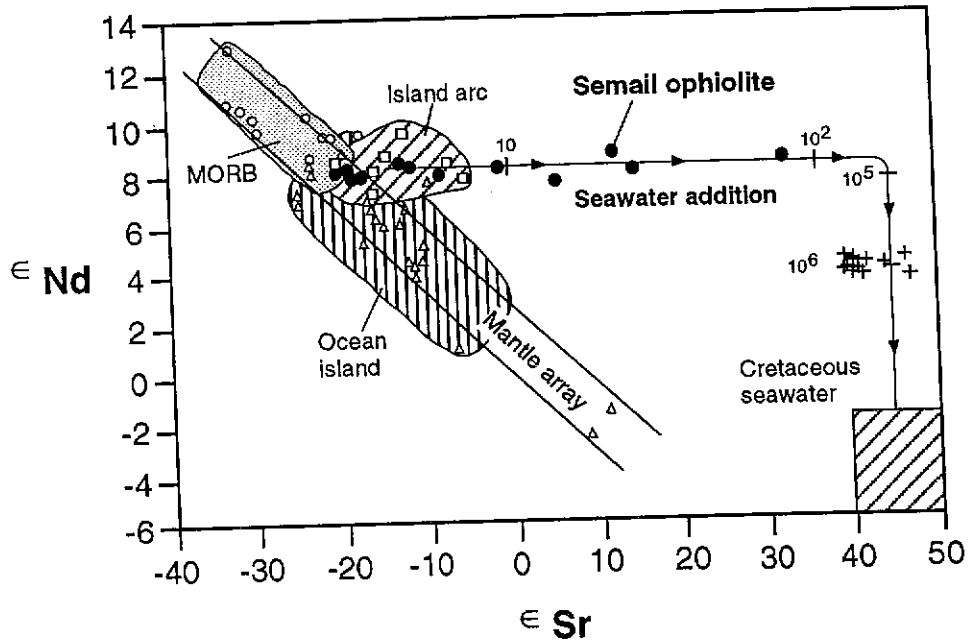

Figure 3.9. ∈ Sr versus ∈ Nd values for the tholeiitic volcanics (cross) in the Mersin ophiolite. Filled circles represent Semail ophiolite data. The arrows indicate the effect of contamination with Cretaceous seawater for different W/R ratios. The ∈ Sr and ∈ Nd values of uncontaminated samples plot on the mantle correlation line (DePaolo and Wasserburg, 1976; O'Nions et al., 1977).

3.3.6. Tectonic implications

In an attempt to identify the past tectonic environment of the basaltic rocks of the Mersin ophiolite, some tectonomagmatic discrimination diagrams based on immobile trace elements have been used. In Nb*2-Zr/4-Y triangular diagram of Meschede (1986), tholeiitic basalts and diabases plot within N-MORB and VAB fields, whereas the alkali basalts lie in the WPA field (Fig. 3.10a). Zr/Y-Zr diagram of Pearce and Norry (1979) divides the volcanic rocks into two different groups, tholeiitic basalts and diabases lie at the junction of MORB and IAB field whereas the alkaline basalts plot in the WPA field (Fig. 3.10b). Shervais (1982) suggested that volatile contents of the magmas erupted in oceanic settings are highest in island arcs. In Figure 3.10c, Ti versus V contents of the tholeiitic basaltic rocks are plotted. They show transitional character between MORBs and arc basalts due to the high V concentrations which are attributed to oxygen fugacity that is higher in volcanic arc magmas (Shervais, 1982).

The differences between the alkali basalts and tholeiitic basalts-diabases, in terms of geochemistry and age, in the Mersin ophiolite, suggest that alkali basalts associated with cherty limestones and radiolarites have the features of an ocean island basalt formed during progressive opening of the ocean as an intraplate seamount on oceanic crust during Late

Jurassic-Early Cretaceous time interval whereas the tholeiitic basalts-diabases presenting island arc characters are thought to have formed as a Late Cretaceous basaltic volcanism cogenetic with the other units of the Mersin ophiolite oceanic lithosphere in a supra-subduction zone tectonic setting.

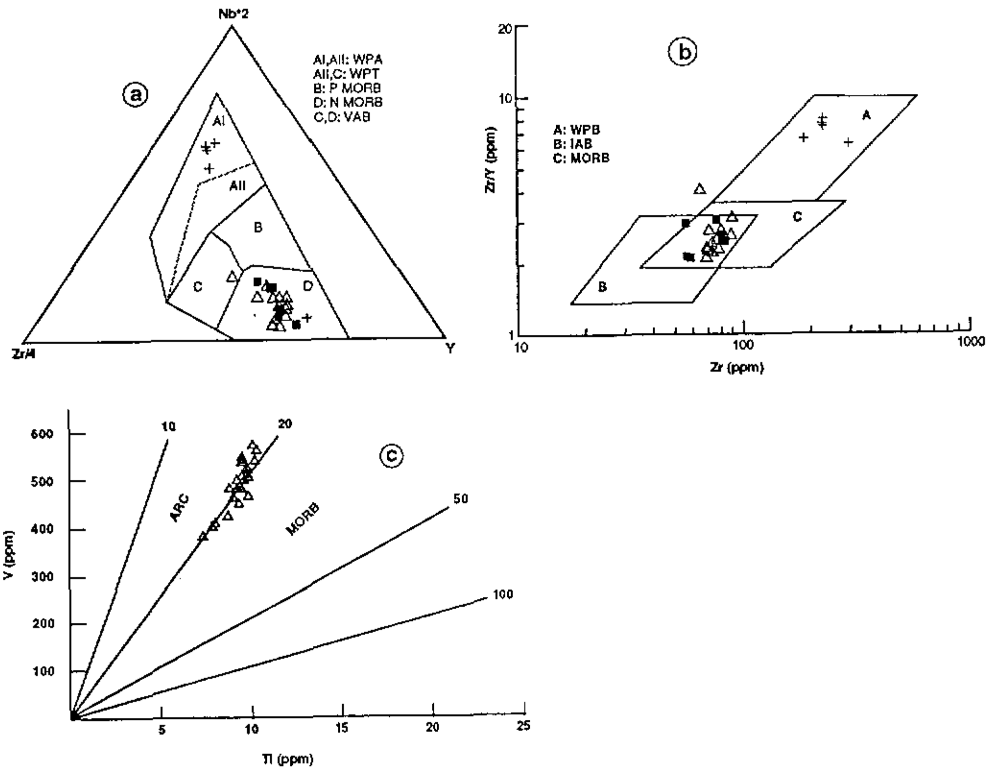

Figure 3.10. a. Nb-Zr-Y tectonomagmatic discrimination diagram of tholeiitic basalts, diabases and alkali basalts in the Mersin ophiolite (after Meschede, 1986). Triangle and filled-square represent tholeiitic basalt and diabase respectively, cross showing alkali basalt. **b.** Zr/Y-Zr discrimination diagram for basaltic rocks (after Pearce and Norry, 1979), symbols same as in a. **c.** Ti versus V for the tholeiitic basalts and diabases (after Shervais, 1982).

3.3.7. Conclusions

The basaltic rocks in the Mersin ophiolite show two suites with distinct geochemical features in terms of major, trace element, REE and mineral chemistry. These are:

a) Late Jurassic-Early Cretaceous basaltic rocks associated with cherty limestones and radiolarites are alkaline in character. Enriched LIL and HFS elements, high fractionated REE patterns and clinopyroxene mineral chemistry clearly shows their alkaline affinity. The tectonic setting of this volcanic association should be an ocean island or seamount environment in which they were derived from a fractionated magma coming from the deeper mantle or probably a plume source.

b) Late Cretaceous basalts and diabases are of tholeiitic character. They are depleted in incompatible elements and enriched in LIL elements. Small degree of fractionation, in terms of REE patterns ($[La/Yb]_N$ ratios between 1.4-1.9), is the main characteristic of this group. Tectonomagmatic discrimination diagrams based on immobile trace elements indicate that these basaltic volcanic rocks formed in an island arc environment. The reason why we accept these volcanics as cogenetic with the formation of oceanic crust in the Mersin ophiolite is that mineral chemistry of ultramafic and mafic cumulates indicate the evidence of high pressure crystallization conditions. These conditions could be present at the base of an island arc such as in Bay of Island ophiolite (Elthon et al., 1982) and Border Ranges ultramafic and mafic complex (Coleman, 1986). The very high $^{87}Sr/^{86}Sr$ ratios and ϵ_{Sr} in the altered volcanic rocks of the Mersin ophiolite are consistent with a high degree of hydrothermal interaction with seawater. Whereas the $^{143}Nd/^{144}Nd$ ratios and ϵ_{Nd} were also shifted. This could be the effect of the subducted Late Jurassic-Early Cretaceous ocean island alkali basalts in the study area.

After the opening of the South Atlantic at about Early-Late Cretaceous time (Smith et al., 1981), a compressional regime started between Afro-Arabia and Eurasia in the eastern Mediterranean region. North dipping subduction of the southern segment of the Neo-Tethyan ocean started during Mid-Cretaceous (Sengör and Yılmaz, 1981; Aktas and Robertson, 1984; Dilek and Moores, 1990). The Mersin ophiolite formed above this intra oceanic subduction zone some time at the beginning of Late Cretaceous. Soon after the formation of the oceanic crust, the Mersin ophiolite was emplaced northwards onto the Tauride active continental margin during Late Cretaceous-Early Paleocene time.

3.4. Ultramafic and mafic cumulate

3.4.1. Field relations

The ultramafic and mafic cumulates are well exposed along roughly the N-S extending Sorgun valley in the western end of the Mersin ophiolite (Fig. 3.1). Detail mapping (1/10.000 scale) and measured stratigraphic section through this cumulate rocks reveal structural, petrologic and petrographic features of lower part of oceanic layer 3 and upper part of oceanic layer 4 in the Mersin ophiolite.

Total thickness of the cumulates is over 3 km (Fig 3.11). The rock association from bottom to top show following sequence: it starts with 60 m thick dunites (ol+cr) (Plate 3.2a) in which stratiform chromite occurrences are present (Plate 3.3c) and gradually passes into 50 m thick dunite (ol+cr)-wehrlite (ol+cpx) alternation zone; each layer in this zone is approximately 10 m thick. A dunitic (ol+cr) layer with 40 m thick comes onto this alternation and is followed by 220 m thick wehrlite (ol+cpx) (Plate 3.2b) within which cm scale dunite layers are present at different levels. A clinopyroxenite layer (Plate 3.2c), 50 m thick, covers the previous rocks. 20 m thick olivine gabbro with a thin sandwiched layer of wehrlite (ol+plg+cpx) are the following units. 450 m thick layered wehrlite (ol+cpx), 310 m thick gabbro (plg+cpx±opx), again 70 m thick wehrlite (ol+cpx), and more than 2000 m thick gabbroic rocks constitute the rest of the section. Within the gabbroic cumulates, olivine gabbro (ol+plg+cpx) (Plate 3.2d), leuco gabbro (plg+cpx) (Plate 3.3a), gabbro (plg+cpx) and anorthosite (plg) (Plate 3.3b) are the most conspicuous lithologies.

The ultramafic cumulates, which generally exhibit adcumulate-heteradcumulate texture, display structures such as igneous lamination, size grading and rhytmic layering (Plate 2d). Mafic cumulates show rhytmic-graded layering and are characterized by adcumulate, mesocumulate and orthocumulate texture (Plate 3.4a-b-c-d). Abundance of monomineralic cumulate layers (dunite, clinopyroxenite) especially in the ultramafic section is an evidence of adcumulate origin (Jackson, 1971). The low concentrations of incompatible trace elements (Zr, Y and REE) and high Mg numbers of mafic minerals in the whole plutonic sequence suggest adcumulate or heteradcumulate growth which expelled trapped intercumulus liquid (Wager et al., 1960). Both mafic and ultramafic cumulates do not show any cross lamination. Size and graded layering are generally upright indicating gravity controlled deposition in cumulates. Igneous lamination, cm-scale rhytmic layering and absence of cross bedding suggest no significant magmatic current in the magma chamber of the Mersin ophiolite. Structures induced from magmatic currents activity such as cross lamination, eroded channel-fill and other type of structures formed by gravitational accumulation in magma chamber such as magmatic lamination, size-graded layering have been documented in number of well known mafic-ultramafic cumulates namely in Oman ophiolite (Pallister and Hopson, 1980; 1981), Antalya ophiolite (Juteau and Whitechurch, 1980), Kalka layered intrusion in central Australia (Goode, 1976) and Skaergaard Intrusion (McBirney and Noyes, 1979).

3.4.2. Petrographic summary

The cumulates of the Mersin ophiolite can be subdivided into two groups namely ultramafic and mafic cumulates. For the classification and nomenclature of the rocks, Streckeisen (1976) definitions have been followed. Ultramafic cumulates are represented by dunite, wehrlite, clinopyroxenite. Rock units of the ultramafic cumulates preserved their primary textures and show adcumulate and mesocumulate textures. Pore-trapped liquid component (as a post-cumulus phase) between cumulus minerals in the rock units of the ultramafic cumulates are very limited.The dunites consist of cumulus euhedral olivine 90-95 vol% (Fo90-85) crystals with grain size of 1.5-3 mm and 1-5 vol% of chromian spinel (Cr# 60-80%) crystals with grain size between 0.7-1 mm. The wherlites are represented by

25-35 vol% olivine and euhedral-subhedral (55-75 vol%) clinopyroxene with grain size of 0.5-5 mm. The composition of the clinopyroxene ranges from (Ens_{45} Fs_{4} Wo_{47}) to (Ens_{48} Fs_{9} Wo_{49}). The clinopyroxenite contains adcumulus coarse grained euhedral (1-8.5 mm) clinopyroxenes.

The mafic cumulates consisting mainly of gabbro, leucogabbro, olivine gabbro and anorthosite constitute more than 2/3 of the whole cumulate section. The mafic cumulative rocks are very fresh and they present adcumulate, mesocumulate and orthocumulate texture. The gabbros consist mainly of 50-55 vol% calcic plagioclase (An_{95-91}) with grain size between 1-3 mm, 35-45 vol% clinopyroxene (En_{40-45} Fs_{8-12} Wo_{46-47}) with 0.5-2 mm grain size and intercumulus unhedral 2-5 vol% orthopyroxene with grain size of 0.5-0.8 mm. The olivine gabbro contains 20-25 vol% cumulus olivine precipitation (Fo_{80-81}) with grain size of 0.8-2.5 mm, 55-60 vol% plagioclase and 15-20 vol% clinopyroxene. The leucogabbros are made of 65-70 vol% cumulus plagioclase and 30-35 vol% clinopyroxene. The anorthosite contains adcumulate (99 vol%) euhedral highly calcic plagioclase ($An_{91.6-95.6}$) with grain size between 2-5.2 mm and 1 vol% post-cumulus clinopyroxene filling the interstices between the cumulus plagioclases.

3.4.3. Analytical method

Twenty-one samples from ultramafic and mafic cumulates have been analysed in terms of major and trace element concentrations. Major and trace element analyses have been carried out by XRF in the Mineralogy Department at the University of Geneva. Major and trace element compositions were determined on glass beads fused from ignited powders to which $Li_2B_4O_7$ was added (1:5), in a gold-platinum crucible at 1150 ^{o}C. 30 representative thin sections have been used for microprobe analysis on a Camebax SX-50 in the Mineralogy Department at Lausanne University. The analytical conditions for the measured elements (K, Si, Mg, Ca, Al, Na, Mn, Ti, Cr, Fe, Ni) were 20 seconds of counting interval, beam current-20 mA, and acceleration voltage-15 kV.

3.4.4. Phase variation

Phase or crystallization layering results from the appearance or disappearance of one or more minerals (Hess, 1989). Phase variation of cumulus and intercumulus minerals in the Mersin ophiolite cumulate suite is illustrated in Figure 3.11. The cumulus phases are olivine, Cr-spinel, clinopyroxene and plagioclase. Post cumulus phases are orthopyroxene, clinopyroxene, plagioclase and olivine. The crystallization order from this phase distribution is as follow; olivine+chromite, olivine+clinopyroxene, clinopyroxene, in the

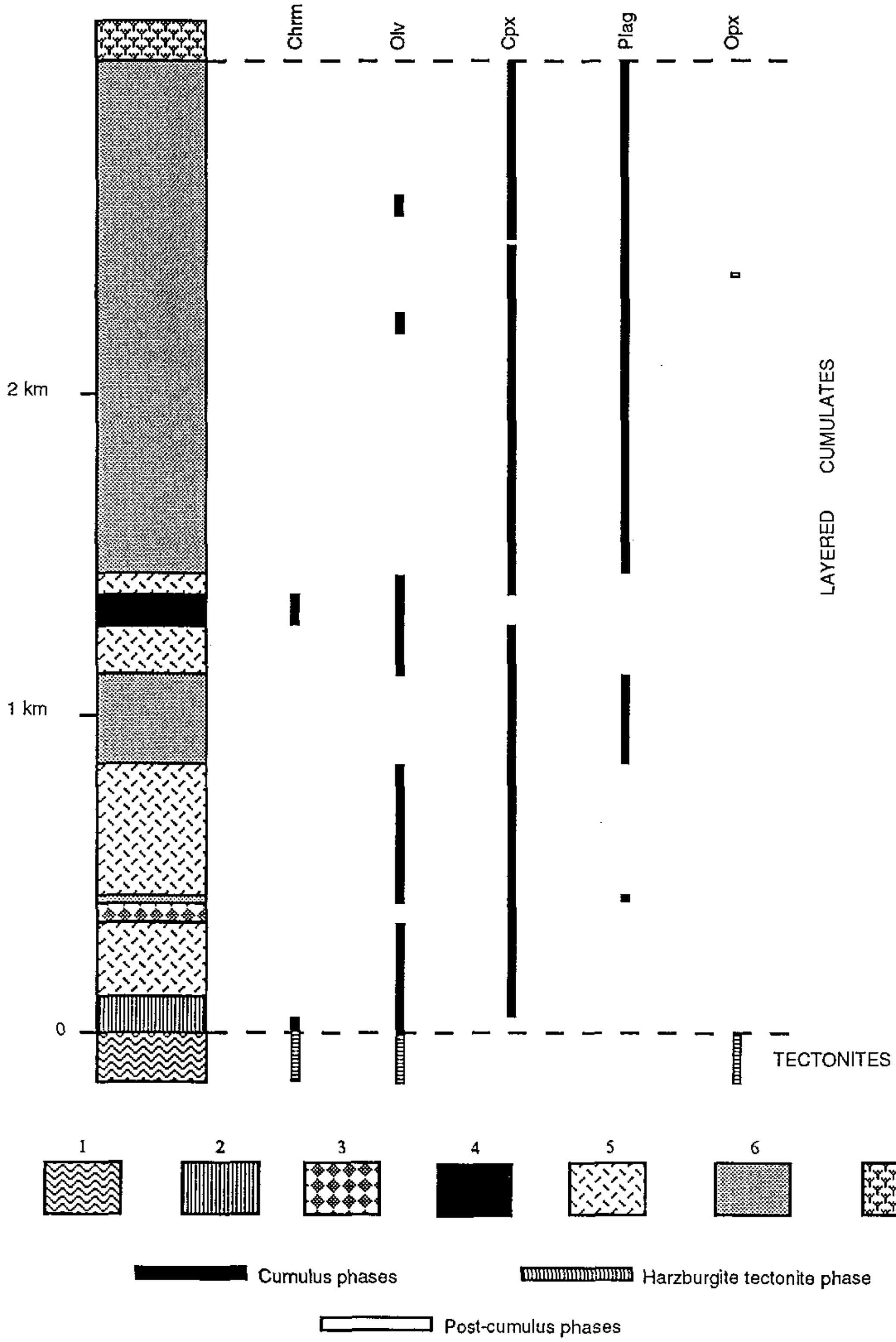

Figure 3.11. Phase distribution within the cumulates. 1-Mantle tectonites, 2-Dunite and wherlite alternation zone, 3-Clinopyroxenite, 4-Dunite, 5-Wherlite, 6- Gabbro, 7-Basalt

ultramafic cumulates, and olivine+plagioclase+clinopyroxene, plagioclase+clinopyroxene, plagioclase+clinopyroxene+orthopyroxene, plagioclase, in the mafic cumulates.

Cr-spinel and olivine are the earliest cumulus phases that crystallized from the liquid in dunite at the base of the plutonic sequence. Occurences of Cr-spinel is restricted to dunites and never observed in wherlites and mafic rocks such as gabbros and olivine gabbros through the Sorgun valley section (Fig. 3.11). Cr-spinel exhibits euhedral-subhedral cumulus minerals with a grain size between 0.7-1 mm and high Cr# (0.6-0.8). Cumulus olivine exists in the ultramafic rocks as well as in the upper part of the gabbroic section suggesting new primitive melt entrance into the magma chamber. Olivine coexists with Cr-spinel in dunites, with clinopyroxene in wehrlites at the base, and disappeared when clinopyroxenite crystallized. Reappearance of olivine in repeated units such as dunites, wehrlites and olivine gabbros is one of the characteristic features of the whole suite (Fig. 3.11). It exhibits highly magnesian composition (Fo_{91-80}) and show variable euhedral-subhedral grain size between 0.8-3 mm. It is obvious from this phase variation in basal dunites that Cr-spinel and olivine co-crystallized as liquidus phases from the primitive melts and Cr-spinel ceased to crystallize when clinopyroxene appeared in the liquids (Pallister and Hopson, 1981).

Clinopyroxene-rich layers rest onto the dunites after a few tens of meters in the basal cumulates. This mineral is present throughout all the mafic rocks (Fig. 3.11). After the cease of Cr-spinel crystallization, clinopyroxene becomes the most conspicuous mineral together with olivine and it is important to note here that appearance of clinopyroxene before plagioclase shows evidence for high pressure crystal fractionation that is common at a base of an immature island arc (Elthon et al., 1982; Pearce et al., 1984; Coleman, 1986; DeBari and Coleman, 1989). Approximately 50 m thick clinopyroxenite layer in which large crystals of clinopyroxene (1-8.5 mm) exist, is the last stage before begining of the three-phase (ol+cpx+plg) cumulates. In gabbroic cumulates, clinopyroxene is seen as cumulus and intercumulus phase in either olivine gabbros or normal gabbros (Fig. 3.11).

Plagioclase in the plutonic suite of the Mersin ophiolite is crystallized after clinopyroxene. Plagioclase generally shows cumulus euhedral and rarely subhedral crystals with very rich in Ca (An_{95-91}) and variable grain size (0.5-5.2 mm). Within the gabbroic cumulates, an anorthositic layer less than 1 m thick, too thin to be shown in Figure 3.11, is seen and shows adcumulate texture with 99% plagioclase and 1% intercumulus clinopyroxene (Plate 3.3b).

Orthopyroxene is not observed as a cumulus mineral but appears as intercumulus phase in the upper part of the gabbroic section (Fig. 3.11). The absence of cumulus orthopyroxene in the ultramafic and mafic cumulates has an importance in constructing phase diagram. Mineral phase variations within the ultramafic and mafic cumulates led us to support the conclusion of a periodic replenishment of the magma chamber by new batches of primitive magma. Periodic replenishment did keep melt composition on olivine liquidus volume and near ol-cpx-plg-liquid cotectic, from this volume olivine was the first phase that crystallized together with Cr-spinel at the base and came to 3-phases cotectic point where ol-cpx-plg crystallized to form the more than 3 km thick cumulate section. Continued fractionation reached the 4-phases cotectic point to be able to crystallize orthopyroxene in the upper part of the gabbroic cumulates. Similar evidence have been observed in the cumulates of the Oman ophiolite by Pallister and Hopson (1981).

3.4.5. Cryptic variation

Cryptic layering demonstrates variation in chemical composition of certain minerals throughout a layered sequence of rocks (Wager and Brown, 1968; Hess, 1989). Representative Olivine, chromite, pyroxene, plagioclase mineral chemistry from cumulates are given in Table 3.5-6-7-8-9. They are represented by Ca-clinopyroxenes, An-rich plagioclases and Fo-rich olivines. Cryptic variation of the ultramafic and mafic cumulates are shown in Figure 3.12 in terms of Cr content (Cr#) in Cr-spinel, forsterite (Fo) content in olivine, Mg content (Mg#) in clinopyroxene, anorthite (An) content in plagioclase and Mg content (Mg#) in orthopyroxene with respect to stratigraphic height.

It is obviously illustrated that there is a limited cryptic variation throughout the cumulate sequence of the Mersin ophiolite. (Fig. 3.12). The cumulus and intercumulus minerals do not show any zoning. Fo compositions of olivines in the basal cumulates (Fo_{89-88}) and underlying mantle tectonites (Fo_{91-89}) are very similar, suggesting that liquids which formed the basal cumulate layers were almost the same as primary magma or that underwent only small degree of fractionation (Elthon et al., 1984). Fo contents of olivines and Mg# in clinopyroxene and An contents of plagioclase decrease from bottom to top (Fig. 3.12). This feature has been interpreted as the result of crystal fractionation (Irvine, 1980; Juteau and Whitechurch, 1980; Pallister and Hopson, 1981; Elthon et al., 1984). After each episodic cryptic layering, Fo content in olivine, Mg# in clinopyroxene and An content in plagioclase reset to higher values subsequently to new influx of primitive melt into the magma chamber of the Mersin ophiolite (Fig. 3.12). Minor element concentrations of the clinopyroxenes in the ultramafic and mafic cumulates clearly well demonstrate the differentiation trend with respect to stratigraphic height (Fig. 3.13). TiO_2, MnO and Na_2O are reversely correlated with Mg# which is chosen as differentiation index, whereas Cr_2O_3 content of clinopyroxenes increases with increasing Mg#. Unzoned nature and uniform composition of clinopyroxenes may indicate either subsolidus reequilibration or slow cooling or both (Flower et al., 1977). Mg-Fe cation exchange during subsolidus reequilibration will affect Mg number in minerals at minor degrees because coexisting olivine (Mg89-81) and clinopyroxene (Mg93-81) have similar Mg numbers (Mori, 1977; Elthon and Scarfe, 1984; Elthon et al., 1984).

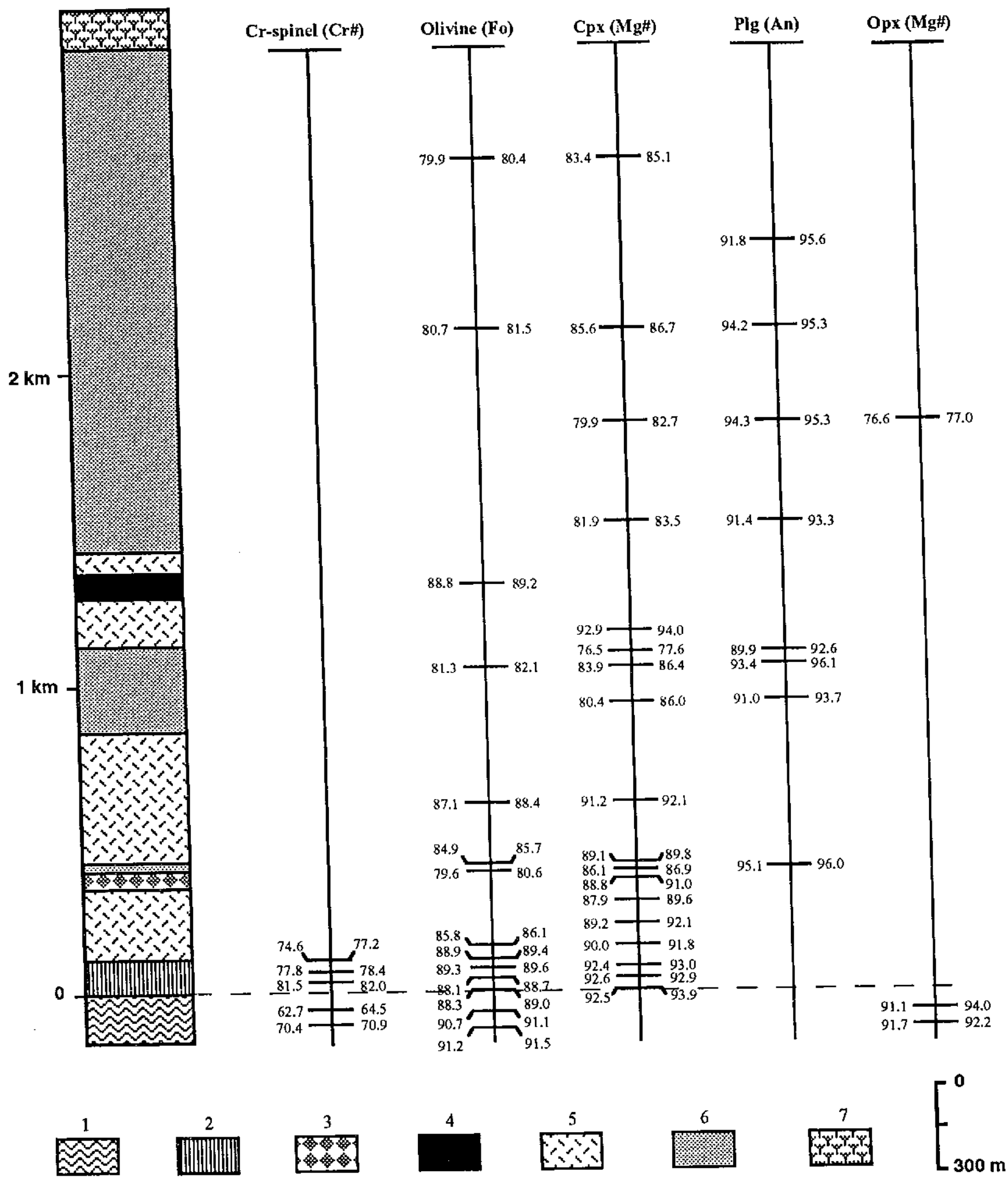

Figure 3.12. Cryptic variation within the cumulative rocks of the Mersin ophiolite (S. Turkey). Legend of the lithologies same as in Fig. 3.11. Numbers represent minimum and maximum values in individual sample.

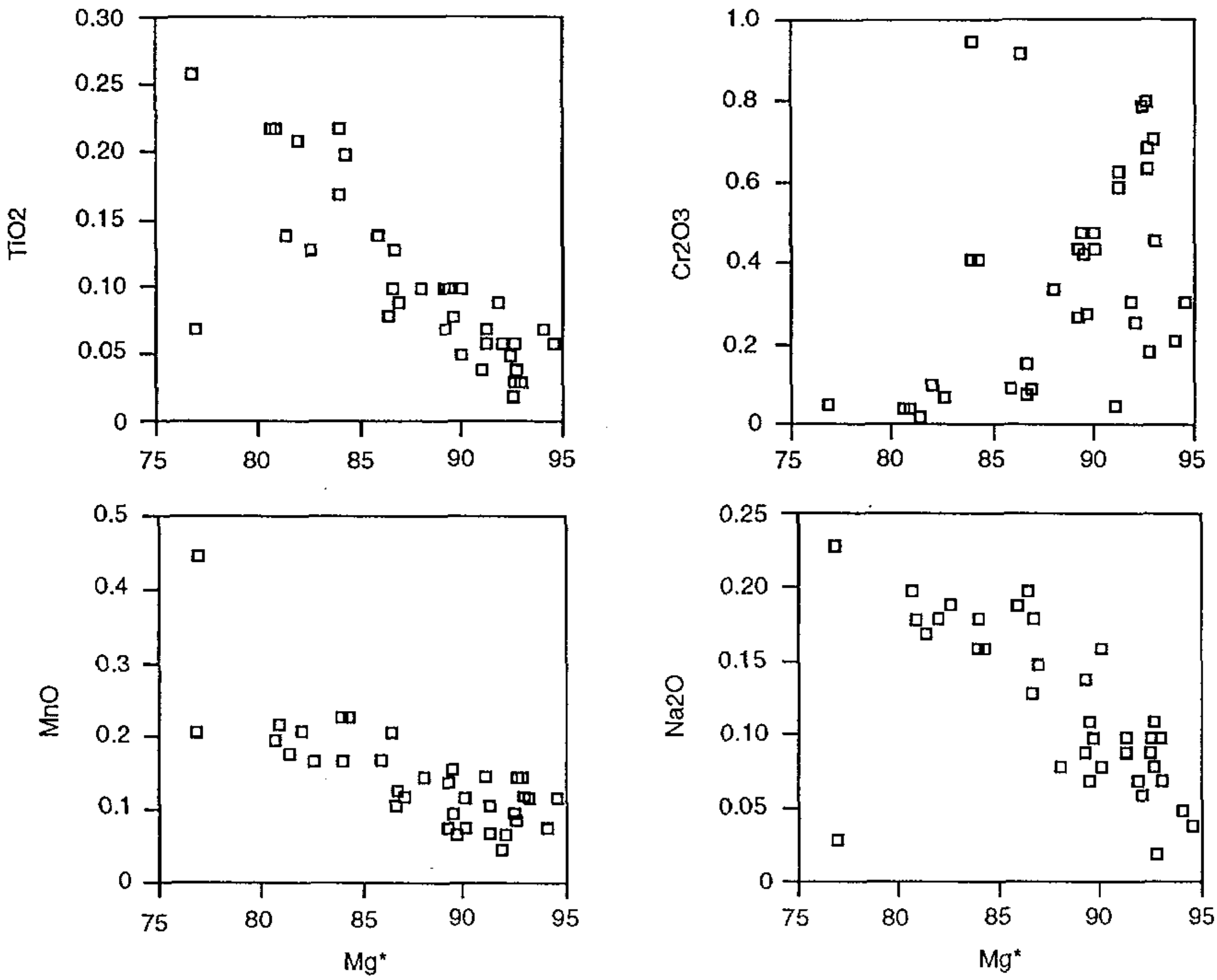

Figure 3.13. Minor element versusMg* (100*Mg/Mg+Fe) variations for clinopyroxene from layered series.

3.4.6. Whole rock chemistry

The cumulative rocks in the Mersin ophiolite range from highly magnesian (40-17 wt%) in dunites, wehrlites and clinopyroxenite to less magnesian (5-10 wt%) in more evolved rocks such as gabbro with olivine, gabbro and anorthosite characterized by high CaO (18-15 wt%) and Al_2O_3 (34-18 wt%) contents (Table 3.4). The overall trend from Mg-rich to Ca- and Al-rich cumulates is directly associated with the formation of the layered sequences by magmatic accumulation of olivines, clinopyroxenes and plagioclases in the Mersin ophiolite magma chamber. Major element compositions of the ultramafic and mafic cumulates are plotted in the AFM diagram (Beard, 1986). The dunites and wehrlites show Mg enrichment while gabbros plot in the arc-cumulate gabbro field (Fig. 3.14). However 2 samples from the ultramafic cumulates plot on the arc-cumulate gabbro field. Trace element abundances vary with both modal mineralogy (amount of post-

Table 3.4. Whole rock (major and trace) chemical analyses of the ultramafic and mafic cumulates

Rock	Whr	D	Whr	Whr	D	D	Whr	Cpxt	Cpxt	G+olv	Whr	Whr	G	Whr	G	G	G	G+olv	Whr	Whr	Anrt
No	11	12	13	14	15	16	17	19	20	21	22	23	24	25	28	31	35	36	37	46	325
SiO2	51.40	35.34	51.39	48.1	35.05	34.47	51.57	50.62	52.82	47.2	49.68	49.04	46.88	41.91	47.6	47.75	47.92	43.88	41.58	52.59	45.15
TiO2	0.05	0.01	0.05	0.05	0.02	0.02	0.07	0.09	0.08	0.06	0.09	0.05	0.08	0.05	0.07	0.06	0.05	0.02	0.08	0.06	0.03
Al2O3	1.15	0.27	1.15	1.06	0.23	0.28	1.85	2.52	2.46	17.37	2.28	1.29	18.14	15.7	22.21	21.6	19.95	27.6	3.51	1.37	33.77
FeO*	4.20	8.67	4.44	5.09	9.48	7.75	4.93	5.13	4.29	4.10	5.04	5.46	6.55	6.92	6.23	3.54	5.48	2.56	12.54	4.43	0.72
MgO	23.28	40.54	23.78	25.50	40.72	42.31	21.28	19.83	18.45	11.39	19.1	23.97	10.58	16.66	7.57	7.72	10.19	5.68	27.25	20.19	0.23
MnO	0.10	0.14	0.11	0.10	0.14	0.11	0.11	0.11	0.10	0.08	0.1	0.11	0.12	0.1	0.11	0.07	0.12	0.04	0.19	0.1	0.01
CaO	18.31	1.60	17.97	14.60	1.13	0.51	19.20	19.38	20.93	18.38	18.66	16.05	14.57	12.8	15.63	17.53	15.25	17.37	8.17	20.38	18.08
Na2O	0.01	0.05	<	<	0.17	0.12	<	<	0.12	0.30	0.16	<	0.55	0.13	0.55	0.44	0.37	0.52	<	0.24	1.09
K2O	<	<	<	<	0.01	0.01	<	<	<	<	<	<	<	<	<	<	<	<	0.04	<	0.01
P2O5	0.01	0.01	0.01	0.01	0.01	<	0.01	0.01	0.01	0.01	0.01	0.01	0.01	0.01	0.01	0.01	0.01	0.01	0.01	0.01	0.01
L.O.I	1.18	13.71	0.76	5.16	13.00	14.68	1.05	2.20	0.81	1.29	4.82	3.32	2.30	5.38	0.51	1.45	0.58	1.91	5.92	0.57	1.07
Total	99.33	100.40	99.66	99.67	99.96	100.30	100.10	99.89	100.10	100.20	99.95	99.3	99.78	99.66	100.30	100.20	99.92	99.59	99.29	99.94	100.10
ppm																					
Ba	<	<	18	<	<	<	<	31	3	<	<	<	<	16	<	3	<	<	39	16	<
Ni	342	1136	367	499	1578	1915	283	192	176	113	385	388	55	416	56	63	36	109	583	239	38
Cr	3658	7480	3963	3446	5542	6698	2456	1663	1665	259	2173	1429	152	1491	92	244	29	140	1307	3213	17
V	98	38	89	85	31	44	153	183	169	115	163	123	151	83	111	98	117	43	146	110	20
Nb	1	1	1	1	5	<	5	0	3	1	1	4	1	<	1	1	1	1	<	3	4
Zr	8	7	4	7	6	6	5	6	8	8	7	6	9	8	11	10	10	13	6	9	13
Y	14	11	13	14	11	4	14	13	5	14	13	14	14	12	14	14	14	14	12	10	<
Rb	5	5	1	1	1	6	4	2	1	<	1	<	5	1	2	1	2	<	<	9	6
Sr	<	<	<	<	<	3	<	0	<	51	<	3	59	42	81	87	69	98	<	<	179

FeO* is expressed as total Fe, "<" is below detection limit

Abbreviations

D: Dunite G: Gabbro Whr: Wehrlite Anrt: Anorthosite

Cpxt: Clinopyroxenite G+olv: Gabbro with olivine cumulus mineral) and Mg number of rock units (Jaques et al., 1983). Trace element concentrations in the ultramafic and mafic cumulates of the Mersin ophiolite are well correlated with the fractionation of olivine, Cr-spinel, pyroxene and Ca-plagioclase. Cr and Ni contents are high in the dunites and wherlites (1900-200 ppm Ni, 7500-1500 ppm Cr) (Fig. 3.15) and decrease to lower values in gabbroic rocks (Ni <60 ppm , Cr <250 ppm). Sr concentrations increase with the modal abundance of plagioclase (40-90 ppm) in the gabbros and reach as high as 179 ppm contents in the anorthosite. Incompatible trace elements (Zr, Ba, Rb, Nb, Y etc.) generally show moderate to low concentrations (Table 3.4), this may be deduced by the high cumulus phase activity in the magma chamber of the Mersin ophiolite .

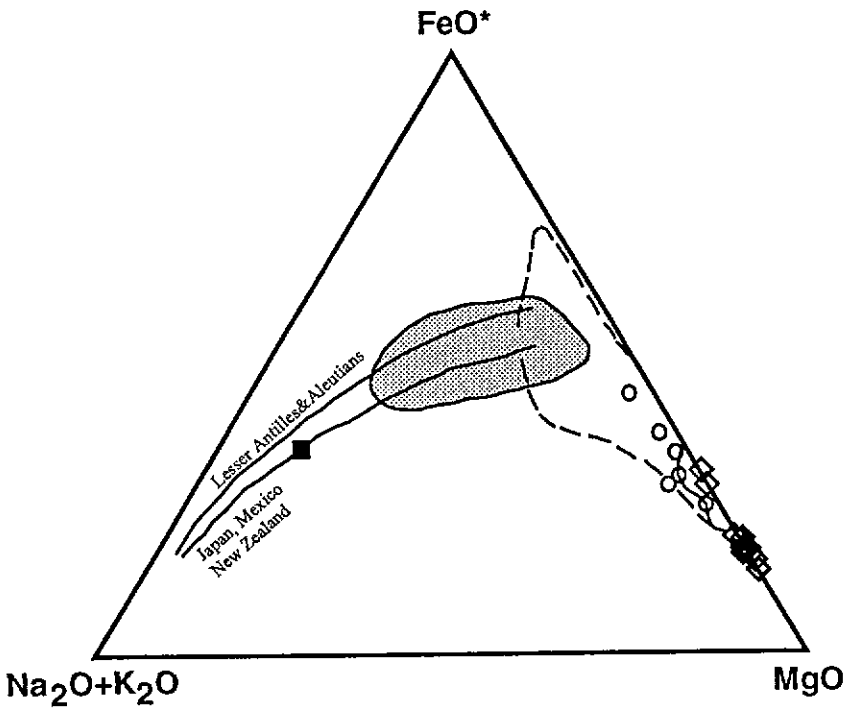

Figure 3.14. AFM composition of ultramafic (diamond) and mafic cumulates [(Gabbro (circle) and anorthosite (filled square)] in the Mersin ophiolite. Dashed line indicates arc-related mafic cumulate field. Solid line represents field of arc-related ultramafic cumulates. Dotted area indicates arc-related non cumulate gabbro and diorite. Fields of cumulate and non cumulate rocks are from Beard (1986), arc volcanic trends from Brown (1982).

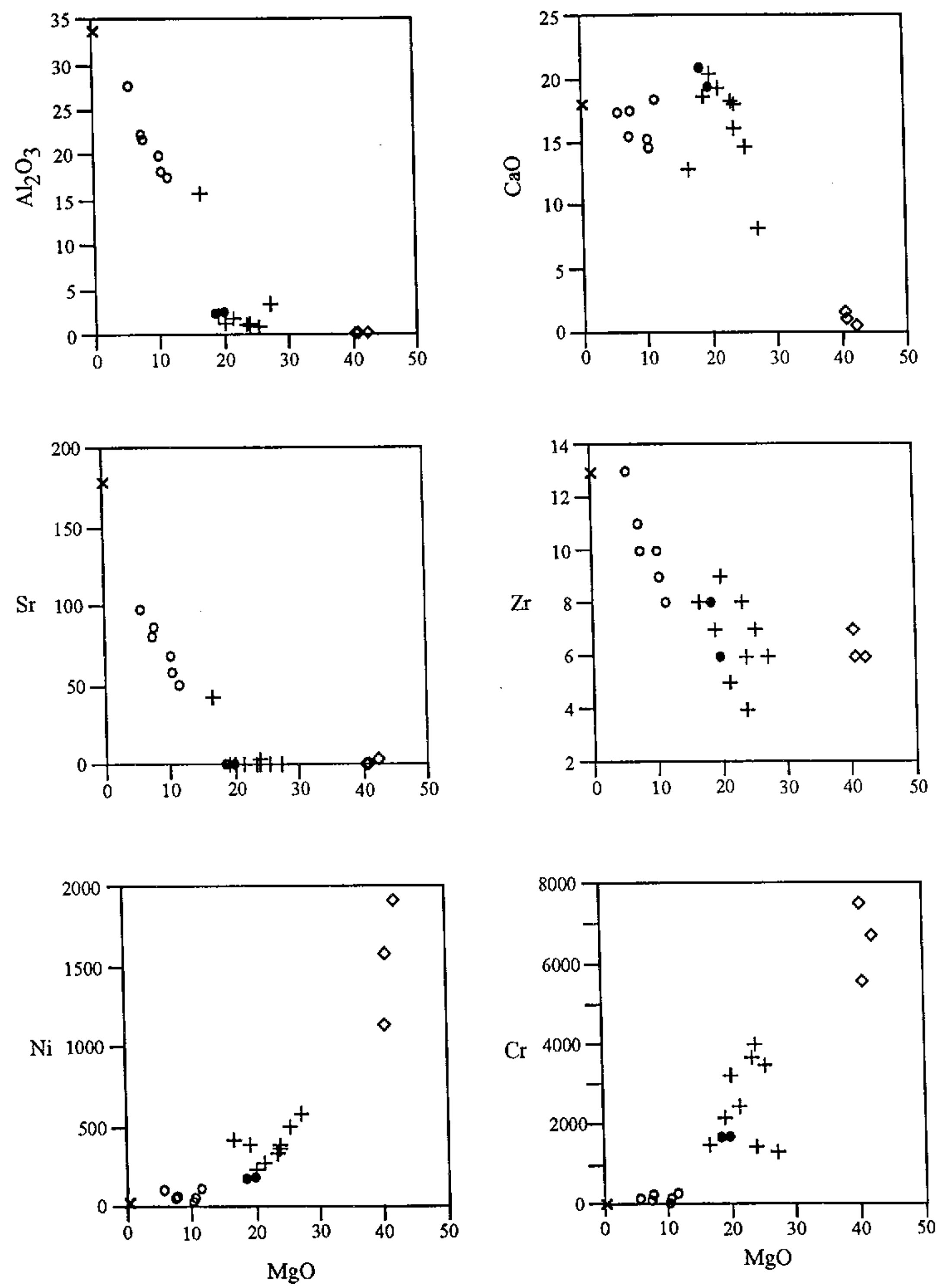

Figure 3.15. Selected major and trace element variations of the ultramafic [Dunite (diamond), wherlite (cross), clinopyroxenite (filled circle)] and mafic cumulates [Gabbro (open circle), anorthosite (x)] with MgO as a differentiation index in the Mersin ophiolite. Ni and Cr are positively correlated whereas Sr, Zr, Al_2O_3 and CaO are negatively correlated with MgO, indicating progressive differentiation in the magma chamber.

3.4.7. Mineral chemistry

3.4.7.1. Olivine

Olivine compositions in the ultramafic-mafic cumulates and mantle tectonites present variations depending mainly on lithology (Table 3.5). Olivine crystals do not show compositional zoning from core to rim and are generally uniform in composition within individual samples. Olivine is highly magnesian in harzburgite tectonites ($Fo_{91.5-90}$), basal dunites-wehrlites ($Fo_{89.5-86}$) and decreases gradually in olivine gabbro ($Fo_{81.5-80}$) with small degree of differentiation in the magma chamber. Similarity of olivine compositions in the lowest cumulates and underlying mantle peridotite suggests that the parental magma for the cumulates equilibrated with mantle type olivine (Pallister and Hopson, 1981). The NiO content is positively correlated with Mg# and higher in harzburgite (0.41-0.34 wt%) compared to the ultramafic cumulates (0.25-0.12 wt%) (Fig. 3.16). The Cr_2O_3 content in olivines is negligable (< 0.1 wt%) both in basal cumulates and olivine gabbros.

In cumulates, olivine is the first crystallizing cumulus mineral phase coexisting together with chromian spinels in dunites. Olivines are also present in plagioclase rich rocks and relatively less magnesian ($Fo_{81.5-80}$) rich. This high Mg nature of olivines in the ultramafic and mafic cumulates of the Mersin ophiolite differ from differentiated oceanic equivalents (Hébert, 1982-1985; Elthon, 1987). The olivine compositions in the cumulative rocks of the Mersin ophiolite show close similarities to those such as Troodos ophiolite (Hébert and Laurent, 1990), Tonsina complex (De Bari and Coleman, 1989), Border Range ultramafic and mafic complex (Burns, 1985), Bay of Island ophiolite (Elthon et al., 1982) which are thought to have formed in an arc environment.

3.4.7.2. Chromian Spinel

The spinel compositions in the basal ultramafic cumulates and in the mantle tectonites of the Mersin ophiolite are rich in Cr_2O_3 (61-49 wt%), low in Al_2O_3 (19-9 wt%) and the Cr# (100*Cr/Cr+Al) ranges from 60 to 80 (Table 3.6). The chromian spinel compositions in the Mersin ophiolite are different from those of oceanic crust (Dick and Bullen, 1984) and stratiform complexes (Irvine, 1967) and similar to chromian spinels from Troodos ophiolite (Hébert and Laurent, 1990) and Border Ranges ultramafic and mafic complex (Burns, 1985). Dick and Bullen (1984) suggested that spinels with high Cr# (> 60%) are restricted to volcanic arcs, stratiform complexes and oceanic plateau basalts whereas low Cr# (< 60%) in spinels is typical of oceanic crust. Thus, on the basis of above-mentioned

Table 3.5. Representative olivine analyses from the ultramafic cumulates and mantle tectonites.

	Mantle tectonite			Ultramafic cumulate															
	Harzburgite			Wehrlite												Dunite			
Sample No	68-2c	68-3c	68-4c	11-1c	13-7c	14-4c	17-3c	22-4c	23-5c	46-1c	46-2c	46-3c	46-4c	46-5c	46-6c	15-2c	30-1c	30-2c	30-3c
SiO2	40.75	40.82	40.99	41.01	40.55	41.29	40.55	40.22	40.91	40.16	40.17	40.12	40.10	39.78	40.24	40.97	40.81	40.43	40.72
TiO2	<	<	<	<	0.03	<	0.01	<	<	0.01	<	0.02	<	0.02	<	<	0.01	0.01	0.02
Al2O3	<	<	0.01	0.02	<	<	0.01	0.01	0.01	<	<	<	<	<	<	<	<	0.02	<
FeO*	8.44	8.31	8.30	10.81	10.93	10.09	13.22	13.97	11.81	12.87	12.79	13.15	13.01	13.03	12.91	10.57	10.54	10.75	10.76
Cr2O3	0.01	<	0.01	0.03	0.05	0.05	0.02	<	<	0.03	<	<	0.00	0.01	<	0.06	<	0.03	0.01
MnO	0.10	0.14	0.07	0.15	0.19	0.13	0.29	0.21	0.22	0.12	0.16	0.20	0.22	0.16	0.14	0.18	0.15	0.18	0.17
MgO	50.24	50.44	50.59	47.73	46.86	47.83	45.81	44.79	47.06	46.80	47.02	47.23	47.12	46.88	46.94	48.05	48.74	48.74	48.51
CaO	0.01	<	0.01	0.01	0.03	0.03	<	<	0.04	0.01	0.01	0.05	0.02	0.03	0.02	0.01	0.03	0.02	0.04
Na2O	<	<	<	<	<	<	0.03	0.01	<	<	<	<	<	<	<	<	<	<	<
K2O	<	<	<	0.02	<	<	<	<	0.01	<	<	<	<	<	<	0.01	<	<	<
NiO	0.39	0.36	0.43	n.d.	n.d.	n.d.	n.d.	n.d.	n.d.	0.15	0.18	0.12	0.14	0.12	0.15	n.d.	0.25	0.19	0.15
Total	99.94	100.08	100.41	99.78	98.64	99.42	99.94	99.21	100.06	100.15	100.33	100.89	100.61	100.03	100.40	99.85	100.53	100.37	100.38
Si	0.99	0.99	1.00	1.01	0.98	1.00	1.01	0.99	1.01	1.00	1.00	0.99	0.99	0.99	1.00	1.00	1.00	0.99	1.00
Ti	<	<	<	<	0.00	<	0.00	<	<	0.00	<	0.00	<	0.00	<	<	0.00	0.00	0.00
Al	<	<	0.00	0.00	<	<	0.00	0.00	0.00	<	<	<	<	<	<	<	<	0.00	<
Fe	0.17	0.17	0.17	0.22	0.22	0.21	0.27	0.29	0.24	0.27	0.27	0.27	0.27	0.27	0.27	0.22	0.22	0.22	0.22
Cr	0.00	<	0.00	0.00	0.00	0.00	0.00	<	<	0.00	<	<	0.00	0.00	<	0.00	<	0.00	0.00
Mn	0.00	0.00	0.00	0.00	0.00	0.00	0.01	0.00	0.00	0.00	0.00	0.00	0.00	0.00	0.00	0.00	0.00	0.00	0.00
Mg	1.83	1.83	1.83	1.74	1.69	1.73	1.70	1.65	1.73	1.73	1.74	1.74	1.74	1.74	1.73	1.76	1.78	1.78	1.77
Ca	0.00	<	0.00	0.00	0.00	0.00	<	<	0.00	0.00	0.00	0.00	0.00	0.00	0.00	0.00	0.00	0.00	0.00
Na	<	<	<	<	<	<	0.00	0.00	<	<	<	<	<	<	<	<	<	<	<
K	<	<	<	0.00	<	<	<	<	0.00	<	<	<	<	<	<	0.00	<	<	<
Ni	0.01	0.01	0.01	n.d.	n.d.	n.d.	n.d.	n.d.	n.d.	0.00	0.00	0.00	0.00	0.00	0.00	n.d.	0.01	0.00	0.00
Fo (100*Mg/Mg+Fe)	91.31	91.41	91.51	88.73	88.43	89.42	86.07	85.11	87.66	86.53	86.62	86.36	86.41	86.39	86.53	89.02	89.09	88.85	88.83
Fa (100*Fe/Fe+Mg)	8.61	8.45	8.43	11.27	11.57	10.58	13.93	14.89	12.34	13.35	13.22	13.50	13.39	13.48	13.35	10.98	10.81	11.00	11.05
Mg*(100*Mg/Mg+Fe)	91.50	91.50	91.50	88.59	88.25	89.30	85.80	84.92	87.46	86.50	86.60	87.00	86.60	86.60	86.50	88.85	89.00	89.00	88.90

Number of ions on the basis of 4 (O), Total Fe is expressed as FeO*, "n.d." is not determined, "<" is below detection limit

Table 3.6. Representative chromian-spinel analyses from the mantle tectonites and ultramafic cumulates

	Ultramafic cumulate			Mantle Tectonite	
	Dunite			Harzburgite	
No	5-1cr	12-1cr	15-1cr	73-1	90-1
SiO2	0.05	0.12	0.08	0.04	0.07
TiO2	0.15	0.21	0.24	0.02	<
Al2O3	8.90	10.27	10.30	15.10	18.90
Cr2O3	60.33	55.60	52.09	53.45	49.93
FeO*	18.99	25.30	28.41	20.14	19.11
MnO	0.34	0.44	0.44	0.29	0.21
MgO	10.69	7.79	7.68	10.25	11.00
CaO	<	0.02	0.01	<	0.02
Na2O	<	0.01	0.01	<	0.03
K2O	0.01	<	<	<	<
Total	99.46	99.76	99.26	99.29	99.27
Si	0.01	0.03	0.02	0.01	0.02
Ti	0.03	0.04	0.05	0.00	<
Al	2.76	3.26	3.28	4.56	5.58
Cr	12.56	11.85	11.12	10.82	9.88
Fe	4.18	5.71	6.41	4.31	4.00
Mn	0.08	0.10	0.10	0.06	0.04
Mg	4.20	3.13	3.09	3.91	4.11
Ca	<	0.01	0.00	<	0.01
Na	<	0.01	0.01	<	0.01
K	0.00	<	<	<	<
Cr# (100*Cr/Cr+Al)	81.97	78.41	77.23	70.37	63.93
Fm# (100*Fe/Mg+Fe)	49.91	64.56	67.48	52.43	49.35

Number of ions on the basis of 32 (O).Total Fe is expressed as FeO*
"<" is below detection limit

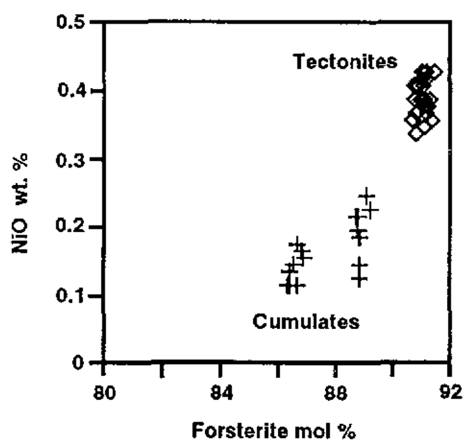

Figure 3.16. NiO versus Fo content of olivines from tectonites and cumulates in the Mersin ophiolite.

interpretations the compositions of chromian spinels in the Mersin ophiolite suggest also arc-related tectonic environment (Fig. 3.17).

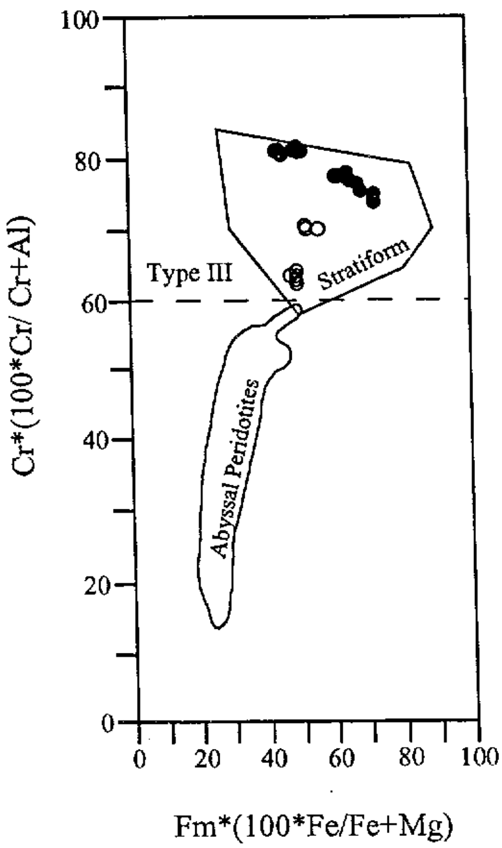

Figure 3.17. Spinel compositions from ultramafic cumulates (filled circles) and peridotites (open circles) in the Mersin ophiolite. Type III spinel field and abyssal peridotite field from Dick and Bullen (1984), stratiform field from Irvine (1967).

3.4.7.3. Clinopyroxene

Representative clinopyroxene compositions from ultramafic and mafic cumulates of the Mersin ophiolite are given in Table 3.7. The clinopyroxenes from ultramafic cumulates demonstrate very restricted compositional variations (En_{49-45} Wo_{50-45} Fs_{6-3}) and are in the diopside field (Fig. 3.18). The clinopyroxenes from gabbroic cumulates show weak Fe enrichment (En_{49-45} Wo_{48-45} Fs_{10-7}) with differentiation and plot in the diopsite field (Fig. 3.18).

The most conspicious feature of the clinopyroxenes in the ultramafic and mafic cumulates is the extremely high Mg number (95-85 and 85-77 respectively). The Cr_2O_3 in clinopyroxene is plotted against the Mg number in Figure 3.19a. Cr_2O_3 content in the clinopyroxenes of the basal cumulate is higher and getting decreased with decreasing Mg#

Table 3.7. Representative clinopyroxene analyses from the ultramafic and mafic cumulates.

	Ultramafic cumulates										Mafic cumulates			
	Wherlite								Cpxt	Cpxt	G+ol	Gabbro		
No	11-1c	13-1c	14-1c	17-1c	18-1c	22-1c	23-1c	25-1c	19-1c	20-1c	21-1c	24-1c	28-1c	31-1c
SiO2	54.47	54.14	55.10	53.65	53.06	53.11	54.48	51.87	53.07	54.46	52.53	52.17	53.01	52.67
Al2O3	1.09	1.06	0.61	1.76	1.95	2.41	0.76	3.55	2.54	0.61	2.81	2.49	1.40	2.22
TiO2	0.06	0.03	0.06	0.10	0.05	0.10	0.04	0.08	0.08	0.04	0.10	0.22	0.07	0.21
FeO*	2.27	2.33	1.78	3.25	3.59	3.52	2.41	4.31	3.45	2.94	4.44	6.64	20.02	6.29
MnO	0.15	0.12	0.12	0.08	0.12	0.10	0.15	0.21	0.07	0.15	0.11	0.20	0.33	0.21
MgO	17.24	17.11	17.26	16.49	16.66	16.56	17.13	15.32	16.18	16.72	15.74	15.09	23.72	15.79
Cr2O3	0.69	0.71	0.31	0.48	0.44	0.43	0.18	0.92	0.28	0.05	0.08	0.04	0.04	0.10
CaO	24.41	24.11	25.29	24.12	23.81	24.27	25.10	23.82	23.84	24.99	23.57	23.01	1.01	22.44
Na2O	0.11	0.10	0.04	0.08	0.16	0.11	0.02	0.20	0.10	0.00	0.13	0.20	<	0.18
K2O	0.02	0.02	<	0.01	0.82	<	0.01	0.01	<	<	0.03	0.14	<	0.09
Total	100.51	99.73	100.57	100.02	100.66	100.61	100.28	100.29	99.61	99.96	99.54	100.20	99.60	100.20
Si	1.97	1.94	1.99	1.96	1.93	1.93	1.98	1.90	1.90	1.98	1.88	1.92	1.91	1.93
Al IV	0.03	0.04	0.01	0.04	0.07	0.07	0.02	0.10	0.10	0.02	0.12	0.08	0.06	0.07
Al VI	0.02	0.00	0.01	0.03	0.01	0.03	0.01	0.05	0.01	0.01	0.00	0.03	0.00	0.03
Ti	0.00	0.00	0.00	0.00	0.00	0.00	0.00	0.00	0.00	0.00	0.00	0.01	0.00	0.01
Fe	0.07	0.07	0.05	0.10	0.10	0.11	0.07	0.13	0.10	0.09	0.13	0.20	0.06	0.19
Mn	0.00	0.00	0.00	0.00	0.00	0.00	0.00	0.01	0.00	0.00	0.00	0.01	0.01	0.01
Mg	0.93	0.92	0.93	0.90	0.90	0.90	0.93	0.84	0.86	0.91	0.84	0.83	1.28	0.86
Cr	0.02	0.02	0.01	0.01	0.01	0.01	0.01	0.03	0.01	0.00	0.00	0.00	0.00	0.00
Ca	0.95	0.93	0.98	0.94	0.93	0.94	0.98	0.93	0.91	0.97	0.90	0.91	0.04	0.88
Na	0.01	0.01	0.00	0.01	0.01	0.01	0.00	0.01	0.01	0.00	0.01	0.01	<	0.01
K	0.00	0.00	<	0.00	0.04	<	0.00	0.00	<	<	0.00	0.01	<	0.00
En. (100*Mg/(Mg+Fe+Ca)	47.70	47.78	47.29	46.20	49.23	45.96	46.80	43.80	45.85	45.92	44.68	43.93	66.14	45.33
Fs. (100*Fe/(Mg+Fe+Ca)	3.76	3.84	2.92	5.23	0.20	5.64	3.93	7.25	5.60	4.76	7.25	7.92	31.83	8.34
Wo. (100*Ca/(Mg+Fe+Ca)	48.54	48.38	49.79	48.56	50.57	48.40	49.28	48.94	48.55	49.32	48.08	48.15	2.02	46.32
Mg* (100*Mg/(Mg+Fe)	92.61	92.90	94.88	89.98	90.00	89.06	92.98	86.53	89.62	90.98	86.59	80.58	95.51	81.90
Cr# (Cr/Cr+Fe)	0.21	0.22	0.15	0.12	0.09	0.10	0.07	0.17	0.07	0.02	0.02	0.00	0.02	0.00

Number of ions on the basis of 6 (O), Total Fe is expressed as FeO*, "<" is below detection limit

Cpxt:Clinopyroxenite, G+ol: Gabbro with olivine

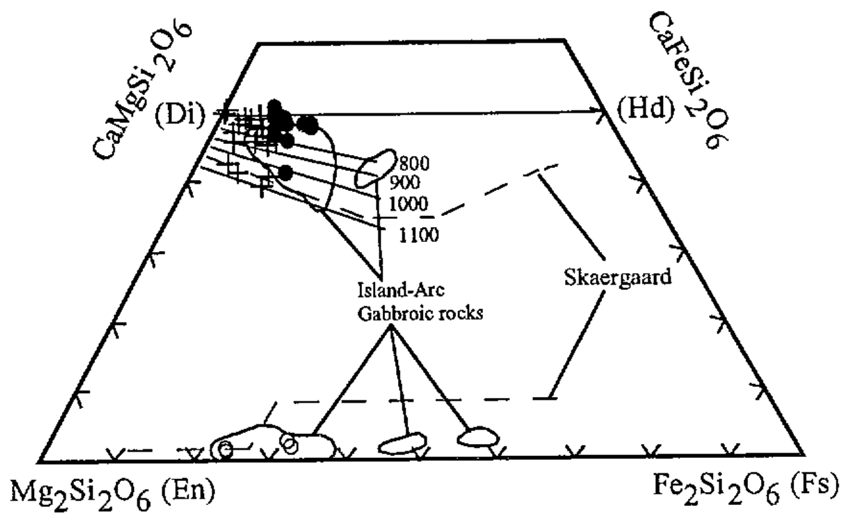

Figure 3.18. Pyroxene ternary diagram showing clinopyroxene and orthopyroxene compositions from ultramafic and mafic cumulates. Cross (+) indicates clinopyroxene from ultramafic and filled circle indicates clinopyroxene from gabbroic cumulates. Open circles (o) are Opx in the gabbroic cumulates. Temperature estimates in degrees celsius from Ross and Huebner (1975). Fields of island arc gabbroic rocks (solid lines) and Skaergaard trend are from Burns (1985).

in the gabbroic clinopyroxenes (Fig. 3.19a). This feature could be related to the gradually Cr impoverishment of the magma (Hodges and Papike, 1976). A similar relationship is observed in the ultramafic and gabbroic cumulates of Troodos (Hébert and Laurent, 1990) and North Arm Mountain Massif of the Bay of Island Ophiolite Complex (Elthon et al., 1982, 1984; Komor et al., 1986).

Mg number versus TiO_2 in the clinopyroxenes of the ultramafic and gabbroic cumulates from the Mersin ophiolite is shown in Figure 3.19b. Elthon (1987) declared that the clinopyroxenes with high Mg numbers have also high TiO_2. This general feature does not fit with the Mersin ophiolite case, because the clinopyroxenes with higher Mg number have generally lower TiO_2 content (< 0.1 wt%) (Fig. 3.19b). The Mersin relation is seen in Bay of Island Ophiolite Complex (Elthon et al., 1982, 1984; Komor et al., 1985) and in Troodos ophiolite (Hébert and Laurent, 1990). TiO_2 content of clinopyroxene generally depends on cooling rate, with faster cooling rates increasing the apparent distribution of Ti coefficient (Coish and Taylor, 1979; Gamble and Taylor, 1980; Elthon, 1987). Consequently, TiO_2 content of clinopyroxenes in the volcanic rocks of the Mersin ophiolite have higher TiO_2 (0.96-0.5 wt%) compared to the cumulative rocks (Fig. 3.19b).

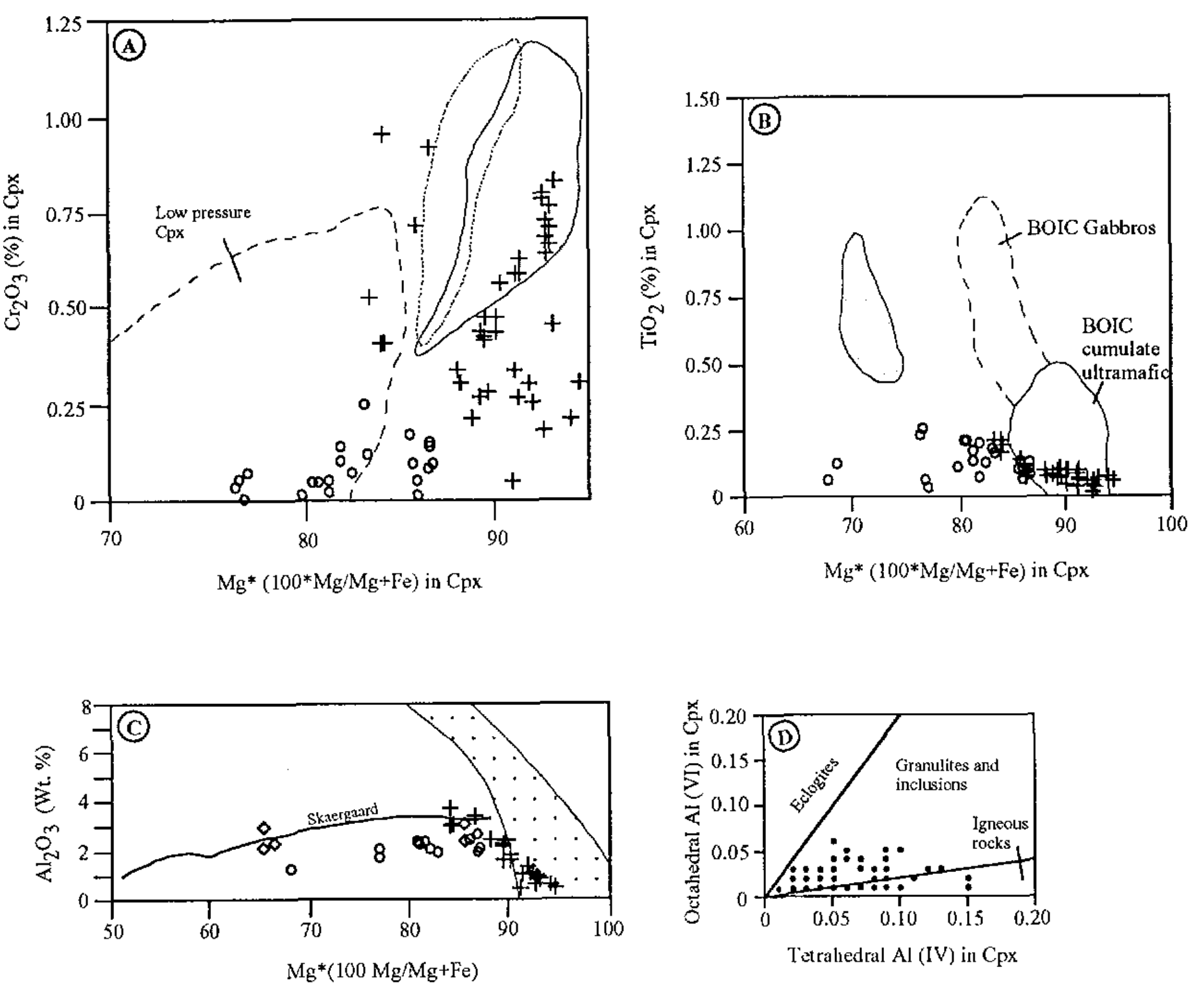

Figure 3.19. a. Cr_2O_3 versus Mg number in clinopyroxene in the ultramafic (+) and mafic (O) cumulates. Low pressure Cpx field from 1-atm experimental studies of N-MORB (Elthon, 1987).Bay of Island ultramafic (solid line) and mafic (dashed line) cumulates are also shown (after Elthon, 1987). **b.** TiO_2 versus Mg number (100*Mg/Mg+Fe) in clinopyroxenes from ultramafic (+) and mafic (o) cumulates. Dotted area is the volcanic clinopyroxene compositions in the Mersin ophiolite. Dashed and solid line indicate gabbro and ultramafic cumulate field of the Bay of Island ophiolite respectively (after Elthon, 1987). **c.** Trend of moderete increasing of Al_2O_3 versus decreasing Mg# number in clinopyroxenes of the ultramafic and mafic cumulates of the Mersin ophiolite. Field of high pressure peridotite (dotted area) after Medaris (1972). Trend of gabbroic cumulates (o) parallel to the trend of low pressure cumulates such as Skaergaard intrusion and Semail ophiolite (open diamond) (from DeBari and Coleman, 1989). **d.** Al in octahedral versus tetrahedral coordination in clinopyroxenes. High octahedral to tetrahedral ratios indicate higher pressures of formation. Fields are from Aoki and Kushiro (1968). Filled circles indicate ultramafic and mafic cumulates of the Mersin ophiolite, plotting in the field of granulite and high pressure xenoliths.

Ti content of clinopyroxene reflects the degree of depletion of mantle source and the Ti activity of parent magma which generated cumulate suite (Pearce and Norry, 1979). The magma source from which the clinopyroxenes crystallized was poor in Ti in the Mersin ophiolite. Absence of zoning and consistent compositions in the cumulus and intercumulus phases indicate slow cooling and extensive subsolidus reequilibration (Burns, 1985). These features support also crystallization at high pressures.

The Al_2O_3 content of the clinopyroxene against Mg number for ultramafic and gabbroic cumulates is plotted in Figure 3.19c. The clinopyroxenes from ultramafic cumulates show low amount of Al_2O_3 (<4 wt%) and plot approximately perpendicularly to the trend of Skaergaard and Semail ophiolite which are thought to be low-pressure crystallization products. The trend of clinopyroxenes is compatible with the trend of those of high-pressure peridotites from southwestern Oregons (Medaris, 1972) as well as the trend of Aleutian lower crustal units (DeBari et al., 1987; Conrad and Kay, 1984) whereas the clinopyroxenes from gabbroic rocks follow Skaergaard and Semail trend (Fig. 3.19c). Furthermore, Al (VI) versus Al (IV) plot of clinopyroxenes, which allows to define high-low pressure crystallization (Aoki and Kushiro, 1968), are in the field of granulites and high pressure xenolites (Fig. 3.19d).

3.4.7.4. Orthopyroxene

Orthopyroxenes are absent in the ultramafic cumulates and rarely observed in the high level gabbroic cumulates as intercumulus phase (Table 3.8). They are hypersthene in composition (Fig. 3.18). The Mg number ($Mg\#_{68-77}$) of orthopyroxenes is lower and they are Fe-enriched. Cr_2O_3 content of orthopyroxenes is negligible again suggesting Cr decrease in the basaltic liquid with differentiation. Al_2O_3 content (1.4-1.9 wt%) is slightly lower than the coexisting clinopyroxenes. The same features have been observed in the Tonsina complex and interpreted as low pressure igneous intrusion (DeBari and Coleman, 1989).

3.4.7.5. Plagioclase

In gabbroic cumulates, plagioclase which is not observed within the ultramafic cumulates is the major crystallizing phase with a highly calcic compositional range (An_{96} to An_{90}) (Table 3.9). This very limited compositional range of plagioclases in the gabbroic rocks of the Mersin ophiolite differs from those plagioclases in mid-oceanic ridge gabbros (Burns, 1985; Hébert, 1982), and similar variations have been observed in the Troodos cumulate sequence (Hébert and Laurent, 1990) and arc-related plutonic rocks (DeBari and Coleman, 1986,1989; DeBari et al., 1987; Arculus and Wills, 1980; Dupuy et al., 1982; Beard, 1986; Fujimaki, 1986). The Or content of plagioclases in the gabbros is negligible (less than 0.1 wt%). Or-poor plagioclases are also reported from the Troodos ophiolite

Table 3.8. Representative orthopyroxene analyses from the mafic cumulates.

	Mafic cumulates					
	Leuco-gabbro					
No	28-1c	28-3c	35-1c	35-4c	35-7c	35-8c
SiO2	53.01	53.05	54.43	54.55	54.53	54.48
Al2O3	1.40	1.62	1.86	1.93	1.63	1.59
TiO2	0.07	0.13	0.07	0.04	0.05	0.08
FeO*	20.02	19.31	14.93	14.54	15.20	14.72
MnO	0.33	0.43	0.45	0.36	0.32	0.38
MgO	23.72	23.65	27.74	27.37	27.83	27.29
Cr2O3	0.04	<	<	0.07	<	<
CaO	1.01	1.28	0.80	0.84	0.74	0.82
Na2O	<	0.02	0.03	<	0.02	<
K2O	<	0.01	<	0.02	0.01	<
Total	99.60	99.50	100.31	99.72	100.33	99.36
Si	1.91	1.90	1.95	1.93	1.95	1.90
Al IV	0.06	0.07	0.05	0.07	0.05	0.07
Al VI	0.00	0.00	0.03	0.01	0.02	0.00
Ti	0.00	0.00	0.00	0.00	0.00	0.00
Fe	0.60	0.58	0.45	0.43	0.45	0.43
Mn	0.01	0.01	0.01	0.01	0.01	0.01
Mg	1.28	1.26	1.48	1.44	1.48	1.42
Cr	0.00	<	<	0.00	<	<
Ca	0.04	0.05	0.03	0.03	0.03	0.03
Na	<	0.00	0.00	<	0.00	<
K	<	0.00	<	0.00	0.00	<
En. (100*Mg/Mg+Fe+Ca)	66.14	66.35	75.09	75.33	75.08	75.07
Fs. (100*Fe/Mg+Fe+Ca)	31.83	31.07	23.36	23.01	23.49	23.31
Wo. (100*Ca/Mg+Fe+Ca)	2.02	2.58	1.56	1.66	1.43	1.62
Mg# (100*Mg/Mg+Fe)	68.03	68.56	76.68	77.05	76.74	76.72

Number of ions on the basis of 6 (O), Total Fe is expressed as FeO*, "<" is below detection limit

(Hébert and Laurent, 1990), the Lesser Antilles (Arculus and Wills, 1980), the Peninsular Ranges Batholiths (Smith et al., 1983).

Origin of calcic plagioclase has been outlined in the literature in following ways such as experimental work carried out on the Albite-Anorthite-water system (Johannes, 1978) showed that high water pressure could cause plagioclase compositions to be anorthite-rich. Moreover Arculus and Wills (1980) also noted that hydrous basaltic melts crystallize more anorthitic plagioclase than anhydrous melts.

Table 3.9. Representative plagioclase analyses from the mafic cumulates.

	Mafic cumulates						
	G+ol		Gabbro		Leuco-gabbro		Anorthosite
No	21-10c	36-5c	24-4c	31-6c	28-2c	35-3c	325-6c
SiO2	43.93	44.30	44.38	44.47	45.02	43.74	44.83
Al2O3	35.53	35.15	35.60	35.13	34.45	35.54	34.41
TiO2	<	0.01	<	<	0.02	0.02	0.02
FeO*	0.16	0.23	0.25	0.21	1.09	0.24	0.44
MnO	<	<	<	<	0.02	0.02	0.05
MgO	<	<	<	<	0.05	0.01	0.04
CaO	20.00	19.66	19.03	18.74	18.64	19.41	18.85
Na2O	0.46	0.61	0.71	0.89	1.08	0.57	0.87
K2O	<	<	0.01	<	0.02	<	<
Total	100.08	99.96	99.98	99.45	100.39	99.55	99.51
Si	2.03	2.05	2.05	2.07	2.07	2.03	2.08
AlIV	0.97	0.95	1.94	1.92	0.93	0.97	0.92
AlVI	0.96	0.96			0.94	0.97	0.96
Ti	<	0.00	<	<	0.00	0.00	0.00
Fe	0.01	0.01	0.01	0.01	0.04	0.01	0.02
Mn	<	<	<	<	0.00	0.00	0.00
Mg	<	<	<	<	0.00	0.00	0.00
Ca	0.99	0.97	0.94	0.93	0.92	0.96	0.94
Na	0.04	0.05	0.06	0.08	0.10	0.05	0.08
K	<	<	0.00	<	0.00	<	<
Ab (100*Na/(K+Ca+Na)	4.00	5.32	6.29	7.92	9.48	5.05	7.71
An (100*Ca/(K+Ca+Na)	96.00	94.68	93.66	92.06	90.41	94.95	92.29

Number of ions on the basis of 16 (O), Total Fe is expressed as FeO*, G+ol: Gabbro with olivine
"<" is below detection limit

3.4.8. Evidence for high pressure fractionation

Several aspects of mineral compositions in the ultramafic-mafic cumulates of the Mersin ophiolite show distinct characteristics relative to low pressure MORB type parental magma (Dungan et al., 1978; Fisk et al., 1980; Elthon, 1981). The main characteristics of low pressure (1-atm) phase relationships are that large amount of olivine fractionation with or without plagioclase prior to pyroxene crystallization depletes the residual liquids in MgO, the Mg# number of coexisting clinopyroxene and olivine is generally low (<82) and orthopyroxene has an even lower Mg# (<74) (Elthon et al., 1982). Moreover low pressure crystallization of MORBs would yield dunites, troctolites and olivine gabbros (Elthon et al., 1982; Pearce et al., 1984). The ultramafic rocks in the Mersin ophiolite are in contradiction with traditional low pressure crystallization order by having dunites, wehrlites, clinopyroxenites and gabbros. The high Mg# of the olivines (89.3-80), clinopyroxenes (95-77) and orthopyroxenes (77-68) in the ultramafic-mafic cumulates and high An content of plagioclase (96-90) in gabbroic rocks clearly demonstrate the incompatibility of crystallization in low pressure MORB type magma. In Figure 3.20, the Mg#'s of coexisting olivines and clinopyroxenes are shown. It can be obviously seen that the data from the Mersin ophiolite differ from the 1-atm experiment field and overlaps with the field of high pressure mantle xenolites (7-10 kbar) and North Arm Mountains which has been thought to have formed in a high pressure arc (Suprasubduction) environment (Elthon et al., 1982; Elthon, 1991). The high pressure crystallization of ultramafic and mafic phases is also supported by very limited cryptic variation through 3 km thick section (Parlak et al., 1995a).

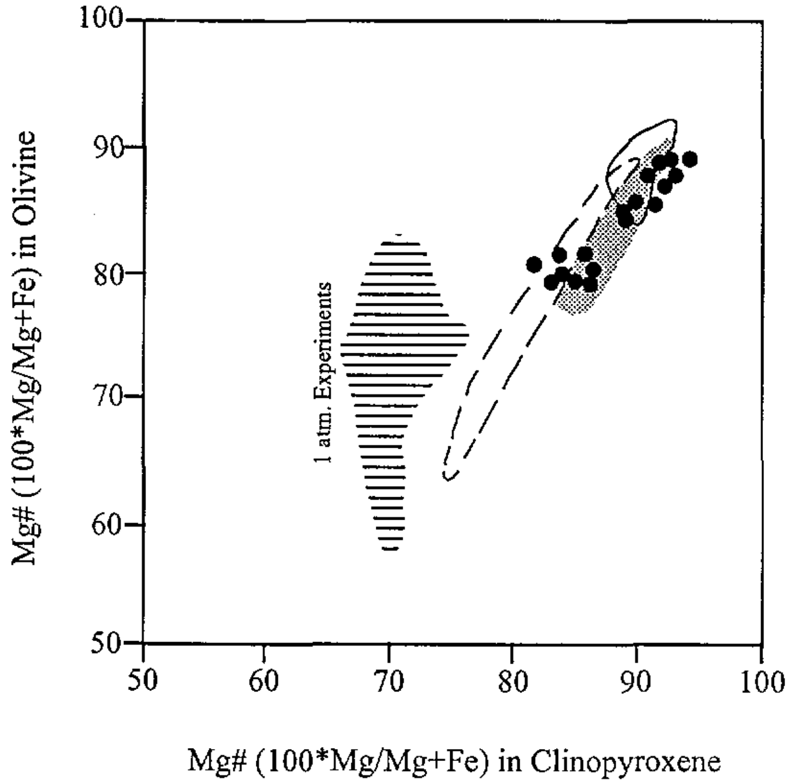

Figure 3.20. Mg# (100*Mg/Mg+Fe) of coexisting olivine and clinopyroxene in the ultramafic and mafic cumulates (filled circle) from Mersin ophiolite. Dashed line represents oceanic ultramafic and mafic cumulates, solid line indicates high-pressure mantle xenoliths. Dotted area shows the Bay of Island ophiolite field. Horizontally lined area shows experimentally determined 1-atm phase equilibria boundaries of MORBs. The fields are after Elthon et al. (1982).

Having unzoned and compositionally constant pyroxenes in cumulus and intercumulus minerals may indicate slow cooling in the magma chamber of the Mersin ophiolite. Flower et al. (1977) concluded that slowly cooling and unzoned minerals may occur in a high pressure crystallization environment likely at the base of an island arc. The existence of high magnesian olivine and pyroxene and the absence of plagioclase in ultramafic rocks may suggest high pressure ($\approx$10 kbars) crystallization of basaltic melt (Green and Ringwood, 1967; Elthon et al., 1982; Burns, 1985). This predicted high pressure crystallization value seems to be compatible with the Mersin ophiolite case.

3.4.9. Tectonic implications

It has been well documented in the study of Pearce et al. (1984) that Cretaceous ophiolites in the eastern Mediterranean including Troodos Massif, Oman, Baer Bassit (Syria), Zagros ophiolites (Iran) and ophiolitic massifs in Turkey show arc affinities, therefore all these massifs are so-called "Supra-Subduction Zone" ophiolites (Pearce et al., 1984; Robertson, 1994).

It was suggested that gabbroic rocks, occurring within an arc-like environment, differ from their oceanic equivalents in terms of their high Ca-content in plagioclase (Burns, 1985). Compositions of co-existing plagioclase and clinopyroxene in the cumulate gabbros are plotted in Figure 3.21a. It is clearly shown that highly calcic plagioclases and magnesian clinopyroxenes in the gabbroic rocks from the Mersin ophiolite are well correlated with arc gabbro field. Figure 3.21b presents the covariation of olivine and plagioclase from the Mersin, Troodos (Hébert and Laurent, 1990) and other well established tectonic settings (Hébert, 1985; Beard, 1986). The mineral compositions of the Mersin plutonic rocks, which present a very a limited fractionation degree in terms of An and Fo content, undoubtly differ from the compositions of the oceanic cumulate spectrum showing high fractionation trend (Fig. 3.21b). The Mersin ophiolite show close similarity to particular trend of Lesser Antilles (Arculus and Wills, 1980), Agrigan volcano in Mariana arc (Stern, 1979) and Troodos trend which is interpreted to have formed in an arc environment (Hébert and Laurent, 1990). The major, trace and REE chemistry as well as the mineral chemistry of the tholeiitic basalts in the Mersin ophiolite also suggest arc affinity (Parlak et al., 1995c). The magma chambers at the base of the immature arc form mafic and ultramafic cumulate sequences that crystallize at high pressures in which olivine+spinel are followed by pyroxene then plagioclase whereas in MORB ophiolites plagioclase crystallizes before pyroxene (Burns, 1985; Coleman, 1986). In the plutonic suite of the Mersin ophiolite, basal dunitic layers pass into wherlites and clinopyroxenites which show the same conditions as at the base of an island arc magma chambers like in Border Range Ultramafic and Mafic Complex (Burns, 1985).

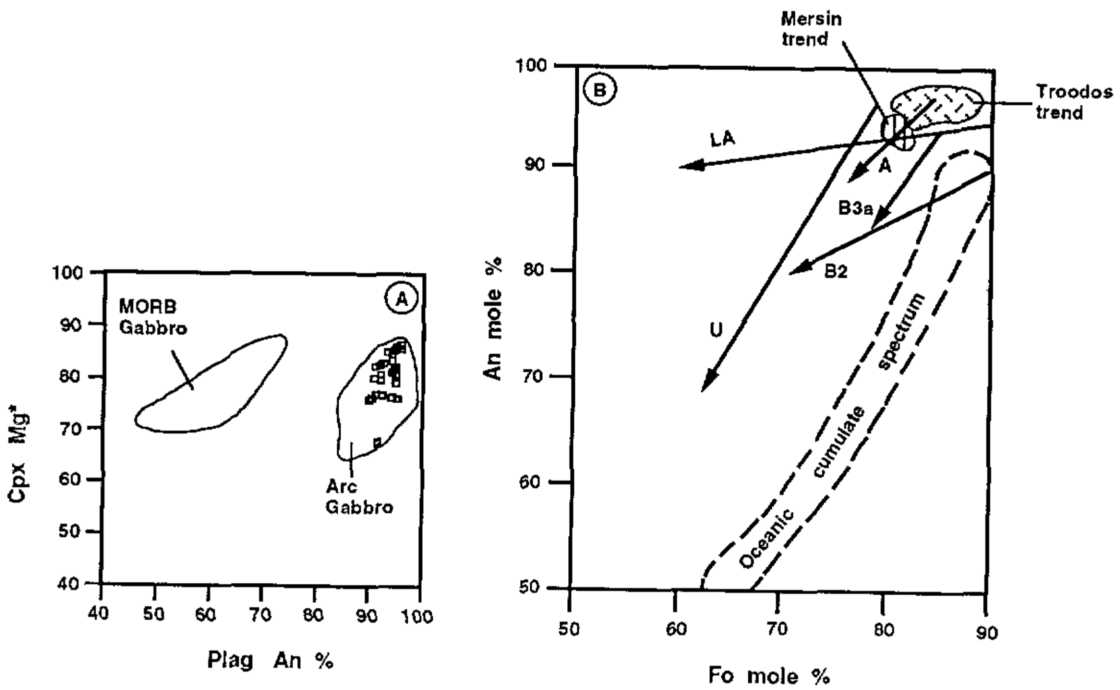

Figure 3.21. a. Composition of coexisting plagioclase and clinopyroxene in the cumulate gabbros (square) from the Mersin ophiolite. Fields of Morb and Arc gabbros are from Burns (1985). Note that cumulate gabbros well fit within the arc-gabbro field. **b.** Co-variation of olivine and plagioclase from the plutonic suite of the Mersin ophiolite and known tectonic settings (Hébert, 1985; Beard, 1986; Hébert and Laurent, 1990). LA: Lesser Antilles (Arculus and Wills, 1980), A: Agrigan volcano-Mariana arc (Stern, 1979), B2 and B3a: Boisa volcano, Papua (Gust and Johnson, 1981), U: Usa volcano, Japan (Fujimaki, 1986).

3.4.10. Conclusions

(1)The phase and cryptic variations in the ultramafic and mafic cumulates show cm- or m-scale repeated cyclicity that is evidence for periodic replenishment of the magma chamber beneath the Mersin ophiolite.

The processes which occurred during the magmatic activity in the Mersin ophiolite magma chamber could be summarized as follows;

a) Grading and size layering suggest gravity-controlled deposition in cumulates. Igneous lamination and cm-scale rhytmic layering are common and no cross-bedding is seen, suggesting no significant magmatic currents in the chamber.

b) Limited overall cryptic variation in the thick cumulate section indicates crystallization from a magma relatively uniform in composition and multiple replenishment of the magma chamber by primitive melt.

c) High Mg/Fe ratios of the mafic-ultramafic phases, highly calcic plagioclase and absence of any evidence of zoning in the cumulus and intercumulus minerals demonstrate a crystallization processes under high temperature conditions.

(2) Major and trace element geochemistry of the ultramafic and mafic cumulates suggest an arc-like tectonic environment for the generation of the Mersin ophiolite oceanic lithosphere. This data is well correlated with the geochemistry of the co-genetic basaltic units that indicates also arc-like/suprasubduction zone tectonic environment.

(3) Mineral chemistry of ultramafic and mafic cumulates indicates high-pressure ($\approx$10kb) crystallization from a basaltic melt. This evidence is based on the crystallization order of the cumulus and intercumulus minerals (olivine$\pm$chromian spinel+clinopyroxene+plagioclase and orthopyroxene), absence of plagioclase in the ultramafic rocks, presence of Ca-rich plagioclase (An_{95-91}), and highly magnesian olivine (Fo_{91-80})-clinopyroxene ($Mg\#_{95-77}$).

(4) Petrological, mineralogical and field evidences suggest following evolutionary scenario for the Mersin ophiolite: Opening of the South Atlantic around Early-Late Cretaceous (Smith et al., 1981), compressional regime started between Afro-Arabia and Eurasia in the eastern Mediterranean region. North dipping subduction of the southern segment of the Neo-Tethyan ocean started during Mid-Cretaceous (Sengör and Yılmaz, 1981; Aktas and Robertson, 1984; Dilek and Moores, 1990). The Mersin ophiolite formed above this intra oceanic subduction zone some time at the begining of Late Cretaceous. Soon after the formation of the oceanic lithosphere, the Mersin ophiolite was emplaced onto the Tauride active continental margin during end of late Cretaceous-early Paleocene time. Neoautochthonous sediments, late Paleocene in age, cap ophiolite body with angular unconformity indicating cessation of the ophiolite obduction in the study area (Avsar, 1992).

3.5. Isolated dike swarms

3.5.1. Petrographic summary

22 diabase dykes were analysed in terms of major, trace and rare earth element concentrations. The primary mineral assemblages of the dykes have been modified by hydrothermal alteration processes characterized by hornblendes that are generally observerd at the rim of clinopyroxenes, albite, sericite, chlorite, epidote. These dykes which generally exhibite doleritic to ophitic textures mainly consist of plagioclase (50-60%), clinopyroxene (25-30%) and brown- to green-amphibole (15-20%). Minor amount of anhedral quartz ($\approx$5%) occupies the interstices of plagioclase and clinopyroxene. The dominantly holocrystalline texture and presence of weak chilled margin features of these diabase dykes

suggest that by the time dyke injection occurred when the main ophiolite body and the metamorphic sole were still hot. This observation is supported by the limited time interval between the formation of the metamorphic sole (96-92 Ma) and beginning of dyke emplacement (≈90 Ma).

3.5.2. Analytical method

Major and trace element analyses have been carried out for 22 isolated dyke swarms. 3 selected dyke samples have been analysed for REE concentrations. Major and trace element analyses were performed by XRF on glass beads fused from ignited powders to which $Li_2B_4O_7$ was added (1:5), in a platinum-gold crucible at 1150^o C. REE analysis was done by ICP-AES technique (Voldet, 1993).

3.5.3. Whole rock chemistry

Major, trace and REE contents of the isolated diabase dykes are presented in Table 3.10. The dyke rocks are characterized by high SiO_2 content (48 to 54%), low TiO_2 (0.7-1.2 %), and high MgO (4.8 to 7.5%). Trace element contents vary in Zr (17-79 ppm), Y (10-36 ppm), Nb (1-7 ppm) and V (253-359 ppm). On the basis of SiO_2 and incompatible trace element ratios (Zr/TiO_2) (Winchester and Floyd, 1977) mafic dyke swarms are defined as sub-alkali basalts (Fig. 3.22a). TiO_2 versus FeO*/MgO plot of the dyke swarms in the Mersin ophiolite exhibit no increase with increasing FeO*/MgO ratios (Fig. 3.22b), showing main trend of island arc tholeiite and calc-alkaline suites (Miyashiro, 1973). Selected incompatible trace elements, in particular Zr, Nb, Y, Ti, V and REE have been shown to be the least mobile during alteration processes (Thompson 1973; Pearce and Cann 1973; Humphris and Thompson 1978; Hart, 1970). These incompatible elements are good indicators to characterize petrological affinities and the past tectonic environment of volcanic rocks (Pearce and Cann 1973; Floyd and Winchester 1975; Pearce and Norry 1979). Abundance of incompatible high field strength elements (Zr, Y, Ti, V) in island arc basalts are thought to be lower than in back-arc basin basalts, whereas incompatible trace element ratios such as Ti/Zr, V/Ti and Sc/Y are higher in island arc basalts (Woodhead et al., 1993). This features are attributed to various reasons such as higher degrees of partial melting of more depleted source compositions or higher bulk (D) solid/liquid distribution coefficient values during partial melting, or effect of both two factors (Woodhead et al., 1993).

Y and Zr contents of the dyke swarms show linear fractionation trend with increasing TiO_2 (Fig. 3.23a,b). These incompatible element abundance in the dyke swarms are clearly lower than in the selected back-arc basin basalts from the western Pacific whereas

Table 3.10. Major, trace and REE analyses of the dike swarms in tectonites, cumulates (*) and metamorphic sole (**) of the Mersin ophiolite.

Sample	7	33	38*	47*	48*	49*	63	80	82	85	87	91	100	104	115	117	121	122**	128**	129**	130**	227**
SiO2	48.10	48.80	52.50	49.60	45.50	52.90	50.00	52.00	52.60	54.40	49.80	50.90	50.00	47.80	50.60	50.80	51.50	52.70	52.90	51.20	51.30	52.30
Al2O3	14.90	15.40	15.70	15.20	15.40	15.50	15.30	15.60	15.30	15.70	16.20	15.80	14.50	15.40	15.30	15.70	15.50	16.00	15.80	15.40	15.40	15.70
TiO2	1.08	1.07	0.92	0.39	0.52	0.39	0.87	1.04	1.06	0.70	0.85	0.78	0.70	0.88	1.20	1.18	0.66	0.72	0.78	0.89	0.92	0.76
FeO	10.20	10.00	10.10	9.35	9.70	9.32	9.82	10.50	10.80	9.82	9.24	11.30	10.10	10.50	11.30	11.20	9.19	9.91	9.40	9.56	9.98	9.79
CaO	13.10	9.94	10.20	13.30	17.60	11.50	9.55	10.50	9.26	9.37	9.32	9.03	7.37	9.52	6.15	9.60	8.45	9.98	9.54	10.20	9.86	9.51
MgO	7.20	7.35	6.23	7.52	7.40	7.28	6.66	5.26	5.62	5.43	6.88	6.02	5.99	6.21	5.93	4.84	5.18	6.31	6.27	7.39	7.25	6.05
Na2O	2.36	3.32	2.54	1.53	0.43	1.37	4.33	2.90	2.86	2.01	4.00	4.70	6.31	5.21	5.68	4.66	5.90	1.11	1.40	1.50	3.41	1.50
K2O	0.10	0.27	0.04	0.29	0.04	0.11	0.14	0.36	0.41	0.41	0.18	0.48	0.14	0.21	0.17	0.50	0.10	0.73	1.18	1.34	0.12	1.49
MnO	0.17	0.16	0.16	0.15	0.16	0.15	0.16	0.17	0.16	0.15	0.15	0.18	0.15	0.16	0.18	0.17	0.14	0.15	0.15	0.16	0.17	0.16
P2O5	0.11	0.10	0.09	0.03	0.04	0.02	0.08	0.09	0.09	0.07	0.08	0.06	0.07	0.08	0.11	0.11	0.06	0.06	0.06	0.07	0.09	0.06
L.O.I.	2.36	2.76	1.98	2.32	3.30	1.26	2.69	1.76	1.27	1.79	3.00	1.60	3.88	3.43	3.02	1.34	3.10	1.98	2.63	1.94	1.58	2.12
Total	99.68	99.20	100.00	99.60	100.00	99.70	99.70	100.00	99.40	99.80	99.70	101.00	99.20	99.40	99.70	100.00	99.80	99.70	100.00	99.60	100.00	99.50
ppm																						
Ba	50	46	35	13	2	43	54	0	89	42	0	0	56	76	78	0	46	57	833	361	62	1456
Ni	57	53	36	56	51	43	54	34	33	34	70	37	40	39	17	21	35	55	52	55	51	50
Cr	107	178	39	117	98	94	103	30	59	38	145	42	36	94	19	18	45	124	157	162	161	155
V	272	285	295	253	260	249	307	307	321	308	255	341	320	323	359	327	278	310	308	270	265	287
Nb	6	1	7	1	7	1	4	1	1	1	1	1	1	1	1	1	1	3	1	0	3	3
Zr	70	79	59	17	19	20	52	63	60	40	66	36	61	47	67	65	41	41	44	56	61	43
Y	28	27	24	14	14	10	17	34	19	24	23	15	25	27	33	36	21	13	16	21	23	16
Sr	242	325	159	91	10	51	151	140	95	82	376	148	502	104	79	144	226	116	93	116	188	100
Rb	1	6	2	7	2	12	7	4	16	5	6	3	6	4	7	1	3	28	28	30	9	32
La	4.1							3.9										3.6				
Ce	8.9							8.4										n.d				
Nd	6.3							7.5										6.2				
Sm	2.2							1.9										1.4				
Eu	0.8							0.8										0.5				
Gd	3.1							3.2										n.d				
Dy	3.6							3.8										2.8				
Ho	0.7							0.8										0.6				
Er	2.4							2.5										1.9				
Tm	0.3							0.4										n.d				
Yb	2.0							2.2										1.7				
Lu	0.3							0.3										0.3				

Total Fe is expressed as FeO, n.d: is not determined

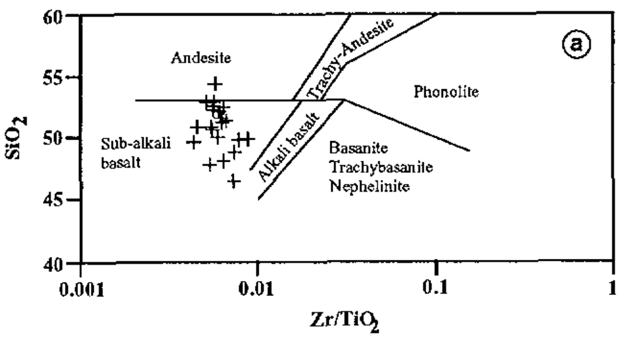

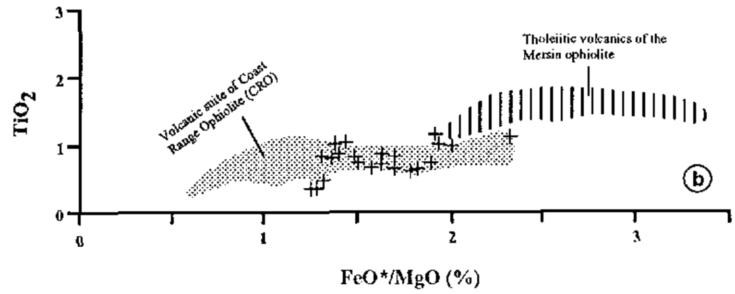

Figure 3.22. a. SiO_2 versus Zr/TiO_2 diagram of the dike swarms in the Mersin ophiolite (After Winchester and Floyd, 1977). **b.** TiO_2 versus FeO*/MgO weight ratio for the dike swarms. Note that dike swarms in the Mersin ophiolites show no increase with increasing FeO*/MgO, similar to volcanic suites of the Coastal Range and Mersin ophiolite.

the concentration of Zr and Y show similar values in Marianas, Vanuatu island-arc basalts (Fig. 3.23a-b). High V/Ti ratios in the dyke swarms range from 0.03 to 0.1. High V content might be explained as a result of high oxygen fugacity of arc magmas due to volatile released from descending lithosphere in subduction zones (Shervais, 1982; 1990). Additional support for the nature of the dyke swarms is that Ti/Zr ratios ranging from 164.1 to 68.8 exhibit progressive decreasing features with increasing Zr content. Tholeiitic dyke swarms of the Mersin ophiolite show transitional character between island arc and back-arc basin basalts of the western Pacific area (Fig. 3.23c).

Chondrite normalized REE patterns of the isolated dyke swarms are presented in Fig. 3.24. REE abundance are generally 17X or 10X higher than chondritic values. They are represented by flat-lying patterns (weak fractionation $[La/Yb]_N$ between 1.3 and 1.5) that do not resemble the depleted REE pattern of N-MORB ($[La/Yb]_N \approx 0.6$; Sun et al., 1979). This REE pattern is in good agreement with the arc-related tholeiitic volcanics ($[La/Yb]_N$ between 1.4 and 1.9) of the Mersin ophiolite (Parlak et al., 1995c). Flat-REE patterns for dyke swarms are documented in several island arc tholeiites namely Papua-New Guinea, Solomon island (Jakes and Gill, 1970). The supra-subduction zone tectonic setting of the eastern Mediterranean ophiolites is mainly represented by LREE-enriched extrusive and intrusive rocks compared to depleted N-MORB due to a subducted slab component, such as seen in Semail (Searle et al., 1980; Alabaster et al., 1982) in Oman, Troodos (Desmons et al., 1980) in Cyprus, Kizildag (Lytwyn and Casey, 1993), Guleman (Aktas and

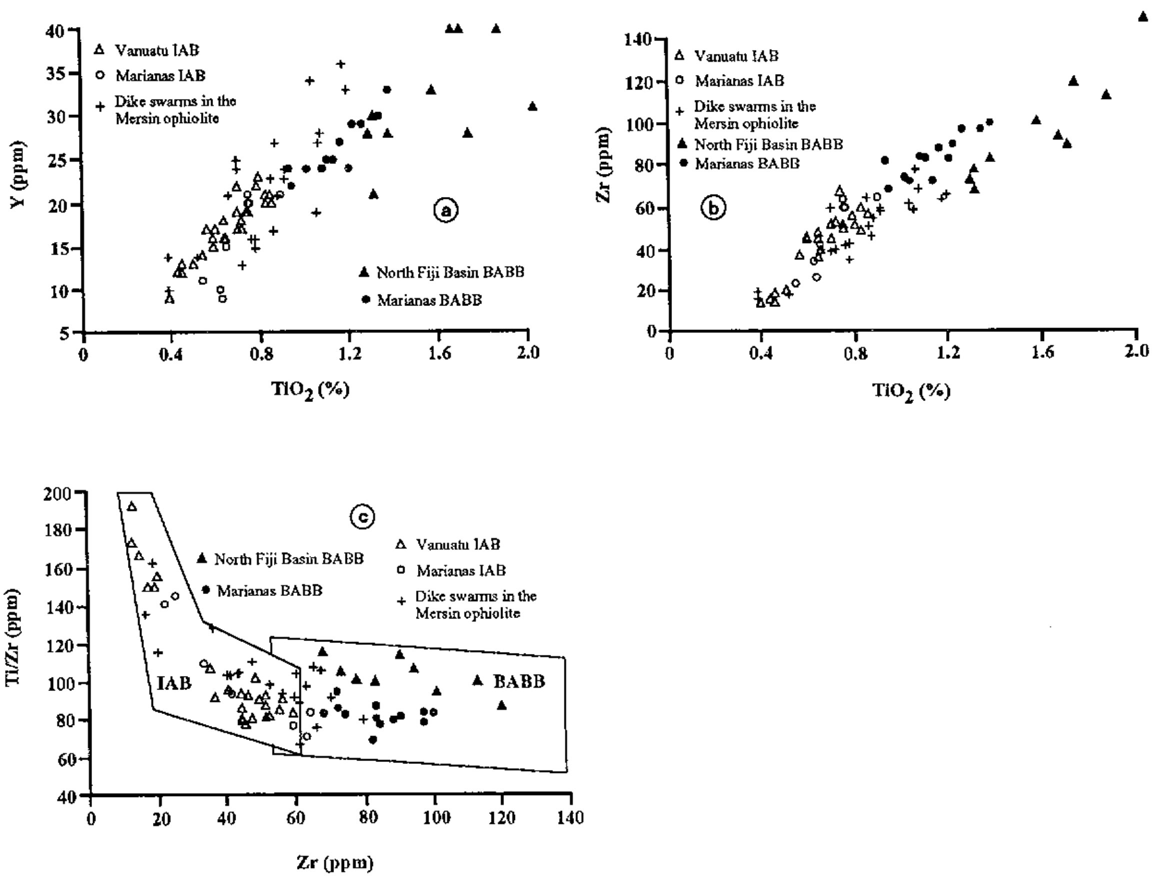

Figure 3.23. a. Y and **b.** Zr versus TiO2 for the dike swarms. Data for IAB and BABB are taken from Knittel and Oles (1995) for comparision. **c.** Ti/Zr versus Zr plot of the dike swarms in the Mersin ophiolite. Fields for IAB and BABB are from Knittel and Oles (1995).

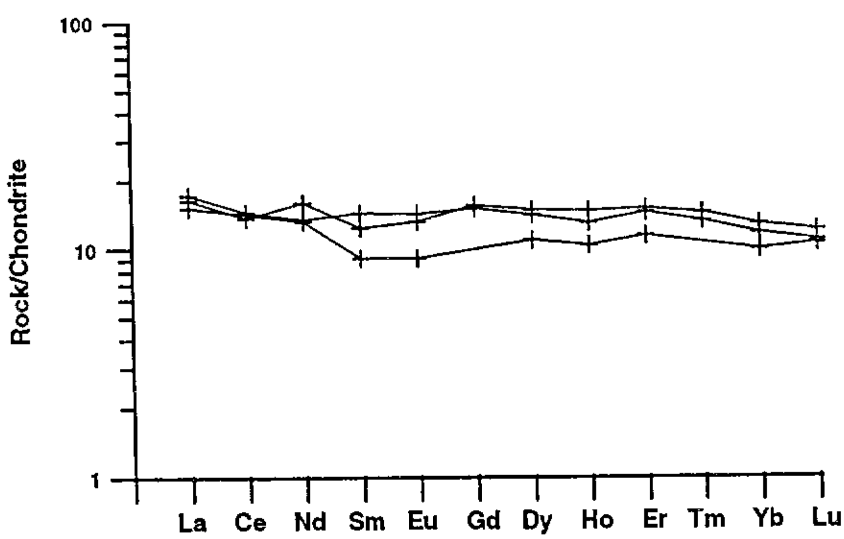

Figure 3.24. Chondrite normalized REE concentrations of the dike swarms. Chondritic values are from Sun and McDonough (1989).

Robertson, 1984) in Turkey and Baer Bassit (Parrot, 1977; Delaloye and Wagner, 1984) in Syria. In particularly Lytwyn and Casey (1995) concluded that the dyke swarms in the Pozanti-Karsanti ophiolite show a close similarity to tholeiitic basalts and basaltic andesites found in modern island-arc environment. Dilek and Thy (1992) also defined similar chemistry for the dikes of the Aladag ophiolite in southern Turkey.

Selected tectonomagmatic discrimination diagrams based on immobile elements have been used in order to determine the tectonic setting of the post-kinematic dyke swarms in the Mersin ophiolite. Ti versus V plot of Shervais (1982), dyke samples show chemical character of arc tholeiites (Fig. 3.25a). High oxygen fugacity of the basaltic magmas in arc environment increases V content due to volatile release from descending lithosphere (Shervais, 1982). Arc-related tholeiitic volcanics in the Mersin ophiolite have higher V concentrations compared to dyke swarms (Parlak et al., 1995c). In the TiO_2-MnO and P_2O_5 triangular diagram of Mullen (1983) the dyke swarms plot in the island arc tholeiite field (Fig. 3.25b).

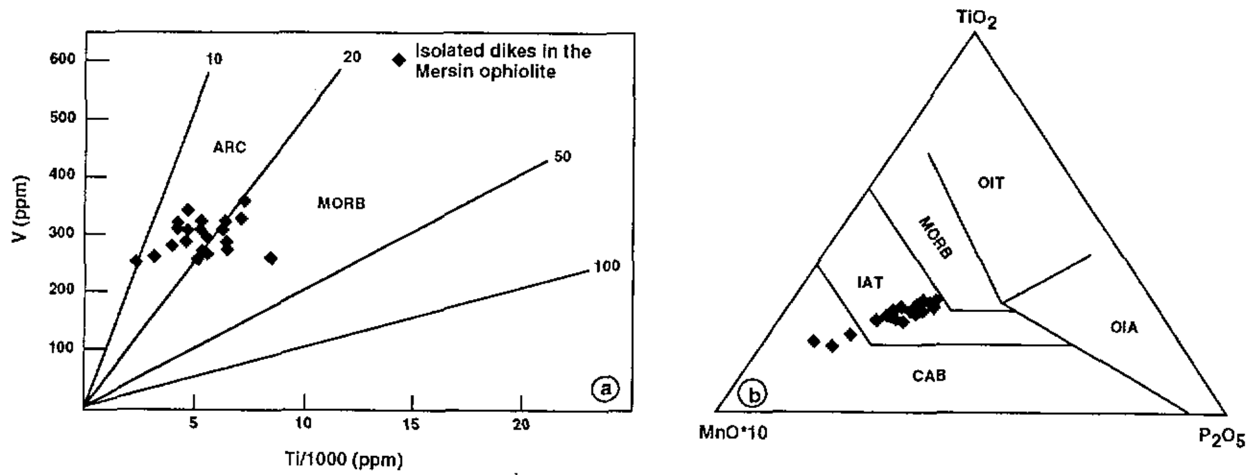

Figure 3.25. a. Plot of Ti versus V for the dike swarms of the Mersin ophiolites (After Shervais, 1982). **b.** TiO_2, MnO and P_2O_5 plot of the tholeiitic dike swarms (After Mullen, 1983).

3.5.4. Discussion and conclusion

Alternative models such as "ridge collapse, ridge subduction, roll-back and subduction zone jumping" for the metamorphic sole formation and the intrusions of mafic dyke swarms were discussed in the studies of the middle and eastern Mediterranean ophiolites (Robertson and Dixon, 1984; Spray et al., 1984; Smith and Spray, 1984). The Mersin ophiolite was generated within a supra-subduction zone environment at the beginning of late Cretaceous (Parlak et al., 1996). Decoupling of the oceanic lithosphere followed weakness zone of the spreading ridge that resulted in the formation of the metamorphic sole derived from the metamorphosed equivalents of the ocean island /or seamount basalts and related sediments (Parlak et al., 1995b). Continuation of the subduction produced dike swarms that intruded already-formed oceanic lithosphere and metamorphic sole of the Mersin ophiolite.

The whole rock geochemical character of the mafic dykes strongly suggest that arc-related melts within the mantle wedge above the intraoceanic subduction zone generated post-metamorphic dyke swarms intruding an already formed basal metamorphic sole and oceanic lithospheric units of the Mersin ophiolite.

PLATE CAPTIONS

Plate 3.1

a) Field view of the late Cretaceous tholeiitic basalts.

b) Field view of the late Cretaceous diabase feeding dikes.

c) Field view of the late Jurassic-early Cretaceous alkali basalts intercalated with cherty limestones.

d) Field view of the folded radiolarites associated with the late Jurassic-early Cretaceous alkali basalts.

Plate 3.2

a) Photomicrograph of adcumulate dunite from the base of the ultramafic cumulate.

b) Olivine-clinopyroxene adcumulate wehrlite.

c) Adcumulate clinopyroxenite, view of the coarse-grained euhedral cpx.

d) Olivine rich level in gabbric rocks showing mesocumulate texture. Olivine and plagioclase cumulus phase whereas clinopyroxene intercumulus phase.

Plate 3.3

a) Orthocumulate leucogabbro, cumulus plg and intercumulus cpx minerals.

b) Adcumulate plagioclase rich anorthosite, cpx is the intercumulus phase.

c) Stratiform choromite banding within dunite rich ultramafic cumulates.

d) Size grading in clinopyroxenite at the base of the ultramafic cumulate.

Plate 3.4

a) Magmatic lamination in the gabbroic rocks and coarse-grained olivine crystals parallel to the lamination.

b) Mineral graded layering in gabbros. Clinopyroxene rich at the bottom and plagioclase rich at the top.

c-d) Rhytmic layering in gabbros. Cm-scale plagioclase and pyroxene alternations.

Plate 3.5

a-b) Field view of the diabase dikes within the metamorphic sole of the Mersin ophiolite.

c) Field view of the diabase dike within the gabbroic cumulate.

d) Field view of the diabase dike within the mantle tectonite.

Plate 3.1

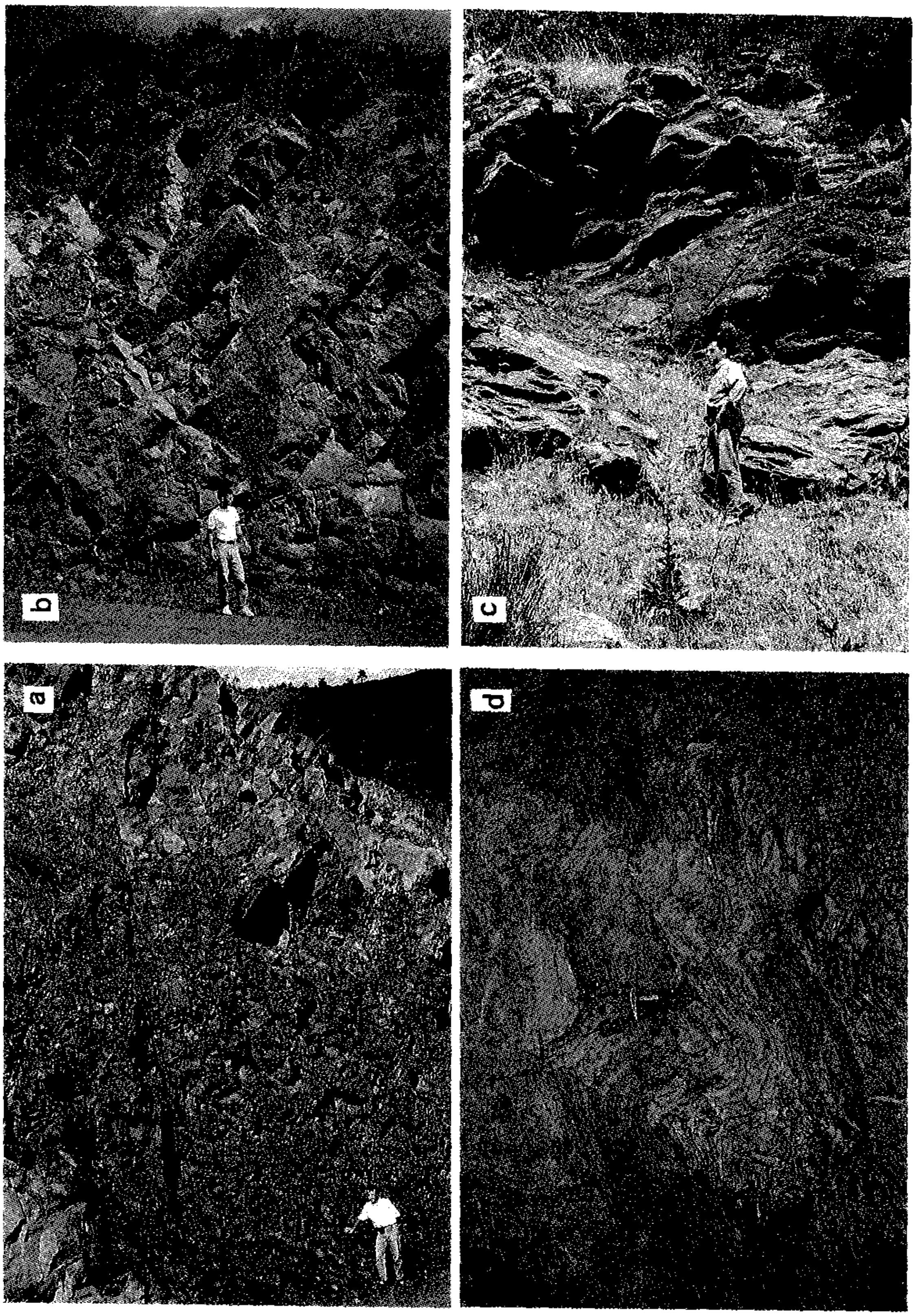

Plate 3.2

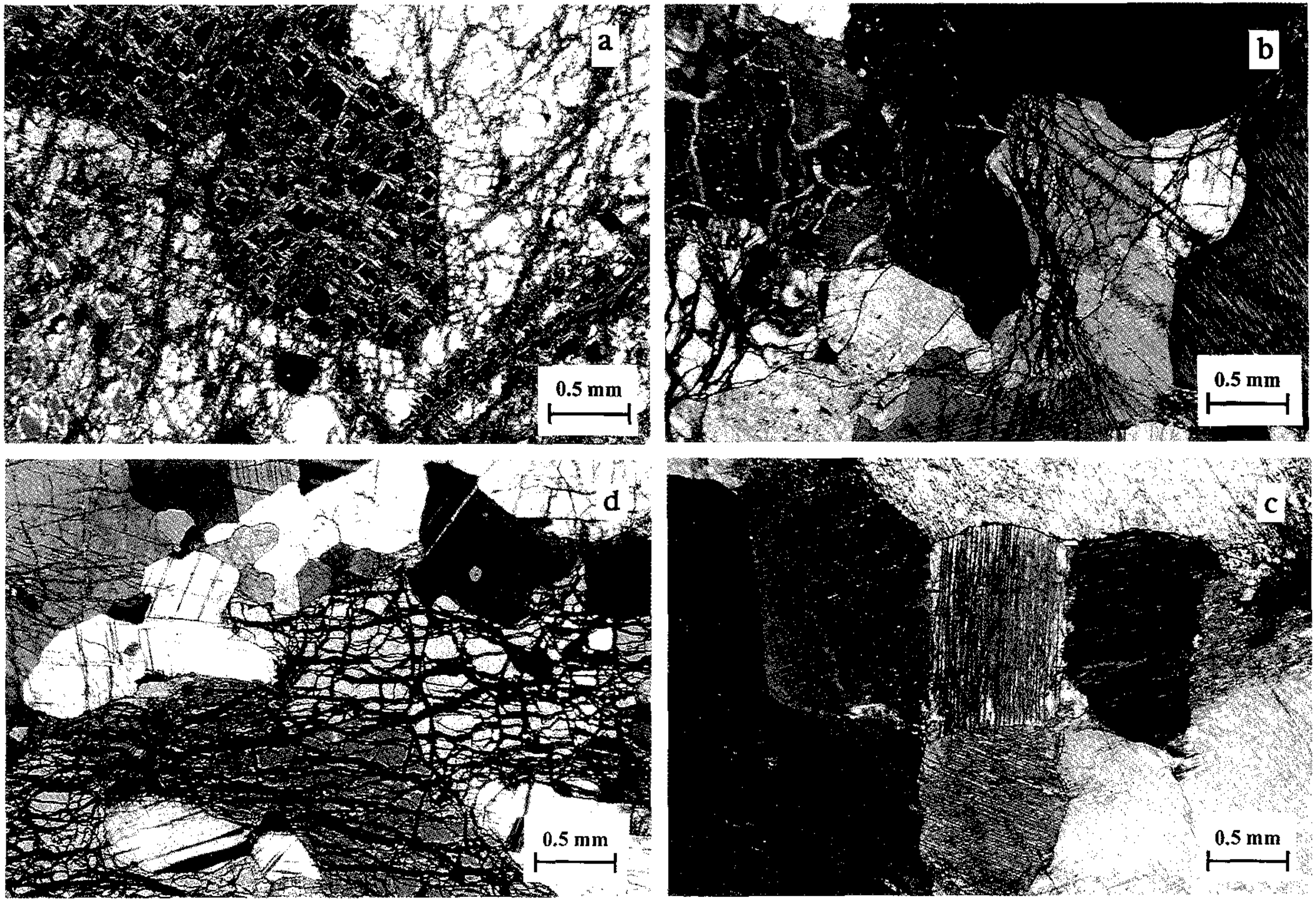

Plate 3.3

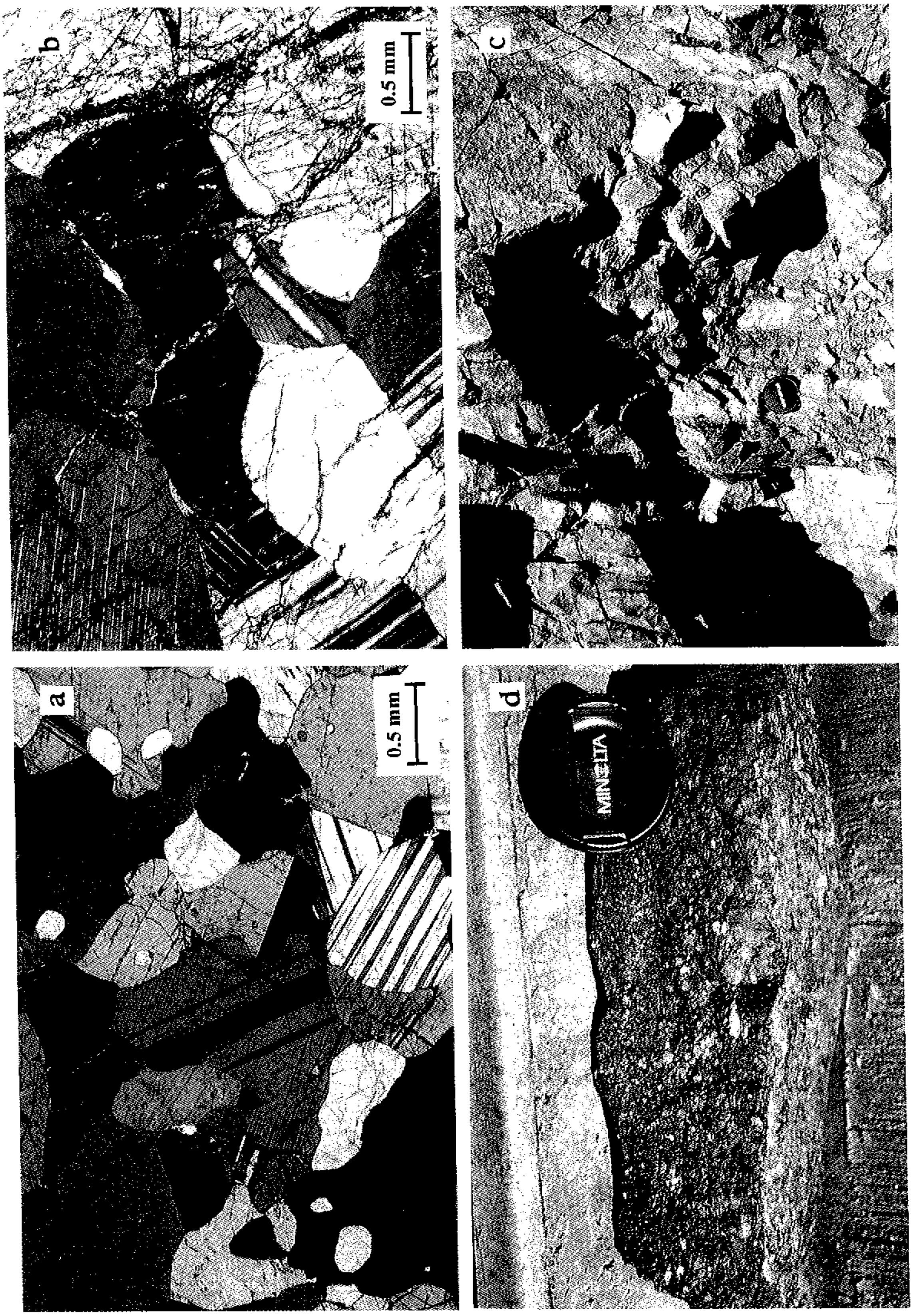

Plate 3.4

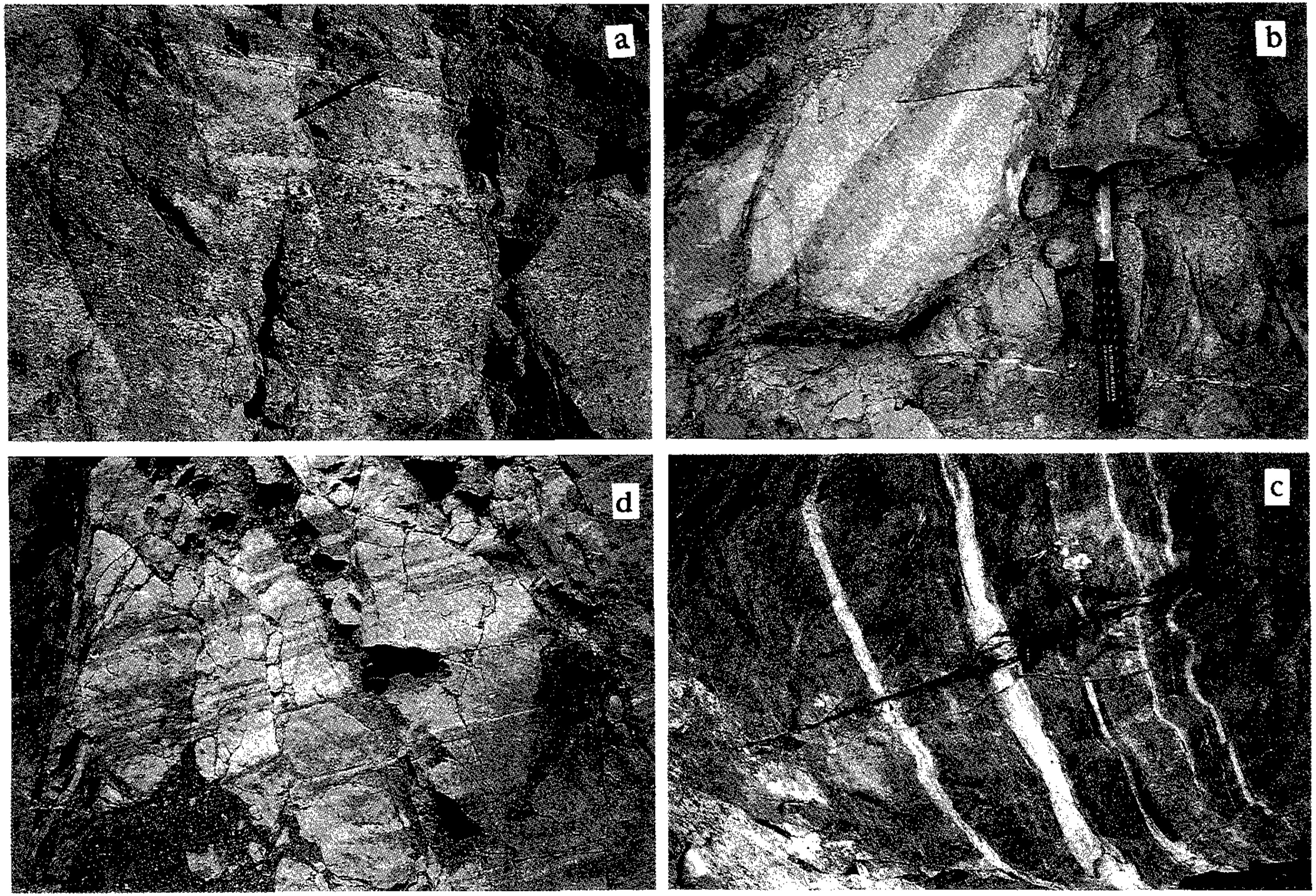

Plate 3.5

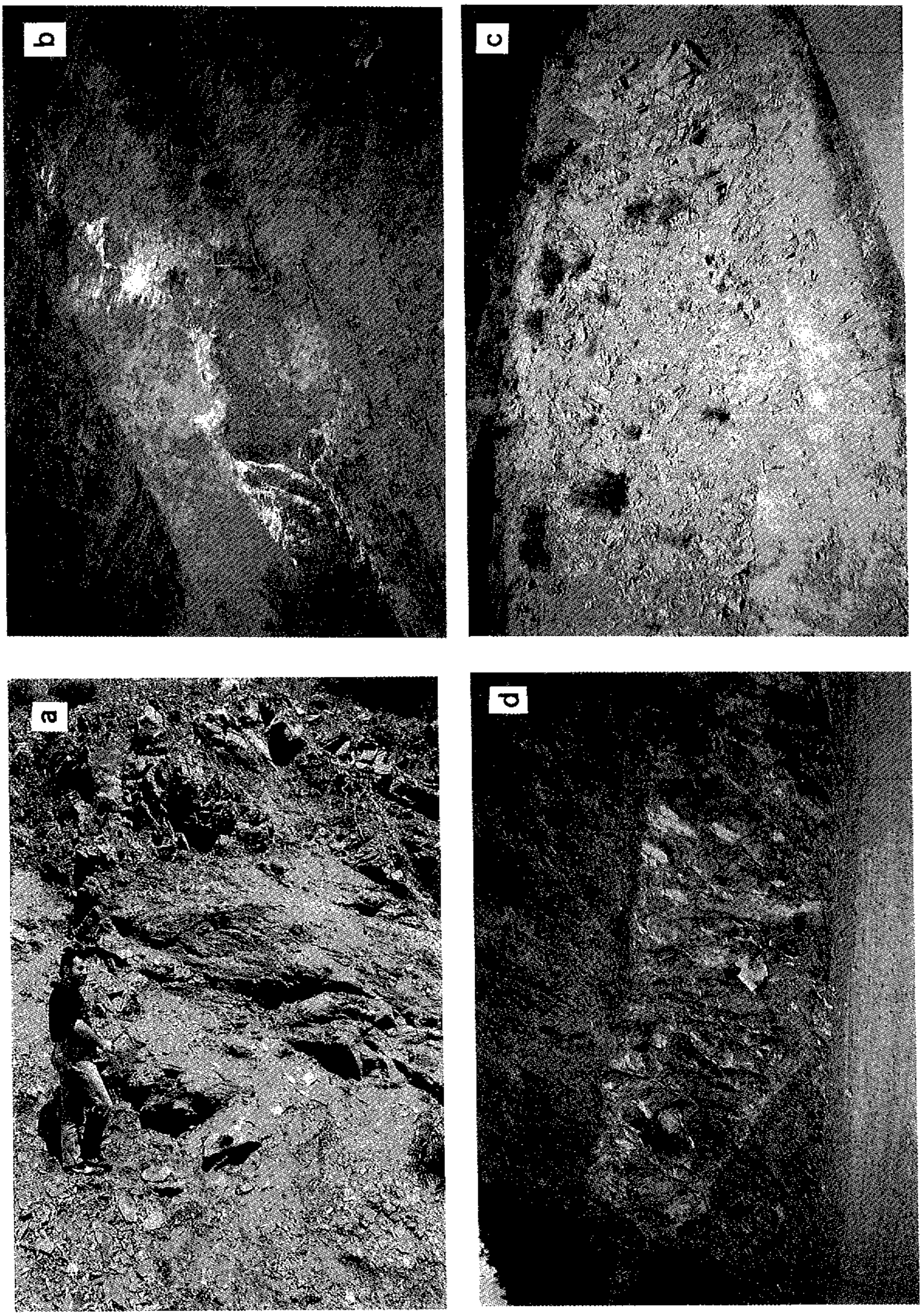

References

Aktas, G., and Robertson, A.H.F., 1984; The Maden complex, SE Turkey: evolution of a Neotethyan active margin. In: Dixon, J.E. and Robertson, A.H.F. (eds), The Geological Evolution of the Eastern Mediterranean, Geol. Soc. London Spec. Publ., 17, 375-403.

Alabaster, T., Pearce, J.A., and Malpas, J., 1982; The volcanic stratigraphy and petrogenesis of the Oman ophiolite complex. Contr. Mineral. Petrol., 81, 168-183.

Aoki, K., and Kushiro, I., 1968; Some clinopyroxenes from ultramafic inclusions in Dreiser Weiher, Eifel. Contr. Mineral. Petrol., 21, 743-749.

Arculus, R.J., and Wills, K.J.A., 1980; The petrology of plutonic blocks and inclusions from the Lesser Antilles island arc. J. Petrol., 21, 743-99.

Avsar, N., 1992; Namrun (Icel) yoresi Paleojen bentik foraminifer faunasi. MTA dergisi 114, 127-144.

Beard, J.S., 1986; Characteristic mineralogy of arc-related cumulate gabbros: Implications for the tectonic setting of gabbroic plutons and for andesite genesis. Geology, 14, 848-851.

Browning, P., 1984; Cryptic variation within the cumulate sequence of the Oman ophiolite: magma chamber dept and petrological implications. In: Gass I.G., Lippard S.J. and Shelton A.W. (eds.) Ophiolites and Oceanic lithosphere. Geol. Soc. London Spec. Publ., 13, 71-82.

Burke, W.H., Denison, R.E., Hetherington, E.A., Koepnick, R.B., Nelson, H.F., and Otto, J.B., 1982; Variation of seawater $^{87}Sr/^{86}Sr$ throughout Phanerozoic time. Geology, 10, 516-519.

Burns, L.E., 1985; The Border Ranges ultramafic and mafic complex, south-central Alaska: cumulate fractionates of island-arc volcanics. Canad. J. Earth Sci., 22, 1020-1038.

Çataklı, A.S., 1983; Assemblage ophiolitique et roches aasociées de la partie occidentale du massif de Pozanti-Karsanti, Taurus Cilicien-Turquie. These de doctorat, Nancy-France, 760p.

Church, W.R., and Riccio, L., 1977; Fractionation trends in the Bay of Island ophiolite of Newfoundland: polycyclic cumulate sequences in ophiolites and their classification. Canad. J. Earth Sci., 14, 1156-1165.

Coish, R.A., and Taylor, L.A., 1979; The effects of cooling rate on texture and pyroxene chemistry in DSDP leg 34 basalt: A microprobe study. Earth and Planet. Sci. Lett., 42, 389-398.

Coleman, R.G., 1971; Plate tectonic emplacement of upper mantle peridotites along the continental edges. J. Geophys. Res., 76, 1212-1222.

Coleman, R.G., 1986; Ophiolites and accretion of the North American Cordillera. Bull. Soc. géol. France, 8, 961-968.

Conrad, W.C., and Kay, R.W., 1984; Ultramafic and mafic inclusions from Adak island: Crystallization history and implications for the nature of primary magmas and crustal evolution in the Aleutian arc. J. Petrol., 25, 88-125.

DeBari, S.M., and Coleman, R.G., 1986; Petrologic aspects of gabbros from the Tosnia complex, Chugach mountains, Alaska: Evidence for deep magma chambers under and island arc. Geol. Soc. Amer. Abstracts and Programs, 18, 99p.

DeBari, S.M., Kay, S.M., and Kay, R.W., 1987; Ultramafic xenoliths from Adagdak Volcano, Adak, Aleutian islands, Alaska: Deformed igneous cumulates from the moho of an island arc. J. Geol., 95, 329-41.

DeBari, S.M., and Coleman, R.G., 1989; Examination of the deep levels of an island arc: evidence from the Tonsina ultramafic-mafic assemblage, Tonsina, Alaska. J. Geophys. Res., 94, 4373-4391.

Delaloye, M., and Wagner, J.J., 1984; Ophiolites and volcanic activity near the western edge of the Arabian plate. In: Dixon, J.E. and Robertson, A.H.F. (eds.). The Geological Evolution of the Eastern Mediterranean. Geol. Soc. London Spec. Publ., 17, 225-233.

DePaolo, D.J., and Wasserburg, G.J., 1976; Inferences about magma sources and mantle structure from variations of $^{143}Nd/^{144}Nd$. Geophys. Res. Lett., 3, 743.

DePaolo, D.J., and Wasserburg, G.J., 1977; The sources of island arcs as indicated by Nd and Sr isotopic studies. Geophys. Res. Lett., 4, 465-468.

Desmons, J., Delaloye, M., Desmet, A., Gagny, C., Rocci, G., and Voldet, P., 1980. Trace and REE abundance in Troodos lavas and sheeted dikes, Cyprus. Ofioliti, 5, 35-56.

Dewey, J.F., and Bird, J.M., 1971; Origin and emplacement of the ophiolite suite: Appalachian ophiolites in Newfounland. J. Geophys. Res., 76, 3179-3206.

Dick, H.J.B., and Bullen, T., 1984; Chromium spinel as a petrogenetic indicator in abyssal and alpine-type peridotites and spatially associated lavas. Contr. Mineral. Petrol., 86, 54-76.

Dilek, Y., and Moores, E.M., 1990; Regional tectonics of the Eastern Mediterranean ophiolites. In: Malpas, J., Moores, E., Panayiotou, A., Xenophontos, C. (eds.). Ophiolites and oceanic crustal analogues. Proceedings of the symposium "Troodos 1987", 295-309.

Dilek, Y., and Thy, P., 1992; Structure, petrology and geochronology of mafic dike intrusions in the Tauride belt (S. Turkey) and implications for the Neotethyan paleogeography. EOS-Amer. Geophys. Union, 73, p.546.

Dungan, M.A., Long, P.E., and Rhodes, J.M., 1978; The petrology, mineral chemistry, and one atmosphere phase relations of basalts from site 395. Init. Rep. Deep Sea Drill. Proj., 45, 461-472.

Dupuy, C., Dostal, J., Marcelot, G., Bougault, H., Joron, J.L., and Treuil, M., 1982; Geochemistry of basalts from central and southern New Hebrides arcs: implication for their source rock composition. Earth Planet. Sci. Lett., 60, 207-225.

Elthon, D., 1981; 1 atm phase equilibria of basalts from the Tortuga ophiolite complex, with implications for magma chamber processes. Chapman Conference on the Generation of the Oceanic Lithosphere-AGU.

Elthon, D., Casey, J.F., and Komor, S., 1982; Mineral chemistry of ultramafic cumulates from the North Arm Mountain massif of the Bay of Island Ophiolite: Evidence for high pressure crystal fractionation of oceanic basalts. J. Geophys. Res., 87, 8717-8734.

Elthon, D., and Scarfe, C.M., 1984; High pressure phase equilibria of a high-magnesia basalt and the genesis of primary oceanic basalts. Amer. Mineralogist, 69, 1-15.

Elthon, D., Casey, J.F., and Komor, S., 1984; Cryptic mineral chemistry variation in a detailed traverse through the cumulate ultramafic rocks of the North Arm Mountain massif of the Bay of Island ophiolite, Newfoundland. In: Gass I.G., Lippard S.J. and Shelton A.W. (eds.) Ophiolites and Oceanic lithosphere. Geol. Soc. London Spec. Publ., 13, 83-97.

Elthon, D., 1987; Petrology of gabbroic rocks from the Mid-Cayman Rise Spreading Center. J. Geophys. Res., 92, 658-682.

Elthon, D., 1991; Geochemical evidence for formation of the Bay of Island ophiolite above subduction zone. Nature, 354, 140-143.

Fisk, M.R., Schilling, J.G., and Sigurdsoon, H., 1980; An experimental investigation of Iceland and Reykjanes Ridge tholeiites, I, Phase relations. Contr. Mineral. Petrol., 74, 361-374.

Floyd, P.A., and Winchester, J.A., 1975; Magma type and tectonic setting discrimination using immobile elements. Earth Planet. Sci. Lett., 27, 211-218.

Floyd, P.A., 1993; Geochemical discrimination and petrogenesis of alkalic basalt sequences in part of the Ankara melange, central Turkey. J. geol. Soc. (London), 150, 541-550.

Flower, M.F.J., Robinson, P.T., Schmincke, H.U., and Ohnmacht, W., 1977; Magma fractionation systems beneath the Mid-Atlantic Ridge at 36-37°N. Contr. Mineral. Petrol., 64, 167-195.

Fujimaki, H., 1986; Fractional crystallization of the basaltic suite of Usu volcano, southwest Hokkaido Japan, and its relationships with the associated felsic suite. Lithos, 19, 129-140.

Gamble, R.P., and Taylor, L.A., 1980; Crystal/liquid partitioning in augite: effects of cooling rate. Earth Planet. Sci. Lett., 47, 21-33.

Gass, I.G., 1967; The ultrabasic volcanic assemblages of the Troodos massif, Cyprus. In Wyllie, P.J. (ed.), Ultramafic and related rocks, John Wiley, Newyork, 121-134.

Gass, I.G., and Smewing, J.D., 1973; Intrusion, extrusion and metamorphism at constructive margins; evidence from the Troodos massif, Cyprus. Nature, 242, 26-29.

Geotimes, 1972; Penrose conference report, ophiolites. 17, 24-25.

Goldberg, E.D., 1965; Minor elements in seawater. In: Riley, J.P. and Skirrow, G. (eds.), Chemical oceanography, 1, Academic, New York.

Goode, A.D.T., 1976; Sedimentary structures and magma currents velocities in the Kalka layered intrusion, central Australia. J. Petrol. 17, 546-558.

Green, TH, and Ringwood, A.E., 1967; Genesis of basaltic magmas. Contr. Mineral. Petrol., 15, 103-190.

Hart, R.A., 1970; Chemical exchange between seawater and deep ocean basalts. Earth Planet. Sci. Lett., 9, 269-279.

Hart, S.R., and Brooks, C., 1974; Clinopyroxene matrix partitioning hemisphere mantle. Nature, 309, 753-757.

Hébert, R., 1982; Petrography and mineralogy of oceanic peridotites and gabbros: some comparisons with ophiolite examples. Ofioliti, 7, 299-324.

Hébert, R., 1985; Pétrologie des roches ignées océaniques et comparison avec les complexs ophiolitiques du Québec, de Chypre et de L'Apennin: Thèse d'Etat, Université de Bretagne Occidentale, Brest, 542p.

Hébert, R., and Laurent, R., 1990; Mineral chemistry of the plutonic section of the Troodos ophiolite: New constraints for genesis of arc-related ophiolites. In: Malpas J., Moores E., Panayiotou A. and Xenophontos C. (eds.) Ophiolites-oceanic crustal analogues. Proceedings of Troodos ophiolite symposium-1987, Cyprus. 149-163.

Hess, H.H., 1960; Stillwater igneous complex, Montana: a quantitative mineralogic study. Mem. geol. Soc. Amer., 80, 230p.

Hess, P.C., 1989; Origins of igneous rocks, Harvard University press, p. 336.

Hodges, F.N., and Papike, J.J., 1976; DSDP site 334: Magmatic cumulates from ocean layer 3. J. Geophys. Res., 81, 4135-51.

Høgdahl, O.T., Bowen, B.T. and Melson, S., 1968; Neutron activation analysis of Lanthanide elements in seawater. Advan. Chem. Ser., 73, 308-325.

Humphris, S.E., and Thompson, G., 1978; Trace element mobility during hydrothermal alteration of oceanic basalts. Geochim. Cosmochim. Acta, 42, 127-136.

Humphris, S. E., and Thompson, G., 1983; Geochemistry of REE in basalts from the Walvis Ridge: implications for its origin and evolution. Earth Planet. Sci. Lett., 66, 223-242.

Irvine, T.N., 1967; Chromian spinel as a petrogenetic indicator, part 2. petrologic applications. Canad. J. Earth Sci., 4, 71-103.

Irvine, T.N., 1980; Magmatic infiltration metasomatism, double-diffusive fractional crystallization, and adcumulus growth in the Muskox Intrusion and other layered intrusions. In: Hargraves R.B. (ed.) Physics of magmatic processes. pp.325-383. Princeton University press.

Jakes, P., and Gill, J., 1970; Rare earth elements and the island arc tholeiitic series. Earth Planet. Sci. Lett., 9, 17-28.

Jackson, E.D., 1961; Primary textures and mineral associations in the ultramafic zone of the Stillwater complex, Montana. U.S. geol. Surv. prof. Paper, 358, 1-106.

Jackson, E.D., 1971; The origin of ultramafic rocks by cumulus processes. Fortschr. Mineral., 48, 128-174.

Jaques, A.L., Chappell, B.W., and Taylor, S.R., 1983; Geochemistry of cumulus peridotites and gabbros from the Marum ophiolite complex, Northenr Papua New Guinea. Contr. Mineral. Petrol., 82, 154-164.

Johannes, M., 1978; Melting of plagioclase in the system Ab-An-H_2O at PH_2O=5 kbars, an equilibrium problem. Contr. Mineral. Petrol., 66, 295-303.

Juteau, T., 1970; Pétrogenèse des ophiolites des nappes d`Antalya (Taurus Lycien oriental, Turquie). Leur liaison avec une phase d`expansion océanique active au Trias supérieur. Sci. de la Terre, Nancy, 15, 265-288.

Juteau, T., Lapierre, H., Nicolas, A., Parrot, J.F., Ricou, L.E., Rocci, G., and Rollet, M., 1973; Idées actuelles sur la constitution, l'origine et l`évolution des assemblages ophiolitiques mésogéens. Bull. Soc. géol. France, 15, 478-493.

Juteau, T., 1980; Ophiolites of Turkey. In Rocci, G. (ed.). Tethyan ophiolites. Ofioliti, 2, 199-237.

Juteau, T., and Whitechurch, H., 1980; The magmatic cumulates of Antalya (Turkey): Evidence of multiple intrusions in an ophiolitic magma chamber. In: Panayiotou, A. (ed.) Ophiolites, proceedings international ophiolite symposium, Cyprus-1979. Geological Survey Department of Cyprus-Nicosia. 377-391.

Komor, S.C., Elthon, D., and Casey, J.F. 1985; Mineralogical variations in a layered ultramafic cumulate sequences at the North Arm Mountain Massif, Bay of Island ophiolite, Newfoundland. J. Geophys. Res., 90, 7705-7736.

Komor, S.C., Elthon, D., and Casey, J.F., 1986; Petrology of layered gabbroic rocks from the North Arm Mountain Massif, Newfoundland. Cont. Mineral. Petrol.

Kretz, R., 1982; Transfer and exchange equilibria in a portion of the pyroxene quadrilateral as deduced from natural and experimental data. Geochim. Cosmochim. Acta, 46, 411-421.

Lapierre, H., and Rocci, G., 1976; Le volcanisme alcalin du sud-ouest de Chypre et le probléme de l'ouverture des régions téthysiennes au Trias. Tectonophysics, 30, 299-313

Leterrier, J., Maury, R.C., Thonon, P., Girard, D., and Marchal, M., 1982; Clinopyroxene composition as a method of identification of the magmatic affinities of paleo-volcanic series. Earth Planet. Sci. Lett., 59, 139-154.

Lytwyn, J.N., and Casey, J.F., 1993; The geochemistry and petrogenesis of volcanics and sheeted dikes from the Hatay (Kizildag) ophiolite, southern Turkey: possible formation with the Troodos ophiolite, Cyprus, along forearc spreading centers. Tectonophysics, 223, 237-272.

Lytwyn, J.N., and Casey, J.F., 1995; The geochemistry of postkinematic mafic dike swarms and subophiolitic metabasites, Pozanti-Karsanti ophiolite, Turkey: evidence for ridge subduction. Bull. geol. Soc. Amer., 107, 7, 830-850.

Marcoux, J., 1976; La fracturation de la plate-forme scythienne et les nappes initiales au dévelopment de la Téthys alpine en Méditerranée. 4th. Annual Meeting Earth Sciences, Societe Géologique de France, abstract volume, p. 285.

McBirney, A.R., and Noyes, R.M., 1979; Crystallization and layering in the Skaergaard Intrusion. J. Petrol., 20, 487-554.

McCulloch, M.T., Gregory, R.T., Wasserburg, G.J., and Taylor, H.P.Jr., 1980; A Neodymium, Strotium, and Oxygen isotopic study of the Cretaceous Semail ophiolite and implications for the petrogenesis and seawater-hydrothermal alteration of oceanic crust. Earth and Planet. Sci. Lett., 46, 201-211.

McCulloch, M.T., Gregory, R.T., Wasserburg, G.J., and Taylor, H.P.Jr., 1981; Sm-Nd, Rb-Sr, and $^{18}O/^{16}O$ isotopic systematics in an oceanic crustal section: Evidence from the Semail ophiolite. J. Geophys. Res., 86, 2721-2735.

McLaughlin, O.M., McArthur, J.M., Thirlwall, M.F., Howarth, R., Burnett, J., Gale, A.S., and Kennedy, W.J., 1995; Sr isotopic evolution of Maastrichtian seawater determined from the chalk of Hemmor, NW Germany.Terra Nova, 7, 491-499.

Medaris, L.G., 1972; High pressure peridotites from in south-western Oregon. Bull. geol. Soc. Amer., 83, 41-58.

Meschede, M., 1986; A method of discriminating between different types of mid-oceanic ridge basalts and continental tholeiites with the Nb-Zr-Y diagram. Chem. Geol., 56, 207-218.

Miyashiro, A., 1973; The Troodos ophiolite complex was probably formed in an island arc, Earth and Planet. Sci. Lett., 19, 218-224.

Mori, T., 1977; Geothermometry of spinel lherzolites. Contr. Mineral. Petrol., 59, 261-279.

Mullen, E.D., 1983; $MnO/TiO_2/P_2O_5$: a minor element discriminant for basaltic rocks of oceanic environments and its implications for petrogenesis. Earth and Planet. Sci. Lett., 62, 53-62.

Nisbet, E.G., and Pearce, J.A., 1977; Clinopyroxene composition in mafic lavas from different tectonic settings. Contr. Mineral. Petrol., 63, 149-160.

O'Nions, R.K., Hamilton, P.J., and Evensen, N.M., 1977; Variations in $^{143}Nd/^{144}Nd$ and $^{87}Sr/^{86}Sr$ ratios in oceanic basalts. Earth and Planet. Sci. Lett., 34, 13-22.

Pallister, J.S., and Hopson, C.A., 1980; Semail ophiolite magma chamber: I. evidence from gabbro phase variation, internal structure and layering. In: Panayiotou, A. (ed.) Ophiolites. Proceedings international ophiolite symposium, Cyprus-1979. Geological Survey Department of Cyprus-Nicosia. 402-404.

Pallister, J.S., and Hopson, C.A., 1981; Samail Ophiolite Plutonic Suite: Field relation, phase variation, cryptic variation and layering, and a model of a spreading ridge magma chamber. J. Geophys. Res., 86, 2593-2644.

Parlak, O., Delaloye, M., and Bingöl, E., 1995a; Magma chamber process in Mersin ophiolite, S. Turkey. Abstracts of International Ophiolite Symposium 109 p, 18-23 September, Pavia-Italy.

Parlak, O., Delaloye, M., and Bingöl, E., 1995b; Origin of sub-ophiolitic metamorphic rocks beneath the Mersin ophiolite, S. Turkey. Ofioliti, 20, 97-110.

Parlak, O., Delaloye, M., and Bingöl, E., 1995c; Geochemistry and tectonic setting of volcanic rocks in Mersin ophiolite, S. Turkey. Abstracts of International Earth Sciences Colloquium on the Aegean Region (IESCA-95) 43p, 9-14 October, Izmir (Güllük)-Turkey.

Parlak, O., Delaloye, M., and Bingol, E., 1996; Mineral chemistry of ultramafic and mafic cumulates as an indicator of the arc related origin of the Mersin ophiolite (southern Turkey). Geol. Rdsch., 85.

Parrot, J.F., 1977; Assemblage ophiolitique du Baer-Bassit et termes effusifs du volcano-sédimentaire. Pétrologie d'un fragment de la croûte téthysienne charriée sur la plate-forme syrienne. Trav. et Doc. ORSTOM Paris, 72, 333 pp.

Pearce, J.A., and Cann, J.R., 1973; Tectonic setting of basic volcanic rocks determined using trace element analysis. Earth and Planet. Sci. Lett., 19, 290-300.

Pearce, J.A., and Norry, M.J., 1979; Petrogenetic implications of Ti, Zr, Y and Nb variations in volcanic rocks. Contr. Mineral. Petrol., 69, 33-47.

Pearce, J.A., 1980; Geochemical evidence for the genesis and eruptive setting of lavas from Tethyan ophiolites. In: Panayiotou, A. (ed.). Ophiolites. Proceedings Int. Ophiolite Symp., Cyprus, 751-757.

Pearce, J.A., Lippard S.J., and Roberts, S., 1984; Characteristics and tectonic significance of supra subduction zone ophiolites. In: Kokelaar B.P. and Howells M.F. (eds.) Marginal Basin Geology, Geol. Soc. London Spec. Publ., 16, 77-96.

Piepgras, D.J., Wasserburg, G.J., and Dasch, E.J., 1979; The isotopic compositions of Nd in different oceanic masses. Earth and Planet. Sci. Lett., 45, 223-236.

Piskin, Ö., Delaloye, M., Moritz, R., and Wagner, J.J., 1990; Geochemistry and geothermometry of the Hatay complex Turkey: Implication for genesis of the ophiolite sequence. In: Malpas J., Moores E.M., Panayiotou A. and Xenophontos C. (eds.) Ophiolites and oceanic crustal analogues. Proceedings of Troodos ophiolite symposium-1987, 329-337.

Ricou, L.E., 1971; Le croissant ophiolitique péri-arabe, une ceinture de nappes mises en place au Crétacé supérieur. Rev. Géogr. phys. Géol. dyn., Paris, 13, 327-349.

Robertson, A.H.F., and Woodcock, N.F., 1981; Godene zone, Antalya complex continental margin, SW Turkey: Volcanism and sedimentation along a Mesozoic marginal ocean crust. Geol. Rdsch., 70, 1177-1214.

Robertson, A.H.F., and Dixon, J.E., 1984; Introduction: aspects of the geological evolution of the eastern Mediterranean. In: Dixon, J.E., and Robertson, A.H.F., (eds.), The geological evolution of the eastern Mediterranean, Geol. Soc. London Spec. Publ., 17, 1-74.

Robertson, A.H.F., and Waldron, J., 1990; Geochemistry and tectonic setting of Late Triassic and Late Jurassic-Early Cretaceous basaltic extrusives from the Antalya Complex, SW Turkey. In Savasçin, Y. and Eronat, A.H. (eds.). IESCA-1990 proceedings, International Earth Sciences Congress on Aegean Regions-Turkey, 2, 279-299.

Robertson, A.H.F., 1994; Role of the tectonic facies concept in orogenic analysis and its application to Tethys in the eastern Mediterranean region. Earth-Sci. Rev., 37, 139-213.

Saunders, A.D., and Tarney, J., 1984; Geochemical characteristics of basaltic volcanism within back arc basins. In: Kokelaar, B.P. and Howells, M.F. (eds.) Marginal Basin Geology. Geol. Soc. London Spec. Publ., 16, 59-76.

Schilling, J.G., 1975; Azores mantle blob: rare earth evidence. Earth and Planet. Sci. Lett., 25, 103.

Searle, M.P., Lippard, S.J., Smewing, J.D., and Rex, D.C., 1980; Volcanic rocks beneath the Semail ophiolite nappe in the northern Oman mountains and their significance in the Mesozoic evolution of Tethys. J. geol. Soc. (London), 137, 589-604.

Sengör, A.M.C., and Yılmaz, Y., 1981; Tethyan evolution of Turkey:a plate tectonic approach. Tectonopysics, 75, 181-241.

Shervais, J.W., 1982; Ti-V plots and the petrogenesis of modern and ophiolitic lavas: Earth and Planet. Sci. Lett., 59, 101-118.

Shervais, J.W., 1990; Island arc and oceanic crust ophiolites: contrasts in the petrology, geochemistry and tectonic style of ophiolite assemblages in the California Coast Ranges. In: Malpas J, Moores E, Panayiotou A, Xenophontos C (eds), Ophiolites-oceanic crustal analogues. Proceedings of Troodos ophiolite symposium-1987, 507-520.

Smith, A.G., Hurley, A.M., and Briden, J.C., 1981; Phanerozoic Palaeocontinental Maps. Cambridge, Cambridge University Press, 102p.

Smith, T.E., Huang, C.H., Wallawender, M.J., Cheung, P., and Wheeler, C., 1983; The gabbroic rocks of the Peninsular Ranges Batholiths, Southern California: cumulate rocks associated with calc-alkalic basalts and andesites. J. Volcan. Geotherm. Res., 18, 249-278.

Smith, A.G., and Spray, J.G., 1984; A half-ridge transform model for the Hellenic-Dinaric ophiolites. In: Dixon, J.E., and Robertson, A.H.F., (eds.), The geological evolution of the eastern Mediterranean, Geol. Soc. London Spec. Publ., 17, 629-645.

Spray, J.G., Bébien, J., Rex, D.C., and Roddick, J.C., 1984; Age constraints on the igneous and metamorphic evolution of the Hellenic-Dinaric ophiolites. In: Dixon, J.E., and Robertson, A.H.F., (eds.), The geological evolution of the eastern Mediterranean, Geol. Soc. London Spec. Publ., 17, 619-629.

Stern, R.J., 1979; On the origin of andesite in the northern Mariana island arc: implications from agrigan. Contr. Mineral. Petrol., 68, 207-219.

Streckeisen, A., 1976; To each plutonic rock its proper name. Earth-Sci. Rev., 12, 1-33.

Sun, S.S., Nesbitt, R.W., and Sharaskin, A.Y., 1979; Geochemical characteristics of Mid-Ocean Ridge Basalts. Earth and Planet. Sci. Lett., 44, 119-138.

Thompson, G., 1973; A geochemical study of the low temperature interaction of seawater and oceanic igneous rocks. Trans. amer. Geophys. Union, 54, 1015-1019.

Thy, P., 1987a; Petrogenetic implications of mineral crystallization trends of Troodos cumulates, Cyprus. Geol. Mag., 124, 1-11.

Thy, P., 1987b; Magmas and magma chamber evolution, Troodos ophiolite, Cyprus. Geology, 15, 316-319.

Thy, P., 1990; Cryptic variation of a cumulate sequence from the plutonic complex of the Troodos ophiolite. In: Malpas J., Moores E., Panayiotou A. and Xenophontos C. (eds.) Ophiolites-oceanic crustal analogues. Proceedings of Troodos ophiolite symposium-1987, Cyprus. 165-172.

Voldet, P., 1993; From neutron activation to inductively coupled plasma-atomic emission spectrometry in the determination of rare-earth elements in rocks. Trends in Analytical Chemistry, 12, 339-344.

Wager, L.R., Brown, G.M., and Wadsworth, W.J., 1960; Types of igneous cumulates. J. Petrol., 1, 73-85.

Wager, L.R., and Brown, G.M., 1968; Layered igneous rocks. W.H. Freeman, San Francisco, California, 588p.

Weaver, B.L., 1991; Trace element evidence for the origine of ocean island basalts. Geology, 19, 123-126.

White, W.M., 1985; Sources of oceanic basalts: radiogenic isotopic evidence. Geology, 13, 115-118.

White, W.M., Tapia, M.D.M., and Schilling, J.G., 1979; The petrology and geochemistry of the Azores islands. Contr. Mineral. Petrol., 69, 201-213.

Whitechurch, H., Juteau, T., and Montigny, R., 1984; Role of the Eastern Mediterranean ophiolites (Turkey, Syria, Cyprus) in the history of the Neo-Tethys. In: Dixon, J.E. and Robertson, A.H.F. (eds.). The Geological Evolution of the Eastern Mediterranean. Geol. Soc. Spec. Publ. London, 17, 301-317.

Winchester, J.A., and Floyd, P.A., 1977; Geochemical discrimination of different magma series and their differentiation products using immobile elements. Chem. Geol., 20, 325-343.

Woodhead, J., Eggins, S., and Gamble, J., 1993; High field strength and transition element systematics in island arc and back-arc basin basalts: evidence for multi-phase melt extraction and a depleted mantle wedge. Earth and Planet. Sci. Lett., 114, 491-504.

Yalınız, M. K., Göncüoglu, M. C., and Floyd, P.A., 1994; Geochemical characteristics and geodynamic interpretation of the Supra-subduction Sarıkaman ophiolite, Central Anatolia. Abstracts of International Volcanological Congress (IAVCEI-94) 162p. 12-16 September, Ankara-Turkey.

CHAPTER 4

SUB-OPHIOLITIC METAMORPHIC ROCKS

Abstract

The Mersin ophiolite crops out on the southern flank of the E-W trending Central Tauride belt as one of the Mesozoic Tethyan oceanic lithospheric remnants obducted onto the Tauride platform during the late Cretaceous-early Paleocene in southern Turkey.

Sub-ophiolitic metamorphic rocks, showing an inverted metamorphic zonation from upper amphibolite facies to greenschist facies, crop out discontinuously along the base of the Mersin ophiolite thrust sheet on the southern flank of the Bolkardag. These metamorphic rocks indicate polyphase deformation and have been folded and imbricated. Major, trace and REE geochemistry suggest that these metamorphic rocks were derived from ocean island/ seamount basaltic rocks and associated sedimentary units. Numerous tholeiitic microgabbroic-diabasic dikes, unaffected by the metamorphism and oriented nearly E-W, intruded the metamorphics. In terms of their trace and REE chemistry, these dikes have the chemical signature of MORB and VAB suggesting supra-subduction zone tectonic setting.

The metamorphics show well developed migmatitic structure and metamorphic banding defined by alternating epidote-rich and carbonate layers. A pronounced regional foliation (S_1), NW-SE trending mineral lineation (L_1) and first-order intrafolial folds (F_1) were produced during their deformation. They are later refolded by NW-vergent asymmetrical folds (F_2). Imbricated structure is also typical in these metamorphics. The meso-structures, such as asymmetry of calcite-augen, vergence and asymmetry of F_1 folds, general trend of brittle-ductile structures such as oblique-slip normal and thrust/reverse faults, and vergence of F_2 folds and thrusts in the imbricate structure, all indicate unambiguous non-coaxial deformation and a shear sense of upper levels moving up to the NE-NW. The structural evidence suggests that the Mersin ophiolite was obducted over the central Tauride belt from SE to NW. The shear sense obtained from the sub-ophioitic metamorphics is compatible with the general trend and vergence of the large scale thrust sheets which comprise the Mersin ophiolite.

K-Ar analyses on hornblendes yield an age of 93.4±2 Ma which represents the initial detachment of the oceanic lithosphere (Mersin ophiolite) during the closure of the Neo-Tethyan ocean in the eastern Mediterranean.

$^{40}Ar/^{39}Ar$ incremental-heating experiments were performed on obduction-related subophiolitic metamorphic rocks, undeformed diabase dikes, and tholeiitic basalts. Highly

altered dike and basalt samples did not yield reliable ages to interpret in any meaningfull way due to ^{39}Ar recoil problem. Seven hornblende samples from the metamorphic rocks yielded isochron ages ranging from 96.0±0.7 Ma to 91.6±0.3 Ma (all errors±1σ). Five of the seven hornblende age determinations are indistinguishable at 95% confidence level and gave weighted mean age of 93.1±0.3 (2σ)Ma. We interpret these ages as the time since cooling below 500°C. Three diabase dike samples postdate the metamorphic sole yielded relatively younger ages 89.6±0.7 Ma, 88.3±0.7 Ma, 86.3±0.5 Ma respectively, suggesting that all the dike swarms postdate the formation of the Mersin ophiolite and the intraoceanic thrusting event in this segment of the Neotethyan ocean. These results suggest that intraoceanic thrusting (compressional event) was completed rapidly (~ 4 Ma) and converted into extensional regime (perhaps in less than 3 m.y.) during which postkinematic dike emplacement occured. Our data show that at least for a single ophiolite (Mersin) in the Tauride belt, high precision ages on the intraoceanic thrusting and the mafic dike emplacement are much better constrained in this study.

4.1. Introduction

The evolution of ophiolites as fragments of oceanic crust and upper mantle can be considered as a series of distinct tectonic events which may finally result in their emplacement onto continental margins (Spray, 1984). The Neotethyan ophiolites in the eastern Mediterranean are situated in two lineaments, one of which including Troodos in Cyprus, Kizildag in Turkey and Baer Bassit in Syria crops out along the continent-continent collision zone informally called the "Bitlis-Zagros crush zone". These ophiolites preserve complete oceanic lithospheric sections (Dilek and Moores, 1990). The second group, that is represented by dismembered and deformed lithological units, is located along the Tauride belt (Juteau, 1980). These ophiolites, so called "Tauride ophiolites" including the Lycian-Beysehir-Alihoca-Mersin-Pozanti-Karsanti, are generally defined by metamorphic soles and tectonic melange (Fig. 4.1).

Many geochemical studies suggest a consistent tectonic setting in which Tethyan ophiolites formed some time during Late Cretaceous (Pearce et al., 1984; Parlak et al., 1996; Robertson, 1994; Yaliniz et al., 1994). Due to the presence of podiform chromite deposits and the crystallization of clinopyroxene before plagioclase which is reflected in the high abundance of wehrlite relative to troctolite in their cumulate sequences, Pearce et al. (1984) suggested that the ophiolites in the eastern mediterranean were formed in a supra-subduction zone tectonic setting. The main controversy for the Neotethyan ophiolites in Turkey and surrounding region concerns the number of root zones from which these

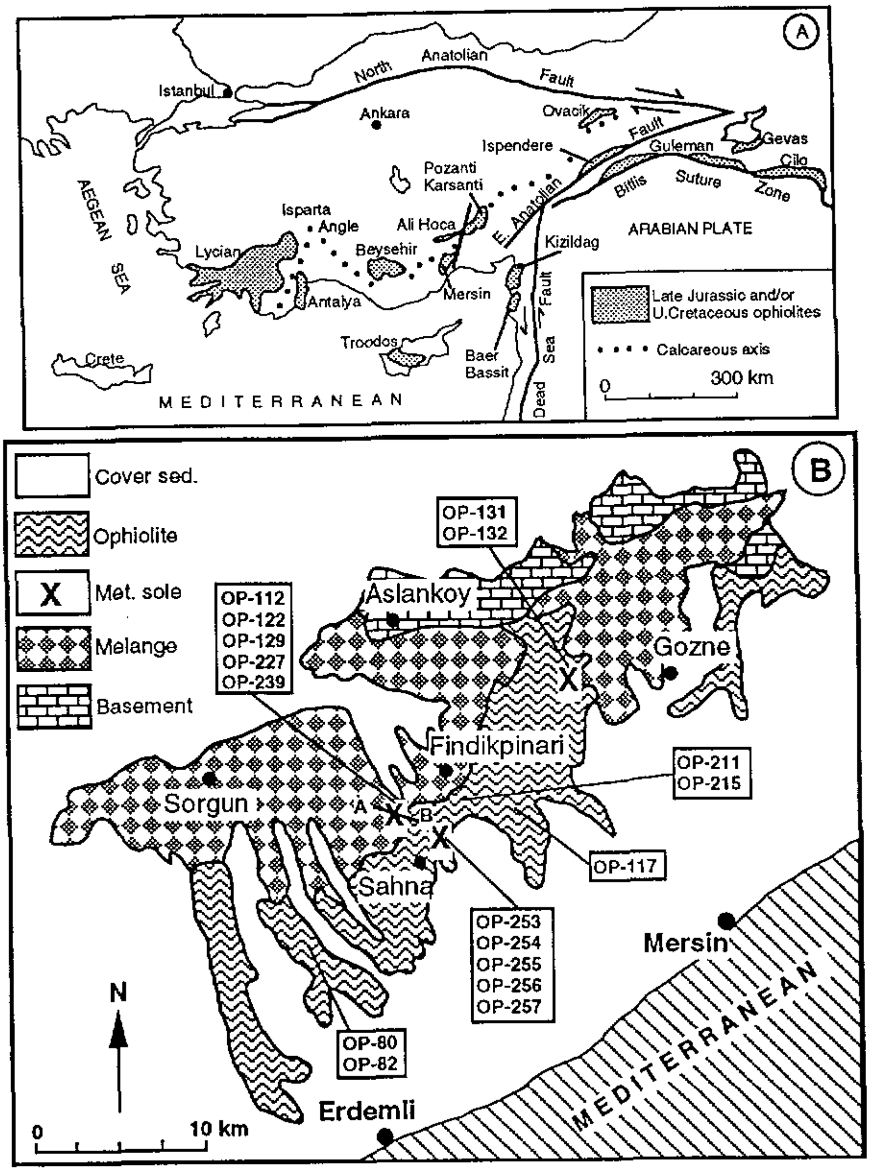

Figure 4.1. a. Ophiolitic massifs in southern Turkey (from Dilek and Moores, 1990).
b. Simplified geological map of the Mersin ophiolite complex (MOC) and the location of the samples used for K-Ar and $^{40}Ar/^{39}Ar$ geochronology.

ophiolites derived. Sengor and Yilmaz (1981) and Robertson and Dixon (1984) suggested that two major ocean basins were present: a multi-armed northern basin and a more simple southern branch of Neotethys, whereas Ricou et al. (1984) and Whitechurch et al. (1984) argued that the ophiolites were formed in a single ocean basin in central Turkey.

The structural analyses in sub-ophiolitic metamorphic soles provides valuable evidence about the tectonic history of ophiolite obduction (Spray, 1984; Shackleton et al., 1990) because the sub-ophiolitic metamorphics are themselves record the deformation and associated metamorphism in the ophiolites themselves (William and Smyth, 1973; Jamieson, 1980; Searle and Stevens, 1984; Robertson et al., 1990; Polat and Casey, 1995).

Although the presence of sub-ophiolitic metamorphics along the Neotethyan belt in Turkey has been known for years, their detail petrographic and structural analysis, except for a recent study by Polat and Casey (1995), have not been studied. The metamorphic sole of, and the underlying mélange beneath, the Mersin ophiolite are considered as an obduction-related Neotethyan accretionary complex and have been choosen for detail petrographic and structural analyses. The structural fabrics in the sub-ophiolitic metamorphics are excellent kinematic indicators and provide valuable information on the types of deformation mechanism and obduction direction during their formation.

Conventional K-Ar and $^{40}Ar/^{39}Ar$ dating have been extensively used on the metamorphic soles of the eastern Mediterranean ophiolites in order to constrain the age of intraoceanic thrusting of the Tethyan oceanic lithosphere before obduction onto continental platform. K-Ar and $^{40}Ar/^{39}Ar$ geochronologic studies of the metamorphic sole of the Oman ophiolite (Lanphere, 1981; Montigny et al., 1988; Gnos and Peters, 1993; Hacker, 1994) yielded cooling ages from 100 to 93 Ma. These ages have been interpreted as the formation age of the Oman ophiolite metamorphic sole during the intra-oceanic thrusting.

Thuizat et al. (1981) documented K-Ar cooling ages from the metamorphic sole of Mersin ophiolite (94±4 to 98±4 Ma), Antalya ophiolite (94±4 to 102±7 Ma), Beysehir nappes (84±3 to 93±3 Ma), Pozanti-Karsanti (92±3 to 95±4 Ma), the Lycian nappes (83±3 to 102±4 Ma) in Turkey and the Baer Bassit (87 Ma) in Syria. He concluded that age of the metamorphism throughout the Tauride belt is about 95 Ma. Thuizat et al. (1978) reported a K-Ar age of 71±3 Ma obtained from the undeformed diabase dike within the metamorphic sole of the Pozanti-Karsanti ophiolite (Fig. 4.2). Whereas Dilek and Thy (1992) reported much older $^{40}Ar/^{39}Ar$ ages from the mafic dike intrusions (140±6 Ma) in Pozanti-Karsanti ophiolite and in Alihoca ophiolite (143±10 Ma). They concluded, on the basis of these age data, that inner zone ophiolites in the Tauride belt are as old as at least Late Jurassic. Further west from the Tauride belt, much older ages from the metamorphic sole of Greek and Yugoslavian ophiolites are between 180 Ma and 160 Ma (Fig. 4.2) (Lanphere et al., 1975; Okrucsh et al., 1978; Thuizat et al., 1978; Roddick et al., 1979; Thuizat et al., 1981; Spray et al.,1984).

Spray (1984) suggested that the age differences between ophiolite igneous crystallization and metamorphic sole formation were less than 10 m.y. based on well-documented geochronologic studies. However, Hacker (1994) proposed much shorter time span for the Oman ophiolite case by comparing U-Pb zircon dates from plagiogranites (Tilton et al.,

1981) and $^{40}Ar/^{39}Ar$ dates from the metamorphic sole; the ocean crust was apparently ~1 My old at the time intraoceanic thrusting began.

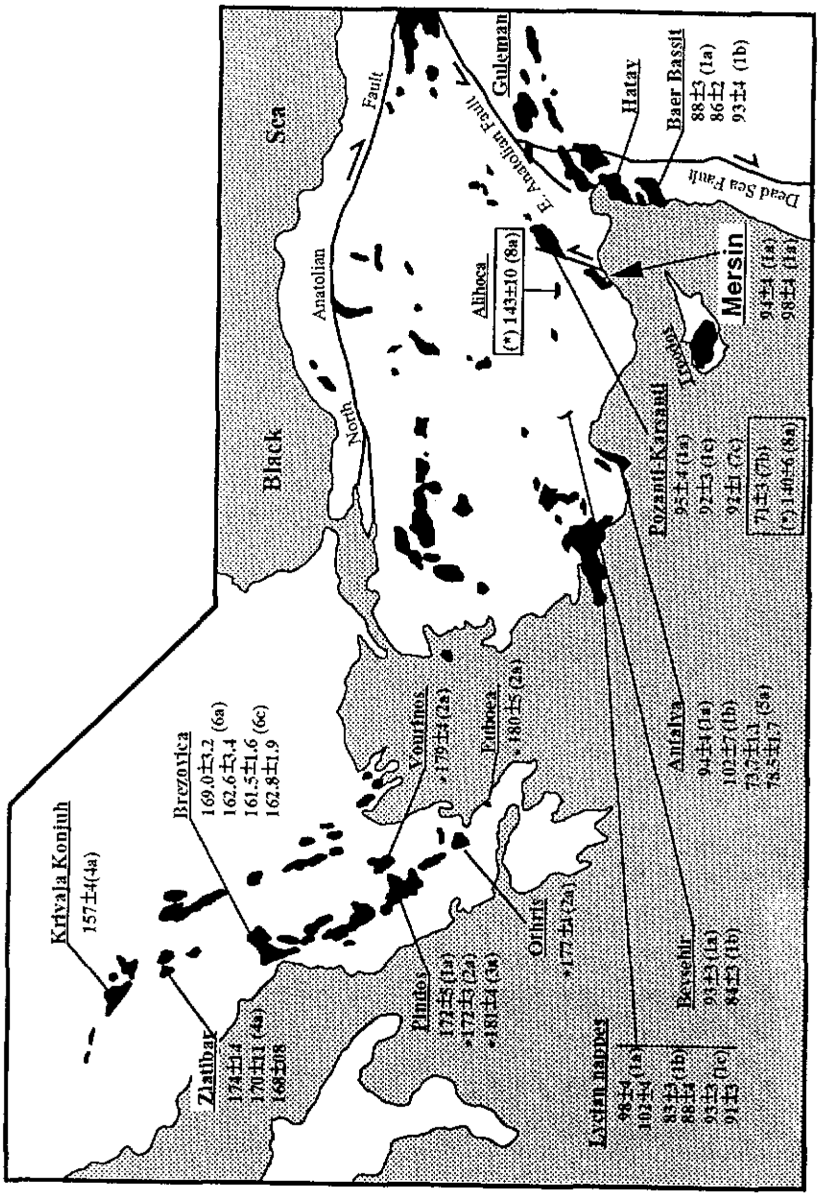

Figure 4.2. Previous K-Ar and $^{40}Ar/^{39}Ar$ [indicated by star (*)] geochronologic studies done on the metamorphic sole of the ophiolites in the eastern Mediterranean. a, b and c represent hornblende, plagioclase and mica analyses respectively. Boxes show post tectonic dyke injection in the Pozantı-Karsantı and Alihoca ophiolites. Numbers indicate references, (1) Thuizat et al. (1981), (2) Spray and Roddick (1980), (3) Roddick et al. (1979), (4) Lanphere et al. (1975), (5) Yilmaz and Maxwell (1982), (6) Okrusch et al. (1978), (7) Thuizat et al. (1978), (8) Dilek and Thy (1992).

The main objective of this study is to discuss geochemistry of metamorphic rocks and define their protholiths, to present the results of K-Ar and $^{40}Ar/^{39}Ar$ incremental heating analyses of hornblendes from the metamorphic sole, and post-metamorphic microgabbroic-diabasic dikes, and to summarize the general characteristics of the structures formed during the deformation and metamorphism of subophiolitic metamorphics, discuss the evidence for the sense of shearing, and propose a model for the origin of, and the kinematic history of, emplacement of Mersin ophiolites.

4.2. Geologic and tectonic setting

The Tauride mountains in Turkey consist of continental and oceanic units (Juteau, 1980; Ricou et al., 1984; Dilek and Moores, 1990). Ophiolitic massifs in the Tauride belt that rest in tectonic contact with underlying platform carbonates are typically dismembered oceanic lithospheric sections, associated with metamorphic soles and ophiolitic melange (Juteau, 1980; Dilek and Moores, 1990).

The Mersin ophiolite is bounded by sinistral Ecemis fault to the east, Bolkardag metamorphic rocks to the north, and is covered by Miocene carbonates to the south and west. The Mersin ophiolite complex (MOC) is an approximately 6 km thick oceanic lithospheric section that rests on the southern flank of the Bolkardag along the Tauride belt in southern Turkey (Fig. 4.1). This complex, which is exposed along strike 60 km in a NE-SW trend, comprises three distinctive structural elements, including ophiolitic mélange, a subophiolitic metamorphic sole and ultramafic+mafic rocks (Juteau, 1980; Parlak et al., 1994-1995b) (Fig. 4.1). Ophiolitic mélange is the lowest part of the tectonic pile and consists of various rock types such as conglomerates, sandstones, shales, mudstones, radiolarites, blocks of limestone of various sizes and ages, serpentinized harburgites-gabbros and basalts, fragments of subophiolitic metamorphic rocks and granitic blocks. Lithological features and structural organization of the units in the mélange suggest the evidence of the openning and closure of the NeoTethyan ocean basin in southern Turkey. This unit is tectonically overlain by a series of rocks that underwent retrogressive metamorphism from upper amphibolite to greenschist facies. These subophiolitic metamorphic rocks formed during intraoceanic thrusting are multiply deformed and are cut by a number of diabasic dikes that are characterized by variable attitude and thickness ranging from 0.4 to 6 m. (Fig. 4.3). The upper tectonic pile, which tectonically overlies the metamorphics in the study area, is represented by oceanic lithospheric section. Except sheeted dike complex, it is represented by harzburgitic tectonites, ultramafic-mafic cumulates and two distinct basalt generations in terms of age and geochemical affinity (Upper Jurassic-Lower Cretaceous alkaline basalts and Upper Cretaceous (?) tholeiitic basalts) (Parlak et al., in review). The harzburgitic tectonites and

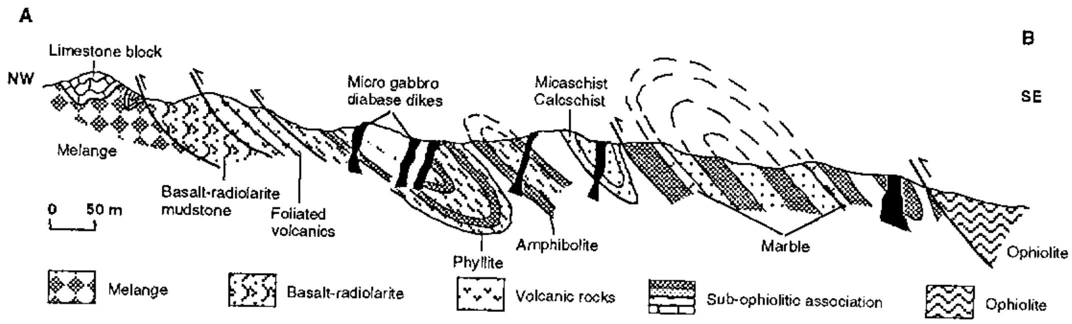

Figure 4.3. Cross section showing the structural relationships of the subophiolitic metamorphic rocks at Fındıkpınarı.

cumulates are intruded by numerous tholeiitic micro gabbroic-diabase dikes. Whole rock and mineral chemistry of cumulates, magmatic affinities of basaltic suite, the regional geological setting all suggest that the Mersin ophiolite formed in a suprasubduction zone setting some time during Late Cretaceous in southern Turkey (Parlak et al., 1996).

4.3. Analytical method

15 amphibolites and 6 diabase dike samples have been analysed in terms of major and trace element concentrations. REE analysis has been carried out for 2 amphibolites and 1 dike sample. Major and trace element analyses have been carried out by XRF. Major and trace element compositions were determined on glass beads fused from ignited powders to which $Li_2B_4O_7$ was added (1:5), in a gold-platinum crucible at 1150 ^oC. REE analysis was done by ICP-AES technique (Voldet, 1993). Microprobe analysis was done on a Camebax SX-50. The analytical conditions for the elements (K, Mg, Ca, Na, Mn, Cr, Al, Si, Fe) were 20 seconds of counting interval, beam current-15 mA and acceleration voltage-15 kV.

9 amphibolite samples have been used for K-Ar analysis. The K content of each mineral separate has been measured with flame spectrophotometry. Ar was extracted by total sample fusion into a pyrex line fitted up with high vacuum metal valves. The resultant gas was mixed with a ^{38}Ar spike to apply the isotopic dilution technique. The contamining gasses have been separated with titanium traps and liquid nitrogen. Measurements are done

in static mode with an AEI MS-10S spectrometer fitted up with a permanent magnet of 4.1 kG and connected to a computer for processing data. Samples were degased at about 100^{o}C for several hours before the analysis to reduce atmospheric contamination. Analytical precision is near 0.5%. For calculating the age, Steiger and Jager (1977) constants were used. The amphibole separates were obtained by crushing hand-sized samples, sieving, and passing the 125-315 μm fractions through heavy liquides. Isotopic measurements were done on the quantities of samples between 200 mg and 1 gr.

Incremental heating experiments were carried out at the University of Geneva $^{40}Ar/^{39}Ar$ Geochronology Laboratory. Seven amphibole separates between 11.7 and 15.6 mg and Three whole-rock samples between 2.5 and 5.8 mg were placed into aluminum foil packets and loaded into 5 mm diameter quartz vials. Nine neutron flux monitors, loaded into copper packets were placed in the 104.5 mm vial. The monitor mineral was HDB-1 Biotite (Fuhrmann et al., 1987). The $^{40}Ar/^{39}Ar$ plateau age of this standard is 24.292 Ma (Wijbrans et al., 1995). The samples were irradiated for 18 hours at the Oregon State University Triga reactor in the unlined inner core facility where they received a total fast neutron dose of $1.62*10^{18}$ n/cm^2. Based on previous analyses of optical grade CaF_2 and Fe-doped K-silicate glass irradiated at Oregon State (Wijbrans et al., 1995), corrections for undesirable neutron-induced reactions on ^{40}K and ^{40}Ca are as follows: $[^{40}Ar/^{39}Ar]_K$= 0.00465; $[^{36}Ar/^{37}Ar]_{Ca}$=0.000268; $[^{39}Ar/^{37}Ar]_{Ca}$= 0.000698. Analytical procedures including gas extraction, isotopic analyses, and system blanks are given in Singer and Pringle (1996).

Incremental heating experiments consisted of 16 to 24 individual steps. For each analysis the $\pm1\sigma$ errors include estimates of the standard deviation of analytical precision on the peak signals, the blank, spectrometer mass discrimination, plus reactor corrections. Inverse-variance weighted mean ages and errors were calculated according to Taylor (1982). J values determined from the mean of 5 to 6 plateau measurements were collected from each monitor (HDB-1) packet. The estimated precision for each monitor point along the J curve suggests that errors in J are $\approx$ 0.3%. This uncertainty was propagated into the final plateau and isochron ages for each analysis. Ages were calculated using the decay constants of Steiger and Jäger (1977). Criteria for the interpretation of the experimental results are outlined in Pringle (1993) and Singer and Pringle (1996).

4.4. Petrographic summary

The dikes intruding metamorphics are dominated by microgabbro-diabase, only one gabbro dike is also observed in this association. Diabase dikes having porphyric texture include plagioclase-clinopyroxene mineral assemblages. The clinopyroxene is generally subhedral with grain size between 0.2-1.3 mm. The matrix is made of plagioclase and pyroxene and chlorite is common as low temperature alteration product. Gabbro dike shows more alteration compared to diabase dikes. Epidote, quartz and chlorite are seen as secondary mineralization products in gabbro. Plagioclase is highly seritized and clinopyroxene is replaced by amphibole.

The metamorphic unit includes following rock association: amphibolites and amphibolitic schists, epidote-amphibolite schists, quartz micaschists, calcschists and marbles (Plate 4.1a-b-c-d).

The most abundant mineral assemblages in sub-ophiolitic metamorphic rocks of the Mersin ophiolite are given in Table 4.1. In thin sections, the amphiboles show granoblastic polygonal texture and they are generally euhedral with grain size between 0.3-2.8 mm. The mineral orientation is in the foliation plane. Representative amphibole analyses are given in

Sample	hb	cpx	pl	ep	chl	qz	bi	rut	sph	cal
108			X							X
109	X		X	X	X	X	X			X
111	X		X		X	X	X		X	
112	X		X	X	X	X	X			
131	X								X	
132	X								X	
133	X	X	X		X					
254	X			X*				X	X	
255	X							X	X	
327	X	X	X	X		X				X

The abbreviations used are as follows:
hb: hornblend, cpx: clinopyroxene pl: plagioclase, ep: epidote, chl: chlorite, qz: quartz, bi: biotite, rut: rutile sph: sphene, cal: calcite. *veins.

Table 4.1. Mineral assemblages in amphibolites and greenschists from the metamorphic rocks in the Mersin ophiolite.

Table 4.2. No systematic zonation from core to rim was observed. Three types of hornblende (Leake, 1978) are distinguished in the studied samples (Fig. 4.4). The first group (OP-131 and OP-132) is generally ferroan pargasitic hornblende and represented by high FeO (12.1-12.6%), low K_2O (0.3-0.4%), low MgO (13.1-14.1%), low SiO_2 (40.5-44.8%) and low Mg*(Mg/Mg+Fe) (0.66). The second group of amphiboles (OP-253, OP-254, OP-255) is dominated by edenite and presents high SiO_2 (46.3-48.8%), high MgO (13.8-15.4%), high Mg* (0.70) low K_2O (0.2-0.4%) and low FeO (10.5-11.4%).

Table 4.2. Representative microprobe analyses of the amphiboles from the metamorphic sole.

Sample	131-1	131-2	131-3	132-3	132-4	132-5	253-1	253-2	253-3	254-1	254-2	254-3	255-1	255-2	255-3	256-1	256-2	256-3	257-1	257-2	257-3
SiO2	44.82	44.58	44.79	43.72	44.14	44.66	47.12	47.03	46.79	46.86	46.85	47.78	46.81	46.95	46.39	44.06	44.10	44.54	44.34	44.84	46.73
Al2O3	11.75	11.99	11.51	11.74	11.01	11.43	9.75	10.16	10.55	10.12	9.81	9.12	10.78	9.80	10.45	12.14	12.31	11.18	12.08	12.11	10.66
TiO2	1.21	1.29	1.07	1.20	1.18	1.45	0.66	0.39	0.50	0.49	0.61	0.68	0.40	0.58	0.52	0.70	0.43	1.01	0.63	0.45	0.38
FeO*	12.36	12.43	12.38	12.82	12.35	12.56	10.52	10.83	10.96	11.43	11.09	10.95	11.61	11.53	11.41	13.15	13.06	13.51	12.94	13.12	12.60
Cr2O3	0.15	0.13	0.17	0.53	0.06	0.07	0.00	0.00	0.00	0.00	0.00	0.00	0.00	0.00	0.00	0.00	0.00	0.00	0.00	0.00	0.00
MnO	0.20	0.23	0.20	0.15	0.18	0.14	0.18	0.15	0.25	0.23	0.20	0.24	0.17	0.21	0.23	0.17	0.15	0.11	0.18	0.14	0.17
MgO	13.76	13.72	14.09	13.19	13.75	13.46	14.78	14.70	14.65	14.27	14.44	14.81	14.19	14.28	13.92	12.14	12.27	12.35	12.47	12.45	13.59
CaO	10.93	11.07	10.95	11.15	11.17	11.25	11.19	11.12	11.05	11.49	11.60	11.59	11.54	11.60	11.58	11.62	11.48	11.63	11.46	11.40	11.54
Na2O	1.94	1.96	1.86	1.98	1.95	2.01	1.99	1.89	2.03	1.80	1.82	1.66	1.91	1.82	1.87	2.06	1.95	1.97	2.07	2.07	1.84
K2O	0.32	0.33	0.32	0.37	0.31	0.34	0.28	0.37	0.24	0.24	0.24	0.20	0.34	0.22	0.31	0.35	0.50	0.40	0.42	0.47	0.38
H2O	2.55	2.26	2.66	3.15	3.91	2.64	2.05	2.06	2.06	2.05	2.05	2.06	2.07	2.05	2.05	2.01	2.01	2.02	2.02	2.03	2.06
Total	99.99	99.99	100.00	100.00	100.01	100.01	98.52	98.70	99.08	98.98	98.71	99.09	99.82	99.04	98.73	98.40	98.26	98.72	98.61	99.08	99.95
Si	6.49	6.48	6.48	6.33	6.32	6.48	6.88	6.86	6.80	6.84	6.85	6.94	6.78	6.86	6.80	6.56	6.57	6.62	6.58	6.61	6.79
AlIV	1.51	1.52	1.52	1.67	1.68	1.52	1.12	1.14	1.20	1.16	1.15	1.06	1.22	1.14	1.20	1.44	1.43	1.38	1.42	1.39	1.21
AlVI	0.50	0.54	0.44	0.33	0.18	0.43	0.56	0.61	0.61	0.58	0.54	0.50	0.62	0.54	0.60	0.69	0.73	0.58	0.69	0.72	0.62
Ti	0.13	0.14	0.12	0.13	0.13	0.16	0.07	0.04	0.05	0.05	0.07	0.07	0.04	0.06	0.06	0.08	0.05	0.11	0.07	0.05	0.04
Fe3+	0.00	0.00	0.00	0.00	0.00	0.00	0.00	0.00	0.00	0.00	0.00	0.00	0.00	0.00	0.00	0.00	0.00	0.00	0.00	0.00	0.00
Fe2+	1.50	1.51	1.50	1.55	1.48	1.52	1.28	1.32	1.33	1.40	1.36	1.33	1.41	1.41	1.40	1.64	1.63	1.68	1.60	1.62	1.53
Cr	0.02	0.01	0.02	0.06	0.01	0.01	0.00	0.00	0.00	0.00	0.00	0.00	0.00	0.00	0.00	0.00	0.00	0.00	0.00	0.00	0.00
Mn	0.02	0.03	0.02	0.02	0.02	0.02	0.02	0.02	0.03	0.03	0.02	0.03	0.02	0.03	0.03	0.02	0.02	0.01	0.02	0.02	0.02
Mg	2.97	2.98	3.04	2.85	2.93	2.91	3.22	3.20	3.18	3.11	3.15	3.21	3.07	3.11	3.04	2.69	2.72	2.74	2.76	2.74	2.95
Ca	1.70	1.73	1.70	1.73	1.71	1.75	1.75	1.74	1.72	1.80	1.82	1.80	1.79	1.81	1.82	1.85	1.83	1.85	1.82	1.80	1.80
Na	0.54	0.55	0.52	0.56	0.54	0.57	0.56	0.53	0.57	0.51	0.52	0.47	0.54	0.52	0.53	0.59	0.56	0.57	0.60	0.59	0.52
K	0.06	0.06	0.06	0.07	0.06	0.06	0.05	0.07	0.04	0.04	0.04	0.04	0.06	0.04	0.06	0.07	0.09	0.08	0.08	0.09	0.07
OH	2.46	2.19	2.57	3.04	3.73	2.55	2.00	2.00	2.00	2.00	2.00	2.00	2.00	2.00	2.00	2.00	2.00	2.00	2.00	2.00	2.00
Mg/(Mg+Fe)	0.66	0.66	0.67	0.65	0.66	0.66	0.71	0.71	0.70	0.69	0.70	0.71	0.69	0.69	0.69	0.62	0.63	0.62	0.63	0.63	0.66
K/Ca	0.03	0.04	0.03	0.04	0.03	0.04	0.03	0.04	0.03	0.02	0.02	0.02	0.04	0.02	0.03	0.04	0.05	0.04	0.04	0.05	0.04

*Total Fe is expressed as FeO. Calculation of chemical formula were done on the basis of 24 (O)

The third group (OP-256, OP-257) of amphiboles is characterized by edenitic hornblende that presents intermediate SiO_2 (43.6-45.5%), high FeO (11.7-13.8%), low K_2O (0.4-0.5%), low MgO (11.9-13.6%) and Mg*=0.64 contents (Fig. 4.4).

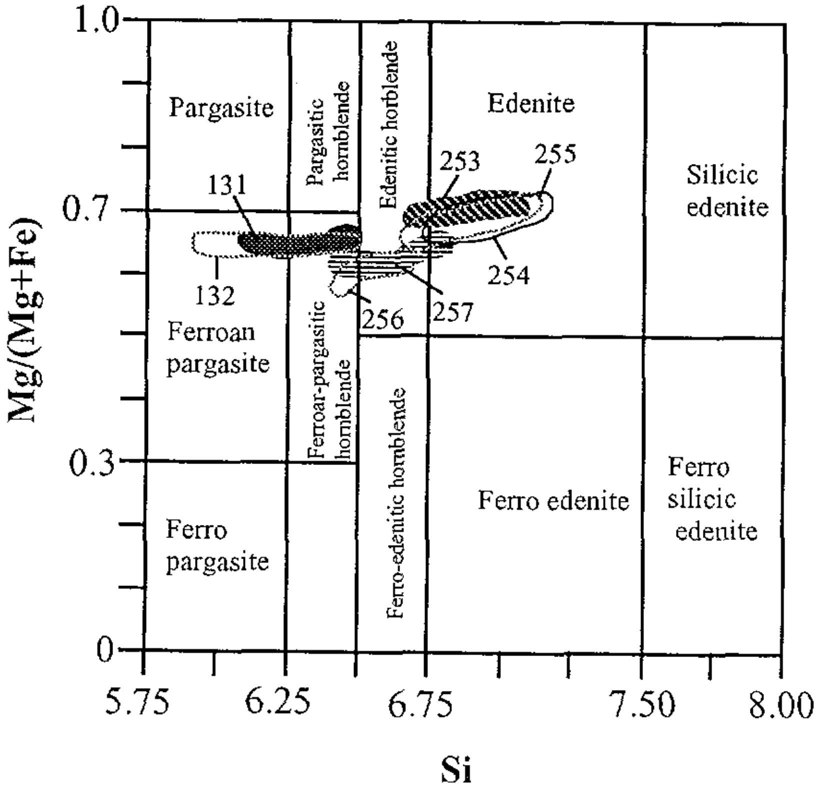

Figure 4.4. Chemical composition of amphiboles in the metamorphic rocks.

Rutile and sphene co-exist with the amphibole. The presence of rutile and sphene in amphibolitic rocks subdivide the facies into two sequences , because sphene is the common Ti-bearing phase in low grade amphibolites, whereas ilmenite, rutile, or hematite are the common phases in higher grade assemblages (Laird, 1977). Absence of garnet in this higher grade assemblage suggests that variations in oxygen fugacity during the metamorphism of amphibolite facies rocks could determine whether hornblende and/or garnet crystallize (Gilbert, 1966).

In thin sections, amphibolitic rocks are rarely cut by inclusions of epidote. The amphiboles associated with the epidote- plagioclase-calcite-quartz-biotite and chlorite exhibit in the field visible schistosity pattern.

Blue-green clinopyroxene is a minor mineral in the assemblage . It belongs to the mineral assemblage of hornblende-epidote-albite-quartz-calcite and appears as anhedral crystals up to 1.2 mm in size. The deformation is very effective on this mineral and uralitization is common.

Epidote occurs as dominant mineral in the greenschist facies and is seen as euhedral-subhedral crystals , ranging from 0.2 to 0.7 mm in grain size. They are often zoned and in the field, schistosity is quite easily underlined by fine-grained green amphiboles and epidotes. Plagioclase is altered to sericite and albite. The crystals are generally parallel to the schistosity.

4.5. Geochemistry of the metamorphic sole

4.5.1. Geochemistry of amphibolites

Major, trace elements and REE analyses of amphibolites are given in Table 4.3. As sphene and rutile are present. TiO_2 content of the amphibolites varies between 1.31 and 2.97 %. Amphibolites are also characterized by high Cr, Zr and Y contents.

REE patterns of amphibolite represent LREE enrichment which may be correlated with WPB (sea mount) (Fig. 4.5) or other ocean island basalts such as those of the Azores (White et al., 1979) and alkali basalts in the Ankara melange (Floyd, 1993).. MORB-normalized trace element patterns of amphibolites are also comparable with WPB and OIB (Pearce, 1982 ; Saunders, 1984). They are enriched in incompatible elements such as K, Ba, Rb, Ce and Nb (Fig. 4.6a).

On the Nb-Zr-Y triangular diagram of Meschede (1986), amphibolites clearly differ from the dike samples. Amphibolites are plotted in the WPB field (Fig. 4.7a). This distinction is also seen on the Ti-Zr-Y diagram of Pearce and Cann (1973): amphibolites are plotted in the WPB field whereas dike samples are plotted in between OFB and arc-tholeiites field (Fig. 4.7b).

4.5.2. Geochemistry of dikes in metamorphics

Major, trace elements and REE analyses of dike samples are given in Table 4.3. All the dike samples are tholeiitic in character. Major oxide contents of dike samples are between for TiO_2= 0.7-0.9%, Al_2O_3= 15.4-16.0%, CaO= 9.5-10%. Some of the trace element contents are between for Y=13-23 ppm, Zr= 41-61 ppm.

Sun et al. (1979) presented existence of correlation between the weight percent of TiO_2, Al_2O_3 and CaO from which degree of partial melting can be estimated. According to their definition, primary MORB with low TiO_2 (≈0.7%), high Al_2O_3 (≈16%) and CaO

Table 4.3. Major, trace and REE analyses of the amphibolites and dikes (122-128-129-130 and 227) in the metamorphic sole.

Sample	111	112	131	132	247	248	249	252	253	254	255	256	382	383	384	122	128	129	130	227
SiO2	48.81	45.29	43.72	43.76	47.94	46.16	45.74	46.02	47.46	45.90	46.84	47.22	42.62	42.30	42.40	52.67	52.87	51.20	51.30	52.29
Al2O3	15.30	14.96	11.86	12.04	13.80	12.80	12.03	11.90	10.71	10.05	9.70	13.09	11.82	11.80	11.93	16.04	15.79	15.37	15.37	15.73
TiO2	2.97	2.53	2.54	2.45	1.43	1.31	1.32	1.83	1.74	1.38	1.62	1.45	2.68	2.73	2.72	0.72	0.78	0.89	0.92	0.76
FeO*	12.75	12.74	14.18	14.04	11.69	12.33	13.07	12.89	12.06	12.30	12.30	12.95	13.76	13.72	13.92	9.91	9.40	9.56	9.98	9.79
CaO	8.69	10.48	10.32	10.72	10.21	10.88	11.01	10.29	10.89	10.80	11.03	9.83	11.13	11.15	11.18	9.98	9.54	10.18	9.86	9.51
MgO	6.50	8.03	13.60	12.98	10.47	12.04	13.16	12.44	13.00	13.35	14.03	10.71	13.81	13.81	13.73	6.31	6.27	7.39	7.25	6.05
Na2O	3.66	2.88	1.63	2.13	3.21	2.40	2.11	2.48	2.00	1.90	1.96	2.92	2.19	2.19	2.14	1.11	1.40	1.50	3.41	1.50
K2O	1.10	1.15	0.32	0.39	0.24	0.29	0.24	0.34	0.23	0.21	0.19	0.40	0.46	0.47	0.47	0.73	1.18	1.34	0.12	1.49
MnO	0.18	0.16	0.19	0.19	0.15	0.18	0.17	0.15	0.17	0.17	0.17	0.14	0.17	0.17	0.17	0.15	0.15	0.16	0.17	0.16
P2O5	0.37	0.33	0.09	0.34	0.13	0.14	0.12	0.20	0.19	0.16	0.18	0.10	0.29	0.30	0.29	0.06	0.06	0.07	0.09	0.06
L.O.I.	0.72	1.33	0.76	0.69	1.00	1.22	1.44	0.70	0.89	2.81	1.20	0.88	0.68	0.74	0.99	1.98	2.63	1.94	1.58	2.12
Total	99.05	99.87	99.20	99.71	100.30	99.74	100.40	99.23	99.35	99.03	99.21	99.70	99.60	99.37	99.93	99.66	100.07	99.60	100.05	99.46
ppm																				
Ba	274				126	118	135	168	109	77	97	250	147	145	151	57	833	361	62	1456
Ni	112	175	272	294	208	347	448	426	480	456	520	340	489	461	459	55	52	55	51	50
V	272	263	280	291	227	217	231	206	203	215	218	220	250	245	250	310	308	270	265	287
Cr	177	371	815	716	340	500	669	774	908	782	1021	770	1088	1082	1052	124	157	162	161	155
Nb	33	33	37	43	15	13	13	18	17	17	19	13	32	35	32	3	1		3	3
Zr	170	160	150	150	76	70	68	110	110	76	102	75	189	195	195	41	44	56	61	43
Y	32	30	21	19	22	17	15	20	15	15	16	18	28	27	27	13	16	21	23	16
Sr	322	4300	150	201	235	165	116	224	219	132	107	453	196	201	203	116	93	116	188	100
Rb	12	13	5	6	7	4	5	2	2	3	2	5	3	2	2	28	28	30	9	32
La			22.20								12.70					3.60				
Ce			49.00								26.10					n.d				
Pr			6.60								n.d					n.d				
Nd			27.00								14.30					6.20				
Sm			5.90								3.20					1.40				
Eu			1.71								0.94					0.53				
Gd			5.50								3.30					n.d				
Tb			n.d								n.d					n.d				
Dy			4.20								2.70					2.80				
Ho			0.75								0.50					0.59				
Er			2.00								1.40					1.90				
Tm			0.25								0.16					n.d				
Yb			1.30								0.90					1.70				
Lu			0.20								0.13					0.27				

*Total Fe is expressed as FeO, n.d: not determined.

(≈12%), high Al_2O_3/TiO_2 (≈20%) and CaO/TiO_2 (≈17%) ratios are generated by a high degree of partial melting (≈25%) of a pyrolite source. On this basis, dikes intruding metamorphics indicate approximately 25% melting of a pyrolite source. The high degree of partial melting is attributed to input of LIL-enriched hydrous fluids and sediments derived from the descending oceanic lithosphere (Saunders and Tarney, 1984).

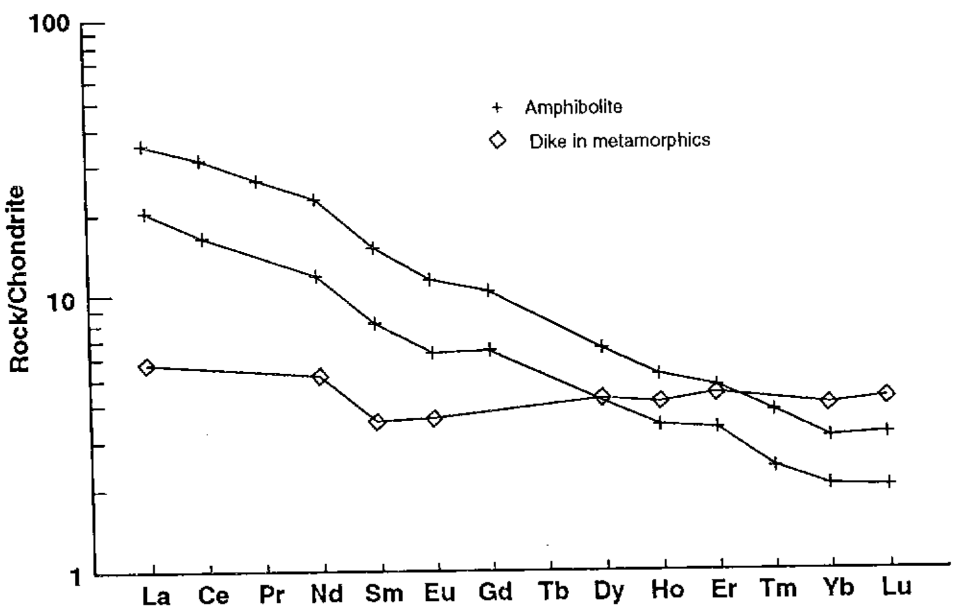

Figure 4.5. Chondrite-normalized REE plots of the amphibolites and dike.

Dikes are more reliable indicators of the original magma composition. REE pattern of a dike sample shows flat pattern (except for negative Sm and Eu anomaly) (Fig. 4.5) similar to back arc basin basalts and island arc tholeiites (Cullers and Graf, 1984). This feature suggests small enrichment in LREE compared to N-MORB source and could be interpreted as volcanic arc component in the formation environment of dike injection. This interpretation is supported by the supra-subduction zone environment of the eastern mediterranean ophiolite complexes (Pearce , 1980; Pearce et al., 1984). MORB-normalized trace element plots of the dikes (Fig. 4.6b) are comparable to trace element patterns of supra-subduction zone ophiolite (Pearce et al., 1984). The enrichment in certain elements such as K, Rb and Ba are interpreted as modification of mantle source by subducted slab component (Pearce et al., 1984; Saunders and Tarney, 1979 and 1984).

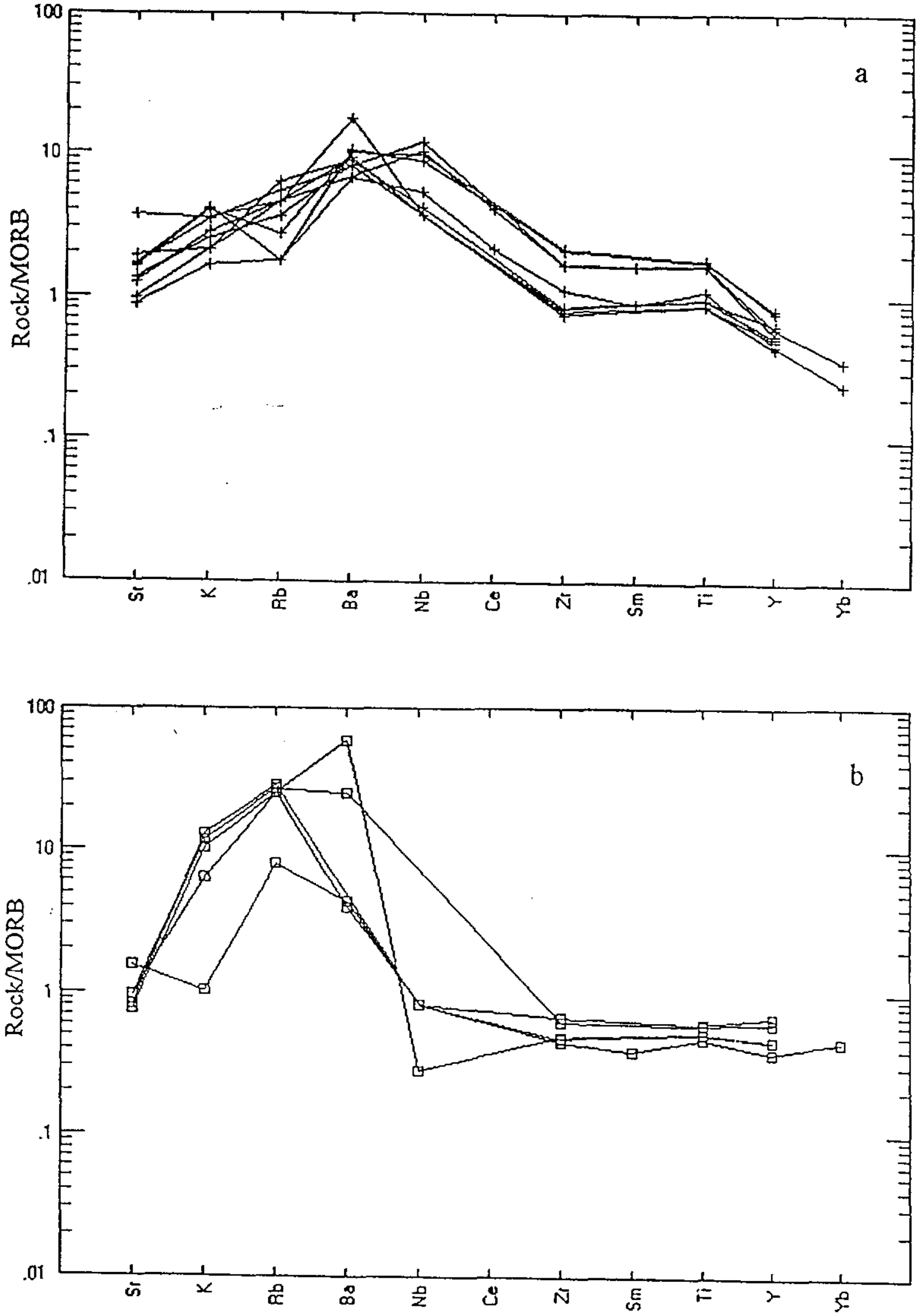

Figure 4.6. MORB-normalized trace element patterns of the amphibolite (**a**) and dike. (**b**) samples (normalizing values from Pearce, 1982).

On the Nb-Zr-Y triangular diagram of Meschede (1986), dike samples plot in N-MORB and VAB field (Fig. 4.7a). On the Ti-Zr-Y triangular diagram of Pearce and Cann (1973) dike samples plot in the arc-tholeiites field (Fig. 4.7b).

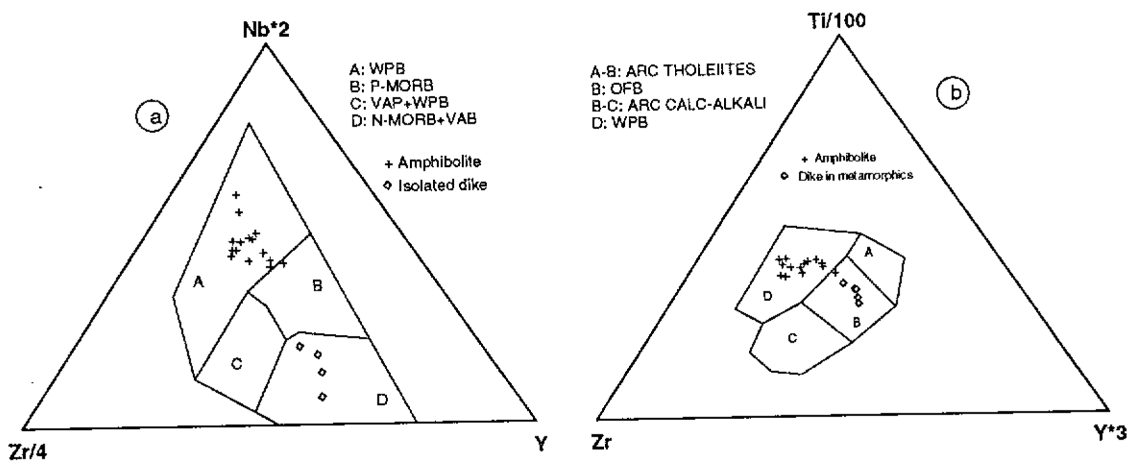

Figure 4.7. a. Nb-Zr-Y tectonomagmatic discrimination diagram for dikes and amphibolites of the Mersin ophiolite (After Meschede, 1986). **b.** Ti-Zr-Y discrimination diagram of dikes and amphibolites in the Mersin ophiolite (After Pearce and Cann, 1973).

4.6. K-Ar age determination of the metamorphic sole

The sub-ophiolitic metamorphic sheet is cut by microgabbro-diabase dikes. These are tholeiitic in composition and plot in the N-MORB and VAB field of Meschede (1986) (Fig. 4.7a). The dikes found in metamorphics are relatively fresh compared to the host rock and are not affected by metamorphism. The interpretation of these relationships may be as follow: the metamorphism took place at a time at which basaltic magma was still beneath the ophiolite sheet and occurred when this rocks were still in an oceanic environment. The same features are seen in Oman (Ghent and Stout, 1981) , in Pozantı-Karsantı (Bingöl, 1978) and in Lycian (Sarp, 1976) ophiolites.

At Fındıkpınarı, the Mersin melange contains slabs of metamorphic rocks indicating that the metamorphism beneath the Mersin ophiolite occurred prior to the formation of the melange. Shallow marine sediments of Paleocene age cap the ophiolitic rocks with an angular unconformity in Namrun area (Avsar, 1992) indicating a minimum age for the emplacement of ophiolite. Ophiolitic rocks are underlain by Upper Cretaceous limestone demonstrating the maximum age of ophiolite obduction in the studied area. K-Ar ages on the hornblendes yield ages of 93 Ma. at Fındıkpınarı, 87-91 Ma. at Gözne and from 77 to 271 Ma. at Sahna respectively (Fig. 4.1b) (Table 4.4). The high age discrepancies obtained

Sample No	Material	Locality	%K	$^{40}Ar/^{36}Ar$ x10^2	$^{40}K/^{36}Ar$ x10^4	^{40}Ar radx10^{-10} moles/g	% Ar rad	Age (Ma)
112	Hornblende	Fındıkpınarı	1.05	17.5868	26.3863	1.7378	83.2	93.0±1.9
131	Hornblende	Gözne	0.26	16.2880	25.7045	0.4288	81.9	87.1±1.8
132	Hornblende	Gözne	0.28	6.7319	6.9561	0.4489	56.1	91.1±1.9
239	Hornblende	Fındıkpınarı	0.85	22.7343	35.7435	1.4006	87.0	92.8±1.9
252	Hornblende	Sahna	0.22	5.7550	4.3992	0.4160	48.7	106.4±2.8
253	Hornblende	Sahna	0.17	0.5500	3.8900	0.8376	24.0	271.3±7.1
254	Hornblende	Sahna	0.17	0.7700	3.8200	0.5734	22.7	183.7±4.4
255	Hornblende	Sahna	0.16	3.3762	0.4684	0.4239	12.5	148.5±3.9
256	Hornblende	Sahna	0.21	6.5041	7.7559	0.2827	54.6	77.1±1.8

Table 4.4. K-Ar ages and analytical data for metamorphic rocks at the base of the Mersin ophiolite, Turkey.

in amphiboles of Sahna may suggest that excess argon and experimental errors can cause such age scattering. However isochron age over all data gives 93.4±2.2 Ma. and no significative argon over-pressure ($^{40}Ar/^{36}Ar$ =325.3±23.3) (Fig. 4.8). This isochron age represents the begining of the compressional regime and the initial detachment of the oceanic lithosphere (Mersin ophiolite) during the closure of the Neo-tethyan ocean in the eastern Mediterranean. The average age for the metamorphism of the sub-ophiolitic metamorphic rocks all over the Tauride belt was presented as 95 Ma by Thuizat et al. (1981).

4.7. Structures and their significance in the metamorphic sole

The metamorphics display a well-developed SE-dipping well-pronounced penetratively developed regional foliation (S_1) that develops parallel or sub-parallel to the original layering or bedding planes S_0 of the parent rock, except along the hinges of F_1 folds. The foliation is invariable associated with a pronounced pervasive NW-SE trending mineral lineation (L_1) that lies in the plane of foliation. Compositional foliation (S_1) is the characteristic planar structures occurring through out the metamorphics. The thickness of widely-spaced compositional domains ranges from a few millimeters to tens of centimeters. In the pelitic rocks, it is defined by the alternation of phyllosilicate domains (P-domain in which planar minerals such as biotite, muscovite and chlorite show remarkable

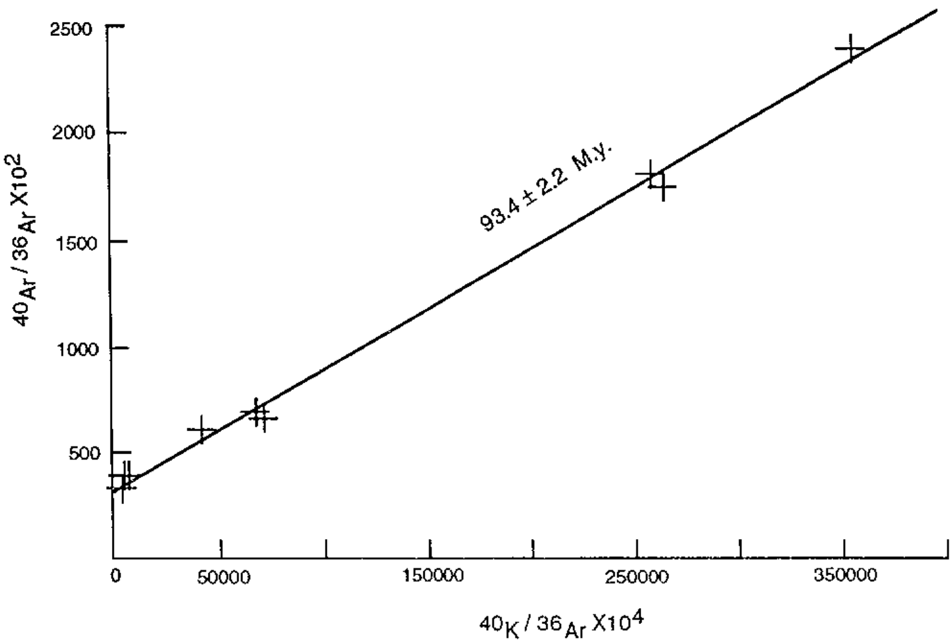

Figure 4.8. Isochron plots of amphibolites in the Mersin ophiolite, Turkey.

preferred parallelism), and quartz-rich domains (Q-domain). In the metavolcanics, the foliation is characterized by the repetition of chlorite-epidote and/or hornblende -rich and quartz-feldspar rich domains, typical of migmatitic structure (Figure 5b,c,d). In the presence of marble intercalations, they display a typical gneisso foliation of alternating marbles and metapelites and/or metavolcanics. The steeply dipping crenulation cleavage (S_2), deforming the pre-existing S_1 foliation, develops as axial surface cleavage along the F_1 folds.

The mineral strecthing lineation (L_1) is penetrative and plunges to the south. It is defined by the preferred parallel alignment of individual elongate platy minerals (such as muscovite, biotite, chlorite) and hornblende, or by the small concentrations of individual mica minerals as hornblende (mineral cluster lineation).

At least two phases of folding (F_1 and F_2) have been recognized in the sub-ophiolitic metamorphics. Their size ranges from microcopic size to tens of meters in wavelenght. F_1 folds are typical asymmetric structures with a SE-dipping axial planes. The F_1 refold earlier S_0 and S_1 regional foliation. They commonly occur as intrafolial folds and vary from tight to isoclinal in style. Most of them are asymmetric-overturned and verge towards NW in the direction of transport and possess a well-developed axial surface cleavage (S_1; see earlier). The presence of F_1 as intrafolial folds suggests that late increments of shearing resulted in the folding of an earlier formed foliation into an intrafolial feature with the axial surface corresponding to the regional foliation of the rock. F_2 folds occur on the limbs of the F_1 folds and are typical S- or Z-shaped, NW-vergent asymmetric folds (Fig.

4.9a). They vary from close to tight in style. The refold earlier S_0 and S_1 regional foliation is commonly associated with a well-developed crenulation cleavage (S_2). The axes of F_2 show remarkable paralellism with those of F_1 folds. This parallelism suggests a genetic relationship between them.

The intensity of their asymmetry of the two phases of folds increases upward towards the boundary with the overlaying mantle tectonites. The close parallelism of F_1 and F_2 fold axes and increase in their asymmetry towards the structurally upper levels suggest that these structures are the product of an essentially continuous progressive single deformation.

Apart from the ductile folds, metamorphic sole is dominated by brittle-ductile structures, such as oblique-slip normal and thrust/reverse faults. Normal faults occur as steeply north-dipping "en èchelon" extension fractures trending in 110^{o}-120^{o} direction (Fig. 4.10). They are usually filled with calcite. Some of them show striated surfaces suggesting an oblique-slip movement along the fractures. The amount of normal offset is variable but usually ranges between a few milimeters to 2-3 centimeters. Small-scale south-dipping reverse and thrust faults trending in 060^{o}-075^{o} direction are also common as much as those of normal faults (Fig. 4.10).

The meso-structures, such as asymmetry of calcite-augen, vergence and asymmetry of F_1 folds, general trend of brittle-ductile structures such as oblique-slip normal and thrust/reverse faults, and vergence of F_2 folds, sigma-type calcite porphyroblasts (Fig. 4.9c), shear band foliation, defined by muscovite and chlorite, and oblique grain-shape foliation of hornblende, all indicate unambiguous non-coaxial deformation and a shear sense of upper levels moving up to the NW. The structural evidence suggests that the Mersin ophiolite was obducted over the Bolkardag Mesozoic carbonates from SE to NW. The shear sense obtained from the sub-ophiolitic metamorphics is compatible with the general trend and vergence of the large scale thrust sheets which comprise the Mersin ophiolite.

4.7.1. Interpretation

Mersin ophiolite in the Central Tauride (southern Turkey) form one of the best exposures to study the emplacement history of a Tethyan-type ophiolite onto an active continental margin during an intra-oceanic subduction event in late Cretaceous.

Non-coaxial fabrics and the general trend of the structures formed during the deformation and associated metamorphism of the sub-ophiolitic metamorphics are consistent with a NNW-directed tectonic transport during the emplacement of Mersin ophiolites onto the passive platform maring in central Taurides. The progressive decrease

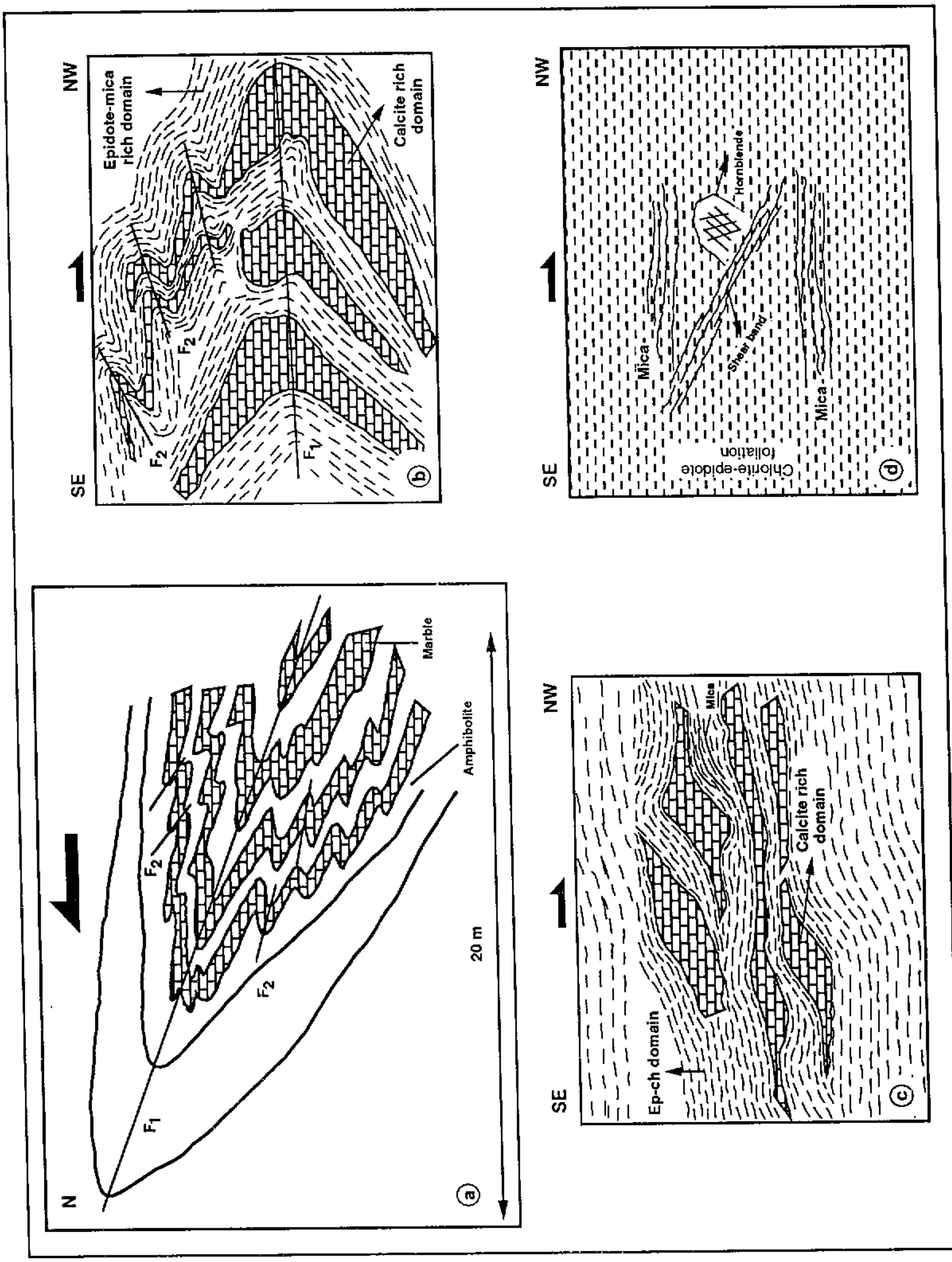

Figure 4.9. a. Field sketch of F_1 and F_2 folds within the metamorphic sole characterized by amphibolite-marble alternation, **(b-d)** line drawings from microscopic observations of various kinematic indicators. **b.** F_1 and F_2 folds in amphibolite comprised by alternating calcite- and epidote-mica -rich domains. **c.** asymmetry of calcite augen (similar to sigma-type porphyroclasts) and **d.** shear band foliation defined by micas, and a grain shape foliation of hornblende. Note that all structures are consistent with a top-to-the-NW shearing. Fold of view is 1.1 cm for (b and c) and is 0.3 cm for (d).

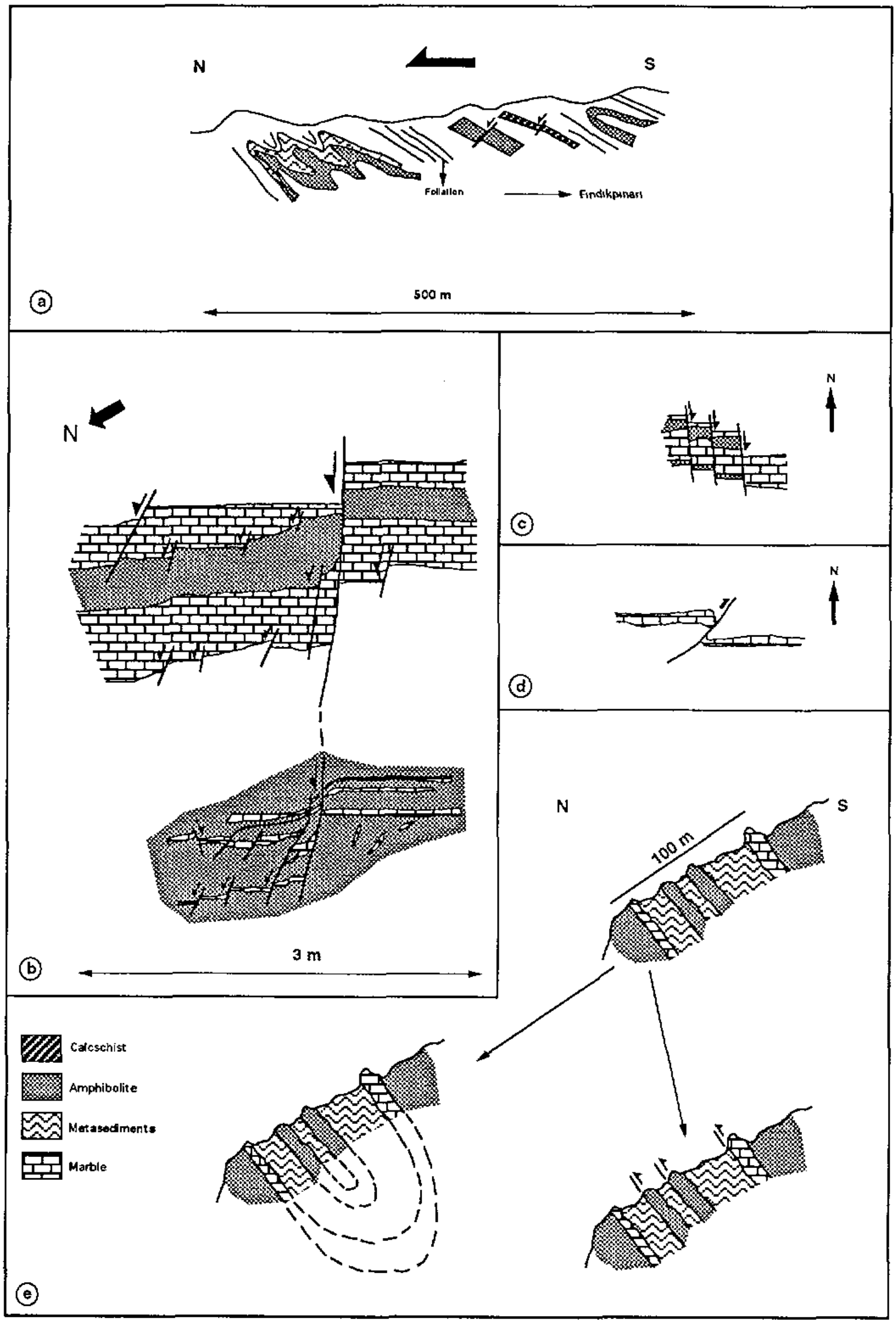

Figure 4.10. Field sketches of some mesostructures in the metamorphic sole.
a. asymmetric, northvergent intrafolial F1 folds. **b-c.** en échelon extensional faults trending in 110-120. **d.** reverse faults trending in 060, and **e.** successive repetition of amphibolite, marble and metasediments and its possible interpretations. Note that it could be interpreted as a fold or a northvergent thrust stacking.

in the grade of metamorphism and in the intensity of deformation from top to bottom within the metamorphic sole is presumably the result of cooling and structural thinning of the overriding plate during intra-oceanic thrusting and indicate that the ophiolite emplacement was a relatively continuous event (cf. Casey and Dewey, 1984).

Parlak et al. (1995b) suggested that the intra-oceanic subduction along the southern branch of the Neotethyan ocean began during Albian-Cenomanian time interval during which the Mersin ophiolites were formed in a supra-subduction zone environment. The subsequent intra- oceanic thrusting resulted in the metamorphism of the subophiolitic amphibolitic sole. The decoupling and obduction of the oceanic lithosphere onto the Tauride belt ceased by the late Paleocene. During the Late Palaeocene, the ophiolites were unconformably capped by clastic sediments, composed mainly of fragments derived from the underlying ophiolites.

4.8. Discussion and conclusion

The evolution of ophiolites in the eastern Mediterranean as a fragment of oceanic lithosphere may be considered as a series of distinct tectonic events which finally result in their emplacement onto the continental margin. Ophiolites in "Tethyan" belt between Yugoslavia and Oman comprise sub-ophiolitic metamorphic rocks showing inverted metamorphic zonation from upper amphibolite to greenschist facies (Woodcock and Robertson, 1977). Alternative heat source mecanisms, namely-heat from serpentinization, -heat from the emplacement of residually hot ophiolite or -frictional heat, have been proposed for the cause of formation of the metamorphic sole beneath allochthonous ophiolite thrust sheet by Woodcock and Robertson (1977).

Metamorphic rocks (amphibolites and dikes cutting metamorphics) of the Mersin ophiolite point out two different sources for the generation of the sub-ophiolitic metamorphic association. The first one is responsible for amphibolite formation whose REE pattern and MORB-normalized trace element features are comparable with ocean island/ seamount basalt (WPB) characteristics. The second one is responsible for the isolated dike generation, demonstrating N-MORB and VAB tendency in terms of trace element and REE geochemistry. These particular features are also clearly seen in the Nb-Zr-Y diagram of Meschede (1986) (Fig. 4.7a) and in the Ti-Zr-Y diagram of Pearce and Cann (1973) (Fig. 4.7b). The possible protholith of amphibolites and metapelitic rocks are ocean island/ seamount basaltic rocks and associated pelagic sediments.

Tectonic setting of the eastern Mediterranean ophiolites is thought to have developed by spreading during the early stages of oceanic subduction (supra-subduction) (Pearce et al., 1984; Robertson, 1994). During the Albian-Cenomanian time interval, intraoceanic subduction may have started in the southern branch of the Neotethyan ocean in the southern Turkey. This event led to the formation of the Mersin ophiolite in the supra-subduction zone environment. Due to the compressional tectonic regime, inception of the intra-oceanic thrusting at 93.4±2 Ma (from K-Ar ages on hornblendes) caused the formation of the amphibolitic sole. The decoupling and obduction of the oceanic lithosphere on the Tauride platform was in progress during the late Cretaceous-early Paleocene. Upper Paleocene ophiolite-derived detritic sediments rest unconformably on the Mersin ophiolite.

Comparison of the amphibolite geochemistry with the other Tethyan ophiolite related metamorphic rocks shows some diversities. Amphibolites in Oman metamorphics are correlated with alkaline and tholeiitic volcanics (Searle and Malpas, 1982) whereas amphibolites of Euboea ophiolite (Greece) show the tendency of island arc tectonic setting (Simantov et al., 1990). The metamorphic sole of the Pindos ophiolite (Greece) presents two major compositional groups such as MORB and WPB (Jones and Robertson, 1991). However, fairly well correlation can be done both for amphibolites and dikes with the ophiolite related metamorphic rocks of Kütahya in Turkey (Önen and Hall, 1993).

4.9. $^{40}Ar/^{39}Ar$ Geochronology

4.9.1. Samples used for $^{40}Ar/^{39}Ar$ geochronology

4.9.1.1. Metamorphic sole

The metamorphic sole crops out at three localities (Fig. 4.1). Samples OP-131 and OP-132 are from Gozne and OP-253, OP-254, OP-255, OP-256, OP-257 are from Sanha (Fig. 4.1). $^{40}Ar/^{39}Ar$ measurements for the metamorphic sole were carried out on pure amphibole separates. The amphibole separates were obtained by crushing hand-sized samples, sieving, and passing the 125-315 µm fractions through heavy liquids. The mineral concentrates were further purified by ultrasonic washings in water, magnetic separation, and hand-picking in order to produce high purity mineral separates (> 99%).

All mineral separates prepared for $^{40}Ar/^{39}Ar$ incremental-heating analysis were analysed for major elements by electron microprobe. Representative amphibole analyses are given in Table 4.2. No systematic zonation from core to rim was observed. Three types of hornblende (Leake, 1978) are distinguished in the studied samples (Fig. 4.4). The first group (OP-131 and OP-132) is generally ferroan pargasitic hornblende and represented by high FeO (12.1-12.6%), low K_2O (0.3-0.4%), low MgO (13.1-14.1%), low SiO_2 (40.5-44.8%) and low Mg*(Mg/Mg+Fe) (0.66). The second group of amphiboles (OP-253, OP-254, OP-255) is dominated by edenite and presents high SiO_2 (46.3-48.8%), high MgO (13.8-15.4%), high Mg* (0.70) low K_2O (0.2-0.4%) and low FeO (10.5-11.4%). The third group (OP-256, OP-257) of amphiboles is characterized by edenitic hornblende that presents intermediate SiO_2 (43.6-45.5%), high FeO (11.7-13.8%), low K_2O (0.4-0.5%), low MgO (11.9-13.6%) and Mg*=0.64 contents (Fig. 4.4).

4.9.1.2. Diabase dikes within metamorphic sole

Three whole rock samples from diabase dikes at Findikpinari (OP-122, OP-129 and OP-227), that intruded the metamorphic sole and are not affected by the metamorphism, have been analysed (Fig. 4.1). Samples OP-129 and OP-227 that show porphyric texture are composed of plagioclase, clinopyroxene and amphibole. Sample OP-122 is characterized by coarse-grained ophitic texture with plagioclase, clinopyroxene, amphibole and quartz. All three samples exhibit same alteration minerals such as chlorite (35%), epidote (1%), sericite (5%), and uralitization (10%).

4.9.1.3. Diabase dikes within mantle tectonites

Three whole-rock diabase samples (OP-80, OP-82 and OP-117) intruding the harzburgitic tectonites were selected for $^{40}Ar/^{39}Ar$ incremental heating analysis (Fig. 4.1). Microscopic studies show that the coarse-grained diabase dikes exhibiting ophitic texture are mainly represented by clinopyroxene, plagioclase and amphibole mineral assemblege. OP-80 and OP-117 samples, that did not give meaningful age spectra, particularly contain low temperature alteration products such as chlorite (20%) and epidote (1%). The results of these samples will not be discussed later in result section. Whereas the OP-82 sample yielded a discordant age spectra that will be discussed later.

4.9.1.4. Tholeiitic basalts

Two samples of tholeiitic basalts (OP-211 and OP-215) located SW of Findikpinari were selected for $^{40}Ar/^{39}Ar$ incremental heating analysis (Fig. 4.1). These basaltic rocks show porphyric texture and consist of augite ($Ca_{37-40}Mg_{41-45}Fe_{16-18}$) and laths of albitized-plagioclase as phenocryst phases. The matrix is characterized by extensive alteration with development of clays and other low temperature phases such as those of chlorite (50%), albite (35%), calcite (5%), and quartz (5%) in tholeiitc basaltic rocks. Two different total fusion ages from stratigraphically same level and the discordant age spectra suggest that either the samples have lost their ^{40}Ar after the crystallization by tectonic or thermal events or chemical alteration. Potassium loss or gain, excess ^{40}Ar, K-derived ^{39}Ar, low temperature loss of radiogenic ^{40}Ar could be the reason for the discordant age spectra in these tholeiitic basaltic rocks (Turner and Cadogan, 1974; Fleck et al., 1977; McDougall and Harrison, 1988). Due to recoil problem causing ^{39}Ar redistribution in K-rich alteration minerals during irradiation at the reactor center, none of these two samples did not yield an age spectra to be able to interpret in any meaningful way. $^{40}Ar/^{39}Ar$ incremental heating analyses of tholeiitic basalts will not be discussed later in results section.

4.9.2. $^{40}Ar/^{39}Ar$ results

4.9.2.1. Sub-ophiolitic metamorphic sole

A summary of the $^{40}Ar/^{39}Ar$ results for the hornblende separates from the metamorphic sole and the whole rocks are presented in Table 4.5. The age spectra, K/Ca ratios and isotope correlation diagrams of the hornblendes from the metamorphic sole are presented in Figure 4.11a-b-c-d-e-f-g. Representative analytical data for $^{40}Ar/^{39}Ar$ incremental heating experiments are given in Table 4.6.

Sample OP-131 from the metamorphic sole yielded an undisturbed age spectra, in which all 20 steps define a plateau with a weighted mean age of 91.9±0.3 Ma. Using an $^{40}Ar/^{36}Ar$ vs $^{39}Ar/^{40}Ar$ isotope correlation diagram the isochron age calculated from the 20 plateau steps is 91.6±0.3 Ma with an $^{40}Ar/^{36}Ar$ intercept of 297.8±1.6 (Fig. 4.11a).

Hornblende from sample OP-132 yielded a plateau, including 11 of 18 steps (57.3% of the total ^{39}Ar released) that gives a weighted mean age of 92.7±0.3 Ma. The inverse isochron age of the 11 plateau steps is 92.9±0.4 Ma with an $^{40}Ar/^{36}Ar$ intercept of 294.6±0.9 (Fig. 4.11b).

The sample OP-253 shows a decrease in low temperature steps (86 to 74 Ma) and then increase to plateau steps, comprising 13 of 17 increments and 83.7% of the total ^{39}Ar released during the analysis. Well constrained inverse isochron age of the 13 plateau steps is 92.3±0.6 Ma with an $^{40}Ar/^{36}Ar$ intercept of 294.6±0.9 (Fig. 4.11c).

The analysis of hornblende OP-254 has a slightly saddle-shaped release spectra, however 12 of the 16 steps (83% of the total ^{39}Ar released) define a plateau that yields a weighted mean age of 93.9±0.4 Ma. Inverse isochron age calculated from the 12 plateau steps is 93.3±0.6 Ma with an $^{40}Ar/^{36}Ar$ intercept of 298.5±2.2 (Fig. 4.11d).

The hornblende separated from OP-255 presents an age spectra that yields generally higher ages at low temperature steps (from 102.8±5 to 95.8±3.5 Ma) and comes down to define plateau steps, consisting of 11 of the 17 increaments (77.7% of the total ^{39}Ar were

				Age spectra			Isochron Analysis			
Whole rock	Unit	Wt. (mg)	Total fusion age (Ma)	Increments used (°C)	^{39}Ar (%) in plateau	Plateau age (Ma)	N	Sums/N-2	$^{40}Ar/^{36}Ar$ Intercept	Age (±1σ) Ma
OP-122	Dike	5.76	89.5±0.3	985-1175	61.4	89.8±0.3	13 of 24	0.58	297.4±7.9	**89.6±0.7**
OP-129	Dike	2.89	89.4±0.5	935-1080	63.8	89.5±0.4	11 of 24	0.73	302.8±3.5	**88.3±0.7**
OP-227	Dike	2.49	82.2±0.3	860-1025	46.4	86.3±0.3	8 of 19	1.14	294.5±5.6	**86.3±0.5**
OP-82	Dike	8.00	59.9±0.4	965-1090	48.8	63.4±0.6	7 of 20	2.60	294.1±4.5	**63.8±0.9**
OP-80	Dike	9.22	51.3±0.3	-	no plateau	-	-	-	-	-
OP-117	Dike	8.55	34.2±0.2	-	no plateau	-	-	-	-	-
OP-211	Basalt	2.73	209.5±0.6	-	no plateau	-	-	-	-	-
OP-215	Basalt	3.62	146.5±0.5	-	no plateau	-	-	-	-	-
Amphibole										
OP-256	Met. sole	12.11	98.2±0.4	1100-1140	61.2	96.1±0.6	7 of 18	1.14	296.0±4.1	**96.0±0.7**
OP-255	Met. sole	12.61	93.9±0.4	1050-1300	77.7	93.6±0.4	11 of 17	0.63	293.3±2.8	**94.0±0.6**
OP-257	Met. sole	12.35	94.4±0.3	1000-1175	68.2	93.7±0.4	11 of 17	1.79	298.5±3.1	**93.4±0.5**
OP-254	Met. sole	11.75	95.1±0.5	1000-1330	83.0	93.9±0.4	12 of 16	1.30	298.5±2.2	**93.3±0.6**
OP-132	Met. sole	11.71	92.4±0.3	700-1135	57.3	92.7±0.4	11 of 18	1.39	294.6±0.9	**92.9±0.4**
OP-253	Met. sole	12.41	91.6±0.4	1000-1350	83.6	91.8±0.4	13 of 17	1.69	292.8±2.8	**92.3±0.6**
OP-131	Met. sole	15.60	91.9±0.3	960-1400	100.0	91.9±0.3	20 of 20	0.98	297.9±1.6	**91.6±0.3**

Table 4.5. Summary table of the $^{40}Ar/^{39}Ar$ incremental heating experiments on samples from the Mersin ophiolite.

released) that yields a weighted mean age of 93.6±0.4 Ma. Inverse isochron age of the 11 plateau steps is 94.0±0.6 Ma with an $^{40}Ar/^{36}Ar$ intercept of 293.3±2.8 (Fig. 4.11e).

OP-256 hornblende separates from the same assemblage has saddle-shaped age spectra that comprises higher ages at low and high temperature steps (130.0±4 Ma and 102.5±1 Ma respectively). The plateau steps comprise 7 of the 18 increments (61.2% of the total ^{39}Ar released), yielding an age of 96.1±0.3 Ma. Inverse isochron age of the 7 plateau steps is 96.0±0.7 Ma with an $^{40}Ar/^{36}$ intercept of 296.0±4.1 (Fig. 4.11f).

Sample OP-257 yielded plateau that consists of 11 steps out of 17 increments. The weighted mean plateau age is 93.7±0.3 Ma and 68.2% of the total ^{39}Ar were released during the plateau steps. The isochron age of the 11 plateau steps is 93.4±0.5 Ma with an $^{40}Ar/^{36}$ intercept of 298.5±3.1 (Fig. 4.11g).

K/Ca ratios of the hornblendes (ranging from 0.01 to 0.1) are similar to those which were obtained from the microprobe analyses (Table 4.2). K/Ca ratios of the hornblende separates yield discordant spectra at low temperature degassing steps possibly due to K-

T (°C)	$^{40}Ar/^{39}Ar$	$^{37}Ar/^{39}Ar$	$^{36}Ar/^{39}Ar$	^{40}Ar (mol)	% ^{40}Ar	K/Ca	% ^{39}Ar	Age (Ma)
Mersin: OP-122 Whole rock (diabase), 5.76 mg, J = 0.0050169, total gas age: 89.5±0.3 Ma								
600	10.657	1.000	0.04689	3.4E-14	43.6	0.490	2.30	93.96 ± 1.44
660	10.341	1.346	0.04351	2.0E-14	44.8	0.364	1.37	91.25 ± 1.48
720	9.803	2.290	0.04120	5.5E-14	44.9	0.214	3.99	86.61 ± 1.07
765	9.952	1.998	0.02762	6.1E-14	55.4	0.245	4.35	87.90 ± 0.79
800	9.975	1.563	0.04277	3.9E-14	44.3	0.313	2.80	88.09 ± 0.61
840	9.982	1.516	0.02534	5.5E-14	57.5	0.323	3.97	88.15 ± 1.54
870	9.657	1.739	0.01290	3.2E-14	72.4	0.282	2.37	85.35 ± 0.75
905	9.863	1.912	0.01700	5.6E-14	66.9	0.256	4.02	87.13 ± 0.83
925	9.651	1.910	0.01278	3.9E-14	72.6	0.256	2.90	85.29 ± 0.68
950	9.897	2.252	0.01380	3.5E-14	71.7	0.217	2.52	87.42 ± 0.59
985	10.188	3.566	0.00956	1.1E-13	80.0	0.137	8.00	89.92 ± 0.52
1000	10.069	5.489	0.01145	7.0E-14	77.3	0.089	4.94	88.90 ± 0.51
1010	10.147	7.623	0.01516	5.2E-14	72.2	0.064	3.68	89.57 ± 0.52
1025	10.226	10.890	0.01368	5.9E-14	76.1	0.045	4.13	90.26 ± 0.47
1040	10.190	10.733	0.01345	5.5E-14	76.4	0.045	3.86	89.95 ± 0.43
1055	10.198	10.874	0.01206	5.8E-14	78.9	0.045	4.08	90.01 ± 0.47
1070	10.228	9.799	0.01229	5.7E-14	78.0	0.050	4.01	90.27 ± 0.56
1085	10.188	7.515	0.00930	6.2E-14	82.4	0.065	4.37	89.93 ± 0.41
1100	10.131	4.624	0.00938	6.2E-14	80.7	0.106	4.39	89.44 ± 0.51
1115	10.152	3.012	0.00794	6.8E-14	82.7	0.162	4.76	89.62 ± 0.36
1130	10.154	2.543	0.00811	7.0E-14	82.2	0.192	4.89	89.63 ± 0.47
1145	10.174	2.727	0.00876	7.0E-14	81.0	0.179	4.92	89.81 ± 0.36
1175	10.150	5.728	0.01719	7.6E-14	68.6	0.085	5.36	89.60 ± 1.07
1250	10.699	15.086	0.03133	1.2E-13	56.8	0.032	8.02	94.32 ± 0.70
Mean weighted plateau age (13 increments, 985 to 1175) = 89.8±0.3 Ma								
Isochron data: Sums/N-2 = 0.58; (40/36) intercept = 297.4±7.9; isochron age = 89.6±0.7 Ma								
Mersin: OP-253 Amphibole, 12.41 mg, J = 0.0041482, total gas age: 91.5±0.4 Ma								
700	11.786	2.999	0.32507	1.1E-14	10.9	0.163	1.12	86.11 ± 7.39
800	10.509	2.888	0.15530	2.1E-14	18.7	0.169	2.47	76.98 ± 3.06
900	10.033	3.081	0.16235	2.5E-14	17.3	0.159	3.11	73.56 ± 2.82
1000	12.606	11.143	0.06908	2.9E-14	39.0	0.044	2.85	91.95 ± 1.56
1060	12.408	22.213	0.05004	4.2E-14	48.4	0.022	4.18	90.54 ± 0.77
1100	12.502	24.253	0.04452	4.6E-14	52.2	0.020	4.64	91.21 ± 1.06
1110	12.609	28.065	0.02859	1.5E-13	66.5	0.017	14.36	91.97 ± 1.00
1113	12.570	28.786	0.02103	8.2E-14	75.8	0.017	8.19	91.69 ± 0.64
1120	12.534	29.155	0.02099	8.1E-14	75.9	0.017	8.02	91.44 ± 0.57
1128	12.772	29.171	0.02091	6.2E-14	76.4	0.017	6.09	93.13 ± 0.68
1135	12.647	28.846	0.01907	6.6E-14	78.7	0.017	6.52	92.24 ± 0.62
1145	12.507	28.485	0.02222	5.1E-14	74.0	0.017	5.06	91.25 ± 0.61
1160	12.483	27.900	0.03184	2.2E-14	62.9	0.017	2.20	91.07 ± 1.05
1200	12.544	29.661	0.04351	3.6E-14	53.9	0.016	3.55	91.51 ± 0.77
1270	12.810	29.269	0.02928	1.1E-13	66.4	0.016	10.87	93.4 ± 0.98
1350	12.977	28.574	0.03543	7.3E-14	60.8	0.017	7.06	94.58 ± 1.27
1420	13.142	28.626	0.05642	1.0E-13	47.2	0.017	9.70	95.76 ± 0.84
Mean weighted plateau age (13 of 17 increments, 1000 to 1350 °C) = 91.8±0.4 Ma								
Isochron data: Sums/(N-2) =1.69; (40/36) intercept = 292.8±2.8; isochron age = 92.3±0.6 Ma								

Table 4.6. Representative $^{40}Ar/^{39}Ar$ analytical data from incremental heating experiments.

rich secondary minerals such as chlorite, and then become constant at high temperature plateau steps.

4.9.2.2. Diabase dikes within the metamorphic sole

The age spectra, K/Ca ratios and isotope correlation diagrams of the whole rock diabase dikes (OP-122, OP-129 and OP-227) that cut the metamorphic sole of the Mersin ophiolite are presented in Figure 4.11h-i-j-k.

OP-122 diabase dike sample yielded a well defined age spectra, including 13 of 24 steps (61.4% of the total ^{39}Ar released) in the plateau that yields a weighted mean age of 89.8±0.3 Ma. Inverse isochron age of the 13 plateau steps is 89.6±0.7 Ma with an ^{40}Ar/^{36} intercept of 297.4±7.9 (Fig. 4.11h).

OP-129 diabase dike samples presents an age spectra that yields young ages (71.9±11.1 Ma) at low temperature steps (650-910 ^{o}C). This analysis is represented by plateau steps, consisting of 11 of the 24 increments between 935 and 1080 ^{o}C and 63.8% of the total ^{39}Ar released. The weighted mean plateau age is 89.5±0.4 Ma and the isochron age is 88.3±0.7 Ma with an ^{40}Ar/^{36} intercept of 302.8±3.5 (Fig. 4.11i).

OP-227 diabase dike sample shows increasing of apparent ages at low temperatures (600-850 ^{o}C) and after the plateau steps progressive decreasing of apparent ages at high temperature steps (1040-1220 ^{o}C). The plateau steps contain 8 of the 19 increments between 860 and 1025 ^{o}C and 46.4% of the total ^{39}Ar released. The weighted mean plateau age is 86.3±0.3 Ma and the isochron age is 86.3±0.5 Ma (Fig. 4.11j).

Whole rock sample of OP-82 yields an age spectra which includes 7 of the 20 increments between 965-1090 ^{o}C and 48.8% of the total ^{39}Ar released during the plateau steps (Fig. 4.11k). Weighted mean plateau age is 63.4±0.6 Ma and inverse isochron age is 63.8±0.9 Ma.

K/Ca ratios of the whole rock samples during ^{40}Ar/^{39}Ar incremental heating analysis yielded discordant spectra, indicating possible recoil problem causing ^{39}Ar redistribution in K-rich alteration minerals (i.e. chlorite) during irradiation at the reactor center. Therefore the ages obtained from whole rock samples should be used with caution.

Some of the samples, such as tholeiitic basalts (OP-211 and OP-215) and isolated dikes (OP-80 and OP-117) from different stratigraphic level of the Mersin ophiolite yielded strongly discordant age spectra that do not suggest any meaningful chronologic informations. Relatively large amounts of microcrystalline matrix (~50%) in these samples suggests that ^{39}Ar recoil may be significant (Turner and Cadogan, 1974; Fleck et al., 1977; McDougall and Harrison, 1988).

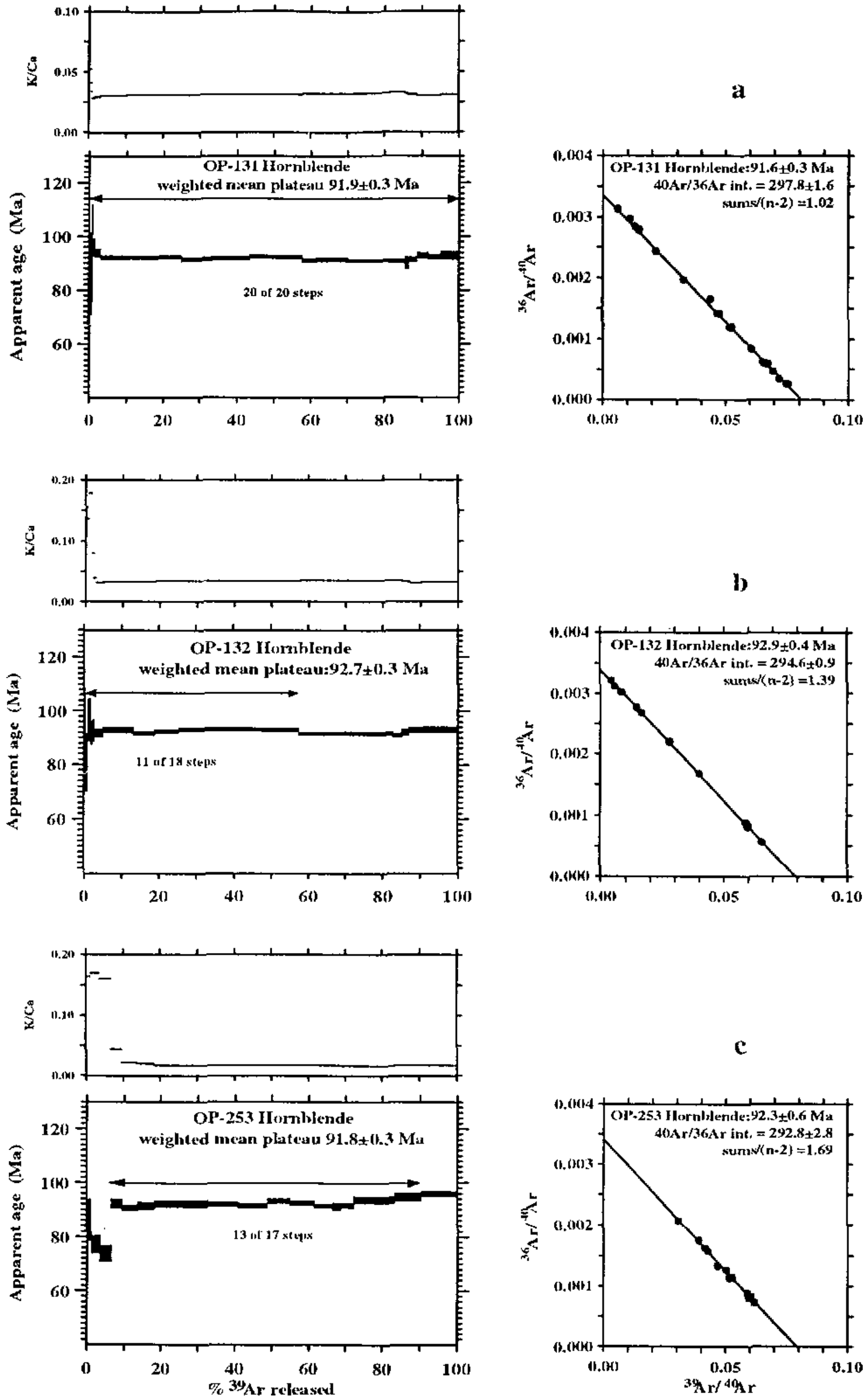

Figure 4.11. Age spectra, inverse isotope correlation diagrams and K/Ca ratios of the amphiboles (from the metamorphic sole) and dike samples in the Mersin ophiolite.

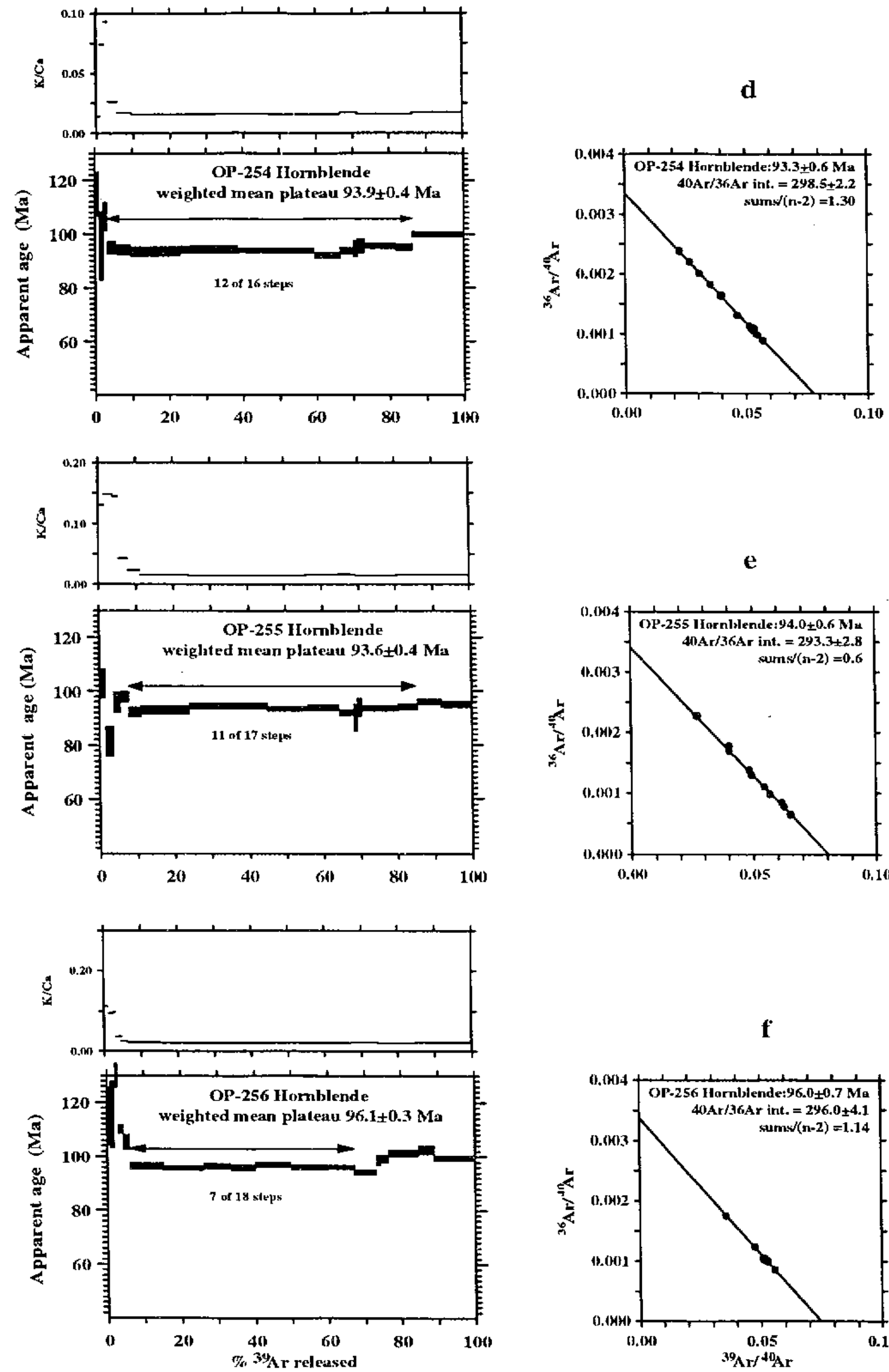

Figure 4.11. (continued).

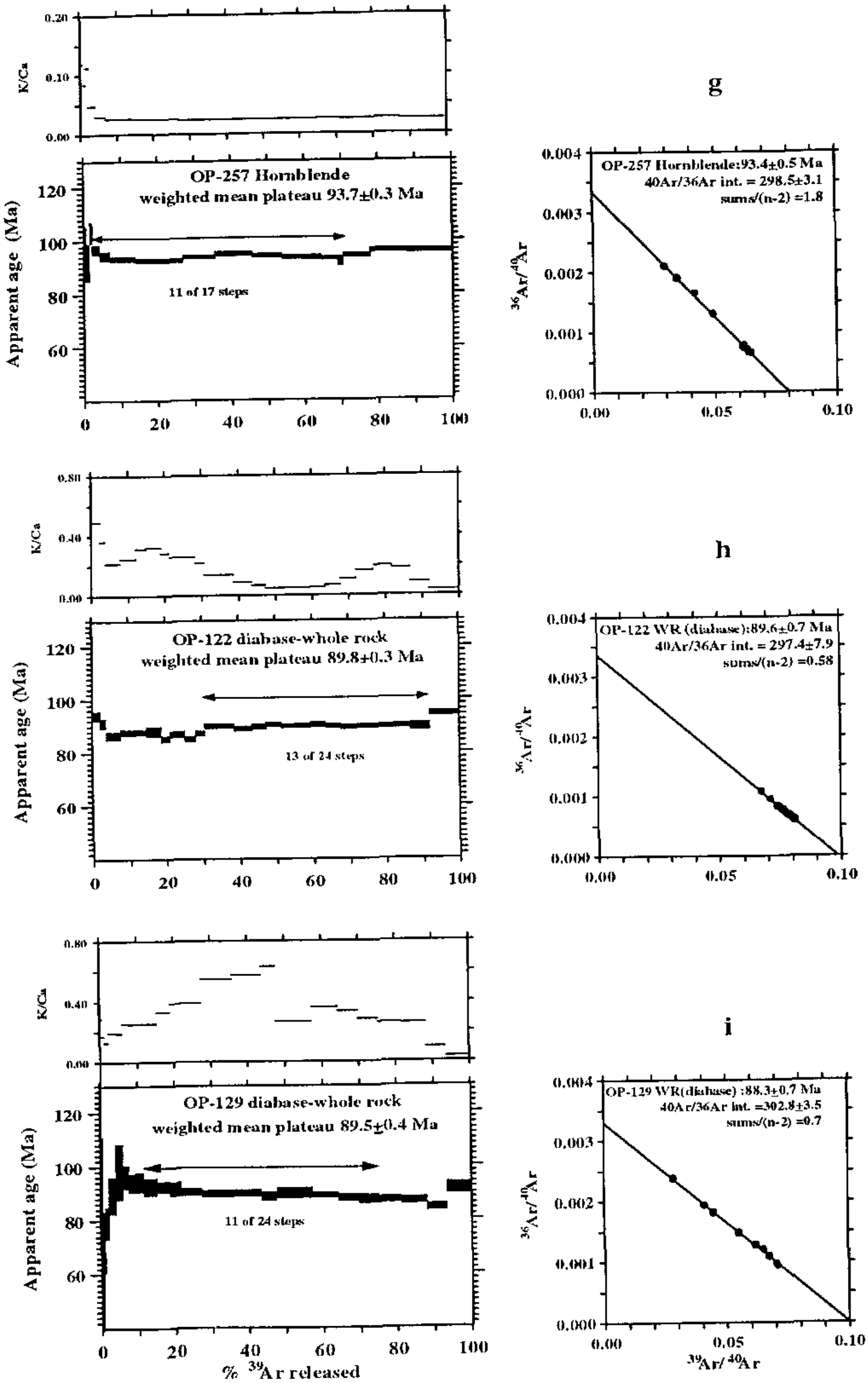

Figure 4.11. (continued).

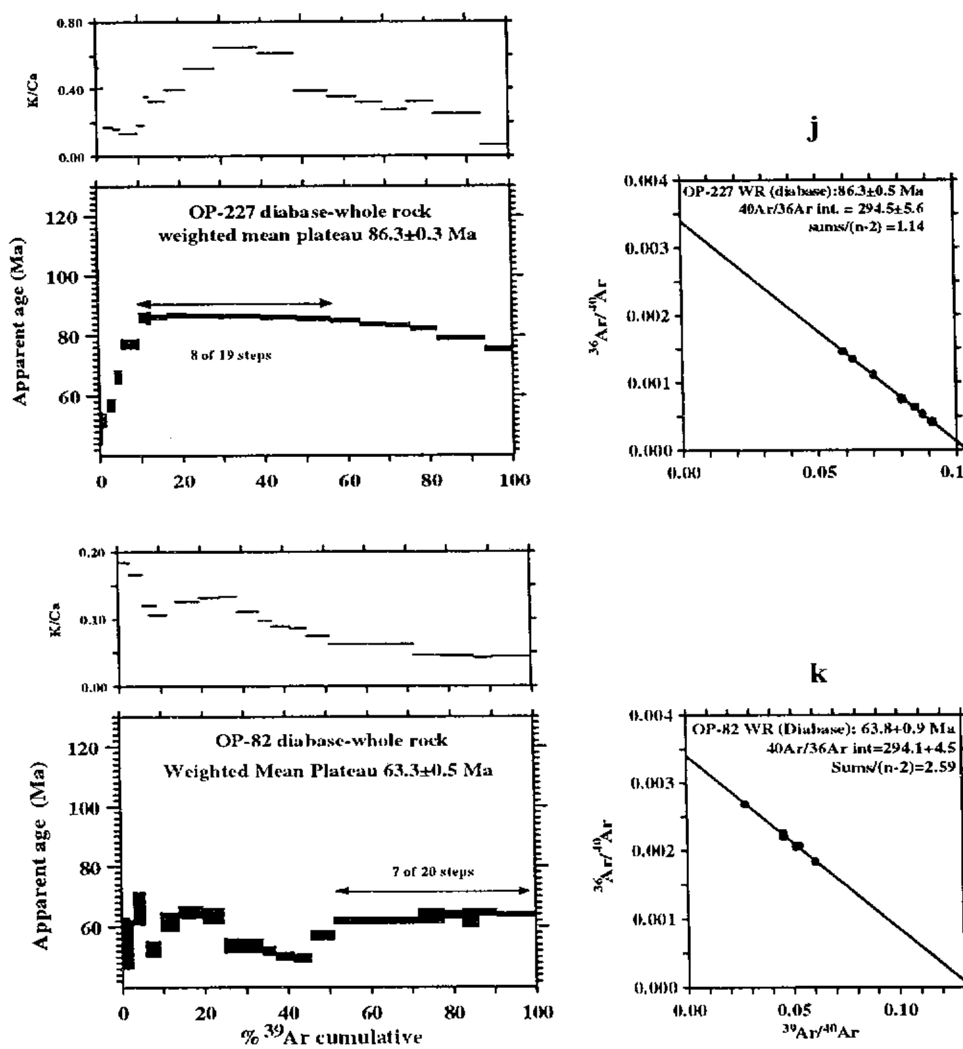

Figure 4.11. (continued).

4.9.3. Discussion

The $^{40}Ar/^{39}Ar$ thermochronology has been widely used for different mineral phases based on the assumption of the argon closure temperatures (Harrison et al., 1979; Berger and York, 1981). Closure temperature for amphiboles we have adopted 510±25 ^{o}C based on the diffusion experiments of Harrison (1981).

All analysed hornblendes are metamorphic in origin and characterized by ferroan pargasitic hornblende, edenite and edenitic hornblende. O'Nions et al. (1969) suggested that the closure temperature for argon in metamorphic hornblendes may be a function of Fe/(Fe+Mg) ratios. However Cosca and O'Nions (1994) showed that composition is probably not an important factor. The ages obtained from hornblendes represent cooling ages whereas the whole-rock samples suggest igneous crystallization age of the dike emplacement in the Mersin ophiolite. The hornblendes formed in amphibolites were subjected to metamorphic temperatures about 800 ^{o}C (Cosca et al., 1991; Gnos and Peters, 1993). All age spectra of the hornblende show generally flat release patterns, suggesting no thermal disturbance after the cooling of the amphibolite facies rocks below 500^{o}C between 96.0±0.7 Ma and 91.7±0.3 Ma. Weighted mean age of the five (except OP-131 and OP-256) of the seven amphiboles yielded 93.1±0.3 (2σ) Ma, indicating the age of the intraoceanic thrusting during which subophiolitic metamorphic rocks formed.

Three whole rock-dike samples (OP-122, OP-129 and OP-227) that cut the metamorphic sole and were not affected by the intraoceanic metamorphism gave isochron ages of 89.6±0.7 Ma, 88.3±0.7 Ma and 86.3±0.5 Ma respectively (Table 4.5). Apart from the low temperature steps yielding younger ages because of the low temperature alteration, age spectra of the diabase dikes, except OP-122, suggest a possible thermal disturbance at about 60-65 Ma may have affected slight argon loss. This effect may reflect thrust tectonic processes that reheated and disturbed the system above argon closure temperature during the obduction onto the Tauride platform around late Cretaceous-Paleocene transition. OP-129 and OP-227 samples show decreasing age spectra, suggesting possible ^{39}Ar recoil problem. The ages of the diabase dikes could be interpreted as the igneous crystallization age of dike emplacement.

Whole rock sample (OP-82) dike within mantle tectonite gave strongly discordant age spectra and are not interpretable with the criteria of Singer and Pringle (1996). The only reasonable interpretation for this sample is that it probably formed before 63 Ma.

$^{40}Ar/^{39}Ar$ cooling ages obtained from the metamorphic sole and dikes in the Mersin ophiolite are shown in Figure 4.12 in order to compare to other K-Ar and $^{40}Ar/^{39}Ar$ ages from similar tectonic units from the Tauride belt and Baer-Bassit ophiolite. New $^{40}Ar/^{39}Ar$ age data from the Mersin ophiolite clearly show that timing of intraoceanic thrusting (92.6±0.2 Ma) and post-metamorphic dike emplacement (87.6±0.4 Ma) are much better constrained in this study.

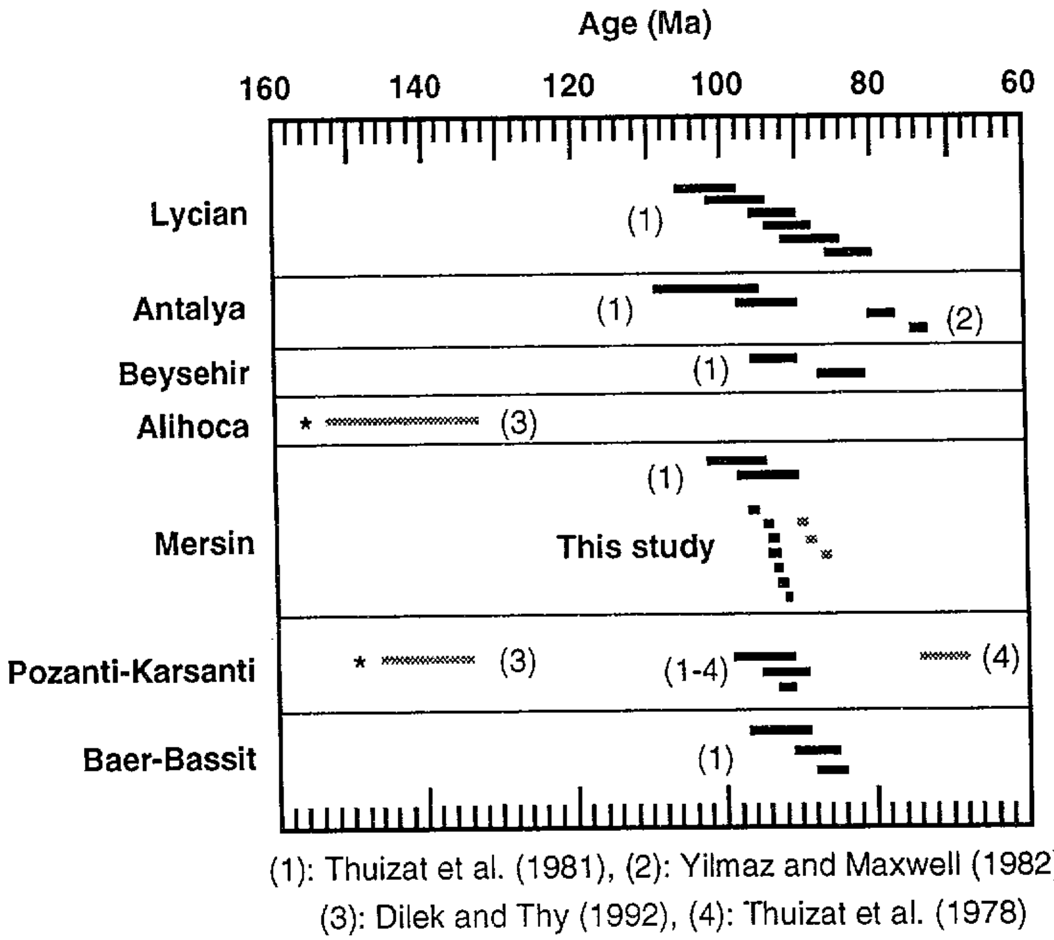

Figure 4.12. Previous K-Ar and $^{40}Ar/^{39}Ar$ (*) ages from the metamorphic sole and mafic dike intrusions in ophiolites, Southern Turkey.

4.9.4. Implications for the evolution of the Neotethyan oceanic crust

Moores (1982) subdivided ophiolites into Tethyan and Cordilleran types. Tethyan ophiolites obducted as a result of continent-continent collision along passive margins are generally associated with tectonic melange and sub-ophiolitic metamorphic soles whereas Cordilleran ophiolites emplaced as a result of arc-continent collisions are represented by dismembered pseudostratigraphy of small ocean basins or island arc/back arc fragments (Moores, 1982; Coleman, 1986; Dilek and Moores, 1990). Most studies of Tethyan ophiolites in Turkey focused on how many root zones exist in which ophiolites were formed and mechanisms by which ophiolites were emplaced onto continental margins.

However there is still debate over these ideas (Sengör and Yılmaz, 1981; Robertson and Dixon, 1984; Ricou et al., 1984; Whitechurch et al., 1984; Sengör, 1990).

The following evolutionary scenario is proposed for the formation of the NeoTethyan oceanic crust based on fossil evidences and $^{40}Ar/^{39}Ar$ geochronology from the Mersin ophiolite case study (Fig. 4.13). Initiation of the rifting of NeoTethyan ocean along the northern margin of the Gondwanaland started during Middle-Late Triassic-Early Jurassic time interval (Sengor and Yilmaz, 1981; Robertson and Dixon, 1984). Micritic limestones intercalated with alkaline volcanics and tuffs croping out in the melange sequence of the Mersin ophiolite yielded following fossils: *Meandrospira sp., Glomospira sp., Aulotortus sp., Duostominidae sp., Frendicularia sp., Involutina sp., Trochammina , Algea* , indicating Upper Triassic (Carnian-Norian) time for the beginning of the oceanization in the study area (Fig. 4.13a). Robertson and Woodcock (1982) reported also Anisian-Carnian time interval for the early stage of crustal extension in the Antalya ophiolite. Upper Triassic plant-bearing sandstones that are exposed in the Tauride belt (Özgül, 1976) support the early stage of crustal extension and shallow water sedimentation in the study area (Fig. 4.13a-b). Continued spreading within rift basins namely southern and multi-armed northern branch of the Neotethys (Sengör and Yılmaz, 1981) was in progress during Jurassic and Early Cretaceous. This period is dominated by calcareous and terrigenous deposition to finer grained siliceous pelagic and hemipelagic sedimentation (Fig. 4.13c) (Robertson and Woodcock, 1982; Özgul, 1976; 1984). Late Jurassic-Early Cretaceous aged extensive ocean island/seamount alkaline basaltic volcanism intercalated with cherty limestone and radiolaria occured in the study area (Fig. 4.13c).

After the opening of the south Atlantic ocean (Smith et al., 1981) in Early-Late Cretaceous, rifting ceased and convergence between Afro-Arabian and Eurasia plates began. As a result of continuous convergence in the southern branch of the Neotethyan ocean, a north dipping subduction at the begining of Late Cretaceous developed arc-related or supra-subduction zone ophiolite bodies in the eastern Mediterranean region (Pearce et al., 1984; Jones et al., 1991; Robertson, 1994). The Mersin ophiolite was formed above subduction zone in the southern branch of the Neotethyan ocean (Fig. 4.13d). Geochemistry of the volcanic rocks and mineral chemistry of the ultramafic and mafic cumulates clearly indicate that the Mersin ophiolite presents the main features of the supra-subduction zone ophiolites in southern Turkey. Soon after the formation of the oceanic lithosphere, continuous compression led oceanic lithosphere to cause intraoceanic thrusting by following weaknesses within the oceanic crust. Numerous weakness possiblities in oceanic lithosphere where detachment could start are explained by ridge subduction (Hacker, 1991), intraoceanic subduction (Hacker, 1990), and feeding zone of seamounts (Gnos and Peters, 1993). Recrystallization during intra-oceanic thrusting created a basal metamorphic sole that cooled below $500^{o}C$ during the period of time between ~ 96-92 Ma

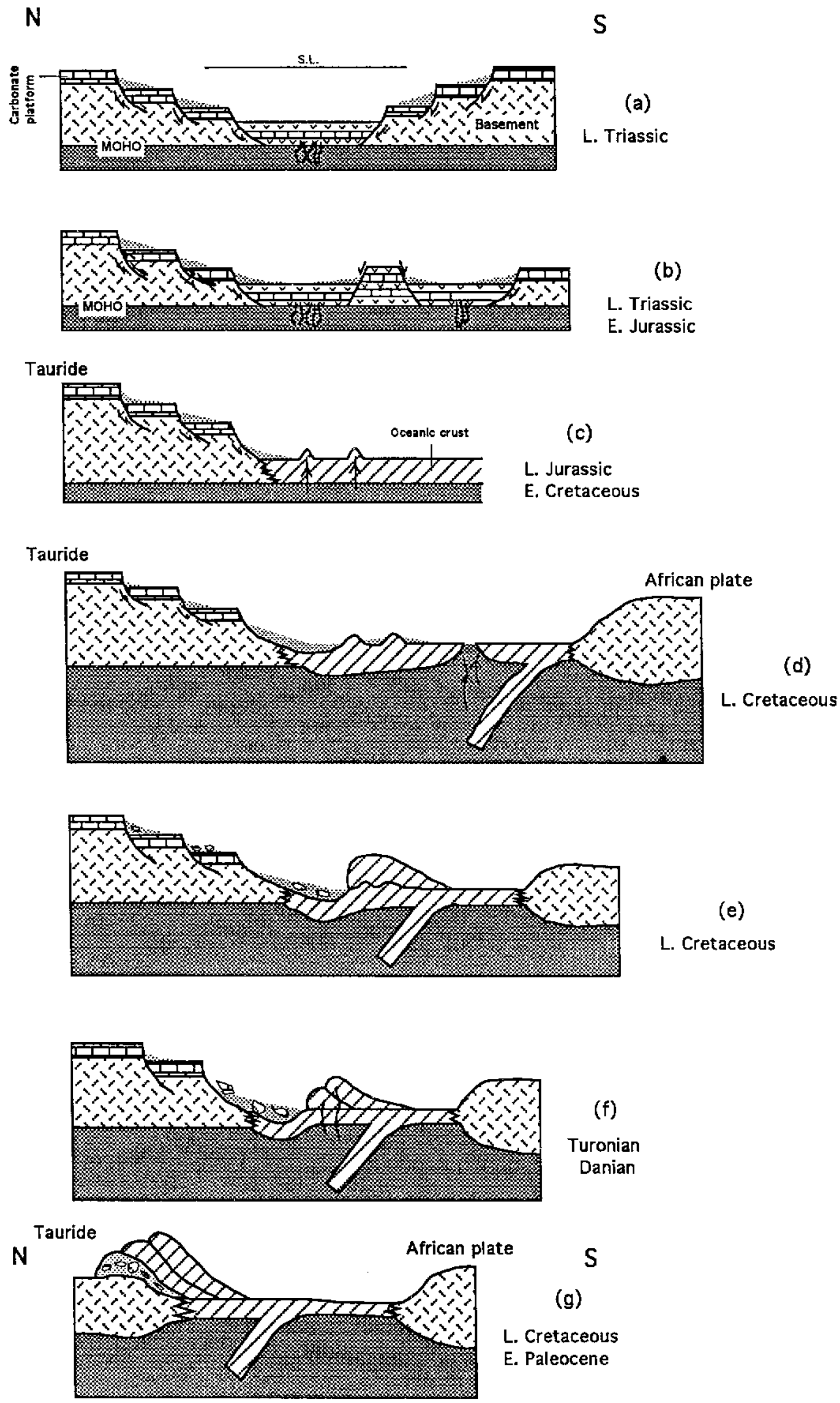

Figure 4.13. Tectonic cartoons illustrating the evolution of the Mersin ophiolite complex (see text for discussions).

(Fig. 4.13e). The geochemistry of basal metamorphic sole suggest the features of ocean island or seamount basaltic rocks from which metamorphic sole was derived (Parlak et al., 1995b). Basaltic melts generated above the subduction zone produced dike swarms intruding the basal metamorphic sole, mantle tectonites, and cumulates of the Mersin ophiolite (Fig. 4.13f). Dike injections occured between 90-86 Ma are younger than the cooling age of the amphibolites in the metamorphic sole. Similar evidence is also seen in the metamorphic sole at the base of the Pozanti-Karsanti ophiolite (Lytwyn and Casey, 1995). The igneous crystallization ages of the dike swarms in the metamorphic sole range from 90 to 86 Ma. These post kinematic dike injections were also in progress in the other part of the oceanic crust during Danian (63.8±0.9 Ma) indicating the presence of an oceanic event in Late Cretaceous-Paleocene before obduction onto the Tauride active continental margin.

The oldest unit resting unconformably upon the ophiolite body is Alveolina-rich Upper Paleocene aged limestones in the eastern part of the Mersin ophiolite (Fig. 4.13g) (Avsar, 1992).

4.9.5. Conclusions

In the light of results of the new $^{40}Ar/^{39}Ar$ incremental-heating analyses on the metamorphic sole and postmetamorphic dike emplacement in the Mersin ophiolite, following conclusions are given;

(1) The cooling ages obtained on amphiboles from the metamorphic sole indicate that these rocks were cooled below 500^{o}C during the period between 96±0.7 Ma and 91.6±0.3 Ma at the base of the Mersin ophiolite. Weighted mean age of the five amphiboles, that do not differ from each other at the 95% confidence level, is 93.1±0.3 Ma. This new $^{40}Ar/^{39}Ar$ age constrains on the metamorphic sole of the Mersin ophiolite does differ from the previously known K-Ar (~ 95 Ma) (Thuizat et la., 1981) in the Tauride belt.

(2) The three diabase dikes cutting metamorphic sole yielded relatively younger ages 89.6±0.7 Ma, 88.3±0.7 Ma, 86.3±0.5 Ma respectively. These ages are interpreted as the igneous crystallization age of the dike emplacement in the Mersin ophiolite.

(3) One important feature of the age spectra of the three dike samples is that all the analyes suggest thermal resetting and ^{40}Ar loose about 60 Ma. This event may correspond with the final obduction of the Mersin ophiolite during late Cretaceous-early Paleocene transition in the study area.

PLATE CAPTION

Plate 4.1

a) Amphibolite schist, calcschist and mica schist intercalation in the metamorphic sole of the Mersin ophiolite at Findikpinari.

b) Epidote- and amphibole-rich layers parallel to main foliation (SE) of the metamorphic sole.

c) Intrafolial folding facing to the NNW in the amphibolites at Sahna valley.

d) Marble-amphibolite intercalation and small scale extensional faults in the metamorphic sole at Sahna valley.

Plate 4.1

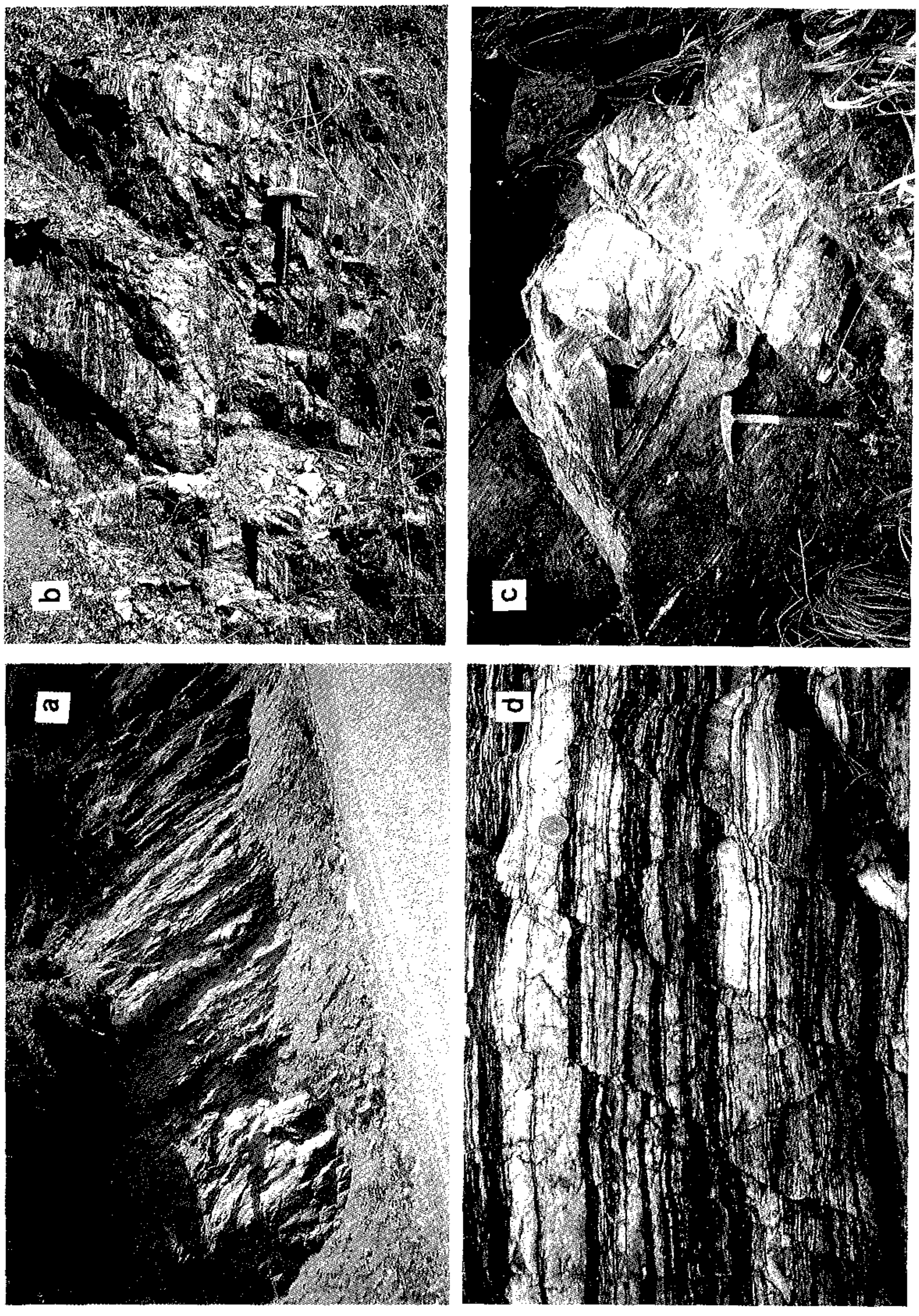

References

Avsar, N., 1992; Namrun (Içel) yöresi Paleojen bentik foraminifer faunası. M.T.A. Dergisi, 114, 127-144.

Berger, G.W., and York, D., 1981; Geothermometry from $^{40}Ar/^{39}$ dating experiments. Geochim. Cosmochim. Acta, 45, 795-811.

Bingöl, A.F., 1978; Pétrologie du massif ophiolitique de Pozantı-Karsantı (Taurus cilicien, Turquie): étude de la partie orientale. Thèse 3e cycle, Univ. Strasbourg, 227 p.

Casey, J.F., and Dewey, J.F., 1984; Initiation of subduction zones along transform and accreting plate boundaries, triple-jonction evolution and forearc spreading centers: implication for ophiolitic geology and obduction. In: Gass, I.G., Lippard, S.J. and Shelton, A.W. (eds.), Ophiolites and oceanic lithosphere. Geol. Soc. Spec. Publ. London, 13, 269-290.

Coleman, R.G., 1986; Ophiolites and accretion of the North American Cordillera. Bull. Soc. géol. France, 8, 961-968.

Cosca, M.A., Sutter, J.F. and Essene, E.J., 1991; Cooling and inferred uplift/erosion history of the Grenville orogen, Ontario: Constraints from $^{40}Ar/^{39}$ thermochronology. Tectonics, 10, 5, 959-977.

Cosca, M.A., and O'Nions, R.K., 1994; A re-examination of the influence of composition on argon retentivity in metamorphic calcic amphiboles. Chem. Geol., 112, 39-56.

Cullers, R.L. and Graf, J.L., 1984; Rare earth elements in igneous rocks of the continental crust: predominantly basic and ultrabasic rocks. In: Henderson (ed.), Rare earth element geochemistry, Elsevier-Amsterdam, 510p.

Dilek, Y., and Moores, E.M., 1990; Regional tectonics of the Eastern Mediterranean ophiolites. In: Malpas, J., Moores, E., Panayiotou, A., Xenophontos, C. (eds.), Ophiolites and oceanic crustal analogues. Proceedings of the symposium "Troodos 1987", 295-309.

Dilek, Y. and Thy, P., 1992; Structure, petrology, and geochronology of mafic dike intrusions in the Tauride belt (S. Turkey) and implications for the Neotethyan paleogeography. American Geophysical Meeting, 73, 43, 546 p. 7-11 December, San Francisco, California.

Fleck, R.J., Sutter, J.F. and Elliot, D.H., 1977; Interpretation of discordant $^{40}Ar/^{39}$ age spectra of Mesozoic tholeiites from Antarctica. Geochim. Cosmochim. Acta, 41, 15-32.

Floyd, P.A., 1993; Geochemical discrimination and petrogenesis of alkalic basalt sequences in part of the Ankara melange, central Turkey. J. Geol. Soc. London, 150, 541-550.

Fuhrmann, U., Lippolt, H.J. and Hess, J.C., 1987; Examination of some proposed K-Ar standarts: $^{40}Ar/^{39}Ar$ analyses and conventional K-Ar data. Chem. Geol., 66, 41-51.

Ghent, E.D. and Stout, M.Z., 1981; Metamorphism at the base of the Semail ophiolite, Southern Oman Mountains. J. Geophys. Res., 86, 2557-2571.

Gilbert, M.C., 1966; Synthesis and stability relations of the hornblende ferropargasite. Amer. J. Sci., 264, 698-742.

Gnos, E., and Peters, T., 1993; K-Ar ages of the metamorphic sole of the Semail ophiolite: implications for cooling history. Contr. Mineral. Petrol., 113, 325-332.

Hacker, B.R., 1990; Simulation of the metamorphic and deformational history of the metamorphic sole of the Oman ophiolite. J. Geophys. Res., 95, 4895-4907.

Hacker, B. R., 1991; The role of deformation in the formation of metamorphic gradients: ridge subduction beneath the Oman ophiolite. Tectonics, 10, 455-473.

Hacker, B.R., 1994; Rapid emplacement of young oceanic lithosphere: Argon geochronology of the Oman ophiolite. Science, 265, 1563-1565, .

Harrison, T.M., Amstrong, R.L., Naeser, C.W. and Harakal, J.E., 1979; Geochronology and thermal history of the Coast plutonic complex, near Prince Rupert, British Columbia. Canad. J. Earth Sci., 16, 400-410.

Harrison, T.M., 1981; Diffusion of ^{40}Ar in hornblende. Contr. Mineral. Petrol., 78, 324-331.

Jamieson, R.A., 1980; Formation of metamorphic aureoles beneath ophiolites: evidence from the St. Anthony complex, Newfoundland. Geology, 8, 150-154.

Jones, G., Robertson, A.H.F. and Cann, J.R., 1991; Supra-subduction zone origin of the Pindos ophiolite, Northwestern Greece. In: Peters, T., Nicolas, A. and Coleman, R.G. (eds.), Ophiolite genesis and evolution of the oceanic lithosphere. Proceedings of the International Conference, Muscat, 7-18 January 1990, 771-801.

Jones, G. and Robertson, A.H.F., 1991; Tectono-stratigraphy and evolution of the Mesozoic Pindos ophiolite and related units, northwestern Greece. J. Geol. Soc. London, 148, 267-288.

Juteau, T., 1980; Ophiolites of Turkey. Ofioliti, 2, 199-235.

Laird, J., 1977; Phase equilibrium of mafic schist and the polymetamorphic history of Vermont. Ph.D thesis, California Inst. Technology, 445p.

Lanphere, M.A., Coleman, R.G., Karamata, S., and Pamic, J., 1975; Age of amphibolites associated with Alpine peridotites in the Dinaride ophiolite zone, Yugoslavia. Earth and Planet. Sci. Lett., 26, 271-276.

Lanphere, M.A., 1981; K-Ar ages of metamorphic rocks at the base of the Samail ophiolite, Oman. J. Geophys. Res., 86, 2777-2782.

Leake, B.E., 1978; Nomenclature of amphiboles. Amer. Mineralogist, 63, 1023-1052.

Lytwyn, J. N., and Casey, J.F., 1995; The geochemistry of postkinematic mafic dike swarms and subophiolitic metabasites, Pozanti-Karsanti ophiolite, Turkey: evidence for ridge subduction. Bull. geol. Soc. Amer., 107, 830-850.

McDougall, I., and Harrison, T.M., 1988; Geochronology and thermochronology by the $^{40}Ar/^{39}Ar$ method. Oxford monographs on geology and geophysics no. 9, 208 p, Oxford University press.

Meschede, M., 1986; A method of discriminating between different types of mid-oceanic ridge basalts and continental tholeiites with the Nb-Zr-Y diagram. Chem. Geol., 56, 207-218.

Montigny R., Le Mer, O., Thuizat, R., and Whitechurch, H., 1988; K-Ar and $^{40}Ar/^{39}Ar$ study of metamorphic rocks associated with the Oman ophiolite: Tectonic implications. Tectonophysics, 151, 345-362.

Moores, E.M., 1982; Origin and emplacement of ophiolites. Rev. Geophys. Space Phys., 20, 735-760.

Okrusch, M., Seidel, E., Kreuzer, H., and Harre, W., 1978; Jurassic age of metamorphism at the base of the Brezovica peridotite (Yugoslavia).Earth and Planet. Sci. Lett., 39, 291-297.

O'Nions, R.K., Smith, D.G.W., Baadsgaard, H., and Morton, R.D., 1969; Influence of chemical composition of argon retentivity in metamorphic calcic amphiboles from south Norway.Earth and Planet. Sci. Lett., 5, 339-345.

Önen, A.P., and Hall, R., 1993; Ophiolites and related metamorphic rocks from the Kutahya region, north-west Turkey. Geol. J., 28, 399-412.

Özgül, N., 1976; Torosların bazı jeoloji özellikleri. T.J.K. Bülteni, 19, 65-78.

Özgül, N., Stratigraphy and tectonic evolution of the central Taurides. In: Tekeli, O. and Göncüoglu, M.C. (eds.), Geology of the Taurus belt. Proceedings of international symposium on the geology of the Taurus belt, 1983, Ankara-Turkey, 77-90.

Parlak, O., Delaloye, M., and Bingol, E., 1994; The main features of the Mersin ophiolite-S. Turkey. Abstracts of International Volcanological Congress (IAVCEI-94) 160p., 12-16 September, Ankara-Turkey, 1994.

Parlak, O., Delaloye, M., and Bingol, E., 1995b; Origin of subophiolitic metamorphic rocks beneath the Mersin ophiolite-Southern Turkey. Ofioliti, 20, 97-110.

Parlak, O., Delaloye, M., and Bingol, E., (in review); Geochemistry of volcanic rocks in the Mersin ophiolite and their tectonic significance in the eastern Mediterranean geology. in IESCA-1995 Proceedings, Int.ernational Earth Sciences Colloquium on the Eagean Region.

Pearce, J.A., and Cann, J.R., 1973; Tectonic setting of basic volcanic rocks determined using trace element analysis. Earth and Planet. Sci. Lett., 19, 290-300.

Pearce, J.A., 1980; Geochemical evidence for the genesis and eruptive setting of lavas from Tethyan ophiolites. In: Panayiotou A. (ed.), Ophiolites. Proceedings of ophiolite symposium, Cyprus, 261-272.

Pearce, J.A., 1982; Trace element characteristics of lavas from destructive plate boundaries. In: Thorpe, R.S. (ed.), Andesites. Wiley and Sons, 525-547.

Pearce, J.A., Lippard, S.J., and Roberts, S., 1984; Characteristics and tectonic significance of supra-subduction zone ophiolites. In: Kokelaar, B.P. Howells, M.F (eds.) Marginal basin geology. Geol. Soc. Spec. publ. London, 16, 77-89.

Polat, A., and Casey, J.F., 1995; A structural record of the emplacement of the Pozanti-Karsanti ophiolite onto the Menderes-Taurus block in the late Cretaceous, eastern Taurides, Turkey. J. Struct. Geol., 17, 1673-1688.

Ricou, L.E., Marcoux, J., and Whitechurch, H., 1984; The Mesozoic organization of the Taurides: one or several ocean basins? In: Dixon, J.E. and Robertson, A.H.F. (eds.), The geological evolution of the eastern Mediterranean. Geol. Soc. Spec. Publ. London, 17, 349-361.

Robertson, A.H.F., and Woodcock, N.H., 1982; Sedimentary history of the south-western segment of the Mesozoic-Tertiary Antalya continental margin, south-west Turkey. Eclogae geol. Helv., 75, 517-562.

Robertson, A.H.F., and Dixon, J.E., 1984; Introduction: aspects of the geological evolution of the eastern Mediterranean. In: Dixon, J.E. and Robertson, A.H.F. (eds.), The geological evolution of the eastern Mediterranean. Geol. Soc. Spec. Publ. London, 17, 1-75.

Robertson, A.H.F., Blome, C.D., Cooper, D.W. J., Kemp, A.E.S., and Searle, P., 1990; Evolution of the Arabian continental margin in the Dibba zone, Northern Oman mountains. In: Robertson, A.H.F., Searle, M.P. and Ries, A.C. (eds.). The geology and tectonics of the Oman region. Geol. Soc. Spec. Publ. London, 49, 251-284.

Robertson, A.H.F., 1994; Role of the tectonic facies concept in orogenic analysis and its application to Tethys in the eastern Mediterranean region. Earth Sci. Rev., 37, 139-213.

Roddick J.F., Cameron, W.E., and Smith, A.G., 1979; Permo-Triassic and Jurassic Ar-Ar ages from Greek ophiolites and associated rocks. Nature, 279, 788-790.

Sarp, H., 1976; Etude géologique et minéralogique du cortège ophiolitique de la région située au Nord-Est de Yesilova (Burdur-Turquie). Thèse Univ. Genève, 373p.

Saunders, A.D., and Tarney, J., 1979; The geochemistry of basalts from a back-arc spreading centre in the East Scotia sea. Geochim. Cosmochim. Acta, 43, 555-572.

Saunders, A.D., and Tarney, J., 1984; Geochemical characteristics of basaltic volcanism within back-arc basins. In Kokelaar B.P. and Howells M.F. (eds.), Marginal basin geology. Geol. Soc. Spec. Publ., London, 16, 59-76.

Saunders, A.D., 1984; The rare earth element characteristics of igneous rocks from the ocean basins. In Henderson, P. (ed.) Rare Earth Element Geochemistry. Elsevier, Amsterdam, 510 p.

Searle, M.P., and Malpas, J., 1982; Petrochemistry and origin of sub-ophiolitic metamorphic and related rocks in the Oman Mountains, J. Geol. Soc. London, 139, 235-248.

Searle, M.P., and Stevens, R.K., 1984; Obduction processes in ancient, modern and future ophiolites. In: Robertson, A.H.F., Searle, M.P. and Ries, A.C. (eds.). The geology and tectonics of the Oman region. Geol. Soc. Spec. Publ. London, 49, 303-320.

Sengör, A.M.C., and Yılmaz, Y., 1981; Tethyan evolution of Turkey: A plate tectonic approach. Tectonopysics, 75, 181-241.

Sengör, A.M.C., 1990; Plate tectonics and orogenic research after 25 years: a Tethyan perspective. Earth Sci. Rev., 27, 1-201.

Shackleton, R.M., Ries, A.C., Bird, R.P., Filbrandt, J.B., Lee, C.W., and Cunningham, J.C., 1990; The Batanian mélange of NE Oman. In: Robertson, A.H.F., Searle, M.P. and Ries, A.C. (eds.). The geology and tectonics of the Oman region. Geol. Soc. Spec. Publ. London, 49, 673-696.

Simantov, J., Economou, C., and Bertrand, J., 1990; Metamorphic rocks associated with the central Euboea ophiolite (Southern Greece): Some new occurences. In: Malpas, J., Moores, E., Panayiotou, A., Xenophontos, C. (eds.), Ophiolites and oceanic crustal analogues. Proceedings of the symposium "Troodos 1987", 285-293.

Singer, B.S., and Pringle, M.S., 1996; Age and duration of the Matuyama-Brunhes geomagnetic polarity reversal from $^{40}Ar/^{39}Ar$ incremental heating analyses of lavas. Earth and Planet. Sci. Lett., 139, 47-61.

Smith, A.G., Hurley, A.M. and Briden, J.C., 1981; Phanerozoic palaeocontinental maps. Cambridge, Cambridge University Press, 102p.

Spray, J.G., 1984; Possible causes and consequences of upper mantle decoupling and ophiolite displacement. In: Lippard, S.J., Shelton, A.W. and Gass, I.G. (eds.), Ophiolites and oceanic lithosphere. Geol. Soc. Spec. publ. London, 13, 255-268.

Spray J.G., Bebien, J., Rex, D.C., and Roddick, J.C., 1984; Age constraints on the igneous and metamorphic evolution of the Hellenic-Dinaric ophiolites. In: Dixon, J.E. and Robertson, A.H.F. (eds.), The geological evolution of the eastern Mediterranean. Geol. Soc. Spec. Publ. London, 17, 619-627.

Steiger, R.H., and Jäger, E., 1977; Subcommision on geochronology: convention on the use of decay constants in geo- and cosmochronology. Earth and Planet. Sci Lett., 36, 359-362.

Sun, S-Su., Nesbitt, R.W., and Sharaskin, A.Y., 1979; Geochemical characteristics of mid-ocean ridge basalts. Earth and Planet. Sci. Lett., 44, 119-138.

Taylor, J.R., 1982; An introduction to error analysis. University Science Books, Mill Valley, California, 270 pp.

Thuizat, R., Montigny, R., Cakir, U., and Juteau, T., 1978; K-Ar investigations on two Turkish ophiolites. In: Zartman, R.E. (ed.), Short papers of the 4th International Conference Geochronology, Cosmochronology, Isotop geology. Geol. Surv. Open-File Report, 78-701, 430-432.

Thuizat R., Whitechurch, H., Montigny, R., and Juteau, T., 1981; K-Ar dating of some infra-ophiolitic metamorphic soles from the eastern Mediterranean: New evidence for oceanic thrusting before obduction. Earth and Planet. Sci. Lett., 52, 302-310.

Tilton, G.R., Hopson, C.A., and Wright, J.E., 1981; Uranium-lead isotopic ages of the Semail ophiolite, Oman, with implications to Tethyan oceanic ridge tectonics. J. Geophys. Res., 86, 2763-2776.

Turner, G., and Cadogan, P.H., 1974; Possible effects of ^{39}Ar recoil in $^{40}Ar/^{39}Ar$ dating. Proc. 5th Lunar Sci. Conf. Geochim. Cosmochim. Acta Suppl., 5, 2, 1601-1615.

Voldet, P., 1993; From neutron activation to inductively coupled plasma-atomic emission spectrometry in the determination of rare-earth elements in rocks. Trends in Analytical Chemistry, 12, 8, 339-344.

Whitechurch, H., Juteau, T., and Montigny, R., 1984; Role of the eastern Mediterranean ophiolites (Turkey, Syria, Cyprus) in the history of the Neo-Tethys. In: Dixon, J.E. and Robertson, A.H.F. (eds.), The geological evolution of the eastern Mediterranean. Geol. Soc. Spec. Publ. London, 17, 301-319.

Wijbrans, M.S., Pringle, M.S., Koppers, A.A.P., and Scheveers, R., 1995; Argon geochronology of the small samples using the Vulkaan argon laserprobe. Proc. (k.) nederl. Akad. Wetensch, 98, 185-218.

Williams, H., and Smyth, W.R., 1973; Metamorphic aureoles beneath ophiolite suites and alpine peridotites: implications with west Newfoundland examples. Amer. J. Sci., 273, 594-621.

Woodcock, N.H., and Robertson, A.H.F., 1977; Origins of some ophiolite-related metamorphic rocks of the Tethyan belt. Geology, 5, 373-376.

Yalınız, M.K., Göncüoglu, M.C., and Floyd, P.A., 1994; Geochemical characteristics and geodynamic interpretation of the Supra-subduction Sarıkaman ophiolite, Central Anatolia. Abstracts of International Volcanological Congress (IAVCEI-94), p162. 12-16 September, Ankara-Turkey.

CHAPTER 5

MERSIN OPHIOLITIC MELANGE

Abstract

The Mersin ophiolite is one of the Neotethyan oceanic crust remnant in the Tauride belt in southern Turkey. It comprises from bottom to top ophiolitic melange, subophiolitic metamorphic rocks showing inverted metamorphism from upper amphibolite to green schist facies, tectonites, ultramafic-mafic cumulates, tholeiitic-alkaline basalts and radiolarites.

The ophiolitic melange in Mersin complex consists of continental margin units, rift assemblages, platform fragments, slabs of ophiolites and metamorphic unit. The contacts between these tectonostratigraphic units are tectonic. Continental margin units present limited outcrop beneath the mantle tectonites of the Mersin ophiolite and are characterized by turbiditic sandstone, mudstone, marls, shales and radiolarites. Platform fragments in ophiolitic melange are represented by rootless E-W oriented limestone blocks ranging from Permian to Upper Cretaceous in age. Rift assemblages in the study area form the most conspicuous unit within the mélange and consist of variable rock fragments such as acidic tuffs intercalated with Carnian-Norian age pelagic limestone indicating initial block-faulting and onset of volcanism in Tauride belt, cherty limestone, radiolarian chert, plant-bearing sandstone, mafic pillow lavas. Sheared serpentinites, highly altered basaltic pillow lavas, gabbros and slabs of deformed metamorphic rocks constitute the other fragments of the ophiolitic melange. A granitic stock, showing the affinity of VAG, is also present in the ophiolitic melange. K-Ar age determinations on muscovite yielded a range between 330-390 Ma.

Continuous rifting and basin extension ceased approximately 94 Ma which marks the formation of amphibolitic sole and the beginnig of closure of the basin. Formation of the ophiolitic melange began in Late Cretaceous during the obduction of the oceanic lithosphere onto continental margin. Transgressive Late Paleocene sediments resting on the ophiolite with angular unconformity indicate that melange formation occurred between Late Cretaceous and Late Paleocene time interval in the Mersin ophiolite complex.

5.1. Introduction

Gansser (1974) described that ophiolitic melange is an association of rock assemblages that consist mainly of an olistostromal and tectonic mixture of ophiolitic material, oceanic sediments and exotic blocks of different age. In Tethyan ophiolites, ophiolitic melanges together with oceanic crust fragments have played an important role in reconstructing plate boundaries in the eastern Mediterranean region during more than last two decade studies. Neotethyan evolution, which began by rifting some time during Carnian-Norian, is dominated by two major ocean basin, namely multi-armed northern branch comprising Intra Pontide, Izmir-Ankara and Inner Tauride oceans and more simple southern branch in Turkey (Sengor and Yilmaz, 1981; Robertson and Dixon, 1984).

Ophiolitic massifs in the Tauride belt are associated with ophiolitic melange and sub-ophiolitic metamorphic rocks (e.g., Lycian nappes, Antalya, Pozanti-Karsanti, Mersin) (Juteau, 1980, Dilek and Moores, 1990). Lycian nappes (Collins and Robertson, 1995), Antalya complex (Juteau et al., 1977; Robertson and Woodcock, 1982; Yilmaz, 1984; Dilek and Rowland, 1993) and Pozanti-Karsanti ophiolites (Juteau, 1980; Tekeli, 1981; Polat and Casey, 1995) were become main focusing terranes of detail examination for determining sedimentological and structural evolution of the Tauride belt. Pampal (1984 and 1987) carried out 1/25000 scale geological mapping in the Mersin ophiolite and associated units and concluded that emplacement of the Mersin ophiolite onto the Tauride platform occurred during Maastrichtian and early Tertiary time interval.

The Mersin ophiolite, croping out as a NE-SW trending belt in the south of Tauride calcareous axis, is located approximately 40-50 km north of Mersin and Erdemli in southern Turkey (Fig. 5.1). The Mersin ophiolite complex (MOC) comprises three nappe packages, of wide-spread ophiolitic melange, subophiolitic metamorphic sole which is either sandwiched between mantle tectonites of the Mersin ophiolite and mélange or beneath the mantle tectonites within deep valleys, and approximately 6 km thick oceanic lithospheric section (Fig. 5.2). Ophiolitic melange in the Mersin ophiolite complex presents a juxtaposed assemblage of different rock units based of age and lithostratigraphic relations. These assemblages are characterized by continental margin units, rift assemlages, platform fragments, slabs of metamorphic rocks, fragments of oceanic lithosphere (Fig. 5.3).

This paper considers the main lithological features of the distinct tectonostratigraphic units and the geochemistry-geochronology of volcanic and granitic rocks in order to reconstruct evolution of the Mersin ophiolite complex (MOC) in southern Turkey.

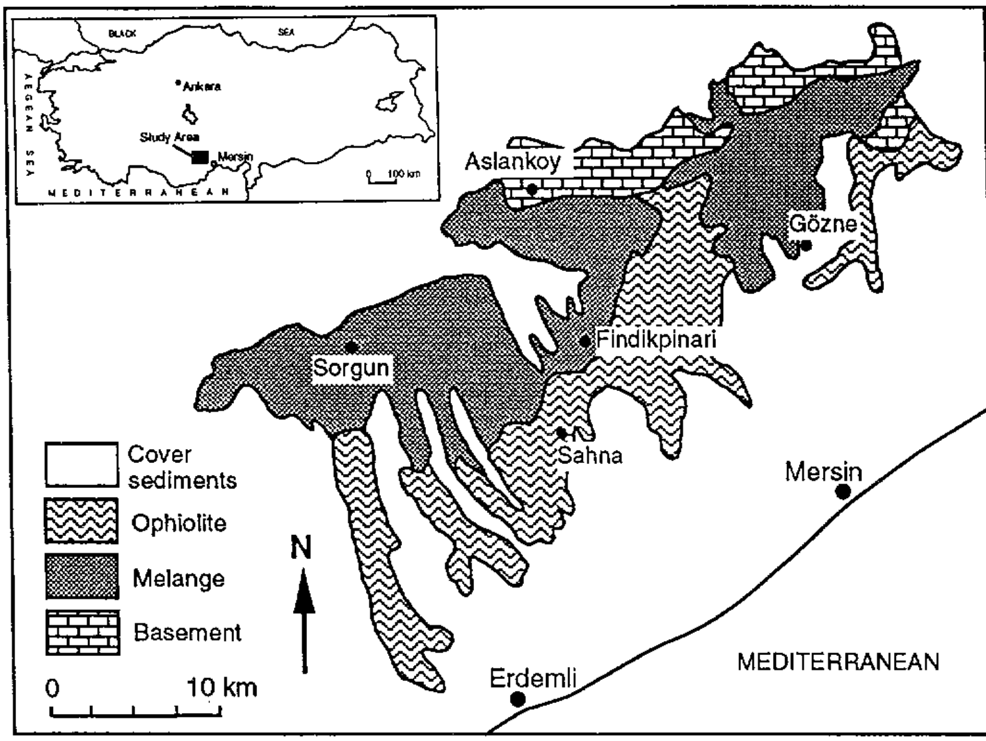

Figure 5.1. Simplified geological map of the Mersin ophiolite complex (MOC).

5.2. Regional geology

The Tauride belt in southern Turkey comprising, on the both side of the calcareous axis (Ricou et al., 1975), a number of dismembered ophiolites (Lycian, Antalya, Beysehir, Mersin, Pozanti-Karsanti) are the remnants of the Neotethyan ocean basin that existed between Afro-Arabian plate to the south and Eurasian plate to the north (Sengör and Yılmaz, 1981; Dilek and Moores, 1990). The initiation of the Neotethyan ocean commenced in Late Triassic time marked by alkaline volcanism and acidic tuffs intercalated with limestones and terrigenous sedimentary rocks (Robertson and Woodcock, 1982; Delaloye and Wagner, 1984; Whitechurc et al., 1984). Whereas the witness of closure of the ocean basin have been documented from sub-ophiolitic metamorphic rocks beneath many ophiolites in the Tauride belt by using conventional K-Ar isotopic age determinations (Delaloye et al., 1980; Thuizat et al., 1978-1981; Yilmaz and Maxwell, 1982). Thuizat et al (1981) concluded that timing of the intra-oceanic thrusting for all over the Tauride belt is 95 Ma.

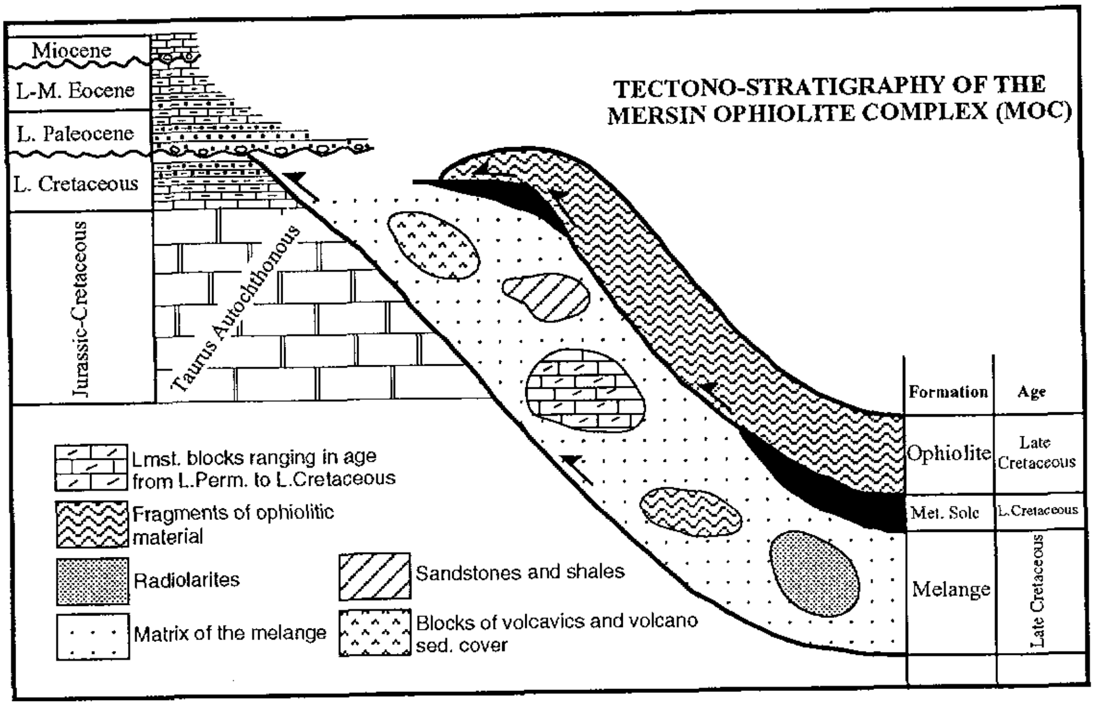

Figure 5.2. The main tectonostratigraphic units of the Mersin ophiolite complex.

The Mersin ophiolite complex (MOC) cropping out on the southern flank of the Bolkardag metamorphics is located in the eastern-end of central Tauride belt in southern Turkey (Fig. 5.1). It is represented by three distinct tectonostratigraphic units namely ophiolitic melange tectonically overlying Tauride platform carbonates of Jurassic-Cretaceous in age, sub-ophiolitic metamorphic sole indicating inverted retrograde metamorphism from upper amphibolite to greenschist facies, intruded by postkinematic diabase dikes and approximately 6 km thick oceanic lithosphere sequences that consist of mantle tectonites, ultramafic-mafic cumulates, and basaltic volcanic suites in association with deep marine sediments.

5.3. Rock units

The Mersin ophiolitic melange in southern Turkey tectonically rests on the southern flank of the Bolkardag to the north and in turn tectonically overlain by Mersin ophiolite to the south. This tectonic assemblage comprises different tectonostratigraphic units all of which have their specific characters. We are going to describe all these units in detail to better reconstruct the evolution of the complex. These units are called as continental margin

Figure 5.3. Detailed geological map of the ophiolitic mélange in the Mersin Ophiolite Complex (S. Turkey).

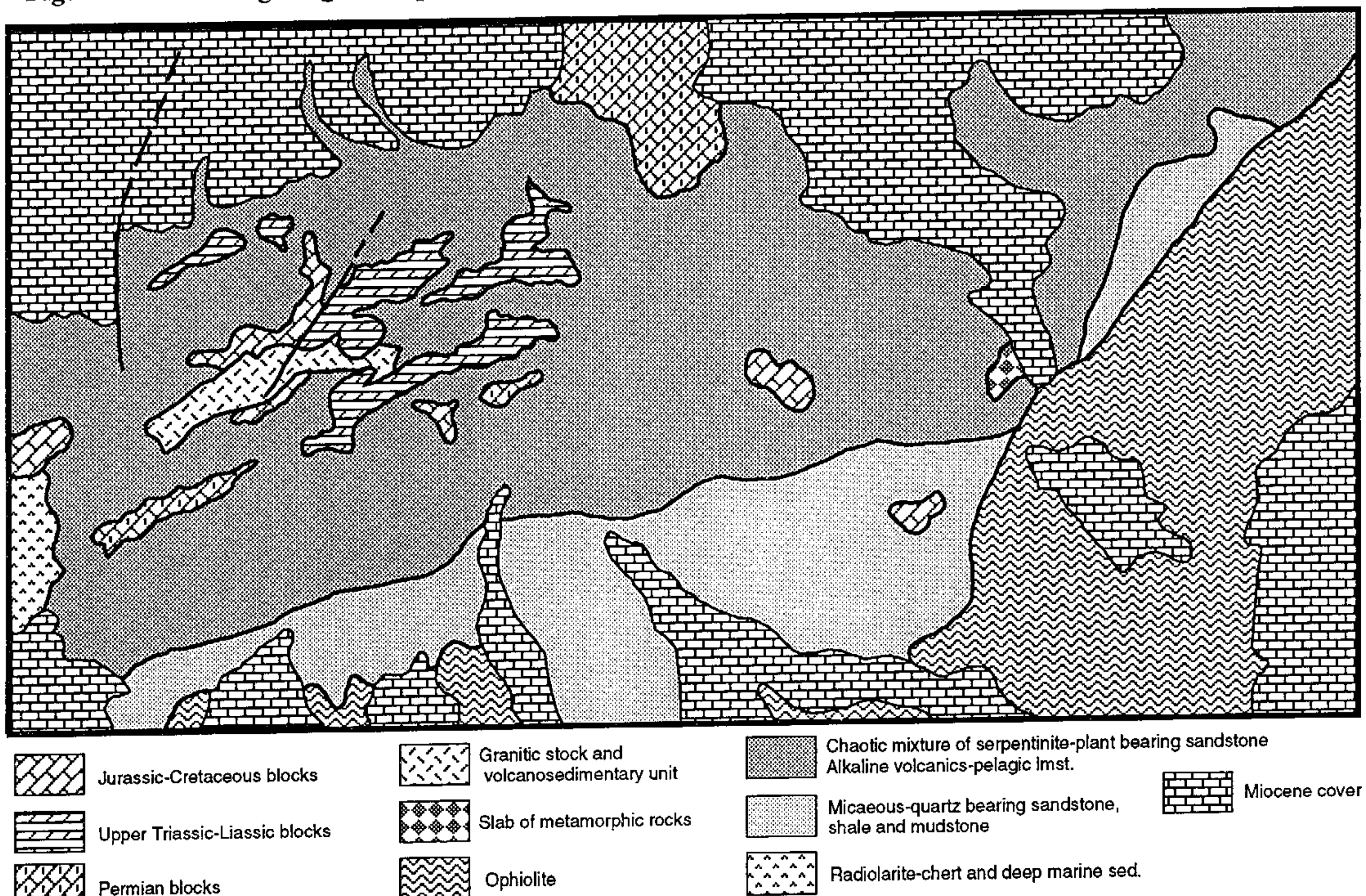

unit, rift assemblage, platform fragments, slabs of ophiolitic and metamorphic units (Fig. 5.3). All these distinct tectonostratigraphic units will be described and a paleogeographic reconstruction for the Mersin ophiolite will be summarized.

5.3.1. Continental Margin Unit

This unit is well exposed beneath the tectonic contact of mantle tectonites between Hacıalanı and Fındıkpınarı (Fig. 5.3). The continental margin unit is represented by turbiditic sandstone, shale, mudstone, marls and radiolarites (Plate 5.1c-d).

Turbiditic sandstones are often intercalated with conglomerate, conglomeratic sandstone, carbonate-cemented sandstone and shale. poorly-graded sandstones are rich in quartz and mica and there is no evidence of ophiolite derived rock fragments. Turbiditic unit might have formed during block faulting of old basement close to continental margin. Rootless limestone blocks ranging from Upper Permian to Jurassic-Cretaceous are present in this unit (Pampal, 1987). This unit tectonically overlies mudstone-marls and radiolarites assemblages to the further north. Because of the imbrication, true thickness of the unit can not be measured. Small-scale north facing folds and thrust faults are dominant structural elements in the unit.

5.3.2. Rift Assemblages

This unit is the most abundant tectonostratigraphic segment of the ophiolitic melange. It comprises acidic tuffs intercalated with Carnian-Norian pelagic limestones, cherty limestone, radiolarian chert, plant-bearing sandstone, black shale and mafic lavas. All these components in the rift assemblages are generally in a chaotic order but locally in a stratigraphic sequence.

The acidic tuffs can be clearly distinguished from other type of volcanic rocks by their green colour. They are generally intercalated with hemi-pelagic limestones (Plate 5.1a). This unit is well seen at the north of Sorgun (Fig. 5.3). The pelagic limestone includes *Duostominidae, Auloteritus sp, Algae, Trochamimina* fossils, indicating Carnian-Norian time interval. The acidic tuffs may be interpreted as the onset of volcanism in the study area. Turbiditic sandstone-conglomerate clastic sedimentation is also present and observed in a unit consisting of pebbles of green-coloured alkaline volcanics due to continuous block faulting along which occurrence of turbiditic sedimentation (Plate 5.2a). New basaltic-diabase lavas, which are interpreted as relatively younger than former acidic tuffs, rest on turbiditic sandstones and conglomerates. Geochemistry of these lavas is presented below. In the north of Hacialani, probable Upper Triassic aged volcanics, black shales and limestone intercalations are seen (Fig. 5.3).

Plant-bearing sandstone, which is exposed all over the Tauride belt (Özgül, 1976; 1984), is seen at Tavusçayiri in the study area (Fig. 5.3) (Plate 5.1b). This unit is intercalated with shales and overlain by Triassic-Liassic limestones. In the area, west of Sorgun, another tectonostratigraphic unit including radiolarite, cherty limestone, pelagic limestone and shale intercalation is present. Fragments of volcanics and serpentinites are included. The age of this unit ranges from Cenomanian to Campanian (Pampal, 1987). This relation shows that these pelagic sediments belong to late stage basinal sequence.

5.3.3. Platform Fragments

This tectonostratigraphic unit represents rootless limestone blocks ranging from Permian to Upper Cretaceous in age (Fig. 5.3-4). These limestone blocks are oriented roughly NE-SW and have faulted contact with underlying rift assemblages and continental margin units (Plate 5.2b-c-d).

Permian aged limestone blocks are seen at Ziyaret Tepe and Sorgun (Fig. 5.3). Upper Triassic fragments are characterized by pelagic limestone blocks intercalated with cherty limestones and radiolarites. These blocks are well exposed at Tavuscayiri and south of Gavuructugu (Fig. 5.3). Within the Upper Triassic sequences, reefal limestone formation is observed in the area between Gavuructugu and Sorgun. At the base of the Jurassic limestones, a brecciated zone is present (at Tavusçayırı), probably due to block faulting and continuous rifting in the region. Jurassic-Cretaceous limestone blocks are seen at Körmenlik Tepe and in the east of Sorgun (Fig. 5.3).

5.3.4. Slabs of Metamorphic rocks

The metamorphic rocks in the ophiolitic melange are seen in the north of Manıt Dagı (Fig. 5.3). These rocks demonstrate polyphase deformation and are folded and imbricated. The metamorphic rocks include amphibolite, amphibolitic schists, quartz-mica schists, calc schists and marbles. Number of microgabbroic-diabasic dikes, which do not show relict of metamorphism, cut these metamorphics. Detailed geochemical features of the metamorphic rocks and intruding dikes have been discussed in Parlak et al. (1995). It has been declared that the protholith of the metamorphics are ocean island/seamount basaltic rocks and associated deep marine sediments. K-Ar analysis on seperated hornblendes yielded an age of 93.4±2 Ma (Parlak et al., 1995). This age corresponds to the initial detachment of oceanic crust during the closure of the Neo-Tethyan ocean in the eastern Mediterranean.

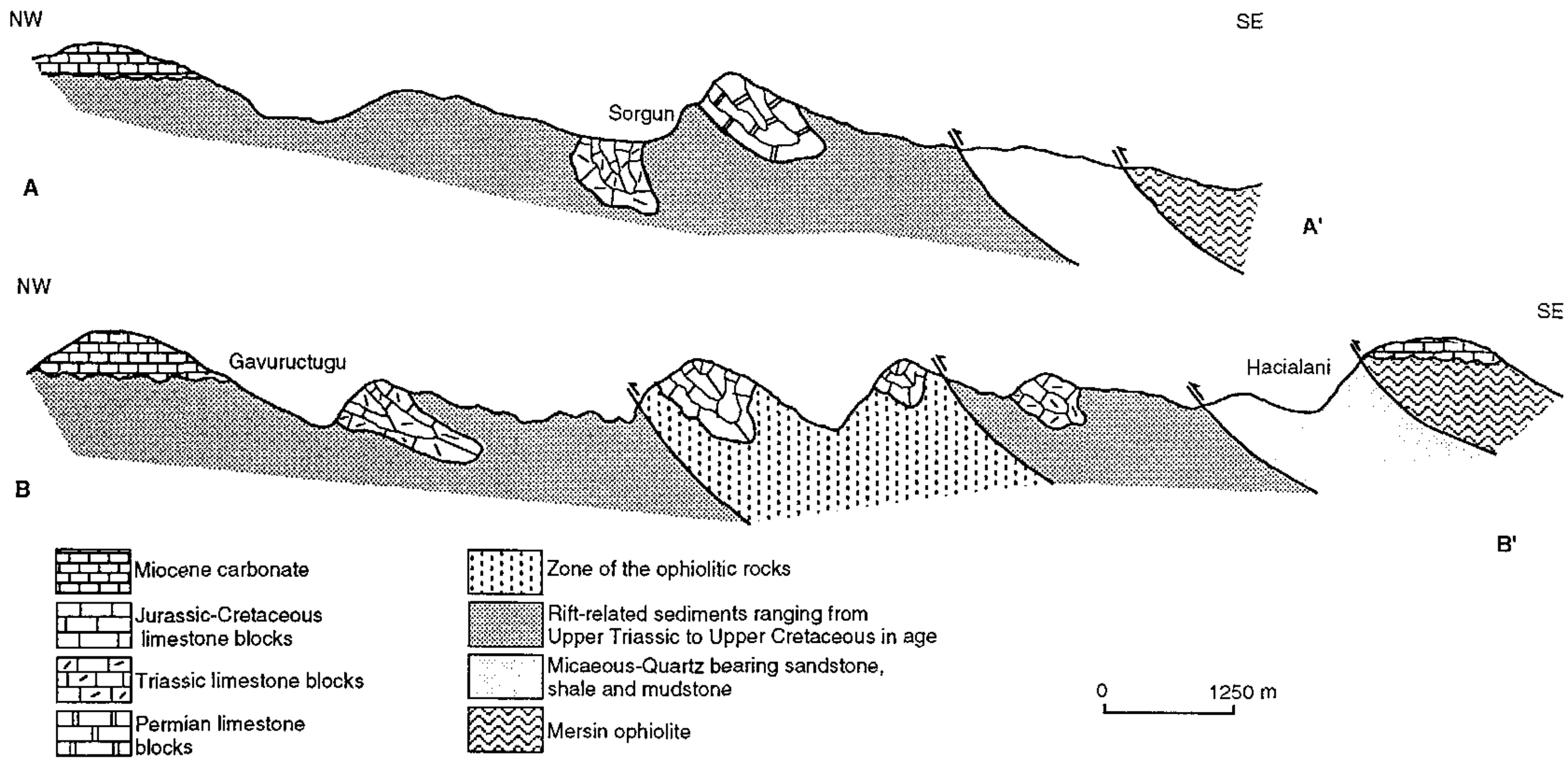

Figure 5.4. Cross-sections showing the relationships of the tectonostratigraphic units in the ophiolitic mélange.

5.3.5. Fragment of oceanic crust

Slabs of ophiolitic rocks are exposed in the area between Asarkayası and Tavusçayırı (Fig. 5.3). They are characterized by serpentinized harzburgite, gabbro, basalt, volcano-sedimentary units and a granitic stock in serpentinites and gabbros. Harzburgites are generally serpentinized and locally preserved in a serpentinzed envelope (Plate 5.3a); olivine-orthopyroxene and chromite are the main mineral phases.

Gabbros are characterized by clinopyroxene and plagioclase. Hornblende and sericite are present as secondary minerals. Due to intensive deformation during the melange formation, gabbros which show some times well preserved foliation pattern are metamorphosed and rarely amphibolitization are seen (Plate 5.3b).

Basaltic rocks and volcanosedimentary unit are the most conspicuous member in this NE-SW trending tectonic zone (Plate 5.3c). Tholeiitic basaltic pillow lavas are highly altered and intercalated with volcanosedimentary unit. The geochemistry of basaltic rocks will be discussed later. The volcanosedimentary unit consists mainly of thin-bedded volcanogenic sandstones, bad-graded conglomerates, shales, mudstones (Plate 5.3d).

5.3.6. Granitic Stock

Granitic rock assemblages are observed within serpentinized harzburgite, gabbro and highly altered basaltic rocks as blocks and lenses (Fig. 5.3). This granitic stock follows an NE-SW trending tectonic linement in further east. They show granular texture and are characterized by following mineral assemblages; quartz (35-40%), alkali feldspar (40%), muscovite (15-20%) and minor amount of biotite (1-5%). Sericitization and chloritization are the main secondary mineral phases. The granitic stock was intensively deformed during amalgamation into the melange unit. As a result of regional metamorphism, granitic rocks have been metamorphosed and garnet-mica schist occurrences were locally observed in some part of the granitic stock. High relief and isotropic nature are the characteristic features of the garnets in the rocks. They are dominated by almandine (>80%) end-member (Table 5.1). Almandines formed during regional metamorphism may show a zoning relations between Fe and Mn. This zoning is marked by Mn-rich core and Fe-rich margin (Deer et al., 1992). The observed almandines in the garnet-mica schist are also characterized by Manganese-rich core and iron-rich rim (Table 5.1).

K-Ar analysis have been done on five muscovite separates from unmetamorphosed granite in order to find out relation with the regional geological context. These K-Ar age determinations yielded an cooling age range from 333-390 Ma. The results are given in Table 5.2. Overall isochron age is 375.7±10.5 Ma (Fig. 5.5). This shows that granitic rocks in the ophiolitic melange belong to an older basement.

Table 5.1. Representative analyses of the garnets from the granitic rocks.

No	271-2c	271-2r	271-3c	271-3r	271-5c	271-5r	271-9c	271-9r	148-1c	148-1r	148-3c	148-3r	148-4c	148-4r	148-5c	148-5r	148-6c	148-6r
SiO2	36.53	36.43	36.54	36.66	36.37	36.68	36.73	36.65	36.66	36.67	36.57	36.80	36.62	36.55	36.69	36.69	36.59	36.49
TiO2	0.00	0.01	0.03	0.00	0.01	0.00	0.07	0.00	0.03	0.00	0.02	0.02	0.05	0.04	0.04	0.01	0.05	0.00
Al2O3	20.93	20.76	20.86	20.71	20.65	20.91	20.78	20.87	20.96	20.82	20.71	20.82	20.91	20.72	20.74	20.99	20.93	20.93
Cr2O3	0.00	0.02	0.00	0.04	0.00	0.00	0.00	0.03	0.00	0.00	0.00	0.00	0.00	0.02	0.02	0.01	0.00	0.03
FeO	37.48	38.09	37.50	38.00	35.02	37.63	35.50	38.21	35.99	36.93	35.60	37.01	34.62	35.24	35.38	36.70	35.21	36.43
MnO	2.28	1.89	2.63	1.88	4.07	2.02	4.48	2.02	3.68	3.44	4.40	3.64	5.19	4.47	4.76	3.46	5.05	3.76
MgO	1.89	1.86	1.88	1.91	1.57	1.87	1.54	1.93	1.81	1.75	1.76	1.81	1.65	1.79	1.76	1.74	1.72	1.78
CaO	1.32	1.16	1.39	1.18	1.70	1.22	1.96	1.18	1.58	1.20	1.58	1.21	1.49	1.40	1.48	1.19	1.51	1.36
Total	100.43	100.22	100.83	100.38	99.95	100.33	101.06	100.89	100.71	100.81	100.64	101.31	100.53	100.23	100.87	100.79	101.06	100.78
Si	5.92	5.92	5.90	5.95	5.74	5.95	5.93	5.92	5.93	5.93	5.92	5.92	5.94	5.94	5.93	5.93	5.90	5.90
Ti	0.00	0.00	0.00	0.00	0.00	0.00	0.01	0.00	0.00	0.00	0.00	0.00	0.01	0.00	0.00	0.00	0.01	0.00
Al IV	0.08	0.08	0.10	0.05	0.26	0.05	0.07	0.08	0.07	0.07	0.08	0.08	0.06	0.06	0.07	0.07	0.10	0.10
Al VI	3.92	3.90	3.88	3.91	3.58	3.95	3.88	3.89	3.92	3.90	3.87	3.88	3.93	3.91	3.88	3.93	3.88	3.89
Cr	0.00	0.00	0.00	0.01	0.00	0.00	0.00	0.00	0.00	0.00	0.00	0.00	0.00	0.00	0.00	0.00	0.00	0.00
Fe3+	0.16	0.17	0.21	0.13	1.26	0.10	0.18	0.19	0.15	0.16	0.20	0.19	0.12	0.14	0.18	0.13	0.21	0.20
Fe2+	4.92	5.01	4.85	5.02	3.36	5.01	4.61	4.97	4.72	4.83	4.62	4.79	4.57	4.65	4.60	4.84	4.54	4.72
Mn	0.31	0.26	0.36	0.26	0.54	0.28	0.61	0.28	0.50	0.47	0.60	0.50	0.71	0.62	0.65	0.47	0.69	0.51
Mg	0.46	0.45	0.45	0.46	0.37	0.45	0.37	0.46	0.44	0.42	0.42	0.43	0.40	0.43	0.42	0.42	0.41	0.43
Ca	0.23	0.20	0.24	0.21	0.29	0.21	0.34	0.20	0.27	0.21	0.27	0.21	0.26	0.24	0.26	0.21	0.26	0.24
End-mem.																		
Alm.	83.13	84.59	82.17	84.44	73.68	84.17	77.73	84.03	79.53	81.43	78.02	80.78	76.94	78.26	77.56	81.47	76.91	80.01
Pyr.	7.71	7.61	7.67	7.77	8.10	7.60	6.24	7.85	7.36	7.11	7.17	7.33	6.71	7.30	7.15	7.07	7.00	7.27
Spes.	5.29	4.39	6.09	4.34	11.92	4.66	10.32	4.67	8.50	7.94	10.19	8.37	11.99	10.35	10.98	7.99	11.68	8.73
And.	3.87	4.11	5.19	3.28	26.02	2.37	4.34	4.56	3.65	4.05	4.88	4.79	2.97	3.38	4.40	3.14	5.03	5.00

Numbers of ions on the basis of 24 (O)

Table 5.2. K-Ar ages and analytical data for the granites in the ophiolitic mélange

Sample No	Material	%K	^{40}Ar*moles/gX10^{-11}	%^{40}Ar*	$^{40}Ar/^{36}Ar$X10^2	$^{40}K/^{36}Ar$X10^4	Age
262	Muscovite	7.5	474.999	98.3	171.51	79.43	332.6±6.5
268	Muscovite	6.7	503.908	97.4	112.18	43.08	390.8±7.5
269	Muscovite	7.5	508.627	98.7	229.41	99.66	354.0±6.9
271	Muscovite	7.5	515.796	97.6	121.04	51.25	358.5±6.9
272	Muscovite	6.8	486.826	93.5	45.15	17.67	370.3±7.1

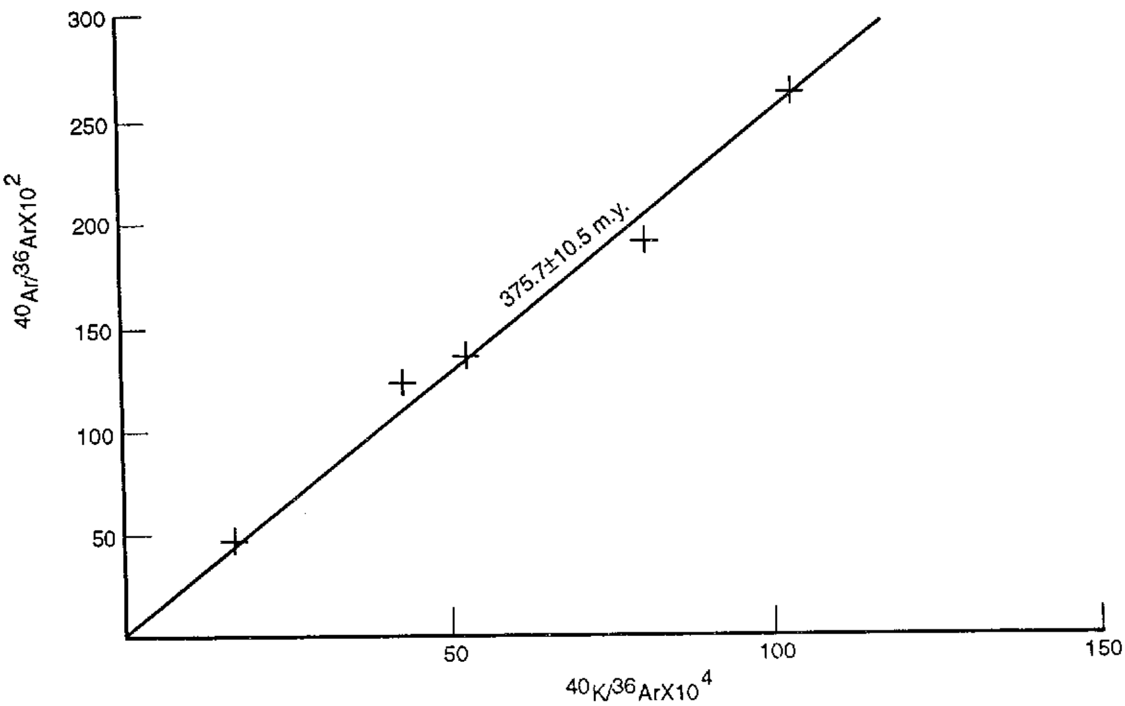

Figure 5.5. Isochron age of the muscovites seperated from the granites.

5.4. Analytical method

Major and trace element analyses have been carried out on 12 tholeiitic basalts-diabases and 12 granite samples. 2 granite samples have been analysed for REE concentrations. Major and trace element analyses have been carried out by XRF on glass beads fused from ignited powders to which $Li_2B_4O_7$ was added (1:5), in a gold-platinum crucible at 1150° C. REE analysis was done by ICP-AES technique (Voldet 1993). Microprobe analysis of pyroxene was carried out by a Camebax SX-50 in the Mineralogy Department at Lausanne University. The analytical conditions for the elements (K, Mg, Ca, Na, Mn, Cr, Al, Ti, Si, Fe) were 30 seconds of counting interval, beam current 20 mA and acceleration voltage 15 kV.

5.5. Geochemistry of Granite

Major, trace and REE analyses of granitic rocks are given in Table 5.3. Intensive deformation during the obduction of the oceanic crust onto the platform carbonates modified major element composition of the granitic rocks. Granitic rocks in the ophiolitic melange are represented by high SiO_2 (74-77%), Na_2O (3-6%), K_2O (0.3-2%), Al_2O_3 (12-15%), MgO (0.3-0.7%). Trace element concentrations are variable, particularly Nb (2-12 ppm), Y (17-34 ppm), Zr (87-180 ppm) and Rb (26-117 ppm).

These granitic rocks show calc-alkaline affinity in AFM diagram of Irvine and Baragar (1971) (Fig. 5.6). Granitic rocks showing calcalkaline tendency are interpreted by some authors as the products of volcanic arc magmatism (Peacock, 1931; Shand, 1951). In the tectonodiscrimination diagrams based on immobile trace elements, the granitic rocks of the ophiolitic melange plot on VAG-SynCOLG field in the Nb-Y ternary diagram and on the VAG field in Rb-Y+Nb ternary diagram of Pearce et al. (1984) (Fig. 5.7a-b). REE pattern is shown in Figure 5.8. They present high LREE/HREE ratios and moderete REE content ranging from 60 to 85 ppm. Eu/Sm ratios are between 0.26 and 0.34 and weak Eu anomalies are seen. Overall REE features may indicate little or no residual plagioclase in the source (Cullers and Graf, 1984). ORG-normalized trace element pattern of the granitic rocks show LIL (K, Rb, Ba) enrichment relative to Nb, Ce, Zr, Sm, Y. These patterns resemble to common trace element patterns seen in VAG (Pearce et al., 1984) (Fig. 5.9).

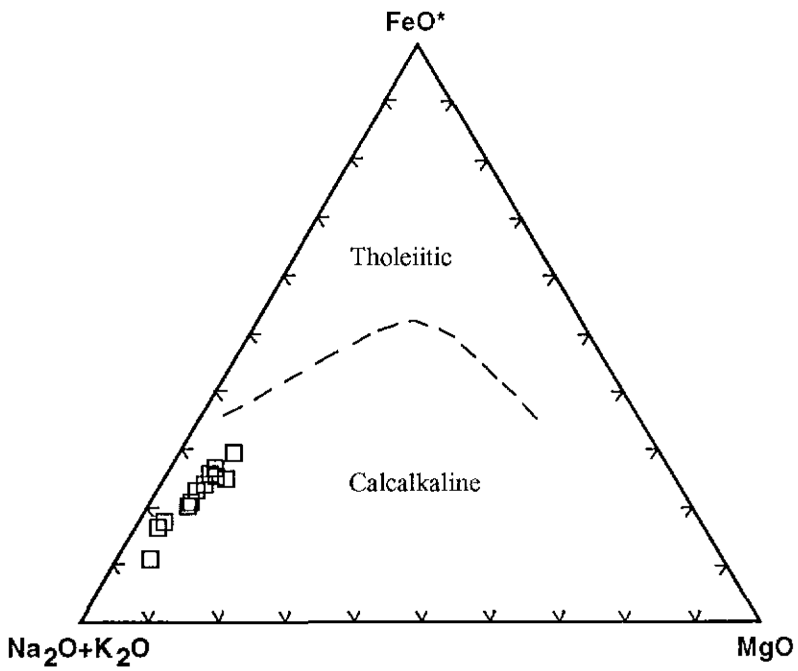

Figure 5.6. AFM diagram of the granitic rocks (after Irvine and Baragar, 1971).

Table 5.3. Major, trace and REE analyses of the granites.

Samp.No	148a	148b	148c	262	264	268	269	272	323	324	337	338
SiO2	77.29	74.72	73.91	74.77	75.27	74.5	76.02	75.36	77.05	77.53	77.34	77.67
Al2O3	13.45	14.95	14.59	14.55	13.41	14.47	14.02	13.96	12.06	12.21	12.38	13.02
TiO2	0.17	0.2	0.24	0.21	0.26	0.23	0.17	0.16	0.13	0.14	0.09	0.1
FeO*	1.79	1.99	2.41	2	2.64	2.17	1.65	1.45	1.46	1.36	1.26	0.88
CaO	0.84	1.34	1.2	1.32	1.07	1.48	1.33	1.32	1.29	2.22	1.67	0.77
MgO	0.63	0.5	0.65	0.47	0.67	0.51	0.37	0.39	0.27	0.37	0.23	0.35
Na2O	2.87	4.53	4.79	3.64	3.65	3.94	3.52	3.62	3.97	4.47	5.82	5.98
K2O	1.85	1.28	1.49	1.64	1.96	1.53	1.6	1.53	2.52	0.5	0.28	0.59
MnO	0.06	0.02	0.02	0.03	0.04	0.03	0.02	0.01	0.02	0.02	0.02	0.01
P2O5	0.03	0.11	0.12	0.08	0.07	0.1	0.1	0.1	0.03	0.02	0.02	0.02
LOI	1.2	0.97	1.01	1.18	1.16	1.09	1.08	1.07	0.84	0.75	0.71	0.57
Total	98.98	100.59	100.4	99.88	100.19	100.05	99.87	98.96	99.63	99.58	99.81	99.95
Ba	619	273	305	632	663	533	622	562	564	145	168	504
Ni	6	7	5	6	16	5	13	38	18	21	38	5
V	28	30	27	25	34	26	21	17	20	18	12	15
Cr	16	52	10	29	32	21	15	22	22	25	26	28
Nb	4	9	6	8	6	8	9	12	5	4	4	2
Zr	92	89	87	90	161	87	87	89	93	180	89	95
Y	20	34	27	34	33	32	29	29	23	17	30	33
Sr	164	274	231	169	182	176	170	180	84	98	56	77
Rb	90	72	91	86	117	82	86	86	65	28	19	26
La	10.2	15.8										
Ce	21.7	31.8										
Pr	2.8	4.1										
Nd	11	15.4										
Sm	2.8	3.7										
Eu	0.74	1.26										
Gd	2.6	3										
Dy	3.3	3.7										
Ho	0.72	0.82										
Er	2	2.4										
Tm	n.d	0.38										
Yb	1.9	2.3										
Lu	0.27	0.34										

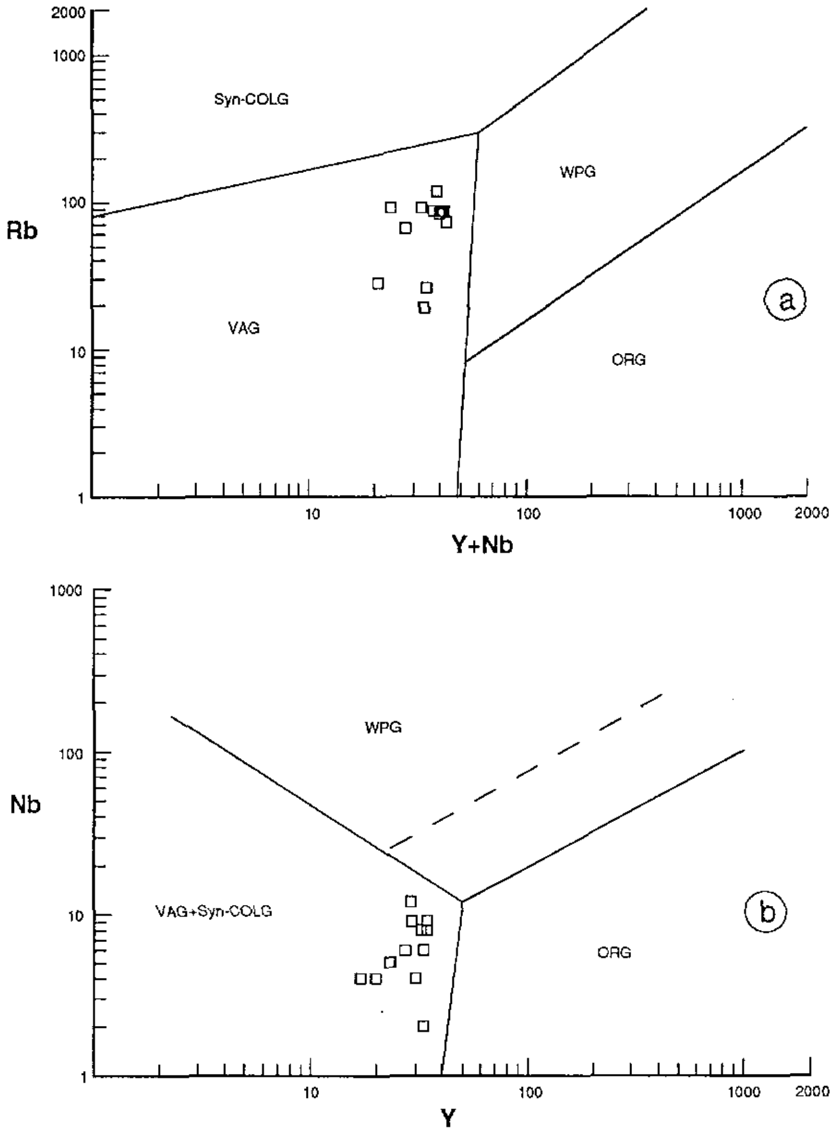

Figure 5.7. a. Rb versus Y+Nb discrimination diagram of the granitic rocks (After Pearce et al., 1984). **b.** Nb versus Y discrimination diagram of the granitic rocks (After Pearce et al., 1984).

5.6. Geochemistry of volcanic rocks

Major and trace element analyses of tholeiitic volcanic rocks are presented in Table 5.4. Volcanic rocks in the ophiolitic melange of the Mersin complex are characterized by tholeiitic basalts and diabases (Fig. 5.10).

The rocks are characterized a wide range of major element compositions, particularly in terms of those elements considered to be mobile during hydrothermal alteration, SiO_2, CaO, Na_2O, K_2O (Humpris and Thompson, 1978). Some trace elements, namely Ti, Nb,

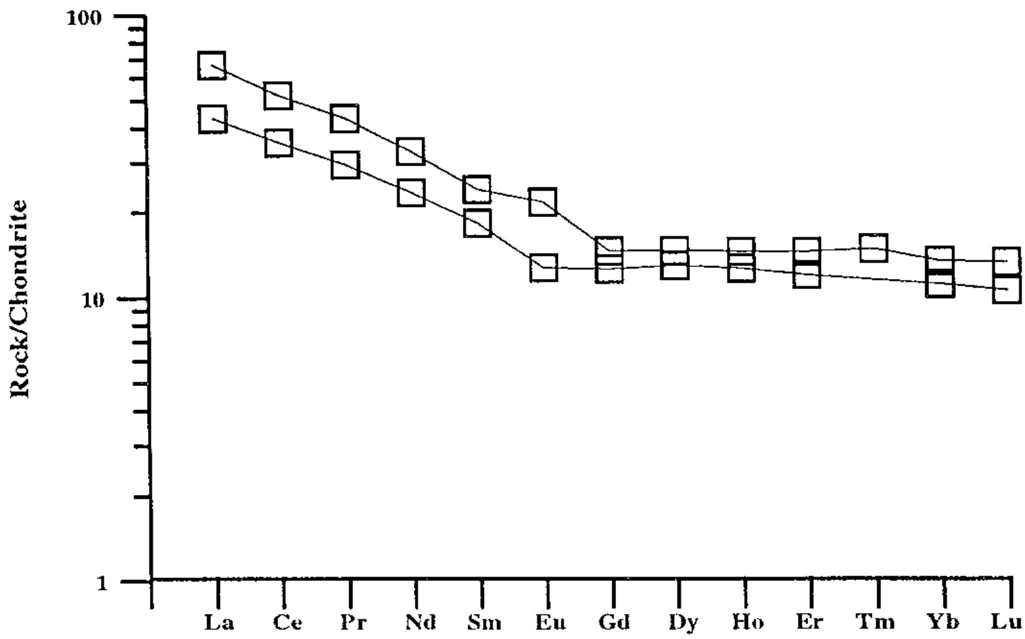

Figure 5.8. Chondrite normalized REE abundance of the granitic rocks (Normalizing values from Sun and McDonough, 1989).

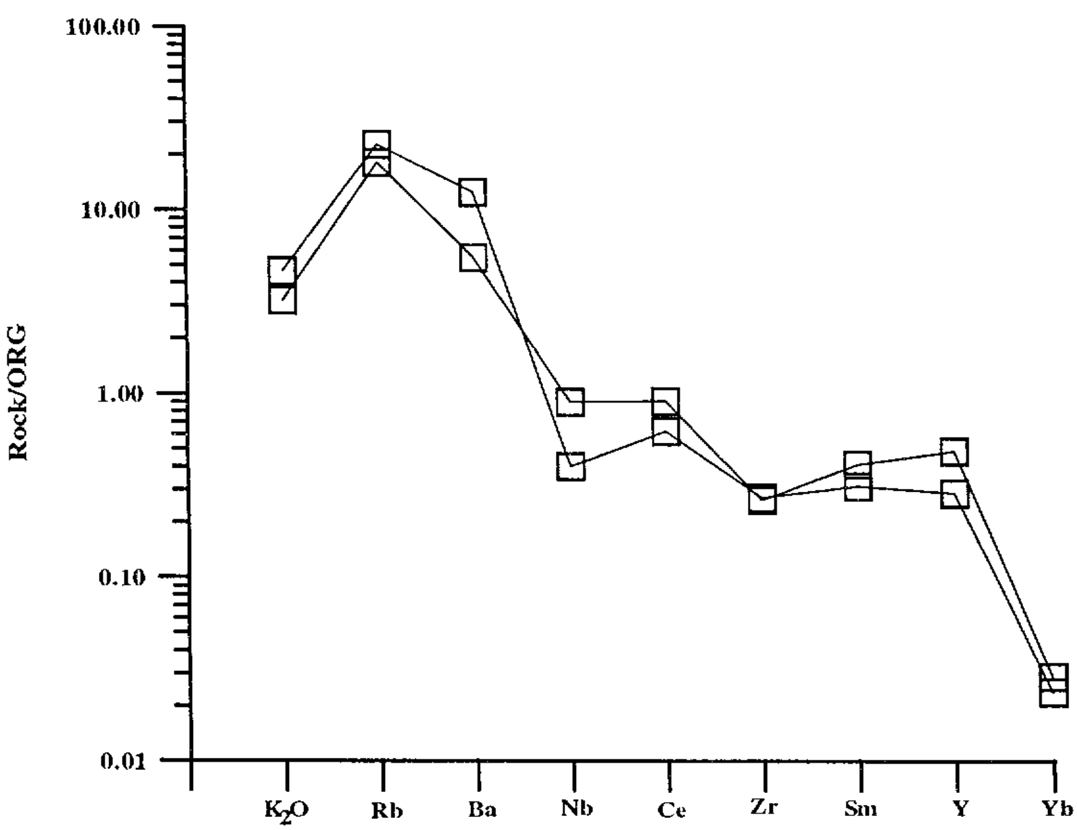

Figure 5.9. Ocean Ridge Granite (ORG) normalised geochemical patterns of the selected granitic rocks in the melange (Normalizing values from Pearce et al., 1984).

Table 5.4. Major and trace element analyses of the basaltic rocks within the mélange.

	Diabases					Basalts						
Samp.No	346	347	348	349	358	359	360	361	362	363	364	365
SiO2	47.25	45.58	48.17	44.09	47.01	56.07	56.37	56.39	59.72	55.53	58.65	59.2
Al2O3	13.59	13.75	14.04	13.59	14.01	15.4	15.33	15.48	13.31	14.41	13.79	13.88
TiO2	1.51	1.61	1.58	1.61	1.64	1.27	1.34	1.32	1.17	1.45	1.23	1.24
FeO*	12.39	13.84	13.48	12.27	13.86	11.26	11.43	11.54	10.12	10.78	11.25	11.36
CaO	6.7	5.63	6.13	8.63	6.29	3.29	3.89	3.31	4.51	6.37	3.37	2.94
MgO	4.01	4.57	3.47	3.52	3.43	2.41	2.6	2.54	2.82	3.26	3.15	3.16
Na2O	5.66	4.94	5.1	5.27	4.8	8.08	7.64	8.08	6.18	7.07	6.42	6.19
K2O	0.21	0.26	0.28	0.22	0.28	0.07	0.07	0.04	0.21	0.03	0.22	0.25
MnO	0.2	0.2	0.17	0.22	0.17	0.08	0.08	0.08	0.08	0.11	0.09	0.09
P2O5	0.16	0.17	0.17	0.17	0.17	0.21	0.21	0.22	0.22	0.18	0.22	0.22
LOI	8.81	8.19	7.95	9.84	8.16	1.11	1.39	0.97	2.34	0.45	1.47	1.21
Total	100.48	99.05	100.55	99.43	99.82	99.39	100.35	99.95	100.7	99.64	99.87	99.75
Ba	101	105	98	72	91	61	53	63	61	51	51	71
Ni						1	4	6	4	2	6	2
V	410	475	460	428	492	254	236	232	172	362	184	190
Cr	7	5	5	1	4	16	23	17	12	4	13	17
Nb	5	5	5	5	4	4	7	2	7	7	6	4
Zr	93	90	93	93	91	133	131	128	125	125	130	130
Y	31	30	29	32	31	55	57	55	56	53	55	54
Sr	397	374	375	627	354	39	36	44	94	47	91	88
Rb	11	7	10	6	11	5	5	6	5	5	9	10

*Total Fe is expressed as FeO

Y, Zr, however, are considered to be virtually immobile during metamorphism and can be used to infer the original compositions and tectonic settings of the volcanic rocks (Winchester and Floyd, 1977; Pearce and Cann, 1973; Pearce and Norry, 1979).

The tholeiitic basalts and diabases present high TiO_2 (1.2-1.6%), high CaO (3.3-8.6%), low SiO_2 (45-59%) compared to the alkaline rocks. The abundance of immobile trace elements in tholeiitic rocks are also depleted and are represented by low Nb (2-7 ppm), low Zr (90-130 ppm) and except high Y (30-56 ppm).

In the discrimination diagrams presented in Figure 5.11a-b, immobile trace elements are used to determine the tectonic setting of the volcanic rocks (Meschede, 1986; Pearce and Norry, 1979). The tholeiitic basalts and diabases show transitional character between MORB and VAB in Zr/Y versus Zr diagram of Pearce and Norry (1979) and MORB-VAB affinity in Nb-Zr-Y triangular diagram of Meschede (1986). MORB-normalized trace element diagram can be used to distinguish different magmatic affinity of the basaltic rocks in the ophiolitic melange of the Mersin complex. Tholeiitic basalts and diabases present mixture of MORB-VAB like pattern (Fig. 5.12). Both discrimination diagrams and Morb-normalized trace element abundance may indicate that tholeiitic basalts and diabases have been formed within a tectonic setting in which subduction influence was present. This particular feature of the eastern Mediterranean ophiolites is well constrained (Pearce et al., 1984; Robertson, 1994).

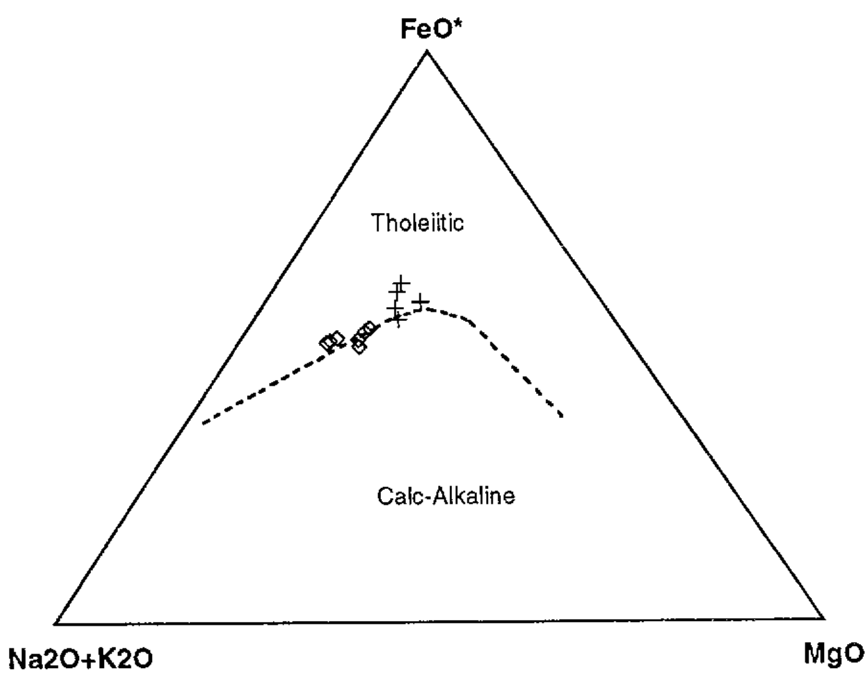

Figure 5.10. AFM diagram of the basalts (◊) and diabases (+) in the melange unit (after Irvine and Baragar, 1971).

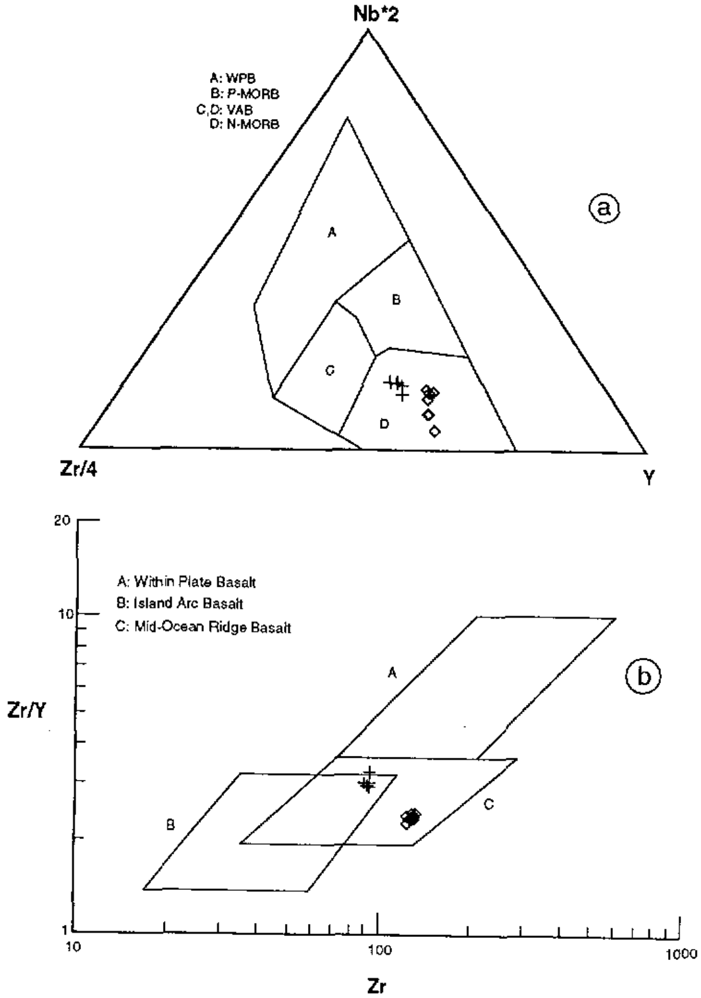

Figure 5.11. a. Nb-Zr-Y triangular diagram of the basalts (◊) and diabases (+) (after Meschede, 1986). **b.** Zr/Y versus Zr discrimination diagram of the basalts (◊) and diabases (+) (after Pearce and Norry, 1979).

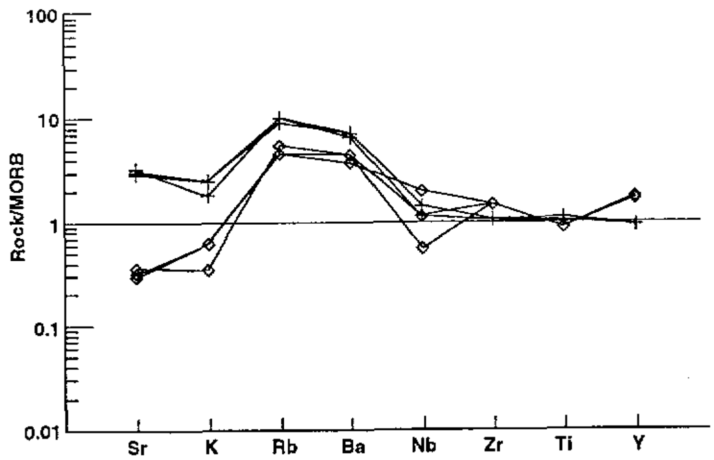

Figure 5.12. Morb-normalized trace element diagram of the basalts (◊) and diabases (+) rocks in the study area (normalizing values from Pearce, 1982).

5.7. Age of the mélange

The ophiolitic melange in Mersin complex includes distinct tectonostratigraphic units ranging in age from Late Paleozoic to Late Cretaceous. Slabs of sub-metamorphic rocks are also present. Therefore melange formation have started approximately in late Cretaceous (~ 94 Ma) based on the K-Ar age data from amphibolitic sole (Parlak et al, 1995). At the east of the study area, Upper Paleocene sediments starting with ophiolite derived pebbly sandstone cap the ophiolite with angular unconformity (Avsar, 1992). This age represents completion of melange and/or final emplacement of oceanic lithosphere onto the Tauride platform in the study area.

5.8. Paleogeographic summary

Mostly Mesozoic aged lithostratigraphic units within the ophiolitic melange sequence have been described on the basis of their age and lithologic characters. It is clearly shown that all these lithostratigraphic units were formed during progressive opening of a basin in the Neotethyan framework some time between late Triassic and late Cretaceous in the study area. A following paleogeographic summary will be given in accordance with the available data from the Mersin ophiolite complex and from surrounding regions.

A clear field evidence of the crustal extension and initiation of rifting in the Mersin ophiolite complex is marked by acidic tuffs and alkaline volcanics that are intercalated with Cornian-Norian aged pelagic limestones. This evidence is well constrained in all over the Tauride belt (Özgül, 1976; Robertson and Woodcock, 1982; Yilmaz, 1984). Block-faulting of older basement rocks have been eroded and quartz-bearing turbiditic sandstone, micaceous sandstone, shales, and conglomeratic sandstone sedimentation took place during that period. Deposition of clastic sediments in turns overlain by deep marine units such as mudstones, marls, plant bearing sandstones and radiolarites show continuous crustal thinning in late Triassic time (Özgül, 1976; 1984). Within this continuous process, Previously-formed alkaline volcanics also became one of the source rocks of conglomeratic sandstones in the region. Due to progressive extension and block-faulting, a brecciated zone was developed at the bottom of the pelagic cherty-limestones during Triassic-Liassic interval in the study area. During the much of the Jurassic-Cretaceous time, basin was subsiding and sedimentation was dominated mainly by siliceous rocks such as radiolarites, mudstones, marls, cherty limestones. Particularly during late Jurassic-early Cretaceous time, alkaline volcanic activity was in progress together with radiolarian cherts in the basin plain (Parlak et al., in review). Basin opening ceased at the begining of the late Cretaceous, as a result of roughly N-S directed compressional tectonic regime caused intraoceanic subduction above which the Mersin ophiolite formed within suprasubduction zone in the southern branch of the Neotethyan ocean (Parlak et al., in review). Soon after the formation of the oceanic lithosphere, intraoceanic subduction led the formation of the amphibolitic sole beneath the mantle tectonite. Postkinematic microgabbroic-diabase dike swarms, which show also geochemical features of the suprasubduction zone setting, intruded metamorphic sole mantle tectonites and ultramafic-mafic cumulates (Parlak and Delaloye, in press). Finally, basin consumption and obduction of the three distinct nappe stacking (ophioliting melange, subophiolitic metamorphic sole and Mersin ophiolite) onto the Tauride continental margin have been completed between late Cretaceous and early Paleocene in the study area.

5.9. Conclusions

The Mersin ophiolite complex (MOC) includes three juxtaposed different tectonic units. Each of which has its specific age and lithological features. The following points will explain the tectonic scenario of the above-mentioned units:

a) The crustal extension and rifting initiated during late Triassic. This evidence is marked by acidic tuffs intercalated with Carnian-Norian aged pelagic limestones in the study area.

b) Before the formation of the Mersin ophiolite, the volcanic activity continued untill Late Jurassic-Early Cretaceous during which ocean island/seamount alkali basalts intercalated with cherty limestones and radiolarites were formed in basin plain (Parlak et al., in review).

c) Regional compression began during Late Cretaceous, yielding formation of the Mersin ophiolite oceanic crust in supra-subduction zone tectonic setting.

d) Continued compression caused intraoceanic thrusting, yielding generation of the metamorphic sole (93.4 Ma) beneath the mantle tectonites. This event was followed by numerous microgabbroic-diabasic dike injections.

e) Formation of the melange and emplacement of the oceanic lithosphere were operating at the same time during late Cretaceous-early Paleocene interval in the study area.

PLATE CAPTIONS

Plate 5.1

a) Pelagic limestones intercalated with the alkaline volcanics and tuffs indicating onset of rifting in the Tauride belt.

b) Plant-bearing sandstones within the rift-related sediments.

c) Overturned carbonate cemented sandstone and siltstone intercalation in continental margin units.

d) Mudstone and radiolarite intercalation in the continental margin sediments.

Plate 5.2

a) Bed-graded conglomerate comprising pebbles of alkaline volcanics indicating relatively younger episode during block faulting and rifting in the continental margin sediments.

b) Brecciated limestone blocks (L.Triassic-Jurassic) due to block faulting.

c) Late Triassic aged cherty limestone blocks.

d) Limestone blocks in the melange of the Mersin ophiolite.

Plate 5.3

a) Serpentinized harzburgite fragments in the melange.

b) Gabbro fragments in the melange.

c) Pillow basalts in the melange.

d) Fragments of the volcano-sedimentary rocks in the melange.

Plate 5.1

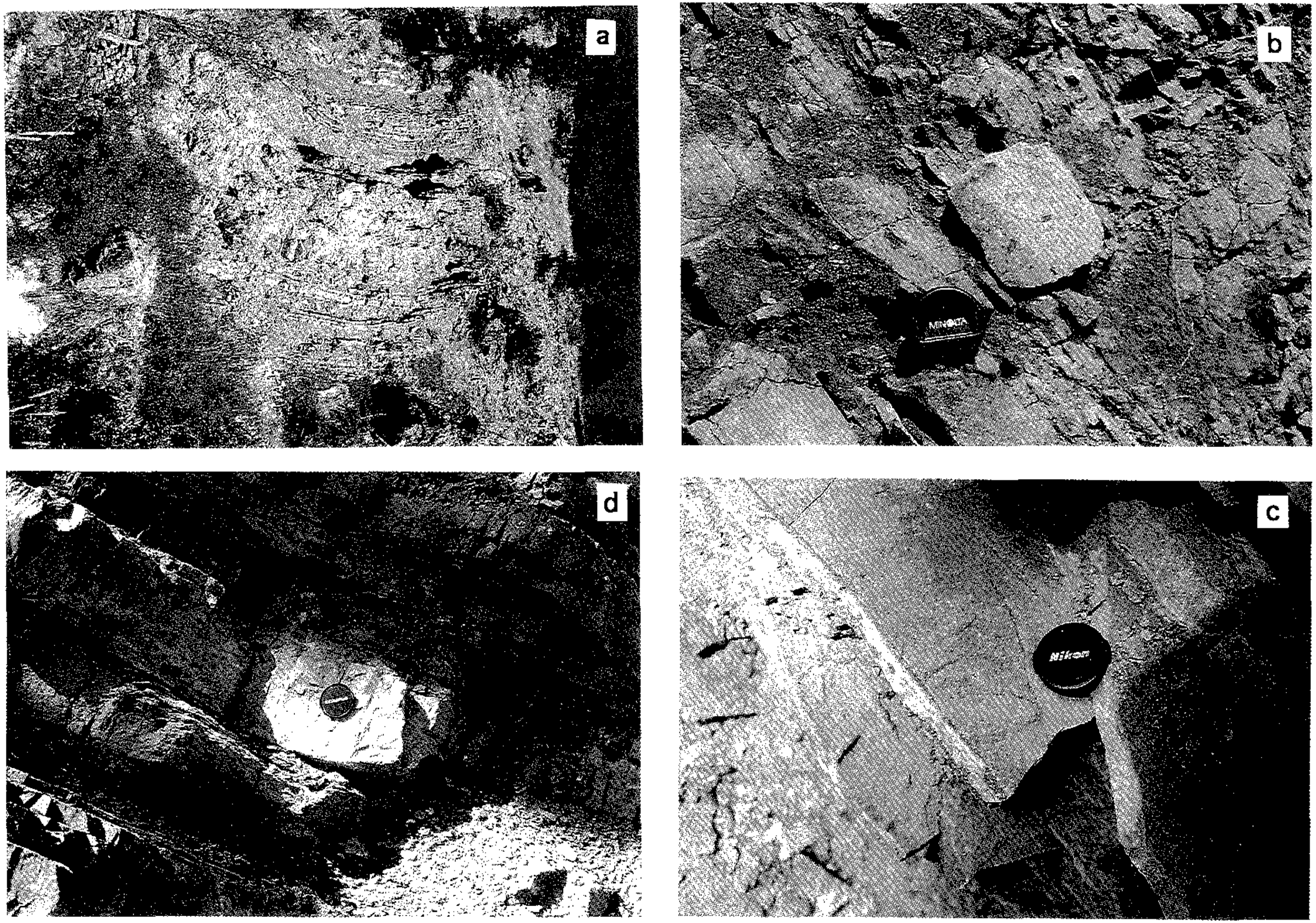

Plate 5.2

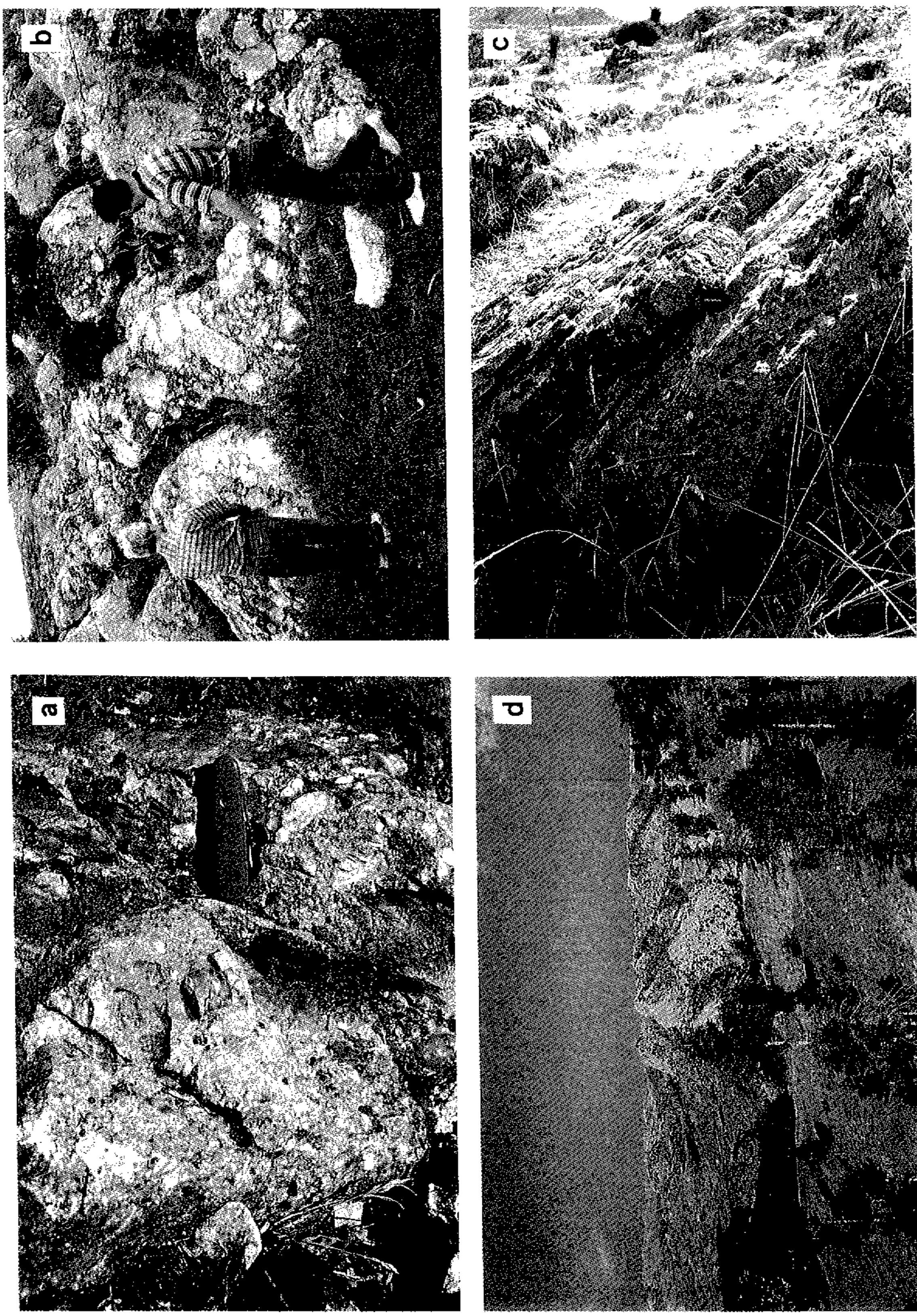

Plate 5.3

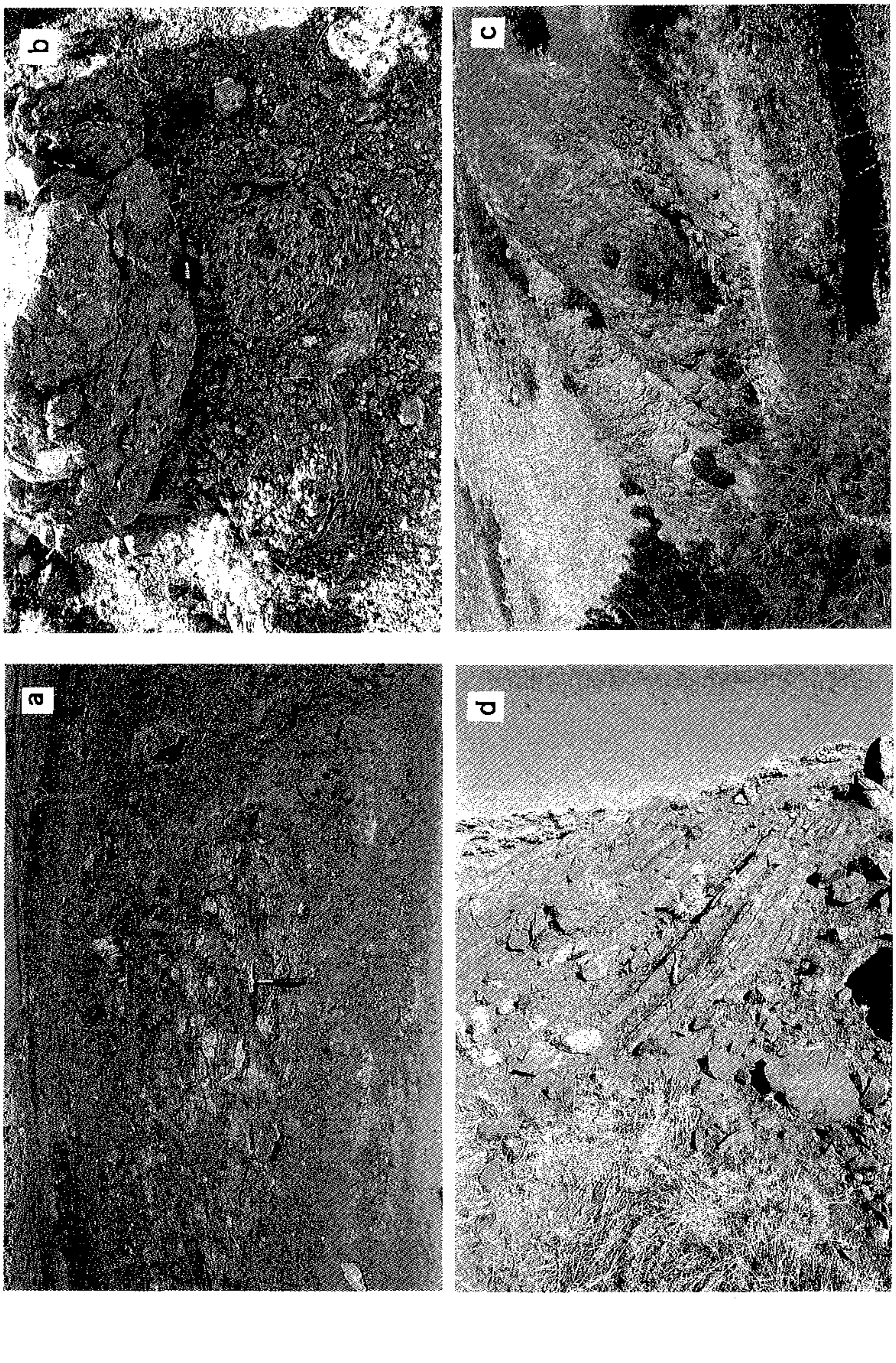

References

Avsar, N., 1992; Namrun (Icel) yoresi Paleojen bentik foraminifer faunasi. M.T.A. Dergisi, 114, 127-144.

Collins, A.S., and Robertson, A.H.F., 1995; Tectonic facies in south-west Turkey: Their contribution to unravelling the Lycian fold and thrust belt. Abstracts of Second International Symposium on the Geology of the eastern Mediterranean region, p.7, 27 August-1 September, Jerusalem, Israel.

Cullers, R.L., and Graf, J.L., 1984; Rare earth element in igneous rocks of the continental crust: intermediate and silicic rocks-ore petrogenesis. In: Henderson, P. (ed.), REE geochemistry, 275-308. Elsevier Sciences Publishers.

Deer, W.A., Howie, R.A., and Zussman, J., 1992; An introduction to the rock forming minerals. 696p., Longman Scientific and Technical.

Delaloye, M., De Souza, H., Wagner, J.J., and Hedley, I., 1980; Isotopic ages on ophiolites from the eastern Mediterranean. In: Panayiotou, A. (ed.), Ophiolites. Proceedings of the International Ophiolite Symposium, Cyprus, 292-295.

Delaloye, M., and Wagner, J.J., 1984; Ophiolites and volcanic activity near the western edge of the Arabian plate. In: Dixon, J.E. and Robertson, A.H.F. (eds.), The geological evolution of the eastern Mediterranean. Geol. Soc. Spec. Publ. London, 17, 225-233.

Dilek, Y., and Moores, E.M., 1990; Regional tectonics of the eastern Mediterranean ophiolites. In: Malpas, J.A., Moores, E.M., Panayiotou, A. and Xenophontos, C. (eds.), Ophiolites and oceanic crustal analogues. 295-309. Geol. Surv. Dept. Nicosia, Cyprus.

Dilek, Y., and Rowland, J.C., 1993; Evolution of a conjugate passive margin pair in Mesozoic southern Turkey. Tectonics, 12, 4, 954-970.

Gansser, A., 1974; The ophiolitic melange, a world-wide problem on Tethyan examples. Eclogae geol. Helv., 67/3, 479-507.

Humphris, S.E. and Thompson, G., 1978; Trace element mobility during hydrothermal alteration of oceanic basalts. Geochim. Cosmochim. Acta, 42, 127-136.

Irvine, T.N. and Baragar, W.R.A., 1971; A guide to the chemical classification of the common volcanic rocks. Canad. J. Earth Sci., 8, 523-548.

Juteau, T., Nicolas, A., Dubessy, J., Fruchard, J.C., and Bouchez, J.L., 1977; Structural relationships in the Antalya ophiolite complex, Turkey: possible model for an oceanic ridge. Bull. geol. Soc. Amer., 88, 1740-1748.

Juteau, T., 1980; Ophiolites of Turkey. Ofioliti, 2, 199-238.

Meschede, M., 1986; A method of discriminating between different types of mid-oceanic ridge basalts and continental tholeiites with Nb-Zr-Y diagram. Chem. Geol., 56, 207-218.

Özgül, N., 1976; Toroslarin bazi temel jeoloji ozellikleri. T.J. K. Bulteni, 19, 65-78.

Özgül, N., 1984; Stratigraphy and tectonic evolution of the central Taurides. In: O. Tekeli and Goncuoglu, M.C. (eds.), Geology of the Taurus belt. Proceedings of the International Symposium, 77-90. Ankara, Turkey.

Pampal, S., 1984; Arslankoy-Tepekoy (Mersin) yoresinin jeolojisi. S.U. Fen-Edebiyat Fakultesi, Fen Dergisi, 3, 247-258.

Pampal, S., 1987; Guzeloluk-Sorgun (Mersin) yoresinin jeolojisi. Gazi Universitesi Muhendislik-Mimarlik Fak. Dergisi, 2, 1, 143-174.

Parlak, O., Delaloye, M. and Bingol, E., 1995; Origin of subophiolitic metamorphic rocks beneath the Mersin ophiolite, southern Turkey. Ofioliti, 20, 2, 97-110.

Parlak, O., Delaloye, M. and Bingol, E., (in review); Geochemistry of volcanic rocks in the Mersin ophiolite and their significance in the eastern Mediterranean geology. IESCA-1995, Proceedings of International Earth Science Colloquium on the Aegean Region, 9-14 October, Izmir-Gulluk, Turkey.

Parlak, O., and Delaloye, M., (in press); Geochemistry and timing of post-metamorphic dike emplacement in the Mersin ophiolite (southern Turkey): New age constraints from $^{40}Ar/^{39}Ar$ geochronology. Terra Nova, 9.

Peacock, M.A., 1931; Classification of igneous rock series. J. Geol., 39, 65-67.

Pearce, J.A. and Cann, J.R., 1973; Tectonic setting of basic volcanic rocks determined using trace element analysis. Earth and Planet. Sci. Lett., 19, 290-300.

Pearce, J.A. and Norry, M.J., 1979; Petrogenetic implications of Ti, Zr, Y and Nb variations in volcanic rocks. Contr. Mineral. Petrol., 69, 33-47.

Pearce, J.A., 1982; Trace element characteristics of lavas from destructive plate boundaries. In: Thorpe, R.S. (ed.), Orogenic andesites and related rocks, Wiley, Chichester, 525-548.

Pearce, J.A., Harris, B.W. and Tindle A.G., 1984; Trace element discrimination diagrams for the tectonic interpretation of granitic rocks. J. Petrol., 25, 4, 956-983.

Pearce, J.A., Lippard, S.J., and Roberts, S., 1984; Characteristics and tectonic significance of supra-subduction zone ophiolites. In: Kokelaar, B.P. and Howells, M.F. (eds.), Marginal basin geology. Geol. Soc. Spec. Publ. London, 16, 77-89.

Polat, A., and Casey, J.F., 1995; A structural record of the emplacement of the Pozanti-Karsanti ophiolite onto the Menderes-Taurus block in the late Cretaceous, eastern Taurides, Turkey. J. Structr. Geol., 17, 12, 1673-1688.

Ricou, L.E., Argyriadis, I., and Marcoux, J., 1975; L'axe calcaire du Taurus, une alignement de fenetres arabo-africaines sous des nappes radiolaritique, ophiolitiques et métamorphiques., Bull. géol. Soc. France, 17, 1024-1043.

Robertson, A.H.F., and Woodcock, N.H., 1982; Sedimentary history of the south-western segment of the Mesozoic-Tertiary Antalya continental margin, south-western Turkey. Eclogae geol. Helv., 75/3, 517-562.

Robertson, A.H.F., and Dixon, J.E., 1984; Introduction: aspects of the geological evolution of the eastern Mediterranean. In: Dixon, J.E. and Robertson, A.H.F. (eds.), The geological evolution of the eastern Mediterranean. Geol. Soc. Spec. Publ. London, 17, 1-75.

Robertson, A.H.F., 1994; Role of the tectonic facies concept in orogenic analysis and its application to Tethys in the eastern Mediterranean region. Earth Sci. Rev., 37, 139-213.

Sengor, A.M.C. and Yilmaz, Y., 1981; Tethyan evolution of Turkey: A plate tectonic approach. Tectonophysics, 75, 181-241.

Shand, S.J., 1951; Eruptive rocks. New York, J. Wiley.

Sun, S.S., and McDonough, W.F., 1989; Chemical and isotopic systematics of oceanic basalts: implications for mantle composition and processes. In: Saunders, A.D. and Norry, M.J. (eds.), Magmatism in the ocean basins. Geol. Soc. Spec. Publ. London, 42, 313-345.

Tekeli, O., 1981; Toroslarda Aladag ofiyolitli melanjinin ozellikleri. T.J.K. Bulteni, 24, 57-64.

Thuizat, R., Montigny, R., Çakir, U., and Juteau, T., 1978; K-Ar investigations on two Turkish ophiolites. In: Zartman, R.E. (ed), Short papers of the 4th International Conference Geochronology, Cosmochronology, Isotop geology. Geol. Surv. Open-File Report, 78-701, 430-432.

Thuizat, R., Whitechurch, H., Montigny, R., and Juteau, T., 1981; K-Ar dating of some infra-ophiolitic metamorphic soles from the eastern Mediterranean: New evidence for oceanic thrusting before obduction. Earth and Planet. Sci. Lett., 52, 302-310.

Voldet, P., 1993. From neutron activation to inductively coupled plasma-atomic emission spectrometry in the determination of rare-earth elements in rocks. Trends in Analytical Chemistry. 12, 8, 339-344.

Whitechurch, H., Juteau, T., and Montigny, R., 1984; Role of the eastern Mediterranean ophiolites (Turkey, Syria, Cyprus) in the history of the Neotethys. In: Dixon, J.E. and Robertson, A.H.F. (eds.), The geological evolution of the eastern Mediterranean. Geol. Soc. Spec. Publ. London, 17, 301-317.

Winchester, J.A. and Floyd, P.A., 1977; Geochemical discrimination of different magma series and their differentiation products using immobile elements. Chem. Geol., 20, 325-343.

Yilmaz, P.O., and Maxwell, J., 1982; K-Ar investigations from the Antalya complex ophiolites, SW Turkey. Ofioliti, 2/3, 527-538.

Yilmaz, P.O., 1984; The Alakircay unit, Antalya complex: a tectonic enigma. In: Tekeli, O. and Goncuoglu, M.C. (eds.), Geology of the Taurus belt, 27-40. Proceedings of the International Symposium, Ankara, Turkey.

CHAPTER 6

GENERAL CONCLUSIONS

The Mersin ophiolite, represented by approximately 6 km thick oceanic lithospheric section on the southern flank of the Taurus calcareous axis, formed in the Mesozoic Neotethyan ocean some time during Late Cretaceous in southern Turkey. It comprises from bottom to top ophiolitic melange, subophiolitic metamorphic rocks showing inverted metamorphism from upper amphibolite to green schist facies, tectonites, ultramafic-mafic cumulates, tholeiitic-alkaline basalts and radiolarites.

Geochemical, geochronological and structural studies let us to make following conclusions:

a) Volcanic rocks present two discrete geochemical and structural features. The first one is represented by alkaline basaltic lavas intercalated with radiolarites and pelagic limestones (Late Jurassic-Early Cretaceous), whereas the second one is represented by basaltic pillow lavas and diabase (Late Cretaceous ?). Major, trace and rare element compositions suggest that these volcanic rocks formed in a within plate basalt setting (WPB). Basalts and diabases of the second group, which exhibit similar geochemical features, differ from the above mentioned group by their tholeiitic affinity. Flat-lying REE patterns of basalts and diabases are also an indication of arc-related environment.

b) Cumulative rocks, occupying an area approximately 15 km^2, crop out only within the N-S oriented Sorgun valley (Mersin) in the western part of the ophiolitic massif. Cumulates, having over 3 km in thickness, start with 800 m of ultramafic rocks at the bottom and continue into 2500 m of gabbroic rocks. Polycyclic cumulative feature is observed between mafic and ultramafic cumulative rocks. Ultramafic cumulates, showing adcumulate texture, are characterized by dunite, wherlite and pyroxenite. Igneous lamination, size grading and rhythmic layering are observed as accumulation features in the ultramafic cumulates. Mafic cumulates consisting mainly of gabbro, leucogabbro, olivine gabbro and anorthosite constitute almost 2/3 of the whole cumulate section. It is observable both in the field and in thin sections that mafic cumulative rocks are very fresh and present adcumulate and mesocumulate texture. Size grading and rhythmic layering are also seen in mafic cumulates. No significant cryptic variation is detected throughout the entire thickness of the layered sequence. Adcumulate-mesocumulate growth in ultramafic and mafic cumulates indicates slow accumulation rate. Absence of zoning in the cumulus and intercumulus phase suggest a crystallization process under constant and high temperature which are confirmed by high Mg/Fe ratio and high Ca content of the plagioclase. Crystallization order is olivine (Fo_{91-80})±chromian spinel (Cr# 0.6-0.8), clinopyroxene

(Mg# 95-77), plagioclase ($An_{95.6-91.6}$) and orthopyroxene (Mg# 68-77). Mineral chemistry of ultramafic and mafic cumulates suggest that highly magnesian olivines, clinopyroxenes and absence of plagioclase in the basal ultramafic cumulates are in good agreement with products of high-pressure crystal fractionation of primary basaltic melts beneath an Island arc environment.

c) Metamorphic sole, showing an inverted metamorphic zonation from upper amphibolite facies to greenschist facies, crop out discontinuously along the base of the Mersin ophiolite thrust sheet on the southern flank of the Bolkardag. These metamorphic rocks indicate polyphase deformation and have been folded and imbricated. Major, trace and REE geochemistry suggest that the metamorphic rocks were derived from ocean island/ seamount basaltic rocks and associated sedimentary units. Numerous tholeiitic microgabbroic-diabasic dikes, unaffected by the metamorphism and oriented nearly E-W, intruded the metamorphics. In terms of their trace and REE chemistry, these dikes have the chemical signature of supra-subduction zone tectonic setting. $^{40}Ar/^{39}Ar$ geochronologic studies have been carried out on obduction related subophiolitic metamorphic rocks that show inverted metamorphic gradient at the base, undeformed diabase dikes intruding metamorphic rocks-mantle tectonites and tholeiitic basalts. Seven hornblende separates from the metamorphic rocks yielded rapid-cooling (500^{o}C) ages ranging from 96.0±0.7 Ma to 91.6±0.3 Ma. Three diabase dike samples postdate the metamorphic sole yielded relatively younger cooling ages 89.6±0.7 Ma, 88.3±0.7 Ma, 86.3±0.5 Ma respectively. One diabase dike within the mantle tectonite yielded a cooling age of 63.8±0.9 Ma, indicating that all the dike swarms postdate the formation of the Mersin ophiolite and the intraoceanic thrusting event in this segment of the Neotethyan ocean.

d) The ophiolitic melange in Mersin complex consists of continental margin units, rift assemblages, platform fragments, slabs of ophiolites and metamorphic unit. The contacts between these tectonostratigraphic units are tectonic. Continental margin units present limited outcrop beneath the mantle tectonites of the Mersin ophiolite and are characterized by turbiditic sandstone, mudstone, marls, shales and radiolarites. Platform fragments in ophiolitic melange are represented by rootless E-W oriented limestone blocks ranging from Permian to Upper Cretaceous in age. Rift assemblages in the study area are the most conspicuous unit and consist of variable rock fragments such as acidic tuffs intercalated with Carnian-Norian age pelagic limestone indicating initial block-faulting and onset of volcanism in Tauride belt, cherty limestone, radiolarian chert, plant-bearing sandstone, mafic pillow lavas. Sheared serpentinites, highly altered basaltic pillow lavas, gabbros and slabs of deformed metamorphic rocks constitute the other fragments of the ophiolitic melange. A granitic stock, showing the affinity of VAG and , is also present in the ophiolitic melange. K-Ar age determinations on muscovite yielded a range between 330-390 Ma.

The overall geochemical, structural and geochronological data support following evolutionary scenario for the Mersin ophiolite in the eastern Mediterranean tectonic framework. Initiation of the rifting of NeoTethyan ocean along the northern margin of the Gondwana land started during Middle-Late Triassic-Early Jurassic time interval (Sengor and Yilmaz, 1981; Robertson and Dixon, 1984). Micritic limestones intercalated with alkaline volcanics and tuffs croping out in the melange sequence of the Mersin ophiolite yielded following fossils: *Meandrospira sp., Glomospira sp., Aulotortus sp., Duostominidae sp., Frendicularia sp., Involutina sp., Trochammina , Algea* , indicating Upper Triassic (Carnian-Norian) time for the oceanization in the study area. Robertson and Woodcock (1982) reported also Anisian-Carnian time interval for the early stage of crustal extension in the Antalya ophiolite. Plant-bearing sandstones of Upper Triassic age, that expose all along the Tauride belt (Özgül, 1976), support the early stage of crustal extension and shallow water sedimentation in the study area. Continued spreading within rift basins namely southern and multi-armed northern branch of the Neotethys (Sengör and Yılmaz, 1981) was in progress during Jurassic and Early Cretaceous. This period is dominated by calcareous and terrigenous deposition to finer grained siliceous pelagic and hemipelagic sedimentation (Robertson and Woodcock, 1982; Özgul, 1976; 1984). Late Jurassic-Early Cretaceous aged extensive ocean island/seamount alkaline basaltic volcanism intercalated with cherty limestone and radiolarites occured in the study area (Parlak et al., in review).

After the opening of the south Atlantic ocean (Smith et al., 1981) in Early-Late Cretaceous, rifting period ceased and convergence between Afro-Arabian and Eurasia plates started. As a result of continuous convergence in the southern branch of the Neotethyan ocean, a north dipping subduction at the begining of Late Cretaceous created arc-related or supra-subduction zone ophiolite bodies in the eastern Mediterranean region (Pearce et al., 1984; Robertson and Dixon, 1984; Jones and Robertson, 1991; Robertson, 1994). The Mersin ophiolite was formed above subduction zone in the southern branch of the Neotethyan ocean. Geochemistry of the volcanic rocks and mineral chemistry of the ultramafic and mafic cumulates clearly indicate that the Mersin ophiolite presents the main features of the supra-subduction zone ophiolites in southern Turkey (Parlak et al., in review). Soon after the formation of the ophiolite body, continuous compression led oceanic lithosphere to cause intraoceanic thrusting. The initiation of intraoceanic thrusting yielded basal metamorphic sole that cooled below 500°C during the period between 96±0.7 Ma and 91.6±0.3 Ma at the base of the Mersin ophiolite. The geochemistry of basal metamorphic sole indicate the features of ocean island or seamount basaltic rocks from which metamorphic sole were driven (Parlak et al., 1995). Arc-related melts generated above the subduction zone produced mafic dike swarms intruding the basal metamorphic sole, mantle tectonites, and cumulates of the Mersin ophiolite. Dike injections are not affected by the metamorphic event and are relatively younger than the cooling age of the amphibolites in the metamorphic sole. The same evidence is also seen in the metamorphic sole at the base of the Pozanti-Karsanti ophiolite (Lytwyn and Casey, 1995). The cooling age of the dike swarms in the metamorphic sole range from 89.6±0.7 Ma to 86.3±0.5 Ma, this post kinematic dike injections were also in progress in the other part of the oceanic crust during Danian (63.8±0.9 Ma) indicating the presence of the oceanic event in Lower Paleocene before obduction onto the Tauride active continental margin. The oldest unit resting unconformably on the ophiolite body is Alveolina-rich Upper Paleocene aged sandy-clayey limestones in the eastern part of the Mersin ophiolite (Avsar, 1992). Shear sense indicaters observed in the metamorphic sole, vergence of large scale faults and vergence of asymmetric folds indicate that Mersin ophiolite were emplaced from southern branch of the Neotethyan ocean onto the Tauride platform some time during end of Early Paleocene in southernTurkey.

References

Avsar, N., 1992; Namrun (Içel) yöresi Paleojen bentik foraminifer faunası, M.T.A. Dergisi, 114, 127-144.

Jones, G., and Robertson, A.H.F., 1991; Tectono-stratigraphy and evolution of the Mesozoic Pindos ophiolite and related units, northwestern Greece. J. Geol. Soc. London, 148, 267-288.

Lytwyn, J. N., and Casey, J.F., 1995; The geochemistry of postkinematic mafic dike swarms and subophiolitic metabasites, Pozanti-Karsanti ophiolite, Turkey: evidence for ridge subduction. Bull. geol. Soc. Amer., 107, 7, 830-850.

Özgül, N., 1976; Torosların bazı jeoloji özellikleri. T.J.K. Bulteni, 19, 65-78.

Özgül, N., 1984; Stratigraphy and tectonic evolution of the central Taurides. In: Tekeli, O. and Göncüoglu, M.C. (eds.), Geology of the Taurus belt. Proceedings of international symposium on the geology of the Taurus belt, 1983, Ankara-Turkey, 77-90.

Parlak, O., Delaloye, M., and Bingol, E., 1995; Origin of sub-ophiolitic metamorphic rocks beneath the Mersin ophiolite, S. Turkey. Ofioliti, 20, 2, 97-110.

Parlak, O., Delaloye, M., and Bingol, E., (in review) Geochemistry of volcanic rocks in the Mersin ophiolite and their tectonic significance in the eastern Mediterranean geology, in IESCA-1995 Proceedings, Int.ernational Earth Sciences Colloquium on the Eagean Region.

Pearce, J.A., Lippard, S.J., and Roberts, S., 1984; Characteristics and tectonic significance of supra-subduction zone ophiolites. In: Kokelaar, B.P. and Howells, M.F. (eds.), Marginal Basin Geology 77-94. Blackwell Scientific-Oxford.

Robertson, A.H.F., and Woodcock, N.H., 1982; Sedimentary history of the south-western segment of the Mesozoic-Tertiary Antalya continental margin, south-west Turkey, Eclogae geol. Helv., 75, 3, 517-562, .

Robertson, A.H.F., and Dixon, J.E., 1984; Introduction: aspects of the geological evolution of the eastern Mediterranean. In: Dixon, J.E. and Robertson, A.H.F. (eds.), The geological evolution of the eastern Mediterranean. Geol. Soc. Spec. Publ. London, 17, 1-75.

Robertson, A.H.F., 1994; Role of the tectonic facies concept in orogenic analysis and its application to Tethys in the eastern Mediterranean region. Earth Sci. Rev. 37, 139-213.

Sengör, A.M.C., and Yilmaz, Y., 1981; Tethyan evolution of Turkey: Plate tectonic approach. Tectonopysics 75, 181-241.

Smith, A.G., Hurley, A.M., and Briden, J.C., 1981; Phanerozoic palaeocontinental maps. Cambridge, Cambridge University Press, 102p.

APPENDIX 1

$^{40}Ar/^{39}Ar$ analytical data from incremental heating experiments

ANALYTICAL METHOD

Incremental heating experiments were carried out at the University of Geneva $^{40}Ar/^{39}Ar$ Geochronology Laboratory. 7 amphibole separates between 15.6 and 11.71 mg and whole-rock samples between 2.49 and 9.22 mg were placed into aluminum foil packets and loaded into 6 mm i.d. quartz vials. Nine neutron flux monitors, loaded into copper packets were placed in the 104.5 mm vial. The monitor mineral was HDB-1 Biotite (Fuhrmann et al., 1987). The $^{40}Ar/^{39}Ar$ plateau age of this standard is 24.292 Ma (Wijbrans et al., 1995). The samples were irradiated for 18 hours at the Oregon State University Triga reactor in the unlined inner core facility where they received a total fast neutron dose of $1.62*10^{18}$ n/cm^2. Based on previous analyses of optical grade CaF_2 and Fe-doped K-silicate glass irradiated at Oregon State (Wijbrans et al., 1995), corrections for undesirable neutron-induced reactions on ^{40}K and ^{40}Ca are as follows: $[^{40}Ar/^{39}Ar]_K$= 0.00465; $[^{36}Ar/^{37}Ar]_{Ca}$=0.000268; $[^{39}Ar/^{37}Ar]_{Ca}$= 0.000698.

At the University of Geneva $^{40}Ar/^{39}Ar$ Geochronology Laboratory, samples were loaded into a glass sedearm over a double vacuum resistance furnace attached to a 225 cm^3 gas cleanup system that employs one SAES AP10-GP ZR-AI getter pump operated at room temperature and one at ~400^oC. All samples were degassed at 600^oC to remove undesirable large quantities of atmospheric argon; this gas was pumped away and not analysed. Following 12 minute heating intervals and an additional 10 minutes of clean-up with a third AP10 GP getter at 400^oC, the purified gas was let into an ultrasensitive rare gas mass spectrometer (Mass Analyzer Products 216 with Bauer-Singer ion source). For each analysis, eight sets of peaks over the mass range 40 to 36 were measured statically on the Johnston secondary electron multiplier and linearly regressed to height at the time of inlet. The instrument was operated at a sensitivity of $8*10^{-15}$ moles ^{40}Ar/V. Each analysis was corrected for mass discrimination and a total system blank that comprised two parts including a small non-atmospheric component contributed by the mass spectrometer plus an atmospheric component from the furnace and clean-up system. These blanks were measured prior to degassing each sample. Total system blanks were typically less than $2.4*10^{-15}$ moles ^{40}Ar and $3.0*10^{-17}$ moles of ^{36}Ar at temperatures below 1200^oC; the spectrometer background was typically less than $2.0*10^{-18}$ moles of ^{40}Ar and $8.0*10^{-18}$ moles of ^{36}Ar.

Incremental heating experiments consisted of 16 to 24 individual steps. For each analysis the $\pm 1\sigma$ errors include estimates of the standard deviation of analytical precision on the peak signals, the blank, spectrometer mass discrimination, plus reactor corrections. Inverse-variance weighted mean ages and errors were calculated according to Taylor (1982). J values determined from the mean of 5 to 6 plateau measurements were collected from each monitor (HDB-1) packet. The estimated precision for each monitor point along the J curve suggest that errors in J are $\approx$ 0.3%. This uncertainty was propagated into the final plateau and isochron ages for each analysis. Ages were calculated using the decay constants of Steiger and Jäger (1977). Criteria for the interpretation of the experimental results are outlined in Singer and Pringle (1996).

Criteria used for determining plateau ages are similar to Pringle (1993). These criteria include: (1) age spectrum plateaus are defined by at least three contiguous steps all concordant in age at the 95% confidence level and comprising >50% of the ^{39}Ar released, (2) a well defined isochron exists for the plateau points as defined by the F-variate statistic SUMS/(N-2) for the York2 regression used here York (1969), (3) the plateau and isochron ages are concordant at the 95% confidence level, and (4) the $^{40}Ar/^{36}Ar$ intercept on the isochron diagram does not differ from the atmospheric value of 295.5 at the 95% confidence level. The isochron ages strongly prefered over the weighted mean plateau ages because they combine quantitative estimates of analytical precision and internal disturbance of the sample (scatter about the isochron), without making any assumption about the trapped argon component (Singer and Pringle, 1996).

Table 1.1. $^{40}Ar/^{39}Ar$ analytical data from incremental heating experiments

T (°C)	$^{40}Ar/^{39}Ar$	$^{37}Ar/^{39}Ar$	$^{36}Ar/^{39}Ar$	^{40}Ar (mol)	% ^{40}Ar	K/Ca	% ^{39}Ar	Apparent Age (Ma)		
Mersin: OP-131 Amphibole (95GE352), 15.6 mg, J= 0.0042104, Total gas age: 91.9±0.3 Ma										
960	12.433	5.119	0.21606	4.4E-15	16.3	0.095	0.23	92.05	±	9.80
1000	11.984	9.390	0.18599	5.8E-15	18.0	0.052	0.31	88.81	±	7.44
1010	11.243	11.907	0.26451	3.5E-15	12.6	0.041	0.21	83.44	±	12.34
1040	12.647	14.164	0.50652	3.0E-15	7.8	0.034	0.15	93.59	±	18.14
1070	12.961	17.160	0.11531	1.3E-14	28.1	0.028	0.65	95.86	±	3.11
1100	12.658	16.824	0.06264	3.0E-14	42.1	0.029	1.54	93.67	±	1.47
1125	12.456	16.392	0.01782	1.3E-13	75.6	0.030	6.80	92.21	±	0.68
1135	12.462	15.901	0.01349	1.7E-13	81.9	0.031	8.80	92.26	±	0.49
1139	12.491	15.721	0.01301	1.2E-13	82.6	0.031	6.25	92.46	±	0.59
1141	12.361	15.583	0.01251	1.6E-13	83.2	0.031	8.27	91.53	±	0.83
1145	12.401	15.553	0.01065	1.9E-13	86.5	0.031	10.27	91.81	±	0.60
1150	12.495	15.422	0.00870	2.7E-13	90.1	0.031	14.25	92.49	±	0.47
1154	12.340	15.196	0.00737	2.4E-13	92.6	0.032	12.53	91.34	±	0.59
1160	12.270	14.975	0.00720	2.1E-13	92.8	0.032	11.14	90.87	±	0.52
1168	12.247	14.791	0.01250	7.5E-14	82.8	0.033	4.02	90.71	±	0.56
1185	12.167	15.151	0.03307	1.7E-14	58.4	0.032	0.93	90.13	±	2.08
1220	12.351	15.875	0.02654	4.5E-14	65.0	0.031	2.38	91.46	±	0.84
1270	12.554	15.914	0.02679	5.7E-14	65.1	0.030	2.96	92.92	±	1.04
1330	12.485	16.001	0.03373	6.7E-14	58.7	0.030	3.49	92.43	±	0.94
1400	12.567	15.766	0.04364	9.2E-14	51.6	0.031	4.81	93.01	±	1.42
Mersin: OP-132 Amphibole (95GE353), 11.71 mg, J= 0.0041751, Total gas age: 92.4±0.3 Ma										
700	14.013	3.184	0.53134	8.8E-15	8.2	0.154	0.41	102.58	±	13.57
800	10.983	3.590	0.65455	8E-15	5.4	0.136	0.48	80.89	±	10.61
900	13.179	2.747	0.36317	1.6E-14	10.9	0.178	0.82	96.63	±	7.62
960	12.499	6.069	0.18701	7.9E-15	18.5	0.080	0.42	91.76	±	4.06
1020	12.628	12.433	0.16181	1.3E-14	21.1	0.039	0.69	92.69	±	3.93
1070	12.511	15.574	0.08114	4.1E-14	35.2	0.031	2.15	91.85	±	1.27
1100	12.662	15.029	0.04506	1.6E-13	50.8	0.032	8.19	92.93	±	0.80
1110	12.487	14.713	0.01849	1.1E-13	74.2	0.033	5.71	91.68	±	0.64
1120	12.591	14.431	0.01698	1.2E-13	76.3	0.034	6.46	92.43	±	0.41
1130	12.679	14.255	0.01691	2.1E-13	76.4	0.034	10.84	93.06	±	0.46
1135	12.684	14.155	0.01209	4.1E-13	83.6	0.034	21.18	93.09	±	0.33
1137	12.464	14.060	0.00883	2.3E-13	89.2	0.035	12.12	91.52	±	0.28
1140	12.483	13.897	0.00939	1.3E-13	88.0	0.035	6.78	91.65	±	0.42
1147	12.453	13.864	0.00848	1.2E-13	89.7	0.035	6.38	91.43	±	0.50
1160	12.386	13.916	0.01419	4.5E-14	79.8	0.035	2.4	90.96	±	0.53
1200	12.512	14.856	0.02635	3.6E-14	65.2	0.033	1.91	91.86	±	1.01
1300	12.644	15.882	0.02610	6.9E-14	65.9	0.031	3.62	92.81	±	0.92
1420	12.682	15.092	0.02465	1.8E-13	67.3	0.032	9.45	93.08	±	0.95
Mersin: OP-253 Amphibole (95GE354), 12.41 mg, J= 0.0041482, Total gas age: 91.5±0.4 Ma										
700	11.786	2.999	0.32507	1.1E-14	10.9	0.163	1.12	86.11	±	7.39
800	10.509	2.888	0.15530	2.1E-14	18.7	0.169	2.47	76.98	±	3.06
900	10.033	3.081	0.16235	2.5E-14	17.3	0.159	3.11	73.56	±	2.82
1000	12.606	11.143	0.06908	2.9E-14	39.0	0.044	2.85	91.95	±	1.56
1060	12.408	22.213	0.05004	4.2E-14	48.4	0.022	4.18	90.54	±	0.77
1100	12.502	24.253	0.04452	4.6E-14	52.2	0.020	4.64	91.21	±	1.06
1110	12.609	28.065	0.02859	1.5E-13	66.5	0.017	14.36	91.97	±	1.00
1113	12.570	28.786	0.02103	8.2E-14	75.8	0.017	8.19	91.69	±	0.64
1120	12.534	29.155	0.02099	8.1E-14	75.9	0.017	8.02	91.44	±	0.57
1128	12.772	29.171	0.02091	6.2E-14	76.4	0.017	6.09	93.13	±	0.68
1135	12.647	28.846	0.01907	6.6E-14	78.7	0.017	6.52	92.24	±	0.62
1145	12.507	28.485	0.02222	5.1E-14	74.0	0.017	5.06	91.25	±	0.61
1160	12.483	27.900	0.03184	2.2E-14	62.9	0.017	2.20	91.07	±	1.05
1200	12.544	29.661	0.04351	3.6E-14	53.9	0.016	3.55	91.51	±	0.77
1270	12.810	29.269	0.02928	1.1E-13	66.4	0.016	10.87	93.4	±	0.98
1350	12.977	28.574	0.03543	7.3E-14	60.8	0.017	7.06	94.58	±	1.27
1420	13.142	28.626	0.05642	1.0E-13	47.2	0.017	9.70	95.76	±	0.84
Mersin: OP-254 Amphibole (95GE355), 11.75 mg, J= 0.0041211, Total gas age: 95.1±0.5 Ma										
700	15.938	4.278	0.37908	8.8E-15	12.5	0.114	0.88	114.76	±	7.97
800	13.21	6.607	0.45677	9.9E-15	8.9	0.074	1.20	95.63	±	12.47
900	14.746	5.28	0.27852	9.2E-15	15.2	0.093	1.00	106.43	±	5.11
1000	13.111	18.804	0.10673	1.9E-14	30.1	0.026	2.35	94.93	±	2.14
1060	13.003	27.592	0.08634	3.2E-14	35.3	0.017	3.92	94.17	±	1.66
1100	12.915	29.587	0.04758	1.1E-13	51.9	0.016	13.57	93.55	±	1.46
1110	12.986	30.068	0.0277	1.3E-13	68.6	0.016	15.69	94.05	±	1.06
1117	12.95	30.27	0.02563	8.8E-14	71.0	0.016	10.91	93.79	±	0.60
1125	12.931	29.941	0.02308	8.1E-14	74.0	0.016	10.02	93.66	±	0.77
1132	12.678	29.434	0.02761	5.5E-14	68.0	0.016	6.92	91.87	±	0.79
1140	12.918	28.656	0.02884	2.9E-14	66.9	0.017	3.61	93.57	±	1.07
1152	13.029	28.554	0.05723	8.7E-15	46.6	0.017	1.06	94.35	±	2.68
1190	13.174	30.399	0.07153	1.5E-14	40.8	0.016	1.79	95.37	±	2.28
1260	13.179	30.576	0.03551	7.2E-14	61.5	0.016	8.74	95.41	±	0.78
1330	13.122	29.228	0.04768	3.7E-14	52.2	0.016	4.47	95.01	±	1.06
1420	13.803	28.854	0.04005	1.2E-13	58.6	0.017	13.88	99.81	±	0.69

T (°C)	$^{40}Ar/^{39}Ar$	$^{37}Ar/^{39}Ar$	$^{36}Ar/^{39}Ar$	^{40}Ar (mol)	% ^{40}Ar	K/Ca	% ^{39}Ar	Apparent Age (Ma)		
Mersin: OP-255 Amphibole (95GE348), 12.61 mg, J= 0.0043054, Total gas age: 93.9±0.4 Ma										
700	13.623	3.759	0.28567	1.3E-14	13.9	0.130	1.41	102.82	±	5.22
800	10.690	3.325	0.24816	1.6E-14	12.7	0.147	2.31	81.18	±	5.42
900	12.667	3.405	0.15957	1.4E-14	21.2	0.144	1.64	95.80	±	3.46
1000	12.951	11.722	0.07927	2.1E-14	36.3	0.042	2.44	97.88	±	1.83
1050	12.173	20.638	0.08742	2.6E-14	33.1	0.023	3.26	92.16	±	1.67
1100	12.279	31.289	0.03581	1.0E-13	59.7	0.015	12.93	92.94	±	1.42
1108	12.473	33.365	0.02558	9.1E-14	71.2	0.014	11.19	94.37	±	0.90
1115	12.496	33.491	0.02543	8.0E-14	71.5	0.014	9.82	94.54	±	0.90
1123	12.349	33.228	0.02080	8.8E-14	77.4	0.014	10.91	93.45	±	0.66
1130	12.403	32.224	0.01821	6.8E-14	81.1	0.015	8.34	93.85	±	0.91
1138	12.169	30.909	0.02148	3.1E-14	75.3	0.015	3.96	92.12	±	1.02
1150	11.890	31.382	0.05082	7.6E-15	48.1	0.015	0.98	90.06	±	4.82
1185	12.406	35.016	0.04979	1.0E-14	50.3	0.014	1.25	93.87	±	3.06
1240	12.378	34.379	0.02866	7.9E-14	67.8	0.014	9.83	93.67	±	0.84
1300	12.469	32.908	0.03411	4.2E-14	62.0	0.015	5.18	94.34	±	1.02
1380	12.728	32.055	0.03348	5.4E-14	62.8	0.015	6.52	96.25	±	0.83
1430	12.570	31.533	0.03082	6.6E-14	65.0	0.015	8.03	95.08	±	0.89
Mersin: OP-256 Amphibole (95GE357), 12.11 mg, J= 0.0040754, Total gas age: 98.2±0.4 Ma										
800	16.138	4.387	0.44967	1.1E-14	10.8	0.111	0.74	114.91	±	10.37
900	16.238	5.180	0.58589	2.0E-14	8.6	0.094	1.36	115.60	±	12.13
960	18.335	5.018	0.19037	1.3E-14	24.6	0.097	0.77	130.00	±	4.08
1020	15.421	13.563	0.11990	2.0E-14	30.8	0.036	1.47	109.96	±	1.32
1060	14.745	19.888	0.10452	2.2E-14	33.2	0.024	1.67	105.27	±	2.39
1100	13.460	21.970	0.05340	1.1E-13	48.6	0.022	9.29	96.34	±	0.90
1110	13.370	22.560	0.03120	1.3E-13	63.9	0.021	10.84	95.71	±	0.47
1114	13.488	22.806	0.02478	8.9E-14	70.6	0.021	7.33	96.54	±	0.69
1120	13.384	22.926	0.02549	8.2E-14	69.7	0.021	6.85	95.81	±	0.59
1128	13.561	22.978	0.02570	1.2E-13	69.8	0.021	9.69	97.04	±	0.60
1135	13.379	22.743	0.02448	1.2E-13	70.8	0.021	9.93	95.77	±	0.46
1140	13.410	22.542	0.02080	8.8E-14	75.1	0.021	7.28	95.99	±	0.37
1150	13.141	22.057	0.02122	7.2E-14	74.1	0.022	6.08	94.11	±	0.48
1160	13.802	21.790	0.04651	1.5E-14	53.1	0.022	1.17	98.72	±	1.41
1200	13.892	22.638	0.04472	2.7E-14	54.5	0.021	2.15	99.35	±	0.95
1270	14.158	22.593	0.03327	1.0E-13	63.4	0.021	8.06	101.20	±	0.67
1340	14.350	22.319	0.04798	5.5E-14	53.2	0.022	4.27	102.53	±	1.16
1420	13.903	22.465	0.04532	1.4E-13	54.1	0.022	11.05	99.42	±	0.66
Mersin: OP-257 Amphibole (95GE350), 12.35 mg, J= 0.004254, Total gas age: 94.4±0.3 Ma										
700	13.081	4.104	0.31273	9.2E-15	12.4	0.119	0.64	97.70	±	7.37
800	12.308	5.813	0.37447	1.0E-14	10.0	0.084	0.77	92.06	±	6.68
900	13.857	4.383	0.17659	1.2E-14	21.0	0.112	0.80	103.32	±	3.48
1000	12.951	10.407	0.07376	2.7E-14	38.0	0.047	1.88	96.74	±	1.53
1050	12.622	16.133	0.05873	3.9E-14	43.7	0.030	2.80	94.36	±	1.49
1080	12.476	18.699	0.03090	9.6E-14	61.7	0.026	6.99	93.29	±	0.61
1100	12.414	19.696	0.01765	1.8E-13	77.0	0.025	12.93	92.84	±	0.62
1107	12.567	20.087	0.01771	1.2E-13	77.3	0.024	8.78	93.95	±	0.50
1115	12.710	20.079	0.01727	1.4E-13	78.1	0.024	9.96	94.99	±	0.60
1120	12.608	20.062	0.01542	1.1E-13	80.7	0.024	8.20	94.25	±	0.48
1125	12.518	19.988	0.01619	8.0E-14	79.4	0.024	5.81	93.60	±	0.57
1130	12.508	19.985	0.01650	6.7E-14	78.9	0.024	4.81	93.52	±	0.59
1145	12.448	19.717	0.01517	6.4E-14	80.7	0.025	4.68	93.09	±	0.39
1175	12.301	19.315	0.04391	1.8E-14	51.5	0.025	1.36	92.01	±	1.44
1250	12.619	19.966	0.02403	1.0E-13	69.3	0.024	7.40	94.33	±	0.54
1340	12.847	19.679	0.02716	1.4E-13	66.2	0.025	9.63	95.99	±	0.61
1430	12.839	19.869	0.02658	1.8E-13	66.8	0.024	12.59	95.93	±	0.63

T (°C)	$^{40}Ar/^{39}Ar$	$^{37}Ar/^{39}Ar$	$^{36}Ar/^{39}Ar$	^{40}Ar (mol)	% ^{40}Ar	K/Ca	% ^{39}Ar	Apparent Age (Ma)
Mersin: OP-122 Whole rock (diabase) (95GE312), 5.76 mg, J= 0.0050169, Total gas age: 89.5±0.3 Ma								
600	10.657	1.000	0.04689	3.4E-14	43.6	0.490	2.30	93.96 ± 1.44
660	10.341	1.346	0.04351	2.0E-14	44.8	0.364	1.37	91.25 ± 1.48
720	9.803	2.290	0.04120	5.5E-14	44.9	0.214	3.99	86.61 ± 1.07
765	9.952	1.998	0.02762	6.1E-14	55.4	0.245	4.35	87.90 ± 0.79
800	9.975	1.563	0.04277	3.9E-14	44.3	0.313	2.80	88.09 ± 0.61
840	9.982	1.516	0.02534	5.5E-14	57.5	0.323	3.97	88.15 ± 1.54
870	9.657	1.739	0.01290	3.2E-14	72.4	0.282	2.37	85.35 ± 0.75
905	9.863	1.912	0.01700	5.6E-14	66.9	0.256	4.02	87.13 ± 0.83
925	9.651	1.910	0.01278	3.9E-14	72.6	0.256	2.90	85.29 ± 0.68
950	9.897	2.252	0.01380	3.5E-14	71.7	0.217	2.52	87.42 ± 0.59
985	**10.188**	**3.566**	**0.00956**	**1.1E-13**	**80.0**	**0.137**	**8.00**	**89.92 ± 0.52**
1000	**10.069**	**5.489**	**0.01145**	**7.0E-14**	**77.3**	**0.089**	**4.94**	**88.90 ± 0.51**
1010	**10.147**	**7.623**	**0.01516**	**5.2E-14**	**72.2**	**0.064**	**3.68**	**89.57 ± 0.52**
1025	**10.226**	**10.890**	**0.01368**	**5.9E-14**	**76.1**	**0.045**	**4.13**	**90.26 ± 0.47**
1040	**10.190**	**10.733**	**0.01345**	**5.5E-14**	**76.4**	**0.045**	**3.86**	**89.95 ± 0.43**
1055	**10.198**	**10.874**	**0.01206**	**5.8E-14**	**78.9**	**0.045**	**4.08**	**90.01 ± 0.47**
1070	**10.228**	**9.799**	**0.01229**	**5.7E-14**	**78.0**	**0.050**	**4.01**	**90.27 ± 0.56**
1085	**10.188**	**7.515**	**0.00930**	**6.2E-14**	**82.4**	**0.065**	**4.37**	**89.93 ± 0.41**
1100	**10.131**	**4.624**	**0.00938**	**6.2E-14**	**80.7**	**0.106**	**4.39**	**89.44 ± 0.51**
1115	**10.152**	**3.012**	**0.00794**	**6.8E-14**	**82.7**	**0.162**	**4.76**	**89.62 ± 0.36**
1130	**10.154**	**2.543**	**0.00811**	**7.0E-14**	**82.2**	**0.192**	**4.89**	**89.63 ± 0.47**
1145	**10.174**	**2.727**	**0.00876**	**7.0E-14**	**81.0**	**0.179**	**4.92**	**89.81 ± 0.36**
1175	**10.150**	**5.728**	**0.01719**	**7.6E-14**	**68.6**	**0.085**	**5.36**	**89.60 ± 1.07**
1250	10.699	15.086	0.03133	1.2E-13	56.8	0.032	8.02	94.32 ± 0.70
Mersin: OP-129 Whole rock (diabase) (95GE313), 2.89 mg, J= 0.0050057, Total gas age: 89.4±0.5 Ma								
625	12.030	1.669	0.91110	3.0E-15	4.3	0.293	0.32	105.49 ± 38.84
650	8.493	1.703	0.67495	1.1E-15	4.1	0.287	0.17	75.11 ± 35.42
710	8.122	2.862	0.31938	4.2E-15	7.9	0.171	0.67	71.90 ± 11.10
760	8.938	3.783	0.18761	7.2E-15	13.9	0.129	1.04	78.96 ± 5.55
810	10.123	2.561	0.22552	1.6E-14	13.2	0.191	2.04	89.17 ± 6.37
840	11.167	2.573	0.27555	1.5E-14	12.1	0.190	1.75	98.12 ± 9.96
860	10.915	1.925	0.16131	1.4E-14	18.7	0.254	1.62	95.97 ± 4.11
885	10.659	1.969	0.14490	1.5E-14	20.0	0.249	1.79	93.78 ± 3.18
910	10.710	1.936	0.12273	1.8E-14	22.8	0.253	2.12	94.21 ± 3.37
935	**10.514**	**1.942**	**0.08292**	**3.3E-14**	**30.1**	**0.252**	**3.99**	**92.53 ± 2.86**
950	**10.476**	**1.499**	**0.04696**	**2.9E-14**	**43.2**	**0.327**	**3.55**	**92.20 ± 1.69**
965	**10.398**	**1.275**	**0.04040**	**2.3E-14**	**46.7**	**0.384**	**2.89**	**91.54 ± 2.07**
990	**10.251**	**1.264**	**0.02681**	**4.4E-14**	**56.7**	**0.387**	**5.47**	**90.27 ± 0.96**
1010	**10.174**	**0.898**	**0.01618**	**6.6E-14**	**68.3**	**0.545**	**8.30**	**89.61 ± 0.84**
1020	**10.222**	**0.857**	**0.01334**	**6.3E-14**	**72.5**	**0.572**	**7.94**	**90.03 ± 0.77**
1030	**10.072**	**0.782**	**0.02053**	**3.2E-14**	**62.6**	**0.626**	**4.04**	**88.73 ± 1.34**
1045	**10.195**	**1.858**	**0.01409**	**7.7E-14**	**71.7**	**0.263**	**9.68**	**89.79 ± 1.56**
1055	**10.107**	**1.369**	**0.01621**	**5.5E-14**	**68.3**	**0.358**	**7.01**	**89.03 ± 0.81**
1065	**9.994**	**1.484**	**0.01842**	**4.4E-14**	**65.2**	**0.330**	**5.62**	**88.06 ± 0.96**
1080	**9.950**	**1.754**	**0.01857**	**4.1E-14**	**65.0**	**0.279**	**5.29**	**87.68 ± 1.39**
1105	9.915	1.904	0.02110	4.7E-14	61.9	0.257	6.12	87.39 ± 0.88
1140	9.860	1.936	0.01676	5.2E-14	67.2	0.253	6.76	86.91 ± 0.86
1190	9.575	5.409	0.02567	4.0E-14	57.1	0.090	5.43	84.46 ± 1.02
1260	10.381	18.947	0.07024	5.2E-14	34.7	0.026	6.39	91.39 ± 2.03
Mersin: OP-227 Whole rock (diabase) (95GE307), 2.49 mg, J= 0.0050875, Total gas age: 82.2±0.3 Ma								
600	5.424	0.927	0.11348	3.1E-15	13.9	0.528	0.52	49.11 ± 5.06
650	5.724	1.207	0.05261	7.3E-15	27.0	0.406	1.17	51.78 ± 2.02
725	6.300	2.867	0.03114	1.4E-14	41.2	0.171	2.07	56.91 ± 1.75
785	7.360	3.024	0.03680	1.3E-14	40.8	0.162	1.61	66.31 ± 1.74
850	8.599	3.657	0.08995	4.1E-14	24.6	0.134	4.32	77.24 ± 1.33
860	**9.618**	**2.663**	**0.02204**	**1.9E-14**	**60.4**	**0.184**	**1.80**	**86.18 ± 1.34**
885	**9.606**	**1.384**	**0.02484**	**1.1E-14**	**57.0**	**0.353**	**1.08**	**86.08 ± 1.80**
925	**9.616**	**1.493**	**0.01600**	**4.1E-14**	**67.6**	**0.328**	**3.92**	**86.17 ± 0.63**
950	**9.701**	**1.238**	**0.00957**	**5.2E-14**	**78.0**	**0.396**	**4.87**	**86.91 ± 0.48**
975	**9.661**	**0.943**	**0.00610**	**7.9E-14**	**84.8**	**0.519**	**7.47**	**86.56 ± 0.32**
995	**9.654**	**0.760**	**0.00459**	**1.1E-13**	**88.1**	**0.645**	**10.43**	**86.49 ± 0.42**
1010	**9.617**	**0.803**	**0.00755**	**9.2E-14**	**81.6**	**0.610**	**8.78**	**86.17 ± 0.42**
1025	**9.563**	**1.266**	**0.00758**	**8.4E-14**	**81.7**	**0.387**	**8.06**	**85.70 ± 0.30**
1040	9.472	1.390	0.00702	7.3E-14	82.8	0.352	7.07	84.90 ± 0.32
1055	9.349	1.536	0.00887	6.5E-14	78.8	0.319	6.39	83.83 ± 0.33
1070	9.291	1.779	0.00776	6.0E-14	81.1	0.275	5.96	83.32 ± 0.36
1090	9.176	1.511	0.00605	6.3E-14	84.6	0.324	6.32	82.31 ± 0.34
1150	8.801	1.941	0.00590	1.1E-13	84.6	0.252	11.54	79.02 ± 0.34
1220	8.402	7.675	0.01287	1.1E-13	72.3	0.064	6.60	75.51 ± 0.42

T (°C)	$^{40}Ar/^{39}Ar$	$^{37}Ar/^{39}Ar$	$^{36}Ar/^{39}Ar$	^{40}Ar (mol)	% ^{40}Ar	K/Ca	% ^{39}Ar	Apparent Age (Ma)
Mersin OP-82 Whole rock (diabase) (95GE325), 8 mg, J= 0.0047965, Total gas age: 59.9±0.4 Ma								
550	6.389	2.658	0.33484	5.5E-15	6.1	0.184	1.92	54.45 ± 8.18
575	6.376	2.677	0.16206	2.4E-15	11.8	0.183	0.86	54.35 ± 7.66
635	7.770	2.954	0.20056	1.0E-14	11.6	0.166	2.99	66.01 ± 4.98
665	6.178	4.092	0.10274	9.7E-15	17.0	0.119	3.50	52.68 ± 2.24
705	7.235	4.638	0.10118	1.5E-14	19.6	0.105	4.50	61.54 ± 2.65
745	7.628	3.907	0.11020	2.0E-14	19.1	0.125	5.81	64.83 ± 1.58
775	7.478	3.713	0.10057	1.7E-14	20.2	0.132	5.05	63.57 ± 2.24
800	6.297	3.670	0.11626	1.1E-14	15.6	0.133	4.04	53.68 ± 1.98
825	6.304	4.459	0.10549	1.5E-14	16.9	0.110	5.33	53.74 ± 1.85
840	6.092	5.036	0.04748	8.1E-15	30.8	0.097	2.96	51.95 ± 1.19
865	5.880	5.520	0.05388	1.2E-14	27.4	0.088	4.46	50.17 ± 1.09
890	5.796	5.739	0.05841	1.1E-14	25.6	0.085	4.08	49.46 ± 1.02
925	6.687	6.578	0.04475	1.7E-14	34.4	0.074	5.67	56.95 ± 1.11
965	**7.273**	**7.863**	**0.04034**	**2.4E-14**	**39.0**	**0.062**	**7.32**	**61.86 ± 0.80**
1010	**7.273**	**7.866**	**0.04034**	**4.2E-14**	**39.0**	**0.062**	**13.03**	**61.86 ± 0.80**
1020	**7.462**	**10.537**	**0.09747**	**2.1E-14**	**20.9**	**0.046**	**6.32**	**63.44 ± 1.94**
1025	**7.514**	**10.928**	**0.05020**	**1.5E-14**	**34.8**	**0.045**	**4.45**	**63.87 ± 0.94**
1032	**7.372**	**10.889**	**0.05099**	**1.3E-14**	**34.0**	**0.045**	**3.85**	**62.69 ± 2.59**
1050	**7.591**	**11.653**	**0.04233**	**1.5E-14**	**39.4**	**0.042**	**4.36**	**64.51 ± 0.86**
1090	**7.513**	**11.159**	**0.03275**	**3.2E-14**	**45.9**	**0.044**	**9.49**	**63.87 ± 0.44**
Mersin: OP-80 Whole rock (diabase) (95GE334), 9.22 mg, J= 0.0046291, Total gas age: 51.3±0.3 Ma								
600	2.421	6.473	0.10478	2.2E-15	7.3	0.075	0.78	20.10 ± 3.66
700	3.689	5.135	0.06021	2.2E-14	17.4	0.095	5.16	30.55 ± 1.01
800	5.243	5.179	0.11961	4.0E-14	13.0	0.094	6.56	43.26 ± 1.85
840	5.419	5.639	0.06838	3.2E-14	21.5	0.087	4.98	44.69 ± 1.08
870	5.115	4.753	0.05243	2.5E-14	25.2	0.103	4.17	42.21 ± 1.33
900	5.447	3.984	0.04045	2.2E-14	31.8	0.123	3.37	44.92 ± 1.19
940	6.153	4.351	0.02886	3.1E-14	42.8	0.112	4.26	50.66 ± 0.74
975	6.647	4.729	0.02576	4.1E-14	47.8	0.103	5.21	54.68 ± 0.58
995	7.280	4.544	0.02548	4.5E-14	50.3	0.108	5.32	59.79 ± 0.72
1005	6.937	4.779	0.02733	3.3E-14	47.3	0.102	4.04	57.02 ± 0.55
1020	6.877	5.677	0.02912	3.2E-14	45.6	0.086	3.99	56.54 ± 0.87
1040	6.932	6.182	0.06922	3.0E-14	25.7	0.079	3.66	56.98 ± 1.75
1055	6.565	6.718	0.02709	4.3E-14	46.6	0.073	5.59	54.01 ± 0.44
1065	6.593	5.862	0.02511	3.5E-14	48.5	0.083	4.59	54.24 ± 0.61
1080	6.464	5.375	0.02326	3.4E-14	49.8	0.091	4.50	53.18 ± 0.60
1095	6.408	4.605	0.02240	3.1E-14	50.5	0.106	4.12	52.74 ± 0.50
1115	6.294	4.037	0.01995	3.7E-14	52.9	0.121	5.06	51.81 ± 0.43
1135	6.261	4.095	0.01912	4.0E-14	53.9	0.119	5.43	51.54 ± 0.48
1150	6.343	5.130	0.02312	3.5E-14	49.6	0.095	4.71	52.20 ± 0.43
1170	6.529	7.773	0.03295	3.6E-14	41.6	0.063	4.73	53.72 ± 1.53
1190	6.949	10.776	0.05015	2.5E-14	33.1	0.045	3.07	57.12 ± 1.55
1250	7.541	21.164	0.06575	5.9E-14	29.5	0.023	6.71	61.90 ± 1.33
Mersin: OP-117 Whole rock (diabase) (95GE337), 8.55 mg, J= 0.0045621, Total gas age: 34.2±0.2 Ma								
640	3.120	2.230	0.06325	6.3E-15	14.4	0.219	1.50	25.50 ± 1.80
690	3.338	2.541	0.04334	1.3E-14	20.9	0.193	2.95	27.26 ± 1.49
740	3.626	3.116	0.03196	2.0E-14	28.2	0.157	3.99	29.60 ± 0.71
780	4.010	3.387	0.04535	1.8E-14	23.3	0.144	3.37	32.70 ± 0.74
810	4.588	2.858	0.06787	2.1E-14	18.8	0.171	3.32	37.37 ± 1.35
825	4.757	4.406	0.05353	2.0E-14	23.5	0.111	3.19	38.73 ± 0.83
840	4.418	5.519	0.05556	1.6E-14	21.6	0.088	2.61	36.00 ± 1.29
865	4.338	3.777	0.05753	1.9E-14	20.6	0.129	3.28	35.36 ± 1.05
915	3.947	2.250	0.02430	2.2E-14	36.0	0.217	4.10	32.20 ± 0.82
950	3.606	2.528	0.02172	2.4E-14	36.6	0.194	4.88	29.44 ± 0.45
990	3.771	3.427	0.01725	3.2E-14	43.8	0.143	6.27	30.77 ± 0.50
1040	4.330	5.627	0.01730	5.5E-14	48.0	0.087	9.40	35.29 ± 0.42
1080	5.473	10.008	0.01533	1.1E-13	59.2	0.049	15.55	44.49 ± 0.41
1100	4.852	10.399	0.01224	7.0E-14	63.3	0.047	10.74	39.50 ± 0.40
1200	3.428	4.499	0.00798	1.2E-13	63.0	0.109	24.85	28.00 ± 0.18
Mersin: OP-211 Whole rock (basalt) (95GE359), 3.62 mg, J= 0.0040196, Total gas age: 146.5±0.5 Ma								
600	25.316	0.707	0.00573	4.0E-13	93.9	0.693	27.90	174.83 ± 0.42
605	22.155	0.935	0.01306	5.4E-14	85.4	0.524	4.28	153.90 ± 1.25
620	21.862	0.928	0.01113	6.8E-14	87.2	0.528	5.48	151.94 ± 1.16
640	21.709	0.910	0.01096	8.2E-14	87.2	0.538	6.68	150.93 ± 0.85
655	22.629	0.840	0.00738	1.3E-13	91.4	0.583	10.01	157.05 ± 0.67
663	23.479	0.682	0.00808	1.2E-13	90.9	0.719	8.64	162.70 ± 0.68
670	23.482	0.582	0.00813	7.9E-14	90.9	0.842	5.93	162.72 ± 0.65
677	22.785	0.715	0.00846	6.2E-14	90.3	0.685	4.76	158.09 ± 0.56
690	21.854	1.037	0.00961	5.1E-14	88.8	0.472	4.08	151.89 ± 0.64
715	20.203	1.810	0.01260	5.0E-14	84.9	0.270	4.37	140.85 ± 0.70
755	15.311	5.534	0.02825	3.3E-14	65.8	0.088	3.83	107.75 ± 0.80
800	6.902	21.693	0.19172	8.1E-15	11.0	0.022	2.06	46.37 ± 3.84
840	3.506	48.697	0.12588	3.6E-15	9.2	0.010	1.78	25.25 ± 1.93
900	1.438	34.185	0.05596	1.9E-15	9.2	0.014	2.34	10.40 ± 1.38
1025	4.561	6.170	0.16341	2.8E-15	8.7	0.079	1.08	32.77 ± 4.21
1200	14.253	22.249	0.07352	5.5E-14	41.3	0.022	6.78	100.50 ± 2.65

T (°C)	$^{40}Ar/^{39}Ar$	$^{37}Ar/^{39}Ar$	$^{36}Ar/^{39}Ar$	^{40}Ar (mol)	% ^{40}Ar	K/Ca	% ^{39}Ar	Apparent Age (Ma)		
Mersin: OP-215 Whole rock (basalt) (95GE304), 2.73 mg, J= 0.0051235, Total gas age: 209.5±0.6 Ma										
520	22.208	0.761	0.05309	1.2E-14	58.7	0.643	0.40	194.40	±	7.08
550	23.570	0.730	0.01212	1.0E-13	87.0	0.671	3.09	205.67	±	1.06
565	25.326	0.676	0.00845	7.0E-14	91.2	0.725	3.58	220.09	±	0.90
570	27.122	0.664	0.00913	9.2E-14	91.1	0.738	2.48	234.73	±	1.34
580	28.335	0.669	0.00884	9.5E-14	91.7	0.732	2.44	244.54	±	1.14
590	28.992	0.677	0.00962	9.8E-14	91.2	0.724	2.46	249.84	±	1.28
605	29.315	0.680	0.00826	1.1E-13	92.5	0.721	2.69	252.44	±	1.06
620	29.013	0.685	0.01850	1.2E-13	84.3	0.715	3.06	250.01	±	1.23
630	28.163	0.706	0.00572	1.5E-13	94.5	0.694	3.92	243.15	±	0.73
640	26.929	0.727	0.00586	1.7E-13	94.1	0.673	4.70	233.16	±	0.75
645	26.254	0.741	0.00521	1.5E-13	94.6	0.661	4.14	227.67	±	0.81
650	25.710	0.735	0.00584	1.3E-13	93.9	0.666	3.58	223.24	±	1.02
660	25.552	0.733	0.00553	1.2E-13	94.2	0.668	3.35	221.94	±	0.85
675	25.539	0.726	0.00590	1.3E-13	93.8	0.674	3.62	221.83	±	0.99
700	26.672	0.725	0.00466	3.4E-13	95.3	0.676	9.42	231.07	±	0.70
710	26.835	0.710	0.00371	2.9E-13	96.3	0.690	7.83	232.40	±	0.76
715	26.558	0.724	0.00525	2.4E-13	94.7	0.676	6.55	230.15	±	0.86
725	26.214	0.734	0.02150	2.7E-14	80.6	0.667	0.76	227.34	±	2.02
745	25.267	0.841	0.00349	2.6E-13	96.3	0.582	7.43	219.61	±	0.84
760	23.982	1.058	0.00460	2.1E-13	94.9	0.463	6.41	209.06	±	0.81
775	22.525	1.457	0.00900	1.5E-13	89.8	0.336	4.98	197.03	±	1.16
795	20.010	2.103	0.02364	8.9E-14	74.5	0.233	3.25	176.07	±	1.15
820	15.766	3.491	0.06507	5.3E-14	45.3	0.140	2.44	140.14	±	1.72
845	8.989	6.036	0.04814	2.2E-14	39.4	0.081	1.75	81.22	±	1.30
880	1.654	7.098	0.01602	7.1E-15	28.3	0.069	3.11	15.23	±	0.60
980	1.634	9.913	0.05371	4.1E-15	9.7	0.049	1.82	15.04	±	2.97
1100	5.996	8.183	0.35264	6.1E-15	5.4	0.060	0.75	54.59	±	11.30

APPENDIX 2

Results of microprobe analysis of the minerals from the mantle tectonites, cumulates, volcanic units and metamorphic sole in the Mersin ophiolite

ANALYTICAL CONDITIONS

Microprobe analysis of the different minerals were done on a Camebax SX50 in the Mineralogy Department at the University of Lausanne.

Standards used for the elements are;
Si= Diopside, olivine, albite
K= Orthose
Mg= Diopside, olivine
Ca= Wollastonite, anorthite
Al= Jadeite, anorthite
Na= Jadeite, albite
Mn= Mns1, $MnTiO_3$
Cr= Cr_2O_3
Ti= Ilmenite, $MnTiO_3$
Fe= Hedenbergite, Fe_2O_3
Ni= NiO

Analytical conditions for the elements are;
Counting interval (seconds): 20
Beam current: 20 mA
Acceleration voltage: 15 kV

Calculation of chemical formula for the minerals is based on;
8 (O) for Plagioclase,
6 (O) for Pyroxene,
4 (O) for Olivine,
32 (O) for Chromian spinelle,
28 (O) for chlorite

APPENDIX 2.1

Microprobe results of the minerals from the mantle tectonites

Table 2.1.1. Results of electron micro-probe analyses of the chromites from harzburgites

Sample	73-1	73-2	73-3	73-4	90-1	90-2	90-3	90-4	90-5
SiO2	0.04	0.07	0.03	0.04	0.07	0.07	0.02	0.02	0.08
TiO2	0.02	0.04	0.05	0.00	0.00	0.02	0.00	0.01	0.04
Al2O3	15.10	14.90	15.13	14.79	18.90	19.66	19.01	18.56	19.51
Cr2O3	53.45	52.83	53.64	53.83	49.93	49.27	50.27	49.97	49.95
FeO	20.14	21.58	20.15	19.97	19.11	18.90	18.23	19.23	19.04
MnO	0.29	0.34	0.34	0.27	0.21	0.24	0.24	0.18	0.26
MgO	10.25	9.43	10.17	10.40	11.00	10.91	11.14	11.00	10.88
CaO	0.00	0.00	0.01	0.00	0.02	0.00	0.00	0.04	0.00
Na2O	0.00	0.01	0.04	0.01	0.03	0.00	0.04	0.01	0.00
K2O	0.00	0.00	0.01	0.01	0.00	0.01	0.00	0.00	0.00
Total	99.29	99.20	99.57	99.32	99.27	99.08	98.95	99.02	99.76
Si	0.01	0.02	0.01	0.01	0.02	0.02	0.00	0.00	0.02
Ti	0.00	0.01	0.01	0.00	0.00	0.00	0.00	0.00	0.01
Al	4.56	4.52	4.59	4.47	5.58	5.76	5.57	5.47	5.79
Cr	10.82	10.76	10.92	10.91	9.88	9.68	9.87	9.87	9.94
Fe	4.31	4.65	4.34	4.28	4.00	3.93	3.79	4.02	4.01
Mn	0.06	0.07	0.07	0.06	0.04	0.05	0.05	0.04	0.06
Mg	3.91	3.62	3.90	3.98	4.11	4.04	4.13	4.10	4.08
Ca	0.00	0.00	0.00	0.00	0.01	0.00	0.00	0.01	0.00
Na	0.00	0.00	0.02	0.00	0.01	0.00	0.02	0.00	0.00
K	0.00	0.00	0.00	0.00	0.00	0.00	0.00	0.00	0.00
Cr*	70.37	70.40	70.40	70.94	63.93	62.70	63.95	64.36	63.20
Fm*	52.43	56.21	52.64	51.85	49.35	49.28	47.86	49.51	49.53
Mg*	47.57	43.79	47.36	48.15	50.65	50.72	52.14	50.49	50.47

Numbers of ions on the basis of 32 (O), c indicates "core"

Table 2.1.2. Results of electron micro-probe analyses of the olivines from harzburgites

Sample	68-1c	68-2c	68-3c	68-4c	68-5c	73-1c	73-2c	73-3c	73-4c	73-5c	90-1c	90-2c	90-3c	90-4c	90-5c	90-6c	98-1c	98-2c	98-3c
SiO2	40.96	40.75	40.82	40.99	40.94	41.16	41.23	41.54	57.83	57.50	41.11	57.32	57.36	57.00	56.89	41.33	40.86	40.77	40.92
TiO2	0.00	0.00	0.00	0.00	0.00	0.00	0.00	0.00	0.03	0.00	0.00	0.00	0.00	0.00	0.00	0.00	0.01	0.00	0.02
Al2O3	0.01	0.00	0.00	0.01	0.00	0.00	0.00	0.00	0.90	1.00	0.00	1.42	1.40	1.45	1.48	0.00	0.00	0.01	0.01
FeO	8.52	8.44	8.31	8.30	8.53	8.93	8.82	9.14	5.73	5.55	9.11	6.02	5.56	5.77	5.52	9.02	8.62	8.94	8.56
Cr2O3	0.00	0.01	0.00	0.01	0.01	0.01	0.00	0.00	0.33	0.44	0.02	0.56	0.57	0.62	0.68	0.00	0.00	0.00	0.02
MnO	0.12	0.10	0.14	0.07	0.12	0.12	0.17	0.12	0.14	0.14	0.13	0.12	0.13	0.10	0.13	0.11	0.13	0.13	0.17
MgO	50.51	50.24	50.44	50.59	50.39	49.03	48.83	49.05	33.95	33.50	48.78	33.59	33.34	33.12	32.72	48.81	50.33	50.31	50.26
CaO	0.02	0.01	0.00	0.01	0.01	0.07	0.00	0.05	0.94	0.92	0.00	1.06	1.60	1.43	1.70	0.01	0.01	0.01	0.00
Na2O	0.00	0.00	0.00	0.00	0.00	0.00	0.01	0.00	0.00	0.01	0.00	0.02	0.02	0.00	0.00	0.01	0.00	0.00	0.00
K2O	0.00	0.00	0.00	0.00	0.00	0.00	0.02	0.00	0.00	0.03	0.01	0.01	0.01	0.00	0.00	0.01	0.00	0.00	0.00
NiO	0.38	0.39	0.36	0.43	0.42												0.35	0.41	0.42
Total	100.52	99.94	100.07	100.41	100.42	99.32	99.08	99.90	99.85	99.09	99.16	100.12	99.99	99.49	99.12	99.30	100.31	100.58	100.38
Si	0.99	0.99	0.99	1.00	0.99	1.00	0.99	1.01	1.32	1.31	0.99	1.32	1.32	1.30	1.30	1.00	0.99	0.99	1.00
Ti	0.00	0.00	0.00	0.00	0.00	0.00	0.00	0.00	0.00	0.00	0.00	0.00	0.00	0.00	0.00	0.00	0.00	0.00	0.00
Al	0.00	0.00	0.00	0.00	0.00	0.00	0.00	0.00	0.02	0.03	0.00	0.04	0.04	0.04	0.04	0.00	0.00	0.00	0.00
Fe	0.17	0.17	0.17	0.17	0.17	0.18	0.18	0.19	0.11	0.11	0.18	0.12	0.11	0.11	0.11	0.18	0.18	0.18	0.17
Cr	0.00	0.00	0.00	0.00	0.00	0.00	0.00	0.00	0.01	0.01	0.00	0.01	0.01	0.01	0.01	0.00	0.00	0.00	0.00
Mn	0.00	0.00	0.00	0.00	0.00	0.00	0.00	0.00	0.00	0.00	0.00	0.00	0.00	0.00	0.00	0.00	0.00	0.00	0.00
Mg	1.83	1.83	1.83	1.83	1.83	1.77	1.76	1.78	1.16	1.13	1.76	1.15	1.14	1.13	1.11	1.76	1.83	1.82	1.82
Ca	0.00	0.00	0.00	0.00	0.00	0.00	0.00	0.00	0.02	0.02	0.00	0.03	0.04	0.04	0.04	0.00	0.00	0.00	0.00
Na	0.00	0.00	0.00	0.00	0.00	0.00	0.00	0.00	0.00	0.00	0.00	0.00	0.00	0.00	0.00	0.00	0.00	0.00	0.00
K	0.00	0.00	0.00	0.00	0.00	0.00	0.00	0.00	0.00	0.00	0.00	0.00	0.00	0.00	0.00	0.00	0.00	0.00	0.00
Ni	0.01	0.01	0.01	0.01	0.01												0.01	0.01	0.01
Fo	91.26	91.31	91.41	91.51	91.22	90.73	90.80	90.54	91.35	91.50	90.52	90.87	91.45	91.10	91.36	90.61	91.12	90.82	91.11
Fa	8.64	8.61	8.45	8.43	8.67	9.27	9.20	9.46	8.65	8.50	9.48	9.13	8.55	8.90	8.64	9.39	8.76	9.06	8.71
Mg*	91.50	91.50	91.50	91.50	91.50	90.62	90.64	90.42	91.16	91.30	90.39	90.70	91.26	90.96	91.17	90.50	91.04	91.00	91.45

Numbers of ions on the basis of 4 (O), c and r indicate core and rim respectively

Continued

Table 2.1.2. (Continued)

Sample	98-4c	98-5c	98-6c	102-1c	102-2c	102-3c	102-4c	102-5c	118-1c	118-1r	118-2c	118-3c	118-4c	118-5c
SiO2	40.79	40.78	40.94	40.78	40.70	40.81	40.79	40.95	41.03	40.83	40.84	41.06	41.08	40.97
TiO2	0.00	0.01	0.00	0.00	0.00	0.00	0.01	0.00	0.01	0.00	0.00	0.00	0.00	0.00
Al2O3	0.00	0.00	0.00	0.00	0.00	0.00	0.01	0.01	0.00	0.00	0.01	0.01	0.02	0.01
FeO	8.83	8.60	8.82	8.58	8.71	8.79	8.56	8.64	9.03	8.91	8.84	8.67	8.73	8.65
Cr2O3	0.00	0.00	0.00	0.00	0.01	0.00	0.00	0.01	0.00	0.03	0.01	0.01	0.00	0.00
MnO	0.15	0.13	0.16	0.12	0.16	0.10	0.11	0.15	0.12	0.11	0.14	0.11	0.10	0.11
MgO	50.37	50.02	50.51	50.26	49.95	50.24	50.03	50.07	49.99	50.13	49.81	50.12	50.24	50.05
CaO	0.01	0.02	0.01	0.04	0.05	0.03	0.04	0.04	0.02	0.02	0.03	0.03	0.03	0.03
Na2O	0.00	0.00	0.00	0.00	0.00	0.00	0.00	0.00	0.00	0.00	0.00	0.00	0.00	0.00
K2O	0.00	0.00	0.00	0.00	0.00	0.00	0.00	0.00	0.00	0.00	0.00	0.00	0.00	0.00
NiO	0.41	0.41	0.39	0.43	0.39	0.39	0.37	0.42	0.36	0.37	0.34	0.43	0.39	0.38
Total	100.56	99.97	100.83	100.21	99.97	100.36	99.92	100.29	100.56	100.40	100.02	100.44	100.59	100.20
Si	0.99	1.00	0.99	0.99	0.99	0.99	1.00	1.00	1.00	0.99	1.00	1.00	1.00	1.00
Ti	0.00	0.00	0.00	0.00	0.00	0.00	0.00	0.00	0.00	0.00	0.00	0.00	0.00	0.00
Al	0.00	0.00	0.00	0.00	0.00	0.00	0.00	0.00	0.00	0.00	0.00	0.00	0.00	0.00
Fe	0.18	0.18	0.18	0.17	0.18	0.18	0.17	0.18	0.18	0.18	0.18	0.18	0.18	0.18
Cr	0.00	0.00	0.00	0.00	0.00	0.00	0.00	0.00	0.00	0.00	0.00	0.00	0.00	0.00
Mn	0.00	0.00	0.00	0.00	0.00	0.00	0.00	0.00	0.00	0.00	0.00	0.00	0.00	0.00
Mg	1.83	1.82	1.83	1.83	1.82	1.82	1.82	1.82	1.81	1.82	1.81	1.82	1.82	1.82
Ca	0.00	0.00	0.00	0.00	0.00	0.00	0.00	0.00	0.00	0.00	0.00	0.00	0.00	0.00
Na	0.00	0.00	0.00	0.00	0.00	0.00	0.00	0.00	0.00	0.00	0.00	0.00	0.00	0.00
K	0.00	0.00	0.00	0.00	0.00	0.00	0.00	0.00	0.00	0.00	0.00	0.00	0.00	0.00
Ni	0.01	0.01	0.01	0.01	0.01	0.01	0.01	0.01	0.01	0.01	0.01	0.01	0.01	0.01
Fo	90.92	91.11	90.94	91.19	91.00	91.00	91.19	91.08	90.70	90.85	90.86	91.09	91.05	91.10
Fa	8.94	8.79	8.91	8.74	8.91	8.93	8.75	8.82	9.20	9.06	9.05	8.84	8.88	8.83
Mg*	91.04	91.00	91.04	91.50	91.00	91.00	91.50	91.00	90.95	91.00	90.95	91.00	91.00	91.00

Table 2.1.3. Results of electron micro-probe analyses of ortho-pyroxenes from the harzburgites

Sample	68-1c	68-2c	68-3c	68-4c	68-5c	68-6c	68-7c	68-8c	68-9c	98-1c	98-1r	98-2c	98-2r	98-3c	98-3r	98-4c	98-4r	98-5c	98-5r	98-6c
SiO2	57.87	57.84	57.62	57.48	57.63	57.94	57.69	57.90	57.78	57.15	57.11	56.94	56.63	57.26	57.35	57.29	57.53	57.06	57.10	56.94
Al2O3	0.76	0.77	0.75	0.71	0.74	0.65	0.72	0.70	0.71	1.48	1.29	1.45	1.46	1.41	1.43	1.44	1.31	1.46	1.40	1.47
TiO2	0.00	0.02	0.00	0.00	0.00	0.00	0.03	0.00	0.02	0.00	0.00	0.03	0.00	0.00	0.00	0.00	0.01	0.03	0.00	0.00
Fe2O3	0.00	0.00	0.11	0.00	0.00	0.00	0.00	0.00	0.00	0.00	0.00	0.00	0.19	0.00	0.00	0.00	0.00	0.00	0.00	0.00
FeO	5.29	5.32	5.16	5.40	4.96	5.17	5.39	5.34	5.18	5.58	5.49	5.63	5.66	5.66	5.69	5.63	5.59	5.50	5.70	5.73
MnO	0.13	0.09	0.13	0.16	0.12	0.14	0.12	0.08	0.14	0.14	0.19	0.15	0.15	0.10	0.15	0.11	0.13	0.14	0.16	0.20
MgO	34.43	34.59	34.15	34.77	33.32	34.76	34.56	34.70	34.30	34.21	34.11	33.56	33.09	34.10	34.36	34.34	34.37	33.32	34.09	34.00
Cr2O3	0.45	0.42	0.43	0.36	0.43	0.32	0.39	0.39	0.49	0.53	0.46	0.58	0.55	0.61	0.57	0.58	0.67	0.66	0.65	0.58
CaO	0.89	0.76	1.65	0.54	2.81	0.58	0.79	0.56	1.15	0.52	0.71	1.08	1.61	0.63	0.50	0.44	0.26	1.96	0.75	0.70
Na2O	0.01	0.01	0.00	0.00	0.02	0.00	0.00	0.00	0.01	0.01	0.00	0.01	0.00	0.00	0.00	0.01	0.01	0.01	0.01	0.01
K2O	0.00	0.16	0.21	0.14	0.00	0.00	0.26	0.01	0.07	0.00	0.07	0.00	0.28	0.00	0.00	0.04	0.08	0.10	0.14	0.08
Total	99.84	99.96	100.21	99.55	100.03	99.57	99.95	99.67	99.85	99.61	99.44	99.43	99.62	99.78	100.06	99.88	99.95	100.25	99.99	99.70
Si	1.99	1.99	1.98	1.98	1.99	1.99	1.99	1.99	1.99	1.97	1.98	1.97	1.97	1.97	1.97	1.97	1.98	1.97	1.97	1.97
Al IV	0.03	0.03	0.03	0.03	0.03	0.03	0.03	0.03	0.03	0.06	0.05	0.06	0.06	0.06	0.06	0.06	0.05	0.06	0.06	0.06
Ti	0.00	0.00	0.00	0.00	0.00	0.00	0.00	0.00	0.00	0.00	0.00	0.00	0.00	0.00	0.00	0.00	0.00	0.00	0.00	0.00
Fe3+	0.00	0.00	0.00	0.00	0.00	0.00	0.00	0.00	0.00	0.00	0.00	0.00	0.01	0.00	0.00	0.00	0.00	0.00	0.00	0.00
Fe2+	0.15	0.15	0.15	0.16	0.14	0.15	0.16	0.15	0.15	0.16	0.16	0.16	0.16	0.16	0.16	0.16	0.16	0.16	0.16	0.17
Mn	0.00	0.00	0.00	0.00	0.00	0.00	0.00	0.00	0.00	0.00	0.01	0.00	0.00	0.00	0.00	0.00	0.00	0.00	0.00	0.01
Mg	1.77	1.77	1.75	1.79	1.71	1.78	1.77	1.78	1.76	1.76	1.76	1.73	1.71	1.75	1.76	1.76	1.76	1.71	1.75	1.75
Cr	0.01	0.01	0.01	0.01	0.01	0.01	0.01	0.01	0.01	0.01	0.01	0.02	0.02	0.02	0.02	0.02	0.02	0.02	0.02	0.02
Ca	0.03	0.03	0.06	0.02	0.10	0.02	0.03	0.02	0.04	0.02	0.03	0.04	0.06	0.02	0.02	0.02	0.01	0.07	0.03	0.03
Na	0.00	0.00	0.00	0.00	0.00	0.00	0.00	0.00	0.00	0.00	0.00	0.00	0.00	0.00	0.00	0.00	0.00	0.00	0.00	0.00
K	0.00	0.01	0.01	0.01	0.00	0.00	0.01	0.00	0.00	0.00	0.00	0.00	0.01	0.00	0.00	0.00	0.00	0.00	0.00	0.00
Ens:	90.33	90.62	89.16	90.85	87.23	91.10	90.44	90.98	90.00	90.53	90.22	89.30	88.22	90.25	90.42	90.66	91.00	87.92	89.91	89.89
Fors.	7.98	7.95	7.75	8.15	7.47	7.81	8.09	7.97	7.84	8.48	8.44	8.63	8.69	8.55	8.62	8.51	8.50	8.36	8.68	8.79
Wol.	1.69	1.43	3.09	1.00	5.30	1.09	1.48	1.05	2.17	0.99	1.35	2.07	3.09	1.20	0.95	0.83	0.50	3.72	1.42	1.32
Mg*	92.19	92.19	92.11	91.79	92.43	92.23	91.71	92.23	92.15	91.67	91.67	91.53	90.96	91.62	91.67	91.67	91.67	91.44	91.62	91.15
Fe*	8.12	8.07	8.00	8.23	7.88	7.90	8.21	8.05	8.01	8.57	8.55	8.81	8.97	8.65	8.70	8.58	8.55	8.68	8.80	8.91

Numbers of ions on the basis of 6 (O), c and r indicate "core" and "rim" respectively

Continued

Table 2.1.3. (Continued)

Sample	98-6r	98-7c	98-7r	98-8c	98-8r	102-1c	102-1r	102-2c	102-3c	102-4c	102-5c	102-6c	102-7c	102-8c	118-1c	118-1r	118-2c	118-2r	118-3c	118-3r
SiO2	57.28	57.11	57.15	57.06	57.10	57.43	57.36	57.34	56.96	57.11	57.73	57.42	56.95	57.47	56.75	57.20	56.56	56.63	56.69	56.80
Al2O3	1.45	1.49	1.40	1.42	1.39	1.23	1.24	1.28	1.27	1.30	1.19	1.31	1.30	1.23	1.77	1.64	1.86	1.81	1.74	1.77
TiO2	0.03	0.04	0.01	0.00	0.00	0.00	0.00	0.00	0.00	0.00	0.04	0.04	0.00	0.01	0.00	0.03	0.00	0.02	0.00	0.05
Fe2O3	0.00	0.00	0.00	0.05	0.00	0.00	0.00	0.00	0.00	0.00	0.00	0.00	0.00	0.00	0.14	0.00	0.00	0.00	0.00	0.00
FeO	5.59	5.50	5.51	5.08	5.59	5.43	5.48	5.36	5.40	5.36	5.41	5.64	5.39	5.46	5.52	5.65	5.68	5.50	5.45	5.53
MnO	0.15	0.17	0.16	0.18	0.14	0.16	0.14	0.15	0.15	0.11	0.15	0.16	0.17	0.17	0.15	0.17	0.11	0.13	0.14	0.09
MgO	34.30	33.76	33.53	32.97	34.06	33.62	34.07	33.62	34.08	34.34	34.33	34.08	33.46	34.04	33.91	33.95	33.59	33.68	33.28	33.74
Cr2O3	0.65	0.60	0.56	0.65	0.61	0.54	0.52	0.52	0.62	0.54	0.47	0.51	0.56	0.51	0.56	0.53	0.63	0.60	0.59	0.62
CaO	0.51	1.22	1.49	2.69	0.76	1.58	0.90	1.61	0.74	0.61	0.66	0.82	1.80	0.91	0.75	0.62	0.81	0.87	1.73	0.83
Na2O	0.00	0.01	0.00	0.00	0.00	0.02	0.00	0.01	0.00	0.02	0.02	0.00	0.01	0.01	0.01	0.00	0.00	0.00	0.01	0.00
K2O	0.00	0.08	0.00	0.25	0.07	0.13	0.01	0.16	0.00	0.00	0.00	0.00	0.00	0.02	0.24	0.00	0.10	0.23	0.19	0.00
Total	99.96	99.96	99.81	100.34	99.73	100.14	99.73	100.06	99.22	99.39	99.98	99.98	99.64	99.82	99.80	99.79	99.32	99.47	99.82	99.43
Si	1.97	1.97	1.97	1.97	1.97	1.98	1.98	1.98	1.97	1.97	1.98	1.98	1.97	1.98	1.96	1.97	1.96	1.96	1.96	1.97
Al IV	0.06	0.06	0.06	0.06	0.06	0.05	0.06	0.05	0.05	0.05	0.05	0.05	0.05	0.05	0.07	0.07	0.08	0.07	0.07	0.07
Ti	0.00	0.00	0.00	0.00	0.00	0.00	0.00	0.00	0.00	0.00	0.00	0.00	0.00	0.00	0.00	0.00	0.00	0.00	0.00	0.00
Fe3+	0.00	0.00	0.00	0.00	0.00	0.00	0.00	0.00	0.00	0.00	0.00	0.00	0.00	0.00	0.00	0.00	0.00	0.00	0.00	0.00
Fe2+	0.16	0.16	0.16	0.15	0.16	0.16	0.16	0.15	0.16	0.15	0.16	0.16	0.16	0.16	0.16	0.16	0.16	0.16	0.16	0.16
Mn	0.00	0.00	0.00	0.01	0.00	0.00	0.00	0.00	0.00	0.00	0.00	0.00	0.00	0.01	0.00	0.00	0.00	0.00	0.00	0.00
Mg	1.76	1.74	1.73	1.69	1.75	1.73	1.75	1.73	1.76	1.77	1.76	1.75	1.73	1.75	1.75	1.74	1.74	1.74	1.72	1.74
Cr	0.02	0.02	0.02	0.02	0.02	0.01	0.01	0.01	0.02	0.01	0.01	0.01	0.02	0.01	0.02	0.01	0.02	0.02	0.02	0.02
Ca	0.02	0.05	0.06	0.10	0.03	0.06	0.03	0.06	0.03	0.02	0.02	0.03	0.07	0.03	0.03	0.02	0.03	0.03	0.06	0.03
Na	0.00	0.00	0.00	0.00	0.00	0.00	0.00	0.00	0.00	0.00	0.00	0.00	0.00	0.00	0.00	0.00	0.00	0.00	0.00	0.00
K	0.00	0.00	0.00	0.01	0.00	0.01	0.00	0.01	0.00	0.00	0.00	0.00	0.00	0.00	0.01	0.00	0.00	0.01	0.01	0.00
Ens:	90.52	89.28	88.74	87.10	90.05	88.74	89.96	88.77	90.35	90.74	90.53	89.86	88.35	89.93	90.12	90.16	89.76	89.90	88.37	89.99
Fors.	8.50	8.40	8.42	7.79	8.50	8.27	8.33	8.17	8.24	8.11	8.22	8.58	8.23	8.35	8.45	8.66	8.67	8.44	8.33	8.41
Wol.	0.97	2.31	2.84	5.11	1.45	2.99	1.71	3.06	1.40	1.15	1.25	1.56	3.42	1.72	1.43	1.18	1.56	1.66	3.30	1.60
Mg*	91.67	91.58	91.53	91.85	91.62	91.53	91.62	92.02	91.67	92.19	91.67	91.62	91.53	91.62	91.62	91.58	91.58	91.58	91.49	91.58
Fe*	8.59	8.60	8.67	8.21	8.63	8.53	8.47	8.43	8.36	8.21	8.32	8.72	8.52	8.50	8.57	8.77	8.81	8.58	8.33	8.55

Continued

Table 2.1.3. (Continued)

Sample	118-4c	118-4r	118-5c	118-6c	118-7c	118-8c	118-9c	118-10c	118-11c	118-12c	118-13c
SiO2	56.54	56.86	56.81	56.85	56.84	56.89	53.56	56.73	56.66	56.88	56.69
Al2O3	1.77	1.65	1.83	1.89	1.84	1.85	1.84	1.77	1.74	1.77	1.72
TiO2	0.00	0.02	0.00	0.00	0.06	0.00	0.00	0.04	0.03	0.00	0.00
Fe2O3	0.00	0.00	0.00	0.00	0.00	0.00	0.27	0.00	0.00	0.00	0.00
FeO	5.35	5.75	5.76	5.77	5.77	5.71	1.63	5.73	5.60	5.54	5.50
MnO	0.14	0.10	0.15	0.17	0.17	0.09	0.07	0.15	0.16	0.15	0.11
MgO	33.08	33.89	33.93	33.78	33.78	33.73	17.38	33.91	33.90	33.88	33.48
Cr2O3	0.57	0.43	0.60	0.63	0.59	0.66	0.79	0.59	0.62	0.62	0.67
CaO	2.18	0.72	0.74	0.78	0.81	0.77	24.28	0.84	0.85	0.95	1.29
Na2O	0.01	0.00	0.00	0.01	0.01	0.00	0.03	0.00	0.00	0.00	0.00
K2O	0.00	0.00	0.16	0.00	0.09	0.14	0.06	0.02	0.00	0.09	0.06
Total	99.65	99.42	99.99	99.89	99.95	99.84	99.86	99.79	99.57	99.89	99.54
Si	1.96	1.97	1.96	1.96	1.96	1.96	1.95	1.96	1.96	1.96	1.96
Al IV	0.07	0.07	0.07	0.08	0.07	0.08	0.08	0.07	0.07	0.07	0.07
Ti	0.00	0.00	0.00	0.00	0.00	0.00	0.00	0.00	0.00	0.00	0.00
Fe3+	0.00	0.00	0.00	0.00	0.00	0.00	0.01	0.00	0.00	0.00	0.00
Fe2+	0.16	0.17	0.17	0.17	0.17	0.16	0.05	0.17	0.16	0.16	0.16
Mn	0.00	0.00	0.00	0.00	0.00	0.00	0.00	0.00	0.00	0.00	0.00
Mg	1.71	1.75	1.74	1.74	1.74	1.73	0.94	1.75	1.75	1.74	1.73
Cr	0.02	0.01	0.02	0.02	0.02	0.02	0.02	0.02	0.02	0.02	0.02
Ca	0.08	0.03	0.03	0.03	0.03	0.03	0.94	0.03	0.03	0.04	0.05
Na	0.00	0.00	0.00	0.00	0.00	0.00	0.00	0.00	0.00	0.00	0.00
K	0.00	0.00	0.01	0.00	0.00	0.01	0.00	0.00	0.00	0.00	0.00
Ens:	87.68	89.92	89.81	89.66	89.61	89.85	48.60	89.66	89.81	89.73	89.14
Fors.	8.17	8.72	8.78	8.84	8.85	8.67	2.66	8.74	8.57	8.46	8.39
Wol.	4.15	1.37	1.41	1.49	1.54	1.48	48.74	1.60	1.62	1.81	2.47
Mg*	91.44	91.15	91.10	91.10	91.10	91.53	94.00	91.15	91.62	91.58	91.53
Fe*	8.53	8.84	8.90	8.98	8.98	8.80	5.18	8.88	8.71	8.61	8.60

APPENDIX 2.2

Microprobe results of the minerals from the cumulates

Table 2.2.1. Results of electron micro-probe analyses of the plagioclases from the mafic cumulates

Sample	21-1c	21-1c	21-3c	21-4c	21-5c	21-6c	21-7c	21-8c	21-9c	21-10c	21-11c	24-1c	24-2c	24-3c	24-4c	24-5c	24-6c	24-7c	25-1c	25-2c
SiO2	44.17	44.01	44.08	44.26	43.68	44.09	43.79	44.06	44.00	43.93	44.07	44.71	44.48	44.55	44.38	44.35	44.53	44.54	43.63	44.16
Al2O3	35.35	35.29	35.35	35.35	35.44	35.48	35.65	35.64	35.36	35.53	35.36	34.93	34.90	34.89	35.60	35.21	35.06	35.03	35.64	34.89
TiO2	0.00	0.02	0.00	0.00	0.00	0.00	0.00	0.01	0.00	0.00	0.00	0.04	0.00	0.01	0.00	0.00	0.00	0.07	0.00	0.01
FeO	0.15	0.20	0.22	0.14	0.17	0.19	0.22	0.22	0.13	0.16	0.19	0.23	0.30	0.16	0.25	0.27	0.20	0.24	0.23	0.08
MnO	0.00	0.00	0.00	0.04	0.00	0.00	0.00	0.00	0.00	0.00	0.03	0.00	0.00	0.00	0.00	0.00	0.00	0.00	0.01	0.06
MgO	0.01	0.01	0.00	0.00	0.01	0.02	0.02	0.00	0.02	0.00	0.03	0.02	0.00	0.02	0.00	0.03	0.00	0.00	0.01	0.01
CaO	19.82	19.78	19.61	19.32	20.00	19.87	19.64	19.52	19.63	20.00	19.61	18.90	18.49	18.77	19.03	18.85	18.87	18.72	19.80	19.61
Na2O	0.53	0.46	0.55	0.61	0.47	0.52	0.49	0.54	0.52	0.46	0.53	0.99	1.01	0.87	0.71	0.86	0.89	0.90	0.43	0.64
K2O	0.00	0.03	0.03	0.01	0.01	0.00	0.00	0.02	0.00	0.00	0.00	0.01	0.00	0.00	0.01	0.01	0.00	0.00	0.03	0.01
Total	100.02	99.80	99.85	99.74	99.78	100.18	99.81	100.02	99.66	100.08	99.82	99.84	99.19	99.27	99.98	99.56	99.55	99.50	99.78	99.47
Si	2.04	2.04	2.04	2.05	2.02	2.03	2.03	2.04	2.04	2.03	2.04	2.07	2.07	2.07	2.05	2.06	2.07	2.07	2.02	2.05
Al	1.92	1.93	1.93	1.93	1.93	1.93	1.94	1.94	1.93	1.93	1.93	1.91	1.92	1.91	1.94	1.93	1.92	1.92	1.95	1.91
Ti	0.00	0.00	0.00	0.00	0.00	0.00	0.00	0.00	0.00	0.00	0.00	0.00	0.00	0.00	0.00	0.00	0.00	0.00	0.00	0.00
Fe2+	0.01	0.01	0.01	0.01	0.01	0.01	0.01	0.01	0.01	0.01	0.01	0.01	0.01	0.01	0.01	0.01	0.01	0.01	0.01	0.00
Mn	0.00	0.00	0.00	0.00	0.00	0.00	0.00	0.00	0.00	0.00	0.00	0.00	0.00	0.00	0.00	0.00	0.00	0.00	0.00	0.00
Mg	0.00	0.00	0.00	0.00	0.00	0.00	0.00	0.00	0.00	0.00	0.00	0.00	0.00	0.00	0.00	0.00	0.00	0.00	0.00	0.00
Ca	0.98	0.98	0.97	0.96	0.99	0.98	0.97	0.97	0.97	0.99	0.97	0.94	0.92	0.94	0.94	0.94	0.94	0.93	0.98	0.98
Na	0.05	0.04	0.05	0.05	0.04	0.05	0.04	0.05	0.05	0.04	0.05	0.09	0.09	0.08	0.06	0.08	0.08	0.08	0.04	0.06
K	0.00	0.00	0.00	0.00	0.00	0.00	0.00	0.00	0.00	0.00	0.00	0.00	0.00	0.00	0.00	0.00	0.00	0.00	0.00	0.00
Or	0.00	0.00	0.00	0.00	0.00	0.00	0.00	0.00	0.00	0.00	0.00	0.05	0.01	0.00	0.06	0.03	0.01	0.00	0.00	0.00
Ab	4.57	4.03	4.86	5.40	4.08	4.52	4.32	4.76	4.57	4.00	4.66	8.68	8.99	7.70	6.29	7.62	7.85	7.96	3.77	5.57
An	95.41	95.80	94.97	94.53	95.89	95.48	95.68	95.12	95.43	96.00	95.34	91.27	91.00	92.30	93.66	92.36	92.13	92.04	96.05	94.37

Numbers of ions on the basis of 8 (O), c and r indicate "core" and "rim" respectively

Continued

Table 2.2.1. (Continued)

Sample	25-3c	25-4c	28-1c	28-2c	28-3c	28-4c	28-5c	28-6c	28-7c	28-8c	31-1c	31-2c	31-3c	31-4c	31-5c	31-6c	31-7c	35-1c	35-2c	35-3c
SiO2	44.42	44.61	44.91	45.02	44.64	45.25	44.94	45.07	44.75	45.31	43.90	43.97	44.26	44.39	43.86	44.47	44.30	43.94	44.18	43.74
Al2O3	35.16	35.19	34.54	34.45	34.54	34.45	34.76	34.49	34.82	34.29	35.10	35.30	35.04	34.98	35.25	35.13	34.96	35.05	35.43	35.54
TiO2	0.02	0.02	0.06	0.02	0.02	0.02	0.04	0.00	0.03	0.08	0.10	0.00	0.00	0.00	0.02	0.00	0.00	0.00	0.00	0.02
FeO	0.16	0.18	0.24	1.09	0.30	0.32	0.38	0.40	0.27	0.35	0.26	0.20	0.31	0.25	0.18	0.21	0.31	0.21	0.30	0.24
MnO	0.00	0.02	0.00	0.02	0.00	0.03	0.00	0.06	0.00	0.00	0.00	0.00	0.00	0.00	0.00	0.00	0.00	0.00	0.01	0.02
MgO	0.00	0.00	0.02	0.05	0.01	0.00	0.01	0.00	0.02	0.02	0.00	0.01	0.01	0.02	0.00	0.00	0.00	0.00	0.00	0.01
CaO	19.23	19.27	18.88	18.64	18.85	18.57	18.87	18.82	19.02	18.69	19.03	19.00	18.52	18.80	19.16	18.74	18.77	19.72	19.37	19.41
Na2O	0.74	0.70	0.97	1.08	0.97	1.13	1.00	0.98	0.84	1.15	0.75	0.79	0.95	0.83	0.78	0.89	0.86	0.52	0.57	0.57
K2O	0.02	0.01	0.00	0.02	0.00	0.02	0.00	0.04	0.00	0.01	0.01	0.01	0.01	0.00	0.01	0.00	0.01	0.02	0.00	0.00
Total	99.75	100.00	99.62	100.39	99.33	99.79	100.00	99.86	99.75	99.90	99.15	99.29	99.09	99.26	99.28	99.45	99.21	99.46	99.86	99.55
Si	2.06	2.06	2.08	2.07	2.07	2.09	2.07	2.08	2.07	2.09	2.05	2.05	2.06	2.07	2.05	2.07	2.07	2.04	2.04	2.03
Al	1.92	1.92	1.88	1.87	1.89	1.87	1.89	1.88	1.90	1.86	1.93	1.94	1.93	1.92	1.94	1.92	1.92	1.92	1.93	1.94
Ti	0.00	0.00	0.00	0.00	0.00	0.00	0.00	0.00	0.00	0.00	0.00	0.00	0.00	0.00	0.00	0.00	0.00	0.00	0.00	0.00
Fe2+	0.01	0.01	0.01	0.04	0.01	0.01	0.01	0.02	0.01	0.01	0.01	0.01	0.01	0.01	0.01	0.01	0.01	0.01	0.01	0.01
Mn	0.00	0.00	0.00	0.00	0.00	0.00	0.00	0.00	0.00	0.00	0.00	0.00	0.00	0.00	0.00	0.00	0.00	0.00	0.00	0.00
Mg	0.00	0.00	0.00	0.00	0.00	0.00	0.00	0.00	0.00	0.00	0.00	0.00	0.00	0.00	0.00	0.00	0.00	0.00	0.00	0.00
Ca	0.95	0.95	0.94	0.92	0.94	0.92	0.93	0.93	0.94	0.92	0.95	0.95	0.93	0.94	0.96	0.93	0.94	0.98	0.96	0.96
Na	0.07	0.06	0.09	0.10	0.09	0.10	0.09	0.09	0.08	0.10	0.07	0.07	0.09	0.07	0.07	0.08	0.08	0.05	0.05	0.05
K	0.00	0.00	0.00	0.00	0.00	0.00	0.00	0.00	0.00	0.00	0.00	0.00	0.00	0.00	0.00	0.00	0.00	0.00	0.00	0.00
Or	0.00	0.00	0.00	0.00	0.00	0.00	0.00	0.00	0.00	0.00	0.08	0.08	0.04	0.00	0.08	0.02	0.04	0.00	0.00	0.00
Ab	6.50	6.16	8.51	9.48	8.52	9.91	8.75	8.59	7.40	10.01	6.65	7.03	8.51	7.39	6.83	7.92	7.65	4.55	5.06	5.05
An	93.38	93.78	91.49	90.41	91.48	89.98	91.25	91.18	92.58	89.93	93.27	92.89	91.44	92.61	93.09	92.06	92.31	95.34	94.94	94.95

continued

Table 2.2.1. (Continued)

Sample	35-4c	35-5c	35-6c	36-1c	36-2c	36-3c	36-4c	36-5c	36-6c	36-7c	325-1c	325-1r	325-2c	325-3c	325-4c	325-5c	325-6c	325-7c	325-8c	325-9c	325-10c	325-11c
SiO2	44.03	44.01	44.03	44.38	44.28	44.35	44.44	44.30	44.02	44.58	45.07	44.95	44.89	45.02	44.95	44.78	44.83	44.91	44.63	44.97	44.89	43.98
Al2O3	35.32	35.33	35.28	34.98	35.57	35.02	35.12	35.15	35.17	35.42	34.35	34.43	34.36	34.60	34.46	34.56	34.41	34.59	34.50	34.67	34.38	35.45
TiO2	0.02	0.00	0.00	0.00	0.00	0.03	0.00	0.01	0.00	0.04	0.00	0.00	0.00	0.00	0.00	0.00	0.02	0.01	0.01	0.00	0.00	0.02
FeO	0.39	0.26	0.20	0.22	0.27	0.21	0.29	0.23	0.30	0.28	0.44	0.63	0.59	0.55	0.54	0.56	0.44	0.50	0.56	0.50	0.61	0.31
MnO	0.05	0.00	0.00	0.01	0.00	0.02	0.01	0.00	0.03	0.00	0.08	0.04	0.00	0.00	0.05	0.04	0.05	0.04	0.02	0.00	0.02	0.03
MgO	0.00	0.00	0.00	0.00	0.01	0.00	0.00	0.00	0.01	0.00	0.02	0.03	0.03	0.03	0.06	0.02	0.04	0.03	0.01	0.02	0.04	0.00
CaO	19.40	19.60	19.54	19.71	19.72	19.73	19.33	19.66	19.67	19.51	19.05	18.95	19.01	19.00	18.94	18.90	18.85	19.00	19.08	18.94	18.85	19.98
Na2O	0.65	0.56	0.60	0.59	0.53	0.63	0.64	0.61	0.63	0.61	0.94	0.93	0.87	0.87	0.96	0.92	0.87	0.85	0.87	0.86	0.91	0.50
K2O	0.00	0.00	0.01	0.00	0.01	0.01	0.02	0.00	0.00	0.02	0.01	0.00	0.01	0.01	0.00	0.00	0.00	0.00	0.00	0.00	0.01	0.02
Total	99.86	99.76	99.66	99.89	100.39	100.00	99.85	99.96	99.83	100.46	99.96	99.96	99.76	100.08	99.96	99.78	99.51	99.93	99.68	99.96	99.71	100.29
Si	2.04	2.04	2.04	2.05	2.04	2.05	2.06	2.05	2.04	2.05	2.08	2.08	2.08	2.08	2.08	2.07	2.08	2.08	2.07	2.08	2.08	2.03
Al	1.93	1.93	1.93	1.91	1.93	1.91	1.92	1.91	1.92	1.92	1.87	1.87	1.87	1.88	1.87	1.88	1.88	1.88	1.88	1.89	1.88	1.93
Ti	0.00	0.00	0.00	0.00	0.00	0.00	0.00	0.00	0.00	0.00	0.00	0.00	0.00	0.00	0.00	0.00	0.00	0.00	0.00	0.00	0.00	0.00
Fe2+	0.02	0.01	0.01	0.01	0.01	0.01	0.01	0.01	0.01	0.01	0.02	0.02	0.02	0.02	0.02	0.02	0.02	0.02	0.02	0.02	0.02	0.01
Mn	0.00	0.00	0.00	0.00	0.00	0.00	0.00	0.00	0.00	0.00	0.00	0.00	0.00	0.00	0.00	0.00	0.00	0.00	0.00	0.00	0.00	0.00
Mg	0.00	0.00	0.00	0.00	0.00	0.00	0.00	0.00	0.00	0.00	0.00	0.00	0.00	0.00	0.00	0.00	0.00	0.00	0.00	0.00	0.00	0.00
Ca	0.96	0.97	0.97	0.98	0.97	0.98	0.96	0.97	0.98	0.96	0.94	0.94	0.94	0.94	0.94	0.94	0.94	0.94	0.95	0.94	0.94	0.99
Na	0.06	0.05	0.05	0.05	0.05	0.06	0.06	0.05	0.06	0.05	0.08	0.08	0.08	0.08	0.09	0.08	0.08	0.08	0.08	0.08	0.08	0.04
K	0.00	0.00	0.00	0.00	0.00	0.00	0.00	0.00	0.00	0.00	0.00	0.00	0.00	0.00	0.00	0.00	0.00	0.00	0.00	0.00	0.00	0.00
Or	0.00	0.00	0.00	0.00	0.00	0.00	0.00	0.00	0.00	0.00	0.00	0.00	0.00	0.00	0.00	0.00	0.00	0.00	0.00	0.00	0.00	0.00
Ab	5.72	4.92	5.26	5.14	4.64	5.46	5.65	5.32	5.48	5.35	8.19	8.16	7.64	7.65	8.40	8.10	7.71	7.49	7.62	7.59	8.03	4.33
An	94.28	95.08	94.68	94.86	95.31	94.48	94.24	94.68	94.52	94.54	91.75	91.84	92.30	92.29	91.60	91.90	92.29	92.51	92.38	92.41	91.91	95.56

Table 2.2.2. Results of electron micro-probe analyses of the ortho-pyroxene from the mafic cumulates

	Leuco-gabbro						
Sample	28-1c	28-3c	35-1c	35-4c	35-4r	35-7c	35-8c
SiO2	53.01	53.05	54.43	54.55	54.55	54.53	54.48
Al2O3	1.40	1.62	1.86	1.93	1.68	1.63	1.59
TiO2	0.07	0.13	0.07	0.04	0.00	0.05	0.08
FeO	20.02	19.31	14.93	14.54	14.61	15.20	14.72
MnO	0.33	0.43	0.45	0.36	0.36	0.32	0.38
MgO	23.72	23.65	27.74	27.37	27.26	27.83	27.29
Cr2O3	0.04	0.00	0.00	0.07	0.00	0.00	0.00
CaO	1.01	1.28	0.80	0.84	1.11	0.74	0.82
Na2O	0.00	0.02	0.03	0.00	0.00	0.02	0.00
K2O	0.00	0.01	0.00	0.02	0.00	0.01	0.00
Total	99.60	99.50	100.31	99.72	99.57	100.33	99.36
Si	1.91	1.90	1.95	1.93	1.92	1.95	1.90
Al IV	0.06	0.07	0.05	0.07	0.07	0.05	0.07
Al VI	0.00	0.00	0.03	0.01	0.00	0.02	0.00
Ti	0.00	0.00	0.00	0.00	0.00	0.00	0.00
Fe3+	0.20	0.24	0.03	0.12	0.19	0.03	0.28
Fe2+	0.40	0.34	0.42	0.31	0.23	0.43	0.15
Mn	0.01	0.01	0.01	0.01	0.01	0.01	0.01
Mg	1.28	1.26	1.48	1.44	1.43	1.48	1.42
Cr	0.00	0.00	0.00	0.00	0.00	0.00	0.00
Ca	0.04	0.05	0.03	0.03	0.04	0.03	0.03
Na	0.00	0.00	0.00	0.00	0.00	0.00	0.00
K	0.00	0.00	0.00	0.00	0.00	0.00	0.00
Ens:	66.14	66.35	75.09	75.33	74.77	75.08	75.07
Fors.	31.83	31.07	23.36	23.01	23.04	23.49	23.31
Wol.	2.02	2.58	1.56	1.66	2.19	1.43	1.62
Mg*	67.87	68.59	76.81	77.04	76.89	76.55	76.77

Numbers of ions on the basis of 6 (O), c and r indicate "core" and "rim" respectively

Table 2.2.3. Results of electron micro-probe analyses of the olivines from the ultramafic and mafic cumulates

	Wherlite																			
Sample	**11-1c**	**11-2c**	**11-3c**	**11-4c**	**11-5c**	**11-6c**	**11-7c**	**13-1c**	**13-2c**	**13-3c**	**13-4c**	**13-5c**	**13-6c**	**13-7c**	**13-8c**	**13-9c**	**13-10c**	**14-1c**	**14-2c**	**14-3c**
SiO2	41.01	40.88	40.61	57.24	41.05	41.04	40.80	40.73	40.88	41.07	40.83	57.37	40.98	40.55	41.06	40.87	41.04	40.93	41.02	40.85
TiO2	0.00	0.00	0.02	0.06	0.01	0.00	0.00	0.01	0.01	0.00	0.02	0.02	0.00	0.03	0.00	0.00	0.00	0.00	0.00	0.04
Al2O3	0.02	0.00	0.00	1.10	0.02	0.00	0.01	0.01	0.00	0.02	0.03	0.76	0.00	0.00	0.01	0.02	0.00	0.02	0.00	0.00
FeO	10.81	11.15	11.07	7.43	10.56	11.23	11.21	11.16	11.32	11.21	11.22	7.46	10.85	10.93	11.08	11.25	11.15	9.95	10.21	10.28
Cr2O3	0.03	0.04	0.00	0.43	0.00	0.00	0.02	0.04	0.05	0.03	0.00	0.26	0.00	0.05	0.00	0.00	0.04	0.05	0.00	0.00
MnO	0.15	0.13	0.14	0.17	0.11	0.13	0.18	0.26	0.18	0.15	0.23	0.19	0.25	0.19	0.15	0.14	0.20	0.22	0.29	0.14
MgO	47.73	47.08	47.10	32.85	47.96	47.67	47.54	47.32	47.16	47.41	47.27	32.81	47.36	46.86	47.30	46.88	47.18	47.92	47.89	48.02
CaO	0.01	0.01	0.02	0.64	0.01	0.00	0.04	0.01	0.03	0.01	0.02	0.37	0.00	0.03	0.01	0.04	0.03	0.01	0.01	0.00
Na2O	0.00	0.01	0.01	0.00	0.00	0.00	0.01	0.01	0.00	0.01	0.00	0.01	0.01	0.00	0.00	0.03	0.01	0.00	0.00	0.00
K2O	0.02	0.01	0.03	0.00	0.02	0.01	0.00	0.00	0.00	0.01	0.00	0.03	0.01	0.00	0.02	0.00	0.00	0.02	0.00	0.00
Total	99.78	99.31	99.00	99.92	99.74	100.08	99.81	99.55	99.63	99.92	99.62	99.28	99.46	98.64	99.63	99.23	99.65	99.12	99.42	99.33
Si	1.01	1.00	0.99	1.32	1.00	1.01	1.00	1.00	1.00	1.01	1.00	1.31	1.00	0.98	1.01	1.00	1.01	0.99	1.00	0.99
Ti	0.00	0.00	0.00	0.00	0.00	0.00	0.00	0.00	0.00	0.00	0.00	0.00	0.00	0.00	0.00	0.00	0.00	0.00	0.00	0.00
Al	0.00	0.00	0.00	0.03	0.00	0.00	0.00	0.00	0.00	0.00	0.00	0.02	0.00	0.00	0.00	0.00	0.00	0.00	0.00	0.00
Fe	0.22	0.23	0.23	0.14	0.22	0.23	0.23	0.23	0.23	0.23	0.23	0.14	0.22	0.22	0.23	0.23	0.23	0.20	0.21	0.21
Cr	0.00	0.00	0.00	0.01	0.00	0.00	0.00	0.00	0.00	0.00	0.00	0.00	0.00	0.00	0.00	0.00	0.00	0.00	0.00	0.00
Mn	0.00	0.00	0.00	0.00	0.00	0.00	0.00	0.01	0.00	0.00	0.00	0.00	0.01	0.00	0.00	0.00	0.00	0.00	0.01	0.00
Mg	1.74	1.71	1.71	1.13	1.75	1.75	1.74	1.73	1.73	1.74	1.73	1.12	1.73	1.69	1.73	1.71	1.72	1.73	1.74	1.74
Ca	0.00	0.00	0.00	0.02	0.00	0.00	0.00	0.00	0.00	0.00	0.00	0.01	0.00	0.00	0.00	0.00	0.00	0.00	0.00	0.00
Na	0.00	0.00	0.00	0.00	0.00	0.00	0.00	0.00	0.00	0.00	0.00	0.00	0.00	0.00	0.00	0.00	0.00	0.00	0.00	0.00
K	0.00	0.00	0.00	0.00	0.00	0.00	0.00	0.00	0.00	0.00	0.00	0.00	0.00	0.00	0.00	0.00	0.00	0.00	0.00	0.00
Fo	88.73	88.27	88.35	88.74	89.01	88.33	88.32	88.32	88.13	88.29	88.25	88.69	88.61	88.43	88.39	88.14	88.30	89.57	89.32	89.28
Fa	11.27	11.73	11.65	11.26	10.99	11.67	11.68	11.68	11.87	11.71	11.75	11.31	11.39	11.57	11.61	11.86	11.70	10.43	10.68	10.72
Mg*	88.59	88.15	88.22	88.51	88.90	88.21	88.15	88.07	87.97	88.15	88.04	88.43	88.38	88.25	88.25	88.01	88.11	89.36	89.05	89.15

Numbers of ions on the basis of 4 (O), c and r indicates "core" and "rim" respectively

continued

Table 2.2.3. (Continued)

	Wehrlite		Dunite						Wehrlite					Gabbro with olivine					
Sample	14-4c	14-5c	15-1c	15-2c	15-3c	15-4c	15-5c	15-6c	17-1c	17-2c	17-3c	17-4c	17-5c	21-1c	21-2c	21-3c	21-4c	21-5c	21-6c
SiO2	41.29	41.18	41.06	40.97	40.93	41.10	40.93	40.86	40.47	40.19	40.55	40.24	40.52	39.62	39.14	39.55	39.17	39.92	39.57
TiO2	0.00	0.03	0.03	0.00	0.00	0.00	0.00	0.00	0.00	0.01	0.01	0.03	0.03	0.00	0.03	0.00	0.00	0.02	0.01
Al2O3	0.00	0.01	0.00	0.00	0.00	0.00	0.01	0.01	0.00	0.01	0.01	0.00	0.01	0.00	0.00	0.01	0.01	0.02	0.03
FeO	10.09	10.14	10.17	10.57	10.30	10.61	10.50	10.24	13.07	13.49	13.22	13.38	13.12	18.56	18.14	18.95	18.50	17.88	17.93
Cr2O3	0.05	0.00	0.00	0.06	0.01	0.06	0.00	0.06	0.01	0.01	0.02	0.00	0.00	0.00	0.00	0.02	0.06	0.00	0.00
MnO	0.13	0.20	0.19	0.18	0.23	0.26	0.20	0.19	0.19	0.13	0.29	0.23	0.21	0.27	0.20	0.32	0.28	0.30	0.21
MgO	47.83	48.23	47.94	48.05	47.69	47.66	47.75	48.05	45.54	45.74	45.81	45.43	45.62	41.95	41.21	41.38	41.13	41.65	41.86
CaO	0.03	0.00	0.01	0.01	0.05	0.06	0.01	0.02	0.04	0.00	0.00	0.06	0.04	0.00	0.00	0.04	0.03	0.01	0.04
Na2O	0.00	0.00	0.00	0.00	0.01	0.00	0.02	0.01	0.02	0.03	0.03	0.01	0.00	0.02	0.03	0.00	0.00	0.02	0.00
K2O	0.00	0.01	0.02	0.01	0.02	0.00	0.01	0.00	0.00	0.01	0.00	0.01	0.00	0.01	0.02	0.02	0.01	0.03	0.04
Total	99.42	99.80	99.42	99.85	99.24	99.75	99.43	99.44	99.34	99.62	99.94	99.39	99.55	100.43	98.77	100.29	99.19	99.85	99.69
Si	1.00	1.01	1.00	1.00	1.00	1.01	1.00	1.00	1.00	1.00	1.01	1.00	1.00	1.01	0.98	1.01	0.99	1.01	1.00
Ti	0.00	0.00	0.00	0.00	0.00	0.00	0.00	0.00	0.00	0.00	0.00	0.00	0.00	0.00	0.00	0.00	0.00	0.00	0.00
Al	0.00	0.00	0.00	0.00	0.00	0.00	0.00	0.00	0.00	0.00	0.00	0.00	0.00	0.00	0.00	0.00	0.00	0.00	0.00
Fe	0.21	0.21	0.21	0.22	0.21	0.22	0.21	0.21	0.27	0.28	0.27	0.28	0.27	0.39	0.38	0.40	0.39	0.38	0.38
Cr	0.00	0.00	0.00	0.00	0.00	0.00	0.00	0.00	0.00	0.00	0.00	0.00	0.00	0.00	0.00	0.00	0.00	0.00	0.00
Mn	0.00	0.00	0.00	0.00	0.00	0.01	0.00	0.00	0.00	0.00	0.01	0.00	0.00	0.01	0.00	0.01	0.01	0.01	0.00
Mg	1.73	1.76	1.74	1.76	1.73	1.74	1.74	1.75	1.67	1.69	1.70	1.67	1.68	1.59	1.54	1.57	1.55	1.57	1.58
Ca	0.00	0.00	0.00	0.00	0.00	0.00	0.00	0.00	0.00	0.00	0.00	0.00	0.00	0.00	0.00	0.00	0.00	0.00	0.00
Na	0.00	0.00	0.00	0.00	0.00	0.00	0.00	0.00	0.00	0.00	0.00	0.00	0.00	0.00	0.00	0.00	0.00	0.00	0.00
K	0.00	0.00	0.00	0.00	0.00	0.00	0.00	0.00	0.00	0.00	0.00	0.00	0.00	0.00	0.00	0.00	0.00	0.00	0.00
Fo	89.42	89.45	89.37	89.02	89.19	88.90	89.02	89.32	86.13	85.81	86.07	85.82	86.11	80.12	80.20	79.56	79.85	80.59	80.63
Fa	10.58	10.55	10.63	10.98	10.81	11.10	10.98	10.68	13.87	14.19	13.93	14.18	13.89	19.88	19.80	20.44	20.15	19.41	19.37
Mg*	89.30	89.26	89.19	88.85	88.98	88.66	88.83	89.14	85.96	85.69	85.80	85.61	85.92	79.88	80.02	79.29	79.61	80.33	80.44

continued

Table 2.2.3. (Continued)

Gabbro with olv.		Wehrlite																			
Sample	21-7c	22-1c	22-2c	22-3c	22-4c	22-5c	22-6c	22-7c	23-1c	23-2c	23-3c	23-4c	23-5c	23-6c	25-1c	25-2c	25-3c	25-4c	25-5c	25-6c	25-7c
SiO2	39.54	40.18	40.33	40.46	40.22	40.08	40.28	40.49	40.90	40.56	40.39	56.75	40.91	40.65	39.59	39.72	39.55	39.80	39.54	39.60	39.78
TiO2	0.00	0.00	0.01	0.03	0.00	0.05	0.03	0.00	0.00	0.04	0.00	0.03	0.00	0.00	0.04	0.00	0.00	0.00	0.01	0.03	0.03
Al2O3	0.00	0.00	0.02	0.00	0.01	0.01	0.01	0.00	0.00	0.00	0.00	1.51	0.01	0.02	0.00	0.01	0.01	0.00	0.00	0.00	0.00
FeO	18.75	13.84	14.13	13.45	13.97	13.68	13.98	13.84	11.86	12.16	11.96	7.63	11.81	12.30	17.33	16.64	17.41	16.86	16.71	16.80	17.04
Cr2O3	0.01	0.00	0.04	0.02	0.00	0.00	0.00	0.04	0.02	0.02	0.00	0.24	0.00	0.02	0.07	0.00	0.00	0.00	0.00	0.00	0.00
MnO	0.25	0.25	0.17	0.26	0.21	0.15	0.11	0.22	0.23	0.21	0.13	0.22	0.22	0.25	0.28	0.24	0.27	0.26	0.32	0.31	0.29
MgO	41.73	44.69	44.65	45.11	44.79	45.28	45.25	44.81	46.75	46.49	46.21	32.66	47.06	46.56	42.45	42.23	42.55	42.58	42.36	43.12	42.68
CaO	0.05	0.02	0.04	0.01	0.00	0.01	0.02	0.02	0.01	0.01	0.02	0.75	0.04	0.03	0.06	0.02	0.00	0.04	0.01	0.01	0.01
Na2O	0.00	0.00	0.01	0.00	0.01	0.00	0.00	0.02	0.01	0.00	0.00	0.01	0.00	0.06	0.00	0.00	0.00	0.00	0.01	0.02	0.01
K2O	0.00	0.00	0.00	0.00	0.00	0.00	0.02	0.00	0.00	0.00	0.00	0.00	0.01	0.00	0.00	0.00	0.00	0.04	0.00	0.00	0.00
Total	100.33	98.98	99.40	99.34	99.21	99.26	99.70	99.44	99.78	99.49	98.71	99.80	100.06	99.89	99.82	98.86	99.79	99.58	98.96	99.89	99.84
Si	1.01	0.99	1.00	1.00	0.99	0.99	1.00	1.00	1.01	1.00	0.98	1.31	1.01	1.01	1.00	0.99	1.00	1.00	0.99	1.00	1.01
Ti	0.00	0.00	0.00	0.00	0.00	0.00	0.00	0.00	0.00	0.00	0.00	0.00	0.00	0.00	0.00	0.00	0.00	0.00	0.00	0.00	0.00
Al	0.00	0.00	0.00	0.00	0.00	0.00	0.00	0.00	0.00	0.00	0.00	0.04	0.00	0.00	0.00	0.00	0.00	0.00	0.00	0.00	0.00
Fe	0.40	0.29	0.29	0.28	0.29	0.28	0.29	0.29	0.24	0.25	0.24	0.15	0.24	0.25	0.37	0.35	0.37	0.35	0.35	0.36	0.36
Cr	0.00	0.00	0.00	0.00	0.00	0.00	0.00	0.00	0.00	0.00	0.00	0.00	0.00	0.00	0.00	0.00	0.00	0.00	0.00	0.00	0.00
Mn	0.01	0.01	0.00	0.01	0.00	0.00	0.00	0.00	0.00	0.00	0.00	0.00	0.00	0.01	0.01	0.01	0.01	0.01	0.01	0.01	0.01
Mg	1.58	1.64	1.65	1.66	1.65	1.67	1.68	1.65	1.72	1.71	1.68	1.12	1.73	1.72	1.60	1.57	1.61	1.60	1.58	1.63	1.61
Ca	0.00	0.00	0.00	0.00	0.00	0.00	0.00	0.00	0.00	0.00	0.00	0.02	0.00	0.00	0.00	0.00	0.00	0.00	0.00	0.00	0.00
Na	0.00	0.00	0.00	0.00	0.00	0.00	0.00	0.00	0.00	0.00	0.00	0.00	0.00	0.00	0.00	0.00	0.00	0.00	0.00	0.00	0.00
K	0.00	0.00	0.00	0.00	0.00	0.00	0.00	0.00	0.00	0.00	0.00	0.00	0.00	0.00	0.00	0.00	0.00	0.00	0.00	0.00	0.00
Fo	79.87	85.20	84.93	85.67	85.11	85.51	85.23	85.23	87.54	87.21	87.32	88.41	87.66	87.09	81.37	81.90	81.33	81.83	81.88	82.07	81.70
Fa	20.13	14.80	15.07	14.33	14.89	14.49	14.77	14.77	12.46	12.79	12.68	11.59	12.34	12.91	18.63	18.10	18.67	18.17	18.12	17.93	18.30
Mg*	79.65	84.97	84.77	85.43	84.92	85.37	85.13	85.03	87.33	87.01	87.20	88.12	87.46	86.86	81.12	81.68	81.10	81.60	81.60	81.79	81.45

continued

Table 2.2.3. (Continued)

	Dunite									Gabbro with olivine						Wehrlite			
Sample	**30-1c**	**30-2c**	**30-3c**	**30-4c**	**30-4r**	**30-5c**	**30-6c**	**30-7c**	**30-8c**	**36-1c**	**36-2c**	**36-3c**	**36-4c**	**36-5c**	**36-6c**	**37-1c**	**37-2c**	**37-3c**	**37-4c**
SiO2	40.81	40.43	40.72	40.30	40.42	40.16	40.64	40.69	40.49	39.53	39.80	39.57	39.74	39.77	39.68	39.39	39.21	39.43	39.31
TiO2	0.01	0.01	0.02	0.03	0.01	0.00	0.00	0.01	0.01	0.00	0.02	0.00	0.00	0.02	0.00	0.02	0.04	0.00	0.00
Al2O3	0.00	0.02	0.00	0.00	0.00	0.00	0.00	0.00	0.00	0.00	0.01	0.00	0.02	0.01	0.00	0.01	0.00	0.00	0.00
FeO	10.54	10.75	10.76	10.85	10.78	10.66	10.87	10.52	10.78	17.46	17.22	17.25	17.41	17.80	17.98	18.06	18.41	18.47	18.69
Cr2O3	0.00	0.03	0.01	0.00	0.02	0.00	0.01	0.01	0.01	0.01	0.04	0.01	0.00	0.04	0.00	0.02	0.07	0.00	0.00
MnO	0.15	0.18	0.17	0.20	0.18	0.18	0.16	0.12	0.15	0.33	0.36	0.20	0.32	0.22	0.29	0.25	0.26	0.29	0.28
MgO	48.74	48.74	48.51	48.81	48.43	48.39	48.89	49.09	48.50	42.15	42.55	42.42	42.26	41.89	42.19	41.60	41.45	41.21	41.64
CaO	0.03	0.02	0.04	0.01	0.02	0.04	0.03	0.02	0.02	0.02	0.04	0.00	0.03	0.03	0.03	0.02	0.03	0.03	0.01
Na2O	0.00	0.00	0.00	0.00	0.00	0.00	0.00	0.00	0.00	0.00	0.00	0.00	0.03	0.01	0.01	0.05	0.00	0.00	0.02
K2O	0.00	0.00	0.00	0.00	0.00	0.00	0.00	0.00	0.00	0.00	0.02	0.00	0.01	0.00	0.03	0.00	0.00	0.00	0.01
NiO	0.25	0.19	0.15	0.22	0.22	0.13	0.20	0.23	0.22										
Total	100.53	100.37	100.38	100.42	100.08	99.56	100.80	100.69	100.18	99.50	100.06	99.45	99.82	99.79	100.21	99.42	99.47	99.43	99.96
Si	1.00	0.99	1.00	0.99	1.00	0.99	0.99	0.99	1.00	1.00	1.01	1.00	1.01	1.01	1.01	1.00	0.99	1.00	1.00
Ti	0.00	0.00	0.00	0.00	0.00	0.00	0.00	0.00	0.00	0.00	0.00	0.00	0.00	0.00	0.00	0.00	0.00	0.00	0.00
Al	0.00	0.00	0.00	0.00	0.00	0.00	0.00	0.00	0.00	0.00	0.00	0.00	0.00	0.00	0.00	0.00	0.00	0.00	0.00
Fe	0.22	0.22	0.22	0.22	0.22	0.22	0.22	0.21	0.22	0.37	0.36	0.36	0.37	0.38	0.38	0.38	0.39	0.39	0.40
Cr	0.00	0.00	0.00	0.00	0.00	0.00	0.00	0.00	0.00	0.00	0.00	0.00	0.00	0.00	0.00	0.00	0.00	0.00	0.00
Mn	0.00	0.00	0.00	0.00	0.00	0.00	0.00	0.00	0.00	0.01	0.01	0.00	0.01	0.00	0.01	0.01	0.01	0.01	0.01
Mg	1.78	1.78	1.77	1.79	1.78	1.78	1.78	1.79	1.78	1.59	1.61	1.59	1.59	1.58	1.60	1.57	1.57	1.56	1.58
Ca	0.00	0.00	0.00	0.00	0.00	0.00	0.00	0.00	0.00	0.00	0.00	0.00	0.00	0.00	0.00	0.00	0.00	0.00	0.00
Na	0.00	0.00	0.00	0.00	0.00	0.00	0.00	0.00	0.00	0.00	0.00	0.00	0.00	0.00	0.00	0.00	0.00	0.00	0.00
K	0.00	0.00	0.00	0.00	0.00	0.00	0.00	0.00	0.00	0.00	0.00	0.00	0.00	0.00	0.00	0.00	0.00	0.00	0.00
Ni	0.01	0.00	0.00	0.00	0.00	0.00	0.00	0.00	0.00										
Fo	89.09	88.85	88.83	88.75	88.75	88.88	88.79	89.19	88.80	81.15	81.50	81.43	81.23	80.75	80.71	80.42	80.06	79.91	79.89
Fa	10.81	11.00	11.05	11.07	11.09	10.99	11.08	10.72	11.07	18.85	18.50	18.57	18.77	19.25	19.29	19.58	19.94	20.09	20.11
Mg*	89.00	89.00	88.90	89.10	89.00	89.00	89.00	89.50	89.00	80.85	81.18	81.25	80.95	80.56	80.45	80.20	79.83	79.66	79.64

continued

Table 2.2.3. (Continued)

	Wherlite									
Sample	**46-1c**	**46-2c**	**46-2r**	**46-3c**	**46-3r**	**46-4c**	**46-4r**	**46-5c**	**46-6c**	**46-7c**
SiO2	40.16	40.17	40.23	40.12	40.19	40.10	40.32	39.78	40.24	40.25
TiO2	0.01	0.00	0.01	0.02	0.01	0.00	0.01	0.02	0.00	0.00
Al2O3	0.00	0.00	0.00	0.00	0.00	0.00	0.00	0.00	0.00	0.00
FeO	12.87	12.79	12.67	13.15	12.88	13.01	12.97	13.03	12.91	12.55
Cr2O3	0.03	0.00	0.01	0.00	0.00	0.00	0.02	0.01	0.00	0.00
MnO	0.12	0.16	0.14	0.20	0.13	0.22	0.17	0.16	0.14	0.14
MgO	46.80	47.02	47.36	47.23	47.03	47.12	46.76	46.88	46.94	47.20
CaO	0.01	0.01	0.02	0.05	0.05	0.02	0.00	0.03	0.02	0.02
Na2O	0.00	0.00	0.00	0.00	0.00	0.00	0.00	0.00	0.00	0.00
K2O	0.00	0.00	0.00	0.00	0.00	0.00	0.00	0.00	0.00	0.00
NiO	0.15	0.18	0.17	0.12	0.12	0.14	0.12	0.12	0.15	0.16
Total	100.15	100.33	100.61	100.89	100.41	100.61	100.37	100.03	100.40	100.32
Si	1.00	1.00	0.99	0.99	1.00	0.99	1.00	0.99	1.00	1.00
Ti	0.00	0.00	0.00	0.00	0.00	0.00	0.00	0.00	0.00	0.00
Al	0.00	0.00	0.00	0.00	0.00	0.00	0.00	0.00	0.00	0.00
Fe	0.27	0.27	0.26	0.27	0.27	0.27	0.27	0.27	0.27	0.26
Cr	0.00	0.00	0.00	0.00	0.00	0.00	0.00	0.00	0.00	0.00
Mn	0.00	0.00	0.00	0.00	0.00	0.00	0.00	0.00	0.00	0.00
Mg	1.73	1.74	1.74	1.74	1.74	1.74	1.73	1.74	1.73	1.74
Ca	0.00	0.00	0.00	0.00	0.00	0.00	0.00	0.00	0.00	0.00
Na	0.00	0.00	0.00	0.00	0.00	0.00	0.00	0.00	0.00	0.00
K	0.00	0.00	0.00	0.00	0.00	0.00	0.00	0.00	0.00	0.00
Ni	0.00	0.00	0.00	0.00	0.00	0.00	0.00	0.00	0.00	0.00
Fo	86.53	86.62	86.85	86.36	86.62	86.41	86.38	86.39	86.53	86.91
Fa	13.35	13.22	13.03	13.50	13.31	13.39	13.44	13.48	13.35	12.97
Mg*	86.50	86.60	87.00	87.00	86.60	86.60	86.50	86.60	86.50	87.00

Table 2.2.4. Results of electron micro-probe analyses of clinopyroxenes from the ultramafic and mafic cumulates

	Wehrlite																			
Sample	**11-1c**	**11-1r**	**11-2c**	**11-3c**	**11-3r**	**11-4c**	**11-4r**	**11-5c**	**11-5r**	**11-6c**	**11-6r**	**11-7c**	**11-7r**	**11-8c**	**11-9c**	**11-10c**	**11-11c**	**13-1c**	**13-1r**	**13-2c**
SiO2	54.47	54.14	54.25	54.36	54.09	53.99	54.23	54.53	54.10	54.21	54.47	54.37	54.54	54.12	54.38	54.21	54.24	54.14	54.44	54.17
Al2O3	1.09	1.14	1.08	1.07	1.12	1.10	1.15	0.60	1.11	1.11	1.12	1.11	1.11	1.12	1.11	1.09	1.10	1.06	1.02	1.11
TiO2	0.06	0.06	0.03	0.05	0.04	0.03	0.04	0.04	0.03	0.03	0.07	0.07	0.05	0.07	0.05	0.05	0.03	0.03	0.03	0.02
Fe2O3																				
FeO	2.27	2.32	2.43	2.46	2.36	2.41	2.23	2.25	2.29	2.51	2.36	2.63	2.25	2.37	2.43	2.15	2.46	2.33	2.41	2.54
MnO	0.15	0.20	0.15	0.05	0.06	0.13	0.05	0.07	0.07	0.05	0.11	0.17	0.09	0.06	0.15	0.11	0.07	0.12	0.11	0.09
MgO	17.24	17.15	17.22	17.58	17.04	17.19	16.99	17.44	16.94	17.23	17.15	17.81	17.17	17.23	17.14	17.19	17.23	17.11	17.10	17.69
Cr2O3	0.69	0.69	0.64	0.69	0.76	0.73	0.68	0.28	0.75	0.75	0.72	0.66	0.67	0.57	0.78	0.66	0.73	0.71	0.73	0.80
CaO	24.41	24.04	24.08	23.65	24.41	24.36	24.44	24.68	24.48	24.26	24.53	23.23	24.50	24.37	24.02	24.20	23.94	24.11	24.31	23.45
Na2O	0.11	0.11	0.08	0.10	0.06	0.09	0.07	0.04	0.10	0.11	0.10	0.11	0.09	0.09	0.09	0.11	0.09	0.10	0.09	0.10
K2O	0.02	0.00	0.02	0.00	0.01	0.02	0.01	0.00	0.01	0.01	0.00	0.01	0.02	0.00	0.00	0.00	0.00	0.02	0.02	0.01
Total	100.51	99.85	99.98	100.01	99.95	100.05	99.89	99.93	99.88	100.27	100.63	100.17	100.49	100.00	100.15	99.77	99.89	99.73	100.26	99.98
Si	1.97	1.96	1.97	1.98	1.96	1.96	1.96	1.97	1.96	1.97	1.97	1.97	1.98	1.97	1.98	1.95	1.96	1.94	1.98	1.97
Al IV	0.03	0.04	0.03	0.02	0.04	0.04	0.04	0.03	0.04	0.03	0.03	0.03	0.02	0.03	0.02	0.05	0.04	0.04	0.02	0.03
Al VI	0.02	0.00	0.02	0.02	0.01	0.01	0.01	0.00	0.00	0.02	0.02	0.02	0.02	0.02	0.03	0.00	0.01	0.00	0.02	0.01
Ti	0.00	0.00	0.00	0.00	0.00	0.00	0.00	0.00	0.00	0.00	0.00	0.00	0.00	0.00	0.00	0.00	0.00	0.00	0.00	0.00
Fe3+	0.00	0.06	0.00	0.00	0.02	0.01	0.03	0.04	0.05	0.00	0.00	0.00	0.00	0.00	0.00	0.00	0.04	0.00	0.00	0.01
Fe2+	0.07	0.01	0.07	0.07	0.05	0.06	0.03	0.03	0.02	0.07	0.07	0.07	0.07	0.07	0.07	0.06	0.03	0.07	0.07	0.07
Mn	0.00	0.01	0.00	0.00	0.00	0.00	0.00	0.00	0.00	0.00	0.00	0.01	0.00	0.00	0.00	0.00	0.00	0.00	0.00	0.00
Mg	0.93	0.92	0.93	0.95	0.92	0.93	0.92	0.94	0.91	0.93	0.93	0.96	0.93	0.93	0.93	0.92	0.93	0.92	0.93	0.96
Cr	0.02	0.02	0.02	0.02	0.02	0.02	0.02	0.01	0.02	0.02	0.02	0.02	0.02	0.02	0.02	0.02	0.02	0.02	0.02	0.02
Ca	0.95	0.93	0.94	0.92	0.95	0.95	0.95	0.96	0.95	0.94	0.95	0.90	0.95	0.95	0.94	0.93	0.93	0.93	0.95	0.91
Na	0.01	0.01	0.01	0.01	0.00	0.01	0.00	0.00	0.01	0.01	0.01	0.01	0.01	0.01	0.01	0.01	0.01	0.01	0.01	0.01
K	0.00	0.00	0.00	0.00	0.00	0.00	0.00	0.00	0.00	0.00	0.00	0.00	0.00	0.00	0.00	0.00	0.00	0.00	0.00	0.00
Ens:	47.70	47.85	47.87	48.86	47.41	47.59	47.42	47.81	47.24	47.73	47.42	49.37	47.58	47.72	47.81	47.95	48.06	47.78	47.52	49.12
Fors.	3.76	3.95	4.03	3.91	3.78	3.95	3.57	3.57	3.69	3.98	3.83	4.36	3.64	3.78	4.04	3.54	3.96	3.84	3.93	4.10
Wol.	48.54	48.20	48.10	47.23	48.81	48.46	49.01	48.62	49.06	48.29	48.74	46.27	48.78	48.50	48.15	48.51	47.98	48.38	48.55	46.79
Mg*	92.61	92.95	92.67	93.16	92.79	92.71	93.14	93.25	92.95	92.45	92.97	93.23	92.98	92.84	93.00	93.89	92.59	92.90	92.97	92.55

Number of ions on the basis of 6(O), c and r indicate "core" and "rim" respectively

continued

Table 2.2.4. (Continued)

	Wehrlite																			
Sample	**13-2r**	**13-3c**	**13-3r**	**13-4c**	**13-4r**	**13-5c**	**13-5r**	**14-1c**	**14-1r**	**14-2c**	**14-2r**	**14-3c**	**14-3r**	**14-4c**	**14-5c**	**14-5r**	**17-1c**	**17-1r**	**17-2c**	**17-2r**
SiO2	54.44	54.06	54.25	54.27	54.28	54.06	54.11	55.10	53.93	54.09	54.24	53.87	55.29	54.08	54.22	54.07	53.65	53.61	53.84	53.68
Al2O3	0.85	1.11	1.12	1.16	1.09	1.10	1.07	0.61	1.19	1.24	1.10	1.20	0.21	1.18	1.14	1.16	1.76	1.71	1.50	1.90
TiO2	0.02	0.01	0.02	0.03	0.07	0.04	0.05	0.06	0.03	0.05	0.01	0.04	0.00	0.06	0.05	0.03	0.10	0.05	0.09	0.14
Fe2O3																				
FeO	2.38	2.26	2.49	2.33	2.26	2.47	2.29	1.78	2.36	2.57	2.29	2.25	1.57	2.41	2.21	2.24	3.25	3.29	2.70	3.16
MnO	0.05	0.03	0.14	0.10	0.13	0.03	0.09	0.12	0.10	0.10	0.08	0.09	0.04	0.09	0.09	0.14	0.08	0.06	0.05	0.16
MgO	17.55	17.00	17.48	17.04	17.27	17.11	17.16	17.26	17.22	17.52	17.34	17.21	17.16	17.56	16.98	17.02	16.49	17.77	16.78	16.72
Cr2O3	0.40	0.77	0.63	0.63	0.73	0.71	0.67	0.31	0.66	0.79	0.65	0.67	0.11	0.72	0.79	0.77	0.48	0.46	0.31	0.52
CaO	24.30	24.20	23.52	24.33	24.00	24.15	24.43	25.29	24.00	23.80	24.01	24.17	25.77	23.28	24.46	24.19	24.12	22.88	24.33	23.91
Na2O	0.09	0.07	0.10	0.11	0.06	0.07	0.09	0.04	0.09	0.09	0.11	0.10	0.03	0.10	0.08	0.11	0.08	0.07	0.07	0.09
K2O	0.01	0.00	0.01	0.01	0.00	0.00	0.00	0.00	0.00	0.00	0.00	0.01	0.00	0.03	0.00	0.00	0.01	0.00	0.00	0.00
Total	100.09	99.51	99.76	100.01	99.89	99.74	99.96	100.57	99.58	100.25	99.83	99.61	100.18	99.51	100.02	99.73	100.02	99.90	99.67	100.28
Si	1.98	1.92	1.95	1.98	1.96	1.94	1.96	1.99	1.92	1.96	1.95	1.92	2.01	1.92	1.97	1.94	1.96	1.94	1.93	1.95
Al IV	0.02	0.05	0.05	0.02	0.04	0.05	0.04	0.01	0.05	0.04	0.05	0.05	0.01	0.05	0.03	0.05	0.04	0.06	0.06	0.05
Al VI	0.01	0.00	0.00	0.03	0.01	0.00	0.01	0.01	0.00	0.02	0.00	0.00	0.00	0.00	0.02	0.00	0.03	0.01	0.00	0.03
Ti	0.00	0.00	0.00	0.00	0.00	0.00	0.00	0.00	0.00	0.00	0.00	0.00	0.00	0.00	0.00	0.00	0.00	0.00	0.00	0.00
Fe3+	0.01	0.00	0.00	0.00	0.03	0.00	0.03	0.01	0.00	0.00	0.00	0.00	0.00	0.00	0.00	0.00	0.00	0.07	0.00	0.00
Fe2+	0.07	0.07	0.07	0.07	0.04	0.07	0.04	0.05	0.07	0.08	0.07	0.07	0.05	0.07	0.07	0.07	0.10	0.03	0.08	0.10
Mn	0.00	0.00	0.00	0.00	0.00	0.00	0.00	0.00	0.00	0.00	0.00	0.00	0.00	0.00	0.00	0.00	0.00	0.00	0.00	0.00
Mg	0.95	0.90	0.94	0.92	0.93	0.92	0.93	0.93	0.91	0.95	0.93	0.92	0.93	0.93	0.92	0.91	0.90	0.96	0.90	0.91
Cr	0.01	0.02	0.02	0.02	0.02	0.02	0.02	0.01	0.02	0.02	0.02	0.02	0.00	0.02	0.02	0.02	0.01	0.01	0.01	0.01
Ca	0.95	0.92	0.91	0.95	0.93	0.93	0.95	0.98	0.92	0.93	0.93	0.92	1.00	0.88	0.95	0.93	0.94	0.89	0.93	0.93
Na	0.01	0.00	0.01	0.01	0.00	0.00	0.01	0.00	0.01	0.01	0.01	0.01	0.00	0.01	0.01	0.01	0.01	0.00	0.00	0.01
K	0.00	0.00	0.00	0.00	0.00	0.00	0.00	0.00	0.00	0.00	0.00	0.00	0.00	0.00	0.00	0.00	0.00	0.00	0.00	0.00
Ens:	48.25	47.65	48.75	47.48	48.16	47.70	47.60	47.29	48.04	48.50	48.27	47.95	46.91	49.20	47.37	47.62	46.20	49.24	46.86	46.75
Fors.	3.75	3.60	4.12	3.80	3.74	3.91	3.70	2.92	3.85	4.15	3.70	3.66	2.47	3.93	3.60	3.74	5.23	5.21	4.31	5.21
Wol.	48.01	48.75	47.14	48.72	48.10	48.39	48.70	49.79	48.11	47.35	48.03	48.39	50.62	46.87	49.03	48.64	48.56	45.56	48.83	48.04
Mg*	92.93	92.79	93.04	92.96	93.16	92.91	93.04	94.53	92.89	92.40	93.01	92.89	94.89	92.98	92.94	92.87	89.98	90.59	91.80	90.42

continued

Table 2.2.4. (Continued)

	Wherlite								Dunite											
Sample	**17-3c**	**17-3r**	**17-4c**	**17-4r**	**17-5c**	**17-5r**	**17-6c**	**17-6r**	**18-1c**	**18-1r**	**18-2c**	**18-2r**	**18-3c**	**18-3r**	**18-4c**	**18-4r**	**18-5c**	**18-5r**	**18-6c**	**18-6r**
SiO2	53.55	54.49	53.39	53.62	53.68	53.61	53.65	54.01	53.06	53.29	52.39	52.74	54.14	53.70	53.62	53.74	53.45	52.99	53.26	54.11
Al2O3	1.73	1.63	1.86	1.75	1.78	1.70	1.76	1.79	1.95	1.87	1.73	2.10	1.22	1.49	1.58	1.39	1.81	2.55	1.99	0.97
TiO2	0.10	0.06	0.08	0.08	0.10	0.03	0.10	0.07	0.05	0.07	0.10	0.12	0.05	0.05	0.09	0.00	0.10	0.14	0.10	0.10
Fe2O3									3.59	1.23	3.83	2.44	0.00	0.72	0.12	0.86	0.00	0.00	0.64	0.31
FeO	3.23	6.02	3.76	3.13	3.23	3.09	3.27	3.57	0.00	1.94	0.00	0.92	2.73	2.19	2.92	2.11	2.83	3.05	2.43	2.48
MnO	0.08	0.13	0.14	0.18	0.17	0.07	0.03	0.14	0.12	0.13	0.08	0.13	0.11	0.15	0.13	0.15	0.15	0.13	0.10	0.11
MgO	16.95	22.56	18.95	16.98	16.85	16.82	16.89	17.45	16.66	17.03	16.71	16.71	16.99	17.03	16.78	17.09	16.71	16.37	16.70	17.04
Cr2O3	0.57	0.38	0.39	0.45	0.39	0.47	0.38	0.43	0.44	0.43	0.44	0.48	0.20	0.34	0.34	0.42	0.43	0.62	0.47	0.20
CaO	23.85	14.77	20.62	23.87	23.79	23.97	23.75	23.09	23.81	23.97	23.45	23.82	24.51	24.36	24.09	24.31	24.00	23.85	23.85	24.68
Na2O	0.09	0.04	0.06	0.12	0.06	0.06	0.07	0.07	0.16	0.14	0.14	0.13	0.05	0.05	0.08	0.06	0.10	0.10	0.12	0.05
K2O	0.02	0.00	0.01	0.01	0.00	0.00	0.01	0.02	0.82	0.00	0.88	0.40	0.00	0.04	0.00	0.04	0.00	0.00	0.13	0.00
Total	100.17	100.08	99.26	100.19	100.05	99.82	99.91	100.64	100.66	100.10	99.75	99.99	100.00	100.12	99.75	100.17	99.58	99.80	99.79	100.05
Si	1.95	1.96	1.86	1.95	1.96	1.94	1.95	1.95	1.93	1.94	1.92	1.92	1.97	1.95	1.96	1.96	1.96	1.94	1.95	1.97
Al IV	0.05	0.04	0.08	0.05	0.04	0.06	0.05	0.05	0.07	0.06	0.07	0.08	0.03	0.05	0.04	0.04	0.04	0.06	0.05	0.03
Al VI	0.02	0.02	0.00	0.02	0.03	0.01	0.02	0.03	0.01	0.02	0.00	0.01	0.02	0.01	0.03	0.02	0.04	0.05	0.04	0.01
Ti	0.00	0.00	0.00	0.00	0.00	0.00	0.00	0.00	0.00	0.00	0.00	0.00	0.00	0.00	0.00	0.00	0.00	0.00	0.00	0.00
Fe3+	0.01	0.01	0.00	0.02	0.00	0.09	0.05	0.00	0.10	0.03	0.11	0.07	0.00	0.02	0.00	0.02	0.00	0.00	0.02	0.01
Fe2+	0.09	0.17	0.11	0.08	0.10	0.01	0.05	0.10	0.00	0.06	0.00	0.03	0.08	0.07	0.09	0.06	0.09	0.09	0.07	0.08
Mn	0.00	0.00	0.00	0.01	0.01	0.00	0.00	0.00	0.00	0.00	0.00	0.00	0.00	0.00	0.00	0.00	0.00	0.00	0.00	0.00
Mg	0.92	1.21	0.99	0.92	0.92	0.91	0.91	0.94	0.90	0.92	0.91	0.91	0.92	0.92	0.91	0.93	0.91	0.89	0.91	0.93
Cr	0.02	0.01	0.01	0.01	0.01	0.01	0.01	0.01	0.01	0.01	0.01	0.01	0.01	0.01	0.01	0.01	0.01	0.02	0.01	0.01
Ca	0.93	0.57	0.77	0.93	0.93	0.93	0.92	0.90	0.93	0.94	0.92	0.93	0.96	0.95	0.94	0.95	0.94	0.93	0.93	0.96
Na	0.01	0.00	0.00	0.01	0.00	0.00	0.00	0.00	0.01	0.01	0.01	0.01	0.00	0.00	0.01	0.00	0.01	0.01	0.01	0.00
K	0.00	0.00	0.00	0.00	0.00	0.00	0.00	0.00	0.04	0.00	0.04	0.02	0.00	0.00	0.00	0.00	0.00	0.00	0.01	0.00
Ens:	47.15	61.59	52.70	47.18	47.00	46.96	47.17	48.30	49.23	48.08	49.71	48.55	46.93	47.69	46.86	47.68	46.90	46.37	47.35	47.04
Fors.	5.17	9.42	6.09	5.16	5.32	4.95	5.17	5.76	0.20	3.28	0.14	1.71	4.40	3.66	4.78	3.55	4.70	5.05	4.03	4.00
Wol.	47.68	28.98	41.21	47.66	47.68	48.09	47.66	45.93	50.57	48.64	50.15	49.74	48.67	48.85	48.36	48.77	48.40	48.57	48.62	48.96
Mg*	90.34	86.98	89.96	90.63	90.29	90.66	90.20	89.71	90.00	91.09	89.22	90.10	92.00	91.09	91.00	92.08	91.00	90.82	91.00	91.18

continued

Table 2.2.4. (Continued)

	Dunite				Clinopyroxenite															
Sample	18-7c	18-7r	18-8c	18-8r	19-1c	19-1r	19-2c	19-2r	19-3c	19-3r	19-4c	19-4b	19-4r	19-5c	19-5r	19-6c	19-6r	19-7c	19-7r	19-8c
SiO2	53.81	53.89	53.98	53.85	53.07	52.96	52.63	53.16	52.86	53.08	53.35	53.15	53.44	52.56	53.14	53.12	53.13	53.30	53.38	53.06
Al2O3	1.32	1.26	0.90	1.13	2.54	2.54	2.61	2.56	2.66	2.61	2.57	2.50	2.56	2.60	2.50	2.46	2.46	2.35	2.48	2.57
TiO2	0.12	0.06	0.03	0.11	0.08	0.11	0.10	0.09	0.08	0.14	0.15	0.08	0.06	0.04	0.08	0.03	0.07	0.06	0.13	0.05
Fe2O3	0.07	0.66	0.14	0.50																
FeO	2.69	2.06	2.51	2.00	3.45	3.75	3.88	3.46	3.88	3.78	3.76	3.84	4.11	3.38	3.80	3.40	3.36	3.54	3.50	3.75
MnO	0.12	0.06	0.14	0.17	0.07	0.17	0.15	0.05	0.20	0.12	0.09	0.19	0.17	0.09	0.08	0.07	0.10	0.00	0.14	0.13
MgO	16.86	17.06	17.11	17.03	16.18	16.31	16.35	16.39	16.25	16.57	16.35	16.51	17.79	16.07	16.62	16.25	16.35	16.35	16.42	16.67
Cr2O3	0.29	0.27	0.17	0.27	0.28	0.39	0.34	0.30	0.31	0.32	0.31	0.36	0.33	0.29	0.31	0.30	0.31	0.30	0.31	0.33
CaO	24.47	24.73	24.42	24.68	23.84	23.49	23.52	23.85	23.84	23.61	23.48	23.28	21.19	24.33	23.51	24.10	24.02	23.93	24.07	23.01
Na2O	0.05	0.06	0.03	0.03	0.10	0.10	0.08	0.11	0.12	0.10	0.08	0.11	0.08	0.09	0.09	0.09	0.11	0.07	0.09	0.07
K2O	0.00	0.00	0.00	0.07	0.00	0.01	0.00	0.02	0.01	0.00	0.00	0.01	0.03	0.00	0.00	0.00	0.00	0.02	0.00	0.00
Total	99.80	100.11	99.43	99.84	99.61	99.83	99.66	99.99	100.21	100.33	100.14	100.03	99.76	99.45	100.13	99.82	99.91	99.92	100.52	99.64
Si	1.96	1.96	1.98	1.96	1.90	1.92	1.89	1.94	1.93	1.93	1.95	1.94	1.92	1.87	1.94	1.92	1.93	1.94	1.94	1.90
Al IV	0.04	0.04	0.02	0.04	0.10	0.08	0.11	0.06	0.07	0.07	0.05	0.06	0.08	0.11	0.06	0.08	0.07	0.06	0.06	0.10
Al VI	0.02	0.01	0.02	0.01	0.01	0.02	0.00	0.05	0.04	0.04	0.06	0.05	0.03	0.00	0.04	0.03	0.03	0.04	0.04	0.01
Ti	0.00	0.00	0.00	0.00	0.00	0.00	0.00	0.00	0.00	0.00	0.00	0.00	0.00	0.00	0.00	0.00	0.00	0.00	0.00	0.00
Fe3+	0.00	0.02	0.00	0.01	0.00	0.10	0.00	0.02	0.03	0.02	0.00	0.01	0.10	0.00	0.01	0.09	0.06	0.04	0.01	0.00
Fe2+	0.08	0.06	0.08	0.06	0.10	0.02	0.12	0.08	0.09	0.10	0.11	0.11	0.02	0.10	0.10	0.01	0.04	0.07	0.10	0.11
Mn	0.00	0.00	0.00	0.01	0.00	0.01	0.00	0.00	0.01	0.00	0.00	0.01	0.01	0.00	0.00	0.00	0.00	0.00	0.00	0.00
Mg	0.92	0.93	0.93	0.93	0.86	0.88	0.87	0.89	0.88	0.90	0.89	0.90	0.95	0.85	0.90	0.88	0.88	0.89	0.89	0.89
Cr	0.01	0.01	0.01	0.01	0.01	0.01	0.01	0.01	0.01	0.01	0.01	0.01	0.01	0.01	0.01	0.01	0.01	0.01	0.01	0.01
Ca	0.96	0.96	0.96	0.96	0.91	0.91	0.90	0.93	0.93	0.92	0.92	0.91	0.82	0.92	0.92	0.93	0.93	0.93	0.94	0.88
Na	0.00	0.00	0.00	0.00	0.01	0.01	0.01	0.01	0.01	0.01	0.01	0.01	0.01	0.01	0.01	0.01	0.01	0.00	0.01	0.00
K	0.00	0.00	0.00	0.00	0.00	0.00	0.00	0.00	0.00	0.00	0.00	0.00	0.00	0.00	0.00	0.00	0.00	0.00	0.00	0.00
Ens:	46.79	47.36	47.33	47.31	45.85	46.09	46.04	46.17	45.55	46.38	46.21	46.51	50.23	45.27	46.57	45.75	45.99	46.01	45.92	47.11
Fors.	4.38	3.31	4.12	3.40	5.60	6.22	6.37	5.55	6.42	6.13	6.10	6.37	6.78	5.48	6.10	5.48	5.46	5.59	5.71	6.15
Wol.	48.83	49.33	48.56	49.29	48.55	47.70	47.59	48.28	48.03	47.49	47.69	47.12	42.99	49.25	47.34	48.76	48.55	48.40	48.37	46.73
Mg*	92.00	92.08	92.08	93.00	89.62	88.58	87.93	89.41	88.19	88.66	88.99	88.46	88.53	89.48	88.63	89.50	89.66	89.17	89.32	89.00

continued

Table 2.2.4. (Continued)

	Clinopyroxenite																				
Sample	**19-8r**	**19-9c**	**19-9r**	**19-10c**	**19-10r**	**20-1c**	**20-1r**	**20-2c**	**20-2r**	**20-3c**	**20-3r**	**20-4c**	**20-4r**	**20-5c**	**20-5r**	**20-6c**	**20-6r**	**20-7c**	**20-8c**	**20-9c**	**20-9r**
SiO2	53.11	53.16	53.98	52.61	53.17	54.46	53.31	53.25	53.05	52.93	53.03	52.95	52.88	52.92	53.22	53.30	53.11	53.48	52.95	53.02	53.96
Al2O3	2.54	2.53	2.38	2.55	2.45	0.61	2.26	2.41	2.35	2.44	2.55	2.35	2.43	2.43	2.35	2.25	2.35	1.18	2.30	2.44	1.21
TiO2	0.11	0.07	0.04	0.04	0.08	0.04	0.13	0.07	0.11	0.09	0.08	0.08	0.08	0.07	0.07	0.07	0.08	0.09	0.06	0.05	0.08
Fe2O3																					
FeO	3.97	3.68	6.54	3.83	3.59	2.94	3.19	3.59	3.45	3.61	3.50	3.28	3.37	3.33	3.37	3.37	3.31	2.96	3.43	3.44	3.03
MnO	0.13	0.22	0.12	0.14	0.10	0.15	0.15	0.14	0.10	0.05	0.09	0.05	0.08	0.06	0.08	0.07	0.17	0.17	0.10	0.18	0.10
MgO	16.88	16.53	21.52	16.90	16.42	16.72	16.82	16.68	16.60	16.50	16.52	16.40	16.59	16.46	16.59	16.76	16.66	16.33	16.37	16.30	16.86
Cr2O3	0.37	0.21	0.37	0.34	0.32	0.05	0.22	0.27	0.19	0.21	0.34	0.23	0.24	0.23	0.36	0.32	0.30	0.09	0.28	0.19	0.22
CaO	22.76	23.60	15.17	23.14	23.79	24.99	23.74	23.61	23.43	23.50	23.51	24.14	23.62	23.95	24.05	23.40	23.69	24.89	24.01	23.82	24.87
Na2O	0.04	0.08	0.06	0.07	0.07	0.00	0.09	0.09	0.09	0.09	0.09	0.10	0.07	0.08	0.11	0.10	0.06	0.07	0.08	0.09	0.02
K2O	0.01	0.00	0.00	0.01	0.01	0.00	0.00	0.00	0.00	0.00	0.01	0.00	0.00	0.01	0.01	0.00	0.00	0.00	0.00	0.01	0.00
Total	99.92	100.08	100.18	99.63	100.00	99.96	99.91	100.11	99.37	99.42	99.72	99.58	99.36	99.54	100.21	99.64	99.73	99.26	99.58	99.54	100.35
Si	1.93	1.94	1.94	1.88	1.94	1.98	1.93	1.94	1.87	1.87	1.91	1.89	1.87	1.89	1.94	1.91	1.91	1.88	1.89	1.89	1.96
Al IV	0.07	0.06	0.06	0.11	0.06	0.02	0.07	0.06	0.10	0.10	0.09	0.10	0.10	0.10	0.06	0.09	0.09	0.05	0.10	0.10	0.04
Al VI	0.04	0.05	0.04	0.00	0.04	0.01	0.03	0.04	0.00	0.00	0.01	0.00	0.00	0.00	0.04	0.00	0.01	0.00	0.00	0.00	0.01
Ti	0.00	0.00	0.00	0.00	0.00	0.00	0.00	0.00	0.00	0.00	0.00	0.00	0.00	0.00	0.00	0.00	0.00	0.00	0.00	0.00	0.00
Fe3+	0.03	0.01	0.00	0.00	0.01	0.02	0.05	0.01	0.00	0.00	0.00	0.00	0.00	0.00	0.02	0.00	0.00	0.00	0.00	0.00	0.02
Fe2+	0.09	0.10	0.19	0.11	0.10	0.07	0.04	0.10	0.10	0.11	0.11	0.10	0.10	0.10	0.08	0.10	1.00	0.09	0.10	0.10	0.08
Mn	0.00	0.01	0.00	0.00	0.00	0.00	0.00	0.00	0.00	0.00	0.00	0.00	0.00	0.00	0.00	0.00	0.01	0.01	0.00	0.01	0.00
Mg	0.91	0.90	1.15	0.90	0.89	0.91	0.91	0.91	0.87	0.87	0.89	0.87	0.87	0.87	0.90	0.89	0.89	0.86	0.87	0.87	0.91
Cr	0.01	0.01	0.01	0.01	0.01	0.00	0.01	0.01	0.01	0.01	0.01	0.01	0.01	0.01	0.01	0.01	0.01	0.00	0.01	0.01	0.01
Ca	0.89	0.92	0.58	0.89	0.93	0.97	0.92	0.92	0.89	0.89	0.91	0.92	0.89	0.91	0.94	0.90	0.91	0.94	0.92	0.91	0.97
Na	0.00	0.01	0.00	0.00	0.00	0.00	0.01	0.01	0.01	0.01	0.01	0.01	0.00	0.01	0.01	0.01	0.00	0.00	0.01	0.01	0.00
K	0.00	0.00	0.00	0.00	0.00	0.00	0.00	0.00	0.00	0.00	0.00	0.00	0.00	0.00	0.00	0.00	0.00	0.00	0.00	0.00	0.00
Ens:	47.50	46.33	59.52	47.26	46.14	45.92	47.04	46.67	46.85	46.56	46.63	46.05	46.73	46.27	46.33	47.20	46.75	45.39	45.98	45.98	46.21
Fors.	6.47	6.14	10.33	6.23	5.82	4.76	5.24	5.86	5.62	5.79	5.69	5.25	5.45	5.35	5.41	5.44	5.48	4.88	5.56	5.73	4.81
Wol.	46.03	47.53	30.15	46.51	48.04	49.32	47.71	47.47	47.52	47.65	47.69	48.71	47.81	48.38	48.26	47.36	47.77	49.72	48.46	48.29	48.98
Mg*	88.35	88.90	85.44	89.12	89.08	91.02	90.39	89.23	89.73	88.79	88.95	89.72	89.72	89.73	89.77	89.94	47.20	90.49	89.72	89.66	90.84

continued

Table 2.2.4. (Continued)

	Clinopyroxenite			Gabbro with olivine										Wehrlite							
Sample	**20-10c**	**20-10r**	**20-11c**	**21-1c**	**21-1r**	**21-2c**	**21-2r**	**21-3c**	**21-4c**	**21-4r**	**21-5c**	**21-5r**	**22-1c**	**22-1r**	**22-2c**	**22-2r**	**22-3c**	**22-3r**	**22-4c**	**22-5c**
SiO2	53.20	53.01	53.06	52.53	52.80	52.86	53.01	52.91	52.88	52.87	52.74	53.19	53.11	53.48	52.86	52.91	52.84	52.87	53.15	53.44
Al2O3	2.42	2.46	2.41	2.81	2.60	2.23	2.27	2.40	2.50	2.32	2.66	2.21	2.41	2.52	2.36	2.48	2.48	2.40	2.45	2.13
TiO2	0.13	0.02	0.11	0.10	0.11	0.09	0.14	0.11	0.11	0.15	0.17	0.11	0.10	0.10	0.10	0.14	0.11	0.12	0.13	0.07
Fe2O3																				
FeO	3.49	3.35	3.26	4.44	5.68	4.41	4.81	4.46	4.62	4.28	4.34	4.13	3.52	4.40	3.46	3.37	3.44	3.25	3.50	3.78
MnO	0.21	0.11	0.16	0.11	0.20	0.12	0.15	0.13	0.18	0.19	0.18	0.17	0.10	0.06	0.16	0.09	0.07	0.06	0.18	0.10
MgO	16.34	16.33	16.50	15.74	17.14	16.12	16.14	15.75	16.00	15.83	15.88	15.97	16.56	17.93	16.34	16.16	16.20	16.21	16.65	17.07
Cr2O3	0.30	0.22	0.27	0.08	0.07	0.09	0.07	0.14	0.05	0.10	0.11	0.08	0.43	0.42	0.48	0.40	0.42	0.37	0.49	0.40
CaO	23.83	23.77	23.93	23.57	20.92	23.51	23.34	23.48	23.37	23.59	23.57	23.66	24.27	21.17	24.09	24.20	23.62	23.86	23.08	22.54
Na2O	0.10	0.11	0.10	0.13	0.13	0.15	0.12	0.16	0.12	0.16	0.17	0.17	0.11	0.08	0.07	0.10	0.09	0.15	0.11	0.10
K2O	0.01	0.00	0.00	0.03	0.02	0.01	0.03	0.02	0.00	0.00	0.02	0.02	0.00	0.01	0.02	0.00	0.00	0.00	0.01	0.00
Total	100.03	99.38	99.80	99.54	99.67	99.59	100.08	99.56	99.83	99.49	99.84	99.71	100.61	100.17	99.94	99.85	99.27	99.29	99.75	99.63
Si	1.94	1.87	1.92	1.88	1.90	1.89	1.94	1.90	1.92	1.89	1.91	1.92	1.93	1.94	1.92	1.92	1.86	1.86	1.91	1.91
Al IV	0.06	0.10	0.08	0.12	0.10	0.09	0.06	0.10	0.08	0.10	0.09	0.08	0.07	0.06	0.08	0.08	0.10	0.10	0.09	0.09
Al VI	0.05	0.00	0.02	0.00	0.01	0.00	0.04	0.00	0.02	0.00	0.03	0.01	0.03	0.05	0.03	0.02	0.00	0.00	0.02	0.00
Ti	0.00	0.00	0.00	0.00	0.00	0.00	0.00	0.00	0.00	0.00	0.00	0.00	0.00	0.00	0.00	0.00	0.00	0.00	0.00	0.00
Fe3+	0.00	0.00	0.00	0.00	0.00	0.00	0.02	0.00	0.10	0.00	0.10	0.00	0.03	0.00	0.05	0.08	0.00	0.00	0.00	0.00
Fe2+	0.10	0.10	0.10	0.13	0.17	0.13	0.12	0.13	0.04	0.13	0.03	0.12	0.07	0.14	0.05	0.02	0.10	0.10	0.11	0.11
Mn	0.01	0.00	0.00	0.00	0.01	0.00	0.00	0.00	0.01	0.01	0.01	0.01	0.00	0.00	0.00	0.00	0.00	0.00	0.01	0.00
Mg	0.89	0.86	0.89	0.84	0.92	0.86	0.88	0.84	0.87	0.84	0.86	0.86	0.90	0.97	0.89	0.87	0.85	0.85	0.89	0.91
Cr	0.01	0.01	0.01	0.00	0.00	0.00	0.00	0.00	0.00	0.00	0.00	0.00	0.01	0.01	0.01	0.01	0.01	0.01	0.01	0.01
Ca	0.93	0.90	0.93	0.90	0.80	0.90	0.91	0.90	0.91	0.90	0.92	0.91	0.94	0.82	0.94	0.94	0.89	0.90	0.89	0.86
Na	0.01	0.01	0.01	0.01	0.01	0.01	0.01	0.01	0.01	0.01	0.01	0.01	0.01	0.01	0.00	0.01	0.01	0.01	0.01	0.01
K	0.00	0.00	0.00	0.00	0.00	0.00	0.00	0.00	0.00	0.00	0.00	0.00	0.00	0.00	0.00	0.00	0.00	0.00	0.00	0.00
Ens:	45.97	46.19	46.33	44.68	48.32	45.34	45.22	44.75	45.09	44.86	44.92	45.13	45.96	50.30	45.79	45.53	46.10	46.03	47.17	48.16
Fors.	5.84	5.49	5.39	7.25	9.30	7.15	7.80	7.32	7.59	7.11	7.17	6.82	5.64	7.02	5.69	5.47	5.60	5.27	5.85	6.14
Wol.	48.18	48.32	48.28	48.08	42.38	47.52	46.99	47.94	47.32	48.04	47.91	48.05	48.40	42.68	48.51	49.00	48.30	48.69	46.98	45.70
Mg*	89.30	89.58	89.88	86.59	84.36	86.87	85.68	86.61	86.06	86.62	86.71	87.72	89.35	87.90	89.38	89.53	89.48	89.48	89.05	89.21

continued

Table 2.2.4. (Continued)

	Wherlite															Gabbro					
Sample	22-5r	22-6c	22-6r	22-7c	22-7r	23-1c	23-1r	23-2c	23-2r	23-3c	23-3r	23-4c	23-4r	23-5c	23-5r	24-1c	24-1r	24-2c	24-2r	24-3c	24-3r
SiO2	53.67	52.94	53.20	53.11	52.84	54.48	53.90	54.25	54.09	53.78	53.79	54.10	53.81	54.00	53.91	52.17	52.43	52.69	52.65	52.49	52.76
Al2O3	2.07	2.34	2.43	2.40	2.60	0.76	1.43	1.21	1.34	1.45	1.49	1.40	1.46	1.41	1.38	2.49	2.46	2.42	2.15	2.16	2.05
TiO2	0.06	0.05	0.11	0.10	0.10	0.04	0.06	0.06	0.06	0.10	0.05	0.05	0.08	0.09	0.08	0.22	0.14	0.22	0.23	0.18	0.24
Fe2O3																2.00	0.82	1.26	0.76	1.36	0.82
FeO	7.12	3.30	3.26	3.44	3.35	2.41	2.80	2.60	3.34	2.91	2.75	2.97	2.74	2.82	2.58	4.64	5.46	5.65	5.46	5.01	5.34
MnO	0.15	0.10	0.08	0.14	0.10	0.15	0.19	0.07	0.07	0.09	0.09	0.12	0.10	0.14	0.06	0.20	0.19	0.22	0.19	0.19	0.19
MgO	23.37	16.42	16.49	16.36	15.91	17.13	17.24	16.92	17.87	17.15	17.24	17.25	17.04	17.04	17.00	15.09	14.97	15.28	15.13	15.07	15.17
Cr2O3	0.46	0.45	0.37	0.48	0.45	0.18	0.22	0.26	0.32	0.27	0.33	0.25	0.26	0.29	0.35	0.04	0.05	0.04	0.01	0.05	0.05
CaO	13.80	24.01	23.78	24.01	23.88	25.10	23.91	24.56	22.76	24.05	24.27	23.68	24.01	23.98	24.25	23.01	23.07	22.52	23.22	23.09	23.27
Na2O	0.04	0.08	0.08	0.07	0.10	0.02	0.09	0.06	0.08	0.12	0.09	0.11	0.11	0.06	0.13	0.20	0.20	0.18	0.17	0.16	0.17
K2O	0.01	0.01	0.00	0.00	0.01	0.01	0.00	0.00	0.01	0.02	0.00	0.00	0.00	0.00	0.00	0.14	0.00	0.14	0.00	0.18	0.05
Total	100.75	99.70	99.80	100.11	99.34	100.28	99.84	99.99	99.94	99.94	100.10	99.93	99.61	99.83	99.74	100.20	99.79	100.62	99.97	99.94	100.11
Si	1.91	1.90	1.92	1.94	1.87	1.98	1.94	1.97	1.96	1.95	1.95	1.96	1.92	1.95	1.94	1.92	1.94	1.93	1.94	1.94	1.94
Al IV	0.09	0.10	0.08	0.06	0.11	0.02	0.06	0.03	0.04	0.05	0.05	0.04	0.06	0.05	0.06	0.08	0.06	0.07	0.06	0.06	0.06
Al VI	0.00	0.00	0.02	0.04	0.00	0.01	0.00	0.03	0.02	0.01	0.02	0.02	0.00	0.01	0.00	0.03	0.05	0.03	0.03	0.03	0.03
Ti	0.00	0.00	0.00	0.00	0.00	0.00	0.00	0.00	0.00	0.00	0.00	0.00	0.00	0.00	0.00	0.01	0.00	0.01	0.01	0.01	0.01
Fe3+	0.08	0.00	0.09	0.01	0.00	0.01	0.00	0.00	0.04	0.05	0.02	0.03	0.00	0.08	0.00	0.06	0.02	0.03	0.02	0.04	0.02
Fe2+	0.13	0.10	0.01	0.10	0.10	0.07	0.08	0.08	0.06	0.04	0.06	0.06	0.08	0.01	0.08	0.14	0.17	0.17	0.17	0.15	0.16
Mn	0.00	0.00	0.00	0.00	0.00	0.00	0.01	0.00	0.00	0.00	0.00	0.00	0.00	0.00	0.00	0.01	0.01	0.01	0.01	0.01	0.01
Mg	1.24	0.88	0.89	0.89	0.84	0.93	0.93	0.92	0.96	0.93	0.93	0.93	0.91	0.92	0.91	0.83	0.82	0.84	0.83	0.83	0.83
Cr	0.01	0.01	0.01	0.01	0.01	0.01	0.01	0.01	0.01	0.01	0.01	0.01	0.01	0.01	0.01	0.00	0.00	0.00	0.00	0.00	0.00
Ca	0.53	0.92	0.92	0.94	0.90	0.98	0.92	0.96	0.88	0.93	0.94	0.92	0.92	0.93	0.93	0.91	0.91	0.89	0.92	0.91	0.92
Na	0.00	0.01	0.01	0.00	0.01	0.00	0.01	0.00	0.01	0.01	0.01	0.01	0.01	0.00	0.01	0.01	0.01	0.01	0.01	0.01	0.01
K	0.00	0.00	0.00	0.00	0.00	0.00	0.00	0.00	0.00	0.00	0.00	0.00	0.00	0.00	0.00	0.01	0.00	0.01	0.00	0.01	0.00
Ens:	62.54	46.15	46.51	45.93	45.45	46.80	47.76	46.91	49.45	47.49	47.53	47.92	47.48	47.42	47.34	43.93	43.11	43.96	43.24	43.57	43.34
Fors.	10.92	5.36	5.29	5.64	5.53	3.93	4.65	4.15	5.29	4.66	4.39	4.82	4.44	4.62	4.12	7.92	9.13	9.47	9.07	8.44	8.86
Wol.	26.54	48.49	48.20	48.43	49.02	49.28	47.60	48.93	45.26	47.85	48.08	47.27	48.08	47.96	48.53	48.15	47.75	46.57	47.69	47.99	47.80
Mg*	85.41	89.79	90.02	89.45	89.33	92.69	92.05	92.07	90.51	91.31	91.79	91.19	91.89	91.51	91.92	80.58	81.19	80.77	81.37	81.37	82.18

continued

Table 2.2.4. (Continued)

	Gabbro										Wherlite										
Sample	**24-4c**	**24-4r**	**24-5c**	**24-5r**	**24-6c**	**24-6r**	**24-7c**	**24-7r**	**24-8c**	**24-8r**	**25-1c**	**25-1r**	**25-2c**	**25-2r**	**25-3c**	**25-3r**	**25-4c**	**25-4r**	**25-5c**	**25-5r**	**25-6c**
SiO2	54.21	54.11	52.00	53.13	52.57	52.90	52.76	52.63	52.79	52.60	51.87	52.00	51.90	53.39	51.75	51.69	51.81	51.52	51.72	52.04	51.29
Al2O3	0.59	0.67	2.34	1.56	2.39	2.08	2.39	2.26	2.24	2.39	3.55	3.36	3.85	3.09	3.41	3.46	3.65	3.52	3.78	3.14	3.85
TiO2	0.07	0.04	0.24	0.18	0.19	0.17	0.26	0.17	0.20	0.22	0.08	0.12	0.17	0.06	0.15	0.09	0.09	0.16	0.16	0.10	0.18
Fe2O3	0.71	0.01	1.29	0.00	0.75	1.06	0.93	1.12	0.74	1.03											
FeO	3.92	4.82	5.14	5.74	5.59	5.25	5.21	5.14	5.63	5.11	4.31	4.70	5.93	8.70	4.33	4.31	4.77	3.97	4.17	3.94	4.25
MnO	0.26	0.20	0.16	0.20	0.21	0.24	0.21	0.20	0.19	0.20	0.21	0.22	0.23	0.19	0.16	0.15	0.17	0.07	0.22	0.24	0.16
MgO	15.85	15.55	14.86	15.31	15.08	14.99	15.26	15.12	15.07	15.18	15.32	15.79	17.38	21.92	14.98	15.43	16.06	15.34	14.92	15.70	15.22
Cr2O3	0.01	0.00	0.04	0.03	0.03	0.06	0.05	0.04	0.06	0.06	0.92	0.82	0.95	0.69	0.72	0.81	0.81	0.90	0.81	0.68	0.96
CaO	24.97	24.88	22.96	23.08	22.95	23.13	23.31	23.13	23.07	23.20	23.82	22.57	19.14	11.69	23.32	23.58	21.99	23.63	23.67	23.82	23.61
Na2O	0.01	0.03	0.18	0.14	0.20	0.26	0.18	0.18	0.19	0.21	0.20	0.20	0.16	0.12	0.24	0.20	0.19	0.19	0.24	0.19	0.19
K2O	0.14	0.00	0.12	0.04	0.00	0.11	0.00	0.11	0.06	0.00	0.01	0.00	0.01	0.00	0.00	0.00	0.00	0.00	0.00	0.00	0.00
Total	100.74	100.31	99.33	99.41	99.96	100.25	100.56	100.10	100.24	100.20	100.29	99.78	99.72	99.85	99.06	99.72	99.54	99.30	99.69	99.85	99.71
Si	1.98	1.99	1.93	1.97	1.94	1.95	1.93	1.94	1.94	1.93	1.90	1.88	1.87	1.91	1.81	1.87	1.85	1.82	1.87	1.89	1.85
Al IV	0.02	0.01	0.07	0.03	0.06	0.05	0.07	0.06	0.06	0.07	0.10	0.12	0.13	0.09	0.14	0.15	0.15	0.15	0.13	0.11	0.15
Al VI	0.01	0.02	0.03	0.04	0.04	0.04	0.03	0.04	0.04	0.03	0.05	0.03	0.03	0.04	0.00	0.00	0.01	0.00	0.03	0.02	0.02
Ti	0.00	0.00	0.01	0.01	0.01	0.00	0.01	0.00	0.01	0.01	0.00	0.00	0.00	0.00	0.00	0.00	0.00	0.00	0.00	0.00	0.00
Fe3+	0.02	0.00	0.04	0.00	0.02	0.03	0.03	0.03	0.02	0.03	0.04	0.13	0.14	0.06	0.00	0.00	0.00	0.00	0.00	0.12	0.00
Fe2+	0.12	0.15	0.16	0.18	0.17	0.16	0.16	0.16	0.17	0.16	0.09	0.01	0.04	0.20	0.13	0.13	0.14	0.12	0.13	0.00	0.13
Mn	0.01	0.01	0.01	0.01	0.01	0.01	0.01	0.01	0.01	0.01	0.01	0.01	0.01	0.01	0.00	0.00	0.01	0.00	0.01	0.01	0.00
Mg	0.86	0.85	0.82	0.85	0.83	0.82	0.83	0.83	0.83	0.83	0.84	0.85	0.93	1.17	0.78	0.83	0.86	0.81	0.80	0.85	0.82
Cr	0.00	0.00	0.00	0.00	0.00	0.00	0.00	0.00	0.00	0.00	0.03	0.02	0.03	0.02	0.02	0.02	0.02	0.03	0.02	0.02	0.03
Ca	0.98	0.98	0.91	0.92	0.91	0.91	0.92	0.91	0.91	0.91	0.93	0.88	0.74	0.45	0.87	0.91	0.84	0.89	0.91	0.93	0.91
Na	0.00	0.00	0.01	0.01	0.01	0.02	0.01	0.01	0.01	0.02	0.01	0.01	0.01	0.01	0.02	0.01	0.01	0.01	0.02	0.01	0.01
K	0.01	0.00	0.01	0.00	0.00	0.01	0.00	0.01	0.00	0.00	0.00	0.00	0.00	0.00	0.00	0.00	0.00	0.00	0.00	0.00	0.00
Ens:	43.85	42.89	43.28	43.45	43.30	43.20	43.54	43.51	43.15	43.56	43.80	45.41	50.24	62.08	43.73	44.24	46.37	44.35	43.38	44.65	43.91
Fors.	6.50	7.78	8.66	9.46	9.34	8.88	8.68	8.62	9.37	8.56	7.25	7.94	9.99	14.13	7.35	7.18	8.00	6.55	7.16	6.67	7.14
Wol.	49.65	49.33	48.07	47.08	47.36	47.91	47.78	47.87	47.48	47.87	48.94	46.65	39.76	23.79	48.92	48.58	45.63	49.10	49.46	48.68	48.95
Mg*	86.00	85.00	80.39	82.52	81.37	81.19	81.37	81.37	81.37	81.37	86.37	85.69	83.94	81.79	85.73	86.47	85.95	87.07	86.06	87.66	86.31

continued

Table 2.2.4. (Continued)

	Wehrlite	Leuco-gabbro					Wehrlite													
Sample	25-6r	28-2c	28-4c	28-5c	28-6c	28-7c	29-1c	29-1r	29-2c	29-2r	29-3c	29-3r	29-4c	29-4r	29-5c	29-5r	29-6c	29-6r	29-7c	29-7r
SiO2	52.37	52.04	52.02	52.26	51.92	51.80	54.17	54.26	54.51	53.66	53.82	53.61	54.12	53.89	54.58	53.65	53.71	53.66	53.74	54.56
Al2O3	3.01	2.21	2.34	2.05	1.86	2.30	0.98	1.18	0.73	1.56	1.48	1.57	0.95	1.61	0.73	1.47	1.47	1.54	1.49	0.83
TiO2	0.08	0.26	0.24	0.24	0.18	0.26	0.00	0.02	0.07	0.03	0.07	0.07	0.04	0.03	0.03	0.03	0.08	0.04	0.07	0.04
Fe2O3							0.67	0.29	0.54	0.05	0.00	0.40	0.32	0.20	0.27	0.20	0.38	1.20	0.00	0.21
FeO	4.15	7.68	7.76	7.34	7.30	7.47	1.52	1.90	1.69	2.25	2.28	1.92	1.95	2.33	1.87	2.11	1.89	1.16	2.16	1.87
MnO	0.13	0.21	0.24	0.14	0.04	0.25	0.12	0.10	0.08	0.12	0.08	0.10	0.09	0.06	0.11	0.10	0.09	0.10	0.08	0.11
MgO	15.85	14.21	14.15	14.28	14.11	14.04	17.32	17.29	17.42	17.02	17.05	17.36	17.23	17.58	17.46	17.11	17.13	17.14	17.01	17.54
Cr2O3	0.71	0.05	0.03	0.06	0.06	0.00	0.46	0.43	0.21	0.81	0.83	0.87	0.38	0.81	0.33	0.74	0.66	0.85	0.83	0.24
CaO	22.90	22.99	23.12	23.00	22.94	23.06	24.79	24.48	24.80	24.18	24.09	23.98	24.63	23.65	24.75	24.20	24.43	24.30	24.40	24.78
Na2O	0.20	0.23	0.23	0.22	0.22	0.20	0.07	0.09	0.05	0.11	0.10	0.10	0.10	0.09	0.05	0.10	0.10	0.10	0.11	0.06
K2O	0.01	0.00	0.01	0.01	0.00	0.00	0.06	0.09	0.14	0.00	0.00	0.00	0.00	0.00	0.09	0.01	0.00	0.26	0.00	0.01
Total	99.41	99.88	100.14	99.60	98.63	99.38	100.16	100.13	100.24	99.79	99.80	99.98	99.81	100.25	100.27	99.72	99.94	100.35	99.89	100.25
Si	1.86	1.92	1.93	1.90	1.80	1.86	1.97	1.97	1.98	1.96	1.96	1.95	1.97	1.95	1.98	1.96	1.96	1.95	1.96	1.98
Al IV	0.13	0.08	0.07	0.09	0.08	0.10	0.03	0.03	0.02	0.04	0.04	0.05	0.03	0.05	0.02	0.04	0.04	0.05	0.04	0.02
Al VI	0.00	0.01	0.03	0.00	0.00	0.00	0.01	0.02	0.01	0.03	0.02	0.02	0.01	0.02	0.01	0.02	0.02	0.02	0.02	0.02
Ti	0.00	0.01	0.01	0.01	0.00	0.01	0.00	0.00	0.00	0.00	0.00	0.00	0.00	0.00	0.00	0.00	0.00	0.00	0.00	0.00
Fe3+	0.00	0.10	0.05	0.22	0.00	0.00	0.02	0.01	0.01	0.00	0.00	0.01	0.01	0.01	0.01	0.01	0.01	0.03	0.00	0.01
Fe2+	0.12	0.14	0.19	0.01	0.21	0.22	0.05	0.06	0.05	0.07	0.07	0.06	0.06	0.07	0.06	0.06	0.06	0.04	0.07	0.06
Mn	0.00	0.01	0.01	0.00	0.00	0.01	0.00	0.00	0.00	0.00	0.00	0.00	0.00	0.00	0.00	0.00	0.00	0.00	0.00	0.00
Mg	0.84	0.78	0.78	0.77	0.73	0.75	0.94	0.94	0.94	0.93	0.93	0.94	0.94	0.95	0.94	0.93	0.93	0.93	0.92	0.95
Cr	0.02	0.00	0.00	0.00	0.00	0.00	0.01	0.01	0.01	0.02	0.02	0.03	0.01	0.02	0.01	0.02	0.02	0.02	0.02	0.01
Ca	0.87	0.91	0.92	0.89	0.85	0.89	0.96	0.95	0.96	0.94	0.94	0.93	0.96	0.92	0.96	0.95	0.95	0.94	0.95	0.96
Na	0.01	0.02	0.02	0.02	0.01	0.01	0.01	0.01	0.00	0.01	0.01	0.01	0.01	0.01	0.00	0.01	0.01	0.01	0.01	0.00
K	0.00	0.00	0.00	0.00	0.00	0.00	0.00	0.00	0.01	0.00	0.00	0.00	0.00	0.00	0.00	0.00	0.00	0.01	0.00	0.00
Ens:	45.67	40.42	40.14	40.79	40.65	40.18	48.03	48.02	48.08	47.64	47.78	48.59	47.75	48.94	48.02	47.87	47.84	48.53	47.50	48.10
Fors.	6.92	12.59	12.73	11.99	11.86	12.40	2.56	3.13	2.71	3.72	3.71	3.18	3.18	3.73	3.05	3.48	3.11	2.01	3.52	3.04
Wol.	47.41	46.99	47.13	47.22	47.49	47.42	49.41	48.85	49.20	48.65	48.51	48.23	49.07	47.33	48.93	48.66	49.05	49.46	48.98	48.86
Mg*	87.49	76.74	76.48	77.62	77.61	77.36	93.07	93.07	94.00	93.00	93.00	93.07	93.07	92.23	93.07	93.00	93.00	93.00	92.93	93.14

continued

Table 2.2.4. (Continued)

	Gabbro																Leuco-gabbro				
Sample	31-1c	31-1r	31-2c	31-2r	31-3c	31-3r	31-4c	31-4r	31-5c	31-5r	31-6c	31-6r	31-7c	31-7r	31-8c	31-8r	35-2c	35-2r	35-3c	35-3r	35-5c
SiO2	52.67	52.80	52.73	52.67	52.55	52.49	52.74	52.69	52.66	52.72	52.94	53.37	52.34	52.82	52.82	52.73	52.45	52.58	52.39	52.44	52.09
Al2O3	2.22	1.62	2.07	2.10	2.35	2.23	2.20	2.28	2.06	1.97	1.57	1.93	2.29	2.08	2.01	1.92	2.48	2.47	2.49	2.37	2.45
TiO2	0.21	0.17	0.13	0.19	0.19	0.15	0.17	0.16	0.24	0.17	0.09	0.15	0.11	0.09	0.15	0.13	0.14	0.14	0.12	0.15	0.14
Fe2O3	1.33	0.78	1.37	0.33	0.97	0.96	0.66	1.05	0.29	0.58	0.23	0.00	0.84	0.57	0.28	0.68					
FeO	4.96	4.67	4.39	5.63	4.64	4.60	5.00	4.68	5.61	5.06	5.01	6.04	4.79	4.83	5.01	4.88	6.16	6.09	7.53	6.27	5.60
MnO	0.21	0.17	0.17	0.18	0.19	0.19	0.17	0.13	0.14	0.16	0.20	0.24	0.16	0.17	0.20	0.17	0.18	0.22	0.23	0.15	0.26
MgO	15.79	15.40	15.46	15.41	15.27	15.26	15.40	15.31	15.31	15.41	15.40	15.53	15.64	15.45	15.35	15.37	15.44	15.36	16.77	15.30	15.32
Cr2O3	0.10	0.11	0.07	0.16	0.25	0.15	0.12	0.10	0.12	0.11	0.09	0.12	0.10	0.10	0.11	0.09	0.02	0.05	0.01	0.01	0.00
CaO	22.44	23.54	23.26	22.67	23.25	23.27	23.11	23.47	22.89	23.16	23.38	22.67	22.57	23.30	23.39	23.06	22.48	22.83	20.12	23.13	23.37
Na2O	0.18	0.14	0.19	0.16	0.18	0.21	0.20	0.18	0.17	0.17	0.17	0.17	0.18	0.16	0.15	0.19	0.17	0.18	0.16	0.20	0.18
K2O	0.09	0.07	0.11	0.04	0.12	0.03	0.02	0.05	0.00	0.01	0.00	0.00	0.03	0.04	0.02	0.10	0.02	0.00	0.00	0.01	0.01
Total	100.20	99.47	99.95	99.54	99.96	99.54	99.79	100.10	99.49	99.52	99.08	100.22	99.05	99.61	99.49	99.32	99.54	99.92	99.82	100.03	99.42
Si	1.93	1.95	1.94	1.95	1.94	1.94	1.94	1.94	1.95	1.95	1.96	1.96	1.94	1.95	1.95	1.95	1.88	1.93	1.91	1.93	1.86
Al IV	0.07	0.05	0.06	0.05	0.06	0.06	0.06	0.06	0.05	0.05	0.03	0.04	0.06	0.05	0.05	0.05	0.11	0.07	0.09	0.07	0.10
Al VI	0.03	0.02	0.03	0.04	0.04	0.04	0.04	0.04	0.04	0.04	0.04	0.04	0.04	0.04	0.04	0.03	0.00	0.03	0.01	0.03	0.00
Ti	0.01	0.00	0.00	0.01	0.01	0.00	0.00	0.00	0.01	0.00	0.00	0.00	0.00	0.00	0.00	0.00	0.00	0.00	0.00	0.00	0.00
Fe3+	0.04	0.02	0.04	0.01	0.03	0.03	0.02	0.03	0.01	0.02	0.01	0.00	0.02	0.02	0.01	0.02	0.00	0.06	0.13	0.04	0.00
Fe2+	0.15	0.14	0.14	0.17	0.14	0.14	0.15	0.14	0.17	0.16	0.16	0.19	0.15	0.15	0.16	0.15	0.19	0.12	0.10	0.15	0.17
Mn	0.01	0.01	0.01	0.01	0.01	0.01	0.01	0.00	0.01	0.01	0.01	0.01	0.01	0.01	0.01	0.01	0.01	0.01	0.01	0.00	0.01
Mg	0.86	0.85	0.85	0.85	0.84	0.84	0.85	0.84	0.84	0.85	0.85	0.85	0.86	0.85	0.85	0.85	0.83	0.84	0.91	0.84	0.81
Cr	0.00	0.00	0.00	0.00	0.01	0.00	0.00	0.00	0.00	0.00	0.00	0.00	0.00	0.00	0.00	0.00	0.00	0.00	0.00	0.00	0.00
Ca	0.88	0.93	0.92	0.90	0.92	0.92	0.91	0.92	0.91	0.92	0.93	0.89	0.90	0.92	0.93	0.91	0.87	0.90	0.78	0.91	0.89
Na	0.01	0.01	0.01	0.01	0.01	0.02	0.01	0.01	0.01	0.01	0.01	0.01	0.01	0.01	0.01	0.01	0.01	0.01	0.01	0.01	0.01
K	0.00	0.00	0.01	0.00	0.01	0.00	0.00	0.00	0.00	0.00	0.00	0.00	0.00	0.00	0.00	0.00	0.00	0.00	0.00	0.00	0.00
Ens:	45.33	43.95	44.51	44.07	44.01	44.00	44.10	43.89	43.75	44.04	43.83	43.93	45.15	44.14	43.73	44.19	43.92	43.50	47.13	43.07	43.27
Fors.	8.34	7.75	7.37	9.32	7.82	7.76	8.32	7.75	9.23	8.37	8.32	9.97	8.02	8.03	8.34	8.16	10.12	10.03	12.24	10.14	9.29
Wol.	46.32	48.30	48.12	46.60	48.17	48.24	47.58	48.36	47.01	47.59	47.85	46.10	46.83	47.83	47.92	47.65	45.96	46.47	40.63	46.79	47.44
Mg*	81.90	84.16	82.52	82.52	83.17	83.17	83.33	83.17	82.35	82.52	83.33	81.73	83.50	83.33	83.33	83.33	81.32	81.81	79.88	81.31	82.73

continued

Table 2.2.4. (Continued)

	Leuco-gabbro					Gabbro with olivine										Wherlite				
Sample	35-5r	35-6c	35-6r	35-9c	35-9r	36-1c	36-1r	36-2c	36-2r	36-3c	36-3r	36-4c	36-4r	36-5c	36-5r	37-1c	37-1r	37-2c	37-3c	37-3r
SiO2	52.82	52.55	52.50	52.31	52.90	52.74	52.90	53.00	52.91	52.87	53.16	53.68	52.93	52.94	53.02	52.05	51.45	51.68	52.17	51.75
Al2O3	2.04	2.40	2.03	2.42	1.88	2.61	2.56	2.06	2.47	2.63	2.17	2.38	2.29	2.57	2.44	3.22	3.18	3.16	2.95	3.06
TiO2	0.13	0.13	0.17	0.14	0.11	0.14	0.12	0.13	0.15	0.11	0.11	0.08	0.09	0.15	0.16	0.20	0.26	0.22	0.22	0.21
Fe2O3																				
FeO	5.65	6.14	5.56	6.38	5.44	4.67	4.53	4.43	4.98	4.71	4.86	9.03	4.26	4.47	4.21	5.31	5.09	5.07	6.08	5.09
MnO	0.31	0.15	0.24	0.24	0.22	0.17	0.12	0.13	0.15	0.15	0.08	0.19	0.09	0.16	0.20	0.23	0.24	0.17	0.18	0.09
MgO	15.49	15.78	15.21	15.58	15.58	15.92	15.80	15.82	16.22	15.72	15.74	22.92	15.99	15.77	15.75	15.92	15.48	15.03	17.14	15.34
Cr2O3	0.00	0.02	0.02	0.08	0.01	0.09	0.16	0.15	0.17	0.17	0.16	0.14	0.16	0.23	0.13	0.41	0.52	0.41	0.53	0.42
CaO	23.22	22.23	23.45	21.93	23.43	23.46	23.75	23.71	22.57	23.19	23.68	11.87	23.55	23.72	23.67	22.52	22.84	23.10	19.96	23.38
Na2O	0.14	0.17	0.17	0.16	0.13	0.19	0.17	0.18	0.16	0.17	0.14	0.07	0.14	0.16	0.16	0.16	0.20	0.18	0.14	0.18
K2O	0.01	0.00	0.01	0.00	0.01	0.03	0.03	0.00	0.00	0.01	0.02	0.01	0.00	0.00	0.01	0.00	0.01	0.00	0.00	0.00
Total	99.81	99.57	99.36	99.24	99.71	100.02	100.14	99.61	99.78	99.73	100.12	100.37	99.50	100.17	99.75	100.02	99.27	99.02	99.37	99.52
Si	1.92	1.89	1.87	1.85	1.91	1.93	1.93	1.90	1.92	1.91	1.95	1.93	1.89	1.94	1.91	1.91	1.82	1.81	1.85	1.85
Al IV	0.08	0.10	0.09	0.10	0.08	0.07	0.07	0.09	0.08	0.09	0.05	0.07	0.10	0.06	0.09	0.09	0.13	0.13	0.12	0.13
Al VI	0.01	0.00	0.00	0.00	0.00	0.04	0.04	0.00	0.02	0.02	0.04	0.03	0.00	0.05	0.02	0.05	0.00	0.00	0.00	0.00
Ti	0.00	0.00	0.00	0.00	0.00	0.00	0.00	0.00	0.00	0.00	0.00	0.00	0.00	0.00	0.00	0.01	0.01	0.01	0.01	0.01
Fe3+	0.11	0.00	0.00	0.00	0.17	0.03	0.02	0.00	0.11	0.14	0.01	0.04	0.00	0.01	0.13	0.03	0.00	0.00	0.00	0.00
Fe2+	0.06	0.18	0.17	0.19	0.00	0.11	0.12	0.13	0.04	0.00	0.14	0.23	0.13	0.12	0.00	0.13	0.15	0.15	0.18	0.15
Mn	0.01	0.00	0.01	0.01	0.01	0.01	0.00	0.00	0.00	0.00	0.00	0.01	0.00	0.00	0.01	0.01	0.01	0.01	0.01	0.00
Mg	0.84	0.85	0.81	0.82	0.84	0.87	0.86	0.85	0.88	0.85	0.86	1.23	0.85	0.86	0.85	0.87	0.82	0.78	0.90	0.82
Cr	0.00	0.00	0.00	0.00	0.00	0.00	0.00	0.00	0.00	0.00	0.00	0.00	0.00	0.01	0.00	0.01	0.01	0.01	0.01	0.01
Ca	0.91	0.86	0.89	0.83	0.91	0.92	0.93	0.91	0.88	0.90	0.93	0.46	0.90	0.93	0.92	0.88	0.87	0.87	0.76	0.90
Na	0.01	0.01	0.01	0.01	0.01	0.01	0.01	0.01	0.01	0.01	0.01	0.00	0.01	0.01	0.01	0.01	0.01	0.01	0.01	0.01
K	0.00	0.00	0.00	0.00	0.00	0.00	0.00	0.00	0.00	0.00	0.00	0.00	0.00	0.00	0.00	0.00	0.00	0.00	0.00	0.00
Ens:	43.61	44.72	43.07	44.45	43.77	44.85	44.54	44.67	45.93	44.77	44.30	62.58	45.23	44.53	44.70	45.21	44.38	43.48	48.98	43.77
Fors.	9.42	10.00	9.22	10.60	8.92	7.65	7.35	7.22	8.15	7.77	7.80	14.12	6.90	7.34	7.02	8.83	8.57	8.51	10.04	8.29
Wol.	46.98	45.28	47.72	44.96	47.30	47.50	48.11	48.11	45.92	47.46	47.90	23.29	47.87	48.13	48.28	45.96	47.05	48.02	40.99	47.94
Mg*	83.02	82.45	82.61	81.22	83.62	85.87	86.15	86.68	85.31	85.61	85.24	81.90	86.73	86.28	86.96	84.24	84.48	83.94	83.41	84.52

continued

Table 2.2.4. (Continued)

	Wehrlite																	
Sample	37-4c	37-4r	37-5c	37-5r	46-1c	46-1r	46-2c	46-2r	46-3c	46-3r	46-4c	46-4r	46-5c	46-5r	46-6c	46-6r	46-7c	46-7r
SiO2	51.69	51.66	51.61	51.52	53.73	53.92	53.91	53.86	54.01	53.90	53.67	54.05	53.38	53.78	53.57	53.95	53.78	53.98
Al2O3	3.43	3.17	3.31	3.37	1.19	1.14	1.18	1.19	1.18	1.16	1.16	1.16	1.19	1.20	1.21	1.17	1.16	1.13
TiO2	0.23	0.25	0.24	0.21	0.06	0.01	0.07	0.07	0.04	0.09	0.04	0.04	0.06	0.07	0.07	0.03	0.05	0.04
Fe2O3					1.14	0.45	0.23	0.18	0.65	0.17	0.48	0.37	1.39	0.80	1.14	0.80	0.17	0.34
FeO	4.75	5.13	5.09	4.77	1.80	2.46	2.69	2.85	2.74	2.60	2.49	3.05	1.80	2.26	2.05	17.26	2.58	2.34
MnO	0.21	0.12	0.11	0.13	0.11	0.12	0.07	0.11	0.11	0.12	0.08	0.11	0.05	0.07	0.10	0.11	0.12	0.06
MgO	15.08	15.47	15.38	15.17	17.14	17.14	17.27	17.38	18.97	17.18	17.19	18.83	17.59	17.58	18.07	17.26	17.13	17.23
Cr2O3	0.55	0.51	0.53	0.48	0.63	0.65	0.59	0.60	0.59	0.57	0.65	0.62	0.58	0.66	0.61	0.61	0.63	0.59
CaO	23.30	22.78	23.05	23.69	23.91	24.10	23.65	23.49	21.20	23.92	23.79	21.46	23.14	23.11	22.84	23.93	23.97	23.85
Na2O	0.21	0.17	0.15	0.14	0.10	0.10	0.09	0.09	0.09	0.12	0.12	0.10	0.11	0.10	0.11	0.11	0.09	0.11
K2O	0.00	0.01	0.00	0.01	0.24	0.00	0.08	0.01	0.12	0.00	0.00	0.00	0.17	0.21	0.00	0.17	0.00	0.14
Total	99.45	99.27	99.47	99.49	100.05	100.09	99.83	99.83	99.70	99.83	99.67	99.79	99.46	99.84	99.77	115.40	99.68	99.81
Si	1.84	1.83	1.85	1.84	1.96	1.96	1.97	1.97	1.96	1.97	1.96	1.96	1.95	1.96	1.95	1.96	1.97	1.97
Al IV	0.14	0.13	0.14	0.14	0.04	0.04	0.03	0.03	0.04	0.03	0.04	0.04	0.05	0.04	0.05	0.04	0.03	0.03
Al VI	0.00	0.00	0.00	0.00	0.01	0.01	0.02	0.02	0.01	0.02	0.01	0.01	0.00	0.01	0.00	0.01	0.02	0.02
Ti	0.01	0.01	0.01	0.01	0.00	0.00	0.00	0.00	0.00	0.00	0.00	0.00	0.00	0.00	0.00	0.00	0.00	0.00
Fe3+	0.00	0.00	0.00	0.00	0.03	0.01	0.01	0.00	0.02	0.00	0.01	0.01	0.04	0.02	0.03	0.02	0.00	0.01
Fe2+	0.14	0.15	0.15	0.14	0.06	0.07	0.08	0.09	0.08	0.08	0.08	0.09	0.05	0.07	0.06	0.06	0.08	0.07
Mn	0.01	0.00	0.00	0.00	0.00	0.00	0.00	0.00	0.00	0.00	0.00	0.00	0.00	0.00	0.00	0.00	0.00	0.00
Mg	0.80	0.82	0.82	0.81	0.93	0.93	0.94	0.94	1.03	0.93	0.94	1.02	0.96	0.96	0.98	0.94	0.93	0.94
Cr	0.02	0.01	0.01	0.01	0.02	0.02	0.02	0.02	0.02	0.02	0.02	0.02	0.02	0.02	0.02	0.02	0.02	0.02
Ca	0.89	0.86	0.88	0.91	0.93	0.94	0.92	0.92	0.83	0.93	0.93	0.84	0.91	0.90	0.89	0.93	0.94	0.93
Na	0.01	0.01	0.01	0.01	0.01	0.01	0.01	0.01	0.01	0.01	0.01	0.01	0.01	0.01	0.01	0.01	0.01	0.01
K	0.00	0.00	0.00	0.00	0.01	0.00	0.00	0.00	0.01	0.00	0.00	0.00	0.01	0.01	0.00	0.01	0.00	0.01
Ens:	43.57	44.47	44.12	43.41	48.41	47.74	48.22	48.38	52.98	47.86	48.10	52.26	49.89	49.53	50.63	48.47	47.75	48.23
Fors.	8.04	8.47	8.37	7.87	3.04	4.03	4.31	4.61	4.47	4.26	4.04	4.92	2.94	3.68	3.38	3.24	4.22	3.77
Wol.	48.38	47.06	47.51	48.72	48.55	48.23	47.47	47.01	42.54	47.88	47.86	42.82	47.17	46.80	45.99	48.29	48.03	48.00
Mg*	85.14	84.46	84.54	85.26	91.18	92.08	91.26	91.26	91.15	92.08	91.26	91.07	91.43	91.43	91.59	92.16	92.08	92.16

Table 2.2.5. Results of electron micro-probe analyses of chromites from ultramafic cumulates

Sample	5-1c	5-2c	5-3c	5-4c	5-5c	5-6c	5-7c	12-1c	12-2c	12-3c	12-4c	12-5c	15-1c	15-2c	15-3c	15-4c
SiO2	0.05	0.04	0.02	0.03	0.40	0.04	0.05	0.12	0.09	0.15	0.14	0.10	0.08	0.09	0.12	0.06
TiO2	0.15	0.12	0.18	0.11	0.16	0.17	0.13	0.21	0.21	0.15	0.23	0.26	0.24	0.22	0.25	0.14
Al2O3	8.90	9.12	8.95	8.94	8.84	9.24	9.16	10.27	10.45	10.46	10.49	10.57	10.30	10.83	11.29	10.83
Cr2O3	60.33	60.95	60.28	59.76	60.08	60.54	61.02	55.60	56.16	55.41	55.45	55.24	52.09	51.51	49.48	50.00
FeO	18.99	16.90	18.63	19.65	19.01	17.37	17.36	25.30	23.55	24.65	24.39	25.33	28.41	28.64	30.88	31.03
MnO	0.34	0.23	0.24	0.36	0.29	0.18	0.27	0.44	0.52	0.40	0.37	0.47	0.44	0.43	0.53	0.48
MgO	10.69	12.10	10.84	10.48	10.89	11.87	11.90	7.79	8.47	8.21	8.29	7.50	7.68	7.37	6.48	6.57
CaO	0.00	0.01	0.02	0.03	0.10	0.00	0.02	0.02	0.00	0.00	0.00	0.00	0.01	0.00	0.00	0.00
Na2O	0.00	0.00	0.00	0.01	0.01	0.01	0.00	0.01	0.00	0.03	0.00	0.01	0.01	0.02	0.03	0.00
K2O	0.01	0.00	0.01	0.00	0.00	0.00	0.01	0.00	0.00	0.01	0.01	0.02	0.00	0.01	0.00	0.00
Total	99.46	99.47	99.17	99.37	99.78	99.42	99.92	99.76	99.45	99.47	99.37	99.50	99.26	99.12	99.06	99.11
Si	0.01	0.01	0.01	0.01	0.11	0.01	0.01	0.03	0.02	0.04	0.04	0.03	0.02	0.02	0.03	0.02
Ti	0.03	0.02	0.04	0.02	0.03	0.03	0.03	0.04	0.04	0.03	0.05	0.05	0.05	0.04	0.05	0.03
Al	2.76	2.80	2.76	2.78	2.75	2.84	2.84	3.26	3.28	3.29	3.29	3.34	3.28	3.43	3.60	3.46
Cr	12.56	12.55	12.46	12.45	12.55	12.48	12.69	11.85	11.82	11.71	11.68	11.72	11.12	10.95	10.58	10.73
Fe	4.18	3.68	4.07	4.33	4.20	3.79	3.82	5.71	5.24	5.51	5.44	5.69	6.41	6.44	6.98	7.04
Mn	0.08	0.05	0.05	0.08	0.06	0.04	0.06	0.10	0.12	0.09	0.08	0.11	0.10	0.10	0.12	0.11
Mg	4.20	4.70	4.23	4.12	4.29	4.61	4.67	3.13	3.36	3.27	3.29	3.00	3.09	2.95	2.61	2.66
Ca	0.00	0.00	0.01	0.01	0.03	0.00	0.01	0.01	0.00	0.00	0.00	0.00	0.00	0.00	0.00	0.00
Na	0.00	0.00	0.00	0.01	0.01	0.01	0.00	0.01	0.00	0.02	0.00	0.01	0.01	0.01	0.02	0.00
K	0.00	0.00	0.00	0.00	0.00	0.00	0.00	0.00	0.00	0.00	0.00	0.01	0.00	0.00	0.00	0.00
Cr*	81.97	81.76	81.88	81.77	82.01	81.47	81.71	78.41	78.29	78.04	78.00	77.81	77.23	76.14	74.62	75.59
Fm*	49.91	43.93	49.08	51.26	49.47	45.08	45.00	64.56	60.93	62.74	62.27	65.45	67.48	68.55	72.77	72.60
Mg*	50.09	56.07	50.92	48.74	50.53	54.92	55.00	35.44	39.07	37.26	37.73	34.55	32.52	31.45	27.23	27.40

Numbers of ions on the basis of 32 (O), c and r indicate "core" and "rim" respectively

APPENDIX 2.3

Microprobe results of the minerals from the volcanic rocks

Table 2.3.1. Results electron micro-probe analyses of the clinopyroxenes from the tholeiitic basalts

Sample	211-1c	211-1b	211-1r	211-2c	211-2b	211-2r	211-3c	211-3b	211-3r	214-1c	214-1b	214-1r	214-2c	214-2b	214-2r	214-3c	214-3b
SiO2	51.01	50.35	50.52	50.05	50.33	50.92	49.74	51.36	51.09	49.82	49.74	51.06	50.30	50.78	51.26	50.36	50.27
Al2O3	2.24	2.79	2.79	3.34	3.32	2.50	3.53	2.08	2.40	3.86	4.09	2.55	3.59	3.12	2.25	3.21	3.19
TiO2	0.52	0.63	0.75	0.64	0.72	0.56	0.81	0.50	0.49	0.87	0.82	0.50	0.79	0.66	0.58	0.73	0.71
FeO	11.34	10.09	10.09	10.68	10.81	10.11	10.90	10.03	10.07	10.97	10.40	10.67	10.95	10.75	10.27	10.20	10.21
MnO	0.24	0.16	0.22	0.32	0.23	0.17	0.28	0.26	0.29	0.32	0.29	0.24	0.25	0.31	0.26	0.32	0.30
MgO	15.61	15.20	15.21	14.64	14.86	15.59	15.19	16.15	15.80	15.27	14.61	15.72	15.32	15.51	15.69	15.38	15.22
Cr2O3	0.03	0.00	0.04	0.00	0.03	0.02	0.13	0.01	0.03	0.12	0.11	0.02	0.14	0.04	0.01	0.08	0.09
CaO	18.20	20.17	20.12	20.01	19.26	19.60	19.28	18.92	19.01	18.44	19.44	19.02	18.43	18.57	19.26	19.34	19.23
Na2O	0.30	0.30	0.26	0.34	0.29	0.27	0.26	0.24	0.26	0.29	0.31	0.25	0.29	0.30	0.30	0.26	0.23
K2O	0.03	0.00	0.01	0.00	0.01	0.03	0.00	0.00	0.00	0.00	0.00	0.02	0.00	0.00	0.00	0.00	0.00
Total	99.52	99.69	100.01	100.02	99.86	99.77	100.12	99.55	99.44	99.96	99.81	100.05	100.06	100.04	99.88	99.88	99.45
Si	1.85	1.84	1.88	1.86	1.86	1.86	1.85	1.86	1.84	1.85	1.83	1.89	1.87	1.88	1.89	1.86	1.81
Al IV	0.09	0.12	0.12	0.14	0.14	0.11	0.15	0.08	0.10	0.15	0.17	0.11	0.13	0.12	0.10	0.13	0.14
Al VI	0.00	0.00	0.00	0.01	0.00	0.00	0.00	0.00	0.00	0.02	0.01	0.00	0.02	0.02	0.00	0.00	0.00
Ti	0.01	0.02	0.02	0.02	0.02	0.02	0.02	0.01	0.01	0.02	0.02	0.01	0.02	0.02	0.02	0.02	0.02
Fe3+	0.32	0.27	0.10	0.12	0.15	0.22	0.12	0.30	0.35	0.12	0.19	0.09	0.08	0.08	0.15	0.16	0.35
Fe2+	0.02	0.04	0.21	0.21	0.18	0.09	0.22	0.00	0.00	0.22	0.13	0.24	0.26	0.25	0.17	0.16	0.00
Mn	0.01	0.00	0.01	0.01	0.01	0.01	0.01	0.01	0.01	0.01	0.01	0.01	0.01	0.01	0.01	0.01	0.01
Mg	0.84	0.83	0.84	0.81	0.82	0.85	0.84	0.87	0.85	0.84	0.80	0.87	0.85	0.86	0.86	0.84	0.82
Cr	0.00	0.00	0.00	0.00	0.00	0.00	0.00	0.00	0.00	0.00	0.00	0.00	0.00	0.00	0.00	0.00	0.00
Ca	0.71	0.79	0.80	0.80	0.76	0.77	0.77	0.73	0.73	0.73	0.77	0.76	0.73	0.74	0.76	0.76	0.74
Na	0.02	0.02	0.02	0.02	0.02	0.02	0.02	0.02	0.02	0.02	0.02	0.02	0.02	0.02	0.02	0.02	0.02
K	0.00	0.00	0.00	0.00	0.00	0.00	0.00	0.00	0.00	0.00	0.00	0.00	0.00	0.00	0.00	0.00	0.00
Ens:	44.36	42.88	42.90	41.60	42.59	43.99	43.01	45.47	44.79	43.81	42.25	44.27	43.96	44.24	44.27	43.72	43.57
Fors.	18.46	16.22	16.32	17.54	17.75	16.27	17.76	16.25	16.48	18.17	17.35	17.24	18.03	17.70	16.67	16.78	16.88
Wol.	37.17	40.89	40.78	40.86	39.66	39.74	39.23	38.28	38.73	38.02	40.40	38.49	38.01	38.06	39.06	39.50	39.56
Mg*	71.05	72.87	72.88	70.96	71.02	73.33	71.30	74.17	73.67	71.28	71.47	72.43	71.38	72.01	73.15	72.89	72.66

Numbers of ions on the basis of 6 (O). C, r and b indicate "core", "between" and "rim" respectively

continued

Table 2.3.1. (Continued)

Sample	214-3r	214-4c	214-4b	214-4r	214-5c	214-5b	214-5r	214-6c	214-6b	214-6r	214-7c	214-7b	214-7r
SiO2	51.22	49.64	49.74	51.32	49.84	51.04	51.35	50.04	50.48	51.04	50.20	49.07	51.47
Al2O3	2.52	3.86	4.08	2.33	4.03	2.83	2.34	3.74	3.39	2.65	3.57	4.00	2.49
TiO2	0.50	0.78	0.73	0.54	0.79	0.60	0.56	0.81	0.68	0.50	0.70	0.96	0.51
FeO	10.31	10.67	10.61	10.08	10.82	10.35	10.19	10.42	10.53	10.46	11.26	10.47	10.14
MnO	0.29	0.18	0.24	0.37	0.19	0.26	0.31	0.27	0.17	0.24	0.30	0.27	0.27
MgO	15.51	15.11	14.67	15.44	14.65	15.45	15.58	15.18	14.91	15.74	14.73	14.71	15.69
Cr2O3	0.00	0.14	0.14	0.04	0.10	0.05	0.03	0.12	0.03	0.04	0.15	0.08	0.03
CaO	19.36	18.99	19.59	19.53	19.20	18.92	19.08	19.61	19.28	18.80	18.39	18.93	18.93
Na2O	0.25	0.24	0.30	0.26	0.27	0.34	0.28	0.31	0.31	0.29	0.52	0.23	0.25
K2O	0.02	0.01	0.00	0.00	0.00	0.01	0.03	0.01	0.00	0.01	0.01	0.02	0.03
Total	99.98	99.62	100.10	99.91	99.89	99.85	99.75	100.51	99.78	99.77	99.83	98.74	99.81
Si	1.90	1.81	1.85	1.90	1.84	1.88	1.88	1.85	1.85	1.87	1.85	1.71	1.89
Al IV	0.10	0.16	0.15	0.10	0.16	0.12	0.10	0.15	0.15	0.11	0.15	0.17	0.11
Al VI	0.01	0.00	0.03	0.00	0.02	0.00	0.00	0.01	0.00	0.00	0.00	0.00	0.00
Ti	0.01	0.02	0.02	0.02	0.02	0.02	0.02	0.02	0.02	0.01	0.02	0.03	0.01
Fe3+	0.09	0.29	0.10	0.12	0.13	0.15	0.20	0.12	0.19	0.19	0.19	0.67	0.16
Fe2+	0.23	0.04	0.23	0.19	0.20	0.17	0.11	0.21	0.14	0.13	0.16	0.00	0.16
Mn	0.01	0.01	0.01	0.01	0.01	0.01	0.01	0.01	0.01	0.01	0.01	0.01	0.01
Mg	0.86	0.82	0.81	0.85	0.81	0.85	0.85	0.84	0.82	0.86	0.81	0.76	0.86
Cr	0.00	0.00	0.00	0.00	0.00	0.00	0.00	0.00	0.00	0.00	0.00	0.00	0.00
Ca	0.77	0.74	0.78	0.77	0.76	0.75	0.75	0.78	0.76	0.74	0.73	0.71	0.74
Na	0.02	0.02	0.02	0.02	0.02	0.02	0.02	0.02	0.02	0.02	0.04	0.02	0.02
K	0.00	0.00	0.00	0.00	0.00	0.00	0.00	0.00	0.00	0.00	0.00	0.00	0.00
Ens:	43.85	43.37	42.11	43.69	42.31	44.14	44.28	43.04	42.88	44.65	42.78	42.84	44.66
Fors.	16.82	17.47	17.47	16.59	17.84	17.01	16.75	17.01	17.27	17.03	18.84	17.55	16.62
Wol.	39.33	39.17	40.41	39.71	39.85	38.85	38.97	39.95	39.85	38.32	38.38	39.61	38.72
Mg*	72.84	71.63	71.14	73.20	70.71	72.69	73.16	72.20	71.63	72.85	69.99	71.47	73.40

Table 2.3.2. Results of electron micro-probe analyses of the clinopyroxenes from alkali basalts

Sample	289-1c	289-1r	289-2c	289-2r	289-3c	289-3r	289-4c	289-4r	289-5c	289-6	289-7c	289-7r	289-8c	289-8r
SiO2	43.60	43.58	49.11	45.81	48.59	47.99	47.27	46.87	48.55	46.28	49.14	44.38	46.80	45.95
Al2O3	8.59	8.59	4.56	6.98	5.14	5.44	6.26	6.86	5.27	7.02	4.42	7.89	6.36	7.17
TiO2	4.20	4.11	1.94	2.79	1.89	2.19	1.91	2.26	1.76	2.65	2.02	3.47	2.52	2.55
Fe2O3	4.09	4.33	2.31	3.93	2.27	3.25	3.18	3.06	2.57	2.86	2.46	3.98	3.22	4.91
FeO	4.68	4.54	4.82	4.13	4.27	3.53	3.32	3.95	3.71	4.05	4.83	4.08	4.22	2.87
MnO	0.15	0.16	0.13	0.10	0.12	0.14	0.10	0.09	0.06	0.13	0.15	0.11	0.11	0.07
MgO	11.29	11.19	13.71	12.27	13.73	13.44	13.23	12.91	13.75	12.70	13.93	11.80	12.82	12.54
Cr2O3	0.00	0.00	0.00	0.00	0.52	0.40	0.64	0.34	0.88	0.37	0.01	0.04	0.18	0.19
CaO	22.08	22.19	22.68	22.65	22.63	22.59	22.62	22.63	22.93	22.67	22.43	22.64	22.64	22.66
Na2O	0.58	0.57	0.43	0.42	0.42	0.46	0.41	0.43	0.38	0.40	0.37	0.42	0.38	0.43
K2O	0.00	0.02	0.00	0.07	0.00	0.22	0.12	0.01	0.08	0.00	0.11	0.00	0.10	0.30
Total	99.25	99.30	99.69	99.15	99.58	99.64	99.04	99.41	99.92	99.12	99.86	98.80	99.36	99.65
Si	1.65	1.65	1.83	1.73	1.81	1.79	1.77	1.75	1.80	1.74	1.83	1.68	1.76	1.72
Al IV	0.35	0.35	0.17	0.27	0.19	0.21	0.23	0.25	0.20	0.26	0.17	0.32	0.24	0.28
Al VI	0.03	0.03	0.03	0.04	0.04	0.03	0.05	0.05	0.03	0.05	0.02	0.03	0.04	0.04
Ti	0.12	0.12	0.05	0.08	0.05	0.06	0.05	0.06	0.05	0.07	0.06	0.10	0.07	0.07
Fe3+	0.12	0.12	0.06	0.11	0.06	0.09	0.09	0.09	0.07	0.08	0.07	0.11	0.09	0.14
Fe2+	0.15	0.14	0.15	0.13	0.13	0.11	0.10	0.12	0.12	0.13	0.15	0.13	0.13	0.09
Mn	0.00	0.01	0.00	0.00	0.00	0.00	0.00	0.00	0.00	0.00	0.00	0.00	0.00	0.00
Mg	0.64	0.63	0.76	0.69	0.76	0.75	0.74	0.72	0.76	0.71	0.77	0.67	0.72	0.70
Cr	0.00	0.00	0.00	0.00	0.02	0.01	0.02	0.01	0.03	0.01	0.00	0.00	0.01	0.01
Ca	0.90	0.90	0.91	0.91	0.90	0.90	0.91	0.91	0.91	0.91	0.89	0.92	0.91	0.91
Na	0.04	0.04	0.03	0.03	0.03	0.03	0.03	0.03	0.03	0.03	0.03	0.03	0.03	0.03
K	0.00	0.00	0.00	0.00	0.00	0.01	0.01	0.00	0.00	0.00	0.01	0.00	0.00	0.01
Ens:	37.78	37.57	41.81	39.67	42.29	42.35	42.12	41.05	42.50	40.51	42.42	38.78	40.66	41.14
Fors.	9.07	8.87	8.48	7.69	7.60	6.49	6.11	7.22	6.54	7.49	8.50	7.72	7.71	5.43
Wol.	53.14	53.56	49.71	52.65	50.11	51.16	51.77	51.74	50.96	52.00	49.08	53.50	51.63	53.44
Mg*	70.33	70.79	78.35	74.19	80.00	78.95	79.57	77.42	80.00	77.17	77.78	73.63	76.60	75.27

Numbers of ions on the basis of 6 (O). c and r indicate "core" and "rim" respectively

Table 2.3.3. Results of electron micro-probe analyses of clinopyroxenes from the tholeiitic diabases

Sample	140-1c	140-1b	140-1r	140-2c	140-2b	140-2r	140-3c	140-3b	140-3r	140-5c	140-5b	140-5r	140-6c	140-6b	140-6r
SiO2	51.46	51.87	51.00	45.55	51.46	51.09	49.50	51.27	51.35	50.79	50.98	50.82	49.41	50.13	51.09
Al2O3	2.37	2.11	2.37	5.04	2.25	2.25	3.93	2.48	1.92	2.55	2.74	2.65	3.94	3.13	2.38
TiO2	0.56	0.47	0.56	0.36	0.48	0.58	0.88	0.52	0.53	0.64	0.67	0.60	0.74	0.67	0.52
FeO	9.92	10.14	10.08	15.07	9.81	10.12	11.44	10.19	10.26	10.47	9.85	10.32	10.34	10.04	10.11
MnO	0.23	0.28	0.28	0.38	0.32	0.32	0.30	0.26	0.34	0.24	0.32	0.27	0.20	0.33	0.28
MgO	16.11	16.31	15.48	14.80	16.13	15.36	15.27	15.89	15.70	15.42	15.68	15.63	14.63	15.24	15.77
Cr2O3	0.12	0.11	0.00	0.07	0.08	0.03	0.16	0.09	0.00	0.03	0.00	0.00	0.15	0.07	0.01
CaO	19.42	18.75	19.35	14.11	18.94	19.55	18.12	18.87	19.29	19.87	19.63	19.34	19.77	19.58	19.21
Na2O	0.20	0.20	0.23	0.71	0.24	0.23	0.28	0.26	0.22	0.26	0.25	0.26	0.28	0.22	0.24
K2O	0.01	0.01	0.00	0.00	0.02	0.00	0.00	0.00	0.00	0.00	0.01	0.01	0.01	0.00	0.02
Total	100.40	100.25	99.35	96.09	99.73	99.53	99.88	99.83	99.61	100.27	100.13	99.90	99.47	99.41	99.63
Si	1.90	1.92	1.83	1.41	1.88	1.85	1.83	1.88	1.87	1.88	1.89	1.87	1.79	1.80	1.85
Al IV	0.10	0.08	0.10	0.18	0.09	0.10	0.17	0.11	0.08	0.11	0.11	0.12	0.16	0.20	0.11
Al VI	0.00	0.01	0.00	0.00	0.00	0.00	0.00	0.00	0.00	0.00	0.01	0.00	0.00	0.14	0.00
Ti	0.02	0.01	0.02	0.01	0.01	0.02	0.02	0.01	0.01	0.02	0.02	0.02	0.02	0.00	0.01
Fe3+	0.08	0.06	0.39	1.83	0.21	0.30	0.17	0.16	0.26	0.11	0.09	0.16	0.37	0.38	0.27
Fe2+	0.22	0.25	0.00	0.00	0.09	0.01	0.18	0.16	0.05	0.21	0.22	0.16	0.00	0.00	0.04
Mn	0.01	0.01	0.01	0.01	0.01	0.01	0.01	0.01	0.01	0.01	0.01	0.01	0.01	0.01	0.01
Mg	0.89	0.90	0.83	0.68	0.88	0.83	0.84	0.87	0.85	0.85	0.86	0.86	0.79	0.82	0.85
Cr	0.00	0.00	0.00	0.00	0.00	0.00	0.00	0.00	0.00	0.00	0.00	0.00	0.00	0.00	0.00
Ca	0.77	0.74	0.74	0.47	0.74	0.76	0.72	0.74	0.75	0.79	0.78	0.76	0.77	0.75	0.75
Na	0.01	0.01	0.02	0.04	0.02	0.02	0.02	0.02	0.02	0.02	0.02	0.02	0.02	0.02	0.02
K	0.00	0.00	0.00	0.00	0.00	0.00	0.00	0.00	0.00	0.00	0.00	0.00	0.00	0.00	0.00
Ens:	45.05	45.78	43.98	44.04	45.53	43.55	43.78	45.00	44.21	43.18	44.18	44.07	42.10	43.38	44.54
Fors.	15.92	16.41	16.51	25.79	16.05	16.61	18.89	16.60	16.75	16.83	16.08	16.75	17.02	16.56	16.47
Wol.	39.03	37.82	39.51	30.17	38.42	39.84	37.33	38.40	39.04	39.99	39.74	39.18	40.88	40.05	38.99
Mg*	74.33	74.15	68.22	27.15	74.56	73.02	70.41	73.55	73.18	72.42	73.95	72.97	68.23	68.20	73.55

Numbers of ions on the basis of & (O): C, b and r indicate "core", "between" and "rim" respectively

Table 2.3.4. Results of electron micro-probe analyses of plagioclases from the tholeiitic basalts

Sample	143-2c	143-2r	143-3c	143-3r	143-3c	143-4c	143-4r	143-5	143-6	143-7	143-8	143-9	143-10	143-11	143-12	143-13	143-14	214-1	214-2
SiO2	68.58	67.86	68.30	68.64	68.58	68.47	68.69	68.51	68.43	68.16	68.60	68.57	68.75	68.60	69.61	74.75	68.38	60.19	67.88
Al2O3	19.72	19.84	19.62	19.69	19.52	19.70	19.59	19.65	19.52	19.62	19.56	19.76	19.69	19.86	18.68	15.73	19.49	18.65	19.65
FeO	0.12	0.13	0.22	0.10	0.09	0.01	0.06	0.04	0.12	0.11	0.00	0.00	0.04	0.23	0.21	0.08	0.14	5.24	0.42
MgO	0.03	0.06	0.03	0.00	0.01	0.00	0.01	0.01	0.00	0.01	0.00	0.00	0.00	0.00	0.02	0.01	0.02	3.79	0.29
CaO	0.10	0.15	0.15	0.10	0.15	0.15	0.15	0.24	0.14	0.14	0.09	0.08	0.10	0.19	0.49	0.09	0.10	0.15	0.10
Na2O	11.82	11.32	11.48	11.92	11.78	11.63	11.83	11.65	11.85	11.56	11.75	11.81	11.72	11.61	11.06	9.80	11.69	9.45	11.62
K2O	0.16	0.24	0.19	0.12	0.14	0.05	0.07	0.02	0.06	0.06	0.04	0.02	0.09	0.01	0.04	0.04	0.04	0.07	0.00
Total	100.53	99.59	99.99	100.57	100.27	100.01	100.40	100.12	100.12	99.66	100.04	100.24	100.39	100.50	100.11	100.49	99.86	97.54	99.96
Si	2.98	2.98	2.99	2.98	2.99	2.99	2.99	2.99	2.98	2.99	2.99	2.98	2.99	2.98	3.06	3.32	2.99	2.72	2.97
AlIV	0.02	0.02	0.01	0.02	0.01	0.01	0.01	0.01	0.02	0.01	0.01	0.02	0.01	0.02	0.00	0.00	0.01	0.28	0.03
AlVI	0.99	1.01	1.00	0.98	0.99	1.00	0.99	1.00	0.98	1.00	1.00	1.00	1.00	1.00	1.02	1.15	1.00	0.71	0.98
Ti	0.00	0.00	0.00	0.00	0.00	0.00	0.00	0.00	0.00	0.00	0.00	0.00	0.00	0.00	0.00	0.00	0.00	0.00	0.00
Fe2+	0.00	0.00	0.01	0.00	0.00	0.00	0.00	0.00	0.00	0.00	0.00	0.00	0.00	0.01	0.01	0.00	0.01	0.20	0.02
Mn	0.00	0.00	0.00	0.00	0.00	0.00	0.00	0.00	0.00	0.00	0.00	0.00	0.00	0.00	0.00	0.00	0.00	0.00	0.00
Mg	0.00	0.00	0.00	0.00	0.00	0.00	0.00	0.00	0.00	0.00	0.00	0.00	0.00	0.00	0.00	0.00	0.00	0.26	0.02
Ca	0.00	0.01	0.01	0.00	0.01	0.01	0.01	0.01	0.01	0.01	0.00	0.00	0.00	0.01	0.02	0.00	0.00	0.01	0.00
Na	0.99	0.96	0.97	1.00	0.99	0.98	1.00	0.99	1.00	0.98	0.99	1.00	0.99	0.98	0.94	0.84	0.99	0.83	0.98
K	0.01	0.01	0.01	0.01	0.01	0.00	0.00	0.00	0.00	0.00	0.00	0.00	0.00	0.00	0.00	0.00	0.00	0.00	0.00
Or	0.88	1.37	1.05	0.66	0.77	0.28	0.39	0.10	0.33	0.34	0.22	0.11	0.50	0.06	0.23	0.27	0.22	0.48	0.00
Ab	98.66	97.91	98.24	98.90	98.54	99.01	98.92	98.76	99.02	99.00	99.36	99.52	99.03	99.05	97.38	99.23	99.31	98.65	99.51
An	0.46	0.73	0.71	0.45	0.69	0.71	0.69	1.14	0.65	0.66	0.42	0.37	0.47	0.90	2.38	0.50	0.47	0.87	0.49

Numbers of ions on the basis of 8(O), c and r indicate "core" and "rim" respectively

continued

Table 2.3.4. (Continued)

Sample	214-3	214-4	214-5	214-6	214-7c	214-7r	214-8	214-9	214-10	214-11	214-12	214-13	214-14	214-15	214-16	214-17
SiO2	67.94	67.21	68.50	68.69	68.53	68.46	68.53	68.12	67.94	68.23	67.22	68.79	68.71	68.70	68.16	68.24
Al2O3	19.64	19.81	19.79	19.74	19.78	19.72	19.76	19.65	19.63	19.88	19.67	19.84	19.72	19.64	19.66	19.55
FeO	0.44	0.54	0.16	0.21	0.15	0.15	0.27	0.47	0.36	0.17	0.57	0.26	0.22	0.15	0.43	0.19
MgO	0.19	0.20	0.02	0.00	0.00	0.00	0.02	0.12	0.07	0.00	0.43	0.03	0.00	0.00	0.07	0.00
CaO	0.19	0.91	0.13	0.09	0.16	0.20	0.16	0.08	0.13	0.10	0.30	0.10	0.07	0.10	0.16	0.13
Na2O	11.80	11.39	11.59	11.89	11.73	11.79	11.91	11.72	11.39	11.94	11.34	12.20	11.85	11.81	11.96	11.53
K2O	0.01	0.03	0.02	0.01	0.01	0.00	0.03	0.02	0.16	0.05	0.09	0.08	0.03	0.02	0.03	0.03
Total	100.21	100.09	100.21	100.63	100.36	100.32	100.68	100.18	99.68	100.37	99.62	101.30	100.60	100.42	100.47	99.67
Si	2.96	2.94	2.99	2.98	2.98	2.98	2.97	2.97	2.98	2.96	2.95	2.96	2.98	2.99	2.96	2.99
AlIV	0.04	0.06	0.01	0.02	0.02	0.02	0.03	0.03	0.02	0.04	0.05	0.04	0.02	0.01	0.04	0.01
AlVI	0.97	0.96	1.01	0.99	1.00	0.99	0.98	0.98	1.00	0.98	0.97	0.96	0.99	0.99	0.96	1.00
Ti	0.00	0.00	0.00	0.00	0.00	0.00	0.00	0.00	0.00	0.00	0.00	0.00	0.00	0.00	0.00	0.00
Fe2+	0.02	0.02	0.01	0.01	0.01	0.01	0.01	0.02	0.01	0.01	0.02	0.01	0.01	0.01	0.02	0.01
Mn	0.00	0.00	0.00	0.00	0.00	0.00	0.00	0.00	0.00	0.00	0.00	0.00	0.00	0.00	0.00	0.00
Mg	0.01	0.01	0.00	0.00	0.00	0.00	0.00	0.01	0.00	0.00	0.03	0.00	0.00	0.00	0.00	0.00
Ca	0.01	0.04	0.01	0.00	0.01	0.01	0.01	0.00	0.01	0.00	0.01	0.00	0.00	0.00	0.01	0.01
Na	1.00	0.97	0.98	1.00	0.99	0.99	1.00	0.99	0.97	1.01	0.96	1.02	1.00	1.00	1.01	0.98
K	0.00	0.00	0.00	0.00	0.00	0.00	0.00	0.00	0.01	0.00	0.01	0.00	0.00	0.00	0.00	0.00
Or																
Ab	99.06	95.61	99.27	99.53	99.20	99.08	99.10	99.51	98.47	99.27	98.05	99.12	99.51	99.42	99.10	99.21
An	0.88	4.22	0.62	0.42	0.75	0.92	0.74	0.38	0.62	0.46	1.43	0.45	0.32	0.47	0.73	0.62

Table 2.3.5. Results of electron micro-probe analyses of plagioclases from the diabase

	Diabase																
Sample	**140-1c**	**140-1r**	**140-2c**	**140-2r**	**140-3**	**140-4**	**140-5**	**140-6c**	**140-6r**	**140-7c**	**140-7r**	**140-8c**	**140-8r**	**140-9**	**140-10**	**140-11**	**140-12**
SiO2	68.72	68.23	68.63	68.55	68.05	68.53	68.85	67.88	68.45	67.98	68.26	68.46	68.28	68.24	68.45	68.11	68.27
Al2O3	19.52	19.63	19.81	19.80	19.67	19.60	19.73	19.75	19.54	19.81	19.64	19.91	19.92	19.83	19.86	19.81	19.86
FeO	0.15	0.02	0.07	0.18	0.13	0.15	0.04	0.08	0.04	0.00	0.09	0.10	0.06	0.06	0.12	0.12	0.03
MgO	0.00	0.00	0.00	0.02	0.00	0.04	0.00	0.00	0.00	0.02	0.01	0.01	0.01	0.04	0.01	0.00	0.04
CaO	0.18	0.21	0.06	0.21	0.17	0.10	0.05	0.40	0.09	0.16	0.15	0.14	0.21	0.24	0.15	0.25	0.20
Na2O	11.74	11.45	11.92	11.81	11.89	11.93	11.76	11.70	11.67	11.86	11.83	11.82	11.66	11.49	11.80	11.55	11.52
K2O	0.04	0.04	0.06	0.06	0.12	0.10	0.00	0.03	0.08	0.07	0.04	0.02	0.05	0.10	0.07	0.02	0.15
Total	100.35	99.58	100.55	100.63	100.03	100.45	100.43	99.84	99.87	99.90	100.02	100.46	100.19	100.00	100.46	99.86	100.07
Si	2.99	3.00	2.98	2.97	2.97	2.97	2.99	2.97	2.99	2.97	2.98	2.97	2.98	2.98	2.97	2.98	2.98
AlIV	0.01	0.00	0.02	0.03	0.03	0.03	0.01	0.03	0.01	0.03	0.02	0.03	0.02	0.02	0.03	0.02	0.02
AlVI	0.99	1.01	0.99	0.99	0.98	0.98	1.00	0.99	1.00	0.98	0.99	0.99	1.00	1.00	0.99	1.00	1.00
Ti	0.00	0.00	0.00	0.00	0.00	0.00	0.00	0.00	0.00	0.00	0.00	0.00	0.00	0.00	0.00	0.00	0.00
Fe2+	0.01	0.00	0.00	0.01	0.00	0.01	0.00	0.00	0.00	0.00	0.00	0.00	0.00	0.00	0.00	0.00	0.00
Mn	0.00	0.00	0.00	0.00	0.00	0.00	0.00	0.00	0.00	0.00	0.00	0.00	0.00	0.00	0.00	0.00	0.00
Mg	0.00	0.00	0.00	0.00	0.00	0.00	0.00	0.00	0.00	0.00	0.00	0.00	0.00	0.00	0.00	0.00	0.00
Ca	0.01	0.01	0.00	0.01	0.01	0.00	0.00	0.02	0.00	0.01	0.01	0.01	0.01	0.01	0.01	0.01	0.01
Na	0.99	0.97	1.00	0.99	1.00	1.00	0.99	0.99	0.99	1.00	1.00	1.00	0.99	0.97	0.99	0.98	0.98
K	0.00	0.00	0.00	0.00	0.01	0.01	0.00	0.00	0.00	0.00	0.00	0.00	0.00	0.01	0.00	0.00	0.01
Or																	
Ab	98.94	98.79	99.39	98.70	98.57	99.00	99.77	97.98	99.13	98.88	99.09	99.24	98.74	98.30	98.92	98.71	98.22
An	0.84	0.99	0.28	0.97	0.78	0.46	0.23	1.85	0.42	0.74	0.69	0.65	0.98	1.13	0.69	1.18	0.94

numbers of ions on the basis of 8(O), c and r indicate "core" and "rim" respectively

Table 2.3.6. Results of electron micro-probe analyses of chlorites from the tholeiitic basalts and diabases

	Diabase		Basalt											
Sample	**140-1**	**140-2**	**211-1**	**211-2**	**211-3**	**211-4**	**211-5**	**211-6**	**211-7**	**211-8**	**211-9**	**211-10**	**211-11**	**211-12**
SiO2	30.92	31.10	29.13	29.27	29.65	29.21	29.32	30.35	32.44	31.17	30.21	31.97	31.36	31.36
TiO2	0.00	0.07	0.02	0.03	0.02	0.00	0.00	0.02	0.01	0.03	0.03	0.00	0.04	0.02
Al2O3	14.90	15.20	14.24	14.70	14.22	15.25	14.09	14.51	14.80	14.58	15.65	14.99	15.63	14.67
Cr2O3	0.02	0.00	0.01	0.00	0.01	0.00	0.01	0.00	0.03	0.00	0.00	0.00	0.03	0.00
FeO	26.36	26.02	22.69	21.32	21.33	21.26	21.59	21.46	22.14	23.00	22.00	22.11	21.82	22.33
MnO	0.23	0.30	0.40	0.31	0.30	0.46	0.35	0.38	0.34	0.44	0.47	0.35	0.35	0.33
MgO	14.97	15.18	16.17	17.83	16.97	17.59	17.47	17.21	17.50	16.92	18.13	17.43	18.18	17.33
CaO	0.69	0.70	0.94	0.67	0.88	0.46	0.93	0.88	0.96	0.93	0.50	0.77	0.64	0.89
Na2O	0.03	0.02	0.07	0.10	0.08	0.08	0.07	0.05	0.08	0.05	0.06	0.09	0.08	0.04
K2O	0.04	0.05	0.14	0.14	0.09	0.09	0.17	0.23	0.14	0.06	0.06	0.12	0.07	0.15
H2O	11.84	11.37	16.19	15.63	16.45	15.60	16.01	14.92	11.56	12.83	12.90	12.16	11.81	12.87
Total	100.00	100.01	100.00	100.00	100.00	100.00	100.01	100.01	100.00	100.01	100.01	99.99	100.01	99.99
Si	6.48	6.47	6.36	6.29	6.43	6.27	6.35	6.46	6.61	6.51	6.28	6.56	6.41	6.52
Al	3.68	3.72	3.66	3.72	3.64	3.86	3.60	3.64	3.56	3.59	3.83	3.63	3.76	3.59
Ti	0.00	0.01	0.00	0.00	0.00	0.00	0.00	0.00	0.00	0.00	0.00	0.00	0.01	0.00
Cr	0.00	0.00	0.00	0.00	0.00	0.00	0.00	0.00	0.00	0.00	0.00	0.00	0.00	0.00
Fe2+	4.62	4.52	4.14	3.83	3.87	3.81	3.91	3.82	3.77	4.01	3.82	3.80	3.73	3.88
Mn	0.04	0.05	0.07	0.06	0.06	0.08	0.06	0.07	0.06	0.08	0.08	0.06	0.06	0.06
Mg	4.68	4.71	5.26	5.71	5.49	5.63	5.64	5.46	5.32	5.26	5.62	5.34	5.54	5.37
Ca	0.15	0.16	0.22	0.15	0.20	0.11	0.22	0.20	0.21	0.21	0.11	0.17	0.14	0.20
Na	0.02	0.02	0.06	0.08	0.07	0.07	0.06	0.04	0.06	0.04	0.05	0.07	0.06	0.03
K	0.02	0.03	0.08	0.08	0.05	0.05	0.09	0.12	0.07	0.03	0.03	0.06	0.04	0.08
OH	16.55	15.76	23.58	22.39	23.79	22.31	23.12	21.16	15.71	17.86	17.88	16.65	16.09	17.84
Fe*	0.50	0.49	0.44	0.40	0.41	0.40	0.41	0.41	0.42	0.43	0.40	0.42	0.40	0.42
Mg*	0.50	0.51	0.56	0.60	0.59	0.60	0.59	0.59	0.58	0.57	0.60	0.58	0.60	0.58
Type	Diabantite	Diabantite	Diabantite	Diabantite	Diabantite	Diabantite	Diabantite	Diabantite	Diabantite	Diabantite	Diabantite	Diabantite	Diabantite	Diabantite

Numbers of ions on the basis of 28 (O)

APPENDIX 2.4

Microprobe results of the minerals from the metamorphic sole

Table 2.4.1. Results of electron micro-probe analyses of the epidotes from the metamorphic sole

Sample	327-1c	327-1b	327-1r	327-2c	327-2b	327-2r	327-3c	327-3b	327-3r	327-4c	327-4b	327-4r	27-4.1c	27-4.2c	27-4.3c	27-4.3r	27-4.4c	27-4.4r	327-5c	327-5b	327-5r
SiO2	37.18	37.44	37.86	37.31	37.41	37.40	37.74	37.49	37.70	37.73	37.68	37.81	37.39	37.94	37.55	37.73	37.69	37.86	37.78	37.96	37.84
TiO2	0.36	0.35	0.30	0.15	0.17	0.21	0.21	0.05	0.18	0.17	0.15	0.25	0.17	0.17	0.18	0.07	0.22	0.11	0.08	0.04	0.05
Al2O3	22.18	22.11	24.04	23.88	24.37	24.58	25.41	24.93	24.64	24.61	24.74	24.71	24.53	24.85	24.01	24.64	25.12	24.67	24.65	25.17	24.82
Cr2O3	0.01	0.00	0.02	0.00	0.05	0.12	0.05	0.23	0.33	0.21	0.19	0.32	0.22	0.21	0.13	0.19	0.21	0.16	0.00	0.01	0.02
FeO	12.95	13.27	11.14	11.35	11.13	10.39	9.75	11.14	10.57	10.83	10.96	10.48	10.30	10.41	11.29	10.78	10.17	10.90	10.92	10.02	10.34
MnO	0.10	0.10	0.16	0.20	0.12	0.12	0.24	0.24	0.16	0.24	0.14	0.33	0.20	0.15	0.25	0.26	0.16	0.24	0.29	0.14	0.15
MgO	0.02	0.00	0.03	0.03	0.09	0.05	0.06	0.07	0.05	0.06	0.06	0.06	0.05	0.04	0.07	0.08	0.00	0.06	0.04	0.00	0.00
CaO	23.99	23.61	23.86	23.99	23.81	23.73	23.76	23.38	23.44	23.56	23.20	23.88	23.96	23.52	23.43	23.05	23.40	23.16	23.75	23.82	23.56
Na2O	0.00	0.03	0.01	0.00	0.00	0.00	0.00	0.02	0.01	0.00	0.00	0.00	0.02	0.00	0.02	0.03	0.00	0.01	0.00	0.01	0.00
K2O	0.02	0.00	0.01	0.00	0.03	0.00	0.00	0.00	0.00	0.00	0.01	0.00	0.00	0.01	0.00	0.00	0.00	0.00	0.01	0.01	0.00
H2O	3.18	3.10	2.58	3.10	2.83	3.40	2.80	2.46	2.93	2.60	2.88	2.17	3.17	2.70	3.08	3.18	3.03	2.84	2.50	2.83	3.24
Total	99.99	100.01	100.01	100.01	100.01	100.00	100.02	100.01	100.01	100.01	100.01	100.01	100.01	100.00	100.01	100.01	100.00	100.01	100.02	100.01	100.02
Si	2.88	2.90	2.91	2.86	2.87	2.84	2.88	2.89	2.88	2.90	2.88	2.92	2.85	2.90	2.88	2.88	2.87	2.90	2.91	2.89	2.88
Ti	0.02	0.02	0.02	0.01	0.01	0.01	0.01	0.00	0.01	0.01	0.01	0.01	0.01	0.01	0.01	0.00	0.01	0.01	0.00	0.00	0.00
Al IV	0.12	0.10	0.09	0.14	0.13	0.16	0.12	0.11	0.12	0.10	0.12	0.08	0.15	0.10	0.12	0.12	0.13	0.10	0.09	0.11	0.12
Al VI	1.90	1.92	2.10	2.03	2.08	2.05	2.16	2.15	2.10	2.13	2.11	2.16	2.06	2.14	2.05	2.09	2.12	2.12	2.14	2.16	2.10
Cr	0.00	0.00	0.00	0.00	0.00	0.01	0.00	0.01	0.02	0.01	0.01	0.02	0.01	0.01	0.01	0.01	0.01	0.01	0.00	0.00	0.00
Fe	0.84	0.86	0.72	0.73	0.71	0.66	0.62	0.72	0.68	0.70	0.70	0.68	0.66	0.67	0.72	0.69	0.65	0.70	0.70	0.64	0.66
Mn	0.01	0.01	0.01	0.01	0.01	0.01	0.02	0.02	0.01	0.02	0.01	0.02	0.01	0.01	0.02	0.02	0.01	0.02	0.02	0.01	0.01
Mg	0.00	0.00	0.00	0.00	0.01	0.01	0.01	0.01	0.01	0.01	0.01	0.01	0.01	0.00	0.01	0.01	0.00	0.01	0.00	0.00	0.00
Ca	1.99	1.96	1.97	1.97	1.96	1.93	1.94	1.93	1.92	1.94	1.90	1.97	1.96	1.93	1.92	1.88	1.91	1.90	1.96	1.95	1.92
Na	0.00	0.00	0.00	0.00	0.00	0.00	0.00	0.00	0.00	0.00	0.00	0.00	0.00	0.00	0.00	0.00	0.00	0.00	0.00	0.00	0.00
K	0.00	0.00	0.00	0.00	0.00	0.00	0.00	0.00	0.00	0.00	0.00	0.00	0.00	0.00	0.00	0.00	0.00	0.00	0.00	0.00	0.00
OH	1.64	1.60	1.32	1.59	1.45	1.72	1.42	1.26	1.49	1.33	1.47	1.12	1.61	1.38	1.57	1.62	1.54	1.45	1.28	1.44	1.64

Numbers of ions on the basis of 12.5 (O). c, b and r indicate "core", "between" and "rim" respectively

Table 2.4.2. Results of electron micro-probe analyses of the amphiboles from the metamorphic sole

Sample	131-1c	131-1r	131-2c	131-2r	131-3c	131-3r	131-4c	131-5c	131-5r	131-6c	131-7c	131-7r	131-8c	131-8r	131-9c	131-9r	131-10c	131-10r	132-1c	132-1r	132-2c
SiO2	44.82	44.63	44.58	44.99	44.79	44.31	44.20	44.73	44.16	44.36	44.34	43.86	43.52	42.86	43.30	42.73	42.78	41.19	40.48	42.71	42.12
Al2O3	11.75	11.77	11.99	11.60	11.51	11.70	11.83	11.51	12.07	11.75	11.92	11.68	11.70	12.10	11.76	11.92	12.13	11.67	11.24	11.59	11.04
TiO2	1.21	1.20	1.29	1.50	1.07	1.33	1.33	1.09	1.18	1.15	1.40	1.50	1.27	1.53	1.33	1.57	1.34	1.41	1.47	1.42	1.24
FeO	12.36	12.64	12.43	12.26	12.38	12.49	12.55	12.29	12.45	12.47	12.59	12.60	12.53	12.43	12.78	12.60	12.44	12.33	12.60	12.75	12.79
Cr2O3	0.15	0.16	0.13	0.13	0.17	0.09	0.11	0.11	0.14	0.20	0.03	0.10	0.06	0.23	0.12	0.17	0.15	0.12	0.09	0.00	0.00
MnO	0.20	0.16	0.23	0.18	0.20	0.15	0.29	0.24	0.15	0.26	0.23	0.18	0.15	0.09	0.21	0.17	0.18	0.25	0.20	0.12	0.23
MgO	13.76	13.72	13.72	14.07	14.09	13.84	13.77	13.88	13.60	13.68	13.49	13.53	13.63	13.50	13.48	13.44	13.41	13.29	13.11	13.29	13.63
CaO	10.93	10.83	11.07	10.99	10.95	10.88	10.84	10.90	10.97	10.96	10.96	11.12	10.98	10.98	10.95	10.88	10.94	11.08	11.27	11.32	11.02
Na2O	1.94	1.95	1.96	1.98	1.86	1.95	1.93	1.89	2.00	1.91	1.98	2.03	1.96	2.05	2.03	2.06	2.05	2.13	1.99	1.93	1.93
K2O	0.32	0.32	0.33	0.33	0.32	0.31	0.31	0.29	0.33	0.32	0.39	0.30	0.34	0.37	0.33	0.32	0.33	0.30	0.32	0.36	0.34
H2O	2.55	2.63	2.26	1.99	2.66	2.98	2.84	3.08	2.95	2.95	2.68	3.09	3.87	3.85	3.72	4.14	4.26	6.24	7.24	4.53	5.66
Total	99.99	100.01	99.99	100.02	100.00	100.03	100.00	100.01	100.00	100.01	100.01	99.99	100.01	99.99	100.01	100.00	100.01	100.01	100.01	100.02	100.00
Si	6.49	6.46	6.48	6.55	6.48	6.39	6.40	6.44	6.38	6.41	6.43	6.34	6.24	6.16	6.23	6.12	6.12	5.80	5.66	6.10	5.96
AlIV	1.51	1.54	1.52	1.45	1.52	1.61	1.60	1.56	1.62	1.59	1.57	1.66	1.76	1.84	1.77	1.88	1.88	1.94	1.85	1.90	1.84
AlVI	0.50	0.47	0.54	0.54	0.44	0.38	0.41	0.39	0.43	0.41	0.46	0.33	0.22	0.20	0.22	0.14	0.16	0.00	0.00	0.05	0.00
Ti	0.13	0.13	0.14	0.16	0.12	0.14	0.14	0.12	0.13	0.12	0.15	0.16	0.14	0.17	0.14	0.17	0.14	0.15	0.15	0.15	0.13
Fe3+	0.00	0.00	0.00	0.00	0.00	0.00	0.00	0.00	0.00	0.00	0.00	0.00	0.00	0.00	0.00	0.00	0.00	0.00	0.00	0.00	0.00
Fe2+	1.50	1.53	1.51	1.49	1.50	1.51	1.52	1.48	1.50	1.51	1.53	1.52	1.50	1.49	1.54	1.51	1.49	1.45	1.47	1.52	1.51
Cr	0.02	0.02	0.01	0.01	0.02	0.01	0.01	0.01	0.02	0.02	0.00	0.01	0.01	0.03	0.01	0.02	0.02	0.01	0.01	0.00	0.00
Mn	0.02	0.02	0.03	0.02	0.02	0.02	0.04	0.03	0.02	0.03	0.03	0.02	0.02	0.01	0.03	0.02	0.02	0.03	0.02	0.01	0.03
Mg	2.97	2.96	2.98	3.05	3.04	2.98	2.97	2.98	2.93	2.95	2.92	2.92	2.91	2.89	2.89	2.87	2.86	2.79	2.73	2.83	2.88
Ca	1.70	1.68	1.73	1.71	1.70	1.68	1.68	1.68	1.70	1.70	1.70	1.72	1.69	1.69	1.69	1.67	1.68	1.67	1.69	1.73	1.67
Na	0.54	0.55	0.55	0.56	0.52	0.55	0.54	0.53	0.56	0.53	0.56	0.57	0.54	0.57	0.57	0.57	0.57	0.58	0.54	0.53	0.53
K	0.06	0.06	0.06	0.06	0.06	0.06	0.06	0.05	0.06	0.06	0.07	0.06	0.06	0.07	0.06	0.06	0.06	0.05	0.06	0.07	0.06
OH	2.46	2.54	2.19	1.93	2.57	2.87	2.74	2.96	2.84	2.84	2.59	2.98	3.70	3.69	3.57	3.96	4.06	5.86	6.75	4.32	5.34
Mg*	0.66	0.66	0.66	0.67	0.67	0.66	0.66	0.67	0.66	0.66	0.66	0.66	0.66	0.66	0.65	0.66	0.66	0.66	0.65	0.65	0.66

Numbers of ions on the basis of 24 (O), c and r indicate "core" and "rim" respectively

continued

Table 2.4.2. (Continued)

Sample	132-2b	132-2r	132-3c	132-3b	132-3r	132-4c	132-4r	132-5c	132-5r	132-6c	132-6r	132-7c	132-7r	132-8c	132-8r	132-9c	132-9r	132-10c	132-10r	253-1c
SiO2	43.01	42.72	43.72	43.84	43.64	44.14	43.34	44.66	44.18	43.61	43.09	43.74	43.87	43.43	43.15	43.92	44.17	42.12	42.05	47.12
Al2O3	11.12	11.26	11.74	11.72	11.36	11.01	11.61	11.43	11.98	11.73	11.56	11.10	10.73	11.54	11.87	11.79	11.62	11.26	11.24	9.75
TiO2	1.23	1.34	1.20	1.23	1.46	1.18	1.58	1.45	1.56	1.32	1.36	1.25	1.40	1.43	1.60	1.31	1.55	1.41	1.40	0.66
FeO	12.48	12.81	12.82	12.88	12.57	12.35	12.50	12.56	12.58	12.26	12.14	12.44	12.65	12.62	13.10	12.49	12.90	12.60	12.72	10.52
Cr2O3	0.03	0.05	0.53	0.31	0.10	0.06	0.05	0.07	0.11	0.86	1.27	0.07	0.00	0.10	0.04	0.13	0.13	0.25	0.38	0.00
MnO	0.28	0.24	0.15	0.21	0.25	0.18	0.14	0.14	0.15	0.16	0.25	0.24	0.17	0.25	0.20	0.30	0.20	0.25	0.13	0.18
MgO	13.56	13.43	13.19	13.43	13.48	13.75	13.30	13.46	13.31	13.19	13.09	13.58	13.79	13.34	13.33	13.32	13.46	13.20	13.27	14.78
CaO	11.12	11.08	11.15	10.99	11.18	11.17	11.11	11.25	11.27	11.16	11.04	11.30	11.32	11.34	11.24	11.15	10.96	11.33	11.24	11.19
Na2O	1.99	1.98	1.98	2.00	2.06	1.95	2.04	2.01	2.14	2.02	2.04	1.89	1.83	1.93	2.11	2.01	2.00	2.04	2.03	1.99
K2O	0.35	0.35	0.37	0.37	0.36	0.31	0.37	0.34	0.35	0.36	0.36	0.36	0.36	0.35	0.39	0.34	0.33	0.37	0.41	0.28
H2O	4.82	4.74	3.15	3.03	3.55	3.91	3.96	2.64	2.38	3.33	3.83	4.03	3.89	3.66	2.98	3.25	2.68	5.16	5.14	2.05
Total	99.99	100.00	100.00	100.01	100.01	100.01	100.00	100.01	100.01	100.00	100.03	100.00	100.01	99.99	100.01	100.01	100.00	99.99	100.01	98.52
Si	6.12	6.10	6.33	6.35	6.29	6.32	6.22	6.48	6.43	6.30	6.20	6.27	6.30	6.26	6.28	6.34	6.42	6.00	5.99	6.88
AlIV	1.87	1.89	1.67	1.65	1.71	1.68	1.78	1.52	1.57	1.70	1.80	1.73	1.70	1.74	1.72	1.66	1.58	1.89	1.89	1.12
AlVI	0.00	0.00	0.33	0.35	0.22	0.18	0.18	0.43	0.49	0.29	0.16	0.14	0.11	0.21	0.31	0.34	0.41	0.00	0.00	0.56
Ti	0.13	0.14	0.13	0.13	0.16	0.13	0.17	0.16	0.17	0.14	0.15	0.13	0.15	0.15	0.18	0.14	0.17	0.15	0.15	0.07
Fe3+	0.00	0.00	0.00	0.00	0.00	0.00	0.00	0.00	0.00	0.00	0.00	0.00	0.00	0.00	0.00	0.00	0.00	0.00	0.00	0.00
Fe2+	1.49	1.53	1.55	1.56	1.51	1.48	1.50	1.52	1.53	1.48	1.46	1.49	1.52	1.52	1.59	1.51	1.57	1.50	1.52	1.28
Cr	0.00	0.01	0.06	0.04	0.01	0.01	0.01	0.01	0.01	0.10	0.14	0.01	0.00	0.01	0.00	0.01	0.01	0.03	0.04	0.00
Mn	0.03	0.03	0.02	0.03	0.03	0.02	0.02	0.02	0.02	0.02	0.03	0.03	0.02	0.03	0.02	0.04	0.02	0.03	0.02	0.02
Mg	2.88	2.86	2.85	2.90	2.90	2.93	2.84	2.91	2.89	2.84	2.81	2.90	2.95	2.86	2.89	2.87	2.91	2.80	2.82	3.22
Ca	1.70	1.69	1.73	1.71	1.73	1.71	1.71	1.75	1.76	1.73	1.70	1.73	1.74	1.75	1.75	1.72	1.71	1.73	1.72	1.75
Na	0.55	0.55	0.56	0.56	0.58	0.54	0.57	0.57	0.60	0.57	0.57	0.52	0.51	0.54	0.59	0.56	0.56	0.56	0.56	0.56
K	0.06	0.06	0.07	0.07	0.07	0.06	0.07	0.06	0.07	0.07	0.07	0.07	0.07	0.06	0.07	0.06	0.06	0.07	0.07	0.05
OH	4.58	4.51	3.04	2.93	3.41	3.73	3.79	2.55	2.31	3.21	3.67	3.85	3.72	3.52	2.89	3.13	2.60	4.90	4.88	2.00
Mg*	0.66	0.65	0.65	0.65	0.66	0.66	0.65	0.66	0.65	0.66	0.66	0.66	0.66	0.65	0.64	0.66	0.65	0.65	0.65	0.71

continued

Table 2.4.2. (Continued)

Sample	253-1r	253-2c	253-2r	253-3c	253-3r	253-4c	253-4r	253-5c	253-5r	253-6c	253-7c	253-8c	253-9c	253-10c	253-11c	253-12c	253-13c	253-14c	253-15c	253-16c	253-17c
SiO2	46.75	47.03	47.77	46.79	47.70	47.90	47.34	47.00	47.66	47.15	46.12	47.83	47.59	45.88	47.00	47.56	47.36	46.88	46.31	47.33	46.88
Al2O3	10.29	10.16	8.88	10.55	9.15	9.13	9.38	10.06	9.17	9.18	10.64	9.26	8.58	11.16	9.99	10.07	10.14	10.40	11.05	9.81	10.29
TiO2	0.48	0.39	0.73	0.50	0.65	0.65	0.77	0.37	0.74	0.84	0.48	0.73	0.72	0.64	0.68	0.59	0.53	0.42	0.38	0.64	0.40
FeO	10.76	10.83	10.99	10.96	11.03	10.83	10.87	10.72	10.75	10.59	10.52	10.56	10.49	10.87	10.74	10.58	10.66	10.88	10.83	11.09	10.73
Cr2O3	0.00	0.00	0.00	0.00	0.00	0.00	0.00	0.00	0.00	0.00	0.00	0.00	0.00	0.00	0.00	0.00	0.00	0.00	0.00	0.00	0.00
MnO	0.20	0.15	0.25	0.25	0.19	0.22	0.18	0.17	0.17	0.22	0.12	0.20	0.19	0.17	0.20	0.15	0.18	0.13	0.16	0.20	0.13
MgO	14.77	14.70	15.25	14.65	15.24	15.27	15.07	14.76	15.17	15.22	14.45	14.99	15.27	14.36	15.03	15.12	15.26	14.68	14.26	14.96	14.61
CaO	11.32	11.12	10.87	11.05	10.78	10.89	10.75	11.38	10.58	10.80	11.02	10.83	10.88	10.99	10.69	10.83	10.67	11.48	10.90	10.54	11.17
Na2O	1.99	1.89	1.81	2.03	1.89	1.87	1.93	1.82	1.89	1.85	2.09	2.07	1.88	2.16	2.07	2.04	2.01	1.88	2.04	1.91	1.90
K2O	0.28	0.37	0.22	0.24	0.17	0.17	0.25	0.34	0.21	0.23	0.36	0.21	0.19	0.32	0.19	0.18	0.22	0.26	0.34	0.21	0.33
H2O	2.06	2.06	2.06	2.06	2.06	2.07	2.06	2.05	2.06	2.05	2.04	2.06	2.04	2.05	2.06	2.07	2.07	2.06	2.04	2.06	2.05
Total	98.90	98.70	98.83	99.08	98.86	99.00	98.60	98.67	98.40	98.13	97.84	98.74	97.83	98.60	98.65	99.19	99.10	99.07	98.31	98.75	98.49
Si	6.81	6.86	6.95	6.80	6.94	6.95	6.90	6.86	6.95	6.91	6.79	6.95	6.98	6.71	6.85	6.88	6.86	6.82	6.78	6.89	6.85
AlIV	1.19	1.14	1.05	1.20	1.06	1.05	1.10	1.14	1.05	1.09	1.21	1.05	1.02	1.29	1.15	1.12	1.14	1.18	1.22	1.11	1.15
AlVI	0.58	0.61	0.48	0.61	0.51	0.51	0.52	0.59	0.53	0.49	0.63	0.54	0.47	0.64	0.56	0.60	0.59	0.60	0.69	0.57	0.62
Ti	0.05	0.04	0.08	0.05	0.07	0.07	0.08	0.04	0.08	0.09	0.05	0.08	0.08	0.07	0.07	0.06	0.06	0.05	0.04	0.07	0.04
Fe3+	0.00	0.00	0.00	0.00	0.00	0.00	0.00	0.00	0.00	0.00	0.00	0.00	0.00	0.00	0.00	0.00	0.00	0.00	0.00	0.00	0.00
Fe2+	1.31	1.32	1.34	1.33	1.34	1.31	1.33	1.31	1.31	1.30	1.29	1.28	1.29	1.33	1.31	1.28	1.29	1.32	1.33	1.35	1.31
Cr	0.00	0.00	0.00	0.00	0.00	0.00	0.00	0.00	0.00	0.00	0.00	0.00	0.00	0.00	0.00	0.00	0.00	0.00	0.00	0.00	0.00
Mn	0.02	0.02	0.03	0.03	0.02	0.03	0.02	0.02	0.02	0.03	0.01	0.02	0.02	0.02	0.02	0.02	0.02	0.02	0.02	0.02	0.02
Mg	3.21	3.20	3.31	3.18	3.30	3.30	3.28	3.21	3.30	3.32	3.17	3.25	3.34	3.13	3.27	3.26	3.30	3.18	3.11	3.25	3.18
Ca	1.77	1.74	1.70	1.72	1.68	1.69	1.68	1.78	1.65	1.69	1.74	1.69	1.71	1.72	1.67	1.68	1.66	1.79	1.71	1.64	1.75
Na	0.56	0.53	0.51	0.57	0.53	0.53	0.55	0.51	0.53	0.53	0.60	0.58	0.53	0.61	0.58	0.57	0.56	0.53	0.58	0.54	0.54
K	0.05	0.07	0.04	0.04	0.03	0.03	0.05	0.06	0.04	0.04	0.07	0.04	0.04	0.06	0.04	0.03	0.04	0.05	0.06	0.04	0.06
OH	2.00	2.00	2.00	2.00	2.00	2.00	2.00	2.00	2.00	2.00	2.00	2.00	2.00	2.00	2.00	2.00	2.00	2.00	1.99	2.00	2.00
Mg*	0.71	0.71	0.71	0.70	0.71	0.72	0.71	0.71	0.72	0.72	0.71	0.72	0.72	0.70	0.71	0.72	0.72	0.71	0.70	0.71	0.71

continued

Table 2.4.2. (Continued)

Sample	253-18c	253-19c	253-20c	254-1c	254-1r	254-2c	254-2r	254-3c	254-3r	254-4c	254-4r	254-5c	254-6c	254-7c	254-8c	254-9c	254-10c	254-11c	254-12c	254-13c	254-14c
SiO2	48.10	46.67	48.73	46.86	47.97	46.85	48.19	47.78	48.05	48.00	47.78	48.59	46.32	47.97	47.45	47.86	47.85	47.07	49.36	52.80	47.78
Al2O3	8.60	10.12	8.41	10.12	8.56	9.81	8.53	9.12	8.48	9.01	8.94	8.26	10.69	8.71	9.93	8.59	9.40	9.78	7.80	4.17	9.02
TiO2	0.63	0.44	0.63	0.49	0.49	0.61	0.75	0.68	0.60	0.51	0.48	0.39	0.39	0.52	0.35	0.58	0.33	0.49	0.51	0.16	0.39
FeO	10.61	10.79	10.57	11.43	10.86	11.09	10.84	10.95	10.93	10.86	10.78	10.77	11.59	10.62	11.26	11.06	11.51	10.83	10.42	9.57	10.85
Cr2O3	0.00	0.00	0.00	0.00	0.00	0.00	0.00	0.00	0.00	0.00	0.00	0.00	0.00	0.00	0.00	0.00	0.00	0.00	0.00	0.00	0.00
MnO	0.14	0.17	0.12	0.23	0.22	0.20	0.18	0.24	0.20	0.18	0.18	0.21	0.20	0.16	0.20	0.19	0.22	0.21	0.22	0.19	0.20
MgO	15.36	14.52	15.36	14.27	14.49	14.44	14.88	14.81	15.00	14.80	14.68	15.21	13.77	14.93	14.33	14.81	14.27	14.43	15.40	17.37	14.78
CaO	10.99	10.93	10.99	11.49	11.61	11.60	11.67	11.59	11.66	11.77	11.69	11.73	11.54	11.69	11.54	11.71	11.34	11.50	11.52	11.89	11.40
Na2O	1.79	1.95	1.70	1.80	1.59	1.82	1.55	1.66	1.58	1.58	1.58	1.47	1.77	1.57	1.67	1.61	1.63	1.68	1.47	0.84	1.64
K2O	0.20	0.31	0.20	0.24	0.25	0.24	0.27	0.20	0.22	0.21	0.29	0.17	0.34	0.15	0.33	0.21	0.31	0.29	0.20	0.06	0.23
H2O	2.06	2.04	2.07	2.05	2.04	2.05	2.06	2.06	2.06	2.06	2.05	2.06	2.04	2.05	2.06	2.05	2.06	2.05	2.07	2.10	2.05
Total	98.48	97.94	98.78	98.98	98.08	98.71	98.92	99.09	98.78	98.98	98.45	98.86	98.65	98.37	99.12	98.67	98.92	98.33	98.97	99.15	98.34
Si	7.01	6.86	7.06	6.84	7.04	6.85	7.01	6.94	7.00	6.98	6.98	7.06	6.79	7.00	6.90	6.99	6.97	6.89	7.14	7.55	6.99
AlIV	0.99	1.14	0.94	1.16	0.96	1.15	0.99	1.06	1.00	1.02	1.02	0.94	1.21	1.00	1.10	1.01	1.03	1.11	0.86	0.45	1.01
AlVI	0.48	0.61	0.50	0.58	0.52	0.54	0.47	0.50	0.46	0.52	0.52	0.47	0.64	0.50	0.60	0.47	0.59	0.58	0.47	0.25	0.54
Ti	0.07	0.05	0.07	0.05	0.05	0.07	0.08	0.07	0.07	0.06	0.05	0.04	0.04	0.06	0.04	0.06	0.04	0.05	0.06	0.02	0.04
Fe3+	0.00	0.00	0.00	0.00	0.00	0.00	0.00	0.00	0.00	0.00	0.00	0.00	0.00	0.00	0.00	0.00	0.00	0.00	0.00	0.00	0.00
Fe2+	1.29	1.33	1.28	1.40	1.33	1.36	1.32	1.33	1.33	1.32	1.32	1.31	1.42	1.30	1.37	1.35	1.40	1.33	1.26	1.14	1.33
Cr	0.00	0.00	0.00	0.00	0.00	0.00	0.00	0.00	0.00	0.00	0.00	0.00	0.00	0.00	0.00	0.00	0.00	0.00	0.00	0.00	0.00
Mn	0.02	0.02	0.01	0.03	0.03	0.02	0.02	0.03	0.02	0.02	0.02	0.03	0.02	0.02	0.02	0.02	0.03	0.03	0.03	0.02	0.02
Mg	3.34	3.18	3.32	3.11	3.17	3.15	3.23	3.21	3.26	3.21	3.20	3.29	3.01	3.25	3.11	3.22	3.10	3.15	3.32	3.70	3.22
Ca	1.72	1.72	1.71	1.80	1.82	1.82	1.82	1.80	1.82	1.83	1.83	1.83	1.81	1.83	1.80	1.83	1.77	1.80	1.79	1.82	1.79
Na	0.51	0.56	0.48	0.51	0.45	0.52	0.44	0.47	0.45	0.45	0.45	0.41	0.50	0.44	0.47	0.46	0.46	0.48	0.41	0.23	0.46
K	0.04	0.06	0.04	0.04	0.05	0.04	0.05	0.04	0.04	0.04	0.05	0.03	0.06	0.03	0.06	0.04	0.06	0.05	0.04	0.01	0.04
OH	2.00	2.00	2.00	2.00	2.00	2.00	2.00	2.00	2.00	2.00	2.00	2.00	2.00	2.00	2.00	2.00	2.00	2.00	2.00	2.00	2.00
Mg*	0.72	0.71	0.72	0.69	0.70	0.70	0.71	0.71	0.71	0.71	0.71	0.72	0.68	0.71	0.69	0.70	0.69	0.70	0.72	0.76	0.71

continued

Table 2.4.2. (Continued)

Sample	254-15c	254-16c	254-17c	254-18c	254-19c	254-20c	255-1c	255-2c	255-2r	255-3c	255-3r	255-4c	255-4r	255-5c	255-5r	255-6c	255-6r	255-7c	255-8c	255-9c	255-10c
SiO2	48.52	47.03	48.67	47.30	47.10	46.64	46.81	46.95	46.76	46.39	47.11	45.69	46.81	48.07	47.68	47.93	48.44	47.67	47.94	46.86	47.60
Al2O3	8.36	9.45	7.86	9.20	9.60	9.94	10.78	9.80	10.06	10.45	9.35	11.43	9.80	8.74	9.12	8.70	8.37	9.19	8.73	9.98	9.45
TiO2	0.66	0.91	0.54	0.84	0.60	0.94	0.40	0.58	0.87	0.52	0.80	0.39	0.60	0.50	0.47	0.39	0.49	0.53	0.40	0.50	0.48
FeO	10.88	11.00	10.90	11.20	11.37	11.62	11.61	11.53	11.84	11.41	11.17	11.76	11.59	11.13	11.09	10.85	10.92	11.25	11.17	11.15	11.17
Cr2O3	0.00	0.00	0.00	0.00	0.00	0.00	0.00	0.00	0.00	0.00	0.00	0.00	0.00	0.00	0.00	0.00	0.00	0.00	0.00	0.00	0.00
MnO	0.13	0.24	0.14	0.20	0.18	0.23	0.17	0.21	0.17	0.23	0.22	0.18	0.18	0.21	0.24	0.27	0.23	0.23	0.18	0.24	0.23
MgO	15.04	14.44	15.24	14.38	14.34	14.05	14.19	14.28	14.21	13.92	14.34	13.55	14.32	14.96	14.90	15.04	15.13	14.72	14.92	14.21	14.45
CaO	11.67	11.59	11.63	11.59	11.63	11.65	11.54	11.60	11.37	11.58	11.52	11.25	11.57	11.58	11.65	11.75	11.71	11.56	11.53	11.56	11.64
Na2O	1.49	1.71	1.50	1.67	1.69	1.80	1.91	1.82	1.85	1.87	1.74	1.97	1.80	1.59	1.66	1.56	1.61	1.71	1.57	1.81	1.75
K2O	0.22	0.29	0.25	0.24	0.22	0.26	0.34	0.22	0.31	0.31	0.26	0.36	0.18	0.17	0.20	0.21	0.21	0.27	0.19	0.21	0.27
H2O	2.07	2.05	2.06	2.05	2.05	2.05	2.07	2.05	2.06	2.05	2.05	2.04	2.05	2.06	2.06	2.06	2.07	2.06	2.06	2.05	2.06
Total	99.04	98.71	98.79	98.67	98.78	99.18	99.82	99.04	99.50	98.73	98.56	98.62	98.90	99.01	99.07	98.76	99.18	99.19	98.69	98.57	99.10
Si	7.04	6.88	7.08	6.92	6.88	6.81	6.78	6.86	6.81	6.80	6.90	6.71	6.84	6.99	6.94	6.99	7.03	6.93	6.99	6.86	6.93
AlIV	0.96	1.12	0.92	1.08	1.12	1.19	1.22	1.14	1.19	1.20	1.10	1.29	1.16	1.01	1.06	1.01	0.97	1.07	1.01	1.14	1.07
AlVI	0.47	0.50	0.43	0.50	0.54	0.52	0.62	0.54	0.53	0.60	0.51	0.69	0.53	0.49	0.50	0.48	0.46	0.51	0.49	0.58	0.55
Ti	0.07	0.10	0.06	0.09	0.07	0.10	0.04	0.06	0.10	0.06	0.09	0.04	0.07	0.05	0.05	0.04	0.05	0.06	0.04	0.06	0.05
Fe3+	0.00	0.00	0.00	0.00	0.00	0.00	0.00	0.00	0.00	0.00	0.00	0.00	0.00	0.00	0.00	0.00	0.00	0.00	0.00	0.00	0.00
Fe2+	1.32	1.34	1.33	1.37	1.39	1.42	1.41	1.41	1.44	1.40	1.37	1.44	1.42	1.35	1.35	1.32	1.32	1.37	1.36	1.36	1.36
Cr	0.00	0.00	0.00	0.00	0.00	0.00	0.00	0.00	0.00	0.00	0.00	0.00	0.00	0.00	0.00	0.00	0.00	0.00	0.00	0.00	0.00
Mn	0.02	0.03	0.02	0.02	0.02	0.03	0.02	0.03	0.02	0.03	0.03	0.02	0.02	0.03	0.03	0.03	0.03	0.03	0.02	0.03	0.03
Mg	3.25	3.15	3.31	3.13	3.12	3.06	3.07	3.11	3.08	3.04	3.13	2.97	3.12	3.24	3.23	3.27	3.27	3.19	3.24	3.10	3.14
Ca	1.81	1.82	1.81	1.82	1.82	1.82	1.79	1.81	1.77	1.82	1.81	1.77	1.81	1.80	1.82	1.83	1.82	1.80	1.80	1.81	1.81
Na	0.42	0.48	0.42	0.47	0.48	0.51	0.54	0.52	0.52	0.53	0.49	0.56	0.51	0.45	0.47	0.44	0.45	0.48	0.44	0.51	0.49
K	0.04	0.05	0.05	0.04	0.04	0.05	0.06	0.04	0.06	0.06	0.05	0.07	0.03	0.03	0.04	0.04	0.04	0.05	0.04	0.04	0.05
OH	2.00	2.00	2.00	2.00	2.00	2.00	2.00	2.00	2.00	2.00	2.00	2.00	2.00	2.00	2.00	2.00	2.00	2.00	2.00	2.00	2.00
Mg*	0.71	0.70	0.71	0.70	0.69	0.68	0.69	0.69	0.68	0.69	0.70	0.67	0.69	0.71	0.71	0.71	0.71	0.70	0.70	0.69	0.70

continued

Table 2.4.2. (Continued)

Sample	255-11c	255-12c	255-13c	255-14c	255-15c	256-1c	256-1r	256-2c	256-3c	256-4c	256-5c	256-6c	256-7c	256-8c	256-9c	256-10c	256-11c	256-12c	256-13c	256-14c	256-15c
SiO2	46.98	48.32	46.15	47.08	48.71	44.06	44.22	44.10	44.54	44.02	43.38	45.03	45.25	44.88	45.99	43.70	45.26	44.54	43.40	45.23	43.39
Al2O3	9.64	8.54	10.79	9.70	7.84	12.14	11.56	12.31	11.18	12.25	13.45	11.15	10.94	11.62	10.37	12.56	10.77	11.80	13.71	11.35	13.04
TiO2	0.83	0.47	0.38	0.60	0.35	0.70	0.96	0.43	1.01	0.87	0.49	0.68	0.71	0.47	0.76	0.78	1.00	0.48	0.49	0.53	0.53
FeO	11.27	11.08	11.55	11.34	10.53	13.15	13.44	13.06	13.51	13.56	13.70	13.11	13.08	13.20	12.95	13.43	13.17	13.29	13.79	13.03	13.43
Cr2O3	0.00	0.00	0.00	0.00	0.00	0.00	0.00	0.00	0.00	0.00	0.00	0.00	0.00	0.00	0.00	0.00	0.00	0.00	0.00	0.00	0.00
MnO	0.18	0.23	0.22	0.17	0.20	0.17	0.10	0.15	0.11	0.21	0.16	0.12	0.12	0.22	0.11	0.20	0.18	0.23	0.15	0.14	0.21
MgO	14.12	15.21	13.71	14.37	15.35	12.14	12.27	12.27	12.35	12.20	11.50	12.65	12.81	12.55	13.19	11.88	12.70	12.41	11.31	12.71	11.82
CaO	11.54	11.54	11.16	11.62	11.66	11.62	11.50	11.48	11.63	11.58	11.38	11.63	11.68	11.47	11.63	11.59	11.61	11.44	11.20	11.54	11.55
Na2O	1.77	1.59	1.91	1.72	1.44	2.06	2.06	1.95	1.97	2.06	2.06	1.89	1.88	1.98	1.77	2.09	1.91	2.04	2.11	1.94	2.11
K2O	0.25	0.20	0.34	0.32	0.17	0.35	0.44	0.50	0.40	0.54	0.50	0.40	0.32	0.42	0.34	0.52	0.44	0.46	0.54	0.35	0.43
H2O	2.05	2.07	2.04	2.05	2.06	2.01	2.01	2.01	2.02	2.03	2.01	2.02	2.03	2.03	2.04	2.02	2.03	2.02	2.02	2.03	2.01
Total	98.63	99.25	98.25	98.97	98.31	98.40	98.56	98.26	98.72	99.32	98.63	98.68	98.82	98.84	99.15	98.77	99.07	98.71	98.72	98.85	98.52
Si	6.88	7.01	6.79	6.87	7.11	6.56	6.58	6.57	6.62	6.51	6.46	6.67	6.69	6.64	6.76	6.50	6.68	6.61	6.45	6.68	6.47
AlIV	1.12	0.99	1.21	1.13	0.89	1.44	1.42	1.43	1.38	1.49	1.54	1.33	1.31	1.36	1.24	1.50	1.32	1.39	1.55	1.32	1.53
AlVI	0.54	0.47	0.66	0.54	0.45	0.69	0.61	0.73	0.58	0.65	0.82	0.62	0.60	0.67	0.56	0.70	0.56	0.67	0.86	0.65	0.76
Ti	0.09	0.05	0.04	0.07	0.04	0.08	0.11	0.05	0.11	0.10	0.05	0.08	0.08	0.05	0.08	0.09	0.11	0.05	0.05	0.06	0.06
Fe3+	0.00	0.00	0.00	0.00	0.00	0.00	0.00	0.00	0.00	0.00	0.00	0.00	0.00	0.00	0.00	0.00	0.00	0.00	0.00	0.00	0.00
Fe2+	1.38	1.34	1.42	1.38	1.28	1.64	1.67	1.63	1.68	1.68	1.71	1.62	1.62	1.63	1.59	1.67	1.63	1.65	1.71	1.61	1.67
Cr	0.00	0.00	0.00	0.00	0.00	0.00	0.00	0.00	0.00	0.00	0.00	0.00	0.00	0.00	0.00	0.00	0.00	0.00	0.00	0.00	0.00
Mn	0.02	0.03	0.03	0.02	0.02	0.02	0.01	0.02	0.01	0.03	0.02	0.02	0.02	0.03	0.01	0.03	0.02	0.03	0.02	0.02	0.03
Mg	3.08	3.29	3.01	3.13	3.34	2.69	2.72	2.72	2.74	2.69	2.55	2.79	2.82	2.77	2.89	2.63	2.80	2.75	2.51	2.80	2.63
Ca	1.81	1.79	1.76	1.82	1.82	1.85	1.83	1.83	1.85	1.84	1.81	1.85	1.85	1.82	1.83	1.85	1.84	1.82	1.78	1.83	1.84
Na	0.50	0.45	0.55	0.49	0.41	0.59	0.59	0.56	0.57	0.59	0.59	0.54	0.54	0.57	0.50	0.60	0.55	0.59	0.61	0.56	0.61
K	0.05	0.04	0.06	0.06	0.03	0.07	0.08	0.09	0.08	0.10	0.09	0.08	0.06	0.08	0.06	0.10	0.08	0.09	0.10	0.07	0.08
OH	2.00	2.00	2.00	2.00	2.00	2.00	2.00	2.00	2.00	2.00	2.00	2.00	2.00	2.00	2.00	2.00	2.00	2.00	2.00	2.00	2.00
Mg*	0.69	0.71	0.68	0.69	0.72	0.62	0.62	0.63	0.62	0.62	0.60	0.63	0.64	0.63	0.64	0.61	0.63	0.62	0.59	0.63	0.61

continued

Table 2.4.2. (Continued)

Sample	257-1c	257-1r	257-2c	257-2r	257-3c	257-3r	257-4c	257-4r	257-5c	257-5r	257-6c	257-7c	257-8c	257-9c	257-10c	257-11c	257-12c	257-13c	257-14c	257-15c	257-16c
SiO2	44.34	45.38	44.84	45.11	46.73	45.73	44.85	45.68	45.25	45.74	45.72	46.11	43.83	46.44	46.09	46.18	45.68	43.61	43.92	43.91	43.58
Al2O3	12.08	10.93	12.11	11.25	10.66	10.65	12.12	10.81	11.49	10.74	10.63	10.44	12.89	10.23	10.87	10.18	10.22	13.85	13.27	13.28	13.53
TiO2	0.63	0.82	0.45	0.84	0.38	0.82	0.48	0.89	0.54	0.91	0.90	0.71	0.47	0.85	0.67	0.74	0.69	0.47	0.46	0.60	0.54
FeO	12.94	12.82	13.12	12.90	12.60	12.57	13.02	12.51	12.86	12.81	12.54	12.43	12.65	12.35	12.42	12.15	12.28	12.58	12.28	12.30	12.82
Cr2O3	0.00	0.00	0.00	0.00	0.00	0.00	0.00	0.00	0.00	0.00	0.00	0.00	0.00	0.00	0.00	0.00	0.00	0.00	0.00	0.00	0.00
MnO	0.18	0.19	0.14	0.18	0.17	0.13	0.22	0.19	0.21	0.20	0.18	0.14	0.14	0.16	0.19	0.19	0.11	0.17	0.19	0.17	0.16
MgO	12.47	12.92	12.45	12.69	13.59	13.23	12.60	13.25	12.90	13.12	13.12	13.47	12.15	13.66	13.41	13.65	13.44	12.25	12.44	12.46	12.20
CaO	11.46	11.59	11.40	11.62	11.54	11.62	11.36	11.48	11.52	11.61	11.61	11.59	11.18	11.42	11.57	11.70	11.36	11.28	11.33	11.45	11.27
Na2O	2.07	1.93	2.07	1.98	1.84	1.94	2.16	1.88	1.94	1.88	1.94	1.85	2.15	1.83	1.90	1.87	1.79	2.16	2.16	2.18	2.20
K2O	0.42	0.42	0.47	0.34	0.38	0.41	0.50	0.38	0.34	0.35	0.43	0.36	0.46	0.38	0.25	0.36	0.33	0.45	0.51	0.51	0.42
H2O	2.02	2.03	2.03	2.03	2.06	2.04	2.04	2.04	2.04	2.04	2.04	2.04	2.01	2.05	2.05	2.04	2.02	2.03	2.03	2.03	2.03
Total	98.61	99.03	99.08	98.94	99.95	99.14	99.35	99.11	99.09	99.40	99.11	99.14	97.93	99.37	99.42	99.06	97.92	98.85	98.59	98.89	98.75
Si	6.58	6.69	6.61	6.66	6.79	6.72	6.60	6.71	6.66	6.71	6.72	6.77	6.53	6.79	6.74	6.78	6.78	6.44	6.49	6.48	6.45
AlIV	1.42	1.31	1.39	1.34	1.21	1.28	1.40	1.29	1.34	1.29	1.28	1.23	1.47	1.21	1.26	1.22	1.22	1.56	1.51	1.52	1.55
AlVI	0.69	0.59	0.72	0.62	0.62	0.57	0.70	0.58	0.65	0.57	0.57	0.57	0.80	0.55	0.61	0.54	0.57	0.85	0.81	0.79	0.81
Ti	0.07	0.09	0.05	0.09	0.04	0.09	0.05	0.10	0.06	0.10	0.10	0.08	0.05	0.09	0.07	0.08	0.08	0.05	0.05	0.07	0.06
Fe3+	0.00	0.00	0.00	0.00	0.00	0.00	0.00	0.00	0.00	0.00	0.00	0.00	0.00	0.00	0.00	0.00	0.00	0.00	0.00	0.00	0.00
Fe2+	1.60	1.58	1.62	1.59	1.53	1.55	1.60	1.54	1.58	1.57	1.54	1.52	1.58	1.51	1.52	1.49	1.52	1.55	1.52	1.52	1.59
Cr	0.00	0.00	0.00	0.00	0.00	0.00	0.00	0.00	0.00	0.00	0.00	0.00	0.00	0.00	0.00	0.00	0.00	0.00	0.00	0.00	0.00
Mn	0.02	0.02	0.02	0.02	0.02	0.02	0.03	0.02	0.03	0.02	0.02	0.02	0.02	0.02	0.02	0.02	0.01	0.02	0.02	0.02	0.02
Mg	2.76	2.84	2.74	2.79	2.95	2.90	2.76	2.90	2.83	2.87	2.88	2.95	2.70	2.98	2.92	2.99	2.97	2.70	2.74	2.74	2.69
Ca	1.82	1.83	1.80	1.84	1.80	1.83	1.79	1.81	1.82	1.83	1.83	1.82	1.79	1.79	1.81	1.84	1.81	1.78	1.80	1.81	1.79
Na	0.60	0.55	0.59	0.57	0.52	0.55	0.62	0.54	0.55	0.53	0.55	0.53	0.62	0.52	0.54	0.53	0.52	0.62	0.62	0.62	0.63
K	0.08	0.08	0.09	0.06	0.07	0.08	0.09	0.07	0.06	0.07	0.08	0.07	0.09	0.07	0.05	0.07	0.06	0.08	0.10	0.10	0.08
OH	2.00	2.00	2.00	2.00	2.00	2.00	2.00	2.00	2.00	2.00	2.00	2.00	2.00	2.00	2.00	2.00	2.00	2.00	2.00	2.00	2.00
Mg*	0.63	0.64	0.63	0.64	0.66	0.65	0.63	0.65	0.64	0.65	0.65	0.66	0.63	0.66	0.66	0.67	0.66	0.63	0.64	0.64	0.63